Université de Sherbrooke

Implications des proprotéines convertases lors d'infections : de l'activation du pathogène au contrôle de l'immunité.

Par
Hugo Gagnon
Département de biochimie

Thèse en cotutelle

Présentée à la Faculté de médecine et des sciences de la santé
de l'université de Sherbrooke, Québec, Canada
en vue de l'obtention du grade de philosophiae doctor (Ph.D.)
Biochimie

et

À l'école doctorale de biologie santé
de l'université de Lille 1, Nord-pas de calais, France
en vue de l'obtention du grade de philosophiae doctor (Ph.D.)
en science de la santé

Sherbrooke, Québec, Canada
février, 2013

Membres du jury d'évaluation
Robert Day Ph. D., département de chirurgie, faculté de médecine et des sciences de la santé de l'université de Sherbrooke, Québec, Canada
Michel Salzet Ph.D., Laboratoire de Spectrométrie de Masse Biologique Fondamentale et Appliquée, EA 4550, Université Lille 1, France.
Martin Bisaillon Ph. D., département de Biochimie, faculté de médecine et des sciences de la santé de l'université de Sherbrooke, Québec, Canada
Philipe Bulet Ph.D., AGIM 3, BioPark Archamps, Université Joseph Fournier Grenoble, France.
Annik Prat Ph. D., Unité de biochimie neuroendocrinienne, Institut de recherche clinique de Montreal, Québec, Canada

À Karine, Édouard et Liliane

RÉSUMÉ

Implications des proprotéines convertases lors d'infections : de l'activation du pathogène au contrôle de l'immunité.

Par
Hugo Gagnon
Programmes de biochimie (Québec)
Et de
Science de la santé (France)

Thèse présentée à la Faculté de médecine et des sciences de la santé en vue de l'obtention du diplôme de Philosophiae doctor (Ph.D.) en biochimie, Faculté de médecine et des sciences de la santé, Université de Sherbrooke, Sherbrooke, Québec, Canada, J1H 5N4

et

À l'école doctorale de biologie santé en vue de l'obtention du grade de Philosophiae doctor (Ph.D.) en science de la santé, Université de Lille 1, Lille, 59650 Villeneuve d'Ascq, France

Les proprotéines convertases (PC) sont d'importantes enzymes principalement impliquées dans l'activation par clivage de précurseurs protéiques dans la voie de sécrétion cellulaire. Ce processus essentiel permet de générer des polypeptides biologiquement actifs qui associent les PC à la régulation d'une diversité de processus de la physiologie animale, dont le système neuroendocrinien. Toutefois, les PC ont un rôle très particulier lors d'infections, puisqu'elles participent à la fois à l'activation de divers pathogènes et au contrôle de la réponse immunitaire induite par ceux-ci. Avec le besoin criant de nouvelles cibles thérapeutiques pour lutter contre les infections virales et bactériennes, les PC deviennent donc une nouvelle cible thérapeutique à investiguer. Néanmoins, si une thérapie antivirale ou antibactérienne ciblant les PC est envisagée, elle devra permettre d'atteindre un équilibre entre inhiber l'activation du pathogène et favoriser une réponse immunitaire appropriée, et ce tout en maintenant les fonctions normales des PC dans le maintien de l'homéostasie. Cette thèse présente donc le développement d'un inhibiteur peptidique de PC à des fins thérapeutiques contre les pathogènes et se penche sur le rôle de PC1/3, qui est principalement associée au système neuroendocrinien, dans le contrôle de la réponse immunitaire au sein des macrophages. Il est important de mieux comprendre ce nouveau rôle de PC1/3 jusqu'ici peu décrit, car il pourrait avoir des implications dans la balance de la réponse immunitaire lors de thérapies ciblant les PC. Dans un premier temps, l'inhibiteur de PC a été optimisé grâce à une approche peptidomimétique afin de bloquer l'activation de deux pathogènes par les PC, l'un viral : l'hémagglutinine (HA5) de la grippe aviaire hautement pathogénique (HPAI) H5N1, et l'autre bactérien : la toxine de Shiga de la forme entérohémorragique d'*E. coli*. La relation structure-activité a été étudiée pour améliorer la stabilité, la puissance d'inhibition et la non-toxicité du peptide dans le but de bloquer de manière efficace la fusion cellulaire induite par HA5 et la toxicité de la toxine de Shiga en essais cellulaires. Dans un second temps, l'utilisation d'outils de contrôle de l'expression génique (shRNA) sur un modèle de macrophages en culture NR8383 et du modèle de souris où PC1/3 est inactivée ont permis de déterminer les conséquences physiologiques et moléculaires de l'inactivation de PC1/3 au sein des macrophages grâce au développement d'une approche par spectrométrie de masse. L'imagerie par spectrométrie de masse a permis de déterminer la distribution moléculaire de médiateurs peptidiques dans la rate de souris KO qui a par la suite été corrélée avec une désorganisation de divers acteurs de la réponse immunitaire. De plus, une approche d'identification protéique Gel LC-MS/MS a permis de faire le pont entre le phénotype immunitaire physiologique et la réponse moléculaire de l'inactivation de PC1/3 grâce à des analyses bio-informatiques. L'approche par spectrométrie de masse s'est avérée être un catalyseur dans cette recherche et a pu être appliquée à l'étude de tissus de patientes atteintes du cancer de l'ovaire, démontrant ainsi tous les avantages de cet outil. En somme, les résultats de cette thèse montrent la faisabilité d'inhiber les PC pour contrôler les infections et ouvrir de nouvelles perspectives sur le contrôle de l'immunité en établissant les bases moléculaires du rôle de PC1/3 dans le maintien de l'homéostasie immunitaire.

Mots clés : proprotéines convertases, inhibiteur, spectrométrie de masse, imagerie, influenza H5N1, sécrétion, macrophage, immunité.

SUMMARY

Involvement of the proprotein convertases during infections: from pathogens activation to immunity control.

By
Hugo Gagnon
Biochemistry Program (Quebec)
and
Life Science (France)

Thesis presented at the Faculty of medicine and health sciences for the obtention of philosophiae doctor (Ph.D.) in biochemistry, Faculty of medicine and health sciences, Université de Sherbrooke, Sherbrooke, Québec, Canada, J1H 5N4

And to

Doctoral school of life science for the obtainement of philosophiae doctor (Ph.D.) in life science, Université de Lille 1, Lille, 59650 Villeneuve d'Ascq, France

The proprotein convertases (PCs) are important enzymes mainly involved in the activation of protein precursors into the cell secretory pathway. This critical activation step that generates various biologically active polypeptides makes the PCs a cornerstone in a variety of biological process, including the neuroendocrine system. However, the PCs are described as very special players during infection, since they both activate various pathogens and control the immune response they induce. With the critical need for new therapeutic targets to fight against viral and bacterial infections, the PCs thus become an interesting therapeutic avenue. However, if PCs are considered for antibacterial or antiviral therapy, it will have to achieve a balance between inhibiting infectious agents activation and promoting an appropriate immune response, while maintaining the critical homeostasis functions of PCs. Therefore, this thesis presents the development of a PCs peptide inhibitor for therapeutic purposes against pathogens and examines the role of PC1/3, which is mainly associated with the neuroendocrine system, in the control of the immune response in macrophages. It is important to understand this new role of PC1/3, because it could have implications in the balance of the immune response during therapies targeting PCs. As a first step, the PC inhibitor has been optimized by a peptidomimetic approach to block pathogens activation by PC for both, a viral pathogen (hemagglutinin of highly pathogenic avian influenza H5N1 (HA5)) and a bacterial pathogen (Shiga toxin form enterohaemorrhagic *E. coli*). The structure-activity relationship has been studied to improve the stability, the inhibition power and a low toxicity profile in order to efficiently block HA5 induced cell fusion and Shiga toxin induced toxicity in cell-based assays. In a second step, gene expression control tools have been used (shRNA) on a macrophage NR8383 cell line combined with the use of PC1/3 inactivated mouse (KO) to determine the physiological and molecular consequences of PC1/3 inactivation in macrophages by the mean of mass spectrometry approaches. Mass spectrometry imaging was used to determine the molecular distribution of peptide mediators in the spleen of KO mice that were subsequently correlated with disorganization of various actors in the immune response. In addition, a gel LC-MS/MS proteomic approach (combined with an appropriated bioinformatics analysis) helped to correlate the immunological phenotype of PC1/3 inactivation to the molecular level. The mass spectrometry approaches were proven to be a catalyst in this research and were further applied on ovarian cancer tissues studies, demonstrating the benefits of these tools. Overall, the results of this thesis demonstrate the feasibility of inhibiting PC to control infections and establish new avenues to modulate immunity by laying the foundations of PC1/3 molecular functions in the maintenance of immune homeostasis.

Keywords: proprotein convertase, inhibitor, mass spectrometry, imaging, influenza H5N1, secretion, macrophages, immunity

TABLE DES MATIÈRES

LISTE DES FIGURES

LISTE DES FIGURES SUPPLÉMENTAIRES

LISTE DES TABLEAUX

LISTE DES TABLEAUX SUPPLÉMENTAIRES

LISTE DES ABRÉVIATIONS

ABRÉVIATION	Descriptif français, *English description*
ACTH	Adrénocorticotrophine, Adrenocorticotropic hormone
ADAM	Disintégrine et métalloprotéinase, *A Disintegrin And Metalloproteinase*
ARNv	ARN virale de simple brin de sens négatif, *negative single strain viral RNA*
BMP10	Protéine de morphogénèse osseuse 10, Bone Morphogenetic Proteins 10
CAAR	Révélation d'antigène par l'acide citrique, *Citric acid antigen retrieval*
CID	Dissociation induite par collision, *Collision Induced Dissociation*
CMH	Complexe majeur d'histocompatibilité, *Major Histocompatibility Complexe*
CPA	Cellules présentatrices d'antigènes, *Antigene presenting cells*
DCSG	Vésicules denses de sécrétion, *Dense Core Secretory Granules*
ECD	Dissociation induite par capture d'électron, *Electron Capture Dissociation*
ESI	Ionisation électro spray, *Electro Spray Ionization*
FDR	Taux de faux positif, *False Discovery Rate*
GDF11	Fracteur de croissance et de différenciation 11, Growth Differentiation Factor 11
GHR	Ghréline, *Ghrelin*
GHRH	Hormone de relâche de l'hormone de croissance, *Growth Hormone Releasing Hormone*
HA	Hemagglutinine, *Hemagglutinin*
HCD	Grippe aviaire hautement pathogénique, *Highly Pathogenic Avian Influenza*
HPAI	Dissociation induite par collision à plus haute énergie, *Higher energy Collision Dissociation*
IGF	Facteur de croissance à l'insuline, *Insulin Growth Factor*
IL	Interleukine, *Interleukin*

IFN-γ	Interféron-γ, *Interferon-γ*
IRF3	Facteur de régulation de l'interféron, *Interferon Regulatory Factor 3*
KO	Gène inactivé, *Knock Out gene*
LDLR	Récepteur de lipoprotéines à faible densité, *Low Density Lipoprotein Receptor*
LPS	Lipopolysaccharide, *Lipopolysaccharide*
M2	Protéine de la matrice 2, *Matrix protein 2*
MALDI	Désorption et ionisation au laser assistées par une matrice, *Matrix Assisted Lazer Desorbtion Ionization*
MMP	Métalloprotéinase de la matrice, *Matrix Metallloproteinase*
MSH	Mélanocortine, *Meloanocortin Stimulating Hormone*
MSI	Imagerie par spectrométrie de masse MALDI, *MALDI mass Spectrometry Imaging*
Myd88	Gène de première réponse de différenciation myéloïde 88, *Myeloid differentiation primary response gene 88*
NA	Neuraminidase, *Neuraminidase*
NEC	Convertase neuroendocrinienne, *Neuroendocine Convertase*
Nf-κB	Facteur de nécrose *κB*, *Necrosis factor-κB*
NK	Cellules naturelles tueuses, *Natural Killer cells*
NS1	Protéine non structurale 1, *Non-Strucutral protein 1*
PACAP	Polypeptide activateur de l'adénylate cyclase de l'hypophyse, *Pituitary Adenylate Cyclase-Activating Polypeptides*
PACE4	Enzyme clivant à une paire de résidus basiques 4, *Paired basic Amino acid residue-Cleaving Enzyme 4*
PAMP	Motif moléculaire associé au pathogène, *Pathogen Associated Molecular Partern*
PB2	Polymérase B2, *Polymerase B2*
PC	Proprotéine convertase, *Proprotein Convertase*
PCA	Analyse en composante principale, *Principal Component Analysis*
PCSK	Proprotéine convertase subtilisine/kexine, *Proprotein Convertase Subtilisin/Kexin*

PS	Peptide signal, *Signal Peptide*
POMC	Pro-opiomélanocortine, *Proopiomleanocorin*
RE	Réticulum endoplasmique, *Endoplasmic Reticulum*
RNPv	Complexe ribonucloprotéique viral, *RiboNucleoProtic complexe*
S1P	Protéase site-1, *Site-1 Protease*
SKI-1	Isozyme 1 subitilisine/kexine, *Subtilisin/Kexin-Isozyme 1*
SRAS	Syndrome respiratoire aigu sévère, *Severe Acute Respiratory Syndrome*
TACE	Enzyme d'activation du facteur de nécrose tumorale alpha, *Tumor necrosis factor-α-Converting Enzyme*
TGF-β1	Facteur de croissance et de transformation, *transforming growth factor* β1 *English description*
TGN	Réseaux trans-Golgien, *Trans-Golgi Network*
TIMP	Inhibiteur tissulaire de métalloprotéinase, T*issu Inhibitor of MetelloProtease*
TIR	TOLL/interleukine-1, *TOLL/interleukin-1*
TLR	Récepteur Toll-like, *Toll-Like Receptor*
TNF	Facteur de nécrose tumorale, *Tumor Necrosis Factor*
TOF	Temps de vol, *Time Of Flight*
TRAM	Molécule adaptatrice associée à TRIF, *TRIF Related Adaptor Molecule*
TRIF	Protéine adaptatrice contenant le domaine TIR induisant l'INF, *TIR-domain-containing adaptor protein inducing IFN*
UNC	Urocortine, *Urocortin*
VIP	Peptide vasoactif intestinal, *Vasoactive Intestinal Peptide*
WT	Souche sauvage, *Wild-Type*

INTRODUCTION

Le système moléculaire cellulaire est, d'une façon simplifiée, constitué de trois composantes majeures qui permettent d'orchestrer la vie soit : le code génétique (ADN), le messager du code (ARNm) et le résultat du code (les protéines). Avec les années, beaucoup d'efforts ont été déployés pour trouver des mutations et des variations génétiques qui pourraient causer ou prédire des maladies. Toutefois, ces mutations génétiques s'avèrent plutôt être l'exception que la règle. En réalité, seulement 5,3 à 7,9 % des maladies diagnostiquées à l'âge de 25 ans seront d'origines génétiques (Baird et al. 1988). Les secrets derrière les maladies se cachent donc à des niveaux de complexités supérieures. Le protéome, qui désigne l'ensemble des protéines, l'illustre bien par sa grande complexité. Les protéines, par leurs structures tridimensionnelles, leurs interactions, leurs changements de conformations et leurs activités catalytiques (si ce sont des enzymes) donnent vie aux cellules. Elles permettent la synthèse et la modification de composés essentiels à la survie cellulaire, mais aussi caractérisent les fonctions et les réponses cellulaires à travers les tissus. De plus, un niveau de complexité supplémentaire est présent au sein du protéome, puisque plusieurs protéines peuvent être elles-mêmes modifiées par diverses classes d'enzymes. Il existe plus d'une centaine de modifications dites post-traductionnelles qui permettent de réguler la fonction, la localisation, l'activité et la structure des protéines de façon réversible ou non (Khoury et al. 2011) (Figure 1). Toutefois, on oublie souvent un type de modification irréversible, mais d'une importance capitale : la protéolyse (Lopez-Otin and Overall 2002).

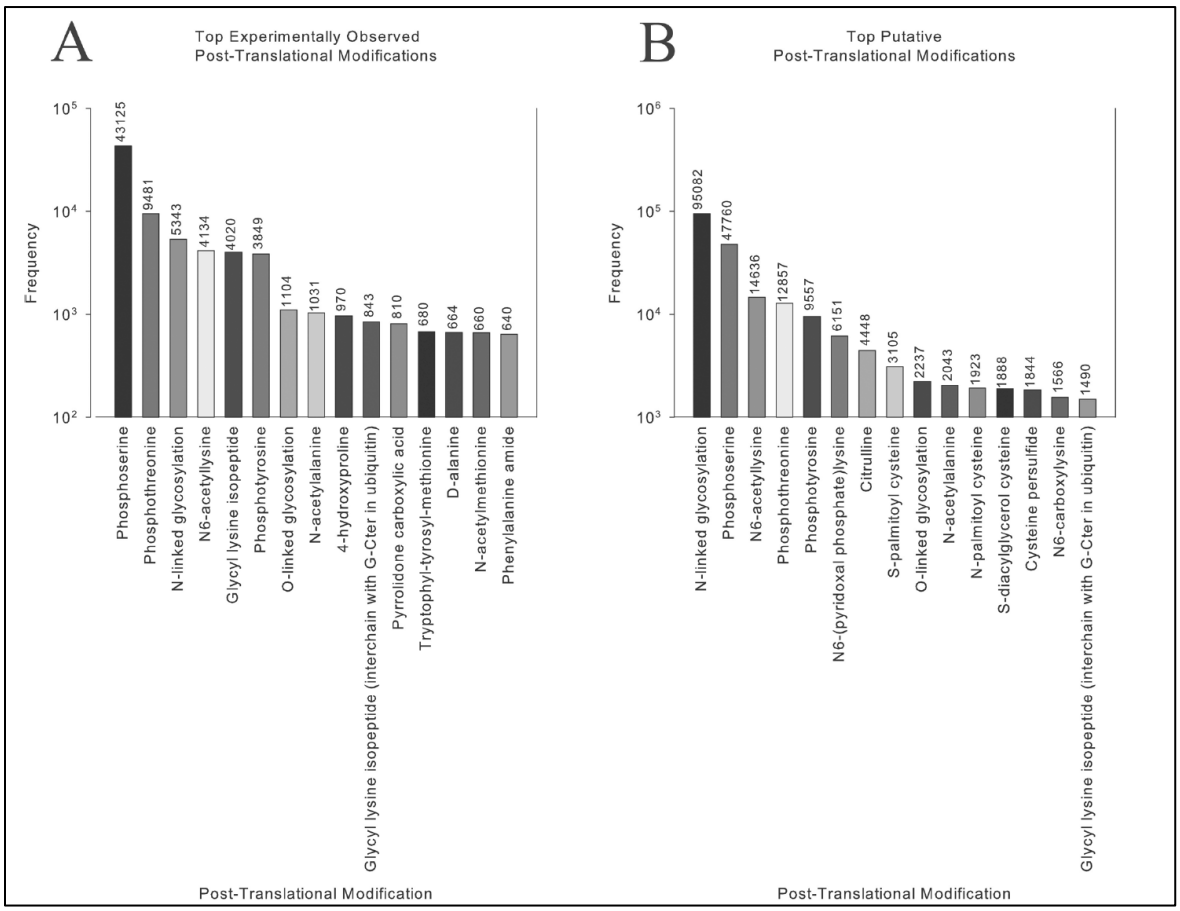

Figure 1 Fréquence des modifications post-traductionnelles des protéines les plus courantes.

À partir d'un vocabulaire contenant 431 modifications post-traductionnelles, la base de données Swiss-Prot a été analysée pour déterminer la fréquence expérimentale (A) et théorique (B) de ces modifications sur le protéome. Tirée de (Khoury et al. 2011).

1.1. Les protéases

Les protéases sont une importante famille de protéines qui compte pour environ 2 % du génome humain, soit plus de 500 protéines, ce qui en fait la 2e plus grande famille de protéines après les ubiquitine ligases (Puente et al. 2003; Rawlings et al. 2012). En soi, les protéases sont des hydrolases spécialisées dans le clivage des liens peptidiques qui relient les acides aminés d'une protéine, cette action est nommée protéolyse. Les protéases sont classées en familles selon leurs homologies de séquence, surtout en ce qui a trait à leur site catalytique. Ainsi, chez l'homme il existe 5 familles de protéases nommées par l'acide aminé conservé et nécessaire à la protéolyse en leur site catalytique (Figure 2A). L'action des protéases peut se faire dans divers compartiments cellulaires, à la membrane plasmique et dans le milieu extracellulaire (Figure 2B). Ainsi, les protéases sont impliquées dans une grande diversité de processus biologiques (Figure 2C), et ce par deux types de protéolyse soit : la protéolyse extensive, par la digestion ou la dégradation partielle ou complète de protéines, ou la protéolyse « ciblée », par un clivage limité à un ou des sites distinctifs. Le premier type de protéolyse s'avère important d'abord pour l'apport en nutriment au corps par les actions successives d'enzymes de digestion du tractus gastro-intestinal (Puente et al. 2003). Mais aussi, elle peut servir à réguler la signalisation cellulaire (ex. par la dégradation d'un récepteur en réponse à son activation (Raiborg et al. 2003)), à maintenir l'homéostasie cellulaire (ex. en dégradant des déchets protéiques (Glickman and Ciechanover 2002)) et à générer des antigènes pour la réponse immunitaire (Watts 2012). Le second rôle, la protéolyse de type « ciblée », est celui sur lequel cette thèse s'est particulièrement attardée. Ce rôle implique la reconnaissance par une protéase d'un substrat présentant une séquence particulière au sein de sa poche catalytique. Ces séquences de substrats sont décrites à l'aide d'une nomenclature qui permet de désigner les positions des acides aminés relatives au site de clivage soit : PX (X=1,2,3…) est assignée aux acides aminés en N-terminal du site de clivage [où P1 est adjacent au site de clivage] et PX' (X=1,2,3…) aux acides aminés en C-terminal (Schechter and Berger 1967). Souvent, la protéolyse « ciblée » consiste en une cascade protéolytique, par analogie aux cascades signalétiques, impliquant une ou plusieurs protéases qui peuvent provenir de différentes familles (Sukharev et al. 1997; Walsh and Ahmad 2002; Sim and Tsiftsoglou 2004). Ainsi, un autre niveau à la complexité biologique des protéases est ajouté.

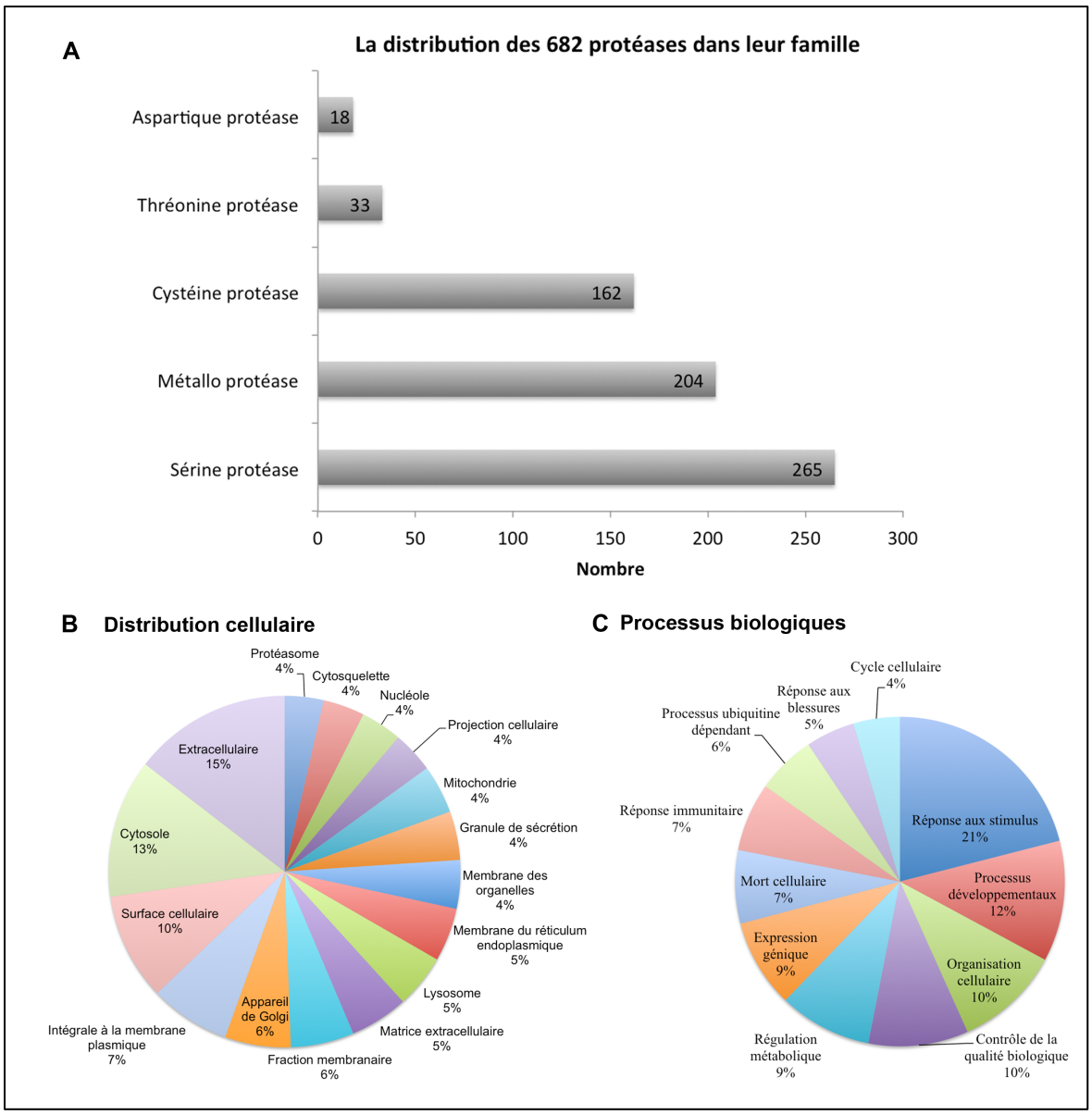

Figure 2 Natures et fonctions des protéases humaines.

(A) Distribution des 682 protéases humaines dans leurs familles respectives répertoriées dans la base de données MEROPS (Rawlings et al. 2012). (B) Distribution cellulaire des protéases humaines tirée de la base de données Uniprot (622 protéases ont été annotées) (UniProt 2012), ainsi que leurs principales fonctions biologiques (C).

1.2. Les proprotéines convertases (PC)

Les sérines protéases sont, à ce jour, la première famille de protéases en importance chez l'homme. Elles se distinguent par leur triade catalytique qui utilise une sérine, coordonnée par une histidine et un acide aspartique, afin de procéder à une attaque nucléophile sur le lien peptidique et engendrer son hydrolyse (Hedstrom 2002). Cette famille se divise en deux sous-familles, appelées clans, soit les homologues à la chymotrypsine et les homologues à la subtilisine Carlsberg (Madala et al. 2010). Cette dernière catégorie se caractérise par un site catalytique qui contient une asparagine supplémentaire qui forme un trou oxyanion qui permet de stabiliser un des états de transition de la réaction catalytique (Robertus et al. 1972; Wells and Estell 1988). Les proprotéines convertases, dont les gènes sont nommés « *proprotein convertase subtilisin/kexin* » (PCSK), font partie de cette dernière catégorie.

Les premières évidences de l'existence de précurseurs qui doivent être clivés par des hydrolases à des paires de résidus basiques remontent aux observations du Dr Michel Chrétien sur les hormones lipotropiques (LPH) provenant de la proopiomélanocortine (POMC) (Li et al. 1965; Chretien and Li 1967) et du Dr Donald Steiner sur l'insuline (Steiner 1967; Steiner et al. 1967; Steiner 2011). Ce n'est qu'en 1984, près de vingt ans plus tard, que l'équipe du Dr Jeremy Thorner identifie la protéine kexin de la levure comme responsable du clivage de précurseurs protéiques à des sites contenant une paire de résidus basiques (Julius et al. 1984; Seidah 2011). S'en est suivi la découverte de 9 gènes de mammifères PCSK (1 à 9) entre les années 1989 et 2003, codant respectivement pour les protéines convertases suivantes (PC) : PC1/3, PC2, furine, PC4, PC5/6, PACE4 (paired basic amino acid residue-cleaving enzyme 4), PC7, SKI-1/S1P et PCSK9 (Hosaka et al. 1991; Creemers et al. 1993; Siezen and Leunissen 1997; Seidah et al. 2006). Les sept premières enzymes, qui seront nommées « PC » dans cet ouvrage, clivent des substrats multibasiques à un motif consensuel R-$(X)_n$-R/K-R↓ (n=0, 2, 4, 6 acides aminés sauf une cystéine et où P4 est préférentiellement une arginine) (Hosaka et al. 1991; Seidah and Chretien 1999; Zhou et al. 1999; Remacle et al. 2008). SKI-1/S1P, la 8e enzyme, reconnait plutôt des substrats qui ont un résidu hydrophobe en P2 avec comme motif consensuel R-X-(V,L)-(T,K,F,L)↓ et est impliquée dans le clivage de facteurs de transcription membranaires (tels Sterol Regulatory Element-Binding Proteins, SREBPs, impliqués dans

le métabolisme des lipides) (Seidah et al. 1999b; Elagoz et al. 2002; Seidah 2011). Finalement, PCSK9 joue sont rôle d'enzyme qu'une seule fois lors d'un clivage autocatalytique au site V-F-A-Q↓ et son rôle principal est d'interagir avec le récepteur de lipoprotéines à faible densité (LDLR) pour promouvoir sa dégradation (Seidah et al. 2003; Benjannet et al. 2004; Yamamoto et al. 2011).

Les proprotéines convertases sont elles-mêmes des proprotéines qui doivent être soumises à des étapes d'activation protéolytique au sein de leur région N-terminale qui contient un peptide signal (PS) et un prodomaine (Figure 3). Le PS, qui permet l'introduction des PC dans les voies de sécrétions au réticulum endoplasmique (RE), est rapidement clivé par des signal peptidases de manière cotraductionnelle (Lindberg 1994). Le prodomaine exerce d'abord un rôle de chaperon veillant au bon repliement de l'enzyme (Bissonnette et al. 2004) et aussi a un rôle d'auto-inhibition sur les PC (Leduc et al. 1992; Anderson et al. 1997). Afin que les PC acquièrent leur pleine activité enzymatique, elles doivent suivre un processus d'activation autocatalytique qui permet la dissociation du prodomaine du site catalytique (Anderson et al. 1997; Feliciangeli et al. 2006). Toutefois dans le cas de PCSK9, le prodomaine restera lié dans la pochette catalytique de l'enzyme par des interactions hydrophobiques fortes empêchant toute activité enzymatique subséquente (Piper et al. 2007). Le dernier des quatre domaines conservés entre les PC est le domaine P contenant un motif RGD, à l'exception de PC7 où le motif est plutôt RGS, qui est essentiel à la stabilité du site catalytique de l'enzyme et permet la dépendance au calcium et l'activité pH dépendant (Gluschankof and Fuller 1994; Lusson et al. 1997; Zhou et al. 1998). D'autre part, les PC se distinguent entre elles principalement par leur région C-terminale qui contribuent essentiellement à la régulation de la localisation et du trafic intracellulaire par l'introduction de domaines, tels que transmembranaire, riche en cystéine ou même d'une hélice alpha amphipatique (Figure 3).

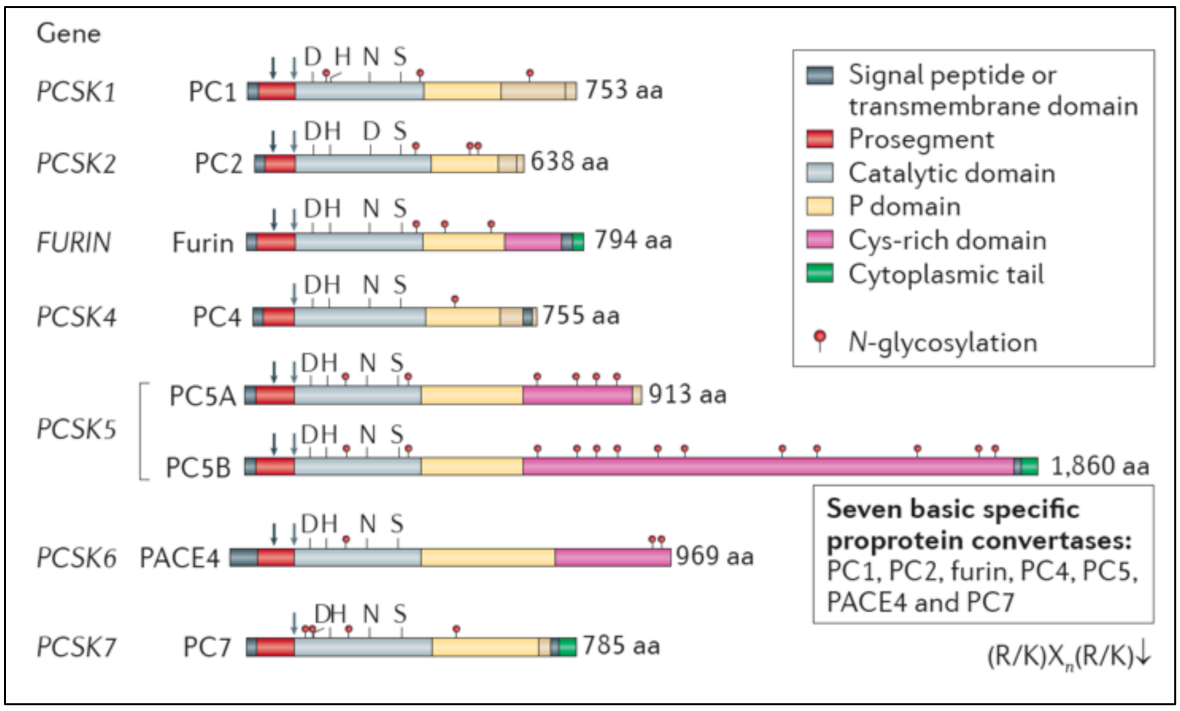

Figure 3 Représentation schématique de la structure primaire des proprotéines convertases.

Structurellement, les PC possèdent toutes quatre domaines communs soit : (i) le peptide signal à l'extrémité N-terminale, responsable de l'entré de l'enzyme dans la voie de sécrétion (ii) le prodomaine qui permet le bon repliement de la protéine et agit comme un inhibiteur intramoléculaire gardant l'enzyme inactive jusqu'à ce que l'enzyme atteigne un compartiment cellulaire où les concentrations de calcium et le pH sont optimaux pour son autoclivage et sa libération de l'enzyme (iii) le domaine catalytique très conservé parmi les PC et qui contient la triade catalytique composée de l'Asp, de l'His et de la Ser ainsi qu'une Asn qui forme un trou oxyanion (Asp pour PC2) (iv) le domaine P qui joue un rôle important dans la stabilité de la poche catalytique et la dépendance au calcium et au pH. Les flèches indiquent les sites de clivage primaire (gris pâle) et secondaire (gris foncé) du prodomaine. PC4 et PC7 possèdent qu'un site de clivage du prodomaine. PC5, souvent nommée PC5/6, est la seule convertase qui est exprimée sous deux isoformes actifs soit, PC5A et PC5B. La région C-terminale variable permet la régulation unique de la localisation cellulaire et du trafic des PC en incluant des régions : transmembranaire (furine, PC4, PC5B et PC7), hélice alpha amphipathique (PC1, PC2 et PC5A) (Dikeakos et al. 2007) et cystéines riches qui permet la liaison aux protéoglycans sulfates d'héparan à la surface cellulaire et dans la matrice extracellulaire (PC5 et PACE4). Tirée de (Seidah and Prat 2012).

1.2.1. Les trois niveaux de complexité de la reconnaissance d'un substrat

Pour une proprotéine donnée, la présence d'un motif consensuel de reconnaissance par les PC reste qu'une approximation du rôle que peut jouer les PC dans son activation. Certaines variations dans la pochette de liaison, dans la localisation cellulaire et dans l'expression tissu spécifique vont permettre aux PC de reconnaitre des substrats de façon spécifique ou redondante.

1.2.1.1. La spécificité de séquence

La structure cristalline de la furine et l'analyse par homologie des autres PC démontrent que la poche de liaison au substrat est très similaire entre les PC et est caractérisée par un nombre élevé de résidus négativement chargés (comme pour la kexine et la subtilisine) qui permettent la reconnaissance des sites contenant de multiples acides aminés basiques (Henrich et al. 2003; Henrich et al. 2005). Toutefois lors d'études de clivage *in vitro*, la spécificité des PC pour les différents substrats qui peuvent découler du motif consensuel de clivage est variable. Ainsi, une large étude utilisant des séquences dérivées de substrats connus des PC a permis de décrire l'affinité des PC envers les différentes variations de leurs substrats (Remacle et al. 2008). Notamment, la distinction entre les PC se fait principalement en P6, P5, P3 et P1'-P4' des substrats. Ainsi, les faibles variations structurelles entre les PC permettent tout de même une certaine spécificité pour leurs substrats. Seule PC2 affiche un caractère unique pour ses substrats préférentiels, ce qui serait attribuable à la substitution de l'asparagine supplémentaire du site catalytique des PC par un acide aspartique. Cette modification change les propriétés du trou oxyanion et par le fait même la propriété enzymatique de PC2 (Henrich et al. 2005).

1.2.1.2. La localisation et distribution intracellulaire

Malgré une affinité similaire pour un même substrat, les PC pourront cliver ce substrat à l'unique condition qu'il y ait colocalisation en un temps et une concentration suffisante. Ainsi, la régulation de la localisation et du trafic intracellulaire des PC, par leurs domaines C-terminaux distinctifs, contribue à la diversité fonctionnelle des PC (Figure 4 et Tableau 1). On retrouve furine, PC4, PC5/6 et PACE4 dans divers compartiments intracellulaires de la voie de sécrétion non régulée, notamment dans le réseau trans-Golgien (TGN), dans les endosomes, à la surface cellulaire et également dans le milieu

extracellulaire. Furine, PC7, PC4 et l'isoforme B de PC5/6 possèdent un domaine transmembranaire qui leur permet d'être retenues à la membrane plasmique (Seidah et al. 2008; Rousselet et al. 2011). Une fois à la membrane plasmique, un clivage permet de relâcher furine, PC5/6B et PC4 dans le milieu extracellulaire (Seidah et al. 1992; Plaimauer et al. 2001). Par leur motif riche en cystéines, les formes sécrétées de PACE4 et PC5/6 peuvent être retenues à la surface cellulaire en liant des groupements sulfates d'héparan sur les protéoglycans et les inhibiteurs tissulaires des métalloprotéinases (TIMP) (Tsuji et al. 2003; Nour et al. 2005). Récemment, il a été démontré que PC7 pouvait se retrouver dans une voie de sécrétion atypique qui transite du RE directement à la membrane plasmique sans emprunter le réseau Golgien (Rousselet et al. 2011).

Quant à elles, PC1/3, PC2 et l'isoforme A de PC5/6 se retrouvent dans la voie de sécrétion régulée (Dikeakos et al. 2007). Cette voie de sécrétion est typique du système neuroendocrinien où divers composés actifs (ex. insuline, glucagon, endorphine) sont emmagasinés dans des granules de sécrétion acides, aussi appelées vésicules denses de sécrétion (DCSG), et seront relâchés dans le milieu extracellulaire (Gauthier et al. 2008; Hou et al. 2009; Zhang et al. 2010). Il a notamment été démontré que le trafic de PC1/3, PC2 et PC5/6 dépend de leur région C-terminale et du domaine P (Ueda et al. 2003b), qui contient une hélice alpha où une région hydrophobique parsemée d'acides aminés chargés est responsable d'acheminer ces PC aux DCSG (Dikeakos et al. 2007; Dikeakos and Reudelhuber 2007; Rabah et al. 2007). Spécialement, PC1/3 requiert une maturation supplémentaire à un site dibasique de sa région C-terminale (Jutras et al. 1997), qui ne sera pas complétée avant les DCSG où l'enzyme aura sa pleine activité pour cliver ses substrats (Rabah et al. 2007).

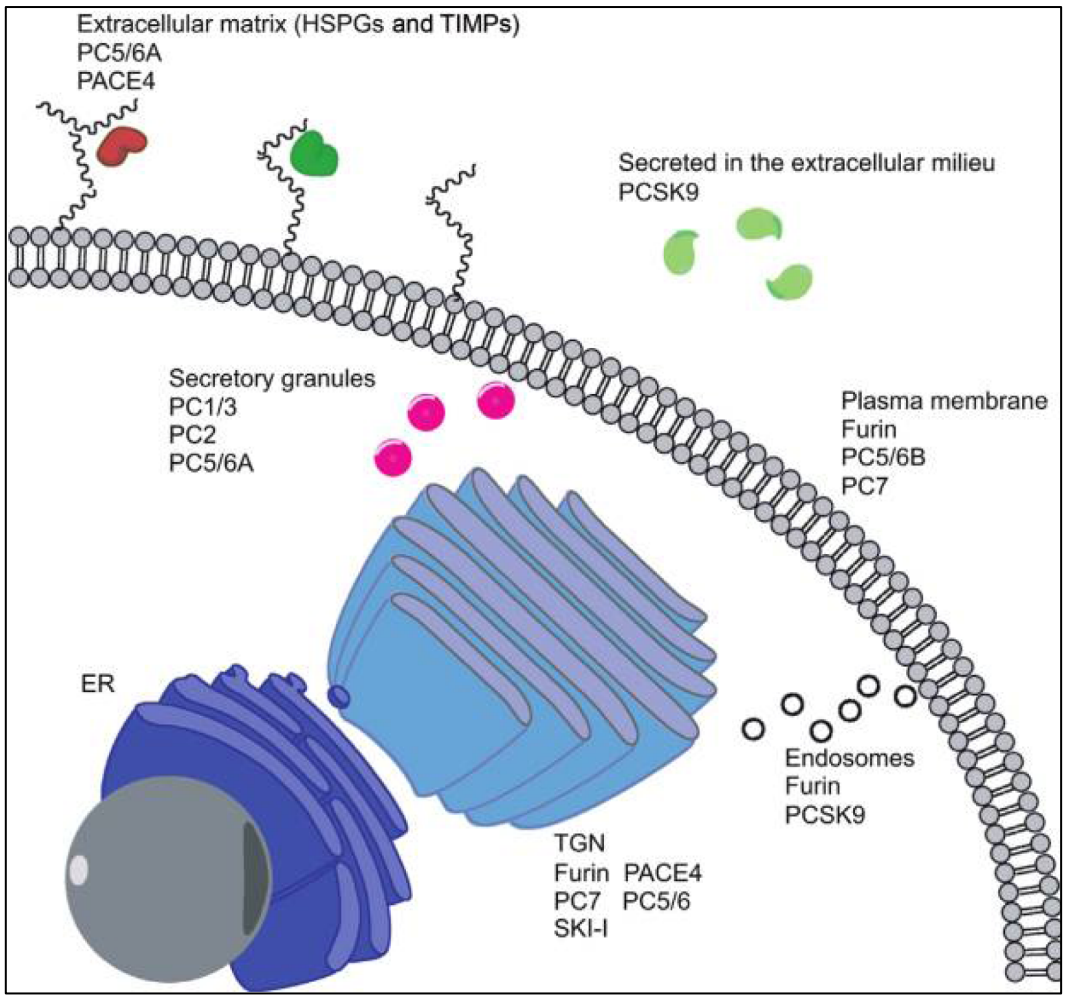

Figure 4 La localisation cellulaire des proprotéines convertases.

Les caractéristiques structurales de la région C-terminale des PC sont responsables de leurs différentes localisations cellulaires. Furine, S1P/SKI-1, PC5/6B et PC7 sont des protéines transmembranaires de type 1 qui vont trafiquer entre le réseau trans-Golgien (TGN) et la surface cellulaire. PC7 peut trafiquer directement du réticulum endoplasmique à la membrane plasmique sans emprunter les compartiments Golgien (non représenté). PC5/6A se retrouve dans la voie de sécrétion régulée, tout comme PC1/3 et PC2. Une fois sécrétées PACE4 et PC5/6 peuvent être retenues à la surface cellulaire ou dans la matrice extracellulaire en s'associant avec des protéoglycans sulfates d'héparan (HSPGs) et aux inhibiteurs tissulaires des métalloprotéinases (TIMPs) par leur domaine riche en cystéines. Tirée de (Couture et al. 2011)

1.2.1.3. Distribution tissulaire

Hormis PC4 (exprimée dans les cellules germinales) et PCSK9 (exprimée seulement dans le foie, les intestins et les reins), l'expression des PC demeure largement répandue (Tableau 1). À ce point, des études portant sur l'expression tissulaire des différentes PC démontrent que furine et PC7 sont exprimées à des niveaux variables dans la majorité des tissus, mais que PACE4 et PC5/6 se retrouvent fortement associées à certains tissus spécifiques voir (Tableau 1) (Bergeron et al. 2000; Seidah and Prat 2012). Un exemple encore plus probant de l'expression tissu spécifique est l'expression de PC1/3 et PC2 souvent associée exclusivement au système neuroendocrinien. Il est à souligner que le nom génique officiel de ces deux protéines est neuroendocrine convertase (NEC1 et NEC2). Lorsque l'on observe l'expression de PC1/3 et PC2 dans le cerveau, certaines régions sont spécifiques à l'une ou l'autre des enzymes (ex. noyau thalamique antérodorsal et hypothalamus : PC1/3, thalamus : PC2), alors que d'autres régions expriment les deux protéines (ex. cervelet et cortex) (Bergeron et al. 2000). Ceci suggère l'importance d'une fonction tissu spécifique de certaines PC pour la reconnaissance de substrats spécifiques qui s'illustre lors de la maturation de POMC (Figure 5A).

Tableau 1 Distribution tissulaire et sécrétion des proprotéines convertase.

Proprotéine convertase	Distribution tissulaire	Sécrétion
PC1/3	Système neuroendocrinien	Sécrétées
PC2		
furine	Ubiquitaire à des niveaux d'expression variables	relâchée
PC4	Germinal	relâchée
PC5/6	Répandue : surrénale, intestin, reins, ovaires	Sécrétée PC5/6A; relâchée PC5/6B
PACE4	Répandue : muscles, cœur, hypophyse, intestin, cervelet, reins	Sécrétée
PC7	Ubiquitaire à des niveaux d'expression variables	Non sécrétée

Tableau adapté de (Seidah and Prat 2012)

1.2.2. Les rôles physiologiques des PC

Souvent, le clivage par les PC (de façon spécifique ou redondante) engendre l'activation, un changement de fonctions ou même l'inactivation d'une protéine qui régulera directement les fonctions cellulaires (Creemers and Khatib 2008). Toutefois, la complexité physiologique des PC va bien au-delà de ce rôle ponctuel. Deux exemples connus décrivent bien le rôle des PC dans la régulation physiologique (Figure 5). Le premier exemple est l'activation du précurseur protéique POMC dans une cascade enzymatique qui intègre tous les niveaux de complexité de la reconnaissance d'un substrat par les PC soit : diverses séquences reconnues spécifiquement par PC1/3 ou PC2, sa localisation cellulaire dans les granules de sécrétion de la voie de sécrétion régulée et l'expression tissu spécifique corrélant avec PC1/3, PC2 ou les deux. Ainsi, la maturation successive ou combinée de POMC par PC1/3 et PC2 permet la libération de plusieurs peptides (ex. adrénocorticotrophine (ACTH), β-LPH, β-endorphine (β-END)) aux fonctions biologiques diverses (Figure 5A). De plus, s'ajoute l'action d'autres enzymes (carboxypeptidase, acétyltransférase et monooxygènase) qui modulent l'activité biologique des divers peptides relâchés (Seidah et al. 1999a; Laurent et al. 2004; Lasaga et al. 2008; Dores and Baron 2011). Le deuxième exemple présente le rôle combiné des PC lors de l'activation de prohormones dans la régulation de larges boucles d'autorégulation juxta/paracrines au sein de divers tissus, soit l'axe hypothalamo-hypophysaire (Figure 5B). Celui-ci permet la régulation neuroendocrinienne de divers organes par la relâche d'hormones trophiques dans la veine porte. D'abord, la sécrétion d'hormones trophiques doit être stimulée par les hormones de relâche sécrétées par hypothalamus. Ensuite, les hormones trophiques auront leurs effets sur les organes cibles qui relâcheront des hormones périphériques. Afin de maintenir la balance de la réponse physiologique, chaque hormone nouvellement sécrétée peut agir comme régulateur négatif des étapes précédentes, souvent nommé rétrocontrôle. À chacune de ces étapes, des précurseurs hormonaux protéiques peuvent être activés par les PC, ce qui illustre l'important rôle des PC dans la régulation de la physiologie animale (Morris and Maisto 2004).

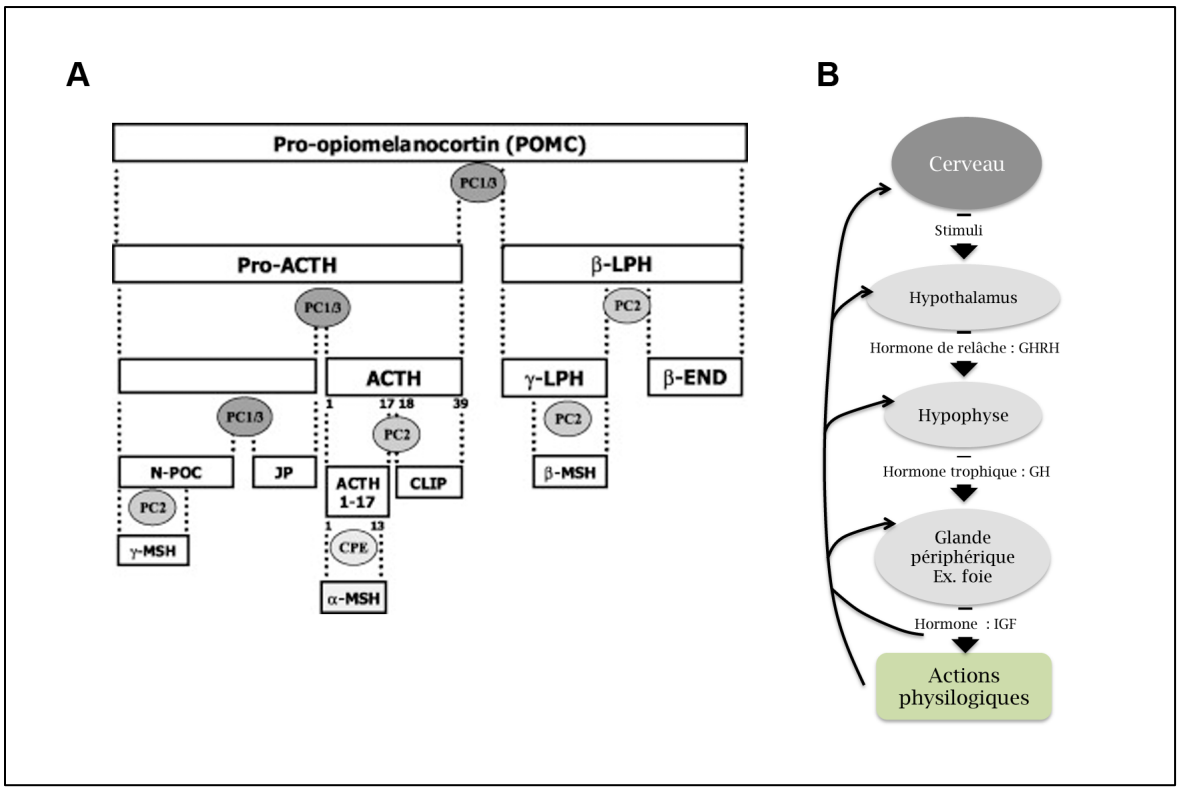

Figure 5 Activation de POMC par PC1/3 et PC2 et rôle des PC dans l'axe hypothalamo-hypophysaire.

A) Diagramme du clivage de POMC. Cette proprotéine est exprimée de façon tissu spécifique, où PC1/3 exercera un premier clivage pour générer la pro-ACTH et la β-lipotropine (β-LPH). La pro-ACTH est par la suite clivée de nouveau par PC1/3 pour générer l'hormone adrénocorticotropique (ACTH), le peptide N-terminal (N-POC) et le « *joining peptide* » (JP). Dans le cerveau, PC2 peut cliver l'ACTH en ACTH 1–17 et en un intermédiaire appelé « *corticotropin-like intermediate lobe peptide* » (CLIP). La caboxypeptidaseptidase E (CPE) est nécessaire pour produire la forme mature de l'« *alpha-melanocyte-stimulating hormones* » (α-MSH) à partir de l'ACTH 1-17. PC2 peut aussi produire : la γ-lipotropine (γ-LPH) et la β-endorphine (β-END) à partir du clivage du β-LPH, la β-MSH à partir de la γ-LPH, et la γ-MSH à partir du N-POC (Lasaga et al. 2008) B) Boucle d'autorégulation juxta/paracrine engendrée par l'axe hypothalamo-hypophysaire. Un stimulus spécifique du cerveau va engendrer la sécrétion d'une hormone de relâche (ex. growth hormone releasing hormone [GHRH]) par l'hypothalamus, qui stimule la sécrétion d'une hormone trophique (ex. growth hormone [GH]) par l'hypophyse dans la veine porte. Une fois dans la circulation périphérique, l'hormone trophique induit une réponse d'organes cibles (ex. le GH stimule la production de l'insulin growth factor [IGF] par le foie). Tous ces exemples d'hormones peptidiques sont maturées par les PC et ont des effets inhibiteurs de façon rétroactive.

1.2.2.1. La détermination du rôle spécifique des PC grâce aux modèles murins KO

Malgré l'importance des études *in vitro* et *ex vivo* pour la découverte des substrats des PC, le développement de modèles murins KO (où un gène spécifique est inactivé) a grandement contribué à la compréhension du rôle individuel des PC (Tableau 2). Toutefois, ces modèles se sont souvent limités aux rôles spécifiques des PC lors du développement embryonnaire. Bien que les études *in vitro* et *ex vivo* démontrent une grande redondance fonctionnelle entre furine, PC5/6 et PACE4, l'inactivation de ses trois PC de la voie de sécrétion constitutive engendre une mortalité à la naissance ou embryonnaire. En fait chez la souris furine KO, une mortalité embryonnaire au jour 11 est observée (Roebroek et al. 1998) qui serait attribuable à un défaut de maturation du facteur BMP10 (*Bone Morphogenetic Proteins 10*) (Susan-Resiga et al. 2011) et du facteur Lefty de la famille du « *transforming growth factor-β* » (TGF-β) (Constam and Robertson 2000b). Normalement, l'activité de ces deux facteurs permet le bon développement embryonnaire du cœur lors de l'inversion et le cloisonnement du cœur. Récemment, un KO de furine spécifique aux cellules endothéliales a confirmé l'importance de furine dans le développement cardiaque. Dans ce modèle, la majorité de la progéniture meurt en moins de 60 h postpartum dû à des malformations cardiaques (Kim et al. 2012). De plus, (Kim et al. 2012) ont démontré que l'endothelin-1, l'adrénomédulline et le TGF-β1 sont des substrats de furine *in vivo*. Malgré tout, l'inactivation génique tissu spécifique de furine, dans le foie chez la souris, n'engendre aucun phénotype apparent et ce KO affecte peu de substrats (Roebroek et al. 2004). Ainsi, furine aurait un rôle redondant avec les autres PC dans le foie des souris adultes, mais serait essentielle au clivage de substrats spécifiques lors du développement embryonnaire (Creemers and Khatib 2008).

Le KO de PACE4 présente une mortalité partielle de la progéniture embryonnaire reliée à des malformations cardiaques, osseuses et des problèmes de développement axial (Constam and Robertson 2000a). Toutefois, ces phénotypes affichent peu de pénétrance selon l'origine génétique des souris (Malfait et al. 2012), mais pourraient être associés au rôle de cette convertase dans la maturation des facteurs de croissance Nodal et Lefty de la famille des TGF-β (Blanchet et al. 2008) .

Le KO de PC5/6 n'engendre pas de mortalité embryonnaire, mais plutôt une mort à la naissance. Les nouveau-nés présentent plusieurs défauts de développement de l'axe

antéropostérieur, dont l'absence de queue et de reins, qui seraient reliés à un défaut de maturation du facteur GDF11 (*Growth Differentiation Factor 11*) (Essalmani et al. 2008; Szumska et al. 2008). Toutefois, le KO spécifique aux cellules endothéliales de PC5/6 ne manifeste pas de phénotype apparent, malgré une diminution de l'activité de la voie de signalisation activant l'autophagie reliée à IGF (*Insuline Growth Factor*). Ceci engendrait une diminution de la déposition de collagène et une hypertrophie cardiaque avec l'âge (Marchesi et al. 2011).

Le KO de PC4 démontre son importance et le peu de redondance des autres PC au niveau des gonades. Les souris mâles PC4 KO présentent une fertilité grandement réduite (Mbikay et al. 1997) qui serait reliée à un défaut de maturation de PACAP (*pituitary adenylate cyclase-activating polypeptides*) au niveau des testicules (Li et al. 1998; Li et al. 2000).

Le KO de PC7 ne présente aucun phénotype apparent ce qui suggère une grande redondance de PC7 avec les autres PC. Toutefois, le Dr Nabil Seidah a observé que les souris PC7 KO affichaient peu d'anxiété (Seidah and Prat 2012) ce qui implique que PC7 affecte les régions du cerveau reliées à l'anxiété soit : l'amygdale, l'hippocampe et le noyau accumbens (Gu et al. 2010).

Tableau 2 Substrats spécifiques et phénotypes des modèles murins KO

Proprotéine convertase	Substrats typiques	Mortalité des souris KO	Phénotypes des souris KO	Commentaires
PC1/3	GHRH, ACTH, GLP1, GLP2	-	Nanisme (proGHRH), proinsulinémie, diarrhée chronique	Collabore souvent avec PC2 (ex. insuline, TRH et MSH)
PC2	β-endorphine, glucagon et α-MSH	-	Retard de croissance, hypoglycémie glucagon non maturé, Phénotype Cushing-like dans la souche 129/SvEv	Collabore souvent avec PC1/3
furine	Facteur de croissance(TGFβ) Récepteur (récepteur de l'insuline) Molécule d'adhésion (α5 integrine et RGMA) Métalloprotéinase (MMP14) Pompe à proton V-ATPase accessory protein Ac45 subunit Glycoprotéines virales (HIV gp160) Toxine bactérienne (anthrax pa83)	Embryon jour ~11	Dimorphisme embryonnaire : pas de rotation axiale, défaut d'inversion du coeur	Redondance *in vitro* et *ex vivo* avec PC5/6 et PACE4

PC4	IGF2 et PACAP	-	Fertilité réduite	Clive des substrats dans les gonades et le placenta
PC5/6	Facteur de croissance (GDF11) Récepteur (PTPRM) Molécule d'adhésion (L1CAM neuronal, α4 integrine)	À la naissance	Défaut de développement antéropostérieur, hyperplasie des membres postérieurs	Redondance *in vitro* et *ex vivo* avec furine et PACE4
PACE4	Facteur de croissance (Nodal et Lefty) Métalloprotéinase (ADAM-TS4) Glycoprotéines virales (HIV Vpr)	25 % de mortalité des embryons au jour 15.5	Malformation cardiaque, isomérisme droit, cyclopie (nodal)	Redondance *in vitro* et *ex vivo* avec furine et PC5/6
PC7	Récepteur (récepteur 1 de la transferrine)	-	Perte de l'anxiété	Redondance partielle avec PC5/6, furine et PACE4

Adapté de (Seidah and Prat 2012) α-MSH, α-melanocyte-stimulating hormone; ACTH, adrenocorticotropic hormone; ADAM-TS4, a disintegrin and metalloproteinase with thrombospondin motif 4; ; GDF11, growth differentiation factor 11; GHRH, growth hormone-releasing hormone; GLP1, glucagon-like peptide 1; gp160, envelope glycoprotein 160; IGF2, insulin-like growth factor 2; L1CAM, L1 cell adhesion molecule; MCH, melanin concentrating hormone; MMP14, matrix metalloproteinase 14; pa83, protective antigen 83; PACAP, pituitary adenylyl cyclase-activating peptide; PTPRM, protein tyrosine phosphatase receptor type M; RGMA, repulsive quidance molecule A; TGFβ, transforming growth factor-β; TRH, thyrotropin releasing hormone.

1.2.2.1.1. Les KO de PC1/3 et PC2

PC1/3 et PC2 sont reconnues pour être fondamentalement liées au système neuroendocrinien, notamment pour la maturation de précurseurs d'hormones peptidiques tels que la proinsuline, le proglucagon (Steiner 2011) et la POMC (Seidah et al. 1999a). Le KO respectif chez la souris de PC1/3 (Zhu et al. 2002b) et PC2 (Furuta et al. 1997; Furuta et al. 2001) n'est pas mortel bien que le KO de PC1/3 engendre une plus faible natalité associée à un retard de croissance (Zhu et al. 2002b). Bien entendu, ces modèles murins ont permis de valider l'important rôle de ces enzymes dans le système neuroendocrinien. Entre autres, les souris PC1/3 KO sont naines, ce qui serait relié à un défaut dans la relâche de la GHRH (*Growth Hormone Releasing Hormone*) qui expliquerait aussi le retard de croissance (Zhu et al. 2002b). De plus, ces souris peuvent développer de l'obésité avec l'âge selon l'origine génétique des souris (observation faite dans le laboratoire du Dr Day) et aussi dans un autre modèle de souris où une mutation homozygote réduit de 60 % l'activité de PC1/3 (Lloyd et al. 2006). Entre autres, ces observations corrèlent les défauts de maturation de la proinsuline (Zhu et al. 2002a; Zhu et al. 2002b). Fait intéressant, les cas observés de délétion ou d'inactivation de PC1/3 chez l'homme présentent aussi de l'obésité, de l'infertilité et des défauts dans l'homéostasie du glucose (Jackson et al. 1997; Farooqi et al. 2007; Creemers et al. 2012). Les souris PC2 KO présentent aussi un retard de croissance, qui serait plutôt relié avec une hypoglycémie chronique et un bas niveau de glucagon circulant (Furuta et al. 1997; Furuta et al. 2001). Il a aussi été observé que le KO de PC2 pouvait être létal, selon l'origine génétique des souris (Peinado et al. 2005). Grâce à ces modèles KO, la coopération entre ces deux PC, bien connue de la littérature, a pu être étudiée *in vivo* notamment lors d'études peptidomiques du cerveau (Wardman et al. 2010; Zhang et al. 2010). Ces études peptidomiques ont démontré que PC1/3 et PC2 avaient un rôle redondant pour environ un tiers des peptides observés et que le reste des substrats étaient spécifiques soit pour PC1/3, soit pour PC2 à parts égales. De plus, on note une augmentation de certains peptides dans le KO de PC1/3, alors que le KO de PC2 induit uniquement une disparition de substrat. Il est alors proposé que PC1/3 masquerait certains substrats à PC2 (ou d'autre PC) dans une sorte de compétition enzymatique. De plus, ces études confirment que PC2 exerce un rôle unique dans la maturation de certains peptides du précurseur POMC, de la pro-enképhaline et de la pro-endorphine et confirment qu'une

partie du précurseur POMC est tout de même maturé en ACTH chez les souris PC1/3 KO (Zhu et al. 2002b). Ce dernier point laisse croire qu'une autre PC peut être responsable du clivage de POMC en ACTH. Finalement, il est confirmé que PC2 est largement responsable de clivages où P2-P1 sont Lys-Arg avec une préférence pour des résidus aromatiques ou une proline en position P1'-P2' et que PC1/3 a une préférence pour les substrats où P2-P1 sont Arg-Arg ou X-Arg. Ces observations corrèlent avec celles décrites *in vitro* par (Remacle et al. 2008).

1.2.2.2. Les PC dans le système immunitaire

Les PC ont un rôle établi dans la modulation de l'inflammation, notamment de façon indirecte par l'activation de plusieurs métalloprotéinases (MMP et ADAM) qui elles-mêmes activent des cytokines et chimiokines (Edwards et al. 2008; Fanjul-Fernandez et al. 2010). Certaines cytokines et protéines modulatrices de l'immunité ont aussi été démontrées pour être clivées par furine, entre autres TACE (*tumor necrosis factor* [TNF]-*α-converting enzyme*) (Srour et al. 2003) et le TGF-β (Dubois et al. 2001). Ce clivage par furine du TGF-β a un rôle primordial pour l'immunité adaptative, puisqu'il est essentiel au maintien de la tolérance périphérique par les cellules T régulatrices (Treg) et T effectrices (Th) (Pesu et al. 2006; Pesu et al. 2008). Non moins, les cytokines APRIL et BAFF, des modulatrices de l'immunité humorale de la famille du TNF, sont de même clivées par furine (Turpeinen et al. 2011). De plus, furine régulerait la présentation d'antigènes par le complexe majeur d'histocompatibilité (CMH) de classe 1 d'une façon non conventionnelle dans la voie de sécrétion (Gil-Torregrosa et al. 1998; Gil-Torregrosa et al. 2000; Leonhardt et al. 2010) et PC7 serait important dans le contrôle de la qualité des peptides présentés par ce même CMH (Leonhardt et al. 2010).

Les proprotéines convertases neuroendocriniennes, PC1/3 et PC2, ont un rôle bien connu au niveau de la modulation de l'inflammation dans système nerveux central par le biais de la maturation de divers neuropeptides. Ces neuropeptides (souvent les mélanocortines (α, β et γ-MSH) dérivées de la maturation du précurseur POMC) ont généralement des propriétés anti-inflammatoires et sont impliqués dans la « régulation croisée » entre le système nerveux central et les cellules immunitaires qui s'y trouvent (Gonzalez-Rey 2010). Entre autres, les récepteurs des MSH sont exprimés dans les cellules immunitaires du cerveau, mais aussi sur les cellules périphériques impliquées dans la

réponse immunitaire (les macrophages, les cellules épithéliales et les lymphocytes), et auraient des capacités anti-inflammatoires bénéfiques dans la réponse immunitaire périphérique (Lasaga et al. 2008). Donc, ces neuropeptides se placent comme des médiateurs importants des maladies inflammatoires, telle l'arthrite, en modulant la voie inflammatoire Nf-κB (*Necrosis factor-κB*) (Muceniece and Dambrova 2010; Zapala et al. 2010). D'autres neuropeptides, tels le « *Vasoactive Intestinal Peptide* » (VIP), l'urocortine (UCN), l'adrénomedulline (AM), la cortistatine (CST) et la ghréline (GHR), ont aussi des activités anti-inflammatoires. Notamment, divers peptides dérivés des précurseurs de l'enképhaline sont capables de contrôler l'inflammation (Salzet and Tasiemski 2001; Schluesener et al. 2012). La majorité de ces neuropeptides exercent leurs effets d'immunomodulation par des récepteurs couplés aux protéines G en activant la voie de signalisation « *cAMP-protein kinase A* » (PKA) immunosuppressive (Gonzalez-Rey 2010).

Plusieurs ont étudié le rôle modulateur de ces peptides et leurs actions reliées à la communication entre le système nerveux central et le système périphérique. À l'opposé, peu d'études se sont penchées sur la provenance exacte de ces peptides et des enzymes participant à leurs biosynthèses, dont les PC. Seulement quelques travaux portent sur l'expression des PC dans le système immunitaire périphérique. On remarque alors que PC7 est hautement exprimée dans le système lymphoïde (Seidah et al. 1996), que PC1/3 est exprimée dans les macrophages et PC2 dans les neutrophiles (LaMendola et al. 1997) (Vindrola et al. 1994). À ce point, les travaux de (Lansac et al. 2006) ont notamment démontré l'expression des différentes PC dans les organes immunitaires (dont la rate et le thymus) et que PC1/3, PC2 et les enképhalines sont sensible à un stimulus de l'immunité innée pro-inflammatoire (le lipopolysaccharide (LPS)) (Figure 6). De ce fait, ces résultats ébranlent certains concepts de l'exclusivité neuroendocrinienne de PC1/3 et PC2 et suggèrent que les cellules immunitaires pourraient exercer des fonctions décrites comme neuroendocrines (Day and Salzet 2002).

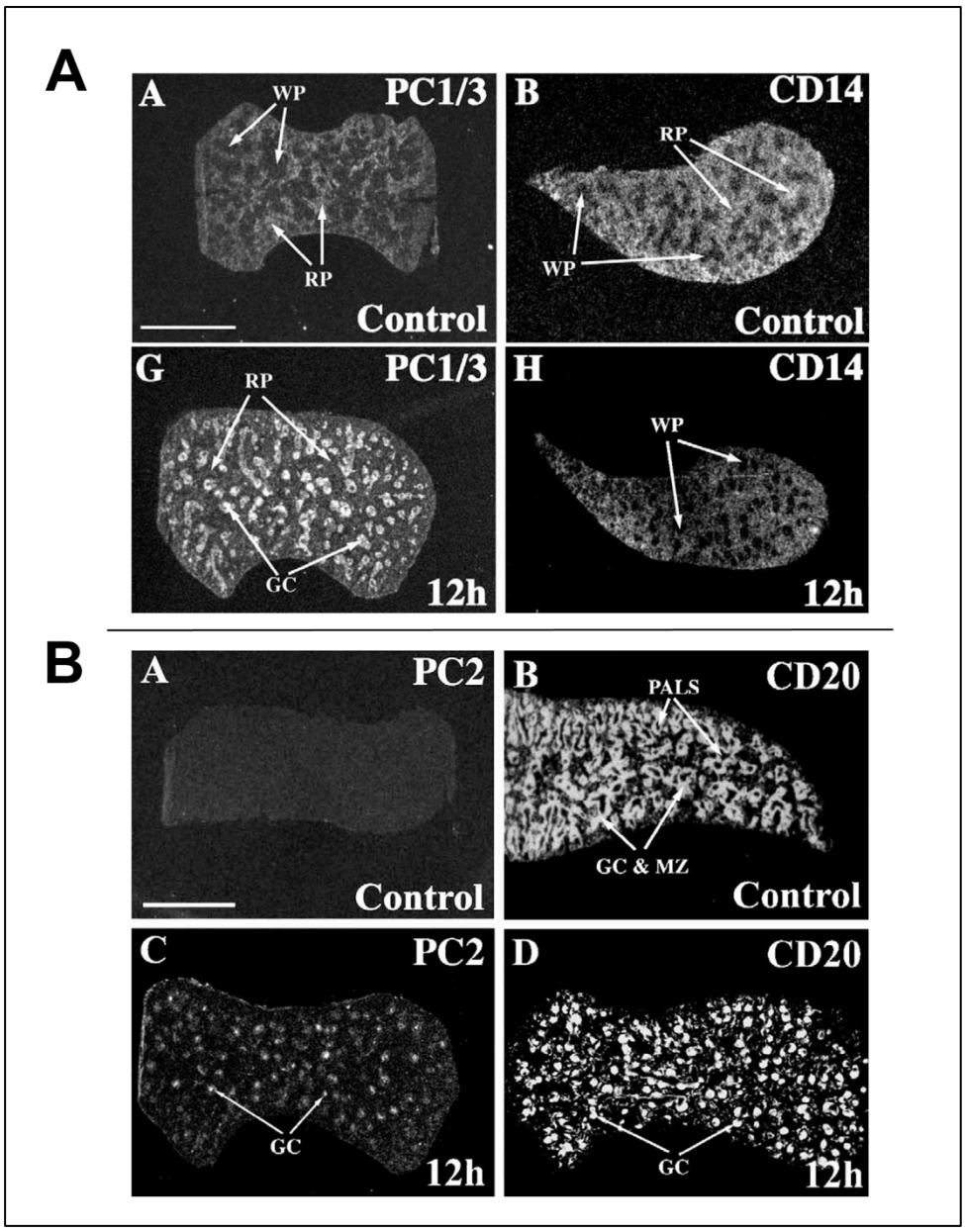

Figure 6 Modulation de l'expression de PC1/3 et PC2 par le LPS.

A) Induction de l'expression de PC1/3 par le lipopolysaccharide (LPS) dans la rate de rat. Autoradiographies montrant la distribution des ARNm correspondant à PC1/3 (A, G) et CD14 (B, H), un marqueur de macrophage, avant (A, B) et après stimulation de 12 h au LPS (G,H). On voit qu'avant stimulation PC1/3 colocalise avec le marqueur de macrophage CD14 dans la pulpe rouge (RP) et qu'après stimulation l'expression de PC1/3 migre vers la pulpe blanche (WP) aux centres germinaux (GC) alors que le marqueur CD14 reste inchangé. B) Induction de l'expression de PC2 par le LPS dans les rates de rat. L'expression des ARNm de PC2 et CD20, un marqueur de cellule B, est révélée par hybridation *in situ*. Après 12 h de traitement au LPS on note l'apparition de l'expression de PC2 au GC marqué par CD20. Bar, 6 mm. Zone marginale (MZ). Tirée de (Lansac et al. 2006).

1.2.2.2.1. La réponse immunitaire innée

La réponse immunitaire innée repose principalement sur la communication entre deux types cellulaires : les cellules présentatrices d'antigènes (CPA) et les cellules T. Les CPA, principalement les cellules dendritiques et les macrophages, sont responsables de la maturation puis de la présentation d'antigènes par les CMH-I et -II (le CMH-I est associé à la présentation d'antigènes du soi et d'infections intracellulaires et le CMH-II est associé à la présentation d'antigènes capturés à l'extérieur de la cellule) qui lieront respectivement leur récepteur CD8 et CD4 sur les cellules T (Murphy et al. 2008). Il s'en suit une réponse qui, par la sécrétion de diverses cytokines, modulera l'immunité adaptative et innée (Figure 7) (Zanoni and Granucci 2009). Ainsi dans le cas de l'intrusion et de la détection d'un pathogène chez l'hôte, les cellules naïves T CD4+ pourront se différencier en cellules Th1 ou Th2 (T effectrices) qui favoriseront respectivement la réponse cellulaire (pro inflammatoire) ou humorale (activation des cellules B et production d'anticorps). Les cytokines, des polypeptides et glycoprotéines de faibles poids moléculaires, sont responsables de caractériser ces voies pro et anti-inflammatoires pour permettre à l'hôte de réagir de manière appropriée aux agents pathogènes (Scott et al. 2002). La voie Th1 se distingue par la sécrétion de cytokines pro-inflammatoires (les plus caractéristiques sont l'IL-12 (interleukine-12) et l'IFN-γ (interféron-γ)) (Schroder et al. 2004). À l'opposé, la voie Th2 est caractérisée par une sécrétion contrôlée de facteurs pro-inflammatoires (IL-1β, IL-6, et TNF-α) notamment modulée par l'IL-10 (Anderson and Mosser 2002). L'IL-10 exerce ses fonctions régulatrices en inhibant l'activité pro-inflammatoire des CPA et la différenciation Th1 (Fiorentino et al. 1991; Cope et al. 2011). De plus, d'autres cellules T sont impliquées dans la régulation de la réponse immunitaire innée, dont les Treg (pour cellule T régulatrice) sécrétant de l'IL-10 (Taams et al. 2005; Cope et al. 2011) et les Th17 qui régulent les lymphocytes, tels les neutrophiles et les «*Natural Killer cells*» (NK), en sécrétant entre autres de l'IL-17 (Korn et al. 2009).

Un élément clef dans l'activation du système immunitaire implique la reconnaissance, par les CPA, des motifs moléculaires non trouvés chez l'hôte et provenant des agents pathogènes, appelés PAMP (PAMP : « *Pathogen Associated Molecular Pattern* ») (Medzhitov and Janeway 1997). On retrouve parmi les récepteurs qui jouent un rôle clef dans la reconnaissance des PAMP : les récepteurs Toll-like (TLR). Ce sont des

protéines transmembranaires de type 1 qui reconnaissent les PAMP par leur exodomaine et induisent la réponse immunitaire innée par un domaine intracellulaire conservé TOLL/interleukine-1 (TIR). Ce domaine permet l'activation de cascades signalétiques menant principalement à l'activation de la voie de transcription inflammatoire Nf-κB (Takeda and Akira 2005) (Figure 8). Il existe au moins treize membres de la famille TLR qui reconnaitront différents types de PAMP pour induire une réponse immunitaire appropriée. Les TLR1-9 sont conservés entre l'homme et la souris, tandis que TLR10 ne se trouve pas sous la forme murine et les TLR 11-13 sont presque exclusivement uniques à la souris (Takeda et al. 2003; Bowie and Haga 2005; Takeda and Akira 2005). Les différents TLR se différencient de trois façons : par leurs localisations cellulaires (Kawai and Akira 2007), par leur spécificité pour divers PAMP et par leurs domaines de signalisation cellulaire qui induisent des voies de signalisations distinctes (Shimazu et al. 1999; Brown et al. 2011). Les TLR1-2, 4 à 6 et 10 à 13 sont connus pour être localisés à la surface cellulaire et les TLR 3 et 7 à 9 ont une localisation dans des vésicules intracellulaires. Il est à noter que la localisation cellulaire correspond aussi au type de ligand reconnu par ces TLR. Ainsi les récepteurs de surface reconnaitront des PAMP localisés à la surface des pathogènes (ex. TLR5 reconnaît les flagellines bactériennes, TLR2 et TLR4 reconnaissent des protéines d'enveloppes bactériennes ou virales) et les récepteurs intracellulaires reconnaîtront des PAMP qui sont libérés lors de la réplication du pathogène (ex. TLR3 : l'ARN double brin viral, TLR9 : l'ADN bactérien riche en CpG) (Elgert 2009). Un cas particulier est le TLR4 qui entre autres lie à la surface cellulaire (avec ses corécepteurs CD14 et MD-2) les lipopolysaccharides des parois de bactéries à Gram négatifs pour ensuite être internalisé dans les endosmes (Akira et al. 2006). De plus, TLR4 est le seul TLR capable d'activé les deux principales voies de signalisation des TLR, soit la voie canonique Myd88 (*Myeloid differentiation primary response gene 88*) et la voie non canonique TRIF (*TIR-domain-containing adaptor protein inducing IFN*) aussi utilisée par TLR3 (Kawai and Akira 2007) (Figure 8). La voie Myd88 est initiée par le domaine conservé TIR qui recrute les protéines adaptatrices Myd88, IRAK-4 et TRAF-6. Ce recrutement permet l'activation des voies MAP kinase (*Mitogen Activated Protein kinase* : ERK, JNK, p38), mais principalement du facteur de transcription NF-κB qui contrôle l'expression des cytokines inflammatoires (dont Il-1β, Il-6 et IL-12) (Blackwell and

Christman 1997). À l'opposé, la voie TRIF est induite par son interaction directe avec le TRL3 ou par l'interaction de TRAM (*TRIF Related Adaptor Molecule*) avec le TLR4 et mène à l'activation des voies MAPK et NF-κB , mais de façon distincte vers la voie du facteur de transcription IRF3 (*Interferon Regulatory Factor 3*) qui est nécessaire à la transcription des gènes de l'interféron de type 1 (ex. IFN-α IFN-β).

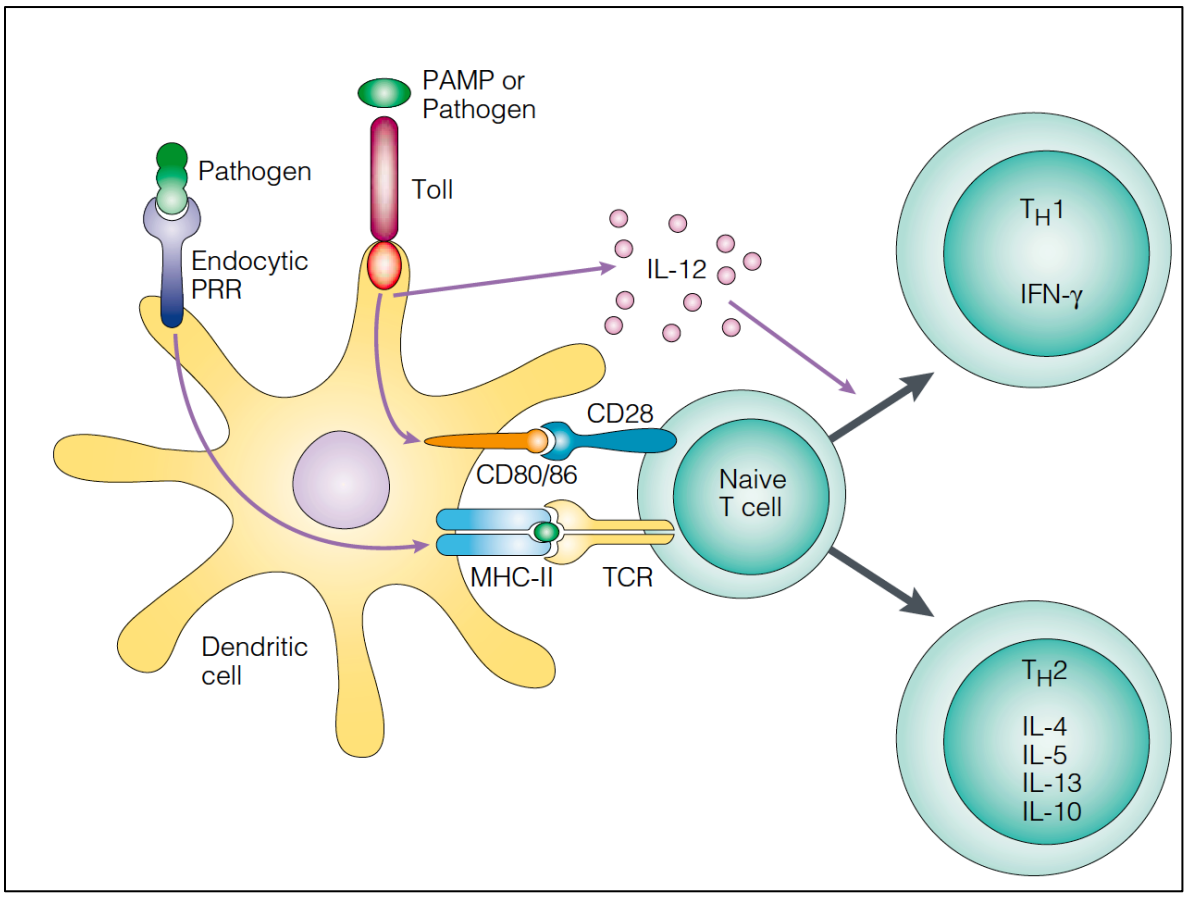

Figure 7 La réponse immunitaire innée.

Les récepteurs Toll-like (TLR) reconnaissent des PAMP distincts et jouent un rôle crucial dans la réponse immunitaire innée. Ils sont la première ligne de défense contre les pathogènes et sont d'importants modulateurs de l'inflammation, de la régulation du système immunitaire, de la survie et de la prolifération des cellules immunitaires. L'activation des TLR induit l'expression de cytokines, telle IL-12, de chimiokines et des récepteurs associés à ces médiateurs de l'immunité. L'induction de l'expression de CD80/86 par les TLR, sur les CPA, combinée à la présentation d'antigènes par les CMH mène à l'activation des cellules T. Subséquemment, les lymphocytes T se différencient en cellules T effectrices Th (T helper). La balance des cytokines, qui sont sécrétées, est importante dans l'activation préférentielle de la voie Th1 ou Th2. PRR (*Pathogen Recognition Receptor*)Tirée de (Medzhitov 2001).

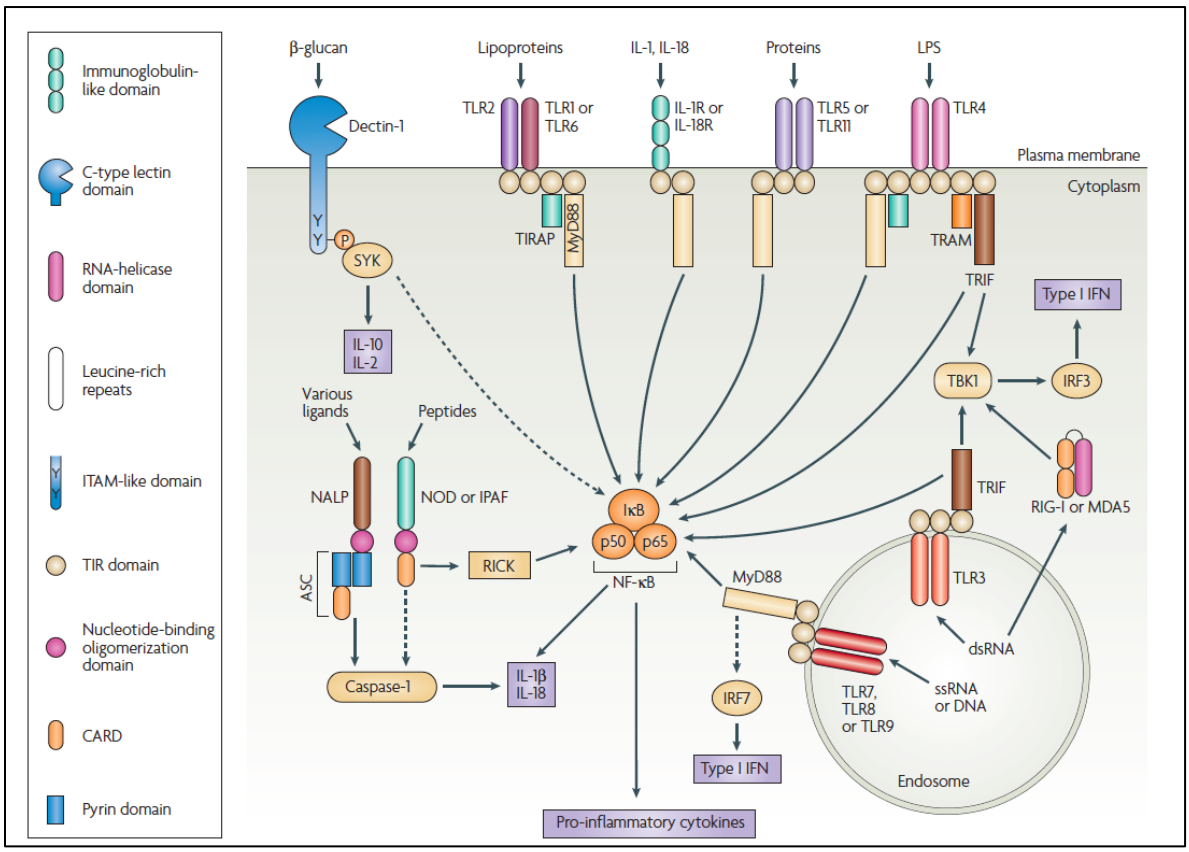

Figure 8 Les voies de signalisations des TLR et l'interaction avec les autres voies de signalisation.

Les TLR1, 2, 4, 5 et 6 se trouvent à la surface cellulaire et les TLR3, 7, 8 et 9 sont localisés dans les compartiments endosomaux/lysosomaux. Seulement les molécules adaptatrices et les principales voies de signalisation qui caractérisent les différentes classes de récepteurs reconnaissant les PAMP sont affichées. En réalité, les voies qui sont activées par ces différents récepteurs sont multiples et complexes. Par exemple, la signalisation des récepteurs TLR implique non seulement l'activation de NF-κB, mais aussi des MAPK, du phosphatidylinositol 3-kinase et plusieurs autres voies qui affectent fortement l'ensemble de la réponse. Dectin-1 (un récepteur de β-glucanes) est montré comme exemple d'autre récepteur PAMP à la surface cellulaire qui peut affecter de façon marquée la signalisation des TLR tout comme l'IL-1R et l'IL-18R. ASC, apoptosis-associated speck-like protein containing a CARD (caspase-recruitment domain); ds, double-stranded; IFN, interferon; IκB, inhibitor of NF-κB; IL, interleukin; IPAF, ICE-protease-activating factor; IRF, IFN-regulatory factor; LPS, lipopolysaccharide; MDA5, melanoma-differentiation-associated gene 5; MyD88, myeloid differentiation primary-response gene 88; NALP, NACHT-, LRR- and pyrin-domaincontaining protein; NOD, nucleotide-binding oligomerization domain; RICK, receptor-interacting serine/threonine kinase; RIG-I, retinoic-acid-inducible gene I; ss, single-stranded; TBK1, TANKbinding kinase 1; TIRAP, Toll/IL-1R (TIR)-domain-containing adaptor protein; TRAM, TRIFrelated adaptor molecule; TRIF, TIR-domain-containing adaptor protein inducing IFN ; SYK, spleen tyrosine kinase. Tirée de (Trinchieri and Sher 2007).

1.2.3. Rôles physiopathologiques des PC

En plus de leurs rôles dans la régulation des fonctions physiologiques par l'activation directe et indirecte de facteurs de croissance, de facteurs neuroendocriniens et de facteurs d'adhésions cellulaires (Creemers and Khatib 2008), les PC sont aussi impliquées dans le développement de physiopathologies. Sans aucun doute, les PC sont d'importantes régulatrices de la croissance tumorale (Cheng et al. 1997; Bassi et al. 2000; Bassi et al. 2001; Bassi et al. 2003; Bassi et al. 2005a; Bassi et al. 2005b; D'Anjou et al. 2011) et sont indicatives de l'agressivité des tumeurs (Bassi et al. 2005b; Scamuffa et al. 2008). Aussi, par la maturation de métalloprotéinase (*matrix metalloproteinases* (MMP) et *a disintegrin and metalloproteinase* (ADAM)) les PC se placent comme d'importantes modulatrices du développement de l'ostéoarthrite (Parks et al. 2004; Edwards et al. 2008; Malfait et al. 2008) et du développement de maladies cardiovasculaires (Stawowy and Fleck 2005; Liu et al. 2010; Marchesi et al. 2011; Turpeinen et al. 2011).

1.2.3.1. Les PC et les infections

Par définition, les pathogènes sont des agents, tels les microorganismes (bactéries, champignons et levures), les particules virales et les prions, qui causent des symptômes néfastes à un hôte. Fait intéressant, les virus et les bactéries ont évolué en utilisant des facteurs moléculaires de l'hôte, à leur propre bénéfice, dans une sorte de parasitisme. Au cours des années, il a été démontré que les PC ont été sélectionnées pour activer divers pathogènes et que cette activation entraine souvent une augmentation de la pathogénicité, de la mortalité et de la sévérité des symptômes (Webster and Rott 1987; Lea et al. 1999; Perdue and Suarez 2000; Hatta et al. 2001). Il existe deux types majeurs de protéines d'agents infectieux qui peuvent être activées par les PC : les glycoprotéines virales et les toxines bactériennes. Chez les virus, les protéines activées sont; les glycoprotéines d'enveloppe permettant l'entrée virale du VIH (gp160) (Hallenberger et al. 1992), du virus Semliki Forest (Zhang et al. 2003), du Chikungunya (Ozden et al. 2008), des arénavirus (Rojek et al. 2010), du virus de la rougeole (Watanabe et al. 1995), des filovirus Ebola (Volchkov et al. 1998; Basak et al. 2001) et Marburg (Volchkov et al. 2000), du coronavirus induisant le syndrome respiratoire aigu sévère (SRAS) (Follis et al. 2006), du cytomégalovirus (Jean et al. 2000) et l'hémagglutinine (HA) du virus de l'influenza hautement infectieux (Stieneke-Grober et al. 1992; Walker et al. 1994). Il a aussi été

démontré que la protéine de la capside du virus du papillome pouvait être clivée par furine (Richards et al. 2006) et que la protéine d'import nucléaire Vpr du VIH pouvait être clivée par PACE4 (Xiao et al. 2008). Dans le cas des toxines bactériennes, il existe trois types de toxines qui peuvent être activées par les PC : les toxines à une chaine où le site de clivage est situé entre les deux futures sous-unités (l'exotoxine de Pseudomonas (Inocencio et al. 1994; Gu et al. 1996), la toxine de la diphtérie (Tsuneoka et al. 1993), la toxine de Shiga (Garred et al. 1995) et Shiga-like (Burgess and Roberts 1993)), les toxines binaires formant un complexe macromoléculaire de deux protéines telles la toxine de l'anthrax (Klimpel et al. 1992; Molloy et al. 1992; Gordon et al. 1997) et les toxines lytiques qui s'assemblent en oligomères protéiques formant des pores (ex. aérolysine (Abrami et al. 1998)).

1.2.3.1.1. Modèle viral : le virus de l'influenza aviaire hautement infectieux

L'influenza est un virus à ARN simple brin de sens négatif (ARNv) qui cause la grippe, soit de la fièvre, des douleurs musculaires, des maux de tête, de la fatigue, des maux de gorge et de la toux (Zambon 2001; Taubenberger and Morens 2008; Whitley 2010). L'influenza est particulièrement fascinante d'un point vu évolutif, car son génome est codé par 7 ou 8 segments d'ARNv qui forment des complexes ribonucleoprotéiques (RNPv) (Figure 9B) plutôt que par un seul ARNv (De Clercq 2002). Cette particularité permet au virus une évolution rapide en échangeant des segments complets de son génome avec un virus parent, et ce dans un hôte commun. Ce mécanisme, appelé réarrangement, est possible pour l'influenza de type A qui est capable d'infecter des hôtes de plusieurs origines animales. Les réarrangements sont d'ailleurs à l'origine des dernières pandémies de grippe et en font un agent infectieux imprévisible et dangereux pour la santé publique (Figure 9A) (Lamb and Takeda 2001; Salomon and Webster 2009).

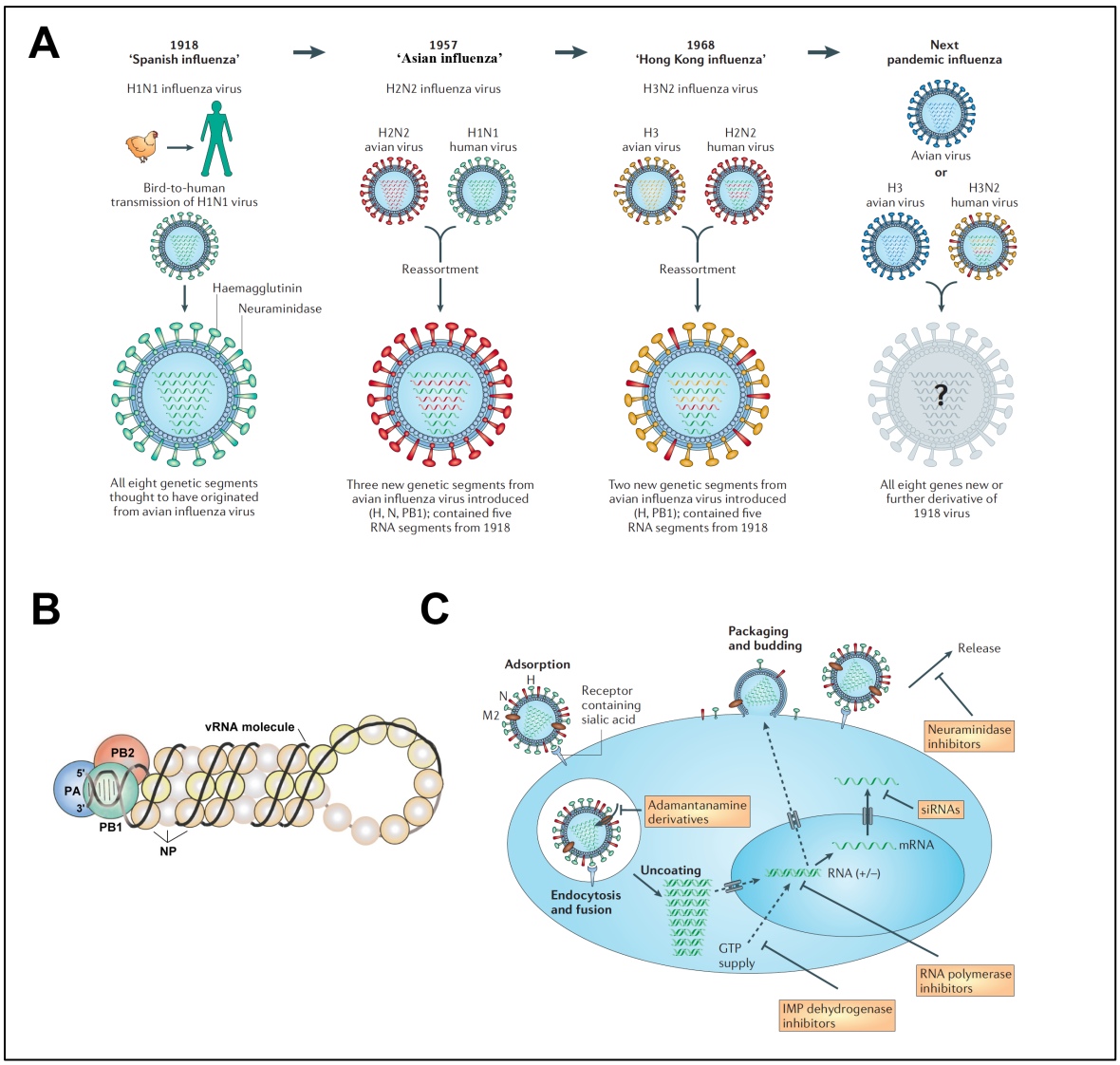

Figure 9 Le virus de l'influenza.

A) Les deux mécanismes à l'origine des pandémies d'influenza. En 1918, un virus de l'influenza H1N1 d'origine aviaire s'est adapté (par mutations) ce qui lui permit alors de se répliquer et se transmettre efficacement chez l'homme et d'engendrer la grippe espagnole « *Spanish influenza* ». En 1957 et 1968, deux évènements de réarrangement ont mené respectivement à l'apparition de la grippe asiatique « *Asian influenza* » par le virus H2N2 et de la grippe de Hong Kong « *Hong Kong influenza* » par le virus H3N2. La grippe asiatique H2N2 provient de l'acquissions de trois segments génétiques d'une espèce d'influenza aviaire (soit l'hémagglutinine (HA), la neuraminidase NA et la polymérase PB1). La grippe de Hong Kong H3N2 a acquis deux segments génétiques d'un virus aviaire (soit HA et PB1). Ainsi, les pandémies futures, dont celle de la grippe porcine H1N1 2009, peuvent provenir de mutation ou de réarrangement viral Tirée de (De Clercq 2006). B) Organisation du complexe de l'ARN ribonucléoprotéique. Les protéines découlant des gènes de polymérase PB1, PB2 et PA retiennent les extrémités 5' et 3' de l'ARNv qui entoure les nucléoprotéines du virus. Tirée de (Naffakh et al. 2008). C) Cycle de réplication

du virus et cibles thérapeutiques actuelles. L'hémagglutinine (HA) lie les acides siacyliques sur des récepteurs à la surface cellulaire qui permettent l'internalisation du virus. À pH acide, induit par l'acidification des endosomes, HA induit la fusion membranaire entre le virus et l'hôte. Il s'en suit la relâche du matériel génétique viral dans la cellule grâce au flux de proton créé par la pompe virale M2 qui permet le désassemblage du virus. Les admantanamines bloquent cette relâche en inhibant l'acidification par la pompe M2. La réplication de l'ARN viral a lieu dans le noyau et peut être bloquée par des inhibiteurs d'inosine 5′-monophosphate (IMP) déshydrogénase. Ces inhibiteurs ont comme effet de bloquer l'apport en GTP, ce qui est requis pour la synthèse de l'ARN. Les protéines virales, synthétisées par la machinerie cellulaire, seront assemblées à la membrane plasmique et le virus sera relâché grâce à l'action de la neuraminidase qui clive les acides siacyliques retenant le virus à la membrane. La relâche peut être inhibée par des bloqueurs de neuraminidase. Tirée de (De Clercq 2006).

La classification des virus de l'influenza se fait par sérotypage des deux protéines membranaires antigéniques du virus, soit l'hémagglutinine (HA/H) et la neuraminidase (NA/N) (ex. un sérotypage HA1 et NA1 sera nommé H1N1) (Hilleman 2002). En plus, pour différencier les différents virus retrouvés, on utilisera la nomenclature suivante : Type d'influenza/localisation/souche/année (sérotype). Ainsi, le premier virus de l'influenza A isolé à Sherbrooke en 2010 qui a un sérotype H3 et N2 sera désigné ainsi : Influenza A/Sherbrooke/1/2010 (H3N2).

Le génome de l'influenza code pour 10 à 11 protéines (décrites dans le Tableau 3) impliquées dans le cycle viral du virus : de l'entrée à la réplication, puis à la relâche du virus (Figure 9C). L'entrée du virus est effectuée grâce à la protéine HA sous sa forme trimérique. HA est la protéine qui lie les acides salicyliques pour permettre l'endocytose récepteur dépendant du virus (De Clercq 2006). Toutefois, HA doit être clivée par une sérine protéase confinée au poumon (à un site contenant une Arg en P1), afin de permettre un changement conformationnel de la protéine dépendant du pH (Figure 10) (Bertram et al. 2010). À pH acide, la protéine expose un peptide de fusion qui interagit avec la membrane endosomale et induit la fusion membranaire entre l'endosome et la membrane virale. Au cours de son passage dans l'endosome, la pompe M2 du virus engendre un flux de proton qui permet le désassemblage de la matrice liée au RNPv. Ainsi, les huit RNPv du virus sont largués dans le cytosol pour ensuite être transportés dans le noyau (De Clercq 2006). Une fois au noyau, le complexe des polymérases virales PB1, PB2 et PA réplique l'ARNv pour permettre la production d'autres RNPv qui seront assemblées pour former de nouveaux virions. Parallèlement, les ARNv sont transcrits en ARNm et traduits par la machinerie cellulaire de l'hôte. Lors de cette étape, l'influenza utilise un mécanisme qui lui permet de stabiliser ses ARNm, mais aussi de dérouter en sa faveur la machinerie de traduction de l'hôte. Dans ce mécanisme appelé « *cap snatching* », la protéine NS1 lie les coiffes (*cap*) des ARNm de l'hôte, puis la protéine PB2 coupe (*snatching*) ces coiffes pour les transférer sur les ARNm viraux (Kawaguchi and Nagata 2006; Nagata et al. 2008). Le virus prend ainsi le contrôle de la cellule hôte en déréglant la réponse immunitaire par divers mécanismes complexes (ex. inhibition des voix de signalisation de la réponse immunitaire, dérégulation des macrophages et apoptose précoce des cellules dendritiques (Peiris et al. 2009; Peiris et al. 2010; Fukuyama and Kawaoka 2011; Karpala et al. 2011; Friesenhagen

et al. 2012)) et en facilitant les co-infections bactériennes (Zambon 2001; Whitley 2010). Quant à elles, les trois protéines membranaires (HA, NA et M2) empruntent la voie de sécrétion suite à leur synthèse. Finalement, les constituants du virus se rencontrent à la membrane plasmique où il y aura assemblage et largage viral par fission membranaire. À cette étape, la protéine NA est essentielle pour la relâche des virions et l'infection des cellules voisines, puisqu'elle détruit les acides salicyliques qui lie HA et retient les virions à la membrane (Das et al. 2010).

Tableau 3 Liste des protéines encodées par le virus de l'influenza et facteurs déterminants pour les HPAI.

Structure virale	Abréviation	Nom	Fonction	Caractéristiques H5N1 (HPAI)
Membrane	HA	Hémagglutinine	Attachement, internalisation et fusion membranaire	Site multibaisque RRRKKR
	NA	Neuraminidase	Salisidase, relâche viral	Tyr 274 plutôt que l'His 274
	M2	Protéine de la matrice 2	Pompe à proton, désassemblage de la matrice et des RNPv	
Ribonucléoprotéine virale (RNPv)	PA	Polymérase A	Transcriptase et réplication virale	
	PB1	Polymérase B1	Transcriptase et réplication virale	
	PB1-FA (facultative)	PB1-Facultatif (Promoteur alternatif du gène PB1)	Induis l'apoptose	Présence avec Ser 66 plutôt que l'Asn 66
	PB2	Polymérase B2	Endonucléase : coupe la coiffe des ARNm de l'hôte pour la lier aux ARNm viraux (cap snatching)	Asn 701 plutôt que l'Asp 701
	NP	nucléoprotéine	Lie l'ARNm, principal constituant du RNPv	
Matrice	M1	Protéine de la matrice 1	Assemblage des RNPv en virion,	

			interaction avec la membrane	
autre	NS1	Protéine non structurelle 1	Lie les ARNm de l'hôte (cap snatching), contribue à la virulence.	Glu 92 Plutôt que l'Asp 92 avec motif C-terminal ESEV
	NS2 ou NEP	Protéine non structurelle 1	Transport du RNPv du noyau vers le cytoplasme	

Adapté de (Tscherne and Garcia-Sastre 2011)

En 1997, une souche aviaire hautement pathogénique de l'influenza A (HPAI) H5N1 est transmise à l'homme et cause sa mort (de Jong et al. 1997). Ce virus se répand rapidement chez la population aviaire du Moyen-Orient et de l'Asie infectant au passage plusieurs hommes (Williams and Peterson 2009). Malgré son faible taux de transmission aviaire/homme et une incapacité de transmission homme/homme, les cas d'infection par ce virus présentent un haut taux de mortalité qui représente toujours un risque important pour la santé humaine mondiale (Writing Committee of the Second World Health Organization Consultation on Clinical Aspects of Human Infection with Avian Influenza et al. 2008). Les déterminants moléculaires derrière ce haut taux de mortalité sont multifactoriels (Tableau 3), mais on note l'apparition d'un site de clivage multibasique (RRRKKR) dans la boucle d'activation de HA plutôt que l'unique Arg en P1 (Figure 10 point 2). Ce site de clivage, reconnu par les PC, (Klenk et al. 1977; Stieneke-Grober et al. 1992; Horimoto et al. 1994) n'avait jamais été observé chez l'homme auparavant. Toutefois, sa présence est un facteur déterminant de la pathogénicité et permet au virus de causer une infection systémique (Webster and Rott 1987; Perdue and Suarez 2000; Basak et al. 2001; Hatta et al. 2001; Shiryaev et al. 2007; Decha et al. 2008; Remacle et al. 2008; Munster et al. 2010).

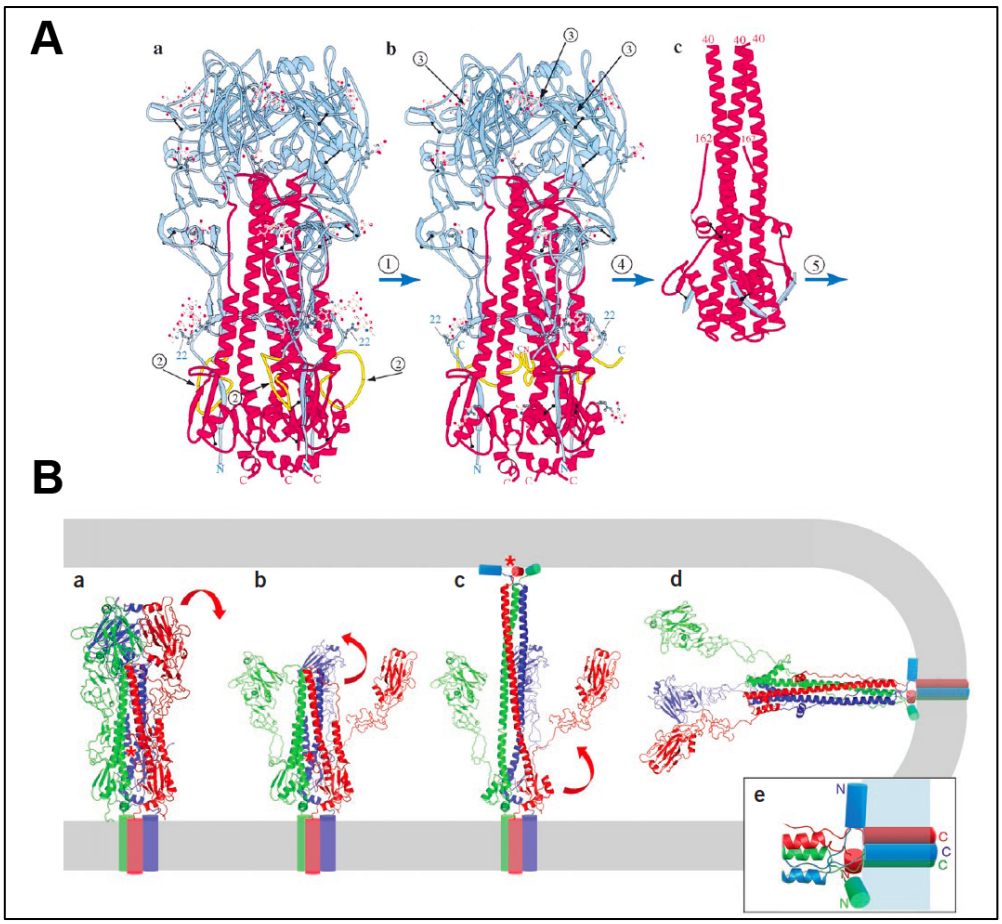

Figure 10 L'hémagglutinine : activation et fusion membranaire.

A) Structure tridimensionnelle de HA. a) Le précurseur non maturé HA0, qui a été produit en introduisant une mutation R329Q au site de clivage et en éliminant le domaine transmembranaire. La flèche 2 indique le site de clivage de chaque monomère dans la boucle qui sépare le domaine HA1 en N-terminal du site de clivage du domaine HA2 en C-terminal du site de clivage (les résidus 323 de HA1 à 12 de HA2 sont en jaune). b) Forme clivée de HA où les flèches 3 indiquent les sites de liaison aux récepteurs c) Conformation induite par le pH acide, solubilisé à la thermolysine. HA1 est en bleu HA2 en rouge et les traits noirs indiquent les ponts disulfures. (Chen et al. 1998). B) Séquence proposée de la fusion induite par HA. a) Conformation «préfusion» en contact avec leurs récepteurs (non représentés) où chaque monomère est d'une couleur différente. On note que les peptides de fusion sont séquestrés au centre du trimère. b) HA1 se dissocie de sa position repliée en conséquence au changement de pH et reste attaché à HA2 par des ponts disulfures. c) Intermédiaire allongé, où les boucles, entre la petite et la grande hélice de HA2, deviennent des hélices ce qui permet l'exposition du peptide de fusion à la membrane endosomale. Les peptides de fusion, marqués par un astérisque, interagissent sous forme d'hélices amphipathiques avec la membrane lipidique. d) L'effondrement de l'intermédiaire étendu génère la conformation postfusion qui provoque le rapprochement entre la membrane endosomal et celle du virus, puis la fusion entre celles-ci. e) Détails de la structure des peptides de fusion encrés aux membranes après la fusion. Tirée de (Harrison 2008).

1.2.4. Les PC comme cibles thérapeutiques

Soupesant le rôle que peuvent jouer les PC dans le développement de physiopathologies, tels le cancer et l'activation de pathogènes, un intérêt certain pour la conception d'inhibiteurs sélectifs aux PC a vu le jour au cours des dernières années. Plusieurs approches ont été utilisées pour en arriver à une liste d'inhibiteurs prometteurs capables de bloquer les infections et la progression tumorale (Tableau 4). Les inhibiteurs de PC ont été développés principalement par : dessin rationnel d'inhibiteur, criblage de peptides par banques combinatoires (PS-SPCL) et bio-ingénierie de macromolécules inhibitrices de protéases (Fugere and Day 2005). L'objectif final est d'obtenir une certaine sélectivité, une puissance d'inhibition, une stabilité in vivo et une faible toxicité (Cardo-Vila et al. 2010; Giordano et al. 2010). Un exemple de bio-ingénierie est la modification de l'antitrypsine en y ajoutant une séquence reconnue par la furine (Jean et al. 1998). Cette dernière approche, tout comme l'utilisation de prodomaines de PC ou la modification d'autres inhibiteurs de protéase endogènes, est capable de produire une certaine sélectivité. Toutefois, la taille des molécules résultantes limite leurs applicabilités cliniques et les confine plutôt à être des outils de biologie moléculaire (Couture et al. 2011). Les approches par dessin rationnel et le criblage de peptides par banques combinatoires sont les démarches qui ont donné les résultats les plus fructueux. La première consiste à utiliser des sites de clivage naturels retrouvés pour dessiner un peptide inhibiteur en effectuant des modifications de séquences afin de permettre l'optimisation de la molécule (ex. en utilisant l'alignement de la molécule à la structure tridimensionnelle de la furine et en appliquant les connaissances acquises sur les déterminants structuraux d'un substrat pour augmenter la sélectivité) (Dreyer et al. 1989). L'autre approche, le criblage de peptides par banques combinatoires, utilise un mélange de peptides ayant des modifications (en acide aminé à chacune de ses positions) pour compiler les positions et les acides aminés importants dans le but d'augmenter la sélectivité et la puissance d'inhibition *in vitro* (Fugere et al. 2007). Une fois sélectionnées, les séquences peptidiques peuvent être modifiées par des acides aminés non naturels, des acides aminés mimétiques et en ajoutant des groupements fonctionnels au peptide. De plus, des approches pour développer des inhibiteurs non peptidiques, sous forme de petites molécules, ont été avancées. L'utilisation de criblage de banques de molécules naturelles ou de synthèses a permis la découverte de molécules qui

ont des profils de sélectivité intéressants pour les PC (Basak et al. 1999; Jiao et al. 2006; Komiyama et al. 2009; Kowalska et al. 2009). Toutefois, la puissance d'inhibition de ces molécules, à l'exception du composé hautement chargé positivement dérivé du 2,5-dideoxystreptamine, est relativement faible comparativement aux inhibiteurs peptidiques (Couture et al. 2011). Malgré tout, le développement d'inhibiteurs peptidiques et de petites molécules synthétiques ont chacun leurs avantages. Les inhibiteurs peptidiques présentent souvent une faible toxicité *in vivo*, car leur composition est reconnue comme des composés naturellement retrouvés dans le corps. De plus, leur structure peut facilement être modifiée de multiples façons afin d'augmenter leur sélectivité, spécificité et stabilité (Abell 1997). L'avantage des petites molécules est principalement leur taille, qui est plus propice à la pénétration cellulaire. Toutefois, leur profile toxicologique est souvent imprévisible.

Tableau 4 Inhibiteurs de PC validés *in vivo*.

Molecules	Type	*In vivo* validated uses	Hits by	Selectivity index (nM)	
TPRARRRKKRT-NH_2 (Shiryaev et al. 2007)	Peptidic	Protects against *Pseudomonas* exotoxin and anthrax infection. Synergism with antibiotics	Extension of the furin cleaving sequence in the HA of avian influenza A H5N1	23 162 441 232 152	furin* PACE4 PC4 PC5/6 PC7
8-amino-octanoyl-RARRRKKRT-NH_2 (Remacle et al. 2010)	Tailed peptide	Protect from anthrax infection *in vivo*. Synergism with antibiotics	Derivation of TPRARRRKKRT peptide with lipid complexion to provide cellular entry	8 3 430 3	furin PC5/6 PC7 PACE4
Hexa-D-arginine (Cameron et al. 2000)† (Fugere et al. 2007)	Peptidic	Prevents and treats PEA sepsis in mice.	PS-SPCL	265 106 13 000 1875 206 580	furin furin† PC1† PC7 PC5/6 PACE4
Nona-D-arginine peptide (Cameron et al. 2000) (Karicherla and Hobden 2009) (Karicherla et al. 2010)	Peptidic	Reduces considerably the corneal damages of the keratitis caused by *Pseudomonas aeruginosa* and prophylaxis uses	Levoratory modification of the nona-L-arginine version previously identified by PS-SPCL of L- and D-hexapeptides	1 19 81	furin* PC5/6 PC7

CMGTINTRTKKC (Hajdin et al. 2010)	Peptidic	Limits rhabdomyosarcoma tumors progression. Synergism with antineoplasic agent	Screening for phage-displayed peptides binding to rhabdomysarcoma cells	N/A	
Decanoyl-RVKR-CMK (Angliker et al. 1993) (Jean et al. 1998) (Fugere et al. 2002) (Bassi et al. 2010)	CMK-peptide	Reduces considerably squamous cell carcinomas (~30%) in TPA induced epidermal proliferation.	Coupling CMK group used to study other proteinases on Arg and Lys peptidic sequences.	1 0.12 0.12 3.6	furin PC5/6 PC7 PACE4

Tiré de (Couture et al. 2011). Basé sur les valeurs de K_i face à la forme recombinante soluble de PC (humaine si non mentionnée) les valeurs avec (*) marquent l'instance sur la sélectivité. PEA : *Pseudomonas aeruginosa* exotoxin A TPA : 12-*O*-tetradecanoylphorbol-13-acetate.

1.2.5. La spectrométrie de masse : un outil pour l'étude des PC

Au cours des dernières années, l'utilisation de plateformes technologiques à haut débit a fait avancer les sciences biologiques à pas de géant. Le séquençage du génome humain a permis d'accumuler une masse de données d'importance capitale pour l'avancement des découvertes biologiques. Une de ces plateformes permet l'étude des molécules de toutes tailles, la détermination de leurs structures et compositions : la spectrométrie de masse. Cet outil est d'une importance particulière pour l'étude des protéines et des peptides, car elle permet le séquençage et l'identification de celles-ci dans des mélanges simples ou complexes et donc le décryptage du protéome et du peptidome. Il est donc pertinent d'utiliser cette technologie pour l'étude des PC, puisque celles-ci agissent directement sur les protéines et les peptides qui composent les systèmes moléculaires et cellulaires.

Les spectromètres de masses sont constitués de quatre parties, soit la source, l'analyseur, le détecteur et l'ordinateur qui permettent de reconstituer les données du détecteur en spectre analysable sous forme d'intensité à une masse/charge donnée (m/z) (Figure 11). L'agencement de différents types de sources, analyseurs et détecteurs va permettre aux appareils d'avoir des propriétés uniques qui seront bénéfiques pour diverses applications. De plus, de nos jours les appareils contiennent souvent des analyseurs en tandem, qui peuvent être hybrides, permettant ainsi de profiter de la combinaison des propriétés de ceux-ci (Tableau 5) (Glish and Vachet 2003).

Tableau 5 Caractéristiques des analyseurs.

Type	Résolution	Précision (ppm)	Gamme de masse (m/z)	Vitesse d'acquisition
FT-ICR	$1x10^6$	1	<6000	Lente
Orbitrap	$1\text{-}2x10^5$	3	<5000	Lente à Moyenne
Temps de vol (TOF)	$2.5\text{-}6x10^4$	50	∞	Moyenne à rapide
TRAP ionique	$2x10^4$	30	<4000	Rapide
Quadripôle	$1.5x10^4$	10	<4000	Moyenne

FT-ICR : *Fourrier Transform- Ion Cyclotron Resonance*

La source est l'élément essentiel pour l'introduction des analytes dans l'appareil. Elle permet d'ioniser les molécules pour leur donner une charge qui est nécessaire pour permettre leur analyse (Gross and Roepstorff 2011). Il existe plusieurs types de sources qui ont leurs avantages et leurs inconvénients. Tandis que certaines sources sont encore au stade de développement, deux types de sources bien établies seront ici décrites : une source permettant l'analyse d'échantillons sous forme liquide dérivée du monde de la chimie (ESI) et une source permettant l'analyse des échantillons sous forme solide (MALDI) dérivée du monde de l'analyse des surfaces de la physique (Figure 11).

La source ESI (*Electro Spray Ionization*) à l'avantage de pouvoir être directement couplée a des appareils de chromatographie afin de préséparer des mélanges complexes pour en obtenir d'avantages d'informations. Le principe de la source ESI repose sur le passage des analytes près d'un faisceau d'électrons qui permet d'induire l'ionisation des molécules à analyser. La source ESI produit des analytes multichargés, on pourra donc déduire leur masse en multipliant la valeur m/z par la charge (ex. pour un ion m/z de 600 où la charge est +2 la masse calculée sera de 1200). Ce type de source peut être modifiée pour s'adapter à des débits d'injection lents (nanoSpay), ce qui permet d'augmenter la sensibilité de détection et le pouvoir de séparation chromatographique pour analyser des échantillons très complexes. Toutefois, la source ESI est très sensible aux contaminants, tels que les

sels, qui inhibent l'ionisation efficace des molécules (Yates et al. 2009). Une attention particulière doit donc être prise durant la préparation des échantillons pour éliminer ces contaminants. La source MALDI (*Matrix Assisted Lazer Desorbtion Ionization*) est quant à elle moins sensible à ce type de contaminants. Cette source, comme son nom l'indique, repose sur l'ionisation par un laser d'un échantillon mélangé dans un excès de matrice. La matrice sous forme de cristal absorbe l'énergie UV du laser qui induit son ionisation et sa désorption par transfert d'énergie. La source MALDI génère des charges par perte ou addition d'un proton générant principalement des analytes monochargés. Cette caractéristique permet entre autres de générer des spectres simples d'interprétation, puisque l'on peut facilement déduire la masse d'un analyte sans calculer sa charge (Yates et al. 2009).

Une fois ionisées, les molécules seront transportées par un champ de force magnétique ou électrique vers l'analyseur. Les analyseurs permettent de séparer les molécules selon leur propriété physicochimique m/z sous deux principes de physiques : 1) la 2e loi de Newton de la physique mécanique 2) la loi de force de Lorentz de la physique électrique. La combinaison de ces deux lois résulte en l'équation classique caractérisant une particule chargée en mouvement : $(\frac{m}{Q})a = E + vB$ ou m est la masse, Q est la charge, a est l'accélération, E est le champ électrique et vB est le produit vectoriel de la vélocité ionique et du champ magnétique (Gross and Roepstorff 2011). Selon cette équation, un analyseur peut donc séparer des molécules ionisées en faisant varier un champ électrique ou un champ magnétique et par leur accélération différentielle (Figure 11). Ainsi, le quadripôle (souvent désigné Q) sépare les ions en exerçant un champ électrodynamique, les secteurs magnétiques utilisent un champ magnétique variable pour sélectionner des ions ayant un moment cinétique particulier ou les mettre en résonnance dans un cyclotron (ICR), les trappes ioniques permettent de créer un champ électromagnétique ou électrodynamique afin de piéger un ion dans un mouvement périodique (TRAP et Orbitrap) et finalement l'analyseur en temps de vol (TOF) utilise un tube sous vide soumis à un champ électrique pour séparer les ions selon leurs accélérations. Ces différents analyseurs permettront aux appareils d'avoir des propriétés uniques au sens du pouvoir résolutif (capacité à séparer deux masses rapprochées, souvent décrites comme le ratio entre la pleine largeur à la base et la largeur à la mi-hauteur du pic), de la précision (décrite en ppm), de leur gamme de

masse en m/z et de leur vitesse d'acquisition (Glish and Vachet 2003; Han et al. 2008; Yates et al. 2009). Voir Tableau 5.

Sauf pour le cas où les ions seront mis en résonnance et analysés par transformée de Fourrier (ICR et Orbitrap), la détection sera faite par des détecteurs capables de mesurer les charges induites, ainsi le courant produit par le passage des ions sera par la suite représenté en spectre d'intensité à une m/z donnée (Gross and Roepstorff 2011).

Les spectromètres de masse sont généralement équipés d'une cellule de collision, souvent appelée spectrométrie de masse en tandem ou MS/MS, qui permettra de briser (appelé CID pour *Collision Induced Dissociation*) les ions introduits dans l'appareil et d'en déduire leurs structures. Des méthodes alternatives existent aussi, telles que la dissociation par capture électronique (ECD) et la dissociation par collision à haute (HCD), qui permettent notamment d'obtenir davantage d'informations structurales sur les ions analysés (Glish and Vachet 2003; Yates et al. 2009).

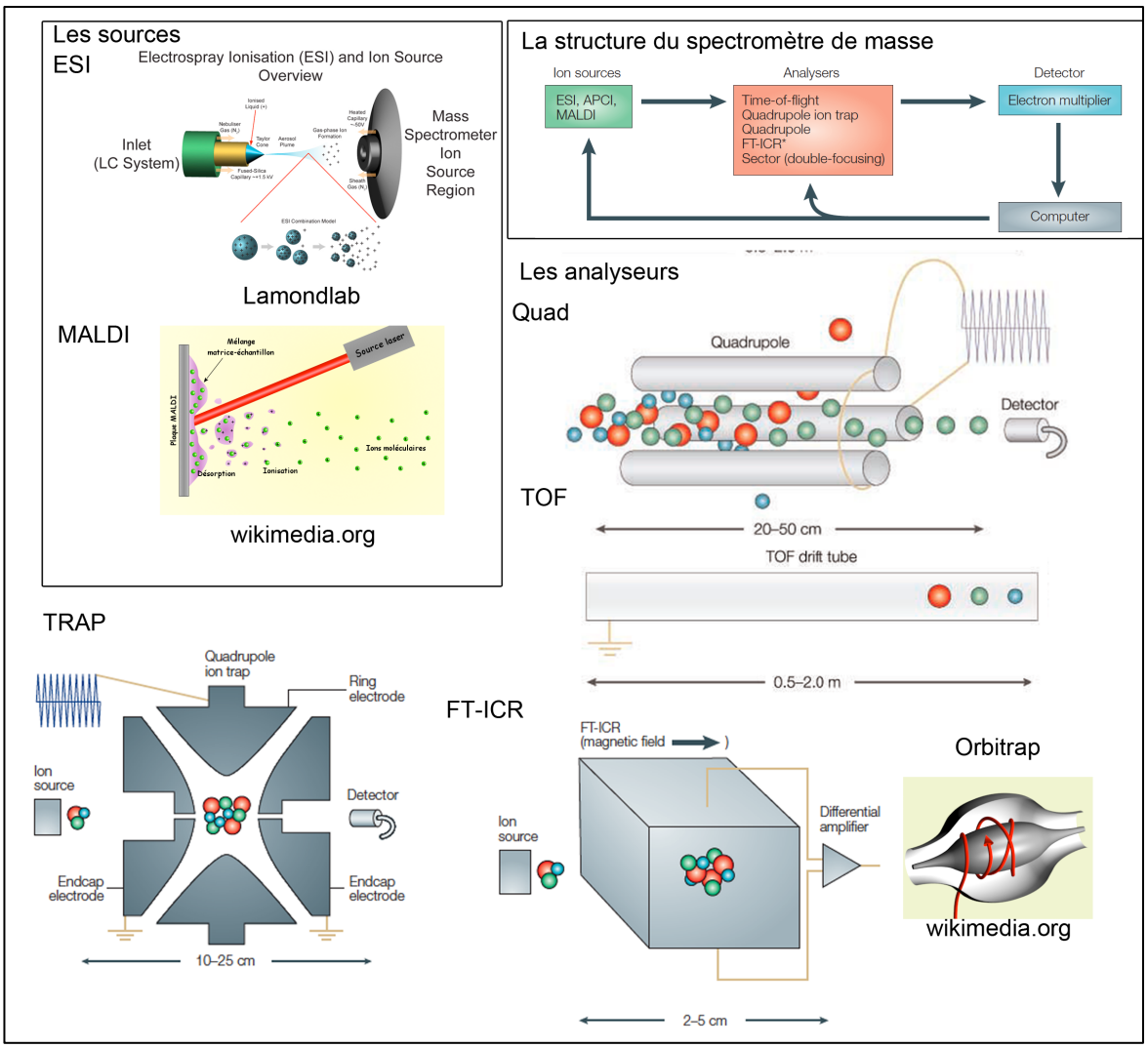

Figure 11 Les spectromètres de masse.

Présentation de la structure des spectromètres de masse. Une schématisation du mode de fonctionnement des sources MALDI et ESI sont présentées, ainsi que les analyseurs les plus courants : le quadrupole (Quad), le temps de vol (TOF), la trappe ionique (TRAP), la cellule de résonnance magnétique (FT-ICR) et la trappe orbitale (Orbitrap). Modifiée de (Glish and Vachet 2003).

1.2.5.1. Protéomique à haut débit de type shotgun

Le terme « *shotgun* » est utilisé en protéomique lorsqu'un échantillon de protéines est digéré et analysé sans passer par une électrophorèse sur gel en deux dimensions. L'approche *shotgun*, dite « bottom-up », utilise couramment deux protocoles: la digestion de l'échantillon suivie de la chromatographie à faible débit (nanoLC) en une ou deux dimensions couplées à un spectromètre de masse hybride (souvent Q-TOF ou LTQ-Orbitrap) ou l'utilisation d'un premier fractionnement de l'échantillon non couplé à l'appareil de spectrométrie de masse (appelé séparation hors ligne). Cette deuxième approche peut utiliser un premier fractionnement chromatographique des peptides digérés ou couramment une électrophorèse par gel sur laquelle on découpe des bandes (appelé Gel LC-MS/MS) qui sont ensuite digérées et analysées par nanoLC-MS/MS. Souvent, la trypsine est utilisée pour digérer les protéines. Cette étape est nécessaire pour réduire les protéines en peptides plus facilement fragmentés et identifiés en mode MS/MS. Des logiciels sont ensuite utilisés pour analyser les spectres MS/MS selon le patron de fragmentation (principalement des ions y et b (Johnson et al. 1987)) des peptides afin de déterminer leur séquence en acide aminé et corréler ces peptides aux séquences protéiques contenues dans une base de données. Ainsi, on peut identifier plusieurs centaines de protéines en une analyse. De plus, diverses approches quantitatives peuvent être utilisées afin de comparer des échantillons de divers groupes (Han et al. 2008). Certaines de ces approches utilisent la dérivation chimique des peptides par l'ajout de molécule isotopique ou isobarique (iTRAQ) (Leitner and Lindner 2009) aux peptides ou même utilisent l'incorporation d'acides aminés isotopique dans les protéines (SILAC) (Ong et al. 2003; McClatchy and Yates 2008). Ces méthodes permettent de combiner les échantillons de deux ou plusieurs traitements et de les quantifier de façon relative dans une même analyse. Il existe aussi des approches sans marquage où l'intensité ou l'aire des spectres est comparée. On peut même convertir le nombre de spectres identifiés pour une protéine à une valeur quantitative relative (Neilson et al. 2011). De plus, les expériences de protéomique s'accompagnent d'analyses bio-informatiques qui permettent de tirer le maximum d'information des données d'identification obtenues. Ainsi, des bases de données contenant les interactions connues ou prédites, les voies de signalisations, les maladies et l'ontologie génique (contenant les localisations cellulaires, les fonctions moléculaires et les fonctions

biologiques) des protéines identifiées peuvent être interrogées. Or donc, grâce à l'intégration de ces informations aux valeurs quantitatives des protéines identifiées, on peut déduire et décrire leurs effets sur les systèmes moléculaires (Suderman and Hallett 2007; Braun 2012; Lemeer et al. 2012; Mostafavi and Morris 2012).

1.2.5.2. L'imagerie par spectrométrie de masse MALDI

En 1994 et en 1997, deux groupes montrent la faisabilité d'utiliser un spectromètre avec source MALDI pour générer une image à partir d'analyses moléculaires sur tissu (Spengler et al. 1994; Caprioli et al. 1997). Exploitant la tolérance aux sels de la source MALDI et la capacité de diriger le laser de la source à des coordonnées précises, ils ont pu rapporter les spectres obtenus point par point sur le tissu et reconstituer une image selon l'intensité d'ion m/z (Figure 52). De cette façon, on peut donc dresser l'histologie moléculaire d'un tissu de façon multiplexée. Depuis, cette méthode a grandement évolué et a été appliquée de façon courante à l'étude de la distribution de petites molécules, de lipides, de peptides et même de protéines. Une description détaillée de l'évolution et de la méthodologie associée à cette technologie est présentée dans le Chapitre 6 - TARGETED MASS spectrometry Imaging: Specific Targeting Mass Spectrometry imaging technologies from history to perspective. Notamment les sections suivantes sont particulièrement utiles à la compréhension de cette technologie : Sample preparation: Tissue Conservation and Imaging Strategies à la p. 256, Frozen tissues à la p. 268, What is the best matrix for MALDI-MSI? à la p. 272, Which method is optimal for matrix deposition? à la p. 274, MALDI-MSI and bioinformatics, à la p. 282, Imaging of peptides and proteins à la p. 284.

1.3. Problématique et hypothèses

Certes, les PC sont des acteurs à considérer lors d'infections, et ce à deux niveaux. Dans un premier lieu, les PC sont décrites comme des protéines activatrices de glycoprotéines virales et de toxines bactériennes. Dans un second temps, les PC peuvent, de façon directe ou indirecte, moduler la réponse immunitaire. Ce sont là deux aspects intimement liés d'un point de vue physiopathologique et qui, dans un contexte où une approche thérapeutique visant les PC est envisagée, doivent respectivement être pris en compte.

Parmi les pathogènes qui exploitent les PC pour leur propagation, figure le virus de l'influenza H5N1 qui possède un site RRRKKR dans sa boucle d'activation de l'hémagglutinine (HA5). Ce gain évolutif du virus fait partie des déterminants qui rendent le virus hautement pathogénique induisant une infection systémique (Hatta et al. 2007) et qui engendre un choc de cytokines relié à une réponse Th1 dérégulée (Peiris et al. 2009; Karpala et al. 2011). Un lien intéressant peut être tissé entre cette réponse Th1 et la régulation de la réponse immunitaire par les PC. Notamment, furine est connue pour réguler la voie Th1 (Pesu et al. 2006; Pesu et al. 2008) et pour être responsable de l'activation de certaines cytokines (Dubois et al. 2001; Turpeinen et al. 2011) et de protéases responsables de la réponse immunitaire (Srour et al. 2003; Edwards et al. 2008; Fanjul-Fernandez et al. 2010). Toutefois, nous avons des évidences que PC1/3 aurait un rôle tout à fait non conventionnel dans la régulation de la voie Th1, non pas par la communication entre le système nerveux central et les cellules immunitaires (Gonzalez-Rey 2010), mais par son expression dans les macrophages et leur régulation (Vindrola et al. 1994; LaMendola et al. 1997; Lansac et al. 2006). Ici, une convertase normalement associée au système neuroendocrinien pourrait directement participer à la régulation des cellules immunitaires, apportant ainsi un nouveau niveau de complexité dans le rôle que jouent les PC relativement aux pathogènes.

Dans l'éventualité où un virus H5N1 (ayant la boucle d'activation sensible au PC) serait capable de se propager d'homme à homme, ce virus pourrait causer l'une des pires pandémies d'influenza de l'histoire (Webby and Webster 2003). Les PC deviennent donc une cible thérapeutique de choix afin de se doter d'outils pouvant contrer ce genre d'évènements qui sont imprévisibles et où le développement d'un vaccin efficace peut

prendre plusieurs mois. Toutefois, une approche thérapeutique ciblant les PC contre les infections devra permettre de faire la balance entre l'inhibition du pathogène et le développement d'une réponse immunitaire appropriée. Ainsi, la compréhension du rôle moléculaire de PC1/3 dans la réponse immunitaire pourrait aider à améliorer les traitements contre les pathogènes. Cette thèse propose donc une validation d'inhibiteurs peptidiques des PC et la découverte du rôle moléculaire de PC1/3 au sein des macrophages, et ce dans l'objectif général d'améliorer les outils et les connaissances pour contrer les agents infectieux.

1.4. Objectifs

1.4.1. Objectif#1

Un bon inhibiteur doit être peu toxique, stable et efficace contre la cible voulue. Toutefois, la validation d'un inhibiteur de PC contre le virus de l'influenza H5N1 est en soi limitée par les risques associés à la manipulation de ce virus. En fait, l'accès à un laboratoire de niveau de confinement trois est nécessaire pour manipuler ce virus. Ces aménagements sont peu accessibles et très couteux, il est donc difficile d'y optimiser des méthodes de validation d'inhibiteurs dans un contexte académique. Afin de valider et d'optimiser un inhibiteur de PC contre l'activation de l'hémagglutinine de H5N1 un essai cellulaire sécuritaire est donc nécessaire. Ainsi, pour mesurer la capacité de peptides inhibiteurs de PC contre l'entrée du virus H5N1, un essai de fusion cellulaire dépendant de l'hémagglutinine HA5 sera développé. Cet essai *ex vivo* permettra de mesurer les paramètres d'efficacité d'analogues peptidomimétiques du peptide Ac-RARRRKKRT-NH_2. De plus, l'efficacité de ces peptides pourra être testée sur un modèle de toxine bactérienne activée par les PC, telle la toxine de Shiga.

L'inhibiteur, ici présenté, a précédemment été développé en dérivant la séquence de clivage de la boucle d'activation de l'hémagglutinine HA5 (Shiryaev et al. 2007). La séquence peptidique sélectionnée, TPRARRRKKRT, a par la suite été optimisée pour obtenir l'inhibiteur Ac-RARRRKKRT-NH_2, un inhibiteur nanomolaire de PC, efficace pour bloquer l'activation de HA *in vitro* (Remacle et al. 2010).

De plus, le rôle individuel des PC dans l'activation HA5 reste flou. Au mieux, des études de coexpression des PC individuelles et de HA5 ont montré que PACE4 ne participe

pas au clivage de HA5 *ex vivo* (Horimoto et al. 1994). Le paramètre de spécificité étant important dans l'élaboration d'un inhibiteur, une approche par répression génétique (shRNA) sera utilisée pour déterminer le rôle individuel des PC dans la maturation de HA5.

1.4.2. Objectif#2

Les données du laboratoire indiquent qu'une stimulation du système immunitaire inné avec un lipopolysaccharide (LPS) de paroi de bactérie Gram négatif de souris où PC1/3 est inactivée (KO) engendre une réaction inflammatoire non contrôlée. Ce phénotype physiologique, associé à une réponse Th1 (caractérisée par la sécrétion IFN-γ), présente une sécrétion accrue de cytokines pro-inflammatoires (IL-12p70, IL-6, IL-1β) et une absence de réponse à la cytokine régulatrice IL-10 par les macrophages. Par conséquent, établir le rôle de PC1/3 dans la régulation des macrophages s'avère un chemin intéressant pour y découvrir de nouveaux mécanismes de régulation de l'immunité qui pourraient être utilisés pour contrôler les infections.

Afin de caractériser les fonctions moléculaires de PC1/3 dans les macrophages, le modèle animal PC1/3 KO sera utilisé pour déterminer les conséquences de l'inactivation de PC1/3 sur les fonctions normales des macrophages dans la sécrétion de cytokine et la régulation d'autres cellules immunitaire. Toutefois, il est difficile de dissocier les fonctions autocrines, paracrines et le rôle que d'autres cellules immunitaires ont dans un phénotype cellulaire particulier dans un modèle animal. Afin de déterminer les conséquences directes de l'inactivation de PC1/3 dans les macrophages, un modèle d'études cellulaires (où l'expression de PC1/3 est réprimée [shRNA]) sera développé. Ce modèle permettra de faire un lien entre le phénotype physiologique, le phénotype moléculaire et les fonctions connues de PC1/3.

1.4.3. Objectif#3

Décrire le rôle moléculaire de PC1/3 dans la régulation du système immunitaire reste une tâche complexe, entre autres parce que PC1/3 a été étudiée exclusivement dans le système neuroendocrinien. L'utilisation d'une approche de caractérisation moléculaire à haut débit s'avère donc un choix judicieux. Puisque PC1/3 est une enzyme et que ses actions se font certainement par la régulation de protéines bioactives dans les voies de signalisations moléculaires, l'utilisation de la spectrométrie de masse (dans des approches

de peptidomique et de protéomique) permettra d'établir un lien entre et le phénotype immunitaire des souris PC1/3KO et les fonctions moléculaires de PC1/3.

D'abord, une approche peptidomique par imagerie par spectrométrie de masse MALDI (MSI) permettra de caractériser la distribution de peptides bioactifs modulateurs de l'immunité dans les rates de souris contrôle (WT) et de souris PC1/3 KO. La rate est un organe complexe responsable de la communication entre les cellules présentatrices d'antigènes, qui détecte les infections circulantes, et les cellules du système lymphatique. Par conséquent, la détermination de la localisation anatomique des peptides permet de les situer dans leurs contextes physiologiques. De plus, une approche protéomique quantitative à haut débit (Gel LC-MS/MS combiné à des analyses bio-informatiques) permettra de caractériser les voies de signalisation et les mécanismes moléculaires impliqués dans le phénotype immunitaire de PC1/3. Cette approche permettra de comparer les voies d'activations moléculaires entre des extrudâts péritonéaux de souris PC1/3 WT et PC1/3 KO.

CHAPITRE 1- OPTIMIZATION OF FURIN INHIBITORS TO PROTECT AGAINST THE ACTIVATION OF INFLUENZA HEMAGGLUTININ H5 AND SHIGA TOXIN.

Auteurs de l'article : Hugo Gagnon, Sophie Beauchemin, Anna Kwiatkowska, François D'Anjou, Frederic Couture, Christine Lévesque, Frederik Dufour, Adamy Roberge Desbiens, Rolland Vaillancourt, Sylvain Bernard, François Malouin, Yves L. Dory, Robert Day.

Statut de l'article : Soumis à Journal of Medicinal Chemistry février 2013

Avant-propos : J'ai écrit le texte à l'exception de la section sur la synthèse chimique. J'ai participé à l'élaboration du design expérimental du projet. J'ai développé l'essai de fusion cellulaire. J'ai fait et analysé les tests de toxicité. J'ai fait les figures 5 et 6A. J'ai analysé les figures 1, 3, 4 5 et 6.

Résumé : L'émergence d'agents pathogènes résistants aux vaccins, aux antibiotiques et aux antiviraux sont une menace persistante pour la santé publique mondiale. D'importantes innovations dans le développement de nouveaux inhibiteurs doivent être accomplies afin de parvenir à un meilleur contrôle des futures éclosions épidémiques de ces pathogènes. Une des nouvelles stratégies pour développer ces nouveaux agents antipathogènes est de cibler des protéines de la cellule hôte nécessaires pour le développement du pathogène et de ses effets indésirables. L'une de ces cibles potentielles, mieux connue pour son rôle dans la maturation de précurseurs protéiques à des sites multibasiques en polypeptides bioactifs, serait une famille de sérine protéase : les proprotéines convertases (PC). Plusieurs travaux démontrent que la maturation par les PC de protéines virales ou bactériennes engendre une augmentation de la pathogénicité, de la sévérité des symptômes et de la létalité. Parmi ces

précurseurs protéiques figurent l'hémagglutinine de la grippe aviaire hautement pathogénique H5N1 (HA5) et les toxines homologues à la toxine de Shiga (SLT) de la bactérie *E. coli* entérohémorragique. Nous avons précédemment développé un inhibiteur peptidique nanomolaire de PC dérivé de la séquence de clivage TPQRERRRKKRT de HA5. Des travaux précédant ont démontré que cet inhibiteur est capable de protéger les souris contre la toxine d'anthrax et bloque la maturation du précurseur HA. Toutefois, si cet inhibiteur doit être utilisé *in vivo* pour prévenir des infections systémiques comme le H5N1 et la SLT, sa stabilité et son innocuité doivent être optimisées tout en maintenant sa puissance. Nous décrivons ici une approche peptidomimétique qui permet de parvenir à ces fins. En utilisant un criblage positionnel d'acide aminé non naturel hydrazine (Aza), nous fournissons également d'importantes informations sur la conformation nécessaire du peptide afin d'inhiber les PC. Nous démontrons la capacité de ce peptide à bloquer la fusogénicité de HA5 et la cytotoxicité de la SLT en essais cellulaires. Nous apportons également un aperçu sur la spécificité requise d'un inhibiteur de PC dans le but de développer un antiviral/antitoxine à large spectre, en testant la participation spécifique des différentes PC au clivage de HA5 *in vitro* et en réduisant l'expression de différentes PC à l'aide de shRNA.

Optimization of furin inhibitors to protect against the activation of influenza Hemagglutinin H5 and Shiga toxin.

Hugo Gagnon[1], Sophie Beauchemin[2], Anna Kwiatkowska[1], François D'Anjou[1], Frederic Couture[1], Christine Lévesque[1], Frederik Dufour[1], Adamy Roberge Desbiens[3], Rolland Vaillancourt[3] Sylvain Bernard[2], François Malouin[3] *, Yves L. Dory[2] *, Robert Day[1,]*

[1]Institut de pharmacologie de Sherbrooke (IPS), Faculté de Médecine et des Sciences de la Santé (FMSS), Université de Sherbrooke 3001, 12e Ave. Nord Sherbrooke, Québec J1H 5N4, Canada, Telephone: (819) 564-5428, Fax: (819) 820-6886.

[2]Institut de pharmacologie de Sherbrooke (IPS), Département de chimie, Faculté des Sciences, Université de Sherbrooke 3001, 12e Ave. Nord Sherbrooke, Québec J1H 5N4, Canada, Telephone: (819) 564-5299.

[3]Centre d'Étude et de Valorisation de la Diversité Microbienne (CEVDM), Département de biologie, Faculté des sciences, Université de Sherbrooke, Sherbrooke, QC, J1K 2R1, Canada.

Abstract

The proprotein convertases (PCs) are crucial in the maturation of viral (e.g. highly pathogenic avian influenza H5N1 hemagglutinin (HA5)) or bacterial protein precursors (e.g. Shiga toxin (Stx)-producing *E. coli* (STEC)) resulting in increased infectivity, severity of symptoms and lethality. We have previously developed a nanomolar peptide inhibitor of PCs intended to block PC activation of infectious agents. Here, we describe a peptidomimetic approach to increase stability of this inhibitor for its eventual use to prevent systemic infections and cellular damages like those caused by influenza H5N1 and Stx. We also provide important gains of knowledge to the needed peptide conformation for PC inhibition using aza-amino acid scan. We demonstrate the ability of the peptides to block influenza HA5 fusogenicity and Stx verotoxicity in cell-based assays. We also bring insight on the required PC specificity for HA5 cleavage in a cell based model using stable shRNA induced PC knock-down.

Introduction

Infectious agents are a persistent threat for public health. While a 40-years innovation gap exists in the development of new antibiotics [1], and most antiviral agents were designed to target HIV and HSV [2], the rapid adaptation of several virus and bacteria has lead to the emergence of antibiotic and antiviral-resistant pathogens [3-5]. Thus, the pharmacopeia to fight those pathogens needs to be developed to counter the increasing risk of major infectious agents outbreaks [6]. Although current therapeutic strategies directly target the pathogens to minimize adverse effects of the treatments, the effectiveness first observed rapidly lowers while resistance occurs [7-9]. Moreover, side effects of the drugs are still present, since anti-infective agents may have off-target effects [7] or even exacerbate the risk of pathologies such as the hemolytic uremic syndrome (HUS) caused by Shiga toxin (Stx)-producing *Escherichia coli* (STEC) [10].

As an alternative concept, targeting host cell proteins has been proposed for various pathogens to develop new anti-infective agents[11-13]. The family of serine protease, the proprotein convertases (PCs), have been suggested as potential therapeutic targets for various pathogens [14, 15]. Seven of nine PCs; namely Furin, PACE4, PC1/3, PC2 PC4, PC5/6 and PC7, recognize a consensus cleavage site R-$(X)_n$-R/K-R↓ (n=0, 2, 4, 6 amino acids except a cysteine) of precursor proteins [16]. The main function of these widespread expressed proteases [17-20] is the activation of the precursor proteins and the production of smaller bioactive products [21, 22]. However through the years, many reports have involve PCs in the maturation of viral (e.g high pathogenic avian influenza (HPAI) hemagglutinin (HA) [23-25]) or bacterial toxins (e.g. Stx [26]).

Interestingly, maturation of pathogens precursor proteins by PCs results in increase infectivity, severity of symptoms and lethality [24, 26-28]. Therefore, human HPAI case of H5N1 leads to around 60% lethal infection with spread of the infection to organ normally unreached by the virus itself [29]. Those highly infectious characteristics are associated with the gain of a multi-basic (RRRKKR) cleavage site in HA recognized by PCs (Furin, PC5/6 and PC7) [14, 23-25, 27, 29-34].Upon cleavage, HA allows virus membrane fusion with host cell membrane leading to the release of virus genetic material and viral replication [13, 28, 35-37]. As for bacterial toxins, a good prototype is the Stx produced by *Shigella dysenteriae* and STEC [38, 39]. Shiga toxins contain, separating the A_1 and the A_2 subunits, a RXXR sequence in a loop stabilized by a disulfide bridge that is very sensitive to cleavage by trypsin but also by

PCs [15, 40, 41]. Furin was proposed as the PC to be responsible for this cleavage needed for rapid intoxication of cells, at low pH in the TGN or the endosomes [42]. Therefore, both targets are particularly interesting to prevent future pandemic and associated economical impacts of those pathogens. Hence, influenza virus rearrangement responsible for last pandemic episodes are unpredictable [7] and the acquisition of this multi-basic cleavage site into human influenza could lead to one of the most deadly pandemic influenza episode [43-45]. Moreover, foodborne STEC, often associated with undercooked ground beef meat and contaminated vegetables, are responsible for thousands of hospitalizations worldwide [46] and cost 405 million$ (in 2003) in the USA [47].

Facing the important role of PCs in the activation of thosepathologies, efforts have been recently made for the development of inhibitors to block harmful effects from viral infections and bacterial toxin activation [14, 48-50]. A peptide derived from the TPQRERRRKKR cleavage sequence of H5N1; TPRARRRKKRT, was found to be a specific nM inhibitor of PCs able to protect mice from antrax inhalation [14]. This peptide was further optimized by C-terminal amidation and N-terminal acetylation modification to give rise to the resulting nM inhibitor; Ac-RARRRKKRT-NH_2, which proved its efficiency to block processing of viral glycoproteins and anthrax toxin without cellular toxicity [15]. Despite those improvements, if the use of this peptide is intended to be use to prevent systemic infection like H5N1 and vascular and renal damages like those caused by Shiga toxin, it needs to be further optimized and characterized to achieve an acceptable therapeutic index as well as a good bioavailability.

Herein, we describe peptidomimetic modifications that enable increased stability with low toxicity. Also, important gain of knowledge on the structural prerequisites of the peptide conformation was provided by aza-β^3-amino acids scan. We demonstrate the ability of this peptide to block HA5-mediated cell fusion as well as Stx Vero cell toxicity. We also bring insights on which specificity PC is required to develop broad-spectrum antiviral/antitoxin PC inhibitor by testing PC specificity for HA cleavage. Notably, we established a sequence specific relationship for HA cleavage and demonstrated that shRNA is a more suitable tool to study PC cleavage specificity in cell-based studies.

Results

Lead peptide properties

In order to optimize our lead PC peptide inhibitor for *in vivo* testing three major points had to be considered: inhibition power (Ki), stability and safety within therapeutic range. Our previously published peptide derived from HA5 multi-basic cleavage sequence was shown to be a nM PC inhibitor with selectivity toward Furin, PACE4, PC5/6 and PC7 [14, 15] (Figure 12A). Stability of the peptide in presence of cultured cells or in mouse plasma had never been determined. Thus, we tested the stability of the peptide in two assays. First, Figure 12B shows the stability of the peptide in cell culture medium in presence, absence of FBS or with FBS alone. Secondly, we tested the peptide stability in *ex vivo* plasma stability assay (Figure 12C). Both results indicate that the peptide is rapidly degraded with a half-life of 3.7 h in plasma, 8h in culture medium with FBS and 10h w/o FBS. FBS alone had a similar degradation activity to plasma with a 4h half-life. By looking at the degradation pattern of the peptide by mass spectrometry (Figure 12D), we could conclude that exopeptidases were responsible for the degradation of the peptide. After 1h incubation, mostly a mass corresponding to Ac-RARRKKR peptide (1167 m/z) was observed. In a second order of degradation ΔRT (1112 m/z), ΔKRT (756 m/z) and ΔKKRT (635 m/z) masses gradually appeared after 3h and 6h of incubation. Our previous report had shown that the peptide had no toxicity up to 100 mM in RAW264.7 measured by ATP release [15]. We wanted to further test the safety of the peptide by measuring long-term cytotoxicity, measured by metabolic activity (MTT assay) after a 24-h incubation on a cell monolayer, and acute cytotoxicity, measured by lactate deshydrogenase (LDH) release after incubation with cells for 4h. We incubated HEK293 cells with peptide concentrations up to 150 mM without significant long-term toxicity (Figure 12E) and up to 100 mM without significant LDH release (values below 5%) after a 4-h incubation. We also determined that the peptide shows low toxicity on other cell line up to 100 mM (Figure S 1). This low toxicity profile encouraged us to determine *in vivo* acute toxicity of the peptide inhibitor. The peptide was injected to mice intravenously (i.v.) up to 10mg/kg and no signs of toxicity were observed.

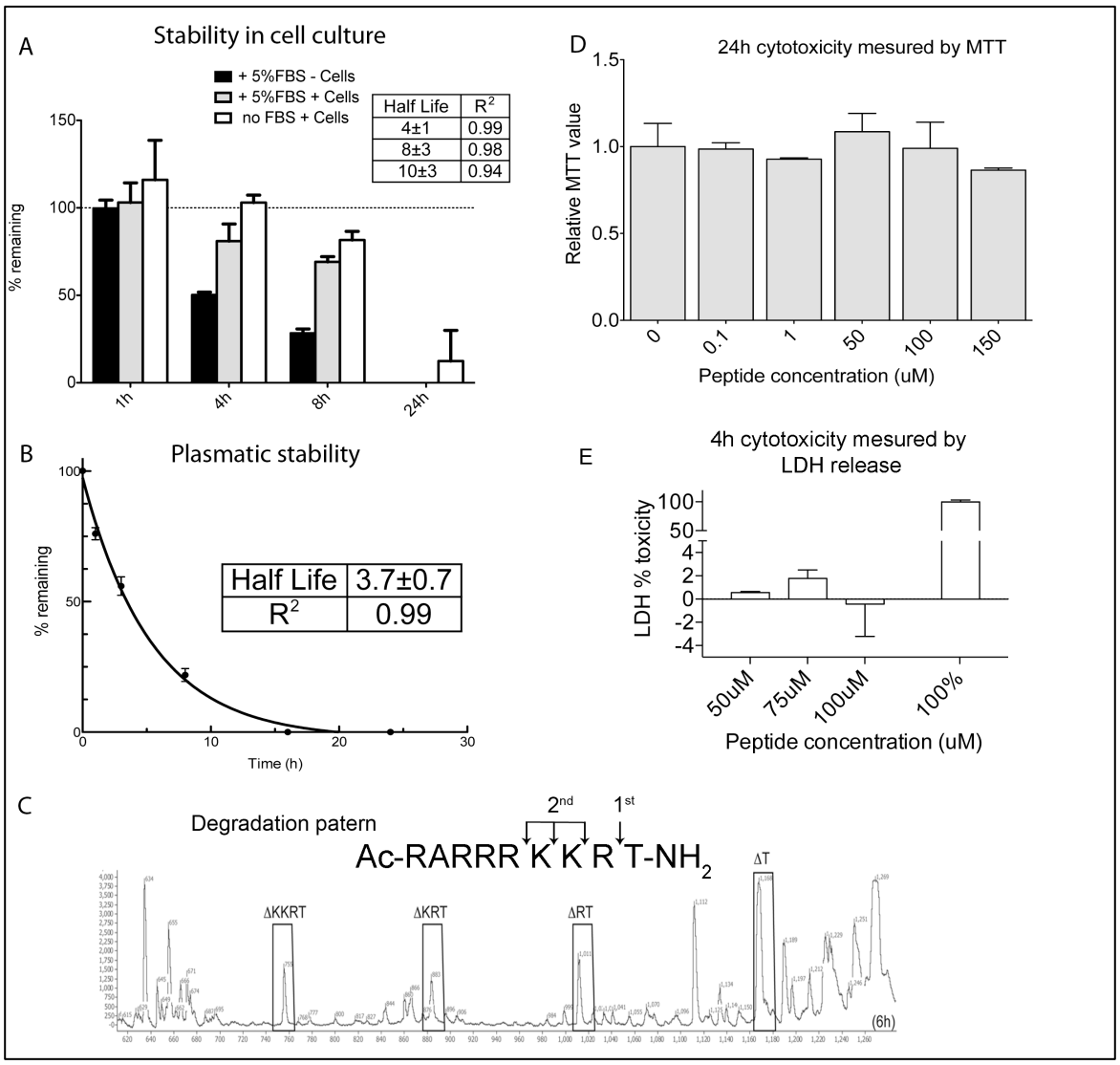

Figure 12 Ac-RARRRKKRT-NH_2 inhibitor K_i, stability and toxicity.

A- Inhibition constant determined against recombinant PC. B- Peptide stability in cell culture (LNCcaP cells) in presence, absence or with FBS alone measured by HPLC. C- *Ex vivo* plasma stability measured by HPLC. D- Peptide degradation pattern, in cell culture medium, analyzed by MALDI-TOF. E- Peptide cytotoxicity on HEK293 after 24h incubation measured by MTT assay. Relative cytotoxicity was normalised against non treated cells F- Acute cytotoxicity, after 4h incubation with HEK293, of peptide at the indicated concentration measured by lactate dehydrogenase (LDH) assay. Relative cytotoxicity was compared with 100% toxicity control.

Peptidomimetic optimization in P1

Clearly if this peptide inhibitor was to be used for *in vivo* testing, its stability needed to be optimized while maintaining low toxicity and nM Ki. Since C-terminal exopeptidase activity was the primary source of degradation of the Ac-RARRRKKRT-NH_2 peptide (Figure 12C), we introduced Arg amino acid mimetic in P1, namely aza-β^3-Arg (aza-R), 4-amidinobenzylamide (AMBA) and 4-aminobut-2-en-1-yl guanidine (which is 4-aminobutyl guanidine, commonly called Agmatine, with an alkene chain thus abbreviated ΔAgm) (Figure 13). Importantly, the AMBA and ΔAgm modification could only be introduced in P1 and resulted in the lost of the P1' threonine because of the lost of the carboxyl that enable the formation of the peptide bound. All modification in P1 leaded to increased stability from 3.7 h half-life to respective half-life of 5.6h, 4.8h and 8.6h for aza-R, ΔAgm and AMBA (Table 6). Still, we hypothesized that exopeptidase activity could also occur from P8 but at a much slower rate and would be responsible of degradation of P1 modified peptide. Accordingly, P8 aza-R modification alone did not significantly change the plasma half-life, however adding aza-R at P8 and P1 resulted in gain in stability form 5.6h half-life (for aza-R P1) to 7.7h half-life for the peptide with P1 and P8 aza-R modification. By looking at the degradation scheme by mass spectrometry (Figure 14) of the P1-P8 aza-R modified peptide we can observe a reduced appearance of the C-terminal degradation pattern after a 6-h incubation in cell culture medium.

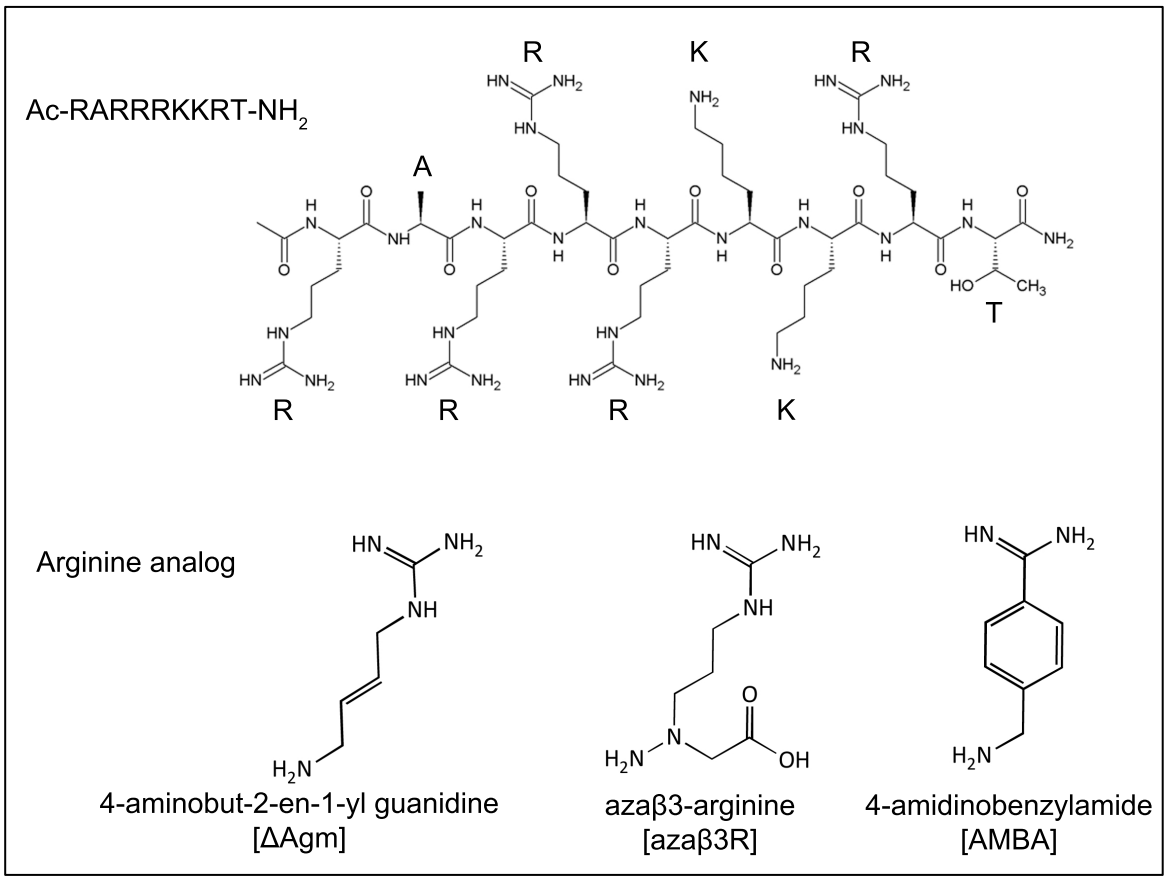

Figure 13 Peptidomimetic modifications of lead peptide.

Structure of the Ac-RARRRKKRT-NH_2 peptide and presentation of peptidomimetic modifications.

Table 6 Peptidomimetic optimization in P1

P8	P7	P6	P5	P4	P3	P2	P1	P1'		Ki Furin (nM)	Plasma Half Life (h)	MTT 24h[a]	LDH 4h 100 µM	*In vivo* toxicity
Ac	**R**	**A**	**R**	**R**	**R**	**K**	**K**	**R**	**T**	**NH2**	25±5	3.7±0.3	**200 uM**	**<5%**	**>10mg/kg**
Ac	Aza-R	A	R	R	R	K	K	R	T	NH2	10±3	2.9±0.9	**100 uM**	**<5%**	**>10mg/kg**
Ac	R	A	R	R	R	K	K	Aza-R	T	NH2	21±5	5.6±0.2	**150 uM**	**<5%**	**≈10mg/kg**
Ac	R	A	R	R	R	K	K	ΔAgm			6±3	4.8±0.7	**150 uM**	**<5%**	**>10mg/kg**
Ac	R	A	R	R	R	K	K	AMBA			1.9±0.7	8.6±0.5	**150 uM**	**<5%**	**[7-10]mg/kg**
Ac	Aza-R	A	R	R	R	K	K	Aza-R	T	NH2	33±9	7.7±0.9	**150 uM**	**<5%**	**≈10mg/kg**

[a]Maximal dose tested without toxicity after 24h incubation

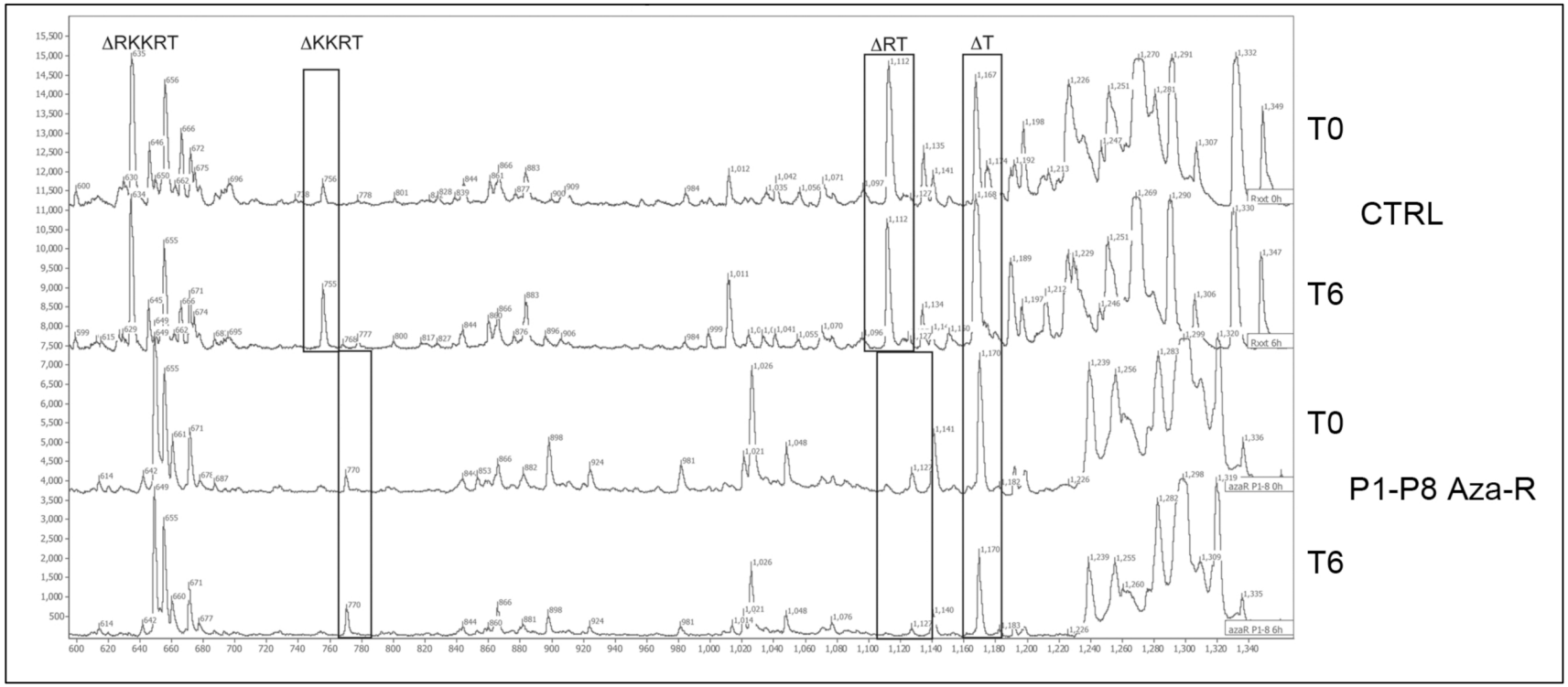

Figure 14 MALDI-TOF analysis of resulting peptide stabilization.

Resulting peptide stabilization of P1-P8 aza-R modified peptide when incubated in cell culture medium analyzed by MALDI-TOF.

Additionally to peptide stability, modification of P1 with AMBA and ΔAgm led to more potent inhibitors with Ki lowered to 1.9 and 6 respectively. Remarkably, P8 aza-R alone lowered the Ki to 10 nM, however addition of aza-R at P1 did not change the inhibition power of the peptide as with the P8-P1 (p-value=0.15). Both gain in stability and potency is an interesting combination since it would reduce the amount of peptide needed to achieve for effective dose *in vivo*. Still, the resulting modification in P1, P8 or both resulted in peptide with low toxicity. MTT assay showed no statistically significant differences on HEK293 cells for all modified peptide up to 150 mM, except for P8 aza-R modification with last non-significant concentration at 100uM. Testing of acute cytotoxicity by LDH release showed that all peptides had less then 5% toxicity after 4h incubation at 100 mM. Finally, *in vivo* acute toxicity showed that only P1 AMBA modification resulted in a notable decreased of tolerable dose lowering it to 7-10 mg/kg and the P1-P8 and P1 aza-R modified peptides also showed some sign of toxicity near 10 mg/kg but did not lead to death and no higher dose were tested.

Aza-amino acids mimetic scan

We next wanted to determine if further optimization could be achieve at the intermediate positions of the peptide. The use of aza scan, that are amino acid lacking stereogenicity, has previously been shown to be particularly insightful on structural requirement of peptide inhibitors [51]. By performing such a scan we could determine that the sole modification of R in the peptide backbone did not improve the peptide stability when incubated in mouse plasma. Even a reduced stability could be observed with half-life near 1h (Table 7). Most interestingly, the modification of P5 to P3 a.a. for aza analogues resulted in a gradual lost of inhibition power with respective Ki of 89, 123 and 591 nM. These results suggest that the peptide backbone need to be highly flexible so that the Arg and Lys side chain of the peptide are properly oriented for enzyme inhibition. P2 was not tested due to low synthesis yield. Interestingly as stated below, the P8 aza-Arg modification resulted in an increased potency of the peptide by lowering its Ki to 10nM. On the opposite, P7 aza-Ala completely reduces the potency of the inhibitor bringing the Ki up to 247 nM. Together these results indicate that the side chain of the Arg at P8 needs to be properly oriented so the peptide can enter in the enzyme binding pocket.

Table 7 Aza-amino acids mimetic scan

	P8	P7	P6	P5	P4	P3	P2	P1	P1'		Ki Furin (nM)	Plasma Half Life (h)
Ac	**R**	**A**	**R**	**R**	**R**	**K**	**K**	**R**	**T**	**NH2**	25	3.7±0.3
Ac	Aza-R	A	R	R	R	K	K	R	T	NH2	8	2.9±0.9
Ac	R	A	Aza-R	R	R	K	K	R	T	NH2	18	1.16±0.04
Ac	R	A	R	Aza-R	R	K	K	R	T	NH2	89	1.00±0.06
Ac	R	A	R	R	Aza-R	K	K	R	T	NH2	123	≈1
Ac	R	A	R	R	R	Aza-K	K	R	T	NH2	591	N.A
Ac	R	A	R	R	R	K	K	Aza-R	T	NH2	21	5.6±0.2

In vitro cleavage of HA spanning peptide

Here we demonstrate that different evolutionary forms of HA5 cleavage site are differently recognized by different PCs. Figure 15D shows the origins of three selected sequences of cleavage from HA5. The first sequence referred as Hong Kong correspond the original sequence of HA5 that was found in infect humans and is still recognized as a factor influencing HPAI infection in human and present in circulating clade 2.3.4 found in human. The second sequence named Vietnam come from avian HA5 clade 2.3.2 with high homology (< 90%) to second generation of HPAI virus that infected human (clade 2.3.4) expect that the cleavage sequence lacking a Lys was never founded in human. Finally, the last sequence referred as Germany comes from a typical avian virus HA clade 2.2 that never infected human based on sequence alignment and information's available at http://www.fludb.org and at http://www.who.int/influenza. Figure 15A shows that Furin cleaves the Hong Kong sequence with a higher rate than PACE4. Notably, the VietNam sequence (Figure 15B) is cleaved more slowly by these PCs compared to the last sequence, but this time PACE4 cleave it faster. Finally, the Germany sequence showed even a slower rate of cleavage then the last two sequences with Furin and PACE4 (Figure 15C). Thus the cleavage sequence that infect human seems to have adapted to be cleaved with a faster kinetics by PCs. Still, both PC are able to cleave all cleavage sequence at some point *in vitro* even though PACE4 was shown to be inefficient to cleave HA5 protein in cell based overexpression models [31, 52].

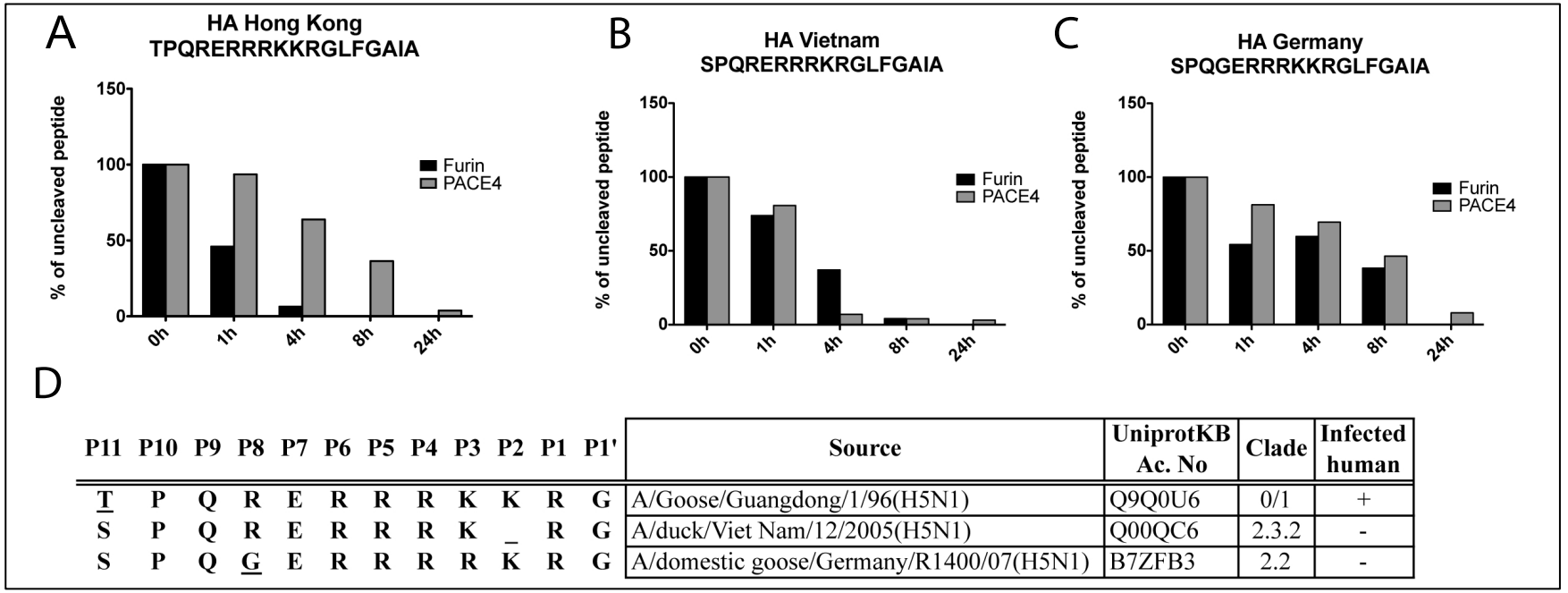

D

P11	P10	P9	P8	P7	P6	P5	P4	P3	P2	P1	P1'	Source	UniprotKB Ac. No	Clade	Infected human
T	P	Q	R	E	R	R	R	K	K	R	G	A/Goose/Guangdong/1/96(H5N1)	Q9Q0U6	0/1	+
S	P	Q	R	E	R	R	R	K	_	R	G	A/duck/Viet Nam/12/2005(H5N1)	Q00QC6	2.3.2	-
S	P	Q	G	E	R	R	R	R	K	R	G	A/domestic goose/Germany/R1400/07(H5N1)	B7ZFB3	2.2	-

Figure 15 Influenza cleavage site evolution and PC specificity.

Spanning peptides of HA5 activating loop, from different H5N1 sources, were incubated with 5nM titrated PC (PACE4, furin or PC7) at the indicated time (A, B, C). D- Source of HA5 activation sequences and clade classification of the used sequences. Only RERRRKKR sequence was found to infect human.

Furin cleaves HA5 in a cell-based model

Thus, a second level of regulation has to be considered since cellular co-localization between HA5 and PCs as to be considered. Here we used down regulation of individual PC expression by stable shRNA expression Figure 16B. We used shRNA against the three PCs that where shown to cleave HA5 when overexpressed: Furin, PC5/6 and PC7 [31, 52]. Figure 16A shows the relative expression of Furin, PC5/6, PC7 and PACE4 in HEK293FT cells. No difference of expressin can be observed between Furin and PC5/6, while PC7 shows little expression in HEK293 cells. It is to note that PACE4 has a high level of expression in those cells, making them ideally suited to confirm that this protease do not participate in HA5 activation. Stable expression of shRNA resulted in a remaining expression of 4% for Furin, 15% for PC5/6 and 25% for PC7 (Figure 16B). Low level of expression of PC7 would explain the poor efficiency of the shRNA. We first wanted to have a good control that shows no cleavage of HA5 when the protein was overexpressed. This control was necessary to show the reaction of the HA5 antibody to non-matured and matured HA5 as well as a negative control to perform cell based assay. Figure 16C shows that WT HA5 present high level of endogenous maturation in HEK293 cells noted by low detection HA_0 and the appearance of matured HA_1. Additionally, mutation of P1 Arg to Ala result in mostly complete abrogation of HA5 cleavage and combination P1 and P5 mutation of Arg to Ala had little additional effect on HA5 maturation. This result was also observed when cells were incubated 48h with 25 μM of dec-RVKR-cmk (Figure S 2). Interestingly P5 Arg mutation to Ala resulted in an increase maturation of HA_0 noted by the total disappearance of the HA_0 precursor. Together these results indicate that even though several RXXR sites and trypsin cleavage sites are present, PCs will mostly recognize P1 R and are responsible of most of the maturation observed. We next overexpressed HA5 in HEK293 down-regulated for Furin, PC5/6 and PC7 by shRNA. Figure 5D shows that only Furin down-regulation results in a mostly complete blockage of HA_0 maturation even with the high level of expression of PACE4 and still shRNA of PC5/6 and PC7 had no effects on HA_0 maturation. Thus, even though Furin and PC5/6 where both shown to mature HA5 [31], only Furin down-regulation is responsible for the maturation of HA5 precursor.

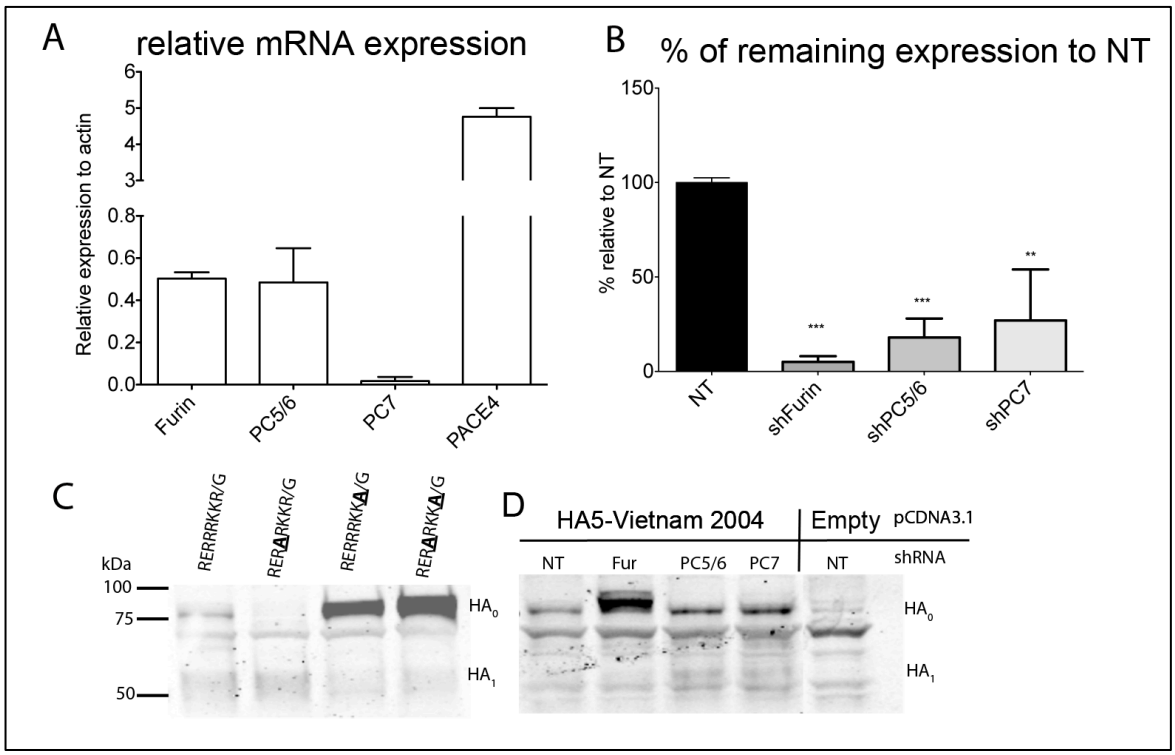

Figure 16 *Ex vivo* HA5 PC cleavage specificity using shRNA.

A- Relative PC expression in HEK293 measured by qPCR. B- Remaining PC expression measured by qPCR after stable shRNA transduction in HEK293. Expression was normalised against non-targeting shRNA transduces HEK293. (Student T-Test **=p<0.001, ***=p<0.0001 C- Western blot using HA5 detecting antibody of HEK293 overexpressing WT HA5 or P5 R/A, P1 R/A, P1-P5 R/A mutants from Influenza A/Vietnam/1203/2004 virus. Antibody show greater affinity for non-matured HA5 (HA_0) compared to mature HA5 (HA_1) D- Western blot using HA5 detecting antibody of HEK293 overexpressing HA5 and stably transduced with indicated shRNA targeting individual PC. Empty vertoc (pCDNA3.1) was used to measure antibody specificity.

Inhibitor efficiency in cell based assays

Since we show that Furin is the major processing enzyme of HA5, we next wanted to test the potential application of the peptidomimetic optimized peptide inhibitors on a HA-mediated membrane fusion assay. Additionally, we wanted to test those inhibitors on a bacterial toxin substrate using Stx-mediated Vero cell toxicity. As mentioned earlier, those two pathogens use PCs for activation of their infectious processes but in a different way. Figure S 3 show the efficiency of a known irreversible PC inhibitor, dec-RVKR-CMK, to block the HA mediated membrane fusion and the Stx Vero cell toxicity. The HA fusion assay exploited the ability of matured HA to induced membrane fusion at low pH [53]. The cell fusion is monitored by the TAT inducible reporter gene (Luciferase or GFP), wherein a first cell line is expressing the TAT inducer and the second cell line is expressing the inducible reporter gene. When PCs are inhibited the maturation does not occur and the low pH treatment fails to induce cell fusion and release the TAT inducer into reporter cells (sup. Data Figure 3). Table 8 shows that the peptidomimetic approach resulted in an increase potency of the peptide inhibitors to block HA-mediated cell fusion. Interestingly, the best inhibitor for this assay was the P1-P8 AzaR. These results were next corroborated by performing dose response curves (Figure 17A) where we show that P1-P8 AzaR is much more efficient to block HA-mediated cell fusion then the unmodified peptide. Also, Table 8 presents the potency of the different inhibitor to block of Stx-induced Vero cell toxicity. Once again the P1-P8 aza-R modified peptide is among the most effective peptide inhibitors with an IC_{50} of 20.8 mM while the control peptide was inefficient to block Stx toxicity (Figure 17B). Noteworthy, this assay is achieved by measuring LDH release from damaged cells, and thus it can also provide an indication of the toxicity of the peptide when combined with Stx. Results show that even though P1 AMBA is a stable and highly potent inhibitor, it resulted in a higher level of toxicity (130%) than that caused by Stx toxin alone when the peptide inhibitor was used at 80 mM; indicative of cellular toxicity of the P1 AMBA peptide on Vero cells. Interestingly, introduction of flexibility going from an aryl to an alkene chain, and switching from amidine to a more basic guanidine by replacing the AMBA with ΔAgm at the P1 position resulted in an increase activity inhibition with no toxicity. Together these results confirm that stabilization of the peptide is a critical step to obtain the best inhibition profile in cell-based assays.

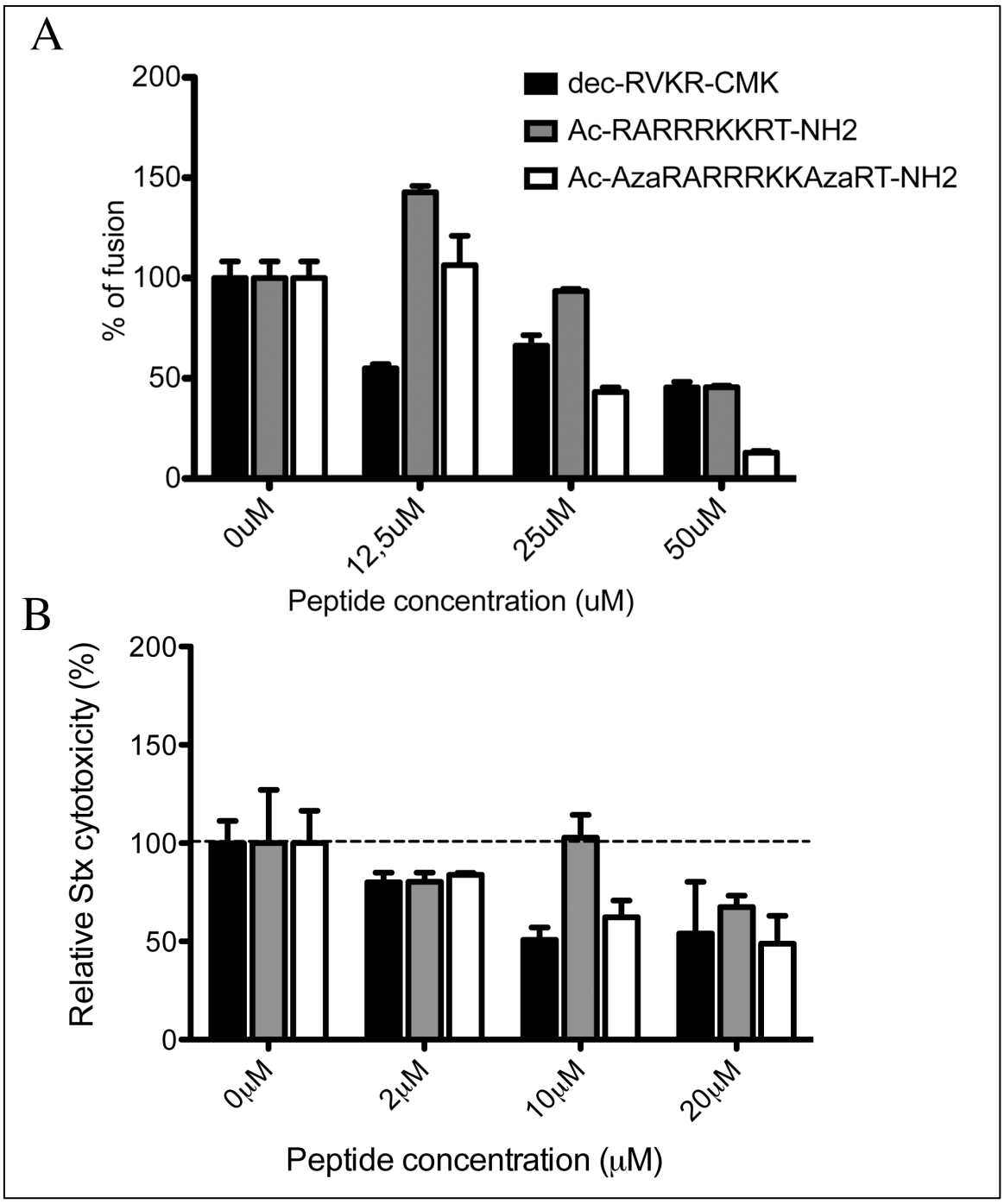

Figure 17 *Ex vivo* HA mediated fusion and Shiga toxin toxicity inhibition by peptidomimetic analogues.

A- Dose-dependent inhibition of HA mediated cell fusion of best candidate peptides. Peptides were incubated 36h before cell fusion induction. A no-fusion control (using P1-P5 R/A HA5 mutant) was used to subtract background and fusion was normalized to 100% with non-treated control. B- Dose-dependent inhibition of Stx cytotoxicity of best candidate peptides. Relative Stx cytotoxicity was measured by LDH release in presence of the indicated peptide concentration normalized to cells challenged with Stx alone.

Table 8 Inhibitor efficiency in cell based assays

	P8	P7	P6	P5	P4	P3	P2	P1	P1'		% fusion[a]	Stx IC50 µM	Relative Stx cytotoxicity (%) with 80 µM inhibitor
Ac	**R**	**A**	**R**	**R**	**R**	**K**	**K**	**R**	**T**	**NH2**	51	> 1000	84
Ac	R	A	R	R	R	K	K	ΔAgm			44	71	87
Ac	R	A	R	R	R	K	K	AMBA			88	> 1000	130
Ac	R	A	R	R	R	K	K	Aza-R	T	NH2	77	314.5	69
Ac	Aza-R	A	R	R	R	K	K	Aza-R	T	NH2	12	20.8	58
				dec	R	V	K	R	CMK		50	11.5	N.D.

[a] 100 µM treatement

Discussion

The feasibility of inhibiting PCs for the purpose of blocking viral glycoprotein and bacterial toxin maturation has previoulsy been tested by mostly focusing on Furin inhibition. However, redundancy between PCs could occur, notably the H5 cleavage site would be sensible to PC5/6 and to PC7 in *in vitro* cleavage assays and after overexpression of selected PCs [30-32]. We report here that cleavage site of different H5N1 clades show different PC sensibility and virus clade that infect human have interestingly evolve for a better cleavage kinetic toward Furin. The presence of Lys at both P2 and P3 seems to be essential for this purpose, which reflects previous findings [31, 32, 54]. On the other side, cellular models take into account cellular localization, thus an enzyme that shows efficient cleavage *in vitro* can result in poor cleavage in cell based models. Hence overexpression studies of PCs have shown that PACE4 was not able to cleave HA5 precursors [31, 54]. Here using shRNA we show that of the PCs that where shown to cleave HA5 when overexpressed, only furin shRNA was able to reduce precursor maturation. Moreover, even though PACE4 is well expressed in those cells it has little activity on HA maturation. It was however hard to conclude for a role for PC7 because of its low expression level in HEK293. These experiments proved to be insightful and should be used on other H5N1 infectable cell lines [55].

Even though PC inhibition could be of concern for toxicity we believe that acute short-term treatment with PC inhibitor should not be harmful. While it is a well established advantage of peptide inhibitor to present low toxicity [56], we present here a low toxicity profile, *ex vivo* and *in vivo*, of the control peptide and most peptidomimetic analogues tested. Interestingly only the AMBA modified peptide showed an increase toxicological profile, which has impaired its efficacy in Stx assays. This modification was previously introduced on PC inhibitors and proved to provide increased inhibition power for Furin [49]. However toxicity of the resulting peptides was not tested. We may suppose that the toxicity observed here would be related to a degradation product that led to the release of toxic AMBA metabolites. On the same note, incorporation of ΔAgm also results in a more stable peptide, as removal the terminal carboxyl group results in peptidase protection, but also a more potent inhibitor. This is indicative that stabilization of the P1 Arg side chain into a more rigid structure form results in a better orientation of the inhibitor in the Furin binding

pocket. However, aza-R modification that favors a beta-turn structure [57-59] had no gain in inhibition activity.

Determining the exact structure of the peptide inhibitor by NMR or by co-crystallization would be of great interest to determine the exact modification that could be tolerated or beneficial on the peptide position P2-P8. Nonetheless, we can establish postulates based on the aza scan we performed. First, beta-turn formation and inclusion of rigidity in position P3 to P5 is not favorable to peptide activity. We can suppose that the peptide will form beta sheet structure from P1 to P5 within the enzyme-binding pocket. P6 would be a position favorable to modification seems little effects on Ki was observed when it was modified for aza-R. One of the most interesting observations is that a P8 aza-R modification resulted in an increased inhibitory activity while P7 aza-A resulted in an increased Ki value. We can conclude that P8 R must be in a particular orientation to provide peptide inhibition activity. The hypothesis would be that aza-A would reverse the side of the beta-turn side. Interestingly this description resembles a lot to the HA5 cleavage loop modeled in to the Furin enzyme pocket [60].

We showed that, amino acids mimetic peptides succeeded to block Stx and HA5 activities in cell-based assays. We observed that the gain in inhibition activity *in vitro* was not predictive of gain in biological activity in cell-based assays. Instead, the protection of amino terminal groups of the peptide and low toxicity profiles were much more important for efficiency in living cells. Before testing therapeutic efficacy in animal models, further peptide modifications that will combine gain in inhibition activity and stability could be beneficial.

Experimental section

Reagents

All solvents and reagents were obtained from commercial suppliers and used without further purification. All the amino acid derivatives and coupling reagents were purchased from Matrix Innovation, Inc. (Montreal, QC) and ChemImpex International (Wood Dale, IL). TentaGel S RAM resin and 2-Chlorotrityl chloride resin were purchased from Rapp Polymere (Tübingen,. Germany), Matrix Innovation**,** Inc. (Montreal, QC), respectively. Recombinant PCs where produced as previously published [61]. Anti-mouse and anti-rabbit IgGs coupled to IRDye800 and IRDye680 were obtained from LI-COR Biosciences. Non-targeting (NT) shRNAs in the MISSION RNAi pLKO.1-puro vector were obtained from Sigma-Aldrich and shRNA against Furin, PC5/6 and PC7 were obtained from Sigma-Aldrich. Sequences were previously published [62]. HA5 (Acc. No HM006759) and NA1 (acc No. EF541467) from Influenza A/VietNam/1203/2004 isolated from Human patient and shown to cause systemic infection [63] was synthetized by Epoch Biolabs and cloned into was cloned into pCDNA3.1 vector. Truefect transfection reagent was used for transfection using provider's recommendation (*UnitedBiosystems*). Tetoff inducible vectors kit containg pLVX-TAT vector and TAT inducible pLVX-Tight-Puro and pLVX-Tight-Puro-Luc were obtained from Clonetech.

Peptide synthesis

The inhibitors containing the Arg or azaR modification at position P1 were obtained manually by solid-phase synthesis on a polystyrene resin TentaGel S RAM (Rapp Polymere, capacity 0.23 mmol/g), according to standard coupling procedures and Fmoc/Bu^t strategy [64]. For protection of the side chain functionalities, Fmoc-Arg(Pbf)-OH, Fmoc-Lys(Boc)-OH, and Fmoc-azaArg(Boc_2) were used. Stepwise synthesis of peptide analogues was achieved with 3-fold excess of Fmoc-amino acid and HATU or PyBOP (with 6-Cl-HOBt) as coupling agents in the presence of DIPEA or NMM (9 equiv) in mixture of DMF/DCM (1:1 v/v). After final Fmoc deprotection, *N*-terminal acetylation was performed in acetic anhydride/DIPEA/DCM(15/15/70 v/v/v) for 20 minutes. After completion of the synthesis, the protected peptidyl resins were treated with TFA/H_2O/TIS (95:2.5:2.5 v/v/v), and stirred for 4 h. The solutions of the released peptides were filtered and evaporated *in vacuo* to a volume of about 1 mL. Then the peptides were precipitated in cold diethyl ether,

centrifuged and washed with diethyl ether, dissolved in H_2O and lyophilized to afford crude products.

Analogues modified with AMBA or ΔAgm were obtained manually by a combination of solid phase peptide synthesis and solution synthesis. Fmoc-Lys(Boc)-OH (1.2 equiv) was dissolved in 15 mL dry DCM and DIPEA (4 equiv), and was immediately poured onto 2-chlorotrityl chloride resin (1g, 1 equiv, resin loading: 0.8 mmol/g). The mixture was shaken for 2 h at RT followed by treatment with DCM/MeOH/DIPEA (17:2:1 v/v/v, 3 × 1 min), washed several times with DCM, DMF, DCM and dried *in vacuo*. The resin loading upon attachment of the first amino acid is typically around 0.4 mmol/g. The synthesis (scale 200 μmol for analogue) proceeded by manual Fmoc SPPS according to standard coupling procedures, using 3-fold excess of Fmoc-amino acids, HATU or PyBOP (with 6-Cl-HOBt) as coupling agent and DIPEA or NMM (9 equiv) in DMF. The Fmoc groups were removed by treatment with 20% piperidine in DMF. After final Fmoc deprotection, *N*-terminal acetylation was performed in acetic anhydride/DIPEA/DCM (15:15:70 v/v/v) for 20 minutes. The protected peptide was cleaved from resin by 1 % TFA in DCM (2 × 30 min) at RT. The solvent was removed *in vacuo*, precipitated in cold diethyl ether, centrifuged and lyophilized from 80 % *tert*-butanol in water. Protected peptide (1 equiv), AMBA· 2 HCl (2 equiv) or ΔAgm(Boc_2) (2 equiv), COMU (2 equiv) and NMM (4 equiv) were dissolved in DMF. The mixture was stirred for 16 h at RT, and the solvent was removed in *vacuo* to yield a brownish oil, which was next dissolved in TFA/TIS/H_2O (95:2.5:2.5 v/v/v). The mixture was stirred for 3 h at RT, precipitated by cold ether, washed two times with ether and lyophilized.

The crude compounds were purified by semi-preparative HPLC and analyzed by SELDI-TOF as previously described [65]. According to both HPLC and MS, the purity of peptides exceeded 95%. Their physicochemical properties are presented in supporting information file.

The synthesis of ΔAgm(Boc_2) was adapted from published procedures [66]. The synthesis started by a monoaddition of phthalimide potassium salt onto *E*-1,4-dibromobut-2-ene (**1**). Addition of hexamethylemetetraamine resulted in the displacement of the residual allylic bromide. Treatment of **3** with ethanolic HCl furnished the ammonium salt **4** that was guanidylated. Deprotection of the phthalimide **5** with hydrazine produced the desired ΔAgm(Boc_2) **6**.

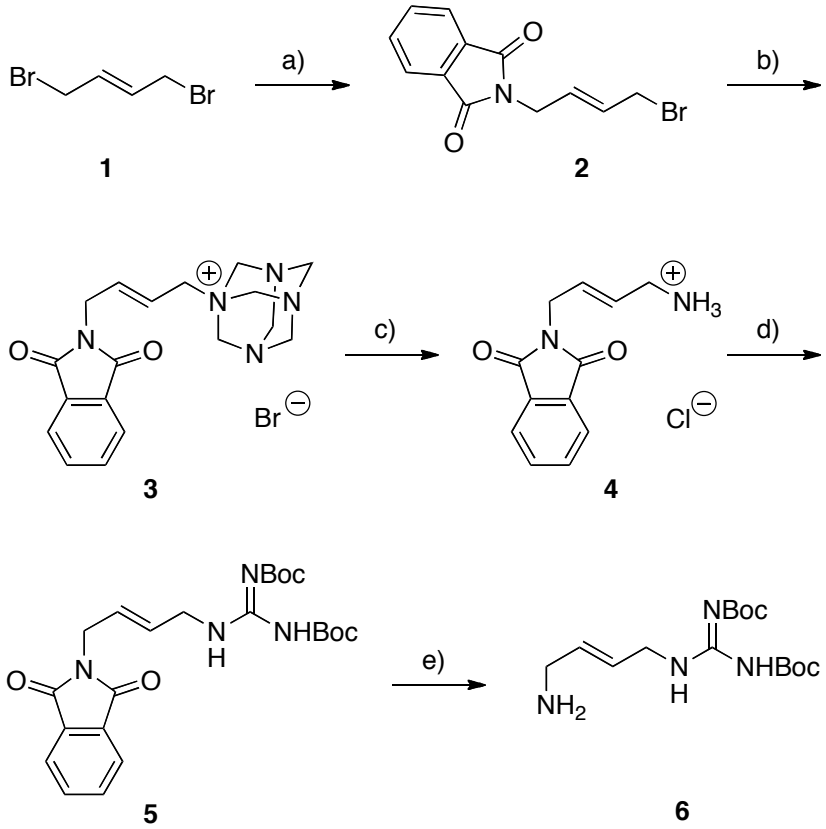

a) PhtlK, DMF, rt, 48h, 66%; b) HMTA, $CHCl_3$, rt, 48h, 100%; c) HCl, EtOH, reflux, 2h, 80%; d) Di(Boc)guanidine, Et_3N, DCM, rt, 93%; e) Hydrazine, $CHCl_3$, MeOH, rt, 4h, 92%.
Experimental procedures for the synthesis of ΔAgm(Boc_2): Fmoc-azab^3-Arg(Boc_2) [67] and AMBA·2HCl [68] were synthesized using protocols described in literature with slight modification for the AMBA·2HCl (Kwiatkowska A. et al. upcoming publication).

Cell culture

Hek293FT cell line was cultured in DMEM medium supplemented with 10% fetal bovine serum (FBS; Wisent Bioproducts, St Bruno, QC) at 37 °C in a humidified atmosphere (5% CO_2). Transfection were performed using Truefect reagent (UnitedBioSystems) according

to vendor is recommendation. Vero cells (ATCC CCL-81) were grown in Dulbecco's Modified Eagle's Medium (DMEM) supplemented with 10% inactivated fetal bovine serum (FBS), penicillin and streptomycin at 37°C with 5% CO_2.

Western blot analysis

After treatment, the cells were detached, centrifuged at 500 g and washed once with ice-cold PBS. The cells were subsequently lysed with radioimmune precipitation assay lysis buffer containing Complete Mini protease inhibitor and processed as previously described [69].

Real-time quantitative PCR

Total RNA was extracted using the Qiagen RNA isolation kit (Qiagen, Valencia, CA, USA). The quality of the total RNA samples was assessed using an Agilent Bioanalyzer with RNA Nano Chips (Agilent Technologies, Palo Alto, CA, USA). Real-time quantitative PCR reactions were performed as previously described [70]. Briefly, 1 μg of RNA was reverse transcribed, and qPCR analysis reactions were performed using a Stratagene Mx3005P5 instrument. Primers for actin, Furin, PC5/6, PC7 and PACE4 are were previously described [62]. The relative expression levels were calculated using β-actin as a reference gene with the formula (1+ amplification efficiency)$^{-\Delta(\Delta CT)}$. All experiments were performed in duplicate in 3 independent experiments (n=3).

Hek293 knockdown using lentivirus transduction

Lentiviral particles containing the MISSION RNAi pLKO.1-puro vector were produced in HEK293FT cells following the manufacturer's instructions (Sigma-Aldrich, St. Louis, MO, USA). Viral titers were calculated in HT1080 cells using a serial dilution approach. Lentiviral transduction was performed in 6-well plates with a cell density of $4x10^5$ cells and a multiplicity of infection (MOI) of 3. After 2 days, the infected cells were selected using growth medium containing 2.5 puromycin/mL. Upon characterization, polyclonal cell populations were selected for further studies to avoid any artifacts associated with individual clone selection and to cross-validate our observations [71].

Enzymatic assays

Inhibitions constant (Ki) were determined as described previously with purified recombinant PCs [72]. Competitive inhibition assays were carried with 100μM of substrate pyroGlu-Arg-Val-Lys-Arg-methyl-coumaryl-7-amide (Bachem, CA) and inhibitory

peptides concentration from 20µM to 10nM. Fluorogenic substrate cleavage was monitored at 37˚C for 60 minutes using a Gemini EM 96-well spectrofluorometer (Molecular Devices, CA) (λ_{EM}:370nm; $\lambda_{EX.}$:460nm; CutOff 435nm). Kinetics assays were analyzed using SoftMaxPro5 and K_i values were determined from IC_{50} using Cheng and Prusoff's equation with Km values of 5.04 µM for furin and 3.5µM for PACE4. Enzyme inhibition assays for furin were performed in 100 mM Hepes pH 7.5, 1 mM CaCl2, 1 mM ß-mercaptoethanol, 1.8mg/mL BSA while assays for PACE4 were performed in 20 mM Bis-Tis pH 6.5, 1 mM CaCl2 1.8mg/mL BSA. Total enzymatic active site were titrated using Decanoyl-Arg-Val-Lys-Arg-Chloro-methyl Ketone inhibitor. The recombinant PCs were produced and purified as described previously [61]. For HA5 peptide assay, HA5 spanning peptide were synthetized with an automated peptide synthesizer using FMOC chemistry and purified by HPLC. Cleavage was analyzed by HPLC, as described in peptide stability in mouse plasma section, by incubating of peptide with 10 nM of enzyme (determined by active site titration with dec-RVKR-cmk as previously described [73]). Statistical analysis was performed using GraphPad Prism 5 software.

Peptide stability and digestion pattern in culture media

DU145 cells were seeded at a density of 6000cells/well in 96-well plate. 24h after, 40µg of peptide (dissolved in water at 10mM) were added to freshly added culture medium. After every time point, media were collected and enzymatic digestion was stopped by adding 20µL of 5%TFA and by keeping the samples at -20˚C until analysis on HPLC on a Hewlett-Packard 1090m C18 Vydac column (218TP104; 4.6mm" 250mm, 10 "m, 300 Å) using a 0-30%ACN gradient (0,5%/min). For MALDI-TOF analysis of peptide fragmentation, 20µg of peptide were incubated with cells/medium for each time point after what salt were removed of a 10µL aliquot using C-18 zip-tip (Millipore). 1µL of the desalted sample was applied on the ProteinChip Gold Array (Bio-Rad) with 1µL of α-cyano-4-hydroxycinnamic acid (HCCA; 10mg/mL;30:70 ACN/water 0,06%TFA) upon analysis on a ProteinChip SELDI system (Bio-Rad).

Peptide stability in mouse plasma

50µL of CD1 mouse plasma from mixed sex animals collected with heparin sodium *Innovative Research* (Novi, MI, USA) was incubated at 37°C with 35µg of peptide added from 20µL of stock solution. At each time point, reaction was stopped by adding 150µL of

1M guanidium-HCl solution followed by 300µL of acetonitrile. Proteins were removed by centrifugation and supernatant were analyzed by HPLC on a Hewlett-Packard 1090m C18 Vydac column (218TP104; 4.6mm" 250mm, 10 "m, 300 Å). Peptides AUC were compared to not incubated samples and percentage remaining were plotted to calculate half-life from one-phase decay fit curves. Each experiment was performed at least three times in duplicate for each time point.

MTT cell toxicity

For cell toxicity assay, cells were seeded at a density of 20 000cells/well in a 96-well plate, which result in a confluent monolayer the day of the experiment. Next day medium was changed with the indicated inhibitor concentration and incubated 24h. MTT assay was next carried as previously described [74].

LDH cell toxicity

For acute cell toxicity, cells were seeded at a density of 4000cells/well in 96-well plate. Next day, medium was changed and incubated with the indicated peptide concentration. LDH assay was carried using CytoxOne LDH assay (Promega) as recommended by the product provider using lysed cells as 100% toxicity control.

HA5 Cell fusion assay

HA5 cell fusion assay was carried as previously described with minor modifications [53]. Cells were transfected with pCDNA3.1-HA5, pCDNA3.1-NA1 and either pLVX-TAT or pLVX-Tight-puro-Luc at a respective ratio 2.5:0.6:1. The ratio between glycoprotein and activator/reporter gene was 2:1. The next day cells were counted and seeded in fibronectine coated 24 wells plate at a ratio of 3:1 of Luc to tat cells. Cell were allowed to adhere and treated 36h with furin inhibitors in medium containing 1% FBS. Cells were finally treated to induce cell fusion by titration of the medium with pH3 citrate solution to a final pH of 5 for 15 minute and neutralised by increasing to pH 7.4 with 100mM HEPES and Bicarbonate supplemented medium and allowed to recover. Medium was change with fresh medium and reporter gene was allowed to developed 48h and revealed using Bright-Glo Luciferase Assay System (Promega) and read with Gemini EM 96-well spectrofluorometer (Molecular Devices, CA). Inhibition of HA cleavage by furin resulted in a decreased fusion between gene and the subsequent non-expression of the reporter gene.

Stx extracts

Stx was isolated from STEC EDL933 (*E. coli* O157:H7, ATCC 43895) based on previously published procedures [75, 76]. Strain EDL933 was originally isolated from raw hamburger meat implicated in a hemorrhagic colitis outbreak. Briefly, for toxin purification, a bacterial culture of EDL933 (37°C, 225 rpm, 23-26 h) was centrifuged and the supernatant was conserved at 4°C until use. The bacterial pellet was suspended in polymyxin B (Sigma-Aldrich Canada Ltd., Nepean, ON, Canada) and after incubation at 37°C for 30 min with agitation, the suspension was centrifuged and the supernatant was combined with the previously collected culture supernatant. The Stx preparation was then filter-sterilized, kept at 4°C and used within 6h.

Vero cells protection assay

Forty-eight hours before the Stx cytotoxicity assay, Vero cells were seeded in 48-well culture plates (5×10^4 cells/well) in DMEM-10% FBS. Vero cells were incubated for two days then washed with serum-free DMEM. In each well, 100 µl of the bacterial toxin preparation (diluted 1:100 in serum-free DMEM) were added to Vero cells in 300 µl of serum-free DMEM and incubated at 37°C with 5% CO_2 for 24 h. A culture extract from *E. coli* K12 (Stx negative) was prepared as for EDL933 and was used as the negative control. Release of LDH by Vero cells was then measured by absorbance (A) readings at 490 nm after 17 min in the cell-free supernatants using a cytotoxicity detection kit (Roche Diagnostics, Indianapolis, IND, USA) according to the manufacturer's recommendations.

To test the ability of peptide inhibitors to protect Vero cells against Stx cytotoxicity, the inhibitors were diluted in serum-free DMEM (generally 0-80 µM, final concentration in the assay) and added to cell cultures 4h prior to the addition of the bacterial toxin preparation as described above. Cytotoxicity values were collected from at least two independent experiments (different toxin extracts and different LDH assays) for a total of 6 replicates. The relative Stx cytotoxicity was expressed as a percentage and calculated as follows: $(A_{EDL933+Inhibitor)} - A_{K12}) \times 100 / (A_{EDL933} - A_{K12})$. The inhibitor IC_{50} (in µM) was defined as the concentration reducing by 50% the relative Stx cytotoxicity in the assay.

Acknowledgements
This work was supported by the Canadian Institutes of Health Research (CIHR to RD), the Ministère du Développement Économique de l'Innovation et de l'Exportation (MDEIE to RD) and the Fond de recherche du Québec-Santé (FRQ-S to RD). RD is a member of the Centre de Recherche Clinique Etienne-LeBel (Sherbrooke, Qc, Canada). HG holds a bursary from CNRS and received the Frontenac mobility grant for a joint thesis (Franco-Quebec) from FQRNT and the French consulate. FC holds a graduate scholarship from the FRQ-S. We also acknowledge funding support from grant 89758-2010 from the Natural Sciences and Engineering Research Council of Canada to FM.

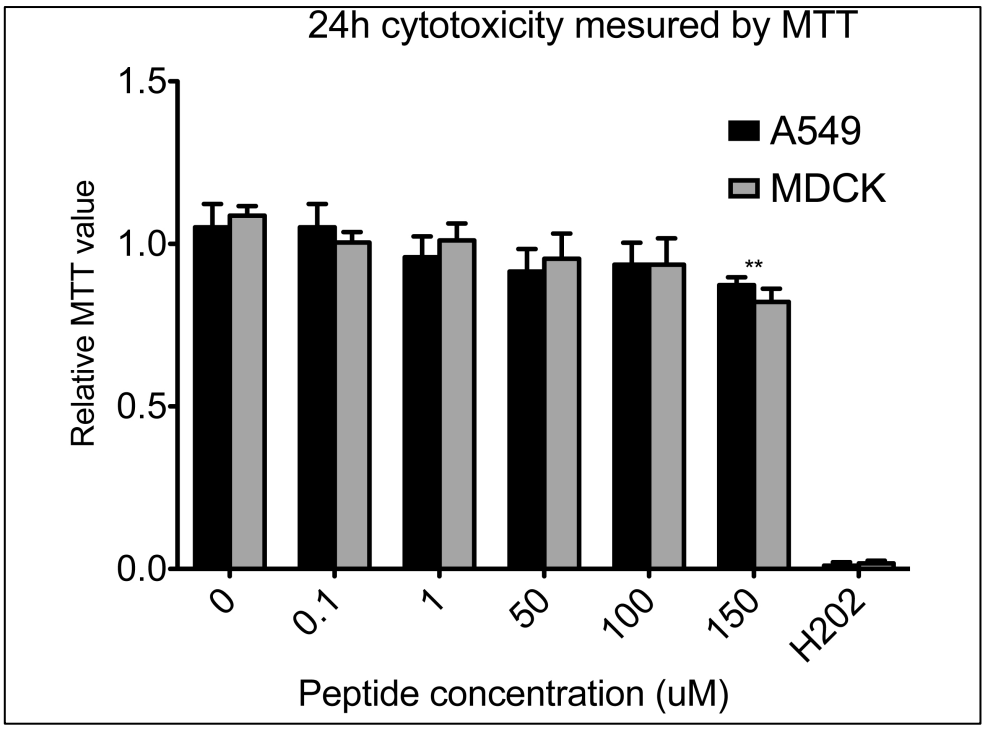

Figure S 1 Cellular toxicity of RARRRKKRT peptide on A549 and MDCK cells.

The peptide was incubated 24h at the indicated concentration on confluent monolayer of A549 and MDCK cells. Toxicity was measured by the MTT assay.

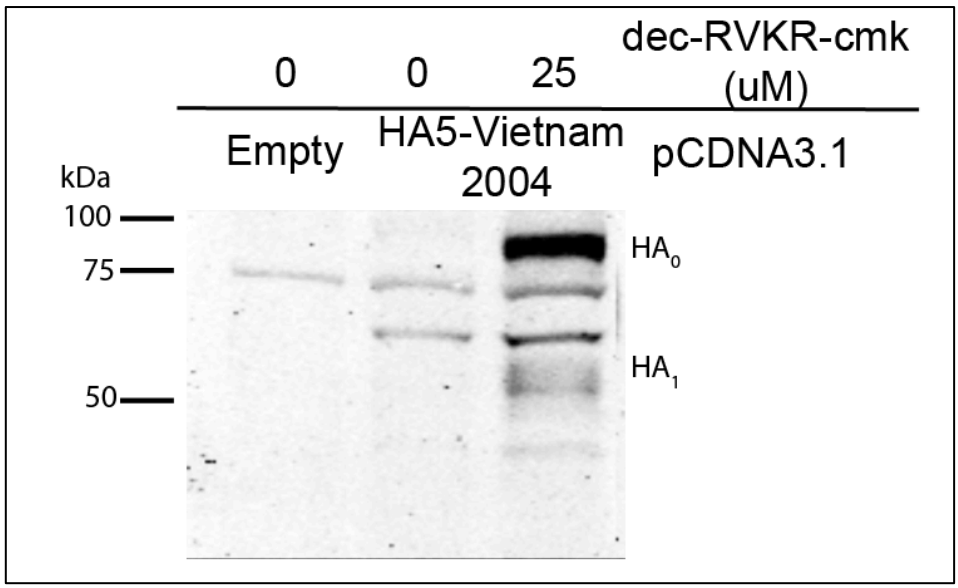

Figure S 2 HA5 expression in presence of dec-RVKR-CMK.

Western blot using HA5 detecting antibody of HEK293 overexpressing HA5 from Influenza A/Vietnam/1203/2004 virus. The antibody shows a greater affinity for non-matured HA5 (HA_0) compared to mature HA5 (HA_1) as shown by 48h incubation with 25 mM dec RVKR-CMR.

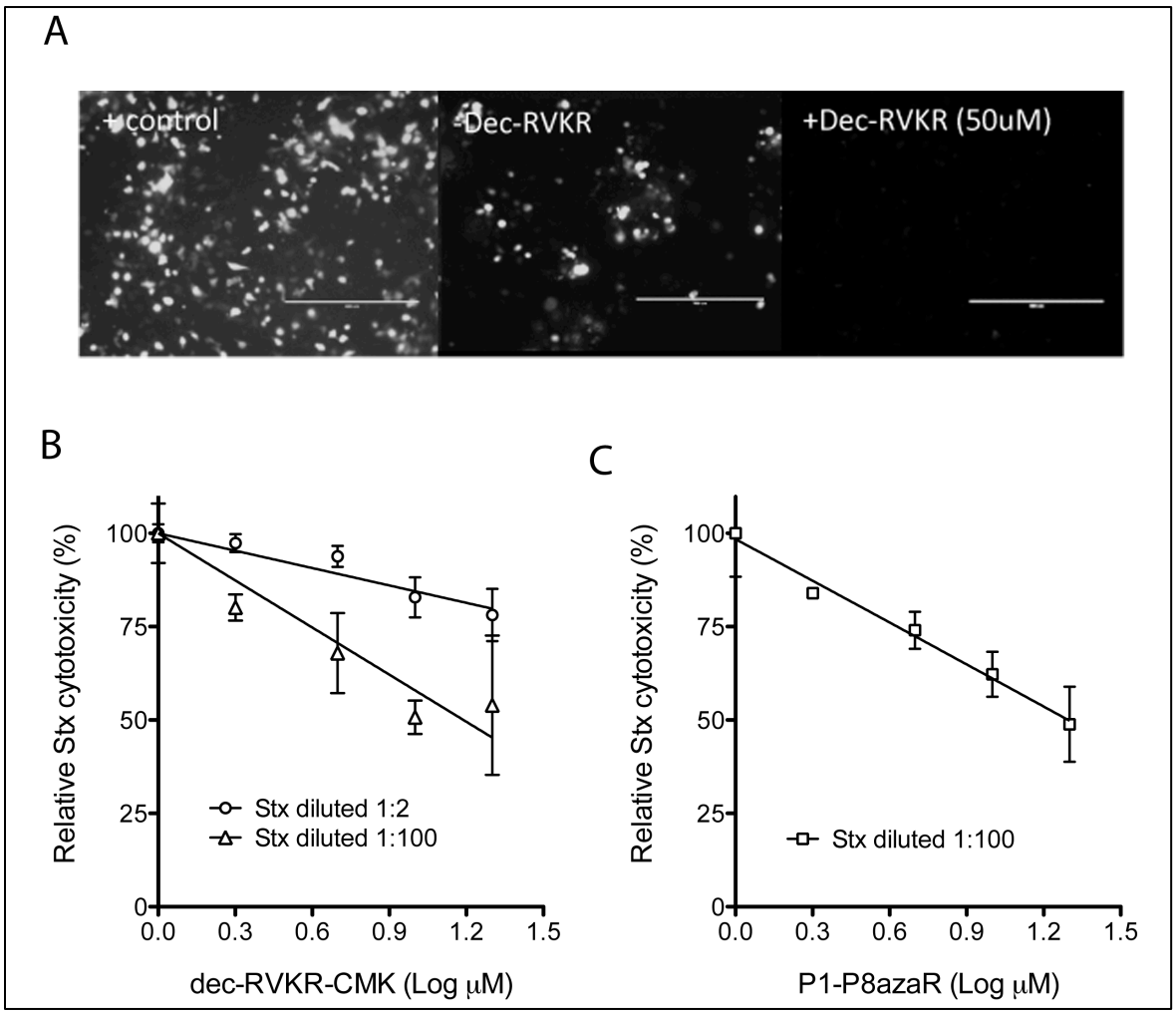

Figure S 3 Cell based assays respond to Furin inhibition by dec-RVKR-CMK.

A- Cell fusion assay was challenged with vehicle or Dec-RVKR-CMK (Dec-RVKR) at 50uM for 24h. Positive control represents cells transfected with activator and reporter plasmid. B- Vero cells were challenged with different concentrations of Dec-RVKR-CMK and two dilutions (1:2 and 1:100) of Stx extracts or in C- with different concentrations of P1-P8azaR in presence of Stx (1:100). In B and C, the relative Stx cytotoxicity measured by LDH release in presence of increasing concentrations of the inhibitor was normalized to cells challenged with Stx alone.

REFERENCES

1. Walsh, C. Where will new antibiotics come from? *Nat Rev Microbiol* **2003,** 1, 65-70.
2. De Clercq, E. Three decades of antiviral drugs. *Nature Reviews Drug Discovery* **2007,** 6, 941-941.
3. Coen, D. M.; Whitley, R. J. Antiviral drugs and antiviral drug resistance. *Curr Opin Virol* **2011,** 1, 545-7.
4. Palumbi, S. R. Humans as the world's greatest evolutionary force. *Science* **2001,** 293, 1786-90.
5. Coates, A.; Hu, Y.; Bax, R.; Page, C. The future challenges facing the development of new antimicrobial drugs. *Nat Rev Drug Discov* **2002,** 1, 895-910.
6. Coates, A. R.; Hu, Y. Novel approaches to developing new antibiotics for bacterial infections. *Br J Pharmacol* **2007,** 152, 1147-54.
7. De Clercq, E. Strategies in the design of antiviral drugs. *Nat Rev Drug Discov* **2002,** 1, 13-25.
8. Shryock, T. R. The future of anti-infective products in animal health. *Nature Reviews Microbiology* **2004,** 2, 425-430.
9. Coates, A. R. M.; Hu, Y. Novel approaches to developing new antibiotics for bacterial infections. *British Journal of Pharmacology* **2007,** 152, 1147-1154.
10. Serna, A. t.; Boedeker, E. C. Pathogenesis and treatment of Shiga toxin-producing Escherichia coli infections. *Curr Opin Gastroenterol* **2008,** 24, 38-47.
11. Sayce, A. C.; Miller, J. L.; Zitzmann, N. Targeting a host process as an antiviral approach against dengue virus. *Trends Microbiol* **2010,** 18, 323-30.
12. Lee, S. M.; Yen, H. L. Targeting the host or the virus: Current and novel concepts for antiviral approaches against influenza virus infection. *Antiviral Res* **2012**.
13. Kido, H.; Okumura, Y.; Yamada, H.; Le, T. Q.; Yano, M. Proteases essential for human influenza virus entry into cells and their inhibitors as potential therapeutic agents. *Curr Pharm Des* **2007,** 13, 405-14.
14. Shiryaev, S. A.; Remacle, A. G.; Ratnikov, B. I.; Nelson, N. A.; Savinov, A. Y.; Wei, G.; Bottini, M.; Rega, M. F.; Parent, A.; Desjardins, R.; Fugere, M.; Day, R.; Sabet, M.; Pellecchia, M.; Liddington, R. C.; Smith, J. W.; Mustelin, T.; Guiney, D. G.; Lebl, M.; Strongin, A. Y. Targeting host cell furin proprotein convertases as a therapeutic strategy against bacterial toxins and viral pathogens. *J Biol Chem* **2007,** 282, 20847-53.
15. Remacle, A. G.; Gawlik, K.; Golubkov, V. S.; Cadwell, G. W.; Liddington, R. C.; Cieplak, P.; Millis, S. Z.; Desjardins, R.; Routhier, S.; Yuan, X. W.; Neugebauer, W. A.; Day, R.; Strongin, A. Y. Selective and potent furin inhibitors protect cells from anthrax without significant toxicity. *Int J Biochem Cell Biol* **2010,** 42, 987-95.
16. Hosaka, M.; Nagahama, M.; Kim, W. S.; Watanabe, T.; Hatsuzawa, K.; Ikemizu, J.; Murakami, K.; Nakayama, K. Arg-X-Lys/Arg-Arg motif as a signal for precursor cleavage catalyzed by furin within the constitutive secretory pathway. *Journal of Biological Chemistry* **1991,** 266, 12127-30.
17. Nakayama, K. Furin: a mammalian subtilisin/Kex2p-like endoprotease involved in processing of a wide variety of precursor proteins. *Biochem J* **1997,** 327 (Pt 3), 625-35.
18. Essalmani, R.; Zaid, A.; Marcinkiewicz, J.; Chamberland, A.; Pasquato, A.; Seidah, N. G.; Prat, A. In vivo functions of the proprotein convertase PC5/6 during mouse development: Gdf11 is a likely substrate. *Proc Natl Acad Sci USA* **2008,** 105, 5750-5.

19. Seidah, N. G.; Hamelin, J.; Mamarbachi, M.; Dong, W.; Tardos, H.; Mbikay, M.; Chretien, M.; Day, R. cDNA structure, tissue distribution, and chromosomal localization of rat PC7, a novel mammalian proprotein convertase closest to yeast kexin-like proteinases. *Proc Natl Acad Sci U S A* **1996,** 93, 3388-93.
20. Tsuji, A.; Mori, K.; Hine, C.; Tamai, Y.; Nagamune, H.; Matsuda, Y. The tissue distribution of mRNAs for the PACE4 isoforms, kexin-like processing protease: PACE4C and PACE4D mRNAs are major transcripts among PACE4 isoforms. *Biochem Biophys Res Commun* **1994,** 202, 1215-21.
21. Rholam, M.; Fahy, C. Processing of peptide and hormone precursors at the dibasic cleavage sites. *Cell Mol Life Sci* **2009,** 66, 2075-91.
22. Seidah, N. G.; Chrétien, M. Proprotein and prohormone convertases: a family of subtilases generating diverse bioactive polypeptides. *Brain Res* **1999,** 848, 45-62.
23. Stieneke-Grober, A.; Vey, M.; Angliker, H.; Shaw, E.; Thomas, G.; Roberts, C.; Klenk, H. D.; Garten, W. Influenza virus hemagglutinin with multibasic cleavage site is activated by furin, a subtilisin-like endoprotease. *EMBO J* **1992,** 11, 2407-14.
24. Hatta, M.; Gao, P.; Halfmann, P.; Kawaoka, Y. Molecular basis for high virulence of Hong Kong H5N1 influenza A viruses. *Science* **2001,** 293, 1840-2.
25. Decha, P.; Rungrotmongkol, T.; Intharathep, P.; Malaisree, M.; Aruksakunwong, O.; Laohpongspaisan, C.; Parasuk, V.; Sompornpisut, P.; Pianwanit, S.; Kokpol, S.; Hannongbua, S. Source of high pathogenicity of an avian influenza virus H5N1: why H5 is better cleaved by furin. *Biophys J* **2008,** 95, 128-34.
26. Lea, N.; Lord, J. M.; Roberts, L. M. Proteolytic cleavage of the A subunit is essential for maximal cytotoxicity of Escherichia coli O157:H7 Shiga-like toxin-1. *Microbiology* **1999,** 145 (Pt 5), 999-1004.
27. Perdue, M. L.; Suarez, D. L. Structural features of the avian influenza virus hemagglutinin that influence virulence. *Vet Microbiol* **2000,** 74, 77-86.
28. Webster, R. G.; Rott, R. Influenza virus A pathogenicity: the pivotal role of hemagglutinin. *Cell* **1987,** 50, 665-6.
29. Writing Committee of the Second World Health Organization Consultation on Clinical Aspects of Human Infection with Avian Influenza, A. V.; Abdel-Ghafar, A. N.; Chotpitayasunondh, T.; Gao, Z.; Hayden, F. G.; Nguyen, D. H.; de Jong, M. D.; Naghdaliyev, A.; Peiris, J. S.; Shindo, N.; Soeroso, S.; Uyeki, T. M. Update on avian influenza A (H5N1) virus infection in humans. *N Engl J Med* **2008,** 358, 261-73.
30. Basak, A.; Zhong, M.; Munzer, J. S.; Chretien, M.; Seidah, N. G. Implication of the proprotein convertases furin, PC5 and PC7 in the cleavage of surface glycoproteins of Hong Kong, Ebola and respiratory syncytial viruses: a comparative analysis with fluorogenic peptides. *Biochem J* **2001,** 353, 537-45.
31. Horimoto, T.; Nakayama, K.; Smeekens, S.; Kawaoka, Y. Proprotein-processing endoproteases PC6 and furin both activate hemagglutinin of virulent avian influenza viruses. *Journal of Virology* **1994,** 68, 6074-6078.
32. Remacle, A. G.; Shiryaev, S. A.; Oh, E. S.; Cieplak, P.; Srinivasan, A.; Wei, G.; Liddington, R. C.; Ratnikov, B. I.; Parent, A.; Desjardins, R.; Day, R.; Smith, J. W.; Lebl, M.; Strongin, A. Y. Substrate Cleavage Analysis of Furin and Related Proprotein Convertases: A COMPARATIVE STUDY. *Journal of Biological Chemistry* **2008,** 283, 20897-20906.
33. Klenk, H. D.; Rott, R.; Orlich, M. Further studies on the activation of influenza virus by proteolytic cleavage of the haemagglutinin. *J Gen Virol* **1977,** 36, 151-61.

34. Munster, V. J.; Schrauwen, E. J.; de Wit, E.; van den Brand, J. M.; Bestebroer, T. M.; Herfst, S.; Rimmelzwaan, G. F.; Osterhaus, A. D.; Fouchier, R. A. Insertion of a multibasic cleavage motif into the hemagglutinin of a low-pathogenic avian influenza H6N1 virus induces a highly pathogenic phenotype. *J Virol* **2010,** 84, 7953-60.
35. Scholtissek, C. Influenza A viruses with noncleaved hemagglutinin are not internalized after adsorption. Brief report. *Arch Virol* **1986,** 90, 159-63.
36. Skehel, J. J.; Waterfield, M. D. Studies on the primary structure of the influenza virus hemagglutinin. *Proc Natl Acad Sci USA* **1975,** 72, 93-7.
37. Skehel, J. J.; Wiley, D. C. Receptor binding and membrane fusion in virus entry: the influenza hemagglutinin. *Annu Rev Biochem* **2000,** 69, 531-69.
38. O'Loughlin, E. V.; Robins-Browne, R. M. Effect of Shiga toxin and Shiga-like toxins on eukaryotic cells. *Microbes Infect* **2001,** 3, 493-507.
39. Sandvig, K. Shiga toxins. *Toxicon* **2001,** 39, 1629-35.
40. Garred, O.; van Deurs, B.; Sandvig, K. Furin-induced cleavage and activation of Shiga toxin. *J Biol Chem* **1995,** 270, 10817-21.
41. Kurmanova, A.; Llorente, A.; Polesskaya, A.; Garred, O.; Olsnes, S.; Kozlov, J.; Sandvig, K. Structural requirements for furin-induced cleavage and activation of Shiga toxin. *Biochem Biophys Res Commun* **2007,** 357, 144-9.
42. Garred, O.; Dubinina, E.; Holm, P. K.; Olsnes, S.; van Deurs, B.; Kozlov, J. V.; Sandvig, K. Role of processing and intracellular transport for optimal toxicity of Shiga toxin and toxin mutants. *Exp Cell Res* **1995,** 218, 39-49.
43. Ilyushina, N. A.; Bovin, N. V.; Webster, R. G. Decreased neuraminidase activity is important for the adaptation of H5N1 influenza virus to human airway epithelium. *J Virol* **2012,** 86, 4724-33.
44. Yen, H. L.; Webster, R. G. Pandemic influenza as a current threat. *Curr Top Microbiol Immunol* **2009,** 333, 3-24.
45. Marinova-Petkova, A.; Georgiev, G.; Seiler, P.; Darnell, D.; Franks, J.; Krauss, S.; Webby, R. J.; Webster, R. G. Spread of Influenza Virus A (H5N1) Clade 2.3.2.1 to Bulgaria in Common Buzzards. *Emerg Infect Dis* **2012,** 18, 1596-602.
46. Scallan, E.; Hoekstra, R. M.; Angulo, F. J.; Tauxe, R. V.; Widdowson, M.-A.; Roy, S. L.; Jones, J. L.; Griffin, P. M. Foodborne Illness Acquired in the United States—Major Pathogens. *Emerging Infectious Diseases* **2011,** 17, 7-15.
47. Frenzen, P. D.; Drake, A.; Angulo, F. J.; Emerging Infections Program FoodNet Working, G. Economic cost of illness due to Escherichia coli O157 infections in the United States. *J Food Prot* **2005,** 68, 2623-30.
48. Zhu, J.; Declercq, J.; Roucourt, B.; Ghassabeh, G. H.; Meulemans, S.; Kinne, J.; David, G.; Vermorken, A. J.; Van de Ven, W. J.; Lindberg, I.; Muyldermans, S.; Creemers, J. W. Generation and characterization of non-competitive furin-inhibiting nanobodies. *Biochem J* **2012**.
49. Becker, G. L.; Sielaff, F.; Than, M. E.; Lindberg, I.; Routhier, S.; Day, R.; Lu, Y.; Garten, W.; Steinmetzer, T. Potent inhibitors of furin and furin-like proprotein convertases containing decarboxylated P1 arginine mimetics. *J Med Chem* **2010,** 53, 1067-75.
50. Becker, G. L.; Lu, Y.; Hardes, K.; Strehlow, B.; Levesque, C.; Lindberg, I.; Sandvig, K.; Bakowsky, U.; Day, R.; Garten, W.; Steinmetzer, T. Highly potent inhibitors of proprotein convertase furin as potential drugs for treatment of infectious diseases. *J Biol Chem* **2012,** 287, 21992-2003.

51. Freeman, N. S.; Tal-Gan, Y.; Klein, S.; Levitzki, A.; Gilon, C. Microwave-Assisted Solid-Phase Aza-peptide Synthesis: Aza Scan of a PKB/Akt Inhibitor Using Aza-arginine and Aza-proline Precursors. *The Journal of Organic Chemistry* **2011,** 76, 3078-3085.
52. Klenk, H. D.; Matrosovich, M. N.; Stech, J. *Avian Influenza*. S Karger Ag: 2008; p 292.
53. Su, B.; Wurtzer, S.; Rameix-Welti, M. A.; Dwyer, D.; van der Werf, S.; Naffakh, N.; Clavel, F.; Labrosse, B. Enhancement of the influenza A hemagglutinin (HA)-mediated cell-cell fusion and virus entry by the viral neuraminidase (NA). *PLoS One* **2009,** 4, e8495.
54. Walker, J. A.; Sakaguchi, T.; Matsuda, Y.; Yoshida, T.; Kawaoka, Y. Location and character of the cellular enzyme that cleaves the hemagglutinin of a virulent avian influenza virus. *Virology* **1992,** 190, 278-87.
55. Li, I. W.; Chan, K. H.; To, K. W.; Wong, S. S.; Ho, P. L.; Lau, S. K.; Woo, P. C.; Tsoi, H. W.; Chan, J. F.; Cheng, V. C.; Zheng, B. J.; Chen, H.; Yuen, K. Y. Differential susceptibility of different cell lines to swine-origin influenza A H1N1, seasonal human influenza A H1N1, and avian influenza A H5N1 viruses. *J Clin Virol* **2009,** 46, 325-30.
56. Mason, J. M. Design and development of peptides and peptide mimetics as antagonists for therapeutic intervention. *Future Medicinal Chemistry* **2010,** 2, 1813-1822.
57. André, F.; Boussard, G.; Bayeul, D.; Didierjean, C.; Aubry, A.; Marraud, M. Aza-peptides. II. X-ray structures of aza-alanine and aza-asparagine-containing peptides. *The journal of peptide research : official journal of the American Peptide Society* **1997,** 49, 556-562.
58. André, F.; Vicherat, A.; Boussard, G.; Aubry, A.; Marraud, M. Aza-peptides. III. Experimental structural analysis of aza-alanme and aza-asparagine-containing peptides. *The Journal of peptide research* **1997,** 50, 372-381.
59. Thormann, M.; Hofmann, H. J. Conformational properties of azapeptides. *Journal of Molecular Structure: THEOCHEM* **1999,** 469, 63-76.
60. Chen, J.; Lee, K. H.; Steinhauer, D. A.; Stevens, D. J.; Skehel, J. J.; Wiley, D. C. Structure of the hemagglutinin precursor cleavage site, a determinant of influenza pathogenicity and the origin of the labile conformation. *Cell* **1998,** 95, 409-417.
61. Fugere, M.; Limperis, P. C.; Beaulieu-Audy, V.; Gagnon, F.; Lavigne, P.; Klarskov, K.; Leduc, R.; Day, R. Inhibitory potency and specificity of subtilase-like pro-protein convertase (SPC) prodomains. *J Biol Chem* **2002,** 277, 7648-56.
62. Couture, F.; D'Anjou, F.; Desjardins, R.; Boudreau, F.; Day, R. Role of proprotein convertases in prostate cancer progression. *Neoplasia* **2012,** 14, 1032-42.
63. Hatta, M.; Hatta, Y.; Kim, J. H.; Watanabe, S.; Shinya, K.; Nguyen, T.; Lien, P. S.; Le, Q. M.; Kawaoka, Y. Growth of H5N1 influenza A viruses in the upper respiratory tracts of mice. *PLoS Pathog* **2007,** 3, 1374-9.
64. Fields, G. B.; Noble, R. L. Solid phase peptide synthesis utilizing 9-fluorenylmethoxycarbonyl amino acids. *Int J Pept Protein Res* **1990,** 35, 161-214.
65. Levesque, C.; Fugere, M.; Kwiatkowska, A.; Couture, F.; Desjardins, R.; Routhier, S.; Moussette, P.; Prahl, A.; Lammek, B.; Appel, J. R.; Houghten, R. A.; D'Anjou, F.; Dory, Y. L.; Neugebauer, W.; Day, R. The Multi-Leu Peptide Inhibitor Discriminates Between PACE4 and Furin And Exhibits Antiproliferative Effects On Prostate Cancer Cells. *J Med Chem* **2012,** 55, 10501-11.

66. Jeon, H. B.; Lee, Y.; Qiao, C.; Huang, H.; Sayre, L. M. Inhibition of bovine plasma amine oxidase by 1,4-diamino-2-butenes and -2-butynes. *Bioorg Med Chem* **2003,** 11, 4631-41.
67. Busnel, O.; Bi, L.; Dali, H.; Cheguillaume, A.; Chevance, S.; Bondon, A.; Muller, S.; Baudy-Floc'h, M. Solid-phase synthesis of "mixed" peptidomimetics using Fmoc-protected aza-beta3-amino acids and alpha-amino acids. *J Org Chem* **2005,** 70, 10701-8.
68. Schweinitz, A.; Sturzebecher, A.; Sturzebecher, U.; Schuster, O.; Sturzebecher, J.; Steinmetzer, T. New substrate analogue inhibitors of factor Xa containing 4-amidinobenzylamide as P1 residue: part 1. *Med Chem* **2006,** 2, 349-61.
69. Refaie, S.; Gagnon, S.; Gagnon, H.; Desjardins, R.; D'Anjou, F.; D'Orleans-Juste, P.; Zhu, X.; Steiner, D. F.; Seidah, N. G.; Lazure, C.; Salzet, M.; Day, R. Disruption of proprotein convertase 1/3 (PC1/3) expression in mice causes innate immune defects and uncontrolled cytokine secretion. *J Biol Chem* **2012,** 287, 14703-17.
70. D'Anjou, F.; Routhier, S.; Perreault, J. P.; Latil, A.; Bonnel, D.; Fournier, I.; Salzet, M.; Day, R. Molecular Validation of PACE4 as a Target in Prostate Cancer. *Transl Oncol* **2011,** 4, 157-72.
71. Yuasa, K.; Masuda, T.; Yoshikawa, C.; Nagahama, M.; Matsuda, Y.; Tsuji, A. Subtilisin-like proprotein convertase PACE4 is required for skeletal muscle differentiation. *J Biochem* **2009,** 146, 407-15.
72. Cheng, Y.; Prusoff, W. H. Relationship between the inhibition constant (K1) and the concentration of inhibitor which causes 50 per cent inhibition (I50) of an enzymatic reaction. *Biochem Pharmacol* **1973,** 22, 3099-108.
73. Jean, F.; Stella, K.; Thomas, L.; Liu, G.; Xiang, Y.; Reason, A. J.; Thomas, G. alpha1-Antitrypsin Portland, a bioengineered serpin highly selective for furin: application as an antipathogenic agent. *Proc Natl Acad Sci U S A* **1998,** 95, 7293-8.
74. Mosmann, T. Rapid colorimetric assay for cellular growth and survival: application to proliferation and cytotoxicity assays. *J Immunol Methods* **1983,** 65, 55-63.
75. Lefebvre, B.; Diarra, M. S.; Vincent, C.; Moisan, H.; Malouin, F. Relative cytotoxicity of Escherichia coli O157:H7 isolates from beef cattle and humans. *Foodborne Pathog Dis* **2009,** 6, 357-64.
76. Maldonado, Y.; Fiser, J. C.; Nakatsu, C. H.; Bhunia, A. K. Cytotoxicity potential and genotypic characterization of Escherichia coli isolates from environmental and food sources. *Appl Environ Microbiol* **2005,** 71, 1890-8.

CHAPITRE 2 - RÔLE DE PC1/3 DANS L'IMMUNITÉ INNÉE : UNE APPROCHE PAR SPECTROMÉTRIE DE MASSE

Par Hugo Gagnon

1.1. Matériel et méthodes

1.1.1. Collection des tissus et des macrophages péritonéaux

Les procédures pour le sacrifice des animaux et la collection des macrophages péritonéaux sont décrites dans la section expérimentale du Chapitre 3 - Disruption of PC1/3 expression in mice causes innate immune defects and uncontrolled cytokine secretion. Brièvement, les animaux ont été sacrifiés par dislocation cervicale après anesthésie. Les macrophages péritonéaux ont été récoltés de souris injectées au thioglycolate 3 % et stimulées ou non 8 h avec 100 µg LPS intrapéritonéale.

1.1.2. Analyse par imagerie par spectrométrie de masse MALDI (MSI)

La procédure pour l'imagerie MALDI a été décrite par (Bonnel et al. 2011). Brièvement, les rates préservées à -80^{o}C ont été équilibrées à -18^{o}C à l'intérieur du cryostat. Les tissus ont par la suite été montés avec un peu de solutions OCT (*optimal cutting temperature*) à la base et des coupes transversales de 12 µm ont par la suite été montées sur une lame conductrice. Les coupes de souris WT et KO étaient adjacentes sur la lame. Les tissus étaient par la suite soumis à une série de lavages à -20^{o}C : EtOH 95 % 15 sec; chloroforme 1 min; acétone 15 sec. Une matrice ionique, composée de 10mg/mL d'acide alpha-cyano-4-hydroxycinnamic (CHCA) et 0,1 µM aniline dans 70 % acétonitrile/H_2O 0,1 % acide trifuloracétique, a par la suite été déposée à l'aide d'un micronébuliseur Imageprep (Bruker). Les tissus ont par la suite été analysés avec un spectromètre masse MALDI-TOF/TOF ultraflex II (Bruker) en mode positif avec une acquisition de 900 m/z à 4000 m/z. Le laser était réglé pour faire l'acquisition point par point afin de couvrir toute la coupe de tissu. À chaque point, 300 spectres étaient acquis de façon aléatoire sur un diamètre de 50 µM et une fréquence de 200Hz.

1.1.3. Analyse des données MSI

Une fois l'acquisition terminée, la matrice a été enlevée par des lavages au méthanol et les rates ont été colorées à hématoxyline et éosine selon un protocole standard, afin de pouvoir déterminer les zones histologiques correspondantes à la pulpe rouge, la pulpe blanche et la zone marginale. L'analyse de données a été décrite par (Bonnel et al. 2011). Brièvement, les spectres des rates ont été classifiés de façon hiérarchique à l'aide du logiciel ClinProTools. Cette étape a permis de tracer les régions où les spectres correspondent à la pulpe rouge, la pulpe blanche et la zone marginale. L'analyse statistique a permis de déterminer que les régions correspondant à la pulpe blanche et la zone marginale présentaient peu de différence, ces régions ont alors été combinées. Finalement, une analyse statistique a permis d'extraire les masses présentant une différence d'intensité de cinq fois entre tissus WT et KO. De plus, une analyse en composante principale (PCA) a été effectuée pour déterminer les masses ayant la plus grande variance entre les tissus WT et les tissus KO.

1.1.4. Analyse par Gel LC-MS/MS

L'analyse par Gel LC-MS/MS a été effectuée comme décrite dans la section expérimentale du Chapitre 3 - Disruption of PC1/3 expression in mice causes innate immune defects and uncontrolled cytokine secretion. Brièvement, le contenu protéique des extrudâts péritonéaux de souris WT et KO stimulées ou non 8 h au LPS ont été fractionnées en fractions membranaires et cytoplasmiques (Figure 18). Chaque échantillon a par la suite été migré sur gel SDS 4-20 % où les lignes de migration étaient découpées en 18 bandes, puis soumises à une digestion trypsique et une analyse nanoLC couplée à un spectromètre de masse LTQ-Orbitrap Velos.

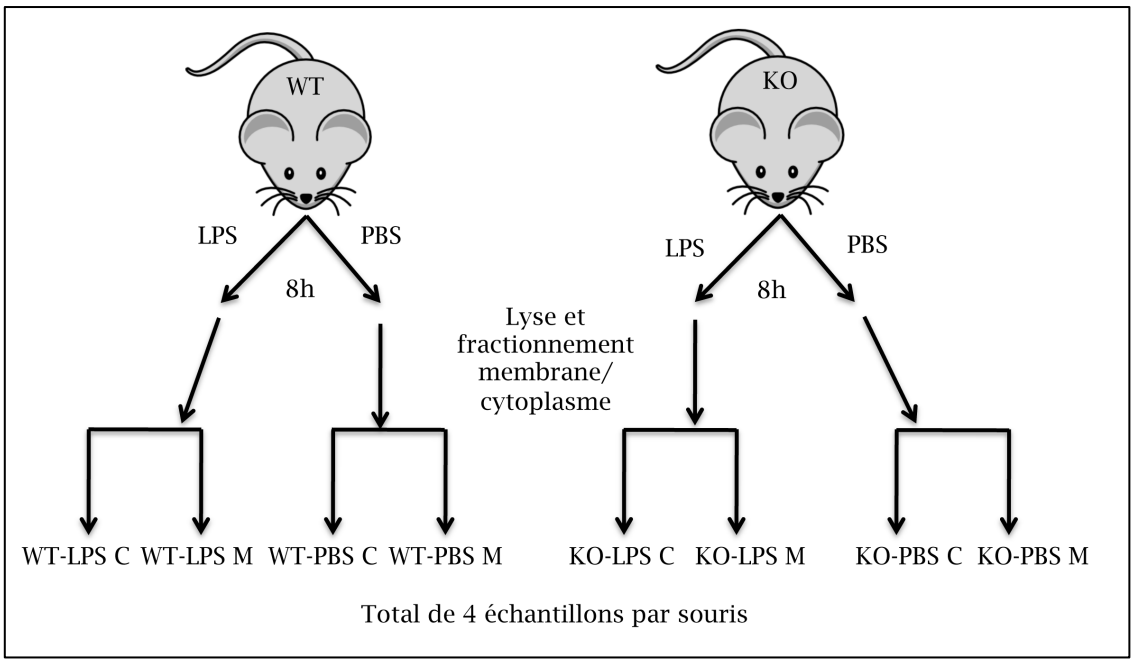

Figure 18 Description des groupes pour l'analyse Gel LC-MS/MS.

Les souris contrôles (WT) et les souris PC1/3 KO (KO) induites au thioglycolate ont été stimulées 8 h au LPS ou avec du tampon physiologique (PBS). Les macrophages péritonéaux ont été récoltés et leur contenu protéique a été séparé en fractions membranaires (M) et cytoplasmiques (C) pour un total de huit échantillons soit : WT-LPS C, WT-LPS, M, WT-PBS C, WT-PBS M, KO-LPS C, KO-LPS M, KO-PBS C et KO-PBS M.

1.1.5. Analyse des données LC-MS/MS

L'organigramme représentant l'analyse LC-MS/MS est présenté à la Figure 19. L'assignation des peptides correspondant aux spectres de masse, l'identification et la validation des identifications protéiques sont décrites dans le Chapitre 3 - Disruption of PC1/3 expression in mice causes innate immune defects and uncontrolled cytokine secretion. La quantification entre les différents échantillons a été faite par compte spectral (Hendrickson et al. 2006; Asara et al. 2008) à l'aide du logiciel Scaffold 3.0 (Searle 2010). L'analyse bio-informatique à l'aide des logiciels Blast2Go, de la base de données STRING et du logiciel Cytoscape est décrite au Chapitre 5 - Proteomic analyses of serous and endometrioid epithelial ovarian cancers: cases studies: molecular insights of a possible histological etiology of serous ovarian cancer. Le test d'enrichissement ontogénique, pour déterminer les fonctions moléculaires les plus affectées par le KO de PC1/3, a été effectué à l'aide de Blast2GO en comparant la liste des protéines surexprimées (KO vs WT membranaire peu importe le traitement) à toutes les protéines identifiées.

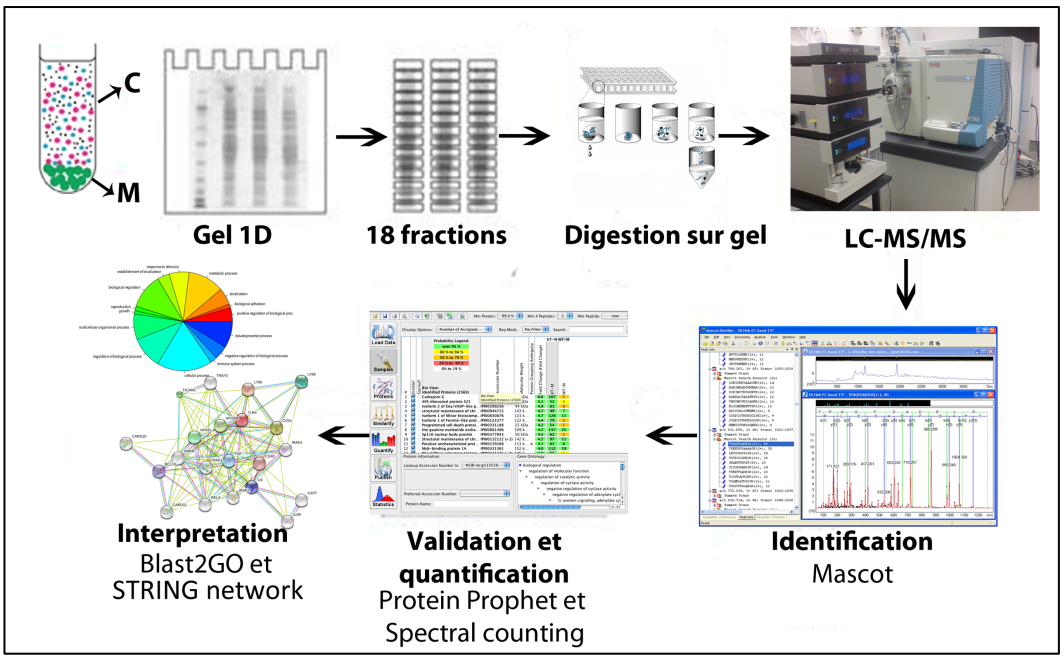

Figure 19 Flux de travail Gel LC-MS-MS.

Les fractions membranaires (M) et cytoplasmiques (C) ont d'abord été séparées sur gel SDS. Chaque bande de migration a par la suite été découpée en 18 fractions puis celles-ci ont été digérées à la trypsine pour être analysées par LC-MS/MS. L'identification des spectres a été faite par l'algorithme Mascot (http://www.matrixscience.com/), puis les identifications protéiques ont été validées par l'algorithme Protien Prophet (Qian et al. 2005). Le logiciel Scaffold (http://www.proteomesoftware.com) a permis d'assigner par compte spectral des valeurs quantitatives à chaque protéine identifiée. Les données ont par la suite été interprétées par analyses bio-informatiques à l'aide du logiciel Blast2GO (http://www.blast2go.com) (qui permet des analyses d'ontologie génique) et de la base de données STRING (http://string-db.org/) (qui permet de tracer les réseaux d'interactions biologiques entre les protéines identifiées).

1.2. Résultats

1.2.1. Analyse par MSI des rates de souris WT et KO PC1/3

Il a précédemment été démontré que PC1/3, le précurseur pro-enképhaline et de ses produits de clivages sont exprimés dans la rate (Lansac et al. 2006). Une approche d'imagerie par spectrométrie de masse (MSI), des peptides dans les rates de souris contrôles (WT) et de souris où PC1/3 est inactivée (KO), permettrait de déterminer le rôle que PC1/3 peut jouer dans la maturation de neuropeptides modulateurs de l'immunité au sein de ce tissu. La détermination de la localisation anatomique des peptides est un avantage afin de les situer dans leur contexte physiologique, puisque la rate est un organe présentant une certaine complexité structurale qui permet la communication entre le système lymphatique et la circulation sanguine.

En utilisant l'imagerie MALDI (MSI) pour analyser une gamme de masse qui correspond à des peptides de 900 m/z à 4000 m/z, le profile moléculaire des rates a été évalué. À la suite de cette imagerie, une coloration hématoxyline et éosine a été effectuée pour discriminer les différentes zones histologiques des rates. Ainsi, des régions d'intérêts correspondantes à la zone marginale, la pulpe blanche et la pulpe rouge des rates ont pu être tracées. Les spectres de chacune de ces zones des rates ont été extraits et analysés par classification hiérarchique afin de déterminer si la MSI permettait de distinguer ces différentes régions sur chaque tissu. Brièvement, l'analyse par classification hiérarchique permet discriminer différentes régions par similitude de profile spectral : deux régions ayant des spectres semblables seront sur une même branche de classification, donc plus les spectres sont différents, plus ils s'éloigneront dans l'arbre de classification. En analysant les différentes branches de classification hiérarchique, il était facile de distinguer les spectres de la pulpe blanche de ceux de la pulpe rouge. Toutefois, les spectres de la pulpe blanche et de la zone marginale se retrouvaient mélangés dans différentes branches homologues, pour en conclure que ces deux zones devaient être traitées comme une seule soit la pulpe blanche. Par la suite, une analyse par classification hiérarchique des spectres a été effectuée pour trouver des ensembles de spectres concordants spécifiquement à des zones histologiques distinctes à la pulpe blanche et à la pulpe rouge sur les tissus WT et KO. Les spectres de ces régions ont par la suite été extraits afin d'effectuer une comparaison entre les tissus KO et WT (Figure 20). Cette approche était nécessaire afin de

réduire le nombre de spectres à analyser par tissu, puisque le logiciel d'analyse ne peut pas analyser plus de 1000 spectres, mais aussi pour s'assurer qu'aucun spectre ne provenait d'un mélange entre deux régions histologiques.

Le résultat fut d'abord étonnant (Figure 20A). La zone de la pulpe rouge de la rate WT était classée dans une branche avec les zones de la pulpe blanche et de la pulpe rouge de la rate KO. En détail, la zone de la pulpe rouge WT (en vert) avait une plus grande similitude envers les spectres de la pulpe blanche KO (en mauve). D'un autre côté, la zone de la puple rouge KO avait une région marquée avec des spectres semblables à la pulpe blanche WT (en rouge). Ces résultats indiquaient soit une délocalisation des ions majoritaires ou un changement important des ions majoritaires observés entre les diverses zones histologiques chez la rate PC1/3 KO par rapport à la rate WT. En examinant les masses dont les intensités des pics affichaient des variations de plus de cinq fois (WT vs KO, test Student $p>0,0001$), on pouvait constater que la majorité des masses étaient surreprésentées chez les WT (Tableau 9). De plus, lorsque l'on reconstituait l'image de ces masses, on pouvait constater que plusieurs ions présentaient une importante délocalisation vers des zones histologiques où ils n'étaient pas observés dans la rate WT. De plus, une analyse statistique multivariée par PCA, qui permet de discriminer les composants des spectres qui sont responsables de la variation entre les échantillons, permettait essentiellement de faire ressortir les mêmes masses que celles identifiées par variation d'intensité. Donc, ces masses sont représentatives des importants changements structuraux de la rate PC1/3 KO, comme en témoigne son hypertrophie, mais aussi des changements au niveau moléculaires. Afin de mieux caractériser ces changements, nous avons effectué une étude histologique avec des marqueurs des différents types de cellule immunitaire présentée au Chapitre 3 - Disruption of PC1/3 expression in mice causes innate immune defects and uncontrolled cytokine secretion.

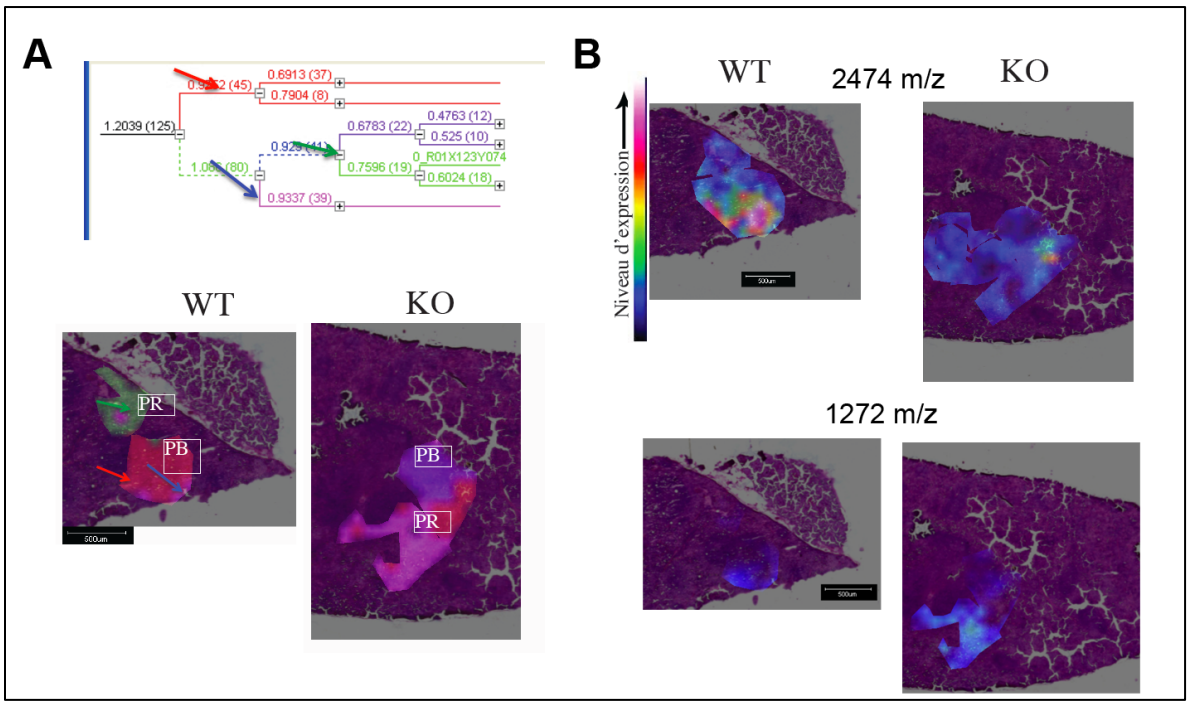

Figure 20 Résultats de la MSI des rates.

A) La classification hiérarchique des spectres de masse a permis de caractériser des zones types de la pulpe rouge (PR) et de la pulpe blanche (PB). En comparant ces zones entre WT et KO on peut voir une désorganisation des spectres pour la gamme de masse observée (900-4000 m/z). Les zones correspondantes à chacune des branches de l'arbre de classification hiérarchique ont été colorées avec la couleur correspondante sur l'image du tissu. La zone de la pulpe blanche de la rate WT est en rouge, la zone de la puple rouge WT est en principalement en vert, la zone de la pulpe blanche KO est en mauve et la zone de la pulpe rouge KO est en rose et en rouge. B) Exemple d'imagerie de l'ion 2475 M/z qui présente une forte différence d'expression et l'ion 1272 m/z identifiés par PCA qui présent une faible différence d'expression, mais un changement de localisation important dans les rates KO.

1.2.1.1. Identification par homologie de masse avec Swepep

Après plusieurs essais infructueux d'identification MS/MS des ions présentant des changements d'expression ou de localisation, l'utilisation d'une banque de données de peptides a permis de corréler certaines de ces masses avec des peptides biologiques connus (Tableau 9). Cette banque, nommée Swepep, contient principalement une liste de neuropeptides et leur masse observée expérimentalement. L'identification est donc biaisée envers ces neuropeptides. De plus, puisque des études peptidomique par LC-MS/MS avaient été réalisées sur des cerveaux de souris PC1/3 KO (Wardman et al. 2010) et PC2 KO (Zhang et al. 2010), les masses identifiées et les niveaux d'expression ont pu être corrélés avec ceux obtenus par MSI. L'assignation des masses à leurs peptides théorique reste qu'une vague approximation, comme en témoigne l'identification d'un fragment qui correspondrait à PC1/3 dans la rate KO. De plus, seulement un peptide, correspondant à la chromogranine B, affiche un profile similaire aux résultats de (Wardman et al. 2010).

Tableau 9 Corrélation des masses observées avec la banque de données Swepep et celles observées dans (Wardman et al. 2010) et dans (Zhang et al. 2010).

Nom	Masse théorique	Masse observée	Expression KO	Localisation	ref PC13	ref PC2	fonction
ocytocine	1009,44	1009,95	+	PR	nd	nd	hormone
chromogranine B	1041,5	1041,00	-	PR	-	=	sécrétion
chromogranine C	1157,52	1158,50	+	PR/PB	nd	nd	sécrétion
PCSK1	1309,5	1311,80	+	PR	-	-	PC
PENK 221-229	1309,5	1311,80	+	PR	nd	nd	produit de clivage
alpha-MSH	1628,7	1627,85	+	PR	nd	nd	hormone
Activation peptide	1655,7	1654,88	+	PR	nd	nd	régulation de la protéine C
Neurotensine	1689	1688,00	+	PR	=	=	hormone
Fibrinopeptide B	1697	1695,00	+/-	délocalisé PB	nd	nd	adhésion cellulaire
PCSK1	1860,5	1862,00	+	PR	-	-	PC
PENK 117-133	1860,8	1862,00	+	PR	nd	nd	produit de clivage
GLUC 32-48	1903	1902,00	+	PR	nd	nd	produit de clivage
Chromogranine B	1910,93	1911,00	+/-	PR/WT++	=	-	sécrétion
POMC 165-181	1911,2	1911,08	+/-	PR/WT++	nd	nd	produit de clivage
Pro SAAS (bigsaas)	2476,4	2273,33	+	PR	+	=	inhibition de PC1/3
Arg-Corticotropin-like intermediary peptide	2505	2507,00	+	PR	nd	nd	hormone/cytokine
Defensin 1	4117	4116,41	-	PR	nd	nd	antimicrobien
Peptide yy	4239	4238,00	-	PR/WT	nd	nd	hormone

Liste de masses identifiées et corrélées avec comme paramètre +/- 2 Da dans l'outil de recherche de la base de données Swepep (http://www.swepep.org/). Ces masses pouvaient avoir une différence d'expression ou une délocalisation.

1.2.2. Analyse Gel LC-MS/MS des extrudâts péritonéaux de souris WT et KO

Au Chapitre 3 - Disruption of PC1/3 expression in mice causes innate immune defects and uncontrolled cytokine secretion, le phénotype immunitaire des souris PC1/3 KO est présenté. D'un point de vue physiologique, l'absence de PC1/3 engendre une réponse immunitaire innée non contrôlée en réponse au LPS qui favorise une réaction inflammatoire forte Th1 (caractérisée par la sécrétion IFN-γ). Cette réponse présente une sécrétion accrue de cytokines pro-inflammatoires par les macrophages (IL-12p70, IL-6, IL-1β) et une absence de réponse des macrophages à la cytokine régulatrice IL-10. De plus, les macrophages péritonéaux extraits des souris PC1/3 KO présentent des changements morphologiques et structuraux importants, notamment des vésicules de leur voie de sécrétion.

Pour comprendre le rôle de PC1/3 dans la régulation physiologique de la réponse immunitaire innée et faire le lien avec les fonctions moléculaires associées, une approche de caractérisation moléculaire à haut débit était de mise. Puisque PC1/3 est une enzyme et que ces actions se font certainement par la régulation de protéines bioactives dans les voies de signalisation moléculaires, l'identification protéique par spectrométrie de masse s'avérait un choix judicieux. Cette approche permet non seulement de détecter des expressions différentielles (présence ou absence de détection), mais aussi de quantifier les protéines identifiées dans les différents échantillons et de détecter des changements de compartiments cellulaires. Aux fins de quantification, une approche sans marquage a été préconisée. Cette approche (nommée compte spectral) s'appuie sur le fait qu'une protéine plus abondante génèrera plus de spectres associés à son identification, déduisant ainsi une information quantitative (Old et al. 2005).

Ainsi, les souris WT et PC1/3 KO ont été stimulées ou non 8 h au LPS, puis les extrudâts péritonéaux contenant les macrophages ont été récoltés. Un fractionnement cellulaire a d'abord été réalisé pour séparer la fraction cytoplasmique de la fraction membranaire. Cette étape permet deux avantages importants : 1) augmenter le nombre d'identifications protéiques, 2) détecter des changements de localisation cellulaire des protéines entre le cytoplasme et des organelles (ex. translocation au noyau, recrutement ou dissociation de la membrane). Grâce à cette approche, nous avons pu identifier 2876 protéines associées à la fraction membranaire et 2717 protéines associées à la fraction

cytoplasmique pour un total de 3750 protéines uniques (avec un taux de faux positif inférieur à 1 % [FDR pour *False Discovery Rate*]) (Figure 21A). En analysant la distribution de ces protéines selon le traitement, on remarque que la majorité des protéines ont été identifiées simultanément dans les échantillons WT et KO. Ce fait indique l'importance d'une approche quantitative afin de tirer le maximum d'informations des identifications protéiques. À titre de contrôle de la qualité, une brève analyse a été réalisée pour déterminer l'efficacité du fractionnement cellulaire. Ainsi, la différence entre le pourcentage des protéines associées à diverses localisations cellulaires des échantillons cytoplasmiques et membranaires a été analysée (Figure 21B). On peut conclure que le fractionnement cellulaire fût efficace, puisque les échantillons membranaires présentent un plus haut pourcentage de protéines associées à des compartiments cellulaires membranaires que les échantillons cytoplasmiques.

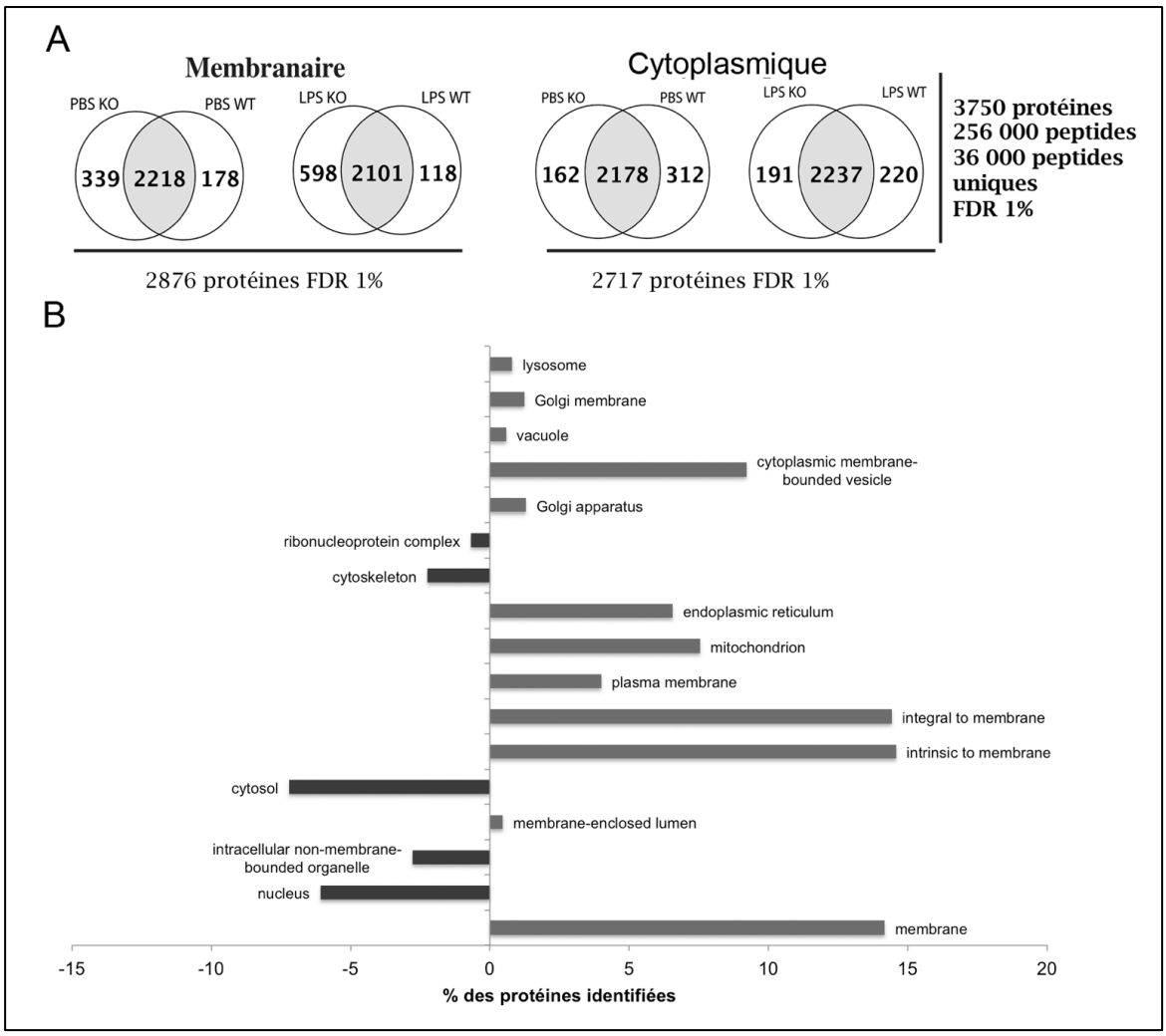

Figure 21 Résultats des identifications Gel LC-MS/MS.

A) Diagrammes de Venn représentant la distribution des différentes protéines identifiées dans les fractions membranaires et cytoplasmiques. L'intersection en gris représente les protéines qui ont pu être quantifiées par compte spectral. Un total de 3750 protéines ont été identifiées avec un FDR (*False Discovery Rate*) inférieur à 1 %. B) Différence du pourcentage de protéines identifiées entre la fraction membranaire (en gris) et la fraction cytoplasmique (en noir) pour différentes localisations cellulaires.

1.2.2.1. Analyse dirigée

Dans un premier temps, une analyse dirigée a été réalisée. Cette analyse consistait à rechercher des voies moléculaires qui pouvaient être associées au phénotype immunitaire observé chez les souris PC1/3 KO. Puisque des termes ontogéniques de la fonction biologique « *LPS response* » étaient associés à plusieurs protéines identifiées, il était de toute évidence d'analyser ce groupe de protéines (Tableau 10). Les résultats de cette analyse indiquent une forte corrélation entre la réponse moléculaire et la réponse physiologique suite à une stimulation au LPS chez les animaux PC1/3 KO. On note d'abord une forte surreprésentation de protéines associées au développement du choc endotoxique et de la réponse inflammatoire. Les facteurs de transduction Stat1, Stat3 et Stat5a sont tous surexprimés dans les extraits KO, que ce soit en présence ou non de LPS, indiquant une forte activité de récepteurs de réponse aux cytokines (Aaronson and Horvath 2002). Quant à elles, les protéines S100a8 et S100a9 sont fortement surexprimées dans les échantillons KO. Ces protéines interagissent pour activer le récepteur du LPS le TLR4 (Ehrchen et al. 2009). Finalement, la protéine Lef1 (*Lymphoid enhancer-binding factor 1*) impliquée dans la différenciation des cellules T en cellules Th1 (Kuo and Leiden 1999) est présente dans les échantillons PC1/3 KO stimulé au LPS, mais n'est pas détectée dans les échantillons LPS WT. De plus, on note aussi la répression de deux protéines impliquées dans l'inhibition de la voie Th1 soit Vsigs4 (*V-set and immunoglobulin domain containing 4*) (Vogt et al. 2006) et la cytokine IL-1α (Helmby and Grencis 2004). Cette forte corrélation entre le phénotype moléculaire et le phénotype physiologique de PC1/3 dans l'immunité innée montre que l'approche protéomique réussit à bien décrire le rôle moléculaire de PC1/3 dans la réponse au LPS.

Tableau 10 Protéines associées à la réponse au LPS.

Fraction	Symbole	Fold PBS	Fold LPS	Fonction
Membranaire	S100a8	+	-2	Développement du choc endotoxique au LPS
Cytoplasmique		64	3	
Membranaire	S100a9	7	1	
Cytoplasmique		20	2	
Membranaire	Stat1	3	4	Traduction du signal et activateur de la voie Interféron
Cytoplasmique		2	2	
Membranaire	Stat3	3	1	Réponse en phase aigue
Membranaire	Stat5a	1	+	Régulation positive de la réponse inflammatoire
Cytoplasmique	Vsig4	-	-	Puissant régulateur négatif de la prolifération des cellules T et de la production d'Il-12
Membranaire	Lef1	1	+	Différentiation des cellules Th1
Cytoplasmique	Il1a	1	-2	Développement de la réponse Th2

Liste de protéines ayant une expression différentielle ou un changement d'expression qui sont associées au terme GO : LPS response. Les niveaux d'expression (*Fold*) sont relatifs au contrôle WT. Les symboles + et – signifient une expression différentielle KO ou WT respectivement.

1.2.2.2. Analyse non dirigée

Afin de découvrir des voies cellulaires affectées par le KO de PC1/3 dans la réponse immunitaire, une analyse non dirigée a été effectuée. Cette analyse consiste en un test d'enrichissement ontogénique entre une liste de protéines à tester et une liste de protéines contrôles. Ainsi, la liste de toutes les protéines surexprimées dans les échantillons membranaires KO, peu importe le traitement, a été comparée à la liste de toutes les protéines identifiées dans les échantillons membranaire. Ce test a comme but d'évaluer les termes ontogéniques qui se trouvent surreprésentés statistiquement dans la liste de protéines d'intérêts. Ainsi, les termes représentant les fonctions des protéines surexprimées dans les échantillons KO ont pu être dressés avec un taux de faux positif inférieur à 0,1 % (FDR<0,1 %) (Figure 22). Parmi les fonctions surreprésentées se trouve un fort pourcentage de protéines impliquées dans la régulation de la transcription. Ce fait n'est pas étonnant étant donné l'ampleur du phénotype physiologique observé chez les souris PC1/3 KO stimulées au LPS. Toutefois, un grand nombre de protéines ayant des activités GTPase semblaient être affectées par le KO de PC1/3, comme en témoigne la surreprésentation de cinq termes ontogéniques reliés au GTPase. La liste des protéines ayant une activité GTPase a donc été extraite et le réseau d'interactions biologiques de ces protéines a été retiré de la base de données STRING (Szklarczyk et al. 2011). Ce réseau a par la suite été analysé à l'aide de l'outil de visualisation Cytoscape (Smoot et al. 2011) et l'outil d'analyse intégré ReactomeFI qui permet de sélectionner des sous-réseaux ayant des fonctions ontogéniques précises (Figure 23). Le réseau d'interaction biologique des protéines GTPase comprenait 202 protéines (identifiées par leur nom génique officiel) qui ont été représentées avec un code couleur (vert pour surexprimée, rouge pour réprimée) représentant leur niveau d'expression relative (KO vs WT) selon le traitement (centre du cercle non traité, contour traité LPS). Parmi les groupes de protéines ayant des fonctions ontogéniques particulières figuraient deux groupes qui affichaient plusieurs membres surexprimés dans les échantillons KO.

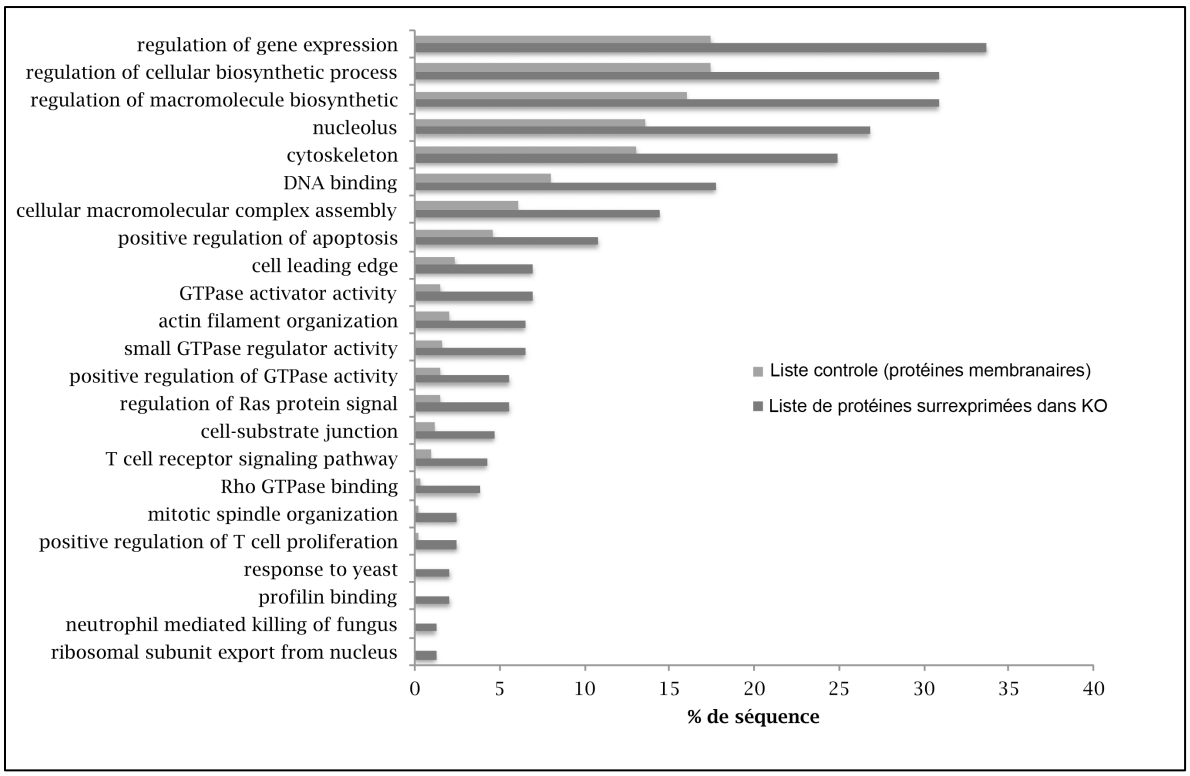

Figure 22 Termes ontogéniques surreprésentés KO vs WT membranaire.

Résultats de l'analyse d'enrichissement des termes ontogéniques en qui compare les protéines membranaires surexprimées dans les échantillons KO par rapport à toutes les protéines membranaires identifiées. Les termes ontogéniques présentés ont été identifiés comme étant surreprésentés avec un FDR de 0,1 %. On note une forte représentation de protéines associées aux GTPase.

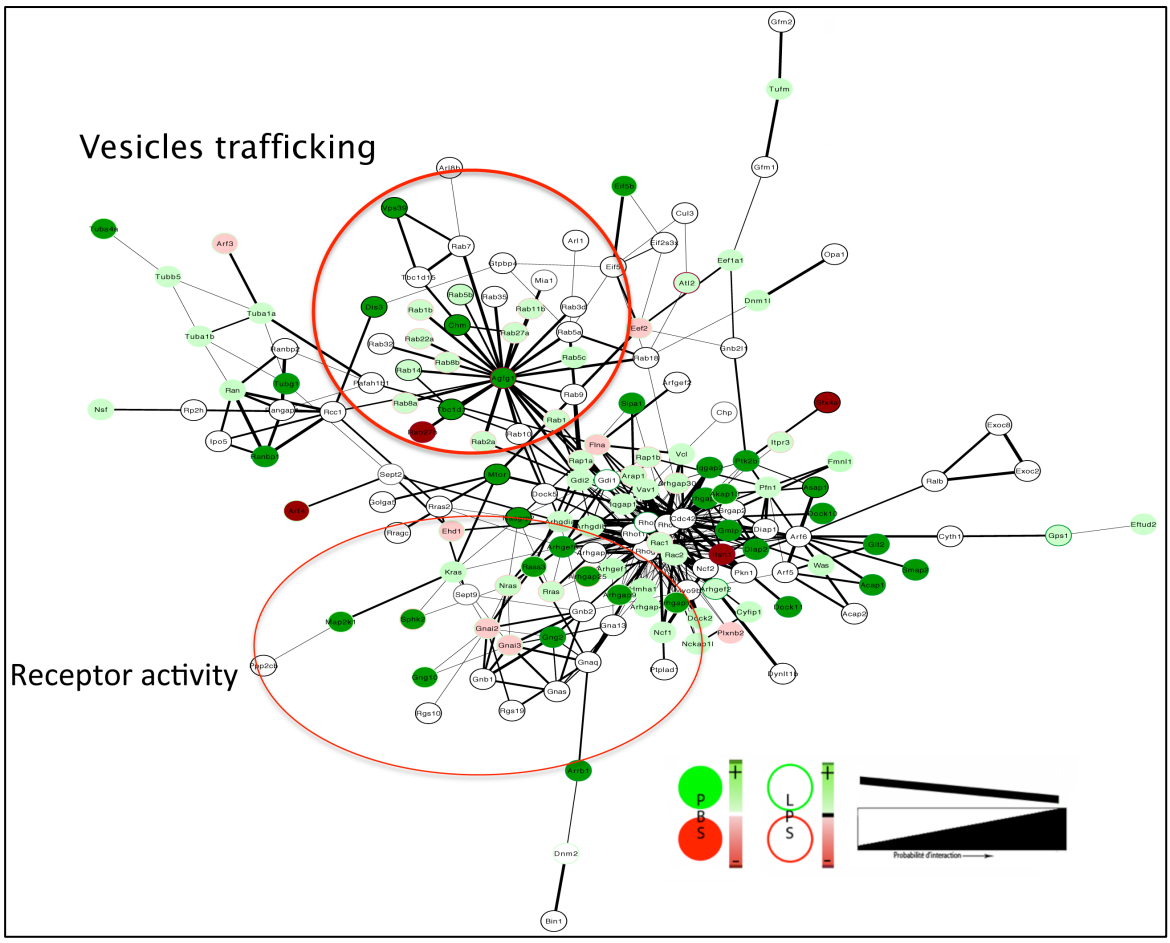

Figure 23 Réseau d'interaction des 202 protéines identifiées qui ont une activité GTPase.

Représentation des interactions extraites de la base de données STRING des 202 protéines associées à l'activité GTPase. La couleur du nœud représente le niveau d'expression KO vs WT non stimulé (PBS), la couleur de la bordure du nœud représente le niveau d'expression KO vs WT stimulé (LPS) et l'épaisseur du trait reliant les nœuds représente la probabilité d'interaction entre les protéines. Deux régions encerclées en rouge indiquent les protéines reliées à une activité biologique associée aux termes ontogéniques « *Receptor activity* » et « *Vesicles trafficking* » (VT).

Le premier groupe consistait en une liste de GTPase impliquées dans la traduction des signaux réceptoriels au sein des cascades signalétiques. D'une part, la voie de signalisation RAS dont les membres identifiés, KRAS, RRAS, NRAS, SphK2, Rasgrp2, RAP1, mTOR, Map2k1, sont pour la plupart surexprimés dans les fractions membranaires PC1/3 KO stimulé ou non. Ce résultat indique une activité accrue de récepteur de type tyrosine kinase. Ces récepteurs sont connus pour induire la réponse de facteurs de croissances et d'hormones, mais aussi de cytokines (Robinson et al. 2000). De l'autre part, la voie de signalisation Gα(i), associée à l'activité des récepteurs couplés aux protéines G (GPCR), semblait affectée. Principalement GNAI2 et GNAI3, qui désigne les protéines Gα(i)2 et 3, affichent une sous-expression dans les échantillons PC1/3 KO non stimulé et une surexpression lorsque stimulé au LPS, indiquant une dérégulation complète de cette voie. Celle-ci est particulièrement intéressante, car elle est responsable de la propagation des signaux induits par plusieurs neuropeptides maturés par PC1/3 (McDonald 2005; Cooray and Clark 2011). Ainsi, une partie du phénotype immunitaire de PC1/3 dans les macrophages pourrait être relié à une activité réceptorielle par la maturation de substrats.

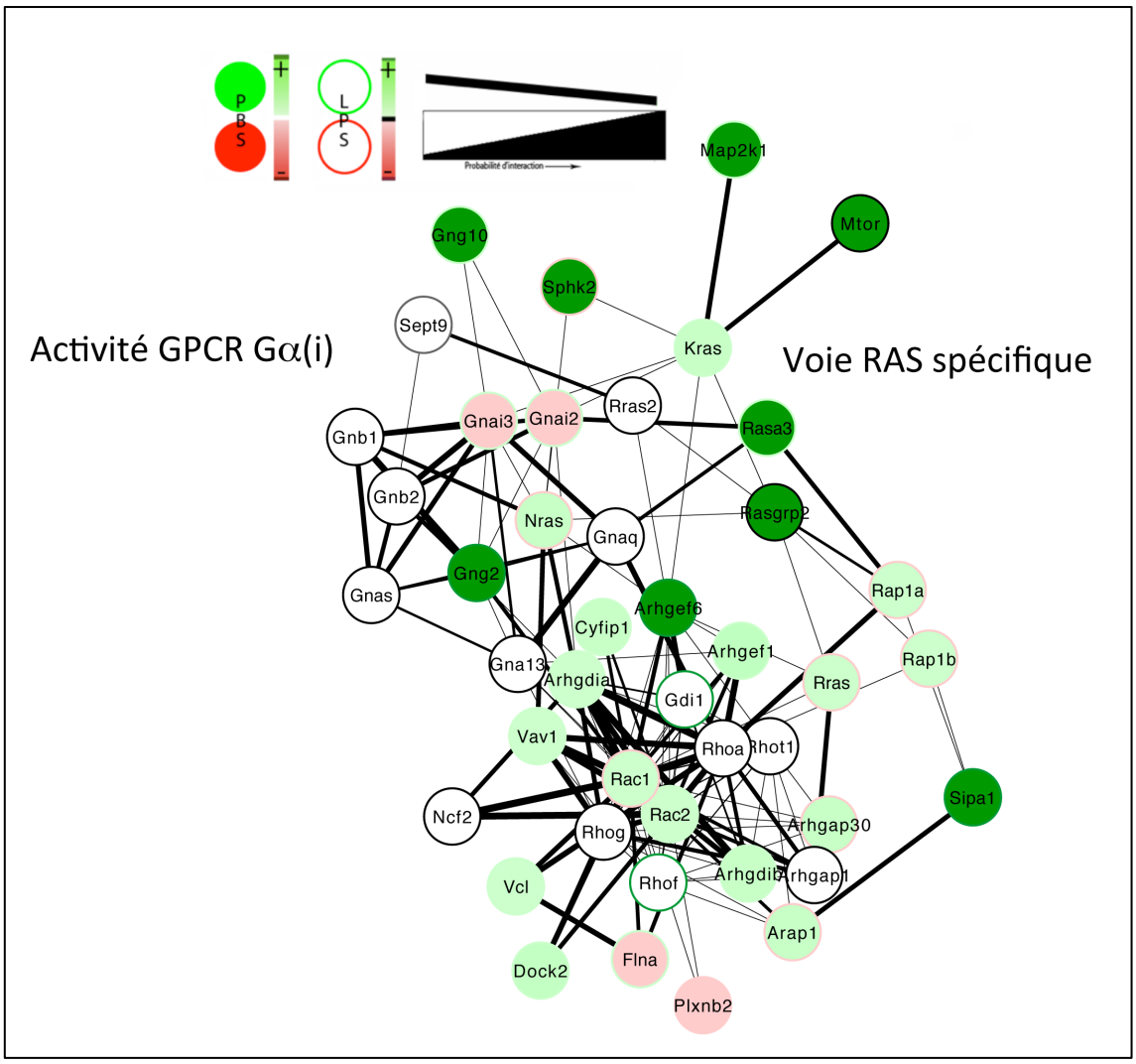

Figure 24 Réseau des protéines GTPase associées à une activité réceptorielle.

Agrandissement de la région associée à l'activité réceptorielle. On peut voir des protéines effectrices de la voie de signalisation RAS associée au récepteur tyrosine kinase (KRAS, RRAS, NRAS, SphK2, Rasgrp2, RAP1, mTOR, Map2k1) et de la voie Gα(i) associé à l'activité GPCR (GNAI2, GNAI3, GNG2, GNG10). Chaque protéine est nommée par son nom génique officiel (*Gene name*).

Le deuxième groupe de GTPase étaient celles responsables de la régulation du trafic intracellulaire. Ce réseau comprend principalement des petites protéines G Rab et des protéines responsables de leurs régulations (Figure 25). Au centre du réseau, la protéine Agfg1 (Arf-GAP domain and FG repeats-containing protein 1) qui à un rôle important dans l'endocytose (Doria et al. 1999; Chaineau et al. 2008). Au pourtour de cette protéine, plusieurs Rab affichent un profile d'expression similaire soit : surexprimées dans l'échantillon KO non stimulé et sous-exprimées lorsque stimulée au LPS. Ces Rab (Rab8, Rab11, Rab14 et Rab27) ont toutes une fonction commune qui est l'exocytose et la sécrétion (Hutagalung and Novick 2011). Cette perturbation moléculaire des voies de sécrétion corrèle avec la sécrétion de cytokine dérégulée, ainsi qu'avec la désorganisation intracellulaire observée chez les macrophages de souris PC1/3 KO et dans le modèle de macrophage NR8383 où PC1/3 est réprimé par shRNA, tel que présentées au Chapitre 3 - Disruption of PC1/3 expression in mice causes innate immune defects and uncontrolled cytokine secretion et au Chapitre 4 - Proprotein convertase 1/3 (PC1/3) in the rat alveolar macrophage cell line NR8383: localization, trafficking and effects on cytokine secretion.

Cette approche d'analyse par bio-informatique s'est donc avérée efficace pour faire le lien entre le phénotype physiologique et moléculaire de la répression de PC1/3 dans les macrophages. La méthodologie a d'ailleurs été appliquée pour analyser des tissus de patientes atteintes du cancer de l'ovaire, afin de décrire des marqueurs protéiques expliquant la progression tumorale, présentée au Chapitre 5 - Proteomic analyses of serous and endometrioid epithelial ovarian cancers: cases studies: molecular insights of a possible histological etiology of serous ovarian cancer.

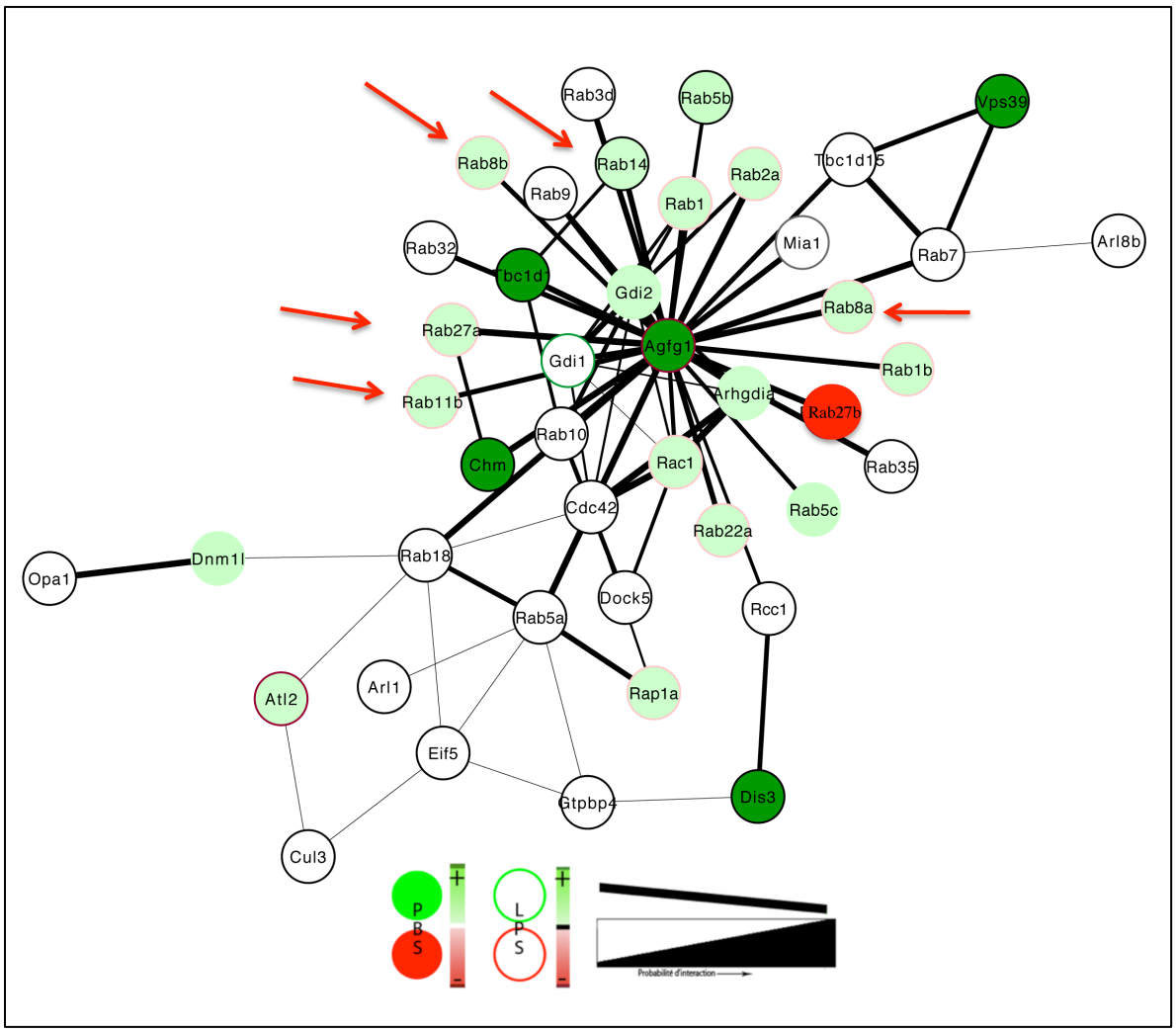

Figure 25 Réseau des protéines GTPase associées au trafic vésiculaire.

Agrandissement de la région associée au trafic vésiculaire. Les flèches indiquent une série de protéines Rab impliquées dans la régulation de la sécrétion. Chaque protéine est nommée par son nom génique officiel (*Gene name*).

CHAPITRE 3 - DISRUPTION OF PC1/3 EXPRESSION IN MICE CAUSES INNATE IMMUNE DEFECTS AND UNCONTROLLED CYTOKINE SECRETION

Auteurs de l'article: Sarah Refaie[#], Sandra Gagnon[#], Hugo Gagnon, Roxane Desjardins, François D'Anjou, Pedro D'Orléans-Juste, Xiaorong Zhu, Donald F. Steiner, Nabil G. Seidah, Claude Lazure, Michel Salzet and Robert Day

[#]Co-auteures

Statut de l'article : publié dans Journal of Biological Chemistry, 287(18), 2012, 14703–14717

Avant-propos : J'ai participé à l'analyse et à la réalisation des figures 1, 10, S1B, S2 à S5. J'ai fait et analysé les figures 5 B, C, et 8. J'ai écrit les parties expérimentales, les résultats et la discussion correspondante à ces résultats.

Résumé : La proprotéine convertase 1/3 (PC1/3) est exprimée dans la voie de sécrétion régulée des cellules neurales et endocrines. Sa fonction principale est la maturation post-traductionnelle menant à l'activation de précurseurs protéiques. Auparavant, des études de tissus neuroendocriniens du modèle de souris PC1/3 KO (KO) ont permis d'élucider ses fonctions physiologiques. Toutefois, PC1/3 est également exprimée dans les cellules du système immunitaire, principalement dans les macrophages. La présente étude explore les effets d'un stimulus de l'immunité innée, le lipopolysaccharide (LPS), chez la souris PC1/3 KO. Ces souris présentent une hypertrophie de la rate et une désorganisation marquée de la zone marginale et de la pulpe rouge. Des études immunohistochimiques utilisant différents marqueurs montrent une déplétion des cellules dendritiques dans la rate PC1/3 KO. Lorsque soumises au LPS, les souris PC1/3 KO sont plus sensibles que les souris contrôles (et que d'autres souris PC KO [PC2 et PC7]) à un choc septique. Ce choc septique s'accompagne d'une augmentation significative des taux plasmatiques des cytokines pro-inflammatoires (IL-6, IL-1β, le TNF-α) chez les souris KO PC1/3, ce qui concorde avec la thèse d'une hypercytokinémie caractérisée par une importante réponse inflammatoire non contrôlée et systémique. À l'appui, le LPS induit préférentiellement la voie pro-

inflammatoire Th1 chez les souris PC1/3 KO. Lorsque traités avec du LPS, les macrophages péritonéaux isolés de souris PC1/3 KO démontrent également une sécrétion élevée de cytokines. Des micrographies électroniques de ces macrophages montrent des caractéristiques morphologiques qui indiquent une activation prolongée de ces cellules après stimulation par le LPS. Nous concluons qu'outre son rôle important dans les fonctions neuroendocriniennes, PC1/3 est importante dans la régulation du système immunitaire inné, et ce très probablement par la régulation de la sécrétion de cytokines chez les macrophages.

Disruption of PC1/3 expression in mice causes innate immune defects and uncontrolled cytokine secretion*

Sarah Refaie[¶1], Sandra Gagnon[¶1], Hugo Gagnon[1, 4], Roxane Desjardins[1], François D'Anjou[1], Pedro D'Orléans-Juste[1], Xiaorong Zhu[2], Donald F. Steiner[2], Nabil G. Seidah[3], Claude Lazure[3], Michel Salzet[4] and Robert Day[1, 5]

[1]Institut de pharmacologie de Sherbrooke, Université de Sherbrooke, Sherbrooke, Québec, J1H 5N4, Canada, [2]Department of Medicine, University of Chicago, Chicago, Illinois 60637, USA, [3]Institut de Recherches Cliniques de Montréal (IRCM), Montreal, Quebec H2W 1R7, Canada, [4]Université Lille Nord de France, Laboratoire de Spectrométrie de Masse Biologique Fondamentale et Appliquée, EA 4550, Université Lille 1, Villeneuve d'Ascq, France.

Running Title : *Innate immunity and PC1/3**

[¶]Equal contributing authors

To whom correspondence should be addressed: Robert Day, PhD Institut de pharmacologie de Sherbrooke (IPS), Faculté de Médecine et des Sciences de la Santé (FMSS), Université de Sherbrooke 3001, 12[e] Ave. Nord Sherbrooke, Québec J1H 5N4, Canada, Telephone: (819) 564-5428, Fax: (819) 820-6886, E-mail: Robert.day@usherbrooke.ca

Keywords: proprotein convertase, innate immunity, macrophage, spleen, pro-inflammatory cytokine, secretion, Toll-like receptor, lipopolysaccharide.

Background: PC1/3 is known for its role in neuroendocrine cells but not for its potential role in innate immunity.

Results: PC1/3 knockout mice express a dysfunctional phenotype when challenged with lipopolysaccaride, characterized by uncontrolled cytokine secretion.

Conclusion: PC1/3 regulates cytokine secretion in macrophages.

Significance: Identifying the role PC1/3 function in macrophages will lead us to a better

understanding of cytokine regulation and innate immunity.

SUMMARY

The proprotein convertase 1/3 (PC1/3) is expressed in the regulated secretory pathway of neural and endocrine cells. Its major function is in the post-translational processing and activation of precursor proteins. The PC1/3 knockout (KO) mouse model has allowed us to elucidate its physiological functions in studies focused primarily on neuroendocrine tissues. However, PC1/3 is also expressed in cells of the immune system, mainly in macrophages. The present study explores the effects of innate immune challenge in the PC1/3 KO mouse. PC1/3 KO mice have an enlarged spleen, with marked disorganization of the marginal zone and red pulp. Immunohistochemical studies using various markers, demonstrate a depletion of dendritic cells in PC1/3 KO spleens. When challenged with lipopolysaccharide, PC1/3 KO mice are more susceptible to septic shock than wild-type controls or other PC KO mice, such as PC2 and PC7 nulls. Plasma levels of pro-inflammatory cytokines (IL-6, IL-1β, TNF-α) were very significantly elevated in PC1/3 KO mice, consistent with a hypercytokinemia, i.e. indicative of a major systemic uncontrolled inflammatory response or cytokine storm. Peritoneal macrophages isolated from PC1/3 KO mice also demonstrate elevated cytokine secretion when treated with LPS. Electron micrographs show morphological features indicating a prolonged activation of these cells following LPS stimulation. We also present evidence that the pro-inflammatory T_h1 pathway is dominant in the PC1/3 KO mouse model. We conclude that aside from its important role in neuroendocrine functions, PC1/3 also has an important role in the regulation of the innate immune system, most likely through the regulation of cytokine secretion in macrophages.

Proprotein convertases (PCs)[6] are a family of enzymes whose main function is the first step of an enzymatic cascade that includes the endoproteolytic cleavage of inactive precursor proteins and the subsequent processing into bioactive proteins and peptides by carboxypeptidases and amidating enzymes (1,2). The PCs form a family of subtilisin-like serine proteinases encoded by 9 genes *PCSK1* to *PCSK9* (PC substilisin/kexin), coding for PC1/3, PC2, furin, PC4, PC5/6, PACE4, PC7, SKI-1/S1P and PCSK9, respectively (3-7).

Seven PCs cleave secretory precursors at single or paired basic amino acids within recognized cleavage site R-X-R/K-R↓ (3), while SKI-1/S1P does not require a basic amino acid at the cleavage site. As for PCSK9, it functions only as a binding protein targeting for degradation in lysosomes, among others, the low-density lipoprotein receptor. PC cleavages result in a diversity of bioactive products, zymogen activation and sometimes inactivation of key proteins (4).

Some PCs are expressed ubiquitously in the organism, such as furin (8,9), or are widespread like PC5/6 and PC7, while others are more organ- or system-specific (10). For example, PC1/3 has been associated with the neuroendocrine system where its expression was first reported (11-13). However, few studies have identified an atypical expression of PC1/3 in cells of the immune system, namely PC1/3 has been detected in a human monocyte-derived macrophage cell line (14), differentiated macrophages (15) and in immune organs such as the spleen, thymus or lymphatic ganglia (16).

In a previous study, we showed that both neuroendocrine-"specific" convertases, namely PC2 and PC1/3, are also expressed in macrophages and lymphocytes *in vivo* (16) and are highly responsive to pathogen-associated molecular patterns (PAMP) challenge. We also showed a coordinated induction of pro-enkephalin (pro-Enk; a PC1/3 and PC2 substrate), PC1/3 and PC2 mRNAs, as well as pro-Enk derived peptides (i.e., enkelytin) in macrophage subpopulations (17,18). While these data support the notion of a neuroendocrine phenotypic plasticity in immune cells (19), they show that their expression is regulated by challenges (e.g. PAMPs) that activate the innate immune system, suggesting a role in innate immunity. Macrophages are crucial in the innate immune system and their activation is mediated via recognition of various PAMPs by specific toll-like receptors (TLR) (20). TLR4, for example, binds and recognizes lipopolysaccharides (LPS) to initiate an immune reaction, including cytokine secretion (21,22). Communication with the acquired immune system is also essential to control the immune response. This is commonly accomplished by activating and recruiting T helper cells (T_h) that can differentiate into T_h1 or T_h2 cells to further activate or attenuate, respectively, the immune response (23,24). Specific cytokine profiles are observed for either the T_h1 cytotoxic pathway, such as IL-12 and IFNγ (25,26), or the T_h2 humoral pathway in which IL-10, IL-4 or IL-5 are secreted (27).

We previously also noted that PC1/3 expression in the spleen (16), was mostly confined to the red pulp regions known to be rich in macrophages (28), and was increased after LPS stimulation. Co-localization of PC1/3 with CD14, a macrophage marker (29), sparked our interest in investigating the role of PC1/3 in macrophages in order to elucidate the function of PC1/3 in the innate immune system. Disruption of the gene-encoding PC1/3 has revealed a phenotype associated with postnatal growth impairment and multiple defects in the processing of neuroendocrine peptide precursors, including hypothalamic growth hormone-releasing hormone (GHRH), pituitary proopiomelanocortin to adrenocorticotropic hormone, islet proinsulin to insulin and intestinal proglucagon to glucagon-like peptide-1 and -2 (30-34). However, in the present study, we hypothesized that an immune phenotype might become more evident in PC1/3 KO mice if they were submitted to a challenge, such as with LPS, which triggers a cascade of events subsequent to the stimulation of TLR4 receptors. Indeed we uncovered a massive cytokine response, which is highly lethal due to a lack of regulation of cytokines secretion *in vivo*. We also demonstrate that the T_h1 pathway, indicative of a pro-inflammatory response, is enhanced in PC1/3 KO mice. Our data thus suggest that PC1/3 plays a vital role in the secretory response of macrophages to pathogen challenge.

EXPERIMENTAL PROCEDURES

Mice experimental models - Transgenic PC1/3, PC2 and PC7 KO as well as wild type (WT) mice used in this study were between 3 and 6 months of age. The mice were held in a pathogen-free environment and were given food and water *ad libitum*. PC1/3 KO and PC2 KO mice have been described (30). PC1/3 KO mice were generated by the deletion of exon 1 and several upstream transcriptional control elements of the *PCSK1* gene, by inserting a neomycin cassette in C57Bl/6 mice background as previously described (30). PC2 KO mice have a mutation in the third exon of the *PCSK2* gene, which leads to the synthesis of a defective enzyme that is subsequently degraded (35). PC7 KO mice were generated by deleting the exons 3 to 7 of the *PCSK7* gene, which yields a protein containing an inactive catalytic site (36). PC1/3, PC2 and PC7 KO mice backgrounds were changed from C57Bl/6 to CD1, with over 20 backcrosses each. All experimental procedures were in accordance with the Canadian Council on Animal Care (CCAC).

Spleen characterization and immunohistochemical staining - WT and PC1/3 KO mice were euthanized by cervical dislocation. Spleens were extracted and weighed. Standard preparation procedure of paraffin-embeded tissues and H&E stain were used. Immunostaining was done with the Dako Autostainer Plus (Dako, Burlington, ON, CAN) using primary antibodies directed against CD3, CD4, CD7, CD15, CD20, CD21, CD22, CD56, CD57, CD68 and IgM (Dako, Burlington, ON, CAN) according to manufacturer's instructions. A secondary antibody coupled to HRP (Dako, Burlington, ON, CAN) was then applied followed by a Harris Hematoxylin counterstain according to manufacturer's specifications. Immunostained spleens were examined using the Axioskop 2 phase-contrast microscope (Carl Zeiss, Inc., Thornwood, NY). Photomicrographs of 1392 x 1040 pixels were captured using 10x or 40x objective and Retiga SRV cooled color digital camera (Qimaging, Burnaby, BC, CAN). The images were processed using Image Pro software (Media Cybernetics, Silver Springs, MD).

Endotoxin shock and determination of plasma cytokine content following LPS in vivo challenge - Mice were injected with *Escherichia coli* 0127:B8 lipopolysaccharide (LPS) (Sigma-Aldrich, St-Louis, MO) at a LD_{100} of 25 mg/kg (*i.p*). Mice were monitored on a 3-day period to observe survival rates. Time course experiments were also performed by injecting 100 μg of LPS *i.p.* into mice for 0, 4, 8 and 24 hours. For plasma cytokine content, blood was collected by cardiac puncture and plasma was isolated by centrifugation. Cytokines were dosed using an ELISA kit (R&D Systems, Minneapolis, MN), specific for mouse IL-6, TNF-α, IL-1β, IL-12p70, IL-10 and IFN-γ. Statistical analysis was performed by applying the t-test parameters (Prism 5, GraphPad software, La Jolla, CA, USA).

Determination of cytokine secretion and cellular content of primary peritoneal macrophages - Mice were injected *i.p.* with 2 mL of sterile 3 % thioglycolate (BD, Sparks, MD) to increase the yield of peritoneal macrophages. Three days later, mice were anesthetized with ketamine/xylazine (87/13 mg/kg; *i.m.*) and then sacrificed by cervical dislocation. Peritoneal cells were collected by peritoneal wash with a phosphate-buffered saline solution (PBS). Red blood cells were lysed by incubating the cells with an hemolysis buffer. Cells were plated in a 6 or 24 well-plate, at 8×10^5 or 2.4×10^6 cells respectively,

for 24 hours at 37°C in humidified atmosphere of 5 % CO_2 in air to allow macrophage adherence, which purifies the peritoneal exudates. The cell medium consisted of RPMI 1640 and penicillin/streptomycin. The following day, the medium was changed and cells were stimulated with PBS 1X or 100ng/mL LPS without serum for 4 hours. Medium was collected and cell lysate was obtained by adding 200 μL of 0.5 N HCl, followed by three freeze-thaw cycles. Protein contents were collected by centrifugation and cytokines were dosed using ELISA kits specific for mouse IL-6, TNF-α and IL-1β as indicated by manufacturer's instructions (R&D Systems, Minneapolis, MN). Statistical analysis was done using a Student t-test algorithm in Prism 5 GraphPad software (La Jolla, CA), which calculated the standard error of the mean (SEM).

Measurement of the arterial blood pressure in mice - Mice were anesthetized with ketamine/xylazine (87/13 mg/kg; *i.m.*). A polyethylene catheter (PE-10) containing a heparin/saline solution was inserted into the common right carotid artery to monitor the arterial blood pressure via transducer linked to a polygraph (Grass instrument company, Baintree, MA). Another catheter (PE-10) was inserted into the left jugular vein to inject LPS at a dose of 2.2 mg/kg.

RNA extraction, Reverse Transcription, Quantitative PCR and PC1/3 sequencing - The RNA of peritoneal macrophages and tissues was extracted with Trizol (Gibco BRL, Burlington, On, CAN) reagent and chloroform. The reverse transcription and quantitative PCR procedure was previously described (37). ProSAAS primers were previously described (38). For PC1/3 cDNA sequencing, the same procedure was used except that the PCR was done with 1 unit of Taq DNA polymerase (Roche Diagnostics, Mannheim, Germany). The resulting cDNA was next cloned in pGEM-T-Easy vector (Promega, Madison, WI) according to the manufacturer's instructions for sequencing. The sequence of the primers used for the PCR reaction was as follows: mIL-6 forward 5'- ACA AGT CGG AGG CTT AAT TAC ACA T -3', reverse 5'- AAT CAG AAT TGC CAT TGC ACA A -3'; mIL-1β forward 5'- GAG AAT GAC CTG TTC TTT GAA GTT GA -3', reverse 5'- TGA AGC TGG ATG CTC TCA TCT G -3'; mTNF-α forward 5'- CGT GGA ACT GGC AGA AGA G -3', reverse 5'- ACA AGC AGG AAT GAG AAG AGG -3'; mPC1/3 91 bp

forward 5'- ATT TTG GTG CTG CTG CTC TT -3', 91 bp reverse 5'- GGA GTG CTC GTC TCA ACC A -3', 252 bp forward 5'- AGC AAA GAG GTT GGA CTC TGC-3', 252 bp reverse 5'- TAT GAA GAG CGC TTC TTC GGG -3', mActin forward 5'- GGG AAA TCG TGC GTG ACA TCA AAG -3', reverse 5'- CAT ACC CAA GAA GGA AGG CTG GAA -3'.

Transmission electron microscopy (TEM) of peritoneal macrophages - Peritoneal macrophages were collected as described above and directly subjected to TEM procedure previously described (39). All images were taken at 60 kV and 3 000X direct magnification. Images were analyzed with ImageJ software (http://rsbweb.nih.gov/). Four different observers, among which three counted the images blindly, analyzed all structural features. An equal variance bilateral Student T-test was performed for statistical analysis.

Western Blotting of PC1/3 – Pituitary glands from WT and KO mice were collected and disrupted in RIPA lysis buffer containing complete mini protease inhibitor (Roche Diagnostics, Mannheim, Germany). Mouse peritoneal macrophages were collected and cultured at 4 x 10^7 cells as described above. The cells were lysed with 500 µL of RIPA lysis buffer containing complete mini protease inhibitor. Equal amount of protein were subjected to 8.5% SDS-PAGE and transferred to nitrocellulose Amersham Hybond ECL (GE Healthcare, Baie d'Urfe, Qc, CAN). The antibody direct against the C-terminal of PC1/3 (#9212) was previously described (40). PC1/3 was reveled by a goat anti-rabbit IgGs coupled to IRdye 800 (Licor Bioscience, Lincoln, NE) with an infrared LICOR Odyssey Imager (Licor Bioscience, Lincoln, NE).

Gel LC-MS/MS identification of PC1/3 - Membrane protein fraction of macrophages was prepared as previously described (41). Briefly, cells were lysed and centrifuged at 16,000xg to pellet membrane proteins. Proteins were solubilized and recovered by standard acetone:methanol precipitation. 20 µg of reconstituted protein were next separated on a pre-cast gradient acrylamide gel 4-12% using freshly made MES buffer according to the manufacturer's protocol. The gel was stained with a MS compatible silverstain (Invitrogen, Carlsbad, CA). The entire gel lane was excised into 18 bands and each band was cut in 1-

mm3 pieces. The in-gel digestion protocol is based on the results obtained by Havlis et al. (42). Briefly, gel pieces were destained, proteins were reduced (10 mM DTT, 100 mM ammonium bicarbonate) and alkylated (55 mM iodoacetamide, 100 mM ammonium bicarbonate) and finally digested with 6ng/ml sequencing grade trypsin (Promega, Madison, WI). The resulting tryptic peptides were purified and identified by reverse phase LC coupled to a LTQ-Orbitrap (ThermoElectron) Protein identification was done with Scaffold V3.1.2 (Proteome Software Inc., Portland, OR) to validate MS/MS based peptide and protein identifications from Mascot V 2.1 (Matrix Science, London, UK) and X! Tandem version 2007.01.01.1 (The GPM, thegpm.org).

RESULTS

Splenic abnormalities in PC1/3 KO mice-Splenomegaly was observed in the PC1/3 KO mice, as shown in Figure 26 (A-B), which was evident by comparing the weight of the spleens (~1.8 fold increase). An HE stain was performed on cross-sections of the spleen to visualize its organizational structure. The staining allows the distinction of red (RP) and white pulp (WP) of the spleen. In PC1/3 KO spleens, the white pulp was more concentrated in the middle of the spleen with apparent fusion of white pulp nodes, which was not observed in WT mice. Some white pulp nodes were observed forming in the periphery of the PC1/3 KO spleen. The marginal zone (MZ), an important area of communication between macrophages and T cells (43,44), shows an abnormal structure and blends with the red pulp in PC1/3 KO mice (Figure 26D-G). This spleen disorganization is also characterized by an increase presence of lymphocytes, represented as small blue cells, in the red pulp of PC1/3 KO spleen. Since, the spleen is an important immune organ that monitors the circulating blood for infections, especially polysaccharide encapsulated bacteria (45) and it requires the proper function of antigen presenting cells (APC) such as macrophages, dendritic cells (DC) and B cells. We also conducted a RT-PCR experiment to confirm PC1/3 expression in spleen as well as its known binding protein proSAAS (Figure 26 **C**). The observation of a structural disorganization in the PC1/3 KO spleen led us to further investigate the role of PC1/3 in the innate immunity using LPS challenge.

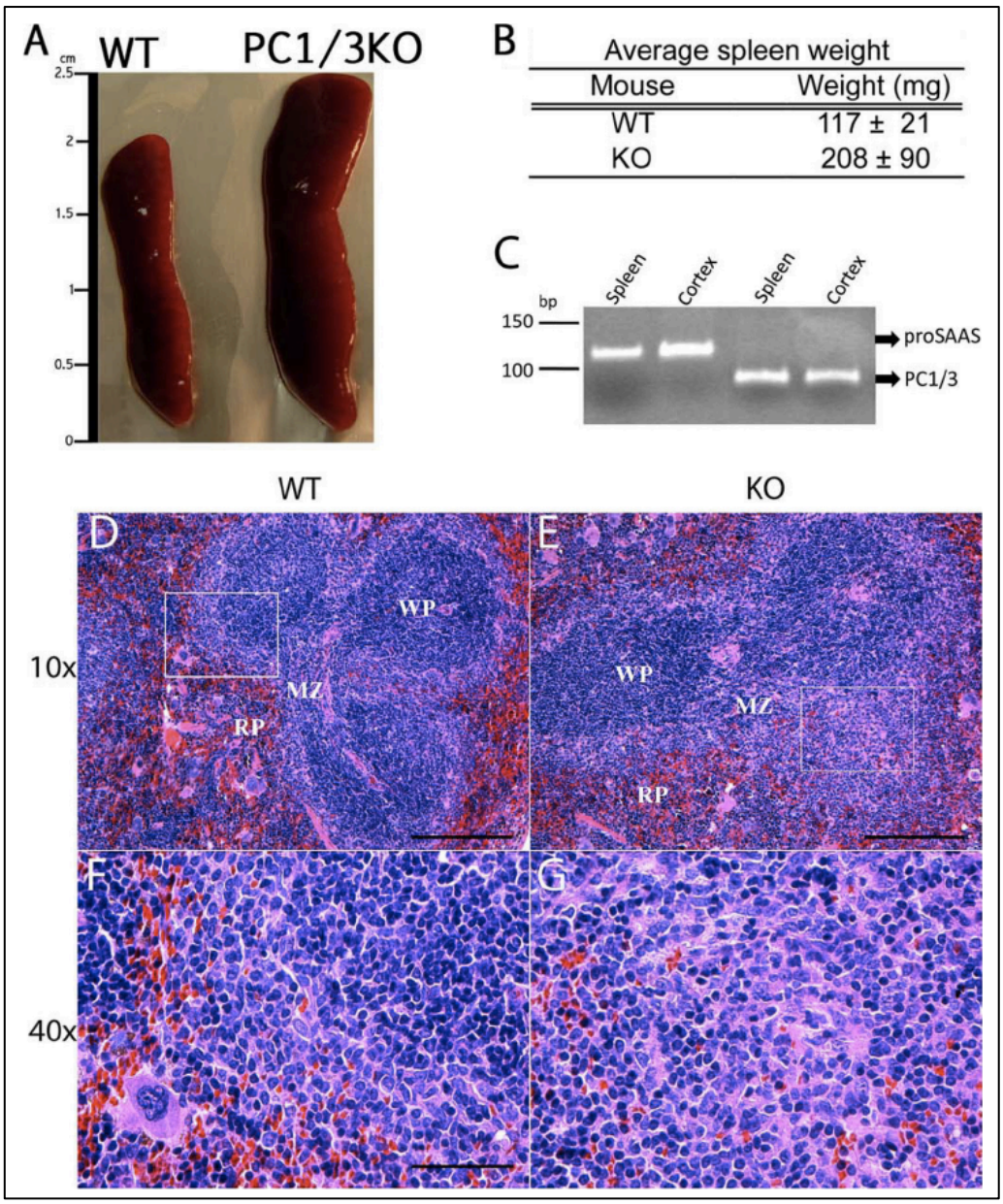

Figure 26 WT and PC1/3 KO mouse spleen characterization and comparison.

A. Relative size of PC1/3 KO (Right) mouse spleen compared to WT (left). B. Average spleen weight from WT and PC1/3 KO mice. Data represent mean ± SD (p-value<0.05; N=7). C. RT-PCR product was obtained using RNA extract from WT mouse spleen and cortex (positive control) and then migrated on 10% acrylamide gel stained with ethidium bromide. 119 bp and a 91 bp fragments were observed correlating with the expected length for proSAAS and PC1/3 respectively. D-G. Hematoxylin and eosin staining of a cross-section of WT (C-E) and PC1/3 KO (D-F) mouse spleen. A magnification at 40x (E-F) represents the framed region shown in the 10x magnification (C-D) of the respective spleen. Spleen regions are indicated including the red pulp (RP), white pulp (WP), marginal zone (MZ).

PC1/3 KO mice are more susceptible to septic shock provoked by LPS - Septic shock is induced by an exaggerated immune response to an infection characterized by an uncontrolled secretion of pro-inflammatory cytokines. During gram-negative bacterial infection, in most cases the initiator of this response is LPS, first recognized by innate immune mediators (i.e., macrophages) via the TLR4 (46). To study the role of PC1/3 in the innate immune system, a sepsis model was used to examine the survival rates of PC1/3 KO mice under endotoxemic conditions. The model consisted of injecting a lethal dose (LD_{100}) of LPS and monitoring the survival rates for 3 days. In the case of WT mice, 50% of the mice were deceased between 24 and 30 hours following LPS treatment and most WT mice did not survive after 72 hours (Figure 27 A). In contrast all the PC1/3 KO mice were deceased 24 hours post-LPS treatment (Figure 27 A).

In order to verify whether this phenotype was shared amongst other PCs, we carried out a similar analysis using available PC2 and PC7 null mice. We observed similar patterns of survival rates in PC2 and PC7 KO mice compared to their associated WT mice in this sepsis model (Figure 27 C). These results indicate that PC1/3 KO mice are more susceptible to septic shock when administered a lethal dose of LPS as compared to WT or even other PC null mice models. Therefore, PC1/3 seems to provide an important protective role during LPS-induced sepsis.

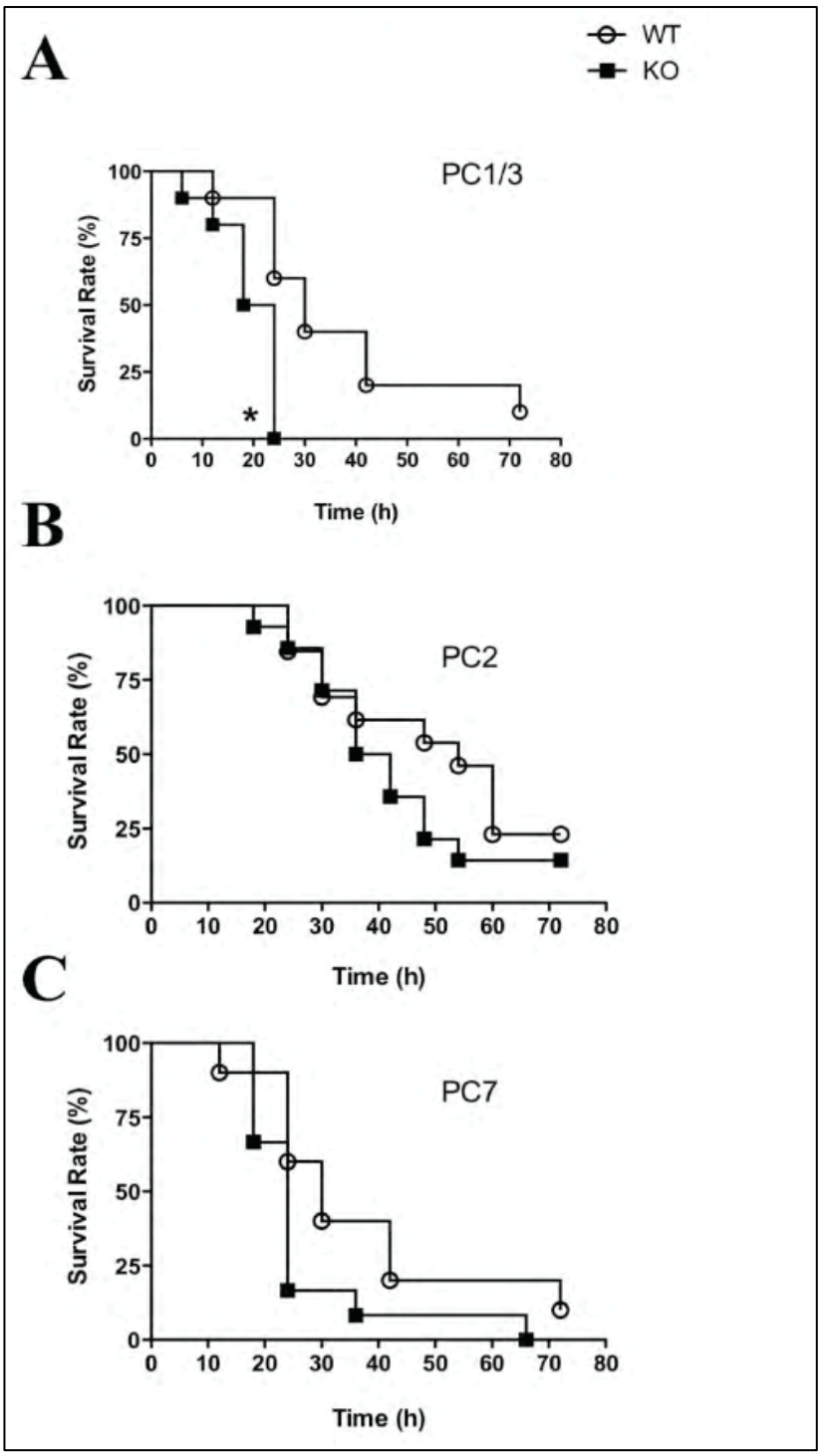

Figure 27 Kaplan-Meier survival rates of mice challenged with LPS stimulation.

Survival curves of A. PC1/3 KO, B. PC2 KO and C. PC7 KO mice, compared to their respective WT mice, injected *i.p.* with a lethal dose of LPS (25 mg/kg). Data represent mean ± SEM (n=10-14, *$p<0.05$)

Effect of LPS stimulation on plasma cytokine concentrations over time - Septic shock is primarily characterized by an unbalanced secretion of pro-inflammatory cytokines causing different symptoms associated with the pathology, such as systemic fever and inducible nitric oxide synthase-dependent vasodilatation (47), resulting in a marked hypotensive response in vivo (48). To verify the effects of LPS on blood pressure in our mouse models, we measured and compared the mean arterial blood pressure (MAP) following LPS stimulation for a period of 60 minutes (Figure 28). We observed a significant decrease of the MAP in PC1/3 KO mice compared to WT mice after 60 minutes of LPS stimulation. Under identical conditions, no such blood pressure drop was observed in PC2 or PC7 KO mice. These results provide further evidence of PC1/3 null mice susceptibility to LPS-induced septic shock.

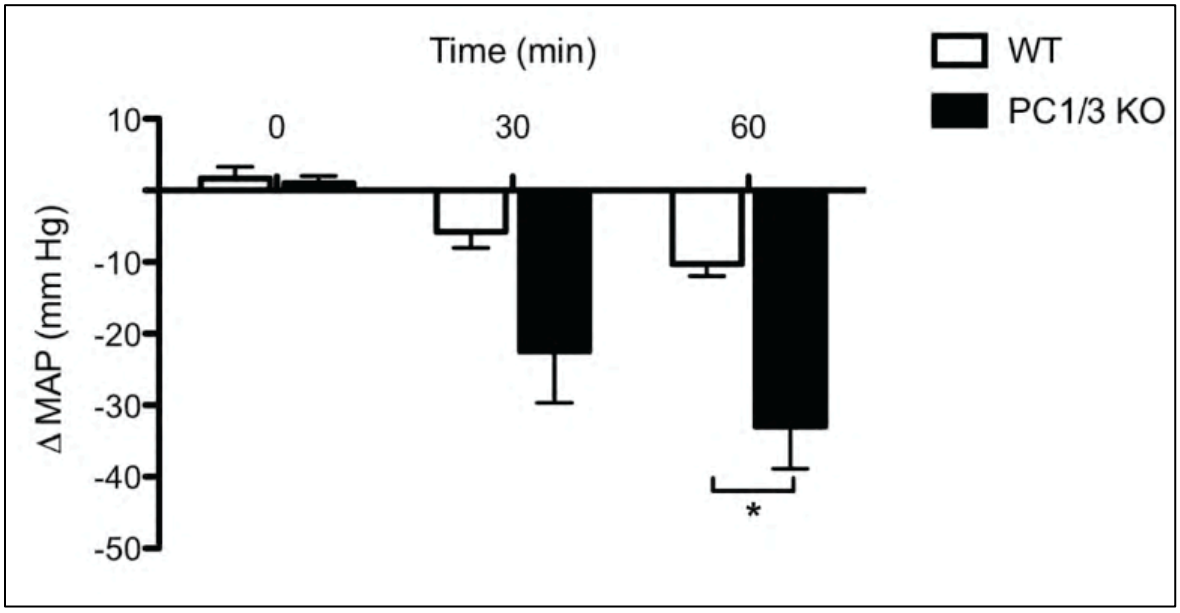

Figure 28 Mean arterial pressure (MAP) measured in mice following LPS stimulation.

MAP observed in WT and PC1/3 KO mice followed by i.v. injection of 2.2 mg/kg of LPS. MAP was measured for a period of 60 minutes after LPS stimulation. Data represent mean ± SEM (n=3-5, *p<0.05)

The most likely explanation for the drop in blood pressure as well as the susceptibility of PC1/3 KO mice to LPS would be due to increased levels of cytokines. We therefore conducted time course experiments to determine the cytokine secretion profiles in the plasma, focusing at first on pro-inflammatory cytokines IL-6, TNF-α and IL-1β. As expected in WT type mice, IL-6 secretion in the plasma reaches its peak after 4 hours of LPS stimulation (Figure 29A) followed by a return towards baseline concentrations 8 hours and 24 hours following LPS stimulation. Similar secretion profiles were observed in the case of TNF-α and IL-1β in WT mice plasma (Figure 29B-C).

However, the time course experiments from PC1/3 KO mice revealed a different profile of cytokine secretion. Four hours following LPS administration, we observed that in the PC1/3 KO mice an IL-6 plasma concentration were 30 times greater than those measured in WT mice (Figure 29 A). Concentrations still increased about two-fold at 8 hours post-LPS stimulation in PC1/3 KO plasma, instead of decreasing as seen in WT mice. In the case of TNF-α, concentrations were recorded to be 8 times higher in PC1/3 KO plasma compared to WT mice following 4 hours of stimulation and continued to rise at 8 hours, similar to IL-6 (Figure 29 B). IL-1β secretion in PC1/3 KO mice was also measured to be 5-fold higher than the concentration observed in WT mice 4 hours post-LPS (Figure 29 C). As concentrations decreased at 8 hours of LPS stimulation in WT plasma, IL-1β secretion rose two times greater in PC1/3 KO mice. No data could be obtained at the 24-hour time point following LPS treatment, as PC1/3 null mice do not survive.

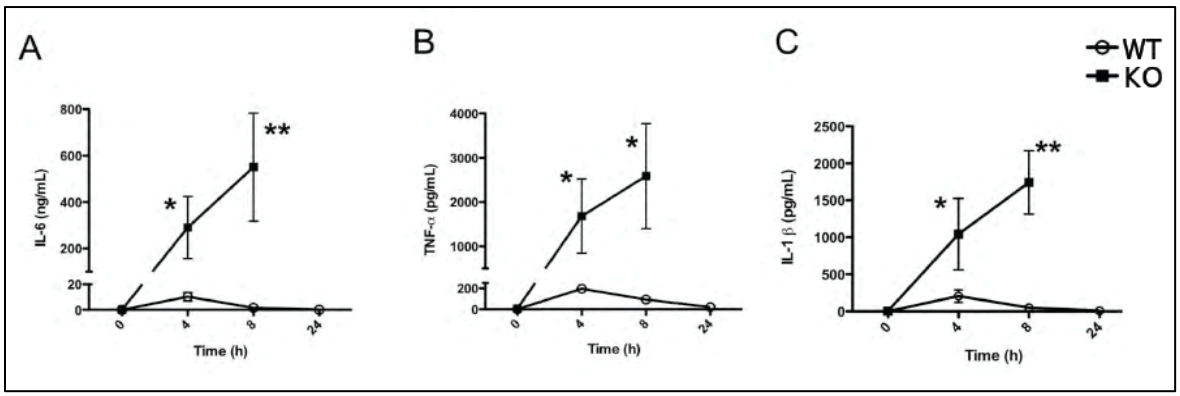

Figure 29 Time course experiment of pro-inflammatory cytokines *in vivo*.

Concentrations of IL-6 (A), TNF-α (B) and IL-1β (C) were dosed in the plasma collected from PC1/3 KO and WT mice injected *i.p.* with 100 µg of LPS. PC1/3 KO mice were deceased following 24 hours of LPS stimulation. Cytokine concentrations were measured using an ELISA kit. Data represent mean ± SEM (n=4-7, *p<0.05, **p<0.01)

Table 11 Comparison of pro-inflammatory cytokine concentrations secreted in PC2 KO and PC7 KO mice.

	PC2		PC7	
Cytokine	WT	KO	WT	KO
IL-6 (ng/ml)				
0 h	ND	ND	ND	ND
4 h	40 ± 20	20 ± 4	20 ± 10	30 ± 10
8 h	7 ± 4	5 ± 1	3 ± 2	5 ± 1
24 h	ND	ND	ND	ND
TNF-α (pg/ml)				
0 h	ND	ND	ND	ND
4 h	430 ± 110	290 ± 40	260 ± 50	780 ± 300
8 h	160 ± 60	90 ± 50	80 ± 30	110 ± 30
24 h	ND	ND	ND	ND
IL-1β (pg/ml)				
0 h	ND	ND	ND	ND
4 h	390 ± 180	150 ± 50	140 ± 40	150 ± 40
8 h	170 ± 160	50 ± 30	70 ± 20	100 ± 20
24 h	50 ± 40	ND	ND	9 ± 9

IL-6, IL-1β and TNF-α was dosed in the plasma of mice following *i.p.* injection of 100 µg LPS. Cytokines were dosed in a time course experiment using an ELISA kit. Data represent mean ± SEM (n=3-4) N.D. means non-detected.

As a comparative measure, we tested available PC2 and PC7 KO mice, in order to determine if those observed effects were PC1/3 specific. No significant differences were observed in the plasma cytokine profiles between KO and WT murine models for both PC2 and PC7 (Table 11). The time course analysis indicated an exaggerated pro-inflammatory cytokine response only in PC1/3 KO mice treated with LPS. This would suggest an implication of PC1/3 in the regulation of pro-inflammatory cytokine secretion *in vivo*.

Expression of PC1/3 gene in peritoneal macrophages - Macrophages are essential APCs in innate immunity since they are part of the first line of defense during an infection and they are a major source of cytokine production. While we have shown that the expression of PC1/3 co-localizes with the spleen macrophage marker CD14 (16), we wanted to establish clear evidence of PC1/3 expression in peritoneal macrophages. An RT-PCR was performed on peritoneal macrophage RNA and the product was analyzed by gel electrophoresis. The observed band yielded the expected 252 bps cDNA fragment (Figure 30**A**). Sequencing of the isolated cDNA confirmed its sequence corresponding to 80-331 nts of the PC1/3 mRNA (GenBank accession number: NM_013628.2). We next conducted a Western blot of proteins extracted from the pituitary gland from WT and KO mice to demonstrate the antibody specificity for PC1/3 Figure 30B panel a). As expected the specific PC1/3 band at approximately 84 kDa was observed in the WT but not in the KO mouse pituitary. A strong non-specific band was always observed at approximately 90 kDa. In Figure 30B panel b, we then analyzed peritoneal macrophages in comparison to AtT-20 cells, known for their very high expression in PC1/3. The strong non-specific band (~90 kDa) was again present, labeled with an asterisk, while the specific 84 kDa PC1/3 band was also observed with an identical migration pattern as that found in AtT-20 and WT pituitary positive controls. We conducted a mass spectrometry experiment to confirm the detection of PC1/3 in peritoneal macrophages. We used a gel LC-MS/MS approach. Membrane proteins extract from LPS or unstimulated WT and KO macrophages were resolved on a SDS-PAGE gel and bands corresponding to the approximate migration of PC1/3 were cut, trypsin digested and analyzed by LC-MS/MS on an LTQ-Orbitrap. We detected PC1/3 only in the WT LPS stimulated sample. This may indicate that in the unstimulated sample the level of PC1/3 was below the detection limit of the technique. The Figure 30**C** show the

sequence of PC1/3 with yellow highlighted section representative of the detected peptides by LC-MS/MS. Three unique peptides (Figure 30 C) of 95% peptide prophet (49) probability were sequenced from three unique spectra (sup Data Figure S 4). A total of 10 spectra where assigned to PC1/3 all from the same gel band. The protein prophet algorithm (50) assigned a probability for PC1/3 detection higher than 99.9% with a protein FDR lower than 0.01% and a peptide FDR of 1.1%. Those results validate the expression of PC1/3 at the protein level in peritoneal macrophages.

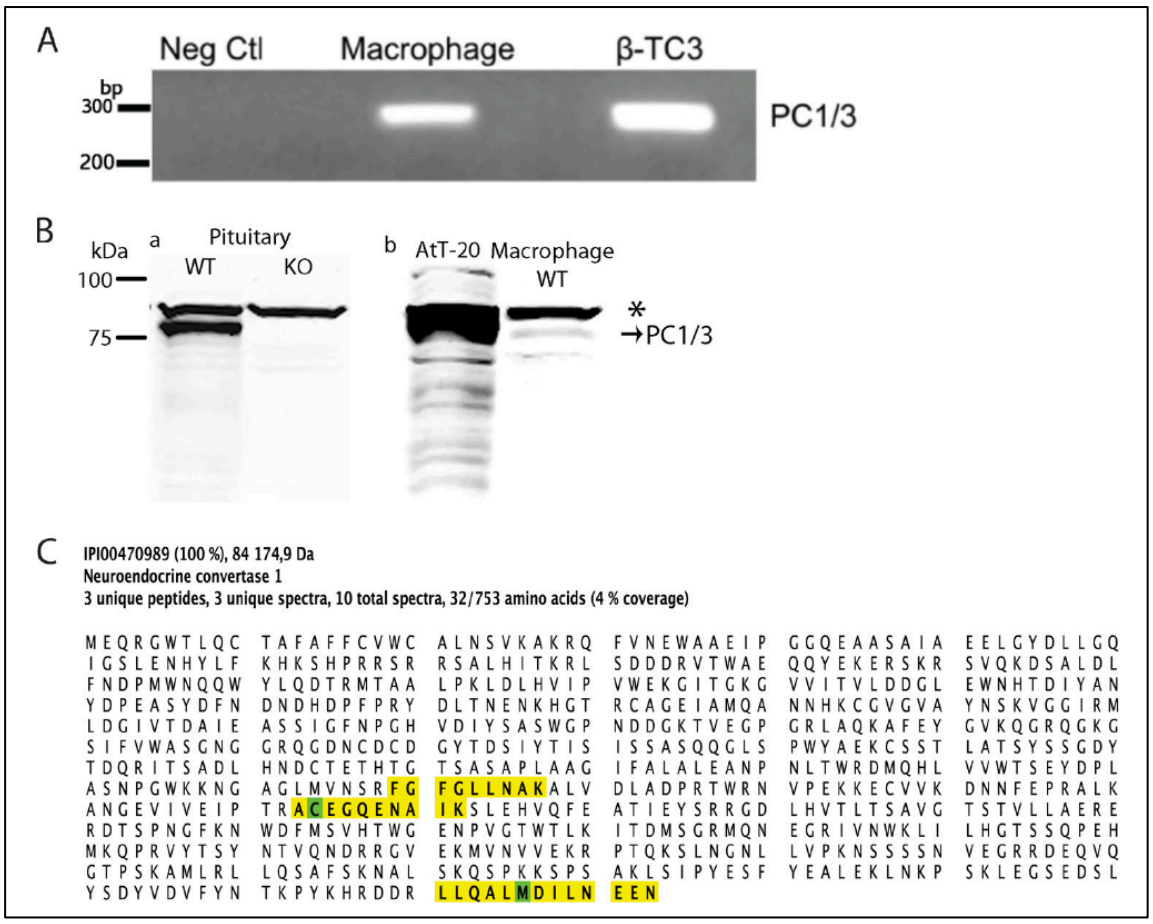

Figure 30 Expression of PC1/3 gene in isolated peritoneal macrophages.

A. RT-PCR product was obtained using RNA extract from peritoneal macrophages and β-TC3 (positive control) that was then migrated on a 1.5% agarose gel colored with ethidium bromide. A 252 bp fragment was observed in the macrophage sample correlating with the expected length for PC1/3 gene. B. a. Western plot of 15 µg of protein extract from PC1/3 on WT and PC1/3 KO mice pituitary gland showing the specificity of the antibody. b. Western blot of PC1/3 from 15 µg of isolated WT peritoneal macrophages. 15 µg of protein form mouse pituitary cells (AtT-20) was used as a positive control. Asterisk indicates a non-specific band. C. Evidence of expression of PC1/3 protein in peritoneal macrophages by mass spectrometry. Peritoneal macrophages where isolated from mice following 8h *i.p.* injection of 100 µg LPS or saline. Membrane fraction was subjected to Gel LC-MSMS. PC1/3 was detected only in stimulated macrophage (99,9% probability) with 3 unique peptides (95% probability) from 3 unique spectra. A total of 10 spectra were assigned to PC1/3 with 4% protein coverage. Yellow highlight represent assigned spectra, while green highlight represent modified amino acids (oxidized methionine and alkyled cysteine).

Effect of LPS stimulation on cytokine production and secretion in primary PC1/3 KO peritoneal macrophages - WT macrophages secreted negligible basal amounts of pro-inflammatory cytokines. While, LPS stimulation caused a significant increase in cytokine secretion (Figure 31 A-C). PC1/3 KO macrophages also secreted low levels of cytokines when incubated with PBS, with the exception of IL-1β. The later is significantly more secreted by PC1/3 KO macrophages compared to WT macrophages, by about 2.5-fold. LPS stimulation resulted in a significantly amplified IL-6 and TNF-α secretion from primary PC1/3 KO macrophages compared to the WT cells. However, no significant difference was observed in IL-1β secretion after 4 hours of LPS stimulation between PC1/3 KO and WT macrophages (Figure 31 C).

Intracellular pro-inflammatory cytokines were also analyzed in primary peritoneal macrophages following a 4-hour LPS treatment (Figure 31 D-F). In the presence of LPS, intracellular cytokine concentrations significantly increased compared to that of basal amounts both in WT and PC1/3 KO macrophages. No significant difference in cytokine concentrations was observed between WT and PC1/3 KO primary macrophages after LPS stimulation. Secretion and intracellular cytokine concentrations were also analyzed in PC2 KO and PC7 KO primary macrophages. No difference was observed in these models in comparison to WT macrophages stimulated with LPS.

Based on the sum of these data we conclude that the lack of PC1/3 results in a deregulated cytokine secretion process, with no observable effect on intracellular cytokines upon short term LPS stimulation. These *ex vivo* studies allowed us to identify an important role of PC1/3 in the control of some pro-inflammatory cytokines secretion (e.g., IL-6 and TNF-a) from LPS-treated macrophages.

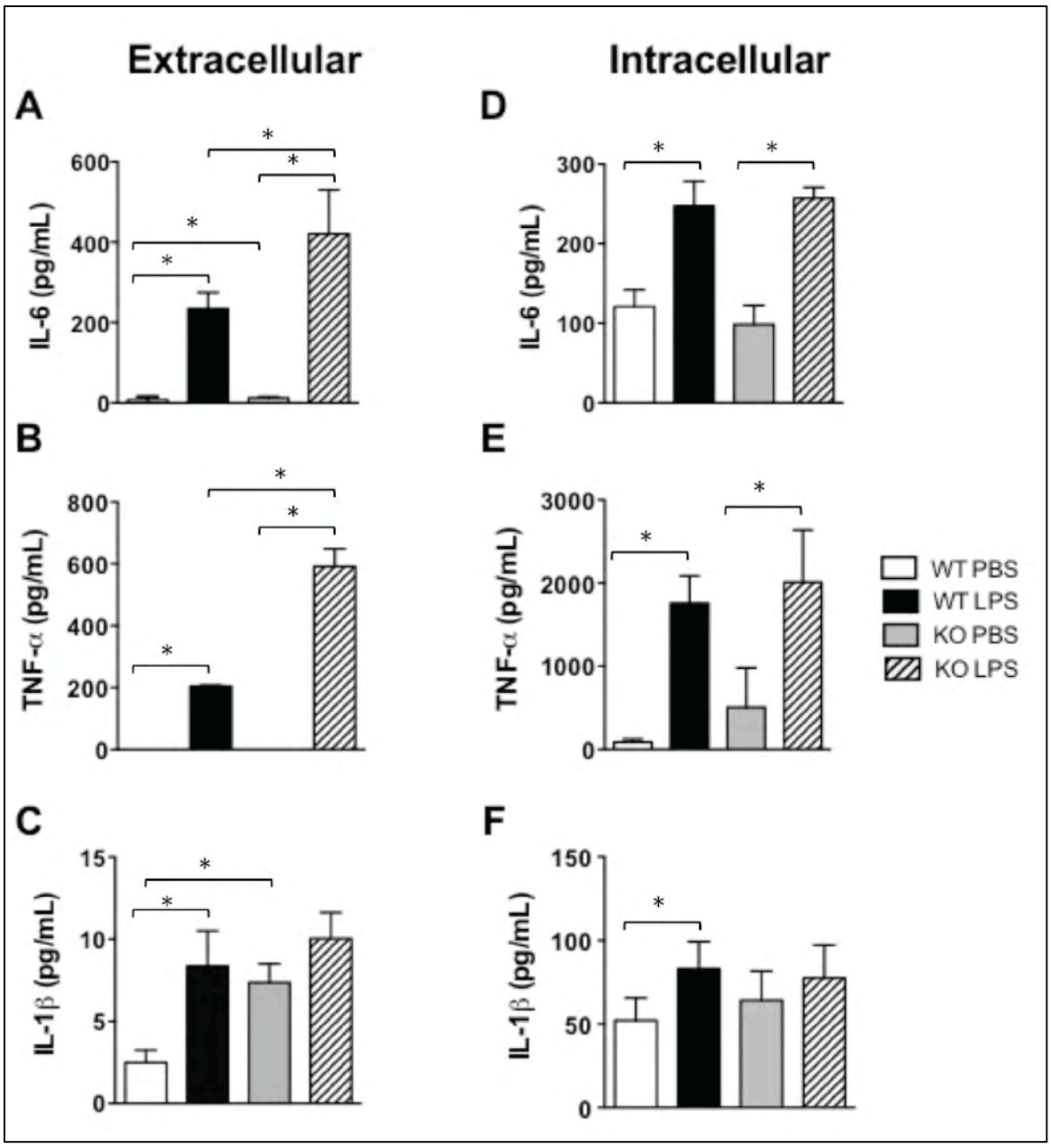

Figure 31 Peritoneal macrophage content and secretion of pro-inflammatory cytokines.

Extracellular (A –C) and intracellular (D-E) proinflammatory cytokine concentrations were dosed in isolated WT and PC1/3 KO peritoneal macrophages stimulated 4 hours with 100ng/mL LPS or PBS. Cytokines were measured using an ELISA assay. Data represent mean ± SEM (n=4, *p<0.05)

We also tested the effects of LPS treatment of WT and PC1/3 KO mice, on the expression profiles of the pro-inflammatory cytokines (IL-6, TNF-α and IL-1β) mRNAs by RT-qPCR. The relative gene expression was calculated by the ratio between RNA expressions of stimulated macrophages (LPS) and that of the control macrophages (PBS). Only IL-6 mRNA was expressed at higher level in both WT and PC1/3 KO LPS-stimulated primary macrophages. Still, no significant changes in relative gene expression were observed in all three cytokines between WT and PC1/3 KO macrophages stimulated with LPS (Figure 32). These results indicate that PC1/3 does not seem to influence macrophages mRNA level of IL-6, TNF-α and IL-1β after 4-hour LPS treatment.

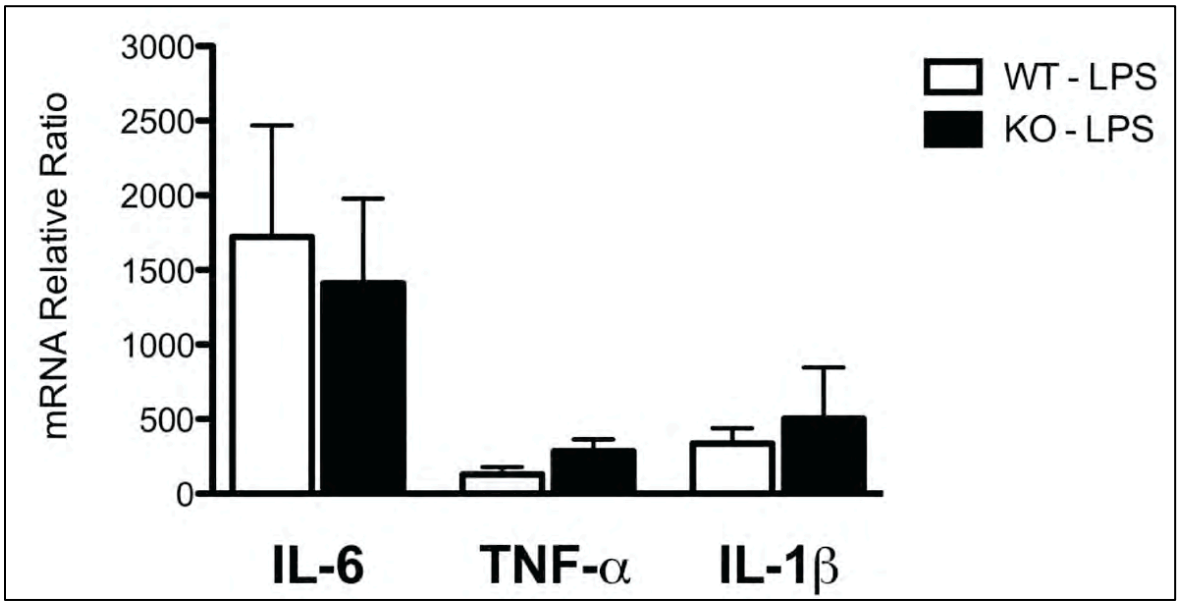

Figure 32 Pro-inflammatory cytokine gene expression in peritoneal macrophages.

Pro-inflammatory cytokine mRNA expression in WT and PC1/3 KO macrophages stimulated 4 hours with 100ng/mL of LPS relative to the expression of these cytokines in control samples stimulated with saline. mRNA was isolated from peritoneal macrophages and quantified by RT-qPCR. All values were normalized to actin mRNA. (n=3)

Effect of PC1/3 KO on the cellular structure of isolated peritoneal macrophages

Since PC1/3 seems to play a role in cytokine secretion, we conducted a transmission electron microscopy experiment to determine if structures involved in cytokine secretion and immune response could be affected by the absence of PC1/3. Peritoneal macrophages

were isolated from WT and PC1/3 null mice following 8 hours of stimulation with LPS or PBS (control) and were then observed by TEM.

At first glance, the general structural aspects appeared to be similar when comparing macrophages from WT mice with that of PC1/3 KO mice (sup. data Figure S 5A). The shape and area of the nucleus were also comparable indicative of the similarity of the cell population observed between each experimental condition (sup. data Figure S 5 B). It has been reported that phagolysosome formation and secretory lysosome trafficking are important features for antigen presentation and cytokine response from APCs (45-47). This led us to conduct a detailed structural analysis of the macrophages by counting electron dense vesicles (EDV) (i.e. lysosomes, heterolysosomes and storage vesicles) (Figure 33 A), vacuoles (i.e. events of pinocytosis, phagosomes and phagolysomes) (Figure 33 B-C) and membrane projections, also known as pseudopods (Figure 33D).

An expected LPS response was observed in WT macrophages (51), which resulted in a 3-fold increase in the ratio of phagolysosomal structures, compared to the total amount of vacuoles, as well as an enlargement of these compartments (Figure 33B). The peripheral vacuole relative ratio, compared to total vacuoles, decreased 2-fold in LPS-stimulated WT macrophages (Figure 33 C).

At basal conditions, no change was observed in the total amount of vacuole in all conditions observed (sup. data Figure S 5 B). Also, no significant difference was observed in the ratio of peripheral (Figure 33 C), internal (data not shown) and phagolysosomal (Figure 33 B) vacuoles between WT and PC1/3 KO macrophages at basal conditions.

Stimulation with LPS caused an alternate structural organization in PC1/3 KO macrophages compared to the WT cells. As described previously, we observed a decrease in the number of peripheral vacuoles accompanied by an increase in the amount of phagolysosomes in WT macrophages following LPS stimulation. In fact, the ratio of peripheral vacuoles remained high in PC1/3 null macrophages (0.45 per cell), while the relative amounts of phagolysosomes were unaffected by the LPS stimulation.

We also examined the EDVs characteristics following LPS stimulation. In WT macrophages, we observed a decrease in EDVs optic densities after 8 hours of LPS stimulation compared to control macrophages. Also, EDVs from LPS-stimulated WT macrophages were often located in or around vacuoles, which suggests that these vesicles

released, or were in the process of releasing, their contents (Figure 33 A, d). An elevated amount of EDVs was observed in control PC1/3 KO macrophages compared to control WT cells, which was calculated at 28 and 21 EDVs per cell, respectively (Figure 33 A, c). Furthermore, the mean radius from EDV measured at basal conditions in PC1/3 KO macrophages (0.24 nm) was larger than that observed in the WT macrophages (0.18 nm). Interestingly, LPS stimulation of macrophages caused a decrease in the amount of EDVs compared to the control cells, leveling the number of EDVs in LPS KO macrophages to the same level of LPS WT macrophages (14 EDVs per cell) (Figure 33 A, e). Also, differences in the morphology of EDVs were detected between PC1/3 KO and WT macrophages at basal conditions. In the former, EDVs appeared as round grey vesicles (Figure 33 A, c) while EDVs in WT macrophages consisted of a heterogenic content (Figure 33 A, a-b).

Further analysis was conducted to examine differences in membrane projections in macrophages, since these structures are important indicators of cell activation and mediate vacuole formation via events of pinocytosis and phagocytosis. Under control and stimulated conditions, PC1/3 KO macrophages showed an increased number of membrane projections compared to WT macrophages, with a respective increased fold of 1,3 and 1,7 per cell (Figure 33 D). Suggesting an increased activation state in those cells.

Taken together these results demonstrate an abnormal structural phenotype of macrophages in the absence of PC1/3, which may affects cytokine secretion and trafficking as well as possible antigen presentation.

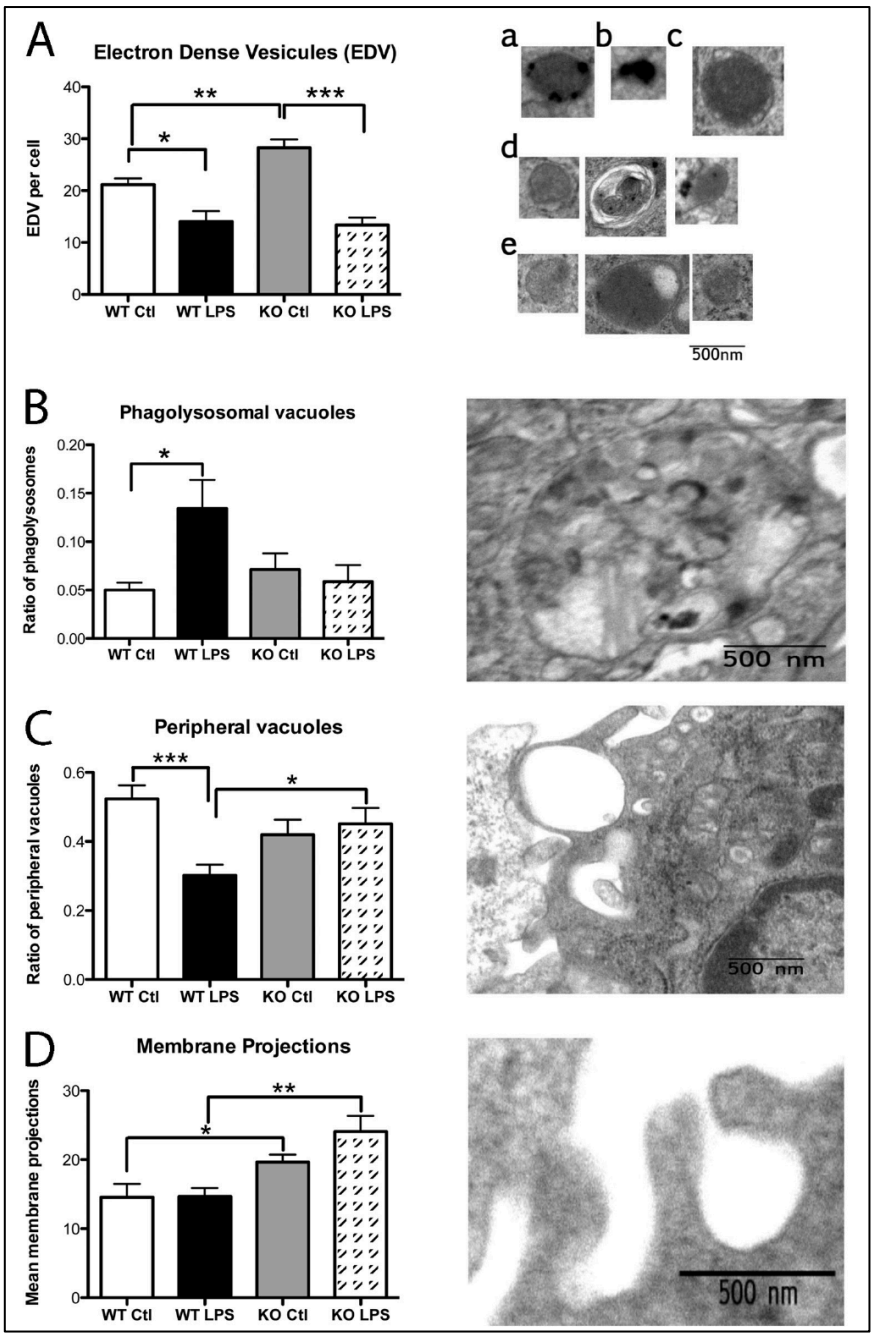

Figure 33 Peritoneal macrophage structure observed by TEM.

Peritoneal macrophages isolated from WT and PC1/3 KO mice stimulated 8h with LPS or PBS (control) were analyzed by transmission electron microscopy (TEM). A. Electron dense vesicles were counted in control WT (a-b) and PC1/3 KO (c), as well as LPS-stimulated WT (d) and PC1/3 KO (e) macrophages. The mean count per cell is reported on the graph. B. The ratio of phagolysosomal vacuoles was counted, relative to the total amount of vacuoles. C. The ratio of peripheral vacuoles was calculated relative to the total vacuoles. D. The mean amount of membrane projections per cell was calculated. Data represent mean ± SEM (n=7-9, *p<0.05, **p<0.01, ***p<0.001)

Implication of PC1/3 in the T_h1/ T_h2 differentiation - An immune response *in vivo* involves the activity of both the innate and adaptive immune system mediated by cells, such as macrophages. These cells can influence the differentiation of T_h cells to T_h1 or T_h2 to propagate a pro- or anti-inflammatory environment, respectively, which is determined mainly by the cytokine profile as well as antigen presentation. To study the effect of PC1/3 on the T_h1/T_h2 differentiation, we use our murine model to perform an LPS stimulation time course and examined the plasma profile of IL-10 IL-12p70 and IFN-γ (Figure 34). IL-10 cytokine secretion profile shows a peak at 4 hours post-LPS administration and levels return to basal amounts at 24 hours in WT mice. PC1/3 KO mice also show a peak of secretion at 4 hours post-LPS and slightly decreased but fail to return to basal levels. At 8 hours following LPS stimulation, IL-10 plasma content in PC1/3 KO mice was significantly higher than in WT (Figure 34 A). These results suggest a failure in IL-10 feedback inhibition on PC1/3 KO innate immunity.

IL-12p70 cytokine plasma content follows a similar profile to IL-10 in WT mice following LPS treatment over time. A peak at 4 hours is also noted in PC1/3 KO mice with a significantly higher plasma concentration compared to WT mice. IL-12p70 levels decrease 8 hours following LPS treatment in PC1/3 KO plasma but still at significantly higher level compared to WT mice (Figure 34 B). An increase in IL-12p70 secretion in PC1/3 KO mice favors the pro-inflammatory T_h1 cell differentiation.

IFN-γ profile concentration in the plasma following a time course of LPS treatment reveals a peak of secretion at 8 hours in WT mice (Figure 34 C). PC1/3 KO and WT mice secrete similar levels of IFN-γ 4 hours post-LPS stimulation. However, plasma contents soar at 8 hours following LPS treatment to 30 times higher than that observed in WT plasma contents (Figure 34 C). This 30-fold increase in IFN-γ secretion observed in PC1/3 KO mice provide further information of the pro-inflammatory cytokine profile secretion in these mice. This balance between IL-10, IL-12 and IFN-γ secretion profile indicates that disruption of PC1/3 promotes T_h1 differentiation.

However, macrophages are not the only immune cells implicated in the induction of T_h1 response. Dendritic cells also secrete IL-12 to favor a T_h1 feedback during an immune reaction (52). Moreover, proper communication between APCs, T cells and B cells is

essential for the development of a T_h2 response and in providing negative feedback on T_h1 response. We thus performed an immunohistochemical analysis with antibodies directed against immune 'Cluster Differentiation' (CD) markers to determine the presence and distribution of these immune cells. As shown, PC1/3 KO has little or no incidence on B, T and NK cells (sup. data Figure S 6-6).

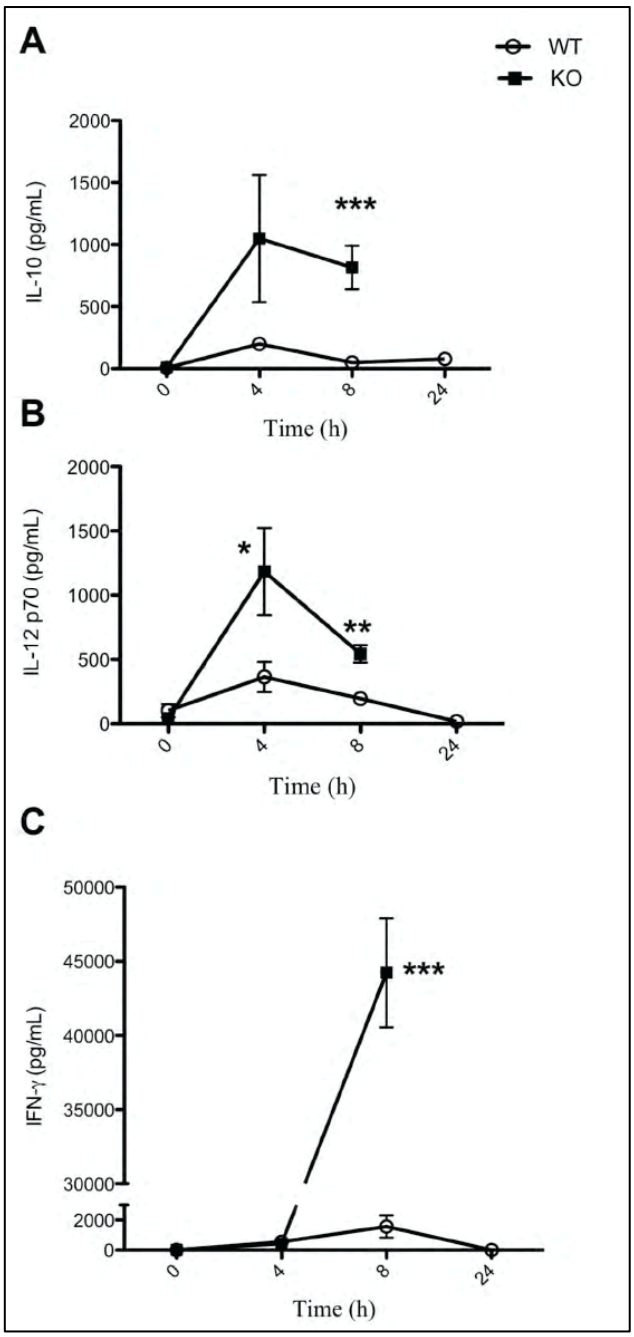

Figure 34 Time course experiment of IL-10, IL-12 and IFN-γ cytokines *in vivo*.

Concentration of IL-10 (A) and IL-12 (B), indicative of T_h2 and T_h1 differentiation respectively, in WT and PC1/3 KO was measured in mouse plasma following 100 μg of LPS stimulation administered *i.p.* C. IFN-γ, a pro-inflammatory cytokine secreted as a result of a T_h1 immune response, was also measured in a similar time course experiment. PC1/3 KO mice were deceased following 24 hours of LPS stimulation. Cytokines were dosed using an ELISA kit specific for mouse IL-10, IL-12 or IFN-γ. Data represent mean ± SEM (n=4-7, *p<0.05, **p<0.01, ***p<0.001)

The marginal zone contains CD20, CD22 and IgM IHC positive B cell markers whereas the nodes contain only CD22 and IgM positive labeling (sup. data Figure S 6). This indicates that the absence of PC1/3 does not alter the B cell trafficking in the spleen, which travels from the MZ to the WP node then to T cell Zone (53). Both the T cells (CD3, CD4, CD7), NKT (CD56, CD7) are present in the WP, specifically in the PALS region, of PC1/3 null spleen but in a slightly lower amount compared to control spleens for some markers (WT) (sup. data Figure S 7-6). The highest impact that can be observed is in regards to the localization of the follicular dendritic cells (CD21 and CD23 not shown), which have mostly disappeared from nodes and the MZ (Figure 35A-B), while macrophage (CD68) and monocyte (CD15) labeling remained unchanged (Figure 35C-F).

Therefore, a decrease of dendritic cells evokes the major contribution of macrophages in PC1/3 KO mice in swaying the T_h immune reaction towards a pro-inflammatory response after LPS stimulation. The early and high secretion level of IL-12 that further promotes IFN-γ secretion by T cells and may outbalance the IL-10 negative feedback. These results contribute additional evidence that PC1/3 plays an essential role in the control of the pro-inflammatory immune response.

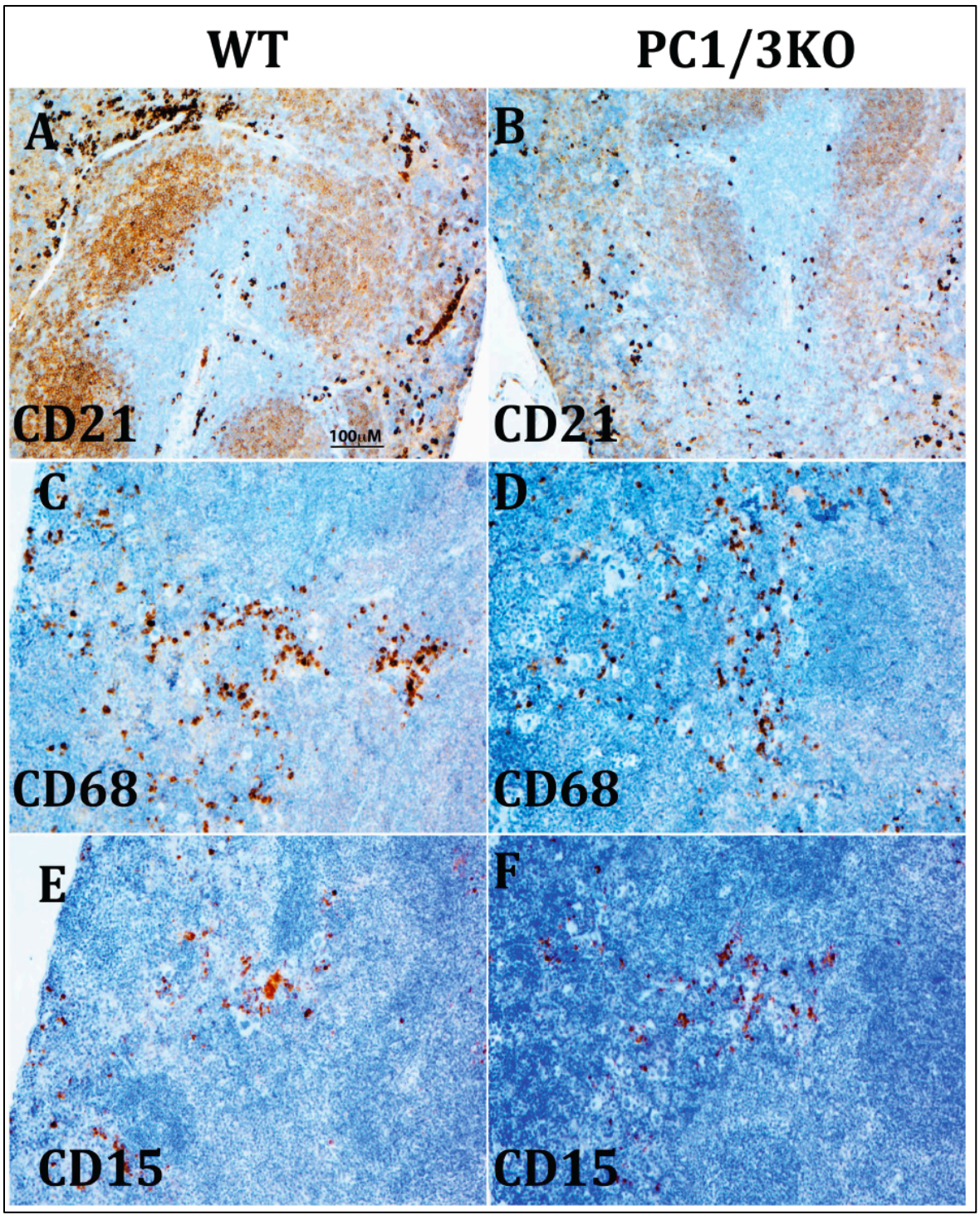

Figure 35 Immunohistochemical staining of untreated WT and PC1/3 KO mouse spleen.

Labeling of dendritic cells, CD21 (A-B), macrophages, CD68 (C-D), and monocytes, CD15 (E-F) is shown at a 10x magnification of the spleen.

DISCUSSION

The use of KO mice has greatly contributed to help elucidate *in vivo* functions of a number of PCs (35,36,54-59). For PC1/3, the discovery of human deficiency cases (17,60-63) has provided important data, which further instigated the development of KO animal models to study the physiological function of this enzyme (30). However, PC1/3 KO mice studies have primarily focused on the study of the neuroendocrine functions of this convertase (17,33,34,64). Since PC1/3 and PC2 are functionally closely related, studies on PC2 KO mice have also focused on its role in the neuroendocrine system (65,66). However, few studies have provided evidence for PC1/3 expression in non-neuroendocrine cells, including macrophages (14, 15). Previous work from our laboratory has demonstrated that PC1/3 expression is regulated by PAMPs, specifically LPS that activates the TLR4 pathway (16). The regulation of the observed expression pattern has encouraged us to explore the PC1/3 KO mouse model from a perspective relating to innate immune mechanisms.

In the present study, we report additional phenotypes in PC1/3 KO mice such as an increase in the spleen size in these animals. We confirmed the expression of PC1/3 and for the first time observed the expression of proSAAS in the spleen. We also observed a spleen disorganization in PC1/3 null mice, which was evident by the overlapping of specific compartments, such as the RP and the MZ. This chaotic phenotype may indicate a lack of proper communication between specific cell types, such as macrophages, B cells and T cells that may lead to an improper immune response (67,68). Moreover, mice challenged with LPS, showed an increase in pro-inflammatory cytokine secretion in the plasma and were much more susceptible to an LPS-induced septic shock compared to WT mice. A decrease in MAP combined with a cytokine storm-like phenotype was detected in the plasma of these mice, which are clear evidence of septic shock (69). These observations suggest that, in the spleen, PC1/3 plays a role in innate immunity, through, for example, the protection against an induced septic shock. We thus attempted to obtain further information about the function of PC1/3 at a cellular level within the PC1/3 KO mouse model.

APCs play an important role in initiating an immune response since they are responsible for the detection of pathogens, such as the recognition of LPS by TLR4, as well as communicating with the adaptive immune system by antigen presentation and cytokine

secretion. Dendritic cells and macrophages are known to collaborate in this task by different cytokine profiles and modulation of adaptive and innate immunity (70). In the present study, spleen immunohistology showed a decrease in dendritic cell markers in PC1/3 KO mice compared to the WT, while the macrophage and monocyte markers are unchanged. Two different DC markers showed this reduction (i.e., CD21 and CD23), suggesting that the most likely explanation is a reduced DC population in the PC1/3 KO spleen. Since three types of DC are present in the mouse spleen (71), it is difficult to ascertain if this change is due to hematopoietic differentiation or a relocation of DC to another lymphoid organ. Based on these and other findings, we hypothesize that the increased LPS sensitivity observed in the PC1/3 KO mice is ostensibly linked to macrophages. Indeed, in previous work we demonstrated PC1/3 expression in splenic macrophages, co-localized with CD14, a macrophage marker (16).

Since peritoneal macrophages are easily obtained, we used these as a cellular model to examine the role of PC1/3 in the macrophage. We established strong evidence that mouse peritoneal macrophages express PC1/3, by using RT-PCR, western blotting and mass spectrometry. This validated our cellular model to study the function of this enzyme in the macrophage.

Furthermore, we examined peritoneal macrophage morphological features. TEM experiments revealed that PC1/3 null macrophages showed a greater number of pseudopods under basal and 8h LPS stimulated conditions compared to the macrophages obtained from WT mice. Pseudopods are membrane extensions essential for sensing the environment and initiating phagocytosis as well as mediating motility, hallmarks of macrophage activation (72,73). Therefore, PC1/3 KO macrophages are primed in the absence of stimulation and remain active longer then the WT cells. We also demonstrated that PC1/3 KO macrophages secreted higher concentrations of pro-inflammatory cytokines, which correlates with the high levels observed in the plasma of these mice.

Since RNA expression levels were unchanged in the null macrophages following LPS treatment, we suggest that PC1/3 may be implicated in a downstream control of cytokine secretion. We also report that PC1/3 KO macrophages show a clear difference in EDV morphology and number, as demonstrated in the TEM experiments, supporting our hypothesis. Indeed heterogeneous contents were observed in WT cells, while homogenous

EDVs were predominant in KO macrophages, implying that the contents of these vesicles differ. These EDVs are most likely secretory lysosomes or late endosomes known to be involved in the canonical (e.g. IL-6 and TNF-α) and non canonical secretion pathway of cytokines (e.g. IL-1β) (74-76). In addition, our data shows that IL-1β secretion is increased in non-stimulated PC1/3 KO macrophages as compared to WT, which fits with the well established data that IL-1β secretion bypasses the TGN (76). In contrast PC1/3 does not appear to affect the TGN retention of cytokines like TNF-α, but rather changes the cytokine turnover in post Golgi transport vesicles upon stimulation. The sum of these data support a role for PC1/3 in the regulation of vesicle trafficking in macrophages, and in this way contribute to the observed phenotype when PC1/3 is disrupted in the KO mouse model.

The question that remains to be answered is the mechanism by which PC1/3 regulates cytokine secretion. It is known that PC1/3 sorting to the regulated secretory pathway depends on its C-terminal, which contains an amphipathic and hydrophobic alpha-helix that anchors the enzyme at the site of formation of dense core secretory granules (DCSG) in the TGN (77). Some studies have implicated PC1/3 as a possible chaperone for proteins to the DCSG by binding the recognition cleavage site composed of paired basic amino acids (78). Adaptor molecules such as EpsinR, are crucial for the sorting of proteins in the recycling endosomes (79) and contain the recognition sequence required to bind PC1/3. Therefore, we speculate that PC1/3 could regulate cytokine secretion by directing trafficking chaperones, while affecting the cytokine secretion and turnover.

An alternative hypothesis would be that PC1/3 affects secretion through cleavage of one or more substrates. Since we only showed the full length form of PC1/3, and the activity of this full length form has been previously demonstrated, it remains likely that processing activity could impact on secretion. It is noted that full-length PC1/3 does not require an acidic environment to be active (80). We cannot exclude that the shorter forms of PC1/3 are also present in peritoneal macrophages, however others have shown a shorter form (i.e., 66 kDa) in alveolar macrophages and spleen monocytes (15). It is well established that the immune and neuroendocrine systems communicate with each other in a paracrine way (17,81,82). The role of neuropeptides as secretion modulators is well known. For example, NPY was shown to modulate IL-6 secretion from macrophages (83) and opioids are known to induce signalling in immune cells We have previously demonstrated

that neuropeptides, such as enkephalin, are co-expressed with PC1/3 in the spleen (16). Others have also observed enkephalin peptides in immune cells and showed that PC1/3 expressing cells lead to the formation of longer peptides (15). Neuropeptides expressed in immune cells could have autocrine activity that regulates secretion. The identification of cognate PC1/3 substrates in macrophages remains an important challenge to better define the mechanisms involved.

Another interesting phenotype observed in the PC1/3 null mice is the global CD4+ T_h1-like response to LPS, as evident by the massive secretion of IFN-γ, indicative of a pro-inflammatory pathway (84). Macrophages are known for their capacity to activate both T_h1 and T_h2, herein M1 and M2 macrophages (70). The former M1 macrophages secrete IL-12 to activate the T_h1 cell to promote a pro-inflammatory response (85). However, LPS alone generally stimulates a T_h2 response leading to protection against LPS toxicity with an inflammatory cytokines profile (e.g. IL-1β, IL6 and TNF-α) controlled by IL-10 (86). The secretion of IL-10 inhibits both the macrophage pro-inflammatory activities and T_h1 differentiation (27,84). However, co-stimulation of macrophage with LPS and IFN-γ gives rise to a M1 response (87 ,88). We show that IL-10 is highly secreted in the PC1/3 KO mouse plasma following LPS stimulation but still IFN-γ and IL-12 surge in PC1/3 null mice indicating a failure of IL-10 to properly inhibit macrophage pro-inflammatory activities. The high IFN-γ and rapid IL-12 over secretion observed in PC1/3 null mice may initiate a positive feedback to further activate the M1 macrophage pro-inflammatory activities and inhibit T_h2 differentiation (89). This would correlates with the observed time course of IL-10, where at 8 hours post-LPS, IL-10 concentration decrease slightly as the amount of IFN-γ increase dramatically. Interestingly, IFN-y is produced by T_h1 (90) cells and it's known that IL-10 regulation of macrophage imply T_{regs} (84,91). We can thus stipulate that PC1/3 would directly or indirectly regulate cytokine secretion in other immune cells, which would contribute to the observed KO mice phenotype.

Apart from the cytokine profile, antigen presentation is also imperative in regulating the T_h1 and T_h2 pathways. By examining once more the macrophages by TEM, PC1/3 KO macrophages show a reduced capacity to form phagolysosomes following 8h LPS stimulation. While phagocytosis seems efficiently performed in WT macrophages since we observed an increase in phagolysosomal vacuoles accompanied by a decrease in peripheral

vacuoles, this pattern of vacuoles is less present in the PC1/3 KO macrophages. This suggests a change in phagocytosis processing in these cells, which may affect many features of the LPS immune response, such as antigen presentation (92). This change in phagocytosis pathway may indicate an increase TLR4 signalling, since it was shown that it slows the rate of phagolysosomes fusion (93). Also, this simple default in lysosome trafficking can contribute to a "cytokine storm-like" phenotype, as reported in the RAB7 KO mouse model (94).

In conclusion, our study has provided evidence for a novel role of PC1/3 in macrophages, by regulating pro-inflammatory immune responses. Since many diseases are related to the APC response and their related T cells balance in cancer (95,96), autoimmune diseases (97) and chronic allergy (98), exploring the role of PC1/3 in immunity may lead to novel insights in these diseases. The development of better tools to study the role of PC1/3 in immune cells and tissues is now justified. The use of conditional KO would be necessary to rule out any paracrine effects from other PC1/3 expressing cells and tissues on immune cells. Also the use of human macrophage-derived cell lines, such as THP-1 which express PC1/3 (14), would be an interesting model to establish the link between the function of PC1/3 in human and mouse immune cells. These would greatly contribute to the advancement in identify molecular mechanisms and pathways by which PC1/3 regulates cytokine secretion.

REFERENCES

1. Rholam, M., and Fahy, C. (2009) Processing of peptide and hormone precursors at the dibasic cleavage sites. *Cell Mol Life Sci* **66**, 2075-2091
2. Seidah, N. G., and Chrétien, M. (1999) Proprotein and prohormone convertases: a family of subtilases generating diverse bioactive polypeptides. *Brain Res* **848**, 45-62
3. Hosaka, M., Nagahama, M., Kim, W. S., Watanabe, T., Hatsuzawa, K., Ikemizu, J., Murakami, K., and Nakayama, K. (1991) Arg-X-Lys/Arg-Arg motif as a signal for precursor cleavage catalyzed by furin within the constitutive secretory pathway. *J Biol Chem* **266**, 12127-12130.
4. Seidah, N. G., Khatib, A. M., and Prat, A. (2006) The proprotein convertases and their implication in sterol and/or lipid metabolism. *Biol Chem* **387**, 871-877
5. Siezen, R. J., and Leunissen, J. A. (1997) Subtilases: the superfamily of subtilisin-like serine proteases. *Protein Sci* **6**, 501-523

6. Creemers, J. W., Siezen, R. J., Roebroek, A. J., Ayoubi, T. A., Huylebroeck, D., and Van de Ven, W. J. (1993) Modulation of furin-mediated proprotein processing activity by site- directed mutagenesis. *J Biol Chem* **268**, 21826-21834.
7. Creemers, J. W., Vey, M., Schafer, W., Ayoubi, T. A., Roebroek, A. J., Klenk, H. D., Garten, W., and Van de Ven, W. J. (1995) Endoproteolytic cleavage of its propeptide is a prerequisite for efficient transport of furin out of the endoplasmic reticulum. *J Biol Chem* **270**, 2695-2702
8. Essalmani, R., Zaid, A., Marcinkiewicz, J., Chamberland, A., Pasquato, A., Seidah, N. G., and Prat, A. (2008) In vivo functions of the proprotein convertase PC5/6 during mouse development: Gdf11 is a likely substrate. *Proc Natl Acad Sci USA* **105**, 5750-5755
9. Nakayama, K. (1997) Furin: a mammalian subtilisin/Kex2p-like endoprotease involved in processing of a wide variety of precursor proteins. *Biochem J* 327 (Pt 3), 625-635
10. Seidah, N. G., Day, R., Marcinkiewicz, M., and Chrétien, M. (1998) Precursor convertases: an evolutionary ancient, cell-specific, combinatorial mechanism yielding diverse bioactive peptides and proteins. *Annals of the New York Academy of Sciences* **839**, 9-24
11. Portela-Gomes, G. M., Grimelius, L., and Stridsberg, M. (2008) Prohormone convertases 1/3, 2, furin and protein 7B2 (Secretogranin V) in endocrine cells of the human pancreas. *Regulatory Peptides* **146**, 117-124
12. Schäfer, M. K., Day, R., Cullinan, W. E., Chrétien, M., Seidah, N. G., and Watson, S. J. (1993) Gene expression of prohormone and proprotein convertases in the rat système nerveux central: a comparative in situ hybridization analysis. *J Neurosci* **13**, 1258-1279
13. Day, R., Schafer, M., Watson, S. J., Chrétien, M., and Seidah, N. G. (1992) Distribution and regulation of the prohomone convertases PC1 and PC2 in the rat pituitary. *Mol Endocrinol* **6**, 485-497
14. LaMendola, J., Martin, S. K., and Steiner, D. F. (1997) Expression of PC3, carboxypeptidase E and enkephalin in human monocyte-derived macrophages as a tool for genetic studies. *FEBS Lett* **404**, 19-22
15. Vindrola, O., Mayer, A. M., Citera, G., Spitzer, J. A., and Espinoza, L. R. (1994) Prohormone convertases PC2 and PC3 in rat neutrophils and macrophages. Parallel changes with proenkephalin-derived peptides induced by LPS in vivo. *Neuropeptides* **27**, 235-244
16. Lansac, G., Dong, W., Dubois, C. M., Benlarbi, N., Afonso, C., Fournier, I., Salzet, M., and Day, R. (2006) Lipopolysaccharide mediated regulation of neuroendocrine associated proprotein convertases and neuropeptide precursor processing in the rat spleen. *J Neuroimmunol* **171**, 57-71
17. Salzet, M., Vieau, D., and Day, R. (2000) Crosstalk between nervous and immune systems through the animal kingdom: focus on opioids. *Trends Neurosci* **23**, 550-555
18. Salzet, M. (2001) Neuroimmunology of opioids from invertebrates to human. *Neuro Endocrinol Lett* **22**, 467-474

19. Day, R., and Salzet, M. (2002) The neuroendocrine phenotype, cellular plasticity, and the search for genetic switches: redefining the diffuse neuroendocrine system. *Neuroendocrinol Lett* **23**, 447-451
20. Akira, S., Takeda, K., and Kaisho, T. (2001) Toll-like receptors: critical proteins linking innate and acquired immunity. *Nat Immunol* **2**, 675-680
21. Lu, Y.-C., Yeh, W.-C., and Ohashi, P. S. (2008) LPS/TLR4 signal transduction pathway. *Cytokine* **42**, 145-151
22. Chow, J. C., Young, D. W., Golenbock, D. T., Christ, W. J., and Gusovsky, F. (1999) Toll-like receptor-4 mediates lipopolysaccharide-induced signal transduction. *J Biol Chem* **274**, 10689-10692
23. Rautajoki, K. J., Kylaniemi, M. K., Raghav, S. K., Rao, K., and Lahesmaa, R. (2008) An insight into molecular mechanisms of human T helper cell differentiation. *Ann Med* **40**, 322-335
24. Cottrez, F., Hurst, S. D., Coffman, R. L., and Groux, H. (2000) T regulatory cells 1 inhibit a Th2-specific response in vivo. *J Immunol* **165**, 4848-4853
25. Schroder, K., Sweet, M. J., and Hume, D. A. (2006) Signal integration between IFNgamma and TLR signalling pathways in macrophages. *Immunobiology* **211**, 511-524
26. Puddu, P., Fantuzzi, L., Borghi, P., Varano, B., Rainaldi, G., Guillemard, E., Malorni, W., Nicaise, P., Wolf, S. F., Belardelli, F., and Gessani, S. (1997) IL-12 induces IFN-gamma expression and secretion in mouse peritoneal macrophages. *J Immunol* **159**, 3490-3497
27. Fiorentino, D. F., Zlotnik, A., Mosmann, T., Howard, M., and O'garra, A. (1991) IL-10 inhibits cytokine production by activated macrophages. *The Journal of Immunology* **147**, 3815
28. Kohyama, M., Ise, W., Edelson, B. T., Wilker, P. R., Hildner, K., Mejia, C., Frazier, W. A., Murphy, T. L., and Murphy, K. M. (2009) Role for Spi-C in the development of red pulp macrophages and splenic iron homeostasis. *Nature* **457**, 318-321
29. Miyake, K. (2003) Innate recognition of lipopolysaccharide by CD14 and toll-like receptor 4-MD-2: unique roles for MD-2. *Int Immunopharmacol* **3**, 119-128
30. Zhu, X., Zhou, A., Dey, A., Norrbom, C., Carroll, R., Zhang, C., Laurent, V., Lindberg, I., Ugleholdt, R., Holst, J. J., and Steiner, D. F. (2002) Disruption of PC1/3 expression in mice causes dwarfism and multiple neuroendocrine peptide processing defects. *Proc Natl Acad Sci U S A* **99**, 10293-10298
31. Dey, A., Xhu, X., Carroll, R., Turck, C. W., Stein, J., and Steiner, D. F. (2003) Biological processing of the cocaine and amphetamine-regulated transcript precursors by prohormone convertases, PC2 and PC1/3. *J Biol Chem* **278**, 15007-15014
32. Marzban, L., Trigo-Gonzalez, G., Zhu, X., Rhodes, C. J., Halban, P. A., Steiner, D. F., and Verchere, C. B. (2004) Role of beta-cell prohormone convertase (PC)1/3 in processing of pro-islet amyloid polypeptide. *Diabetes* **53**, 141-148
33. Ugleholdt, R., Poulsen, M. L., Holst, P. J., Irminger, J. C., Orskov, C., Pedersen, J., Rosenkilde, M. M., Zhu, X., Steiner, D. F., and Holst, J. J. (2006) Prohormone convertase 1/3 is essential for processing of the glucose-dependent insulinotropic polypeptide precursor. *J Biol Chem* **281**, 11050-11057

34. Wardman, J. H., Zhang, X., Gagnon, S., Castro, L. M., Zhu, X., Steiner, D. F., Day, R., and Fricker, L. D. (2010) Analysis of peptides in prohormone convertase 1/3 null mouse brain using quantitative peptidomics. *J Neurochem* **114**, 215-225
35. Furuta, M., Yano, H., Zhou, A., Rouillé, Y., Holst, J. J., Carroll, R., Ravazzola, M., Orci, L., Furuta, H., and Steiner, D. F. (1997) Defective prohormone processing and altered pancreatic islet morphology in mice lacking active SPC2. *Proc Natl Acad Sci USA* **94**, 6646-6651
36. Villeneuve, P., Feliciangeli, S., Croissandeau, G., Seidah, N. G., Mbikay, M., Kitabgi, P., and Beaudet, A. (2002) Altered processing of the neurotensin/neuromedin N precursor in PC2 knock down mice: a biochemical and immunohistochemical study. *J Neurochem* **82**, 783-793
37. D'Anjou, F., Routhier, S., Perreault, J., Latil, A., Bonnel, D., Fournier, I., Salzet, M., and Day, R. (2011) Molecular Validation of PACE4 as a Target in Prostate Cancer. *Translational Oncology* **4**, 157-172
38. Wardman, J. H., Berezniuk, I., Di, S., Tasker, J. G., and Fricker, L. D. (2011) ProSAAS-derived peptides are colocalized with neuropeptide Y and function as neuropeptides in the regulation of food intake. *PLoS One* **6**, e28152
39. Grenier, C., Bissonnette, C., Volkov, L., and Roucou, X. (2006) Molecular morphology and toxicity of cytoplasmic prion protein aggregates in neuronal and non-neuronal cells. *J Neurochem* **97**, 1456-1466
40. Benjannet, S., Rondeau, N., Paquet, L., Boudreault, A., Lazure, C., Chretien, M., and Seidah, N. G. (1993) Comparative biosynthesis, covalent post-translational modifications and efficiency of prosegment cleavage of the prohormone convertases PC1 and PC2: glycosylation, sulphation and identification of the intracellular site of prosegment cleavage of PC1 and PC2. *Biochem J* **294 (Pt 3)**, 735-743
41. Polati, R., Castagna, A., Bossi, A., Campostrini, N., Zaninotto, F., Timperio, A. M., Zolla, L., Olivieri, O., Corrocher, R., and Girelli, D. (2009) High resolution preparation of monocyte-derived macrophages (MDM) protein fractions for clinical proteomics. *Proteome Sci* **7**, 4
42. Havlis, J., Thomas, H., Sebela, M., and Shevchenko, A. (2003) Fast-response proteomics by accelerated in-gel digestion of proteins. *Anal Chem* **75**, 1300-1306
43. Cesta, M. F. (2006) Normal structure, function, and histology of the spleen. *Toxicologic Path.* **34**, 455-465
44. You, Y., Myers, R. C., Freeberg, L., Foote, J., Kearney, J. F., Justement, L. B., and Carter, R. H. (2011) Marginal zone B cells regulate antigen capture by marginal zone macrophages. *J Immunol* **186**, 2172-2181
45. Jia, T., and Pamer, E. G. (2009) Immunology. Dispensable but not irrelevant. *Science* **325**, 549-550
46. Takahashi, K., Shibata, T., Akashi-Takamura, S., Kiyokawa, T., Wakabayashi, Y., Tanimura, N., Kobayashi, T., Matsumoto, F., Fukui, R., Kouro, T., Nagai, Y., Takatsu, K., Saitoh, S.-I., and Miyake, K. (2007) A protein associated with Toll-like receptor (TLR) 4 (PRAT4A) is required for TLR-dependent immune responses. *Journal of Experimental Medicine* **204**, 2963-2976

47. MacMicking, J. D., Nathan, C., Hom, G., Chartrain, N., Fletcher, D. S., Trumbauer, M., Stevens, K., Xie, Q. W., Sokol, K., Hutchinson, N., and et al. (1995) Altered responses to bacterial infection and endotoxic shock in mice lacking inducible nitric oxide synthase. *Cell* **81**, 641-650
48. Sriskandan, S., and Altmann, D. M. (2008) The immunology of sepsis. *J. Pathol.* **214**, 211-223
49. Keller, A., Nesvizhskii, A. I., Kolker, E., and Aebersold, R. (2002) Empirical statistical model to estimate the accuracy of peptide identifications made by MS/MS and database search. *Anal Chem* **74**, 5383-5392
50. Nesvizhskii, A. I., Keller, A., Kolker, E., and Aebersold, R. (2003) A statistical model for identifying proteins by tandem mass spectrometry. *Anal Chem* **75**, 4646-4658
51. Nacife, V., Soeiro Mde, N., Gomes, R., D'avila, H., Castro-Faria Neto, H., and Meirelles Mde, N. (2004) Morphological and biochemical characterization of macrophages activated by carrageenan and lipopolysaccharide in vivo. *Cell Struct Funct* **29**, 27-34
52. Moser, M., and Murphy, K. M. (2000) Dendritic cell regulation of TH1-TH2 development. *Nat Immunol* **1**, 199-205
53. Mebius, R. E., and Kraal, G. (2005) Structure and function of the spleen. *Nat Rev Immunol* **5**, 606-616
54. Roebroek, A. J., Umans, L., Pauli, I. G., Robertson, E. J., van Leuven, F., Van de Ven, W. J., and Constam, D. B. (1998) Failure of ventral closure and axial rotation in embryos lacking the proprotein convertase Furin. *Development* **125**, 4863-4876
55. Mbikay, M., Tadros, H., Ishida, N., Lerner, C. P., De Lamirande, E., Chen, A., El-Alfy, M., Clermont, Y., Seidah, N. G., Chrétien, M., Gagnon, C., and Simpson, E. M. (1997) Impaired fertility in mice deficient for the testicular germ-cell protease PC4. *Proc Natl Acad Sci USA* **94**, 6842-6846
56. Constam, D. B., and Robertson, E. J. (2000) SPC4/PACE4 regulates a TGFbeta signaling network during axis formation. *Genes Dev* **14**, 1146-1155
57. Essalmani, R., Hamelin, J., Marcinkiewicz, J., Chamberland, A., Mbikay, M., Chrétien, M., Seidah, N. G., and Prat, A. (2006) Deletion of the gene encoding proprotein convertase 5/6 causes early embryonic lethality in the mouse. *Mol Cell Biol* **26**, 354-361
58. Yang, J., Goldstein, J. L., Hammer, R. E., Moon, Y. A., Brown, M. S., and Horton, J. D. (2001) Decreased lipid synthesis in livers of mice with disrupted Site-1 protease gene. *Proc Natl Acad Sci USA* **98**, 13607-13612
59. Abifadel, M., Varret, M., Rabès, J.-P., Allard, D., Ouguerram, K., Devillers, M., Cruaud, C., Benjannet, S., Wickham, L., Erlich, D., Derré, A., Villéger, L., Farnier, M., Beucler, I., Bruckert, E., Chambaz, J., Chanu, B., Lecerf, J.-M., Luc, G., Moulin, P., Weissenbach, J., Prat, A., Krempf, M., Junien, C., Seidah, N. G., and Boileau, C. (2003) Mutations in PCSK9 cause autosomal dominant hypercholesterolemia. *Nat Genet* **34**, 154-156
60. O'Rahilly, S., Gray, H., Humphreys, P. J., Krook, A., Polonsky, K. S., White, A., Gibson, S., Taylor, K., and Carr, C. (1995) Brief report: impaired processing of

prohormones associated with abnormalities of glucose homeostasis and adrenal function. *N Engl J Med* **333**, 1386-1390

61. Jackson, R. S., Creemers, J. W., Ohagi, S., Raffin-Sanson, M. L., Sanders, L., Montague, C. T., Hutton, J. C., and O'Rahilly, S. (1997) Obesity and impaired prohormone processing associated with mutations in the human prohormone convertase 1 gene. *Nat Genet* **16**, 303-306
62. Jackson, R. S., Creemers, J. W. M., Farooqi, I. S., Raffin-Sanson, M.-L., Varro, A., Dockray, G. J., Holst, J. J., Brubaker, P. L., Corvol, P., Polonsky, K. S., Ostrega, D., Becker, K. L., Bertagna, X., Hutton, J. C., White, A., Dattani, M. T., Hussain, K., Middleton, S. J., Nicole, T. M., Milla, P. J., Lindley, K. J., and O'Rahilly, S. (2003) Small-intestinal dysfunction accompanies the complex endocrinopathy of human proprotein convertase 1 deficiency. *J. Clin. Invest.* **112**, 1550-1560
63. Farooqi, I. S., Volders, K., Stanhope, R., Heuschkel, R., White, A., Lank, E., Keogh, J., O'Rahilly, S., and Creemers, J. W. M. (2007) Hyperphagia and early-onset obesity due to a novel homozygous missense mutation in prohormone convertase 1/3. *Journal of Clinical Endocrinology & Metabolism* **92**, 3369-3373
64. Ugleholdt, R., Zhu, X., Deacon, C. F., Ørskov, C., Steiner, D. F., and Holst, J. J. (2004) Impaired intestinal proglucagon processing in mice lacking prohormone convertase 1. *Endocrinology* **145**, 1349-1355
65. Furuta, M., Zhou, A., Webb, G., Carroll, R., Ravazzola, M., Orci, L., and Steiner, D. F. (2001) Severe defect in proglucagon processing in islet A-cells of prohormone convertase 2 null mice. *J Biol Chem* **276**, 27197-27202
66. Pan, H., Che, F.-Y., Peng, B., Steiner, D. F., Pintar, J. E., and Fricker, L. D. (2006) The role of prohormone convertase-2 in hypothalamic neuropeptide processing: a quantitative neuropeptidomic study. *J Neurochem* **98**, 1763-1777
67. Pasparakis, M., Alexopoulou, L., Episkopou, V., and Kollias, G. (1996) Immune and Inflammatory Responses in TNFa-deficient Mice: A Critical Requirement for TNFa in the Formation of Primary B Cell Follicles, Follicular Dendritic Cell Networks and Germinal Centers, and in the Maturation of the Humoral Immune Response. *J Exp Med* **184**, 1397-1411
68. Tumanov, A., Grivennikov, S., Shakhov, A., Rybtsov, S., Koroleva, E., Takeda, J., Nedospasov, S., and Kuprash, D. (2003) Dissecting the role of lymphotoxin in lymphoid organs by conditional targeting. *Immunol Rev* **195**, 106-116
69. Rittirsch, D., Flierl, M. A., and Ward, P. A. (2008) Harmful molecular mechanisms in sepsis. *Nat Rev Immunol* **8**, 776-787
70. Zanoni, I., and Granucci, F. (2009) Dendritic cells and macrophages: same receptors but different functions. *Current Immunology Reviews* **5**, 311-325
71. Kamath, A., Pooley, J., O'Keeffe, M., Vremec, D., Zhan, Y., Lew, A., D'Amico, A., Wu, L., Tough, D., and Shortman, K. (2000) The development, maturation, and turnover rate of mouse spleen dendritic cell populations. *J Immunol* **165**, 6762-6770
72. Rittig, M. G., Wilske, B., and Krause, A. (1999) Phagocytosis of microorganisms by means of overshooting pseudopods: where do we stand? *Microbes and Infection* **1**, 727-735

73. Isaac, B. M., Ishihara, D., Nusblat, L. M., Gevrey, J.-C., Dovas, A., Condeelis, J., and Cox, D. (2010) N-WASP has the ability to compensate for the loss of WASP in macrophage podosome formation and chemotaxis. *Experimental Cell Research* **316**, 3406-3416
74. Blott, E. J., and Griffiths, G. M. (2002) Secretory Lysosomes. *Nature Reviews Molecular Cell Biology* **3**, 122-131
75. Duitman, E. H., Orinska, Z., and Bulfone-Paus, S. (2011) Mechanisms of cytokine secretion: A portfolio of distinct pathways allows flexibility in cytokine activity. *European Journal of Cell Biology* **90**, 476-483
76. Stow, J. L., Low, P. C., Offenhäuser, C., and Sangermani, D. (2009) Cytokine secretion in macrophages and other cells: pathways and mediators. *Immunobiology* **214**, 601-612
77. Dikeakos, J. D., Di Lello, P., Lacombe, M.-J., Ghirlando, R., Legault, P., Reudelhuber, T. L., and Omichinski, J. G. (2009) Functional and structural characterization of a dense core secretory granule sorting domain from the PC1/3 protease. *Proc Natl Acad Sci USA* **106**, 7408-7413
78. Dikeakos, J. D., and Reudelhuber, T. L. (2007) Sending proteins to dense core secretory granules: still a lot to sort out. *The Journal of Cell Biology* **177**, 191-196
79. Saint-Pol, A., Yélamos, B., Amessou, M., Mills, I. G., Dugast, M., Tenza, D., Schu, P., Antony, C., McMahon, H. T., Lamaze, C., and Johannes, L. (2004) Clathrin adaptor epsinR is required for retrograde sorting on early endosomal membranes. *Dev Cell* **6**, 525-538
80. Jean, F., Basak, A., Rondeau, N., Benjannet, S., Hendy, G. N., Seidah, N. G., Chretien, M., and Lazure, C. (1993) Enzymic characterization of murine and human prohormone convertase-1 (mPC1 and hPC1) expressed in mammalian GH4C1 cells. *Biochem J* **292 (Pt 3)**, 891-900
81. Haddad, J. J., Saadé, N. E., and Safieh-Garabedian, B. (2002) Cytokines and neuro-immune-endocrine interactions: a role for the hypothalamic-pituitary-adrenal revolving axis. *J Neuroimmunol* **133**, 1-19
82. Sternberg, E. M. (2006) Neural regulation of innate immunity: a coordinated nonspecific host response to pathogens. *Nat Rev Immunol* **6**, 318-328
83. Straub, R. H., Schaller, T., Miller, L. E., Von Horsten, S., Jessop, D. S., Falk, W., and Scholmerich, J. (2000) Neuropeptide Y cotransmission with norepinephrine in the sympathetic nerve-macrophage interplay. *J Neurochem* **75**, 2464-2471
84. Cope, A., Le Friec, G., Cardone, J., and Kemper, C. (2011) The Th1 life cycle: molecular control of IFN-γ to IL-10 switching. *Trends in immunology* **32**, 278-286
85. Hsieh, C. S., Macatonia, S. E., Tripp, C. S., Wolf, S. F., O'Garra, A., and Murphy, K. M. (1993) Development of TH1 CD4+ T cells through IL-12 produced by Listeria-induced macrophages. *Science* **260**, 547-549
86. Anderson, C. F., and Mosser, D. M. (2002) Cutting edge: biasing immune responses by directing antigen to macrophage Fc gamma receptors. *J Immunol* **168**, 3697-3701

87. Mantovani, A., Sica, A., Sozzani, S., Allevena, P., Vecchi, A., and Locati, M. (2004) The chemokine system in diverse forms of macrophage activation and polarization. *Trends Immunol* **25**, 677-686
88. Gordon, S. (2003) Alternative activation of macrophages. *Nat Rev Immunol* **3**, 23-35
89. Murray, H. W., Spitalny, G. L., and Nathan, C. F. (1985) Activation of mouse peritoneal macrophages in vitro and in vivo by interferon-gamma. *J Immunol* **134**, 1619-1622
90. Schroder, K., Hertzog, P. J., Ravasi, T., and Hume, D. A. (2004) Interferon-gamma: an overview of signals, mechanisms and functions. *J Leukoc Biol* **75**, 163-189
91. Taams, L. S., van Amelsfort, J. M., Tiemessen, M. M., Jacobs, K. M., de Jong, E. C., Akbar, A. N., Bijlsma, J. W., and Lafeber, F. P. (2005) Modulation of monocyte/macrophage function by human CD4+CD25+ regulatory T cells. *Hum Immunol* **66**, 222-230
92. Harding, C. V. (1995) Phagocytic processing of antigens for presentation by MHC molecules. *Trends Cell Biol* **5**, 105-109
93. Blander, J. M., and Medzhitov, R. (2004) Regulation of phagosome maturation by signals from toll-like receptors *Science* **304**, 1014-1018
94. Wang, Y., Chen, T., Han, C., He, D., Liu, H., An, H., Cai, Z., and Cao, X. (2007) Lysosome-associated small GTPase Rab7b negatively regulates TLR4 signaling in macrophages by promoting lysosomal degradation of TLR4. *Blood* **110**, 962-971
95. Wang, Y. C., He, F., Feng, F., Liu, X. W., Dong, G. Y., Qin, H. Y., Hu, X. B., Zheng, M. H., Liang, L., Feng, L., Liang, Y. M., and Han, H. (2010) Notch signaling determines the M1 versus M2 polarization of macrophages in antitumor immune responses. *Cancer Res* **70**, 4840-4849
96. Kim, R., Emi, M., and Tanabe, K. (2005) Cancer cell immune escape and tumor progression by exploitation of anti-inflammatory and pro-inflammatory responses. *Cancer Biol Ther* **4**, 924-933
97. Baecher-Allen, C., and Hafler, D. (2006) Human regulatory T cells and their role in autoimmune disease. *Immunol Rev* **212**, 203-216
98. Gereda, J. E., Leung, D. Y., Thatayatikom, A., Streib, J. E., Price, M. R., Klinnert, M. D., and Liu, A. H. (2000) Relation between house-dust endotoxin exposure, type 1 T-cell development, and allergen sensitisation in infants at high risk of asthma. *Lancet* **355**, 1680-1683

FOOTNOTES

*This work was supported by the Canadian Institutes of Health Research. RD is a member of the Centre de Recherche Clinique Etienne- Le Bel (Sherbrooke, Québec, Canada).

¶Equal contributing authors

[1]Institut de pharmacologie de Sherbrooke, Université de Sherbrooke, Sherbrooke, Québec, J1H 5N4, Canada

[2]Department of Medicine, University of Chicago, Chicago, Illinois 60637, USA

[3]Institut de Recherches Cliniques de Montréal (IRCM), Montreal, Quebec H2W 1R7, Canada, [4]Université Lille Nord de France, Laboratoire de Spectrométrie de Masse Biologique Fondamentale et Appliquée, EA 4550, Université Lille 1, Villeneuve d'Ascq, France.

[5]To whom correspondence should be addressed: Robert Day, PhD Institut de pharmacologie de Sherbrooke (IPS), Faculté de Médecine et des Sciences de la Santé (FMSS), Université de Sherbrooke 3001, 12[e] Ave. Nord Sherbrooke, Québec J1H 5N4, Canada, Telephone: (819) 564-5428, Fax: (819) 820-6886, E-mail: Robert.day@usherbrooke.ca

[6]Abreviation used here : PC1/3, proprotein convertase 1/3; KO, knockout; PCSK, PC substilisin/kexin; PAMP, pathogen-associated molecular patterns; TLR, toll-like receptors; T_h,T helper cells; GHRH, hypothalamic growth hormone-releasing hormone; WT, wild type; PBS, phosphate-buffered saline solution ; TEM, transmission electron microscopy; RP, red pulp; WP, white pulp; MZ, marginal zone; APC, antigen presenting cells; DC, dendritic cells; NKT, natural killer T cell; LD_{100} lethal dose; MAP, mean arterial blood pressure; EDV, electron dense vesicles; DCSG dense core secretory granules.

ACKNOWLEGMENTS - We thank Dany Gauthier for technical expertise and Denis Faubert for LC-MS/MS analyses.

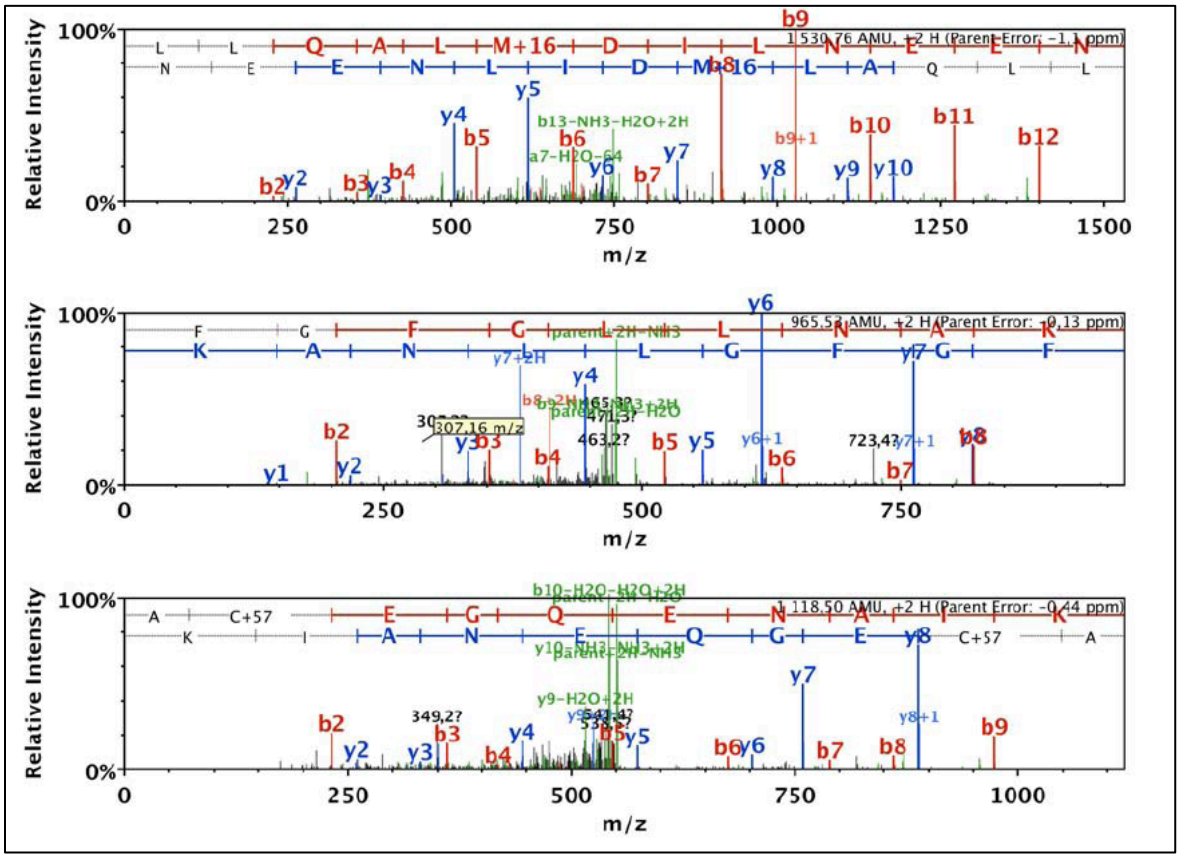

Figure S 4 Unique LC-MS/MS spectra identifying PC1/3.

Representation of the three unique spectra indentifying PC1/3 with their ion fragmentation sequences.

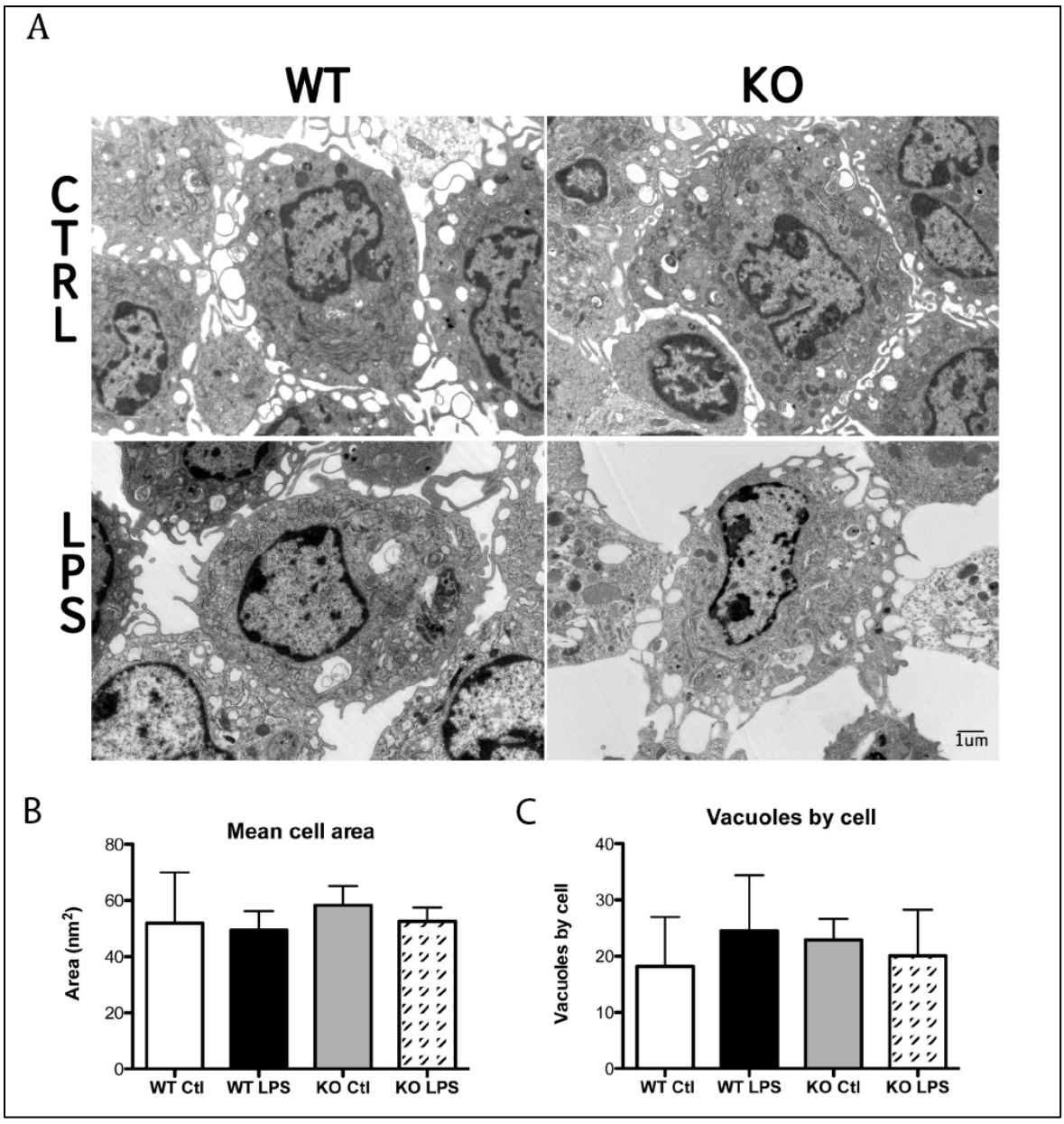

Figure S 5 TEM on peritoneal macrophages.

A. General aspect of WT and KO macrophages under control (PBS) or LPS (8h) condition.

B. Mean area of cells. C. Mean number of vacuoles by cells.

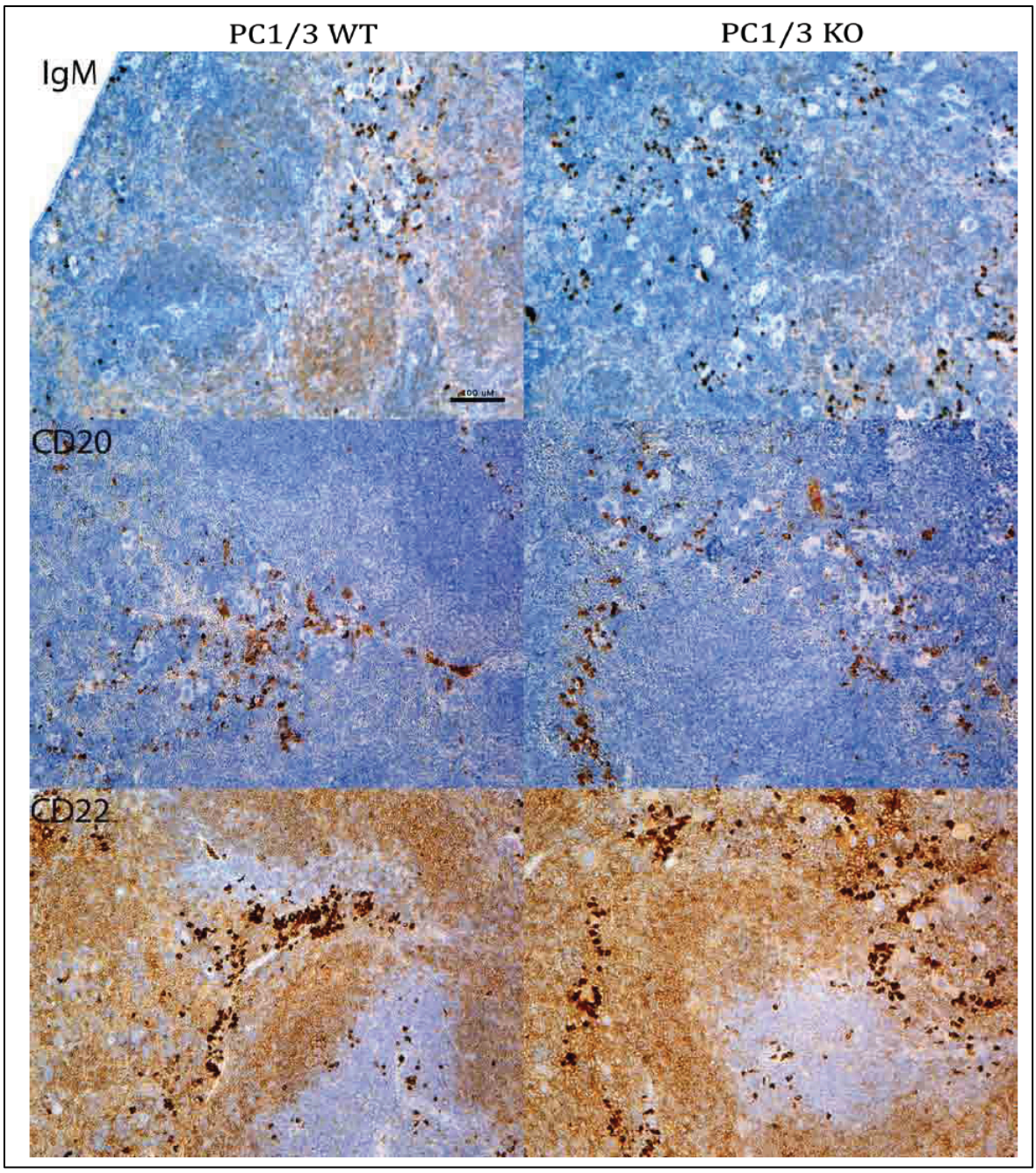

Figure S 6 Immunohistology of B-cells markers.

Parafilm embedded spleen from WT and KO mice were analyzed for B-cell markers (IgM, CD20, CD22) by immunohistology.

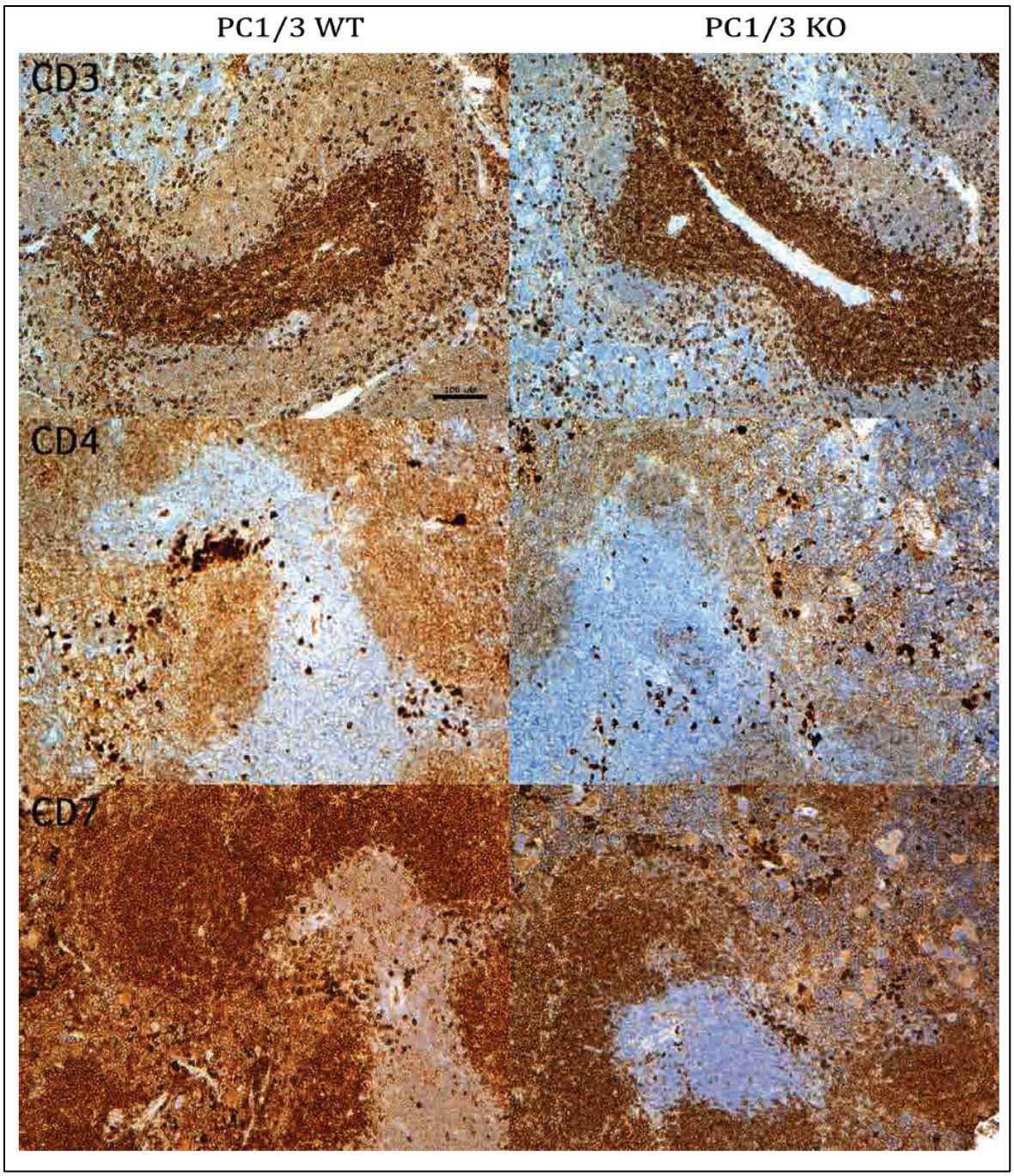

Figure S 7 Immunohistology of T-cells markers.

Parafilm embedded spleen from WT and KO mice were analyzed for B-cell markers (CD3, CD4, CD7) by immunohistology.

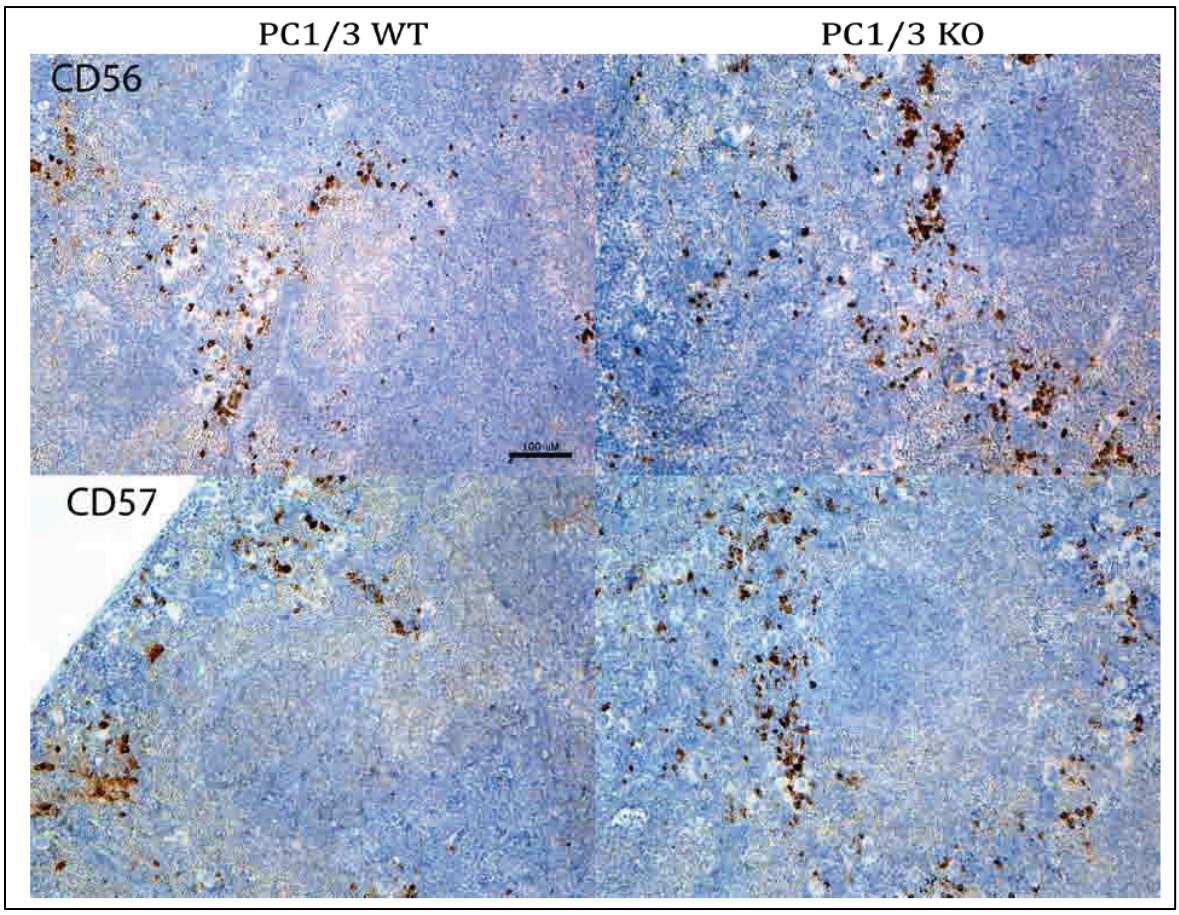

Figure S 8 Immunohistology of Natural Killer cells markers.

Parafilm embedded spleen from WT and KO mice were analysed for B-cell markers (CD56, CD57) by immunohistology.

CHAPITRE 4 - PROPROTEIN CONVERTASE 1/3 (PC1/3) IN THE RAT ALVEOLAR MACROPHAGE CELL LINE NR8383: LOCALIZATION, TRAFFICKING AND EFFECTS ON CYTOKINE SECRETION

Auteurs de l'article: Hugo Gagnon, Sarah Refaie, Sandra Gagnon, Roxane Desjardins, Michel Salzet, Robert Day

Statut de l'article : soumis (en révision) à PlosOne

Avant-propos : J'ai fait et analysé toutes les figures à l'exception des figures 1, 4, et S1. J'ai écrit l'article.

Résumé : La proprotéine convertase 1/3 (PC1/3) est une importante enzyme qui effectue des modifications post-traductionnelles en activant par clivage des précurseurs protéiques dans la voie de sécrétion régulée. Bien caractérisée pour son rôle dans le système neuro-endocrinien, nous avons récemment rapporté un rôle non conventionnel de PC1/3 comme modulateur de la réponse immunitaire induite pour les récepteurs de type Toll-like. Ce nouveau rôle va de pair au peu de littérature qui rapporte l'expression de PC1/3 dans les macrophages. Il est donc maintenant nécessaire d'étudier plus en détail cette nouvelle fonction. Connaissant l'importance des lignées cellulaires en culture pour acquérir des connaissances fondamentales sur des modèles spécifiques, cette étude vise à caractériser PC1/3 dans un modèle cellulaire de macrophages afin de déterminer si un lien peut être fait entre le rôle de PC1/3 dans le contrôle de l'immunité et ses fonctions connues. Nous décrivons la lignée de macrophage alvéolaire de rat, NR8383, qui exprime PC1/3 et la plupart des récepteurs de type Toll-like. Dans ces cellules, PC1/3 est majoritairement localisée au niveau du réseau trans-Golgi et trafic vers des vésicules lysosomales lors de stimulations au lipopolysaccharide. En outre, nous démontrons une colocalisation de PC1/3 et du « *Toll-like receptor 4* » lors de cette stimulation. L'utilisation de shRNA pour réduire l'expression de PC1/3 dans les NR8383 permet de reproduire un phénotype similaire à celui rapporté dans les macrophages péritonéaux isolés de souris PC1/3 KO. Le shRNA de

PC1/3 induit des changements dans l'organisation cellulaire et l'expression de certaines Rab GTPase : des régulatrices du trafic intracellulaire. En conséquence, la répression de l'expression de PC1/3 dans les NR8383 engendre un profil anormal de sécrétion de cytokines. Nous concluons que la lignée cellulaire NR8383 représente un bon modèle pour étudier la fonction de PC1/3 dans les macrophages et que PC1/3 agit comme un régulateur important du trafic vésiculaire et de la sécrétion dans les macrophages.

Proprotein convertase 1/3 (PC1/3) in the rat alveolar macrophage cell line NR8383: localization, trafficking and effects on cytokine secretion

Hugo Gagnon[1,2], Sarah Refaie[1], Sandra Gagnon[1], Roxane Desjardins[1], Michel Salzet[2,#], Robert Day[1,#]

[1]Institut de pharmacologie de Sherbrooke, Université de Sherbrooke, Sherbrooke, Québec, J1H 5N4, Canada

[2]Université Lille Nord de France, Laboratoire de Spectrométrie de Masse Biologique Fondamentale et Appliquée, EA 4550, Université Lille 1, Villeneuve d'Ascq, France.

[#]To whom correspondence should be addressed: Robert Day PhD, Institut de pharmacologie de Sherbrooke (IPS), Faculté de Médecine et des Sciences de la Santé (FMSS), Université de Sherbrooke 3001, 12[e] Ave. Nord Sherbrooke, Québec J1H 5N4, Canada, Telephone: (819) 564-5428, Fax: (819) 820-6886, E-mail: Robert.day@usherbrooke.ca and Michel Salzet, Laboratoire de Spectrométrie de Masse Biologique Fondamentale et Appliquée, EA 4550, Université de Lille 1, Cité Scientifique, 59650 Villeneuve D'Ascq, Telephone: +33 3 2043 41 94; Fax: +33 3 2043 4057, E-mail: Michel.salzet@univ-lille1.fr,

Abstract

The proprotein convertase 1/3 (PC1/3) is an important post-translational processing enzyme for the activation of precursor proteins within the regulated secretory pathway. Well characterized for its role in the neural and endocrine system, we recently reported an unconventional role of PC1/3 as a modulator of Toll-like receptor innate immune response. Adding up to few reports of PC1/3 expression in macrophages, investigation are needed to better characterize this new function. Knowing the benefit of culture cell line to gain fundamental knowledge on specific models; this study aimed to characterized PC1/3 in a model macrophage cell line and to determine if a link between what is known of PC1/3 can be translated to this new immune related function. We describe a rat alveolar cell line, NR8383, as expressing PC1/3 and most common Toll-like receptors. In those cells PC1/3 is mostly localized at the Trans-Golgi network and traffic to lysosome related vesicles upon lipopolysaccharide stimulation. Moreover, we report co-localization of PC1/3 and Toll-like receptor 4 upon lipopolysaccharide stimulation. Down regulation of PC1/3 by shRNA produce similar phenotype in NR8383 to what we report in isolated peritoneal macrophages. PC1/3 shRNA induce changes in cellular organization and expression of specific trafficking regulator Rab GTPase. As a consequence NR8383 down-regulated for PC1/3 present abnormal cytokines secretion profile. We conclude that NR8383 cell line represent a good model to study PC1/3 in macrophages and present PC1/3 as an important regulator of vesicle trafficking and secretion in macrophages.

Introduction

Post-translational modifications are important processes that contribute to the biological regulation of proteins. One such modification is the endoproteolysis of precursor proteins, which can lead to activation, inactivation or functional changes [1]. This cleavage process can be extensive or limited to a few bonds by specific convertases and is followed by amino-terminal, internal and carboxy-terminal modification into smaller biologically active polypeptides [2,3]. Among them Proprotein convertases (PCs) a family of subtilisin-like serine proteinases encoded by 9 PC subtilisin/kexin genes (*PCSK1* to *PCSK9*) that encode PC1/3, PC2, furin, PC4, PC5/6, PACE4, PC7, SKI-1/S1P and PCSK9 respectively [4-8]. Seven PCs cleave secretory precursors at single or paired basic amino acids within the cleavage site R-X-R/K-R↓ [4]. PC2 and PC1/3 represent a particular subtype of PCs because they operate within the regulated secretory pathway and are sorted into secretory granules. The expression of PC2 and PC1/3 is widely associated with neuroendocrine tissues; however, we previously reported that both of these neuroendocrine-"specific" convertases are also expressed in macrophages and lymphocytes *in vivo* [9] and are highly responsive to pathogen-associated molecular pattern challenge. This study supports other reports that illustrate the atypical expression of PC1/3 in cells of the immune system. Specifically, PC1/3 has been detected in a human monocyte-derived macrophage cell line [10] and in differentiated macrophages [11]. In a recent study [12], we characterized the innate immune phenotype in PC1/3 knockout (KO) mice challenged with lipopolysaccharides (LPS), which triggers a cascade of events following the stimulation of Toll-like receptor 4 (TLR4) [13-15]. We identified a massive cytokine response and demonstrated that the T_h1 pathway is enhanced in PC1/3 KO mice, which is indicative of a pro-inflammatory response. Our data also suggest that PC1/3 plays a vital role in the secretion of bioactive proteins from macrophages. Notably, we used electron microscopy to demonstrate a drastic change in the number and morphology of secretion-related vesicles in macrophages derived from PC1/3 KO mice. We concluded that PC1/3 regulates the cytokine response and the innate immune response. The innate immune responses observed in the absence of PC1/3 underscore its importance in this system.

This previous discovery described a novel and unconventional innate response control mechanism mediated by the enzyme PC1/3. Imbalance in the innate immune

response is associated with many physiopathologies [16-18], and therapies that target the innate immune response are emerging as potential treatment avenues [19]. Nevertheless, additional knowledge in this field would aid in the development of new therapies and may overcome barriers in this field [20]. This new role of PC1/3 as a modulator of innate immunity is exciting because the mechanism of action of this protein has been extensively characterized in neuroendocrine tissues and cells [21,22]. Although mouse models have proven useful for the study of PC physiology [23], *in vitro* models provide a more straightforward way to characterize molecular and cellular mechanisms. Thus, cellular models must be established to build solid postulates that can be subsequently transferred to *in vivo* models.

This study reflects the need to examine the role of PC1/3 in innate immunity, establish a cellular model to study innate immunity and determine whether the known cellular biology of PC1/3 is applicable to this specific system. Here, we report that the NR8383 model exhibits similar features in terms of PC expression when compared to rat-isolated macrophages [11], where PC1/3 expression levels were high whereas PC2 was not expressed. NR8383 cells were previously shown to be sensitive to LPS [24], and we took this finding a step further by characterizing the expression of the most common TLRs. By establishing the cellular localization of PC1/3 in this cell line, we also found that PC1/3 trafficking is affected by LPS stimulation. Using shRNA, we investigated the consequences of PC1/3 down-regulation on vesicle trafficking and cytokine secretion. Thus, in this study, we have established the rat alveolar NR8383 cell line as a good model in which to study the role of PC1/3 in innate immunity, described LPS-regulated PC1/3 trafficking and provided evidence for how PC1/3 can modulate macrophage activation by affecting molecular trafficking.

Materials and Methods

Reagents and antibodies

UltraPure *E.coli* 0111:B4 LPS was obtained from Sigma-Aldrich. We obtained the Alexa Fluor® 488 donkey anti-rabbit and Alexa Fluor® 546 goat anti-mouse secondary antibodies from Molecular Probes. Anti-mouse and anti-rabbit IgGs coupled to IRDye800 and IRDye680 were obtained from LI-COR Biosciences. The rabbit anti-PC1/3 (Fus) antibody was previously described [25]. The rabbit anti-PC1/3 targeted against the catalytic domain of PC1/3 was provided by cell signalling technologies (No. 11914). The other commercially available antibodies used in this study included anti-TLR4 (ProSci No. 49-321), anti-actin (NeoMarkers, Clone ACTN05), anti-TGN46 (Novus Biologicals No. NB110-60520), anti-EEA1 (BD Transduction Laboratories No.610456), anti-LAMP1 (University of Iowa, Clone H4A3) and the following antibodies from CellSignaling Technology: anti-RAB5 (No. 3547), anti-RAB7 (No.9367), anti-RAB8 (No. 6975), anti-RAB9 (No. 5118), anti-RAB11 (No. 5589) and anti-EEA1 (No. 3288). Non-targeting (NT) shRNAs in the MISSION RNAi pLKO.1-puro vector were obtained from Sigma-Aldrich. Several shRNA sequences targeting rat PC1/3 (accession number NM_017091) were tested. TRC sequences for shRNAs against human and mouse PC1/3 were modified to target the rat PC1/3 sequence using the Addgene pLKO shRNA design recommendation (see web link below). The most effective sequence used in this paper was 5'-AATTATGACCCAGAGGCTAGC-3', which targets 21 nucleotides starting at position 757 in the gene and corresponds to a modified version of TRCN0000032922. This sequence was cloned into the pLKO.1 vector using the protocol available at http://www.addgene.org/tools/protocols/pLKO/. We used the following previously described probes: furin [26], PC2 [27], PC1/3 [28], PACE4 [29], PC5/6 [30] and PC7 [31].

Cell culture

The rat alveolar macrophage NR8383 cell line [32,33] was cultured in Ham's F12K medium supplemented with 15% fetal bovine serum (FBS; Wisent Bioproducts, St Bruno, QC) at 37 °C in a humidified atmosphere (5% CO_2). For LPS stimulation, the cells were starved overnight, the medium was replaced with fresh medium and the cells were stimulated with 100 ng/ml LPS for the indicated times.

Confocal microscopy and co-localization

The NR8383 cells were grown in culture flasks on coverslips and treated as described. The cells were treated and observed with an Olympus FV1000 inverted confocal laser-scanning microscope as previously described with minor modifications to the protocol [34]. Primary antibodies were incubated in a moist chamber overnight at 4° C. Coverslips were mounted with SlowFade Gold Antifade Reagents (Life Technologies). Olympus Fluoview software (version 1.6b) was used for image acquisition. The images were further processed and analyzed using ImageJ [35,36] with Bio-Formats plugin [37]. Statistical analysis was performed using GraphPad Prism 5 software.

Western blot analysis

After treatment, the cells were detached, centrifuged at 500 g and washed once with ice-cold PBS. The cells were subsequently lysed with radioimmune precipitation assay lysis buffer containing Complete Mini protease inhibitor and processed as previously described [12]. ImageJ software was used to quantify bands and statistical analysis was performed using GraphPad Prism 5 software.

Northern blot

Total RNA was extracted from tissues using a guanidium isothiocyanate method that includes a lithium chloride precipitation step [38]. Northern blotting was performed as previously described [9].

Real-time quantitative PCR

Total RNA was extracted using the Qiagen RNA isolation kit (Qiagen, Valencia, CA, USA). The quality of the total RNA samples was assessed using an Agilent Bioanalyzer with RNA Nano Chips (Agilent Technologies, Palo Alto, CA, USA). Real-time quantitative PCR reactions were performed as previously described [39]. Briefly, 1 μg of RNA was reverse transcribed, and qPCR analysis reactions were performed using a Stratagene Mx3005P5 instrument. To amplify actin, we used the following primers: forward 5'-GCGTCCACCCGCGAGTACAAC-'3 and reverse 5'-CGACGACGAGCGCAGCGATA-'3. To amplify PC1/3, we used the following primers: forward 5'-

GGTGAATGTTGTGGAGGAGAAGC-‘3 and reverse 5’-AGCACTTTGTAGGAGCCGTAGC-‘3. To amplify ProSAAS, we used the following primers: forward primer (5_-TGCTGCTCTTGGGTCTTCTG-3_), reverse primer (5_-GAGTGCTCGTCTCAGCCAA-3_). The relative expression levels were calculated using β-actin as a reference gene with the formula $(1+ \text{amplification efficiency})^{-\Delta(\Delta CT)}$. All experiments were performed in duplicate in 3 independent experiments (n=3).

NR8383 knockdown using lentivirus transduction

Lentiviral particles containing the MISSION RNAi pLKO.1-puro vector were produced in HEK293FT cells following the manufacturer’s instructions (Sigma-Aldrich, St. Louis, MO, USA). Viral titers were calculated in HT1080 cells using a serial dilution approach. Lentiviral transduction was performed in 12-well plates with a cell density of $5x10^5$ cells/mL and a multiplicity of infection (MOI) of 1.5. After 2 days, the infected cells were selected using growth medium containing 12.5 puromycin/mL. Upon characterization, 2 polyclonal cell populations were selected for further studies to avoid any artifacts associated with individual clone selection and to cross-validate our observations [40].

ELISA

Cells were plated at densities of $2.5x10^5$ or $5x10^5$ cells/ml in serum-free F12K medium overnight at 37 °C in a humidified atmosphere containing 5% CO_2. The medium was subsequently changed, and the cells were stimulated with vehicle or 100 ng/ml LPS without serum for the indicated times. The medium was collected and cleared of cells and cell debris by centrifugation at 800 g for 5 min. Cytokines were measured using ELISA kits specific for rat TNF-α (BD biosciences), IL-1β and IL-6 (R&D Systems) according to the manufacturers’ instructions. Statistical analysis was performed using GraphPad Prism 5 software.

RESULTS

PC1/3 and most common TLRs are expressed in NR8383 cells.

Although various macrophage cell lines are available, little information was available regarding their PC1/3 expression. The human macrophage cell line THP-1 was shown to express PC1/3; however, THP-1 cells need to be stimulated with phorbol 12-myristate 13-acetate (PMA) to induce PC1/3 expression [10]. We have screened various cell lines and discovered that NR8383 cells, originally derived from rat alveolar macrophages [32,33], express PC1/3 but not PC2 (Figure 36B). We confirmed that the resulting RT-PCR product was PC1/3 by sequencing (Figure S 9). This observation agrees with previous data obtained using isolated rat alveolar macrophages and splenic macrophages [11]. Moreover, NR8383 cells were shown to be sensitive to TLR ligands, notably LPS [24] and polyI:C [41], making them a good cellular model in which to examine the role of PC1/3 in TLR-based activation of macrophages. However, previous reports have not addressed which of the most common TLRs are expressed in NR8383. We thus used RT-PCR (Figure 36A) to detect the expression of the intracellular TLR receptors TLR3 and TLR9 and the cell surface receptors TLR2 and TLR4. We did not detect the expression of TLR5. To our knowledge, this is the first time that TLR expression profile has been characterized in NR8383 cells. We also used RT-PCR to examine the expression of other PCs and detected the expression of Furin, PC5/6 and PC7 but not PACE4 (Figure 36B). Moreover, as the expression of proSAAS may be relevant to regulate the activity of PC1/3, we tested its expression. We conducted a qPCR experiment to amplify rat proSAAS and rat PC1/3 and ran the product on gel (Figure 36C). Accordingly, proSAAS expression was detected and its expression level was 2.5 times lower then the level of PC1/3. We also further confirmed PC1/3 expression in NR8383 macrophages using northern blot analysis (Figure 36D), and confirmed the probe specificity in the known PC1/3-expressing cells beta-TC3 [42] and PMA-differentiated THP-1 macrophage cells [10].

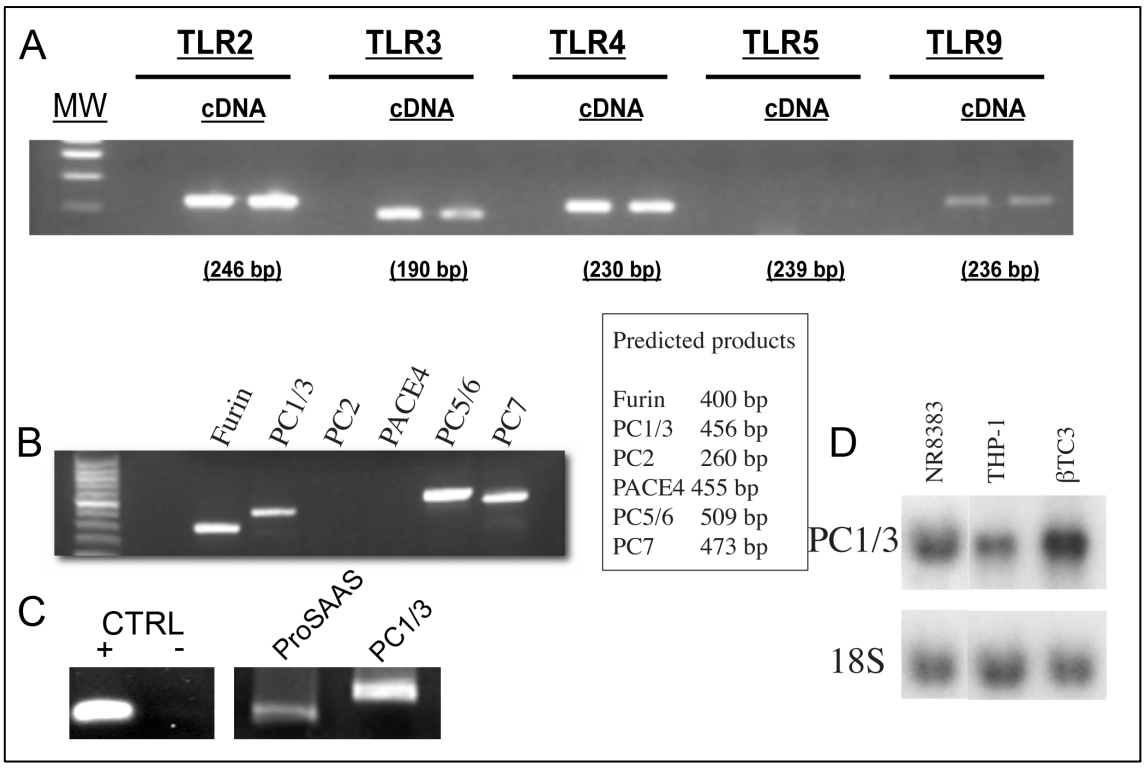

Figure 36 Characterization of the NR8383 cell line.

A. Expression of TLR in NR8383 by RT-PCR. B. Expression of PCs in NR8383 by RT-PCR with the expected band length in base pairs (bp). C. Expression of proSAAS and PC1/3 by qRT-PCR. Negative control (CTRL –) is a non template control and positive control (CTRL +) is 10 pg of rat proSAAS cloned into pCDNA3.1 vector. D. Northern blot analysis of PC1/3 in NR8383, PMA-induced THP-1 and control β-TC3.

PC1/3 down-regulation by shRNA and PC1/3 protein expression in NR8383 cells.

The successful down-regulation of PC1/3 by shRNA was essential in our experiments for 2 major reasons. First, cells that exhibit PC1/3 down-regulation were used as negative controls to ensure that the antibodies we used to detect PC1/3 were specific, and second, these cells were used to confirm our previous observations using macrophages isolated from PC1/3 KO mice. We induced stable PC1/3 knockdown using lentiviral delivery of shRNA. Using this method, we induced stable knockdown of PC1/3 with a multiplicity of infection of 1.5, which resulted in an average reduction of 98% in PC1/3 mRNA expression (Figure 37A). We next determined PC1/3 protein levels. The principal antibody used in this study, which was raised against the C-terminal region of PC1/3, better recognize full-length PC1/3 but also can detect C-terminal matured form of PC1/3 (referred here as ΔCT) (Figure 37C). We have previously confirmed the specificity of this antibody [12]. Using this antibody on 15 ug of AtT-20 cells protein extract, we can detect full-length PC1/3, but also at a weaker intensity 66kDa ΔCT-PC1/3. We detected PC1/3 as a weak band of approximately 88 kDa NR8383 cells; however, a large amount of protein (50 µg) needed to be loaded to achieve this detection, which resulted in increased non-specific band detection. This protein species likely corresponds to the full-length form of PC1/3. We previously characterized this band and confirmed it as PC1/3 by mass spectrometry [12]. We also show that PC1/3 down-regulation by shRNA resulted in the disappearance of the PC1/3 specific band (Figure 37C). We have also used another antibody directed against the catalytic domain of PC1/3 with better sensitivity for the matured forms of PC1/3. Using this antibody we were able to detect, pro-PC1/3, full-length PC1/3 and ΔCT-PC1/3 on 15 ug of AtT-20 protein extract (Figure 2B). Still in NR8383 the protein was hard to detect, a specific band corresponding to full-length PC1/3 and reduced by PC1/3 shRNA was detected. Because the antibody lacked high selectivity in western blotting, we wanted to test it in indirect immunofluorescence labeling (IF). In AtT-20 cells, where PC1/3 is known to accumulate in dense core secretory granules (DSCG) and in TGN [43,44], specific labeling of structures that can be described as DSCG was observed (Figure 37C, c) as well as TGN like region could be recongized by reconstructing vertical confocal plane ((Figure 37C, d). Moreover, when we performed IF on control NR8383 cells and on NR8383 cells stably expressing an shRNA directed against PC1/3, we easily observed the consequences of reduced PC1/3 expression. Specifically, we observed that our PC1/3 shRNA clearly

reduced PC1/3 expression because we could no longer detect PC1/3 using IF. These data indicate that our antibody is much more specific for IF than for western blotting and encouraged us to further characterize the PC1/3 intracellular localization in NR8383 cells.

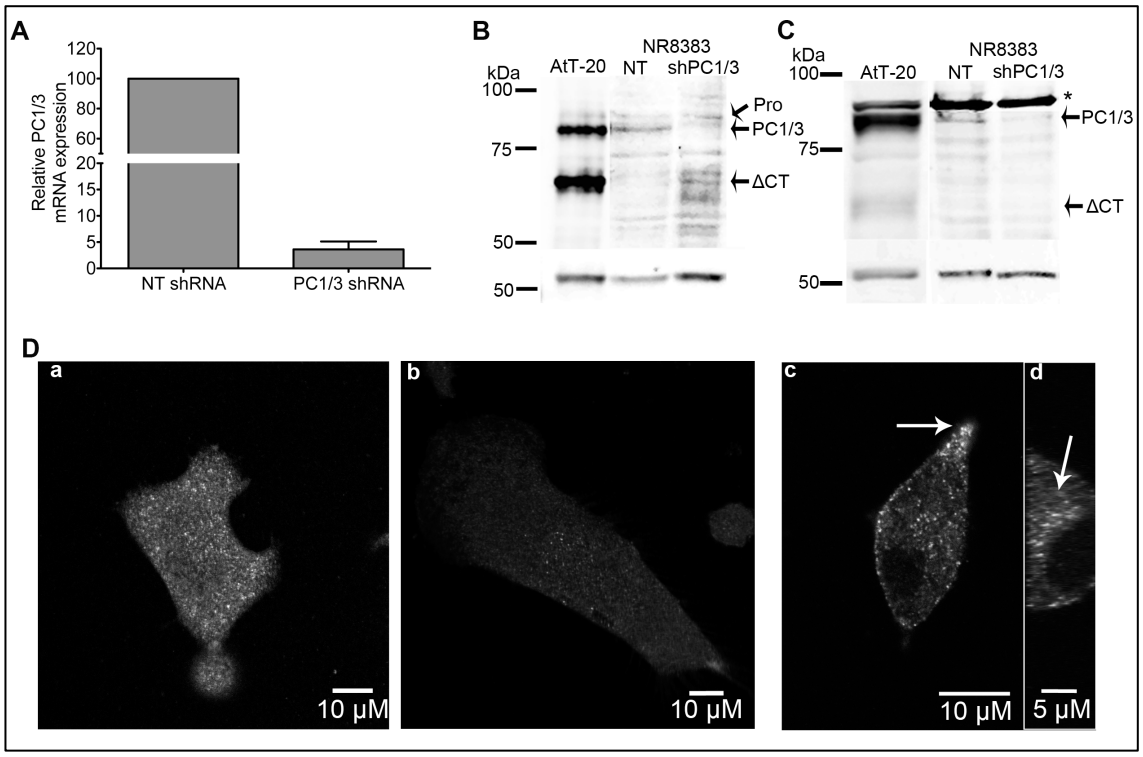

Figure 37 PC1/3 protein expression and down-regulation by shRNA in NR8383 cells.

A. qPCR analysis of the relative expression of PC1/3 in NR8383 cells stably transduced with non-target (NT) shRNA and PC1/3 shRNA. Relative expression was normalized on β-actin (*n*=3). B-C. Western blot of PC1/3 in NR8383 cells stably transduced with NT shRNA or PC1/3 shRNA. as well as AtT-20 cells using a PC1/3 antibody targeted against the catalytic domain (B) or the C-terminal domain (C). 15 µg of AtT-20 protein and 50 ug of NR8383 cells was loaded. Pro-PC1/3 is detected around 90 kDa, full-length PC1/3 (PC1/3) is detected at 87 kDa and fully c-terminally matured PC1/3 (ΔCT PC1/3) is detected at 66 kDa. C. Confocal microscopy of PC1/3 by indirect immunofluorescence on NR8383 cells expressing PC1/3 shRNA (b) and NT shRNA (a) using anti-PC1/3 directed against the C-terminal domain. A positive control (AtT-20) is shown, which exhibits specific secretory granule-like labeling (c) (3x magnification in the rectangle inset). d- is a Z-stack reconstruction of confocal plane from (c) showing TGN labeling of PC1/3 in AtT-20 cells.

PC1/3 cellular localization in NR8383 cells.

As mentioned above, the main characteristic of PC1/3 in neuroendocrine cells is its typical accumulation in DSCG [43,44] (Figure 37, c). In our first observations, PC1/3 mainly accumulated in the Golgi/TGN structure in NR8383 cells (Figure 37C, a) and shows labeling of vesicles like structures throughout the cells. We therefore wanted to better characterize the PC1/3 distribution using an IF confocal co-localization study. Our data indicate that PC1/3 co-localizes with TGN46, which is a well-described TGN marker [45,46] (Figure 38A). Additional PC1/3 showed perinuclear localization, which may represent endoplasmic reticulum (ER), and localization to vesicle-like structures. To identify the vesicle-like structures, we performed co-localization experiments and determined that PC1/3 co-localized with the lysosomal marker LAMP1 (Figure 38C), especially when phagosomal structures were developing into cells. LAMP1 is known to be a marker of late endosomes, lysosomes [47] and phagolysosomes [48]. The remaining PC1/3-containing vesicles were most likely recycling endosomes and secretory vesicles because little or no co-localization was observed with the early endosome marker EEA1 [49,50] (Figure 38B). To confirm our immunofluoresence results and fully map PC1/3 localization in NR8383 cells, we performed immunogold labeling of PC1/3 and electron microscopy. PC1/3 was obviously located in the ER and Golgi (Figure 39a,b) but also showed extensive accumulation at the periphery of structures corresponding to endosomes (Figure 39c) and lysosomes (Figure 39f) as well as inside multivesicular structures corresponding to late endosomes (Figure 39d) and phagolysosomes (Figure 39e). To our knowledge, this is the first time that PC1/3 localization has been so extensively characterized in non-neuroendocrine cells. It is likely that PC1/3 does not accumulate in specialized secretory granules but instead is retained in the TGN and migrates at least partially to lysosomal or secretory lysosomes. This is not surprising because macrophage secretion has been demonstrated to be regulated quite differently compared to specialized secretory cells [51,52].

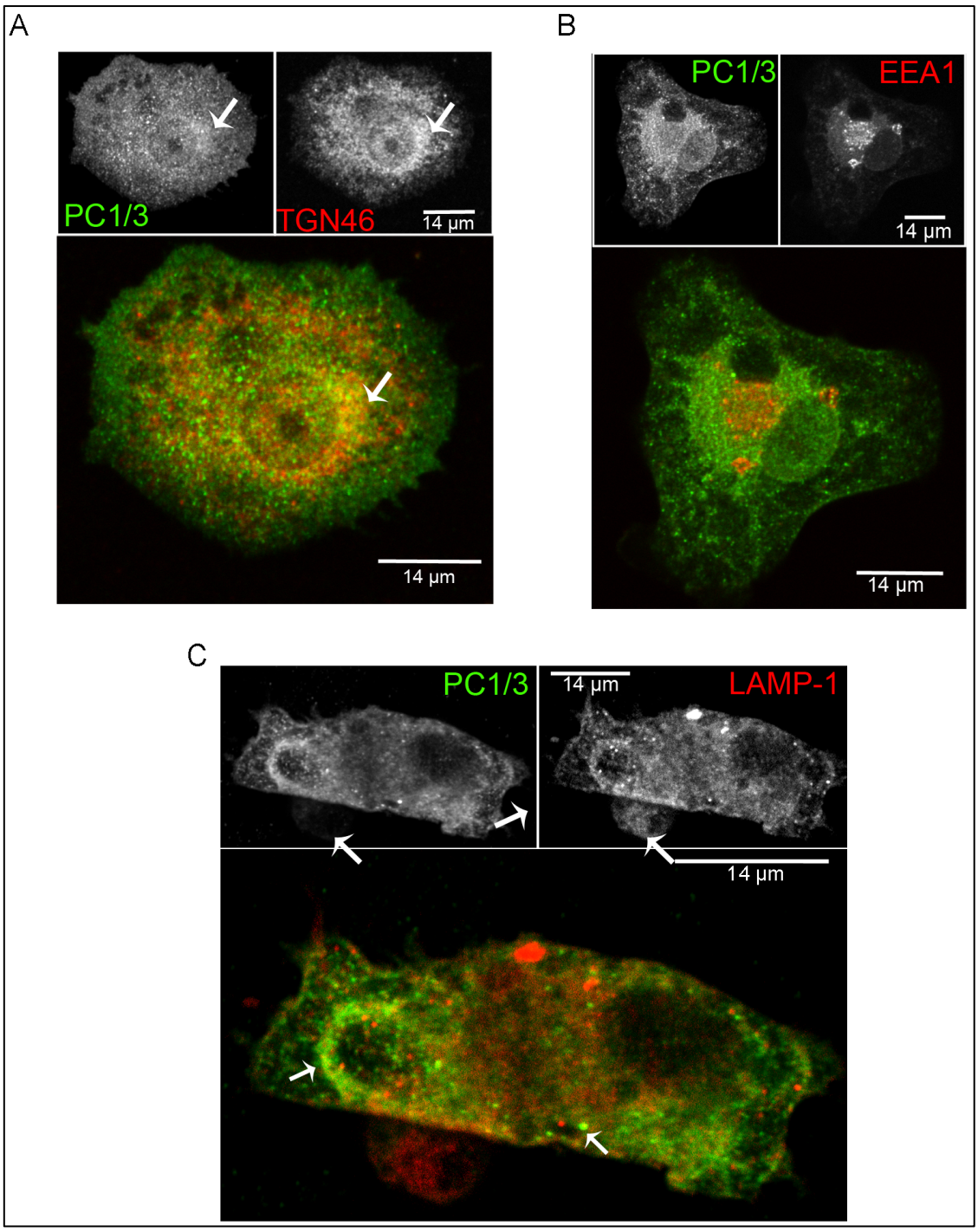

Figure 38 PC1/3 cellular distribution in NR8383 cells as examined by immunofluorescence.

Indirect immunofluorescence confocal microscopy with anti-PC1/3 (green), (A) anti-TGN46 (red), (B) anti-EEA1 (red) and (C) anti-LAMP1 (red). A. The arrow indicates the TGN region where PC1/3 and TGN46 co-localize. C. The left arrow indicates the phagocytic structure and the lower right arrow indicates the lysosome-like structure where PC1/3 and LAMP1 are partially co-localized.

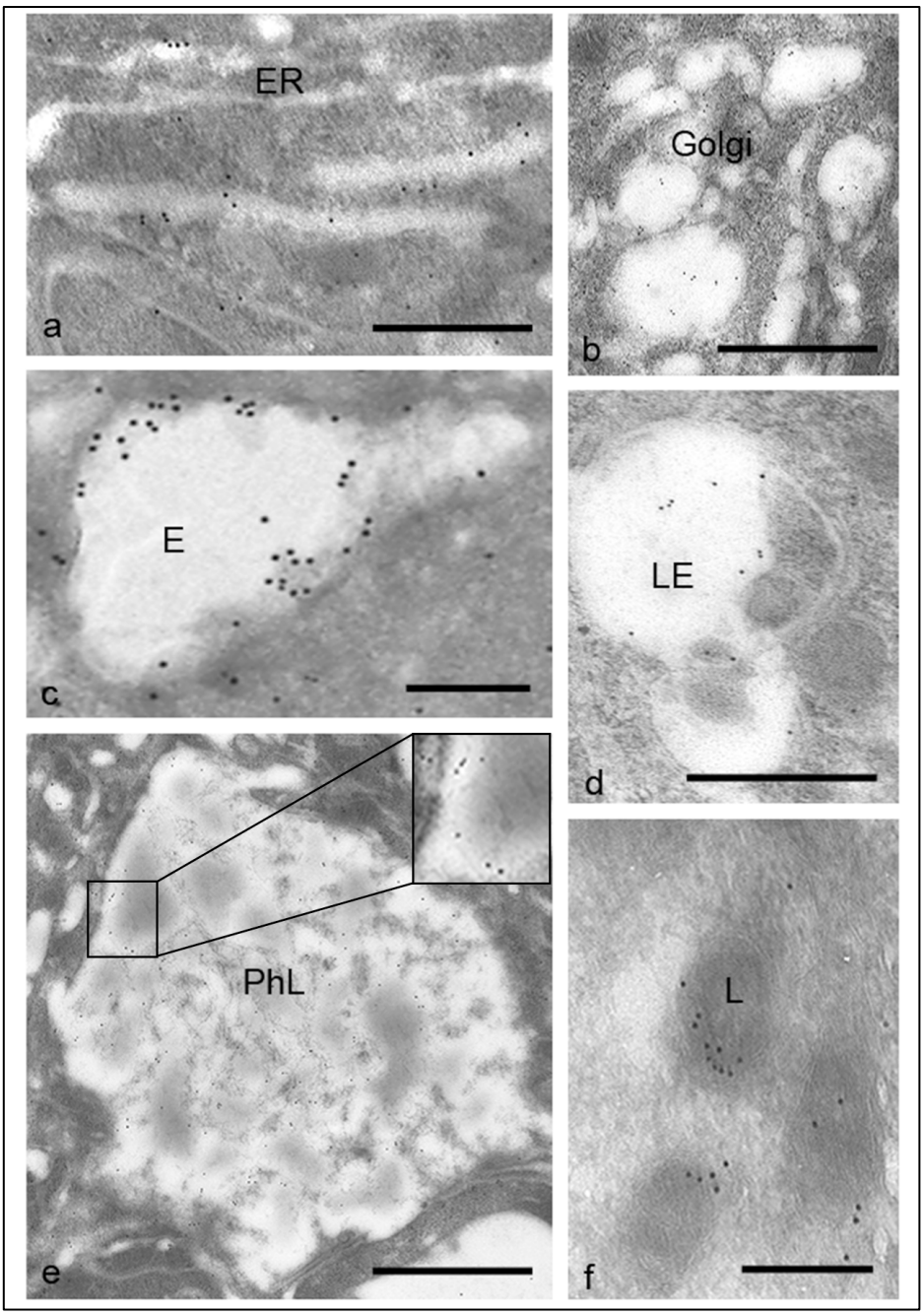

Figure 39 Cellular distribution of PC1/3 in NR8383 determined by immuno-gold electron microscopy.

Electron micrographs of NR8383 cells immunolabeled for PC1/3. Gold particles can be observed in: (a) endoplasmic reticulum (ER), bar = 500 nm; (b) Golgi apparatus, bar = 1 µm; (c) endosome (EE), bar = 250 nm; (d) late endosome (LE), bar = 500 nm; (e) phagolysosome (PhL), bar = 1 µm inset is a 2x magnification; (f) lysosomes (L), bar = 250 nm.

LPS induces PC1/3 trafficking and co-localization with TLR4.

Similar to neuroendocrine secretory cells, macrophages are known to secrete several factors (mostly cytokines) in a regulated fashion following innate immune stimulation. Thus, we postulated that LPS, which is a gram-negative bacterial stimulus, would induce PC1/3 trafficking. We thus used LPS to stimulate TLR4 in NR8383 macrophages. We show that LPS induced the time-dependent translocation of PC1/3 toward a phagolysosomal-like structure that co-localized with TLR4 (Figure 40). As soon as 30 min after initial LPS stimulation, PC1/3 showed good co-localization with TLR4 on these phagolysosomal-like structures. This co-localization is sustained over time. After 4 h of stimulation, increased accumulation of PC1/3 was observed within phagolysosomal structures as if the PC1/3 was now contained into multivesicular bodies being internalized. We also observed this phenomenon using a different PC1/3 antibody that recognizes the N-terminus of PC1/3 (Figure S 10), which reinforces the validity of our observation. Noteworthy, PC1/3 accumulation in vesicles near the PM was observed after LPS stimulation.

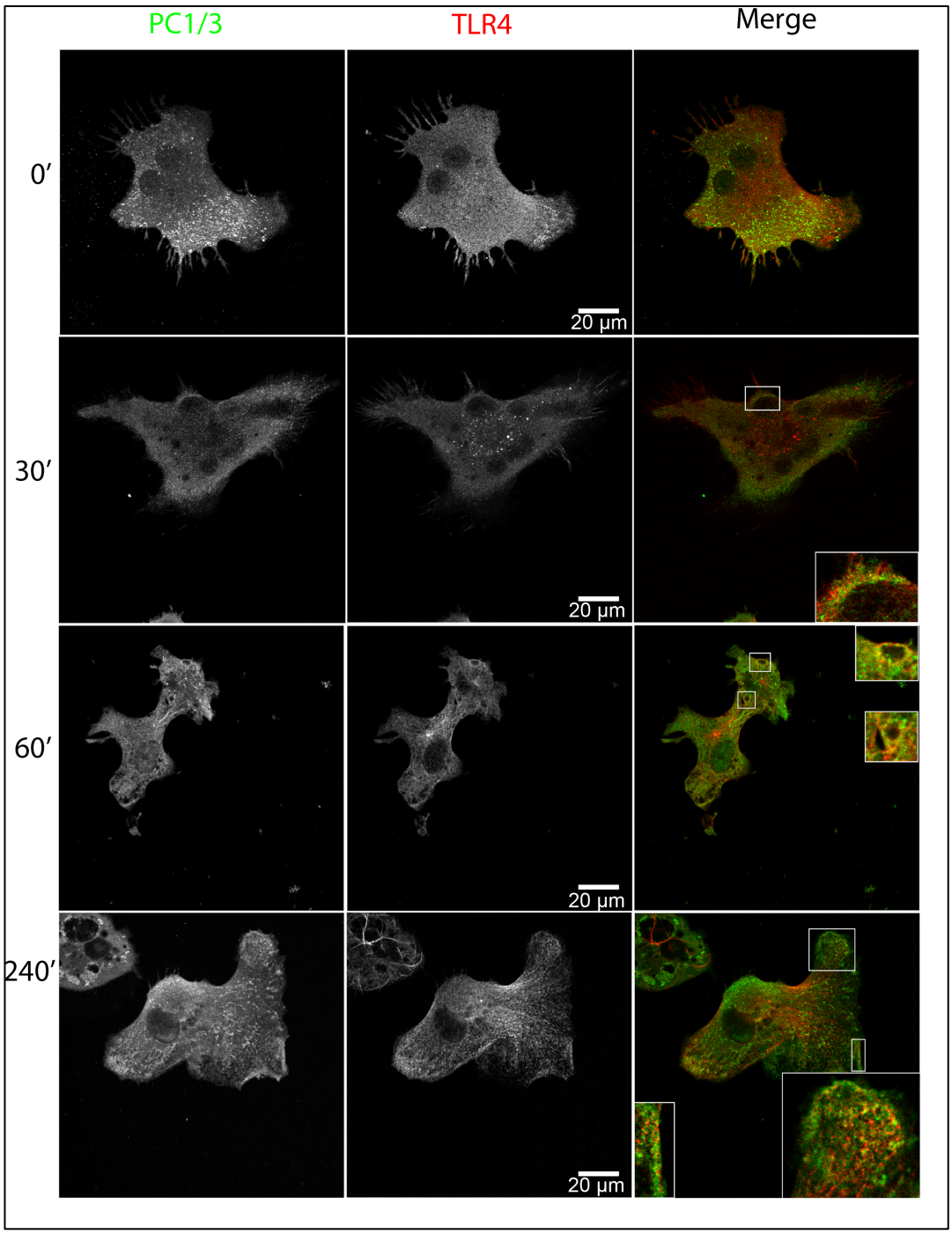

Figure 40 LPS induces PC1/3 trafficking and co-localization with TLR4.

Confocal images of NR8383 cells double-labeled with anti-PC1/3 (green) and anti-TLR4 (red) and incubated with 100 ng/ml LPS for the indicated time. Insets represent 3x magnification of regions where PC1/3 and TLR4 show partial co-localization.

LPS stimulation induces PC1/3 translocation from TGN46 to LAMP1 compartments

We next wanted to fully characterize this LPS-induced PC1/3 trafficking. We therefore conducted an immunofluorescence confocal microscopy co-localization study with PC1/3 and different organelle markers. After 60 min of LPS stimulation, PC1/3 still co-localized with TGN46 (Figure 41A). We also observed that LPS induced a clear reorganization of TGN46 such that this marker became like a round ball in the center of a vacuolar structure. PC1/3 was observed to localize to both the middle and the surrounding areas of these structures. After 240 min of LPS stimulation, PC1/3 no longer co-localized with TGN46 marker but rather localized near the PM and in vesicles surrounding large vacuolar structures. This vacuolar structures would correspond to where PC1/3 and TLR4 co-localize. PC1/3 co-localized with LAMP1 in the vesicles surrounding vacuolar structures only after 240 min of LPS stimulation and not after 60 min of stimulation (Figure 41B). Which support the observation that PC1/3 and LAMP1 co-colocalize (Figure 38C), mostly when phagosomal structures are present into cells. Little or no co-localization was observed with the early endosome marker EEA1 after 60 and 240 min of stimulation (Figure S 11).

Together, these results indicate that LPS induces PC1/3 trafficking into TLR4-containing structures and that LPS induces the exit of PC1/3 from TGN structures toward lysosomal and phagolysosomal vesicles. Another interesting observation is the drastic change in the distribution of TGN46, which is indicative of TGN reorganization after macrophage activation by LPS as previously described [53].

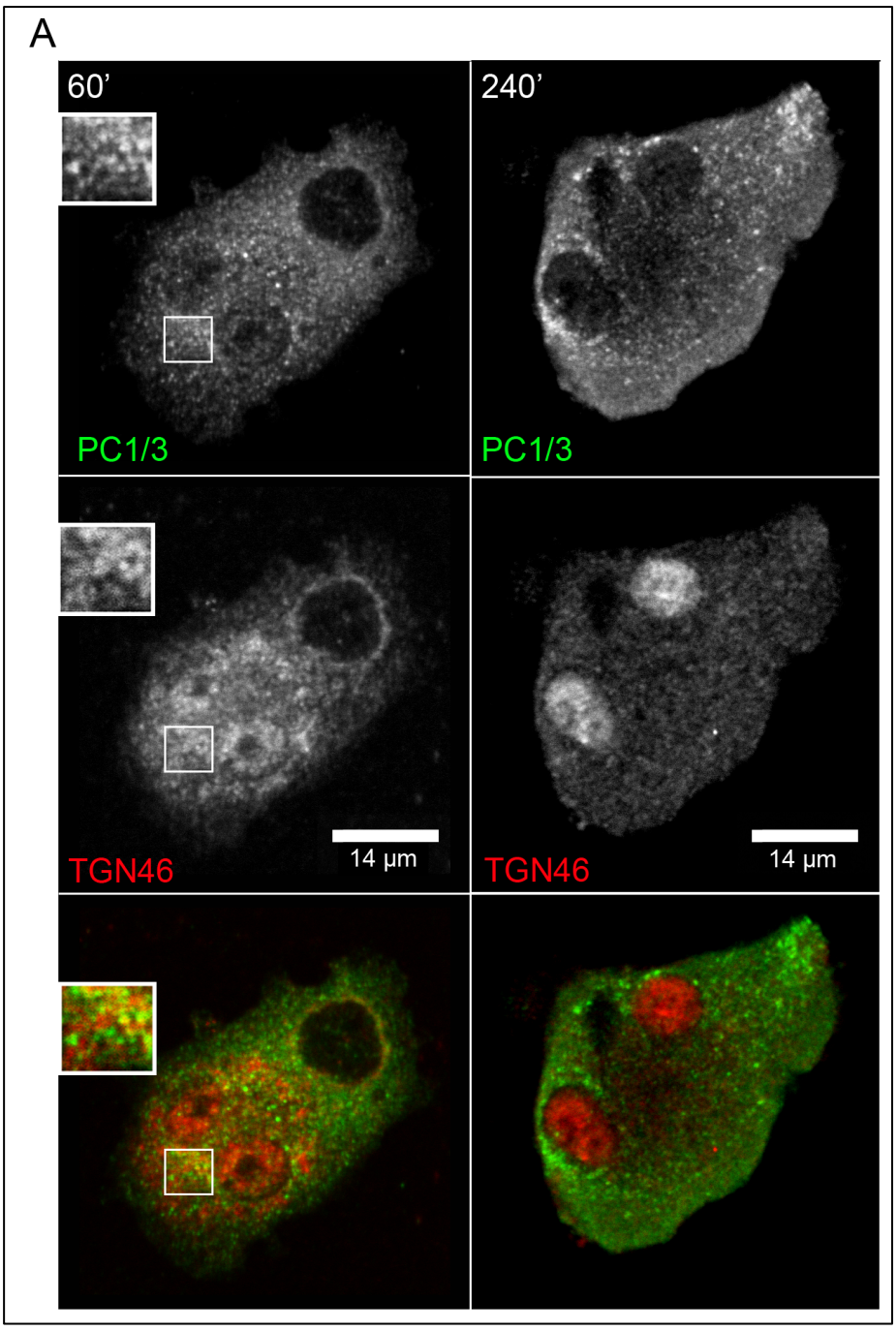

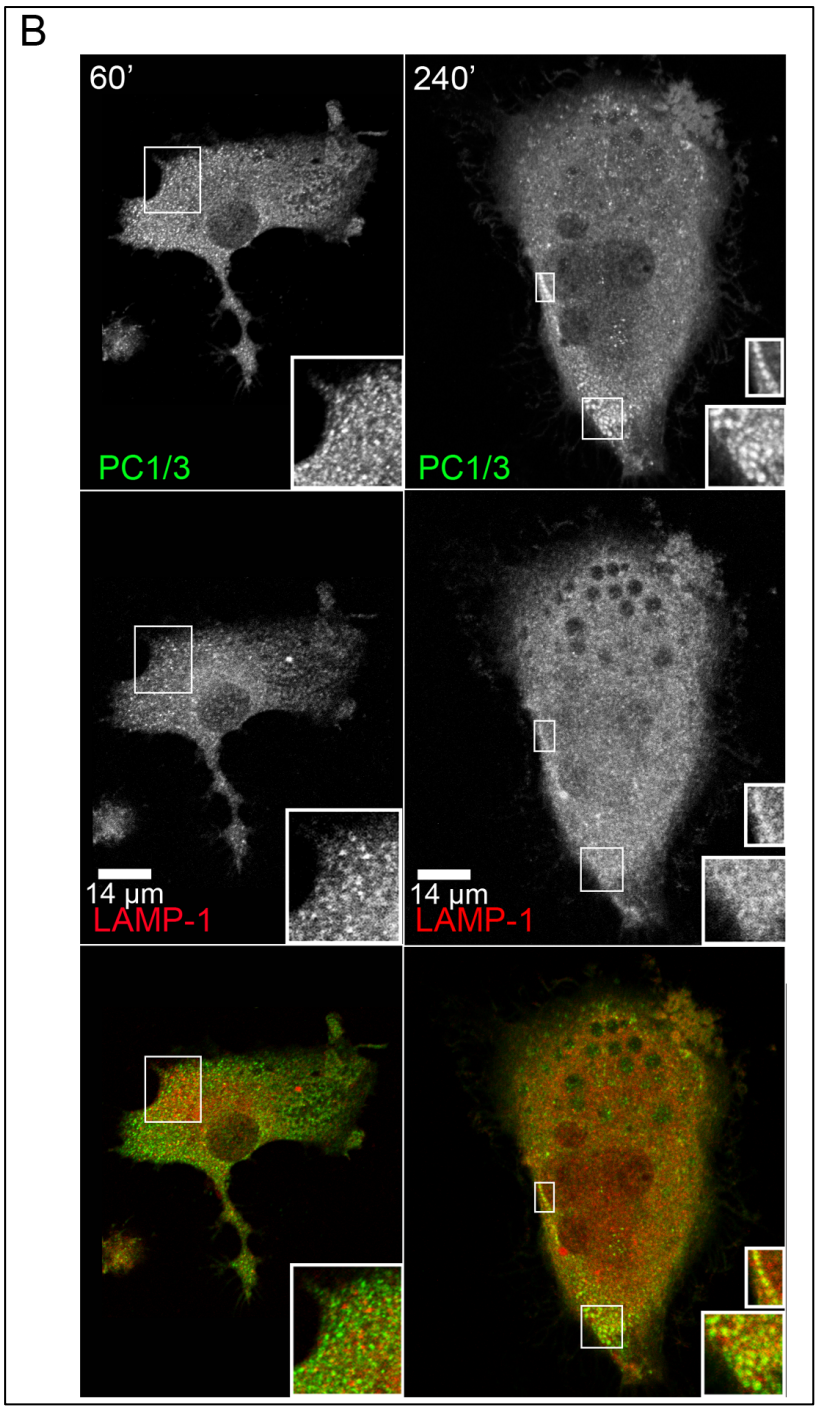

Figure 41 LPS induces PC1/3 trafficking into LAMP1 phagolysosomal structures.

Confocal images of NR8383 cells doubly labeled with anti-PC1/3 (green) co-localizing with (A) anti-TGN46 (red) and (B) anti-LAMP1 (red) after 60 and 240 min of stimulation with LPS (100 ng/mL). A. The inset shows the remaining co-localization between TGN46 and PC1/3 after 60 min of stimulation. B. The inset shows a low level of co-localization with LAMP1 after 60 min of LPS stimulation and increased co-localization with LAMP1 after 240 min of LPS stimulation.

Down-regulation of PC1/3 disrupts the spatial organization of vesicle trafficking markers in NR8383 cells.

One of our most interesting observations using isolated macrophages derived from PC1/3 KO mice was the drastic change in the number, shape and density of vesicles [12]. This observation, which was made using transmission electron microscopy (TEM), was a sign of several events that affect vesicle trafficking. We thus conducted a confocal microscopy study to determine whether the down-regulation of PC1/3 would affect vesicle trafficking markers in NR8383 cells. Little or no difference was observed in recycling vesicle maker RAB11 [54,55], lysosome to TGN recycling maker RAB9 [56,57] and TGN marker TGN46 [45,46] (Figure S 12). However, we observed notable changes (Figure 42A) in the early endosome markers Rab5 [49,58] and EEA1 [49,50] (Figure 42B), the baso-lateral transport marker RAB8 [59-61] and the lysosomal marker RAB7 [62,63] (Figure 42C). In NT cells, the early endosome markers EEA1 and RAB5 labeled the TGN region and areas near the PM. RAB5 labeling was stronger near the PM, and EEA1 labeling was stronger near the TGN region. Both markers indicated the formation of medium-sized vesicles (Figure 42A, inset). In shPC1/3 cells, one of the most important observations was the increased number of medium-sized vesicles and this observation correlate with an increase average size (Figure 7B-C) of the vesicles labelled by both markers (1.5±0.3 vs 0.28±0.05 μm^2 for RAB5 and 0.68±0.08 vs 0.47±0.05 μm^2 for EEA1). As well, a more diffuse distribution pattern of both markers was observed and a higher density of vesicles forming near the PM, especially when examining EEA1 (Figure 42A, arrows). In fact, while the integrated optic density remained comparable between NT shRNA and PC1/3 shRNA, mean intensity was lower in PC1/3 shRNA (66±8 vs 42±3, p=0.009 Student's t-test, indicative of a broader distribution since cell area was unchanged) and accompanied with an increased peripheral labelling ratio in PC1/3 shRNA cells (33±6 vs 22±4 %, p=0.01 Student's) . However, peripheral labelling ratio for RAB5 was unchanged. It is important to note that RAB5 labeling appeared to be much less intense in shPC1/3 cells, and this observation was confirmed by western blotting (Figure 43B). Western blots also illustrated a notable increase in EEA1 expression (Figure 43A) that was not easily observable in IF, most likely because of the dispersal of the marker throughout the cell. RAB8 labeling was mostly present at the basal PM of NT cells, and it exhibited tubular labeling and slight labeling of vesicle-like structures (Figure 42D, inset). RAB8 also labeled the TGN/Golgi

region. In shPC1/3 cells, the tubular labeling at the basal PM was much more intense accompanied with and increased tubular structures per cells (9±3 vs 2±1 tubules per cells, p=0.008 Student's t-test). Additionally, many cells showed strong and dense labeling of small vesicle-like structures near the PM as well as decreased and diffuse labeling of the TGN/Golgi. The latter observation was confirmed by an increase peripheral labelling ratio for RAB8 in shPC1/3 cells (34±1 vs 22±4 %) and could be explained by the decreased RAB8 expression observed in western blots (Figure 43D). RAB7 exhibited most intense labeling of all RAB proteins observed in NR8383 cells and was distributed throughout the cell with strong labeling near the TGN/Golgi region (Figure 42F). RAB7 also labeled large vesicle-like structures (Figure 42F, inset). In shPC1/3 cells, RAB7 labeling was even more intense, although this finding was not significant in western blot (Figure 43C). This increased labelling intensity was most likely related to the increased RAB7 integrated intensity in the peri nuclear region in PC1/3 shRNA (Figure 42H) (while the labeling ratio remained unchanged), where it appeared in multiple large well-formed vesicles (Figure 42F, inset) that were also an increased in size in PC1/3 shRNA (Figure 42G). Some weakly labeled large vesicles were also observed near the PM. Although we didn't observe any change in RAB9 and RAB11 localization (Figure S 12), western blotting revealed a notable decreased of RAB11 expression in PC1/3 shRNA cells (Figure 43F).

Based on these data, we can conclude that PC1/3 down-regulation results in dramatic changes in organization and trafficking activity in NR8383 cells. These results agree with our previously published data obtained in isolated PC1/3 KO peritoneal macrophages [12].

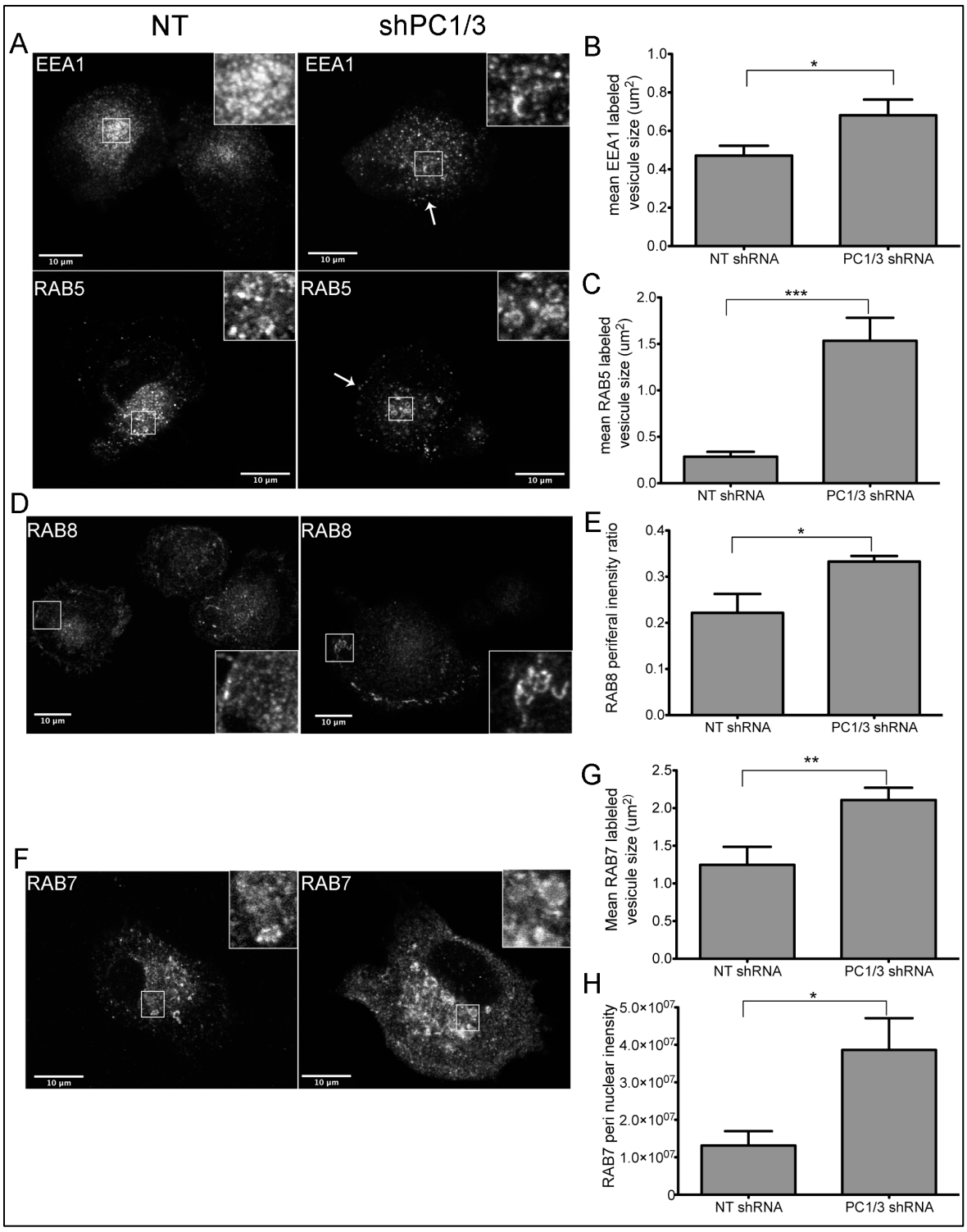

Figure 42 Effects of PC1/3 down-regulation on vesicle trafficking markers.

Confocal images of NR8383 cells stably transformed with control shRNA (NT) and shRNA directed against PC1/3 labeled with (A) early endosome marker EEA1 or RAB5. (D) baso-lateral membrane transport marker RAB8 and (F) late endosome/lysosome marker RAB7. In (A), arrows indicate punctate labeling near the plasma membrane. Insets

represent 3x magnification. (B-C, G) EEA1 (B), RAB5 (C) and RAB7 (G) labelled vesicles area was estimated using ImageJ software. Vesicles where considered as ovals and area was calculated using the following formula: π x a x b where a and b are the two largest diameters. E. The ratio between peripheral and total integrated intensity of RAB8 labeling is represented. H. RAB7 peri nuclear integrated intensity is represented. *=0.05 **=0.001 ***<0.0001, p-values, Student's t-test. Quantification was performed on randomly selected field of view on two independent shRNA cell lines n=4-6.

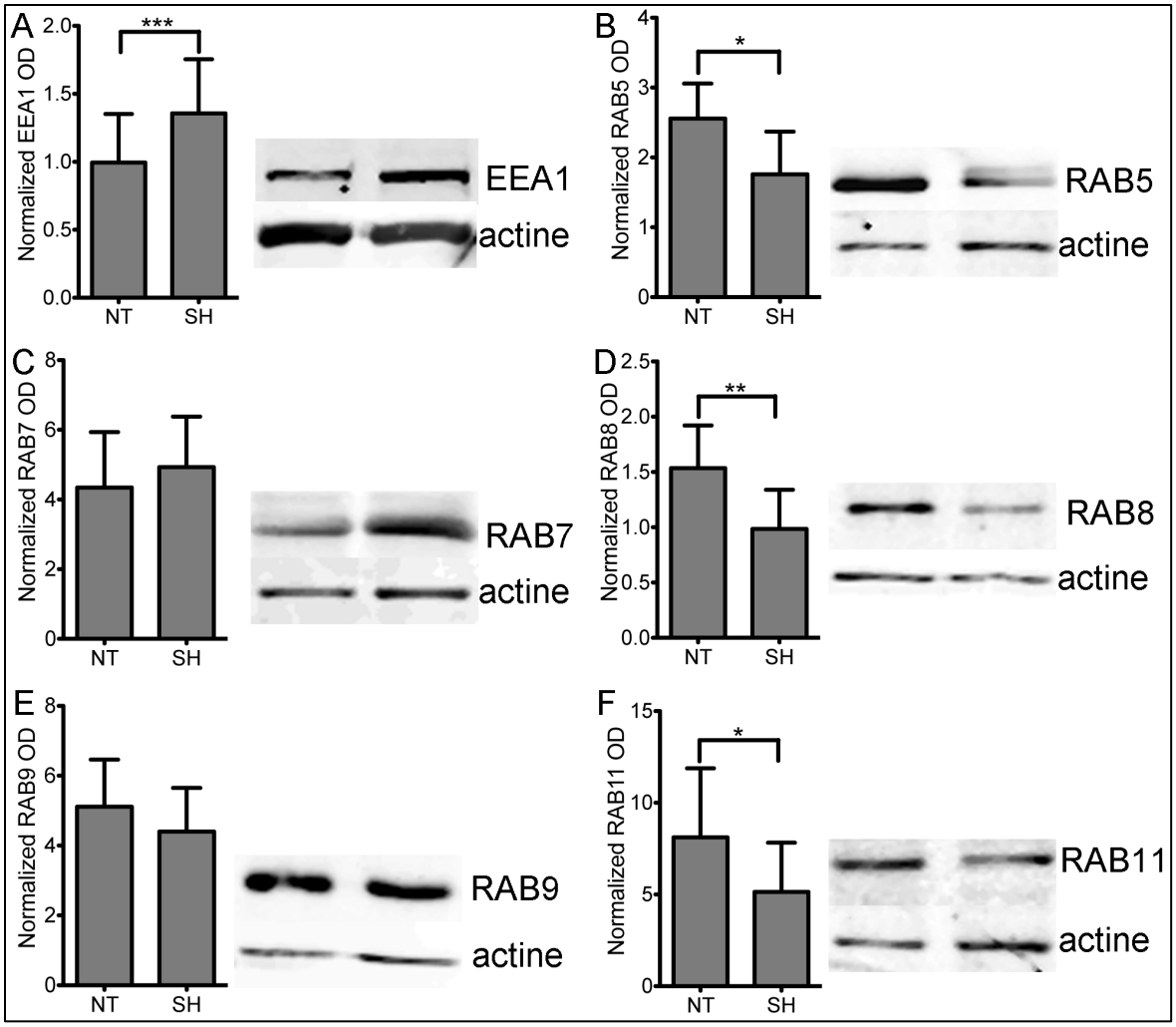

Figure 43 Effects of PC1/3 down-regulation on vesicle trafficking markers protein expression.

Representative western blots (20 µg of protein) and gels optic density (OD) quantification showing the relative levels of vesicle trafficking markers EEA1 (A), RAB5 (B), RAB7 (C), RAB8, RAB9 (D) and RAB11 (E) between NR8383 cells expressing control shRNA (NT) and those expressing shRNA directed against PC1/3 (SH). The actin loading control is included. *=0.05 **=0.001 ***<0.0001 p-values, Student's t-test n=5-8.

PC1/3 down-regulation modulates cytokine secretion in NR8383 cells.

Because an acute secretion of cytokine characterized the major innate immune phenotype of PC1/3 KO cells, we wanted to determine whether PC1/3 shRNA would induce the same phenotype in the NR8383 model. We observed a 4-fold increase in basal TNF-alpha secretion at 4 h and a 1.6-fold increase at 24 h in NR8383 cells expressing PC1/3 shRNA (NR8383 shPC1/3 cells) (Figure 44A-B). LPS stimulation did not have any effect on TNF-alpha secretion when compared with the control condition. However, when we examined the fold changes induced by ratios (LPS/basal), PC1/3 shRNA did in fact reduce TNF-alpha LPS induced secretion in NR8383 shPC1/3 cells; consequences of increased basal secretion level. When we examined the inflammasome-related cytokine IL-1β [64], we observed a similar increase in basal secretion at 4 h and 24 h with a respective increase in secretion of 1.7- and 3.5-fold in NR8383 shPC1/3 cells (Figure 44C-D). The main difference was the approximately 2.7-fold IL-1β increased secretion after 24 h of LPS stimulation in shPC1/3 cells. However, this represents an equivalent 3-fold increased LPS induced secretion in both NT and shPC1/3 cells. For IL-6, it was difficult to detect basal secretion at 4 h and 24 h as well as secretion after 4 h of LPS stimulation (Figure 44E). However, after 24 h of LPS stimulation, we were able to detect a 3.5-fold decrease in Il-6 secretion in shPC1/3 cells. We also examined other inflammatory cytokines such as IL-12p70 [65] and regulatory cytokine IL-10 [66]; however, we failed to observe reproducible and detectable levels of either cytokine (data not shown). Taken together, these results reflect a cytokine-dependent effect of PC1/3 down-regulation and indicate the complexity of the role of PC1/3 in macrophages. Although IL-6 showed a decrease in secretion upon LPS stimulation, TNF-α did not appear to be affected, and IL-1β was drastically up-regulated. The most consistent data obtained were the increased basal secretion of TNF-α and IL-1β, and we note that these were the only cytokines that could be measured when basal secretion was examined at 4 and 24 h.

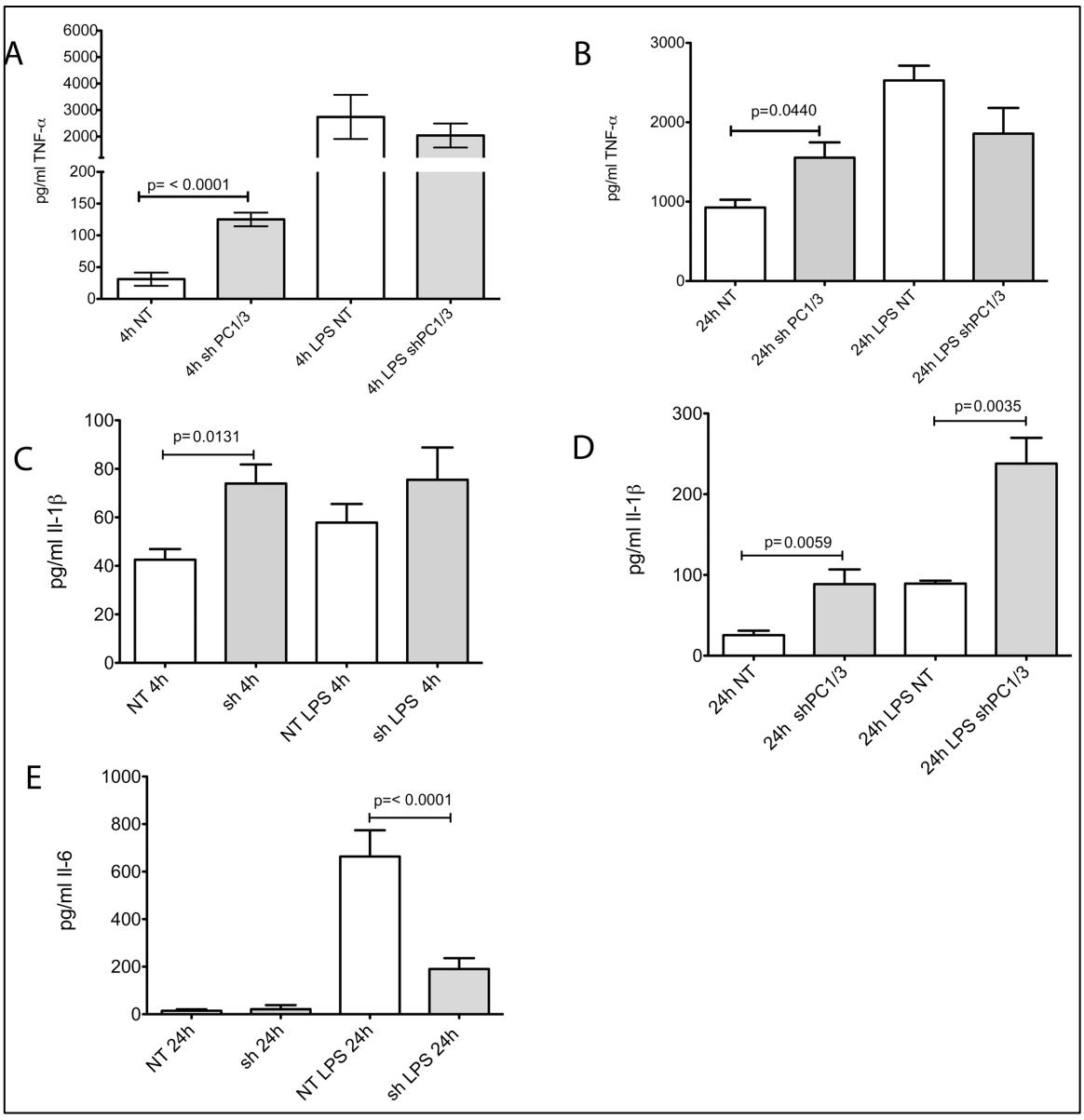

Figure 44 **Effects of PC1/3 down-regulation on cytokine secretion in NR8383 cells.**

Cytokine secretion measured by ELISA in control NR8383 cells expressing control shRNA (NT) and shRNA directed against PC1/3 in culture media with or without LPS stimulation (100 ng/mL) at various time points. A. TNF-alpha 4 h, B. TNF-alpha 24 h, C. IL-1beta 4 h, D. IL-1beta 24 h and E. IL-6 24 h. p-values were obtained using Student's t-test (n=4-6)

Discussion

PC1/3 plays a critical role in the neuroendocrine system, and our knowledge regarding PC1/3 has benefited from several cellular models, notably AtT-20 [67] and β-TC3 [42]. The discovery of human PC1/3 deficiency [68] and the generation of the PC1/3 KO mouse model [69] have allowed the fundamental data on PC1/3 to be further validated. In a recent study using PC1/3 KO mice [12], we clearly established a role for PC1/3 in the maintenance of immune homeostasis, which adds to the growing body of evidence indicating a role for PC1/3 in macrophages [9,11,70]. Thus, elucidation of the cellular biology and biochemistry of PC1/3 in macrophages would be highly valuable, and we report here that NR8383 cells are perfectly suited to do so. NR8383 cells express most TLRs and were previously shown to be sensitive to LPS [24] and Poly:IC [41]. NR8383 cells express PC1/3 but not PC2 and the know PC1/3 regulator ProSAAS [71,72], and PC1/3 expression is detectable at the protein level. This finding agrees with findings previously reported in rat-isolated macrophages [11]. Interestingly, the widely used RAW 264.7 cells did not express PC1/3 (data not shown). Macrophage-dependent expression of PC1/3 may have occurred; RAW264.7 cells are derived from ascites [73], and NR8383 cells are more similar to resident alveolar macrophages [33]. Alternatively, this phenomenon may reflect an artefact of the cell line itself. Indeed, THP-1, a human cell line, was previously shown to express PC1/3 [10], but THP-1 cells need to be induced with PMA to differentiate into macrophages. We believe that PMA treatment may introduce variability to the response; thus, it would be difficult to predict the stability and efficiency of knockdown strategies such as shRNA.

The regulated secretory pathway in macrophages, where PC1/3 is stored in neuroendocrine cells [74-77], is not conventional [51,52,78-80]. Thereby, this report indicates marked differences in PC1/3 cellular distribution when compared with neuroendocrine cells. In NR8383 cells, PC1/3 was mostly retained at the TGN in a pool that translocate to LAMP1-related vesicles. This pool was especially visible when macrophages exhibited phagocytic-like activities or where LPS stimulated. PC1/3 did not appear to accumulate in specialized secretory vesicles and showed no signs of PM-to-endosome trafficking. We can thus hypothesize that the TGN is where PC1/3 is primarily retained in NR8383 cells. EM confirmed these data and showed that PC1/3 was still widely

distributed in NR8383 cells with a preference for ER, TGN, phagolysosomes and late endosome vesicles. It is noteworthy that LPS triggers PC1/3 exit from the TGN toward LAMP1-labeled vesicles as well as co-localization with the LPS receptor TLR4. PC1/3 expression in macrophages [11] and tissue distribution in immune tissues [9] were already shown to be sensitive to LPS. The novel LPS-triggered trafficking of PC1/3 is what most closely resembles the well-known stimulus-dependent PC1/3 secretion and could be regulated by the phosphorylation mannose moieties in the N-glycosylation sites of PC1/3 by the phosphomannose receptor pathway [81]. However, LPS stimulation is known to induce dramatic changes in the organization of organelles within macrophages [53,82,83], and the intracellular reorganization of TGN46 that we observed as well as the previously reported reorganization [53] help to confirm this point. It remains unclear whether LPS-induced PC1/3 trafficking is tightly regulated or is simply part of a general cell reorganization mechanism.

Questions remain regarding whether PC1/3 plays a functional role in the cellular compartments to which it localizes, i.e., whether it is LPS-specific or whether other TLR ligands could induce similar changes in its localization. The change in localization of PC1/3 from the TGN toward LAMP1-labeled compartments provides an important hint. If PC1/3 was able to reach acidic vesicles, it must have been converted to shorter and more active forms [84]. Moreover, lysosomes and phagolysosomes are well known to be a part of the secretory pathway in macrophages [51,52,78]. Thus, this trafficking event may imply changes in PC1/3 secretion that could affect any paracrine role involved in the immune response. So far, we have only detected full-length PC1/3 in our experiments, but “granule rich” like fraction from THP-1 stimulated or not with LPS detected mostly ΔCT PC1/3 [10] and isolated rat alveolar macrophage and spleen monocytes present also ΔCT PC1/3 [11]. Unfortunately, the low level of PC1/3 expression in macrophages and the lack of specificity of our antibody in western blots prevented us from obtaining more detailed data for the characterization of PC1/3 maturation in NR8383 cells and further PC1/3 maturation and trafficking studies needs to be carried on these cells..

In this report, shRNA allowed us to corroborate a previous observation obtained in macrophages isolated from PC1/3 KO mice [12]. The most striking phenotype observed in PC1/3 KO mice was the deregulation of the LPS-induced secretion of pro-inflammatory

cytokines. This deregulated cytokine secretion was also observed in isolated PC1/3 KO macrophages. Here, we report somewhat similar findings in NR8383 cells with down-regulation of PC1/3, where the basal secretion of TNF-α and IL-1β was augmented, and 24 h of LPS stimulation drastically increased IL-1β secretion. However, 24 h of LPS stimulation had no effect on TNF-α secretion and reduced IL-6 secretion. The time course used to observe differences in cytokine secretion and the specific cytokine that exerted this effect in NR8383 shPC1/3 cells differ from what was reported for macrophages isolated from PC1/3 KO mice. The purity of the peritoneal extract, the long-term potentiation of peritoneal macrophages by other immune cells and the origin of the macrophage itself may explain these disparities. However, regarding the global effects on cytokine secretion, it is clear that PC1/3 is involved in the control of cytokine secretion in macrophages.

Part of the reason why cytokine secretion was deregulated was previously explained by EM studies on peritoneal isolated macrophages from KO mice. These studies uncovered drastic changes in the cellular organization of PC1/3 KO macrophages. In macrophages, constant transformation occurs between tubuloreticular and vesicular formations [85]. This process involves ligand-receptor binding, intricate signal transduction networks, focal cytoskeleton rearrangement and a dynamic series of membrane fusion/fission and remodelling events [86]. We investigated the effect of PC1/3 down-regulation on these processes. NR8383 shPC1/3 cells showed expression changes and intracellular re-organization of RAB7-, RAB8- and EEA1/RAB5-related markers. Interestingly the effect seemed to be constrained to specific markers and vesicles because no effects were observed for RAB9, RAB11 or TGN46. These results are highly similar to previous findings in isolated KO macrophages and are indicative of the regulatory mechanisms of cytokine secretion. Thus, we propose two hypotheses to explain these changes. First, PC1/3 may affect the activity of a substrate and trigger signalling events that could regulate the expression and activation of RAB proteins. It was previously reported that substrates of PC1/3 are secreted by macrophages, notably proopiomelanocortin and somatostatin [10,11,70,87,88]. Given the cellular localization of PC1/3, it may even play a role within the phagocytic synapse, where several signalling events are initiated [89,90]. The second hypothesis implies that PC1/3 could act as a binding partner or a possible chaperone within the secretory pathway. It was proposed that PC1/3 could sort proteins to DCSGs by binding

to the recognition cleavage site composed of paired basic amino acids [43,91-93]. Knockout models have revealed that in absence of PC1/3 some neuropeptide substrates tend to be overrepresented [94]. Thus, without the need for processing a specific substrate, PC1/3 could use paired basic amino acids as a sorting motif and could regulate several trafficking events.

The establishment of the rat alveolar NR8383 cell line as a good model to study the role of PC1/3 in innate immunity is a step toward achieving a better understanding of this non-conventional role of PC1/3. Future studies on the expression of PC1/3 substrates as well as activation and trafficking regulation in NR8383 cells will provide clues regarding how the knockout of PC1/3 causes a global deregulation of the innate immune response.

Acknowledgements

We are extremely grateful to Drs. Marc Pallardy (CEA, Paris) and Sandrine Lacour for providing the NR8383 cell line used in this study, to Dr. Christine Lavoie (UdeS, Sherbrooke) for providing material and assistance for confocal microscopy and to Christian Slomianny (Université Lille 1) for electronic microscopy.

References

1. Turk B, Turk du SA, Turk V (2012) Protease signalling: the cutting edge. EMBO Journal 31: 1630-1643.
2. Rholam M, Fahy C (2009) Processing of peptide and hormone precursors at the dibasic cleavage sites. Cellular and Molecular Life Sciences 66: 2075-2091.
3. Seidah NG, Chretien M (1999) Proprotein and prohormone convertases: a family of subtilases generating diverse bioactive polypeptides. Brain Research 848: 45-62.
4. Hosaka M, Nagahama M, Kim WS, Watanabe T, Hatsuzawa K, et al. (1991) Arg-X-Lys/Arg-Arg motif as a signal for precursor cleavage catalyzed by furin within the constitutive secretory pathway. Journal of Biological Chemistry 266: 12127-12130.
5. Seidah NG, Khatib AM, Prat A (2006) The proprotein convertases and their implication in sterol and/or lipid metabolism. Biological Chemistry 387: 871-877.
6. Siezen RJ, Leunissen JA (1997) Subtilases: the superfamily of subtilisin-like serine proteases. Protein Science 6: 501-523.
7. Creemers JW, Siezen RJ, Roebroek AJ, Ayoubi TA, Huylebroeck D, et al. (1993) Modulation of furin-mediated proprotein processing activity by site-directed mutagenesis. Journal of Biological Chemistry 268: 21826-21834.
8. Creemers JW, Vey M, Schafer W, Ayoubi TA, Roebroek AJ, et al. (1995) Endoproteolytic cleavage of its propeptide is a prerequisite for efficient transport of furin out of the endoplasmic reticulum. Journal of Biological Chemistry 270: 2695-2702.
9. Lansac G, Dong W, Dubois CM, Benlarbi N, Afonso C, et al. (2006) Lipopolysaccharide mediated regulation of neuroendocrine associated proprotein convertases and neuropeptide precursor processing in the rat spleen. Journal of Neuroimmunology 171: 57-71.
10. LaMendola J, Martin SK, Steiner DF (1997) Expression of PC3, carboxypeptidase E and enkephalin in human monocyte-derived macrophages as a tool for genetic studies. FEBS Letters 404: 19-22.
11. Vindrola O, Mayer AM, Citera G, Spitzer JA, Espinoza LR (1994) Prohormone convertases PC2 and PC3 in rat neutrophils and macrophages. Parallel changes with proenkephalin-derived peptides induced by LPS in vivo. Neuropeptides 27: 235-244.
12. Refaie S, Gagnon S, Gagnon H, Desjardins R, D'Anjou F, et al. (2012) Disruption of proprotein convertase 1/3 (PC1/3) expression in mice causes innate immune defects and uncontrolled cytokine secretion. Journal of Biological Chemistry 287: 14703-14717.
13. Lu YC, Yeh WC, Ohashi PS (2008) LPS/TLR4 signal transduction pathway. Cytokine 42: 145-151.
14. Chow JC, Young DW, Golenbock DT, Christ WJ, Gusovsky F (1999) Toll-like receptor-4 mediates lipopolysaccharide-induced signal transduction. Journal of Biological Chemistry 274: 10689-10692.
15. O'Neill LA (2008) 'Fine tuning' TLR signaling. Nat Immunol 9: 459-461.
16. Mantovani A, Sica A (2010) Macrophages, innate immunity and cancer: balance, tolerance, and diversity. Current Opinion in Immunology 22: 231-237.

17. Gereda JE, Leung DY, Thatayatikom A, Streib JE, Price MR, et al. (2000) Relation between house-dust endotoxin exposure, type 1 T-cell development, and allergen sensitisation in infants at high risk of asthma. Lancet 355: 1680-1683.
18. Baecher-Allen C, Hafler D (2006) Human regulatory T cells and their role in autoimmune disease. Immunological Reviews 212: 203-216.
19. Ulevitch RJ (2004) Therapeutics targeting the innate immune system. Nat Rev Immunol 4: 512-520.
20. Guha M (2012) Anticancer TLR agonists on the ropes. Nat Rev Drug Discov 11: 503-505.
21. Seidah NG, Day R, Benjannet S, Rondeau N, Boudreault A, et al. (1992) The prohormone and proprotein processing enzymes PC1 and PC2: structure, selective cleavage of mouse POMC and human renin at pairs of basic residues, cellular expression, tissue distribution, and mRNA regulation. NIDA Research Monograph 126: 132-150.
22. Hook V, Funkelstein L, Lu D, Bark S, Wegrzyn J, et al. (2008) Proteases for processing proneuropeptides into peptide neurotransmitters and hormones. Annual Review of Pharmacology and Toxicology 48: 393-423.
23. Scamuffa N, Calvo F, Chretien M, Seidah NG, Khatib AM (2006) Proprotein convertases: lessons from knockouts. FASEB Journal 20: 1954-1963.
24. Ren W, Hu L, Hua F, Jin J, Wang Y, et al. (2011) Myeloid differentiation protein 2 silencing decreases LPS-induced cytokine production and TLR4/MyD88 pathway activity in alveolar macrophages. Immunology Letters 141: 94-101.
25. Seidah NG, Marcinkiewicz M, Benjannet S, Gaspar L, Beaubien G, et al. (1991) Cloning and primary sequence of a mouse candidate prohormone convertase PC1 homologous to PC2, Furin, and Kex2: distinct chromosomal localization and messenger RNA distribution in brain and pituitary compared to PC2. Molecular Endocrinology 5: 111-122.
26. Day R, Schafer MK, Cullinan WE, Watson SJ, Chretien M, et al. (1993) Region specific expression of furin mRNA in the rat brain. Neuroscience Letters 149: 27-30.
27. Seidah NG, Chretien M, Day R (1994) The family of subtilisin/kexin like pro-protein and pro-hormone convertases: divergent or shared functions. Biochimie 76: 197-209.
28. Lanoue E, Day R (2001) Coexpression of proprotein convertase SPC3 and the neuroendocrine precursor proSAAS. Endocrinology 142: 4141-4149.
29. Dong W, Marcinkiewicz M, Vieau D, Chretien M, Seidah NG, et al. (1995) Distinct mRNA expression of the highly homologous convertases PC5 and PACE4 in the rat brain and pituitary. J Neurosci 15: 1778-1796.
30. Lusson J, Vieau D, Hamelin J, Day R, Chretien M, et al. (1993) cDNA structure of the mouse and rat subtilisin/kexin-like PC5: a candidate proprotein convertase expressed in endocrine and nonendocrine cells. Proc Natl Acad Sci U S A 90: 6691-6695.
31. Seidah NG, Hamelin J, Mamarbachi M, Dong W, Tardos H, et al. (1996) cDNA structure, tissue distribution, and chromosomal localization of rat PC7, a novel mammalian proprotein convertase closest to yeast kexin-like proteinases. Proceedings of the National Academy of Sciences of the United States of America 93: 3388-3393.

32. Helmke RJ, German VF, Mangos JA (1989) A continuous alveolar macrophage cell line: comparisons with freshly derived alveolar macrophages. In Vitro Cell Dev Biol 25: 44-48.
33. Helmke RJ, Boyd RL, German VF, Mangos JA (1987) From growth factor dependence to growth factor responsiveness: the genesis of an alveolar macrophage cell line. In Vitro Cell Dev Biol 23: 567-574.
34. Brodeur J, Larkin H, Boucher R, Theriault C, St-Louis SC, et al. (2009) Calnuc binds to LRP9 and affects its endosomal sorting. Traffic 10: 1098-1114.
35. Schneider CA, Rasband WS, Eliceiri KW (2012) NIH Image to ImageJ: 25 years of image analysis. Nat Methods 9: 671-675.
36. Girish V, Vijayalakshmi A (2004) Affordable image analysis using NIH Image/ImageJ. Indian Journal of Cancer 41: 47.
37. Linkert M, Rueden CT, Allan C, Burel JM, Moore W, et al. (2010) Metadata matters: access to image data in the real world. J Cell Biol 189: 777-782.
38. Day R, Schafer MK, Watson SJ, Chretien M, Seidah NG (1992) Distribution and regulation of the prohormone convertases PC1 and PC2 in the rat pituitary. Mol Endocrinol 6: 485-497.
39. D'Anjou F, Routhier S, Perreault JP, Latil A, Bonnel D, et al. (2011) Molecular Validation of PACE4 as a Target in Prostate Cancer. Transl Oncol 4: 157-172.
40. Yuasa K, Masuda T, Yoshikawa C, Nagahama M, Matsuda Y, et al. (2009) Subtilisin-like proprotein convertase PACE4 is required for skeletal muscle differentiation. J Biochem 146: 407-415.
41. Meng L, Zhu W, Jiang C, He X, Hou W, et al. (2010) Toll-like receptor 3 upregulation in macrophages participates in the initiation and maintenance of pristane-induced arthritis in rats. Arthritis Res Ther 12: R103.
42. Benjannet S, Rondeau N, Paquet L, Boudreault A, Lazure C, et al. (1993) Comparative biosynthesis, covalent post-translational modifications and efficiency of prosegment cleavage of the prohormone convertases PC1 and PC2: glycosylation, sulphation and identification of the intracellular site of prosegment cleavage of PC1 and PC2. Biochemical Journal 294 (Pt 3): 735-743.
43. Dikeakos JD, Mercure C, Lacombe MJ, Seidah NG, Reudelhuber TL (2007) PC1/3, PC2 and PC5/6A are targeted to dense core secretory granules by a common mechanism. Febs J 274: 4094-4102.
44. Lindberg I (1994) Evidence for cleavage of the PC1/PC3 pro-segment in the endoplasmic reticulum. Molecular and Cellular Neurosciences 5: 263-268.
45. Ponnambalam S, Girotti M, Yaspo ML, Owen CE, Perry AC, et al. (1996) Primate homologues of rat TGN38: primary structure, expression and functional implications. Journal of Cell Science 109 (Pt 3): 675-685.
46. Prescott AR, Lucocq JM, James J, Lister JM, Ponnambalam S (1997) Distinct compartmentalization of TGN46 and beta 1,4-galactosyltransferase in HeLa cells. European Journal of Cell Biology 72: 238-246.
47. Saftig P, Klumperman J (2009) Lysosome biogenesis and lysosomal membrane proteins: trafficking meets function. Nat Rev Mol Cell Biol 10: 623-635.
48. Huynh KK, Eskelinen EL, Scott CC, Malevanets A, Saftig P, et al. (2007) LAMP proteins are required for fusion of lysosomes with phagosomes. EMBO Journal 26: 313-324.

49. Christoforidis S, McBride HM, Burgoyne RD, Zerial M (1999) The Rab5 effector EEA1 is a core component of endosome docking. Nature 397: 621-625.
50. Mu FT, Callaghan JM, Steele-Mortimer O, Stenmark H, Parton RG, et al. (1995) EEA1, an early endosome-associated protein. EEA1 is a conserved alpha-helical peripheral membrane protein flanked by cysteine "fingers" and contains a calmodulin-binding IQ motif. Journal of Biological Chemistry 270: 13503-13511.
51. Blott EJ, Griffiths GM (2002) Secretory lysosomes. Nat Rev Mol Cell Biol 3: 122-131.
52. Tapper H (1996) The secretion of preformed granules by macrophages and neutrophils. Journal of Leukocyte Biology 59: 613-622.
53. Tian Y, Pate C, Andreolotti A, Wang L, Tuomanen E, et al. (2008) Cytokine secretion requires phosphatidylcholine synthesis. Journal of Cell Biology 181: 945-957.
54. Ullrich O, Reinsch S, Urbe S, Zerial M, Parton RG (1996) Rab11 regulates recycling through the pericentriolar recycling endosome. Journal of Cell Biology 135: 913-924.
55. Chen W, Feng Y, Chen D, Wandinger-Ness A (1998) Rab11 is required for trans-golgi network-to-plasma membrane transport and a preferential target for GDP dissociation inhibitor. Molecular Biology of the Cell 9: 3241-3257.
56. Lombardi D, Soldati T, Riederer MA, Goda Y, Zerial M, et al. (1993) Rab9 functions in transport between late endosomes and the trans Golgi network. EMBO Journal 12: 677-682.
57. Riederer MA, Soldati T, Shapiro AD, Lin J, Pfeffer SR (1994) Lysosome biogenesis requires Rab9 function and receptor recycling from endosomes to the trans-Golgi network. Journal of Cell Biology 125: 573-582.
58. Bucci C, Parton RG, Mather IH, Stunnenberg H, Simons K, et al. (1992) The small GTPase rab5 functions as a regulatory factor in the early endocytic pathway. Cell 70: 715-728.
59. Chen YT, Holcomb C, Moore HP (1993) Expression and localization of two low molecular weight GTP-binding proteins, Rab8 and Rab10, by epitope tag. Proceedings of the National Academy of Sciences of the United States of America 90: 6508-6512.
60. Henry L, Sheff DR (2008) Rab8 regulates basolateral secretory, but not recycling, traffic at the recycling endosome. Molecular Biology of the Cell 19: 2059-2068.
61. Huber LA, Pimplikar S, Parton RG, Virta H, Zerial M, et al. (1993) Rab8, a small GTPase involved in vesicular traffic between the TGN and the basolateral plasma membrane. Journal of Cell Biology 123: 35-45.
62. Feng Y, Press B, Wandinger-Ness A (1995) Rab 7: an important regulator of late endocytic membrane traffic. Journal of Cell Biology 131: 1435-1452.
63. Meresse S, Gorvel JP, Chavrier P (1995) The rab7 GTPase resides on a vesicular compartment connected to lysosomes. Journal of Cell Science 108 (Pt 11): 3349-3358.
64. Dinarello CA (1996) Biologic basis for interleukin-1 in disease. Blood 87: 2095-2147.
65. Hsieh CS, Macatonia SE, Tripp CS, Wolf SF, O'Garra A, et al. (1993) Development of TH1 CD4+ T cells through IL-12 produced by Listeria-induced macrophages. Science 260: 547-549.
66. Akuffo H, Alexis A, Eidsmo L, Saed A, Nylen S, et al. (1999) Natural killer cells in cross-regulation of IL-12 by IL-10 in Leishmania antigen-stimulated blood donor cells. Clinical and Experimental Immunology 117: 529-534.

67. Smeekens SP, Avruch AS, LaMendola J, Chan SJ, Steiner DF (1991) Identification of a cDNA encoding a second putative prohormone convertase related to PC2 in AtT20 cells and islets of Langerhans. Proc Natl Acad Sci U S A 88: 340-344.
68. Jackson RS, Creemers JW, Ohagi S, Raffin-Sanson ML, Sanders L, et al. (1997) Obesity and impaired prohormone processing associated with mutations in the human prohormone convertase 1 gene. Nature Genetics 16: 303-306.
69. Zhu X, Zhou A, Dey A, Norrbom C, Carroll R, et al. (2002) Disruption of PC1/3 expression in mice causes dwarfism and multiple neuroendocrine peptide processing defects. Proceedings of the National Academy of Sciences of the United States of America 99: 10293-10298.
70. Saravia F, Padros MR, Ase A, Aloyz R, Duran S, et al. (1998) Differential response to a stress stimulus of proenkephalin peptide content in immune cells of naive and chronically stressed rats. Neuropeptides 32: 351-359.
71. Basak A, Koch P, Dupelle M, Fricker LD, Devi LA, et al. (2001) Inhibitory specificity and potency of proSAAS-derived peptides toward proprotein convertase 1. J Biol Chem 276: 32720-32728.
72. Lee SN, Prodhomme E, Lindberg I (2004) Prohormone convertase 1 (PC1) processing and sorting: effect of PC1 propeptide and proSAAS. J Endocrinol 182: 353-364.
73. Ralph P, Nakoinz I (1977) Antibody-dependent killing of erythrocyte and tumor targets by macrophage-related cell lines: enhancement by PPD and LPS. Journal of Immunology 119: 950-954.
74. Hornby PJ, Rosenthal SD, Mathis JP, Vindrola O, Lindberg I (1993) Immunocytochemical localization of the neuropeptide-synthesizing enzyme PC1 in AtT-20 cells. Neuroendocrinology 58: 555-563.
75. Malide D, Seidah NG, Chretien M, Bendayan M (1995) Electron microscopic immunocytochemical evidence for the involvement of the convertases PC1 and PC2 in the processing of proinsulin in pancreatic beta-cells. Journal of Histochemistry and Cytochemistry 43: 11-19.
76. Bailyes EM, Shennan KI, Seal AJ, Smeekens SP, Steiner DF, et al. (1992) A member of the eukaryotic subtilisin family (PC3) has the enzymic properties of the type 1 proinsulin-converting endopeptidase. Biochem J 285 (Pt 2): 391-394.
77. Tanaka S, Kurabuchi S, Mochida H, Kato T, Takahashi S, et al. (1996) Immunocytochemical localization of prohormone convertases PC1/PC3 and PC2 in rat pancreatic islets. Archives of Histology and Cytology 59: 261-271.
78. Duitman EH, Orinska Z, Bulfone-Paus S (2011) Mechanisms of cytokine secretion: a portfolio of distinct pathways allows flexibility in cytokine activity. European Journal of Cell Biology 90: 476-483.
79. Stow JL, Low PC, Offenhauser C, Sangermani D (2009) Cytokine secretion in macrophages and other cells: pathways and mediators. Immunobiology 214: 601-612.
80. Chapman HA, Jr. (1991) Role of enzyme receptors and inhibitors in regulating proteolytic activities of macrophages. Annals of the New York Academy of Sciences 624: 87-96.
81. Zandberg WF, Benjannet S, Hamelin J, Pinto BM, Seidah NG (2011) N-glycosylation controls trafficking, zymogen activation and substrate processing of proprotein convertases PC1/3 and subtilisin kexin isozyme-1. Glycobiology 21: 1290-1300.

82. Zhao Z, Fux B, Goodwin M, Dunay IR, Strong D, et al. (2008) Autophagosome-independent essential function for the autophagy protein Atg5 in cellular immunity to intracellular pathogens. Cell Host Microbe 4: 458-469.
83. Rittig MG, Wilske B, Krause A (1999) Phagocytosis of microorganisms by means of overshooting pseudopods: where do we stand? Microbes Infect 1: 727-735.
84. Zhou Y, Lindberg I (1994) Enzymatic properties of carboxyl-terminally truncated prohormone convertase 1 (PC1/SPC3) and evidence for autocatalytic conversion. Journal of Biological Chemistry 269: 18408-18413.
85. Knapp PE, Swanson JA (1990) Plasticity of the tubular lysosomal compartment in macrophages. Journal of Cell Science 95 (Pt 3): 433-439.
86. Desjardins M (2003) ER-mediated phagocytosis: a new membrane for new functions. Nat Rev Immunol 3: 280-291.
87. Lolait SJ, Lim AT, Toh BH, Funder JW (1984) Immunoreactive beta-endorphin in a subpopulation of mouse spleen macrophages. J Clin Invest 73: 277-280.
88. Dalm VA, van Hagen PM, van Koetsveld PM, Achilefu S, Houtsmuller AB, et al. (2003) Expression of somatostatin, cortistatin, and somatostatin receptors in human monocytes, macrophages, and dendritic cells. Am J Physiol Endocrinol Metab 285: E344-353.
89. Murray RZ, Kay JG, Sangermani DG, Stow JL (2005) A role for the phagosome in cytokine secretion. Science 310: 1492-1495.
90. Dustin ML (2012) Signaling at neuro/immune synapses. Journal of Clinical Investigation 122: 1149-1155.
91. Feliciangeli S, Kitabgi P, Bidard JN (2001) The role of dibasic residues in prohormone sorting to the regulated secretory pathway. A study with proneurotensin. Journal of Biological Chemistry 276: 6140-6150.
92. Brechler V, Chu WN, Baxter JD, Thibault G, Reudelhuber TL (1996) A protease processing site is essential for prorenin sorting to the regulated secretory pathway. Journal of Biological Chemistry 271: 20636-20640.
93. Bundgaard JR, Birkedal H, Rehfeld JF (2004) Progastrin is directed to the regulated secretory pathway by synergistically acting basic and acidic motifs. Journal of Biological Chemistry 279: 5488-5493.
94. Pan H, Nanno D, Che FY, Zhu X, Salton SR, et al. (2005) Neuropeptide

Figure S 9 Alignment between PC1/3 RT-PCR product from NR8383 and sequence of rat NR8383 NM_017091.

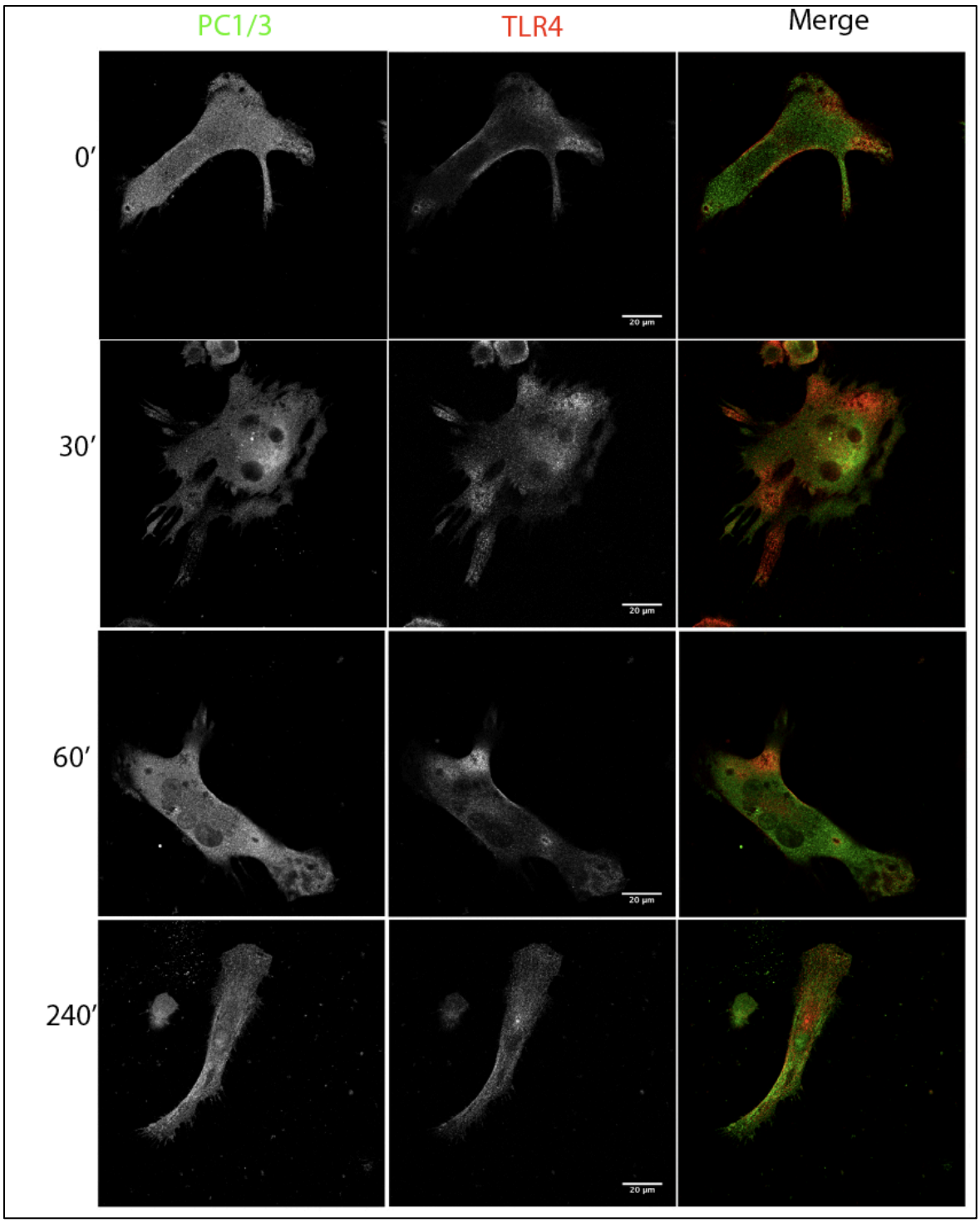

Figure S 10 TLR4 and PC1/3 (using C-Terminal antibody) co-localize during LPS stimulation.

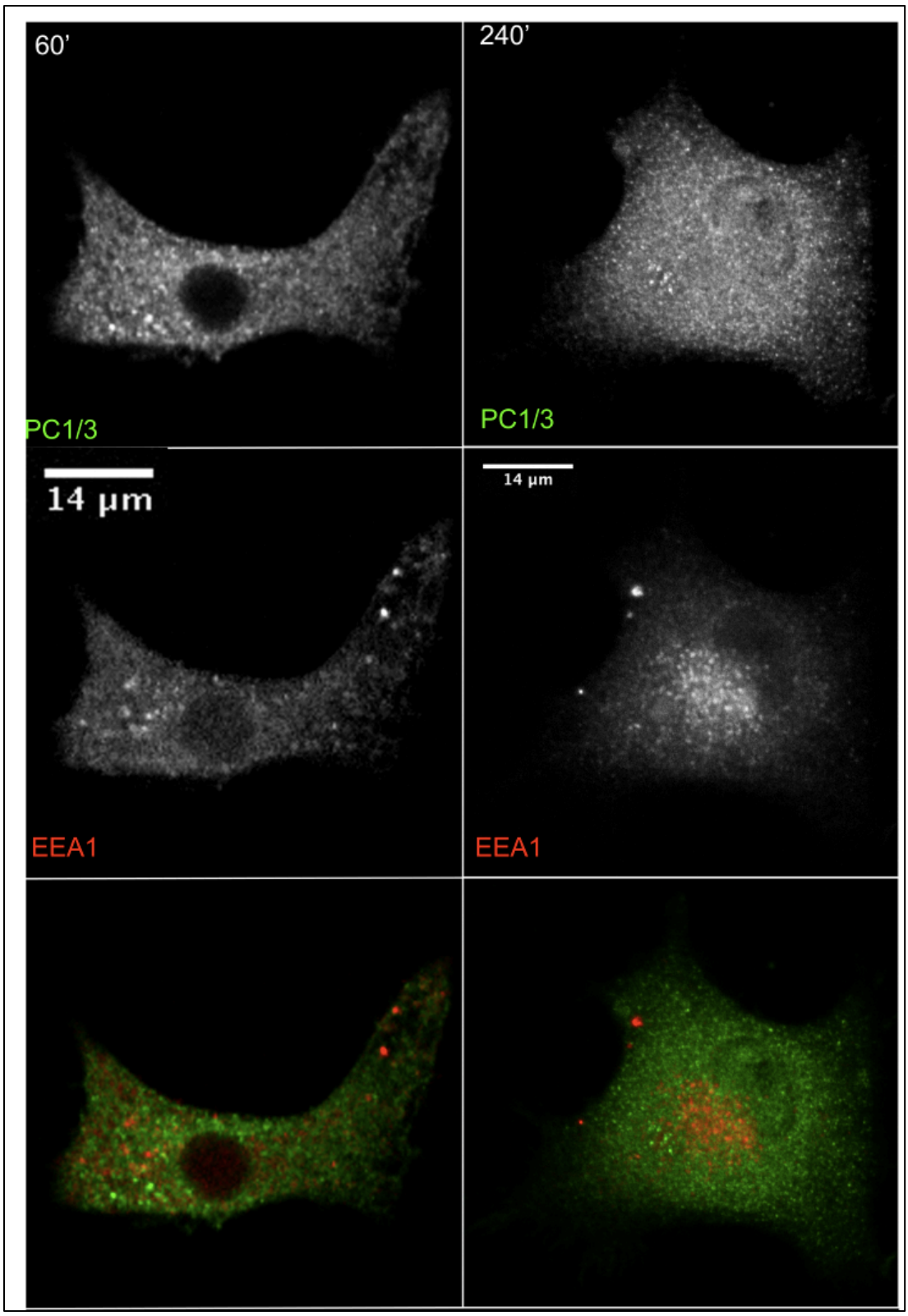

Figure S 11 PC1/3 and EEA1 do not co-localize during LPS stimulation.

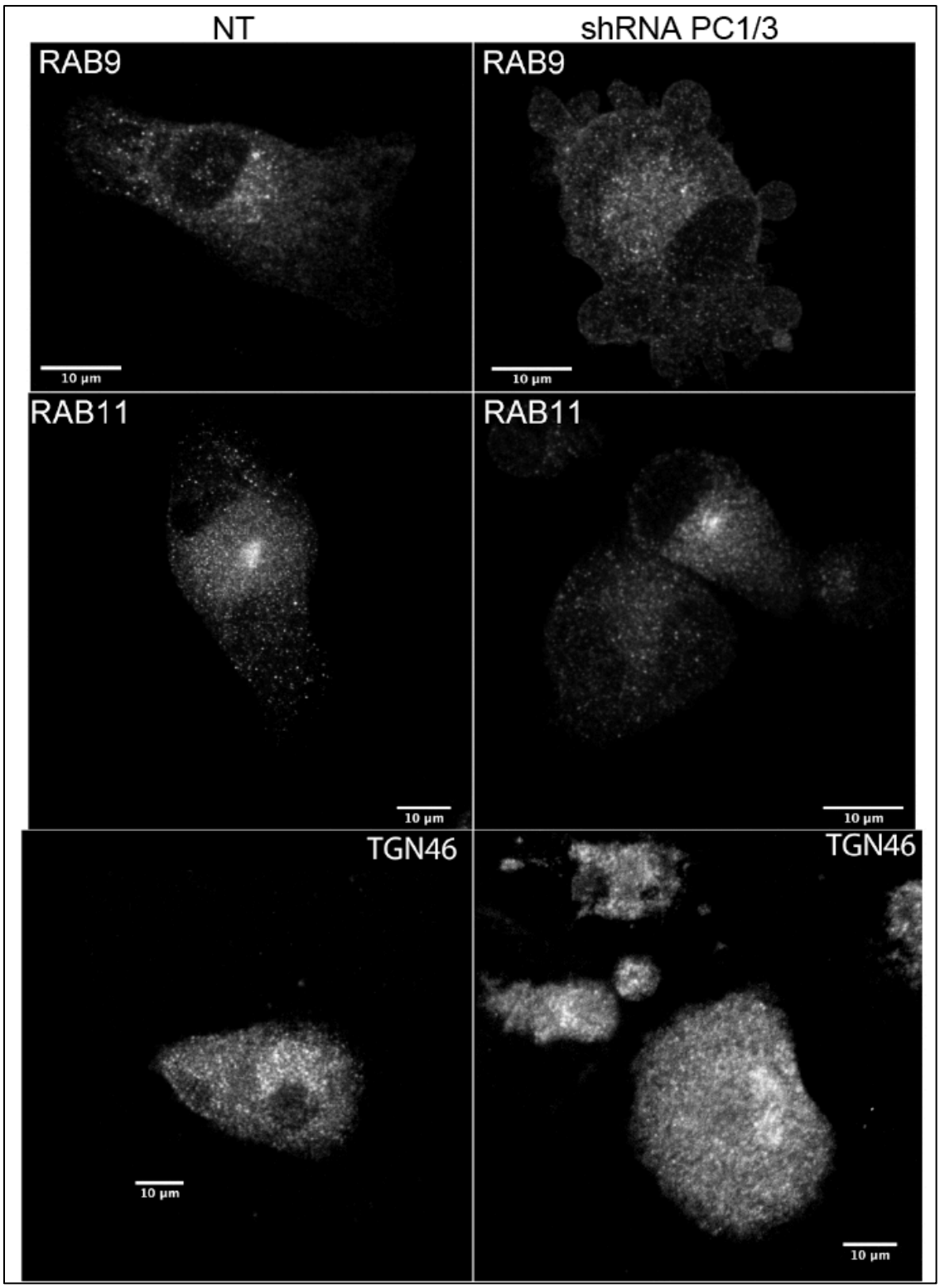

Figure S 12 PC1/3 shRNA in NR8383 do not affect RAB9, RAB11 and TGN46 distribution.

CHAPITRE 5 - PROTEOMIC ANALYSES OF SEROUS AND ENDOMETRIOID EPITHELIAL OVARIAN CANCERS: CASES STUDIES: MOLECULAR INSIGHTS OF A POSSIBLE HISTOLOGICAL ETIOLOGY OF SEROUS OVARIAN CANCER.

Auteurs de l'article : Rémi Longuespée[*], Hugo Gagnon[*], Charlotte Boyon, Kurstin Strupat, Claire Dauly, Olivier Kerdraon, Adesuwa Ighodaro, Annie Desmons, Jocelyn Dupuis, Maxence Wisztorski, Denis Vinatier, Isabelle Fournier, Robert Day, Michel Salzet
[*]Co-auteurs

Statut de l'article : accepté dans Protomics clinical applications 2013

Avant-propos : Cet article est le fruit d'une collaboration avec mon collègue Rémi Longuespée dont le sujet de thèse était le cancer ovarien. L'inclusion de cet article dans ma thèse a pour but de démontrer l'universalité de la méthode d'analyse de donnée par bio-informatique présentée au Chapitre 2 - Rôle de PC1/3 dans l'immunité innée : une approche par spectrométrie de masse. J'ai participé à l'analyse et à la réalisation des figures 5 à 7, la figure S2, S3 et des tableaux S1 à S5. J'ai participé à la rédaction et aux corrections du manuscrit en ce qui a trait aux sections correspondantes à ces figures et tableaux.

Résumé : La carcinogenèse épithéliale ovarienne peut se produire *de novo* à la surface des ovaires au niveau des cellules mésoépithéliales ou par l'établissement de cellules provenant d'autres organes. L'intrusion de cellules de Müller dans l'environnement ovarien figure parmi les hypothèses pour expliquer ce dernier scénario. L'utilisation du profilage par spectrométrie de masse MALDI a permis de fournir des indications concernant ce potentiel mécanisme. Grâce à cette technique, les signatures moléculaires de différentes biopsies de cancers ovariens épithéliaux séreux et endométrioïde ont été dressées dans leur contexte anatomique. Nous avons ensuite appliqué des méthodes bio-informatiques et une stratégie d'identification protéique par analyses LC-MS/MS. Des extraits digérés de tissus FFPE de certaines régions (un adénocarcinome ovarien séreux, un adénocarcinome séreux de la trompe de Fallope, un cancer ovarien endométrioïde, de l'endomètre sain et de l'ovaire

sain) ont été analysés. La comparaison des protéines identifiées à partir de l'endomètre sain ou des trois types de cancer de l'ovaire fournit de nouvelles évidences d'une corrélation possible entre la carcinogenèse des trompes de Fallope et des ovaires séreux. Ici, nous proposons une méthodologie composée de la comparaison de plusieurs tissus dans leur contexte anatomique chez un patient donné dans le but de fournir de nouvelles connaissances sur les similitudes moléculaires entre ces tissus. Cette méthodologie permettrait ainsi de discriminer des marqueurs hautement spécifiques dans un contexte de diagnostic et de prise en charge personnalisée des patients.

Proteomic analyses of serous and endometrioid epithelial ovarian cancers: cases studies :molecular insights of a possible histological etiology of serous ovarian cancer

Rémi Longuespée[1,7*], Hugo Gagnon[1,7*], Charlotte Boyon[1,2], Kurstin Strupat[3], Claire Dauly[4], Olivier Kerdraon[5], Adesuwa Ighodaro[1,6], Annie Desmons[1], Jocelyn Dupuis[4], Maxence Wisztorski[1], Denis Vinatier[1,2], Isabelle Fournier[1], Robert Day[7], Michel Salzet[1**]

1: Université Nord de France, Laboratoire de Spectrométrie de Masse Biologique Fondamentale et Appliquée, MALDI Imaging Team, EA 4550, Université de Lille 1, Cité Scientifique, 59650 Villeneuve D'Ascq

2: Hôpital Jeanne de Flandre, service de Chirurgie Gynécologique, CHRU de Lille, 59037 Lille Cedex.

3: Thermo Fisher Scientific (Bremen) GmbH, Hanna-Kunath-Strasse 11, 28199 Bremen, Germany

4: Thermo Fisher Scientific (France), 16 Avenue du Quebec, SILIC 765, 91963 COURTABOEUF CEDEX

5 Laboratoire d'Anatomie et de Cytologie Pathologiques, CHRU de Lille, 59037 Lille Cedex

6: OWNIP fellow, SUNY College at Old Westbury, Old Westbury, NY.

7: Institut de pharmacologie de Sherbrooke et Département de chirurgie/urologie, Faculté de médecine et des sciences de la santé, Université de Sherbrooke, Sherbrooke, Québec, J1H 5N4, Canada

***Co-authors, **corresponding author.**

Abstract

Epithelial ovarian carcinogenesis may occur *de nov*o on the surface of ovarian mesothelial epithelial cells or from cells originating in other organs. Foreign müllerian cell intrusion into the ovarian environment has been hypothesized to explain the latter scenario. MALDI mass spectrometry (MS) profiling technology was used to provide molecular insights regarding these potentially different mechanisms Using this technique, the molecular disease signatures were established in their molecular context. MALDI MS profiling was used on serous and endometrioid cancer biopsies to investigate cases of epithelial ovarian cancer. We then applied bioinformatic methods and identification strategies on the LC-MS/MS analyses of extracts from digested FFPE tissues. Extracts from selected regions (*i.e.*, serous ovarian adenocarcinoma, fallopian tube serous adenocarcinoma, endometrioid ovarian cancer, benign endometrium and benign ovarian tissues) were performed, and peptide digests were subjected to LC-MS/MS analysis. Comparison of the proteins identified from benign endometrium or three ovarian cancer types (*i.e.,* serous ovarian adenocarcinoma, endometrioid ovarian adenocarcinoma and serous fallopian tube adenocarcinoma) provided new evidence of a possible correlation between the fallopian tubes and serous ovarian adenocarcinoma. Here, we propose a workflow consisting of the comparison of multiple tissues in their anatomical context in an individual patient. The present study provides new insights into the molecular similarities between these two tissues and an assessment of highly specific markers for an individualized patient diagnosis and care.

Introduction

The origin of epithelial ovarian cancers (EOC) is a critical clinical issue. Currently, patients with a mutation in the BRCA gene, who are at higher risk for EOC, are surgically treated with a prophylactic bilateral salpingo-oophorectomy (BSO), which is the complete removal of the ovary and fallopian tubes. This procedure decreases the patients' quality of life because the total removal of the ovaries induces menopause, consequently making those women infertile.

There are two hypotheses for the origin of epithelial ovarian cancers (EOCs), *i.e.*, the intrinsic and extrinsic (1, 2). Ovarian cancer may develop *de novo* from the mesothelial epithelial cells located on the surface of the ovary or from cells originating in other organs (1-3) (Figure 45). If the Müllerian origin of serous ovarian cancer theory is valid, then the surgical removal of the junction of the fallopian tube and the ovary would reduce the risk of developing serous ovarian cancers to the same extent as a BSO. A fimbriectomy, which consists of the removal of the fallopian tube and the junction between the fimbria and the ovary, has been proposed by some surgeons (4) for patients who have BRCA mutations. The theory of *de novo* EOC appearance is supported by HOX gene expression, which regulates the Müllerian duct differentiation in epithelial ovarian cancer, but not in normal ovarian surface epithelium (OSE). The ectopic expression of the HOX genes in mouse OSE leads to the development of tumors that resemble EOC. In this scenario, different HOX genes give rise to distinct EOC histological subtypes (*i.e.*, Hoxa9 for serous, Hoxa10 for endometrioid and Hoxa11 for mucinous cancer (1)). However, several studies have reinforced the second and newer theory, and the principal types of ovarian cancer tissues share similar characteristics with normal Müllerian-type tissues. Serous cancer tissue strongly resembles fallopian tube tissue, endometrioid tissue is similar to endometrial tissue, and mucinous tissue resembles intestinal tissue (1-3). Recent studies on serous adenocarcinoma, the most common type of ovarian cancer, have shown that 80% of these adenocarcinomas are associated with *in situ* cancerous lesions of the tubal epithelium called "serous tubal intraepithelial carcinoma" (STIC), which may be the source of ovarian cancer (5-12). Moreover, genomic signatures that may be associated with STICs, such as mutations in the p53 gene, have been observed (13-19). Additional studies have identified other common serous ovarian and fallopian tube cancer signatures, indicating that some

Müllerian markers, such as PAX8, are commonly found in fallopian tubes and ovarian cancers and not in the mesothelial epithelium of the ovary. Further studies have shown that mesothelial markers such as calretinin are absent (17).

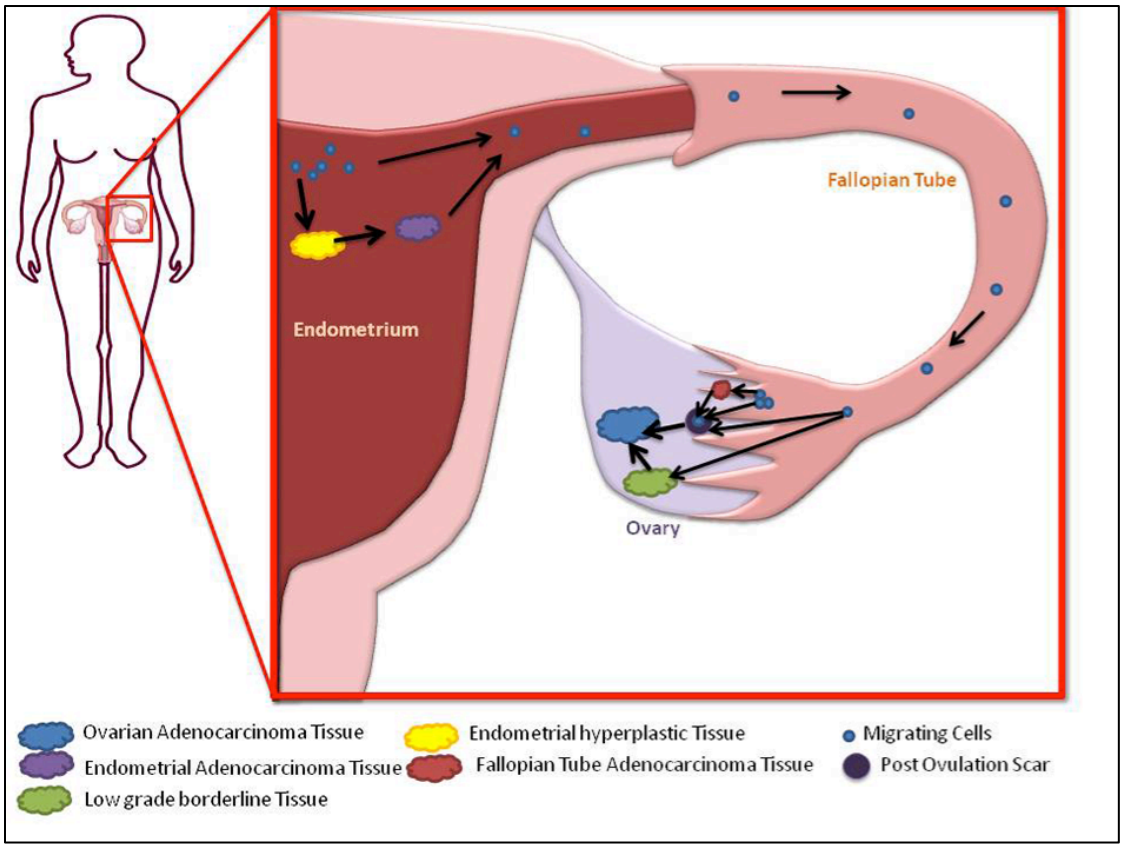

Figure 45 Recapitulation of the Müllerian origin of ovarian cancer type theories.

Neoplastic processes may originate in Müllerian-related tissues and spread to the ovaries via post-ovulation scars or can directly evolve from benign cells. For endometrioid tissues, retrograde menstruation may play a role in disseminating cells from the endometrium to the ovaries. In serous cases, cells may come from the STICs evolving at the junctions between the fallopian tubes and the ovaries. Each tissue subtype and evolution grade is represented by a color that corresponds with the colors used for the PCA spectra spots in the following figures.

The origin of serous ovarian cancer is still under debate, but evidence elucidating the molecular nature of the tissues may be provided by mass spectrometric strategies. In the early 1990s, MALDI (matrix-assisted laser/desorption ionization) mass spectrometry profiling, which consists of the direct molecular analysis of hundreds of biological compounds in tissues, was proposed (20). Since the beginning of the last decade, many institutions have invested in molecular histological screening (20-25), including that of ovarian cancer samples (22, 25-31). Thus, MALDI MS molecular profiling is considered a new and important "molecular histology" tool. We proposed to investigate the molecular nature of serous and endometrioid cancers using the novel MALDI MS profiling technology (Figure 46 A, 2B). This technology provides a comparison of the molecular profiles from different ovarian cancer tissues with the corresponding reference tissues.

In this present study, we first evaluated the use of MALDI MS on tissues on endometrioid low grade ovarian cancer cases. Using PCA calculations on acquired spectra, we compared the global molecular profiles of the different tissues involved in the evolution of this pathology, *i.e* between the endometrium and the ovaries.

This first examination allowed us to observe in a handly view of the global similitudes and dissimilitudes of endometrial and ovarian tissues.

The second part of the study is a more extensive analysis aiming to bring new clues for the tubal origin of serous ovarian cancer. Indeed, we first evaluated the global profiles of tubal and ovarian tissues by PCA analyses on MALDI MS spectra using the same procedure in the first part.

We then aimed to identify the potential molecular actors implicated in the close relationship between ovarian serous cancer tissues and tubal tissues. To do so, we performed a solvent-based extraction on previously analyzed regions of interest in the different tissues and conducted LC-Orbitrap MS analyses. The use of bioinformatics for analyzing the proteomics information allowed us to depict the common molecular functions for the cancerization of different organs and gave us access to the organs' specific molecular content. (Figure 46 C).

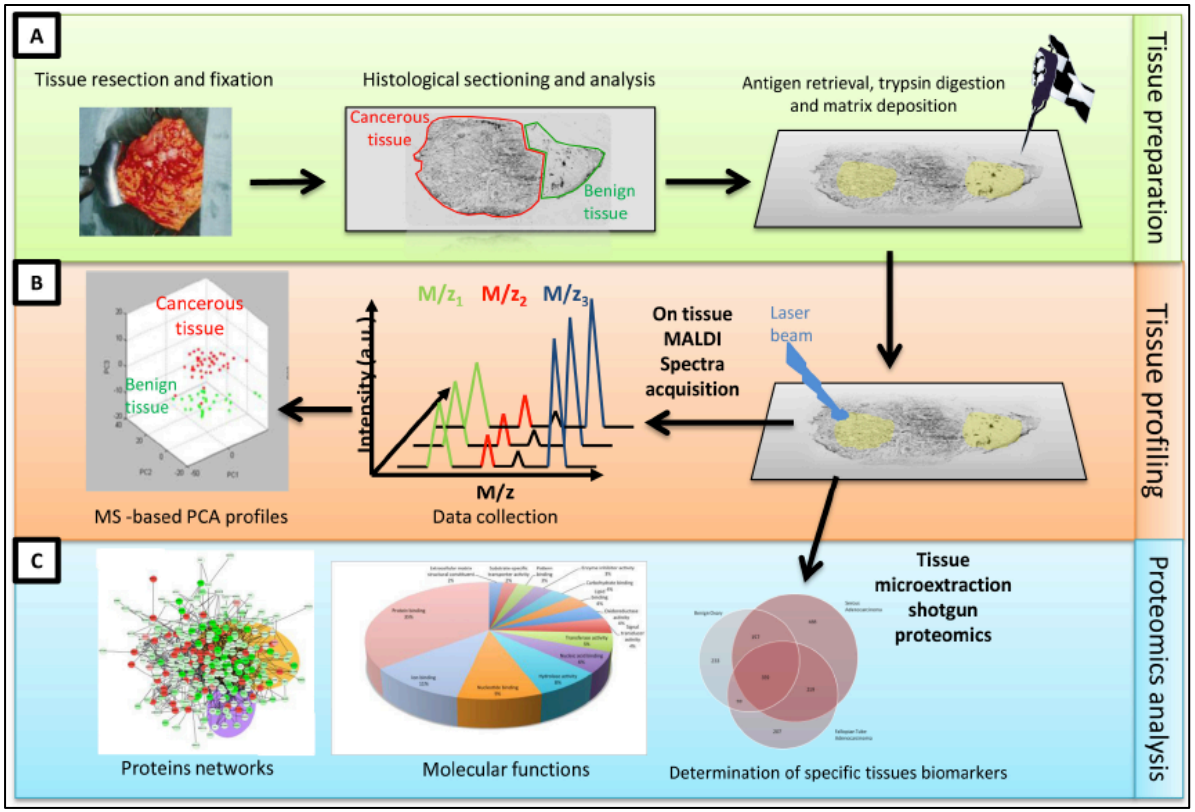

Figure 46 Proteomic workflow.

A: The tissue preparation and analysis workflow for MALDI imaging. The resected organs or tissues were sliced with a microtome for FFPE tissues or a cryostat for fresh frozen tissues. The sections were mounted on conductive slides, the matrix was dropped onto the section, and the mass spectrometric analysis was performed on the tissue area. The positions and intensities of the ions are represented in a visual format called "image." **B**: The corresponding PCA of the tissue with normal and carcinomatous endometrium. The PC1/PC2, PC1/PC3, and PC2/PC3 analyses are shown, illustrating the best 2D-space separation of the ions. **C**: After PCA analysis, the tryptic digests were extracted for the tissue sections by solvents washes. These digests were submitted to proteomic analyses. The use of specific software allowed us to determine the proteins' molecular functions and biological processes. It was also possible to elaborate the interaction networks of the proteins of interest.

Materials and methods

Materials

Alpha-cyano-4-hydroxycinnamic acid (HCCA) and trifluoroacetic acid (TFA) were obtained from Sigma-Aldrich and used without further purification. Trypsin was purchased from Promega. Acetonitrile p.a. and methanol p.a. were obtained from J.T. Baker.

Samples

FFPE tissues were obtained from the CHRU de Lille pathology department. An institutional review approval (CPP Nord Ouest IV 12/10) was obtained without requiring informed consent from patients. The ethical committee considered contacting the patients, often many years after surgery, to be unnecessary. Our reference pathologist (O.K.) selected the FFPE blocks that included ovarian cancer tissue and tissue from the potential Müllerian precursor. To avoid inter-patient variability, each figure in the Results section represents tissue from the same patient. The International Federation of Gynecology and Obstetrics (FIGO) stages for each specimen were determined, and the results of the histological examinations were recorded. For the histological imaging prior to MALDI analysis, 4-µm-thick tissue sections were cut from the formalin-fixed, paraffin-embedded (FFPE) whole-mount ovarian tissue blocks. The sections were placed on ITO-coated slides and heated for 60 min at 58°C (29). The tissue was counterstained with hematoxylin, eosin and safranin (HES), dehydrated using a graded ethanol series, and air-dried for histological examination by our staff pathologist. The tissues appeared heterogeneous and contained cancerous, hyperplastic, and normal regions, with stromal tissue in each region (29, 32).

Hematoxylin, eosin and safranin (HES) staining

The following procedure was used for the HES staining. The sections were heated for 5 minutes, stained with hematoxylin for 3 minutes, rinsed with water, washed twice in a solution of 156 mL EtOH (95%), 44 mL H_2O and 80 µL HCl, washed in water, washed in a solution of 0.48 mL NH_4OH (35%) and 200 mL H_2O, washed with water for 5 minutes, washed in ethanol (80%), colored with eosin for 10 seconds, washed twice with ethanol (95%), washed twice with ethanol (100%), stained with safranin (10 g/L in ethanol (100%)) for 6 minutes, and then washed twice in ethanol (100%) and once in xylene for 1 minute (29, 33).

Tissue de-waxing. Ovarian FFPE tissues were used for the retrospective studies. Tissue sections (6 μm) were generated using a microtome and were placed on conductive glass slides coated with ITO (indium tin oxide) on one side. The paraffin was removed by submersion in toluene twice for 5 min followed by a light rehydration in ethanol baths (100%, 96%, 70% and 30%) before the slides were dried in a desiccator at room temperature (29, 33).

Antigen retrieval. FFPE tissues have well-conserved tissue morphology and the capacity to prevent molecular degradation. Due to methylene bridge formation during conservation, trypsin digestion is often necessary to retrieve protein information. Because cross-linking continues over time in FFPE tissue blocks, protein accessibility becomes increasingly difficult. Enzymatic cleavage may be affected, which may lead to poor enzymatic yields. Therefore, it is necessary to establish processes that facilitate protein access, and many such protocols exist (33, 34). However, the associated molecular changes of these so-called antigen retrieval (AR) processes remain poorly understood. The most reasonable hypothesis is that AR allows changes in the conformation of cross-linked proteins and thus facilitates access to sites within proteins. Due to the variation among protocols, systematic tests of different AR techniques are required for an optimized protocol, so several protocols were tested here. Citric acid antigen retrieval (CAAR) provides good results with prostate tissue sections (33). CAAR protein unmasking was performed by immersing the slides in 10 mM of citric acid for 20 min at 90°C and drying them in a desiccator for 10 min. Prior to enzymatic digestion, the slides were incubated twice in 10 mM NH_4HCO_3 to remove the remaining AR solution and condition the tissue for effective enzyme activity.

Trypsin digestion and matrix digestion

Ten milliliters in total of a solution containing 40 mM trypsin in 50 mM ammonium bicarbonate was dropped onto each tissue discrete region of interest using gel loader tips (the ten microliters have been dropped in 5 times using 2 microliters of solution). This procedure avoid the drop to spread and thus to have a mixed up of different cell types. The slides were then incubated for 4 hours at 37°C in a customized humidity chamber (a 10 cm x 15 cm box filled with water to one quarter of the box height and placed in a 37° incubator). After the trypsin digestion, 10 μl of a 10 mg/ml HCCA solution in aqueous TFA 0.1%/ACN (3:7) was dropped onto each section (35, 36).

MALDI mass spectrometry profiling methodology

The mass spectrometry profiling approach is presented in Figure 46 (22, 25). The first step includes the sectioning and preparation of tissue using standard methods. The preservation of tissue integrity while avoiding molecular composition changes (*e.g.*, enzymatic activation) is of utmost importance. The second and third steps are based on MALDI-MS technology. The second crucial step is the deposition of the matrix onto the tissue section. The importance of the matrix for mass spectra quality is well established, and the proper matrix choice is crucial for a successful MALDI experiment. It is also important that the MALDI-MSI matrix does not induce molecular delocalization across the tissue sample. Such delocalization must not spread further than the area analyzed by one laser pulse. The third step is the tissue data acquisition. This step depends on the mass analyzer and involves optimizing various parameters; the acquisition step requires the automation of the analytical process. The final step consists of data processing via informatics tools.

Tissue profiling using MALDI

For each tissue, 50 spectra were acquired on spots homogeneously distributed across the analysis surface. The profiles were acquired using an UltraFlex II MALDI-TOF/TOF instrument (Bruker Daltonics, Bremen, Germany) equipped with a smart beam laser with a 200 Hz repetition rate and controlled by FlexControl 2.5 software (Bruker Daltonics, Bremen, Germany). The mass spectra profiles were acquired in the positive reflection mode in the 500 to 5,500 Da mass range. One thousand spectra were acquired at each position using a 200 Hz laser frequency. The images were recorded and reconstructed using FlexImaging II 2.5 software (Bruker Daltonics, Bremen, Germany).

Statistical data analysis

The data obtained using FlexImaging II 2.5 software (Bruker Daltonics, Bremen, Germany) were loaded into the ClinProTools v2.5 software (Bruker Daltonics, Bremen, Germany) to conduct principal component analysis (PCA) and hierarchical clustering analysis. After standardization of the data, the unsupervised PCA method was selected. The PC1 and PC2 components were found to have the largest variance (33, 37).

LC MS/MS Analyses

Trypsin-digested peptides from the FFPE tissue after the antigen retrieval procedure were manually extracted from specific tissue regions after PCA. Using a micropipette, specific regions were subjected to 20 successive washes with 100 µL of 80% ACN in water. The extract solution was then dried with a SpeedVac (Savent). The dried peptides were re-dissolved in 10 µL 0.1% TFA. The salts were removed from the solution, and peptides were concentrated using a solid-phase extraction procedure with a Millipore ZipTip device in 10 µL 80% ACN elution solution. The solution was dried again using a SpeedVac, and the dried samples were resuspended in a solution of 5% acetonitrile and 0.1% formic acid. The samples were separated by online reversed-phase chromatography using a Thermo Scientific Proxeon Easy-nLC system equipped with a Proxeon trap column (100 µm ID x 2 cm, Thermo Scientific) and a C18 packed-tip column (100 µm ID x 15 cm, Nikkyo Technos Co. Ltd). The peptides were separated using an increasing concentration of acetonitrile (5%-40% over 110 minutes) at a 300 nL/min flow rate. The LC eluent was electrosprayed directly from the analytical column, and a 1.7 kV voltage was applied via the liquid junction of the nanospray source. The chromatography system was coupled to a Thermo Scientific Orbitrap Elite mass spectrometer, which was programmed to acquire in a data-dependent mode. The survey scans were acquired in the Orbitrap mass analyzer operating at 120,000 (FWHM) resolving power. A mass range of 400 to 2000 m/z and a target of 1E6 ions were used for the survey scans. The precursors observed with an intensity of over 500 counts were selected “on the fly” for the ion trap collision-induced dissociation (CID) fragmentation with an isolation window of 2 amu and a normalized collision energy of 35%. A target of 5000 ions and a maximum injection time of 200 ms were used for CID MS^2 spectra. The method was set to analyze the 20 most intense ions from the survey scan, and a dynamic exclusion was enabled for 20 s. Each sample has been analyzed three times. The limit of detection of the instrumentation is 25000 peptides for an LC-MS/MS run.

Analysis

Tandem mass spectra were processed using the Thermo Scientific Proteome Discoverer software version 1.3. Resultant spectra were matched against the Swiss-Prot® Human database (version January 2012) using the SEQUEST® algorithm. The search was

performed by selecting trypsin as the enzyme with two missed cleavages allowed. The precursor mass tolerance was 10 ppm, and the fragment mass tolerance was 0.5 Da. N-terminal acetylation, methionine oxidation and arginine deamination were set as the variable modifications. Peptide validation was performed using the Percolator algorithm. The peptides were filtered based on a q-value of 0.01, which corresponds to a 1% false discovery rate (FDR).

Only proteins with a score of over 5, which represents the proteins identified with 2 or more unique peptides, were kept for analysis. The relative protein expression was calculated based on the protein score, which was shown to be an adequate relative indicator of the relative differential expression (38, 39). We compared the acquired results with an analysis using the Scaffold 3 software (40). We considered this method to be quite accurate because it gave similar results when a quantitative comparison of the different tissues' proteins relied on spectral counting (data not shown). Gene ontology (GO) analysis was performed using Blast2go (41). The network analysis was performed as follows: The gene names of identified proteins were used as input to retrieve a network from STRING (42), and this network was then loaded into Cytoscape 2.8 (43) with relative expression data using Id mapper. The Reactome FI pluggin was used to select a sub network of GO terms and NCI database-associated disease specific proteins.

Results and discussion

The study presented here is composed of two separated parts. The first one consists in the determination of molecular signatures of tissues from patients afflicted by low grade endometrioid cancers, using PCA calculations applied to mass spectra. A solvent extraction has then been performed on the ovarian endometrioid cancer tissue, followed by a LC MS/MS analysis. This analysis has been used to support the second part of the investigation.

The second part of the investigation consists in the exanimation of serous cancer cases. We also present the molecular profiles of the different tissues. We then focused on one case to perform an extensive proteomic analysis comparing different tissues of interest. This part of the study is devoted to the finding of clues of the potential tubal origin of ovarian cancer in this specific clinical case.

Before any analysis, we aimed for the proper selection of the tissues areas for the molecular comparisons. The methods presented here allowed us to make the examination of the molecular content of whole tissue areas without fastidious steps of laser capture microdissections for cell types selections. In order to avoid any analytical artifacts due to the analysis of mixed cells types, a first meticulous tissue area selection have been performed by our reference pathologist (O.K.). Between any tissues to compare, we aimed to have the same amount of vessels. For normal tissue tubal, ovarian and endometrial tissues, we selected representative regions of interest of the whole tissue areas, *i.e* with the average proportion of stromal and epithelial cells. For cancerous tissue area selection, we also aimed for the selection of ROI with average proportion of cancerous epithelia and surrounding stromal cells.

The cancerous epithelia proportion is the most represented cell types (80-90% of the cells types), and absolutely absent from the other tissues which are by almost 100% stomal cells. We then estimate that the comparison of the cancerous tissues with normal tissues controls is free of the analytical artefacts that we could have without a previous selection of the tissues.

Part 1:Molecular signature profiling and proteomic analysis of endometrioid ovarian cancer tissues

In this first part of the investigation, we selected low grade endometrioid tissues in order to test the feasibility of the PCA procedure to compare molecular profiles of selected tissues of interest. Indeed we compare the possible similitude and dissimilitude between normal, cancerous, hyperplastic endometrium with borderline and cancerous ovaries.tissues that our pathologist found for this case.

Due to the large amount of data acquired using the MALDI MSI method, data reduction and multivariate analyses were necessary to extract the information of interest. Among the multivariate methods available, principal component analysis (PCA) provides a proven method for automatic feature extraction (26, 33, 37). Several studies have shown that PCA is a data reduction method that is useful for MALDI MSI in disease applications (26, 33, 37, 44, 45). Therefore, PCA was applied to the data from several spectral

acquisitions. In this bioinformatics spectral data processing, each peak was considered to be a single dimension, and each group of spectra was considered to be a multi-dimensional space. This process reduces the multi-dimensional space to two or three dimensions. The PCA approach provides access to m/z, which demonstrates differences between or within samples. PCA is often combined with hierarchical clustering (HC) because HC classifies the mass spectra according to similarities between their profiles, thus highlighting the regions containing differing molecular content. In these ways, the different molecular content profiles may be easily compared among the different tissue types. As shown in supplementary Figure S 13, the mass spectra observed in normal, borderline, and adenocarcinoma ovarian tissues contain a high number of peaks that appear to present some intensity differences that could not be precisely quantified manually. PCA analysis thus evaluates the relative intensity of all peaks and provides insight into differential molecular signatures.

The correlations between each cellular phenotype were tracked across the m/z detected in each tissue type. The endometrioid cancer origin hypothesis posits that cells from retrograde menstruation and endometriosis or endometriotic cysts reach the ovary, develop in the endometrial tissue and eventually become cancerous (46). For each case, the ovarian biopsy was studied concurrently with its respective case-matched control (*i.e.*, the endometrial tissues). We focused on the cases whose endometrioid cancers were associated with endometrial lesions (Figure 47). HES staining and pathological analysis were used to study the FFPE sections from different organs of the same patient. To facilitate the analysis and determine the nature of the tissues, we retained the annotations added by the pathologist on the tissue section slides.

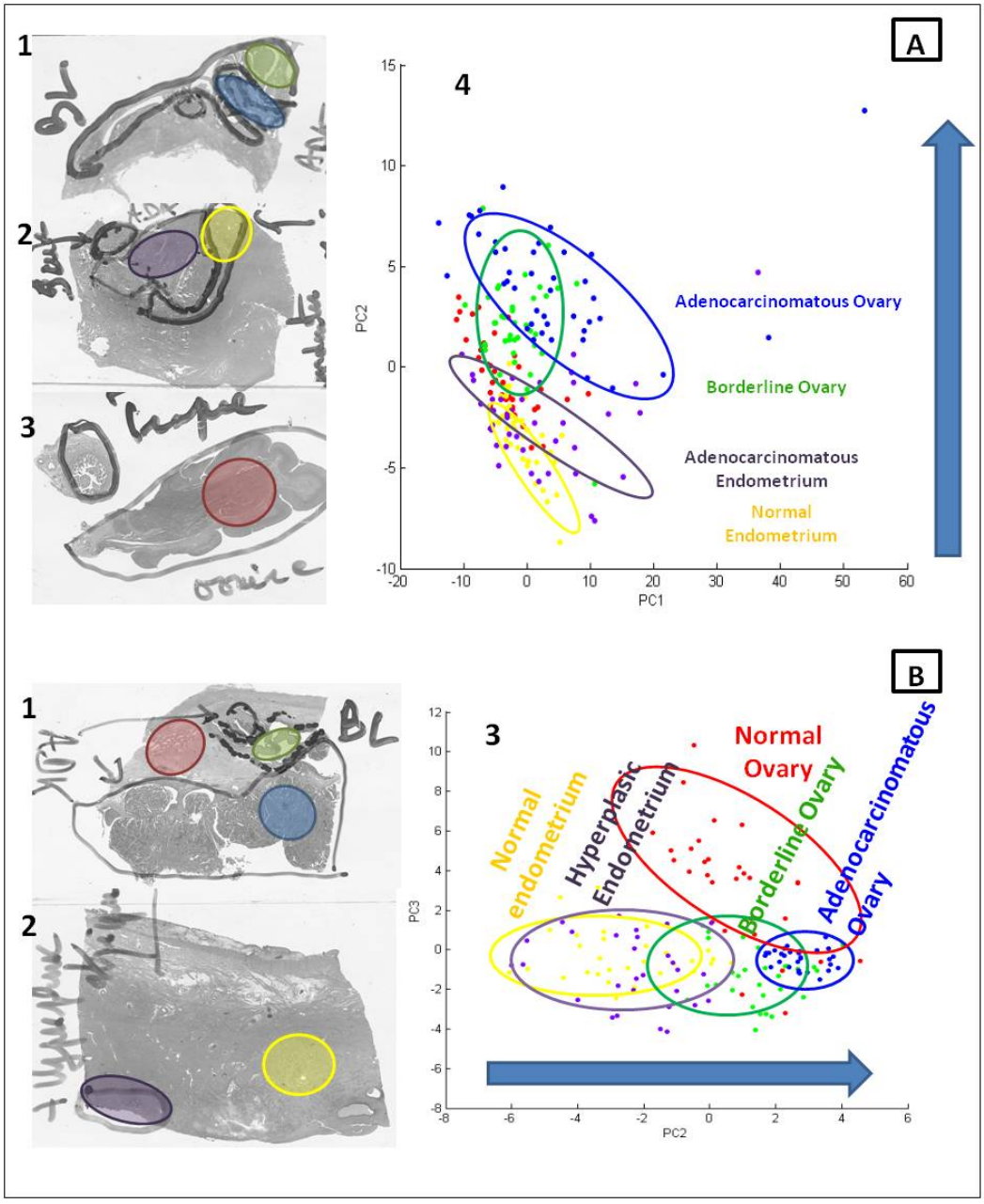

Figure 47 PCA analysis of the two patient tissues with endometrioid ovarian cancer.

CAAR was applied to FFPE tissue sections. Ten microliter trypsin droplets were then deposited on each tissue region of interest (ROI) and HCCA matrix. Fifty MALDI/TOF spectra were then acquired for each region of interest, and the acquired data were submitted to PCA for a molecular-based comparison.**A**: First patient case, HES sections (1, 2, 3) and PCA analyses of normal, adenocarcinomatous ovarian tissues and normal and adenocarcinomatous endometrial tissues.**B**: Second patient case, HES sections (1, 2) and PCA analyses of normal, borderline and adenocarcinomatous ovarian tissues and normal and hyperplasic endometrial tissues.

Two patients were selected because they presented with ovarian endometrioid and endometrial cancers or hyperplasic lesions. These tissue sections included borderline (BL) ovarian tissue (in green) and a portion of an adenocarcinoma (ADK, in blue) (Figure 47), endometrial tissue (in yellow) (Figure 47) and its contralateral normal ovary tissue (in red) (Figure 47) and adenocarcinomatous or hyperplastic endometrial tissues (in purple). Adjacent sections were subjected to the MALDI profiling procedure after Citric Acid Antigen Retrieval and trypsin digestion to demask the peptide and protein markers. Principal component analysis (PCA) was performed for each region of interest in the sections; the data are presented in Figure 47 for the two patient cases in the A and B insets. Figure 47 A depicts the analysis of the first patient. Borderline (green) and cancerous (blue) tissue sections were found in the carcinomatous ovary (Figure 47 A1). These tissues were compared with normal endometrium (Figure 47 A2), carcinomatous endometrium (Figure 47 A2), and normal contralateral ovary (Figure 47 A3). For this patient, the normal endometrium is weakly proliferative. In this case, it is easy to distinguish the spectral profile scatters in the regions of interest, which are circled in the same colors used to highlight the HES scan sections. The profiles have a specific order in 2D space, which is determined by the first PCs (*i.e.*, PC1 and PC2), ranging from normal endometrial tissue to ovarian carcinoma. Endometrial carcinoma showed close similarities with normal endometrial tissue (Figure 47 A4). It seems that normal and adenocarcinomatous endometrial tissues share common ions with borderline ovarian tissue and that borderline ovarian tissue share common ions with and adenocarcinomatous ovarian tissue. In this context, the blue arrow represents a possible continuum in the different molecular contents of the tissues through the different organs and tissue types. The inset in Figure 47 B demonstrates the analysis of the second endometrioid ovarian cancer case. In this second case, we found normal, borderline and carcinomatous tissues in the ovarian biopsy sections (Figure 47 B1).Is this case, the patient present an atrophic normal endometrium. In parallel, this patient presented with an atypical hyperplastic zone detected near the endometrial tissue that was considered a region of interest (Figure 47 B2). We found that the PC2-PC3 dimensions indicated a close similitude in the molecular profiles of the normal endometrial and hyperplastic tissues (Figure 47 B3). In this case, the normal ovarian molecular profile was different from the pre-invasive and invasive profiles. In the 2D PC space, the

molecular-based profiles of the ovarian borderline and carcinomatous tissues were placed after the hyperplastic endometrial tissue. From these observations, we suggest that endometrial hyperplasia may be a latent state for carcinoma progression. With this global molecular information, we predict that an endometrial hyperplasic cell may nest in the ovarian environment and evolve to borderline and lead to a carcinomatous state.

A solvent extraction of the tryptic peptides from the endometrial adenocarcinoma has then been performed and LC MS/MS analyses as mentioned in Material and Methods. These analyses have then been used in part 2. These results gave us insights in the histological resemblance between the tissues involved in endometrioid ovarian cancer progression, and in the possible histological etiology of this type of cancer. We also got a first clue of the usefulness of this method for the evaluation of this specific issue.

Part 2: Molecular signature profiling of the tissues and proteomic analysis of serous ovarian cancer tissues: insights of a possible histological origin

In this part, we focused on serous ovarian cancers because the proof of a fallopian tube tissue origin may represent the most relevant context for further clinical application. Furthermore, serous ovarian cancers represent the most prevalent cases. We then applied the MALDI profiling method on serous ovarian cancer tissues. The results of these analyses are presented in Figure 48. The tissue regions of interest are labeled pink for the normal fallopian tube, red for normal ovary, blue for ovarian adenocarcinoma and turquoise for tubal adenocarcinoma (Figure 48). Three patient cases were selected. For a more defined view of the molecular profiles, we added the hierarchical clustering results of the tissues of interest. The first patient did not present with any tubal lesions. Therefore, we aimed to compare the ovarian carcinomatous regions with the normal fallopian tube tissue. The tubal origin of serous ovarian tissue theory also states that a normal cell from the fallopian tube may evolve into cancer in the ovarian environment. The first case is presented in the inset in Figure 48 A. The PCAs in the first two axes (Figure 48 A2) demonstrated that the normal fallopian tube and normal ovarian tissues presented similar molecular profiles that were different from normal contralateral ovarian tissue. The hierarchical clustering (HC) data demonstrated that the fallopian tube spectra presented an intermediate profile that was between the ovarian cancer and normal ovarian tissue profiles. (Figure 48A3)

The last patient presented fallopian tube adenocarcinoma (Figure 48 B1 and B2). The patient has been diagnosed for the presence of adenocarcinomatous cells after gynecological examination. A diagnostic coeliscopy revealed the presence of carcinomatous annexes. A radical annexectomy has been performed in both the tubal and the ovarian tissues have been analyzed by the pathologist. After the microscopic examination, the pathologist stated that the tube, that have been taken in totality, presented an invasive adenocarcinomatous proliferation, mostly solid, measuring 8mm in length on the longer axe. Otherwise the fimbria was dotted with serous tubal intraepithelial carcinoma (STIC). The pathologist clearly stated that ovarian lesion corresponded to a metastasis of the tubal adenocarcinoma. The PCA (Figure 48 B3) shows that ovarian cancer presents the following order of molecular profiles: normal ovary, normal fallopian tube, fallopian tube adenocarcinoma and ovarian serous adenocarcinoma. This observation is in agreement with the molecular origin of ovarian cancer theory. HC (Figure 48 B4) also confirms the similar characteristics among ovarian adenocarcinoma and fallopian tube adenocarcinoma and normal tissues.

These analyses were easy to perform and allowed a quick survey on the global differential molecular content between the tissues. Therefore, because the identification of the proteins responsible for molecular differentiation is difficult to obtain using the MALDI TOF device, we performed an in-depth analysis of the molecular content of the tissues of interest in the serous ovarian cancer case.

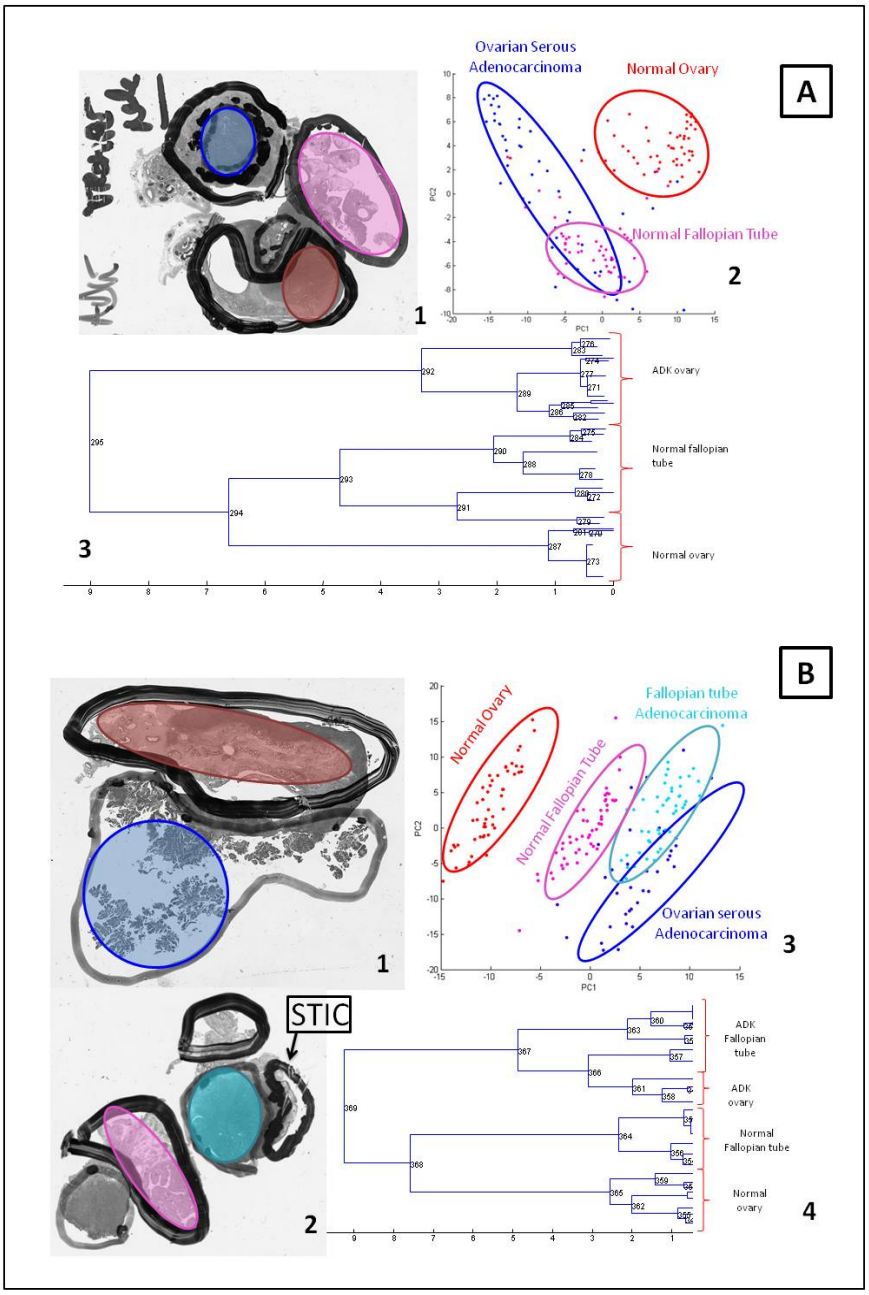

Figure 48 PCA analysis of the two patient tissues with serous ovarian cancer.

CAAR was applied on FFPE tissue sections. Ten microliter trypsin droplets were then deposited on each tissue region of interest (ROI) and HCCA matrix. Fifty MALDI/TOF spectra were then acquired for each region of interest, and the obtained data were submitted to PCA for a molecular-based comparison. **A**: First patient case, HES sections (1), PCA analyses of normal, and adenocarcinomatous ovarian tissues and normal tubal tissue (2), HC of spectra (3). **B:** Second patient case, HES sections (1, 2) and PCA analyses of normal and adenocarcinomatous ovarian tissues and normal and cancerous fallopian tissue.

Proteomics analyses of serous ovarian cancer and tubal cancer tissues.

For the proteomics analyses, peptide extractions from normal endometrium and endometrioid ovarian cancer of the case were performed, and peptide digests were then subjected to LC MS/MS analyses.

Among the identified proteins, those with a score under 5 were removed for subsequent analyses because they were identified from the MS/MS to have less than two peptides. We then evaluated the number of common peptides between the tissues of interest. Each accession number, proteins description, gene name and relative score associated with the selected proteins are reported in Supplementary Table 1. The selected tissues are serous ovarian adenocarcinoma, fallopian tube serous adenocarcinoma, and benign ovarian tissues. The Venn diagram presented in Supplementary Figure S 14 illustrates the common identification between each cancer tissue. The obtained overlapping identifications provide an insight into the molecular similarities of the tissues. Primarily, the number of specific proteins in the serous ovarian adenocarcinoma samples appears higher than any of the other specific proteins, suggesting that many cellular processes involving several proteins may be mandatory for ovarian cancer progression. The number of proteins in the two other cancers was similar. We then observed that the number of common proteins identified between serous EOC and fallopian tube serous cancer was higher than that between the endometrioid EOC type, and the number of common proteins identified between endometrioid EOC and tubal cancer was more than 3-fold less than that between serous EOC and fallopian tube serous cancer. These observations suggest that serous EOC has a molecular profile that is more similar to tubal cancer than any other type of EOC. This point also supports the ectopic origin of EOC hypothesis. Although these data provide interesting information regarding the relative molecular nature of each cancer, this comparison lacks accuracy because it relied on two patient cases. Thus, the comparison may be partially influenced by the inter-patient variability.

We then focused on a single patient case of ovarian serous cancer. We compared the tissues of interest illustrated in Figure 49B. The Venn diagram in Figure 49 A demonstrates the common identified proteins in benign ovary, serous ovarian cancer and serous tubal cancer for the same patient. As illustrated, more proteins are shared in common between tubal cancer and serous ovarian cancer than between serous cancer and the benign ovary. This may suggest that processes implicated in serous related cancers (*i.e.*, ovarian and tubal)

require numerous molecular actors, and a portion of these is in common between ovarian and tubal serous cancers.

The protein identification (id) score was compared between the different tissue regions. The differential protein ids between ovarian cancer and benign tissues were selected as proteins specifically implicated in the cancerous processes. Some of these demonstrated highly similar id scores between ovarian cancer and fallopian tube cancer tissues. These proteins were selected as proteins possibly implicated in ovarian and tubal serous cancers processes.

The molecular function of each of the specific proteins was determined using Blast2GO. Figure 7 shows pie charts demonstrating the proteins' cellular localization (Figure 49 B), the biological processes in which they are involved (Figure 49 C) and their molecular functions (Figure 49 D). In these representations, we observed that the functions principally found in common between ovarian and tubal cancer have been found in other cancers. Therefore, we demonstrated that the major molecular functions were related to molecular binding, with 35% of protein binding, and metabolism (Figure 49 D). With regards to cellular processes (Figure 49 C), the most represented corresponds with well-known processes associated with cancer. Processes such as growth, cell proliferation, cellular component organization, biological adhesion, response to stimulus and signaling and metabolic processes correspond with classically described functions in tumorigenesis phenomena. These elements provide an initial clue to the underlying mechanisms related to these two cancers.

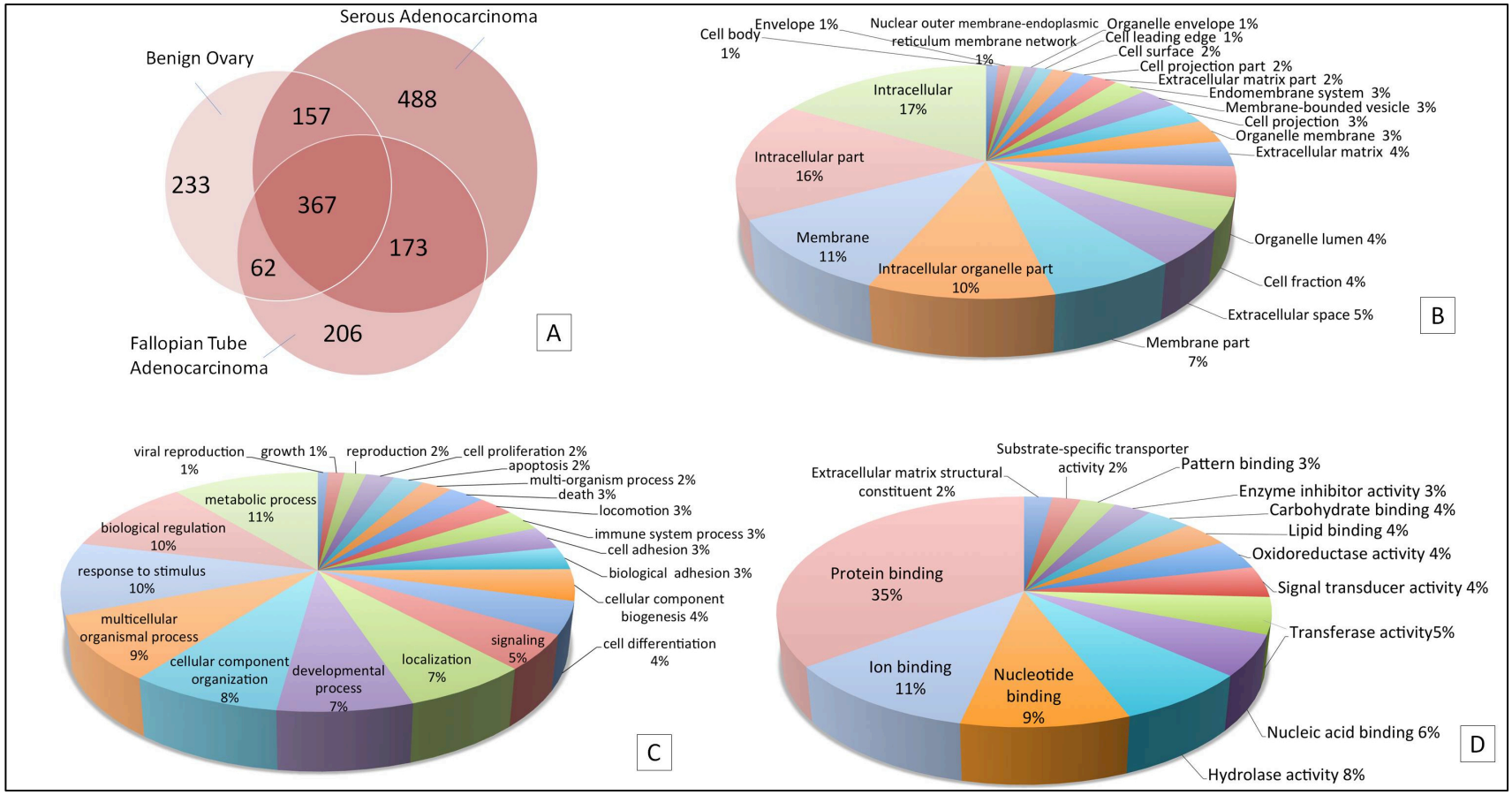

Figure 49 Analysis of common proteins identified by LC-MS/MS between serous ovarian and tubal cancers.

Venn diagram of protein ids from ovarian, tubal cancer and normal ovarian tissues in the same patient case **(A)**. Blast2Go was then used to determine the gene ontology (GO) of proteins with similar id scores between the ovarian cancer and fallopian tube cancer tissues and pie charts for cellular localization **(B)**, cellular processes **(C)** and molecular functions **(D)** were drawn.

All of these proteins have been reported in a network representing the functional interaction between these proteins based on the String database interaction probability (Figure 50). In this network, a score based on the up and down regulation of each of the proteins in common with ovarian and tubal cancers compared with the normal ovary is represented by a color code; the green shade represents negative score changes, and the red shade represents positive score changes. Thus, we postulated that this change in the score ranking reflects expression changes, *i.e.*, a negative score change represents down regulation (Green), and positive score change represents up regulation (Red). From this global network (Figure 50 A, enlarged in supplementary Figure S 15 Enlarged full network from), sub networks can be extracted, corresponding to proteins with functions of interest or related to physiopathological events. The first observation was that down regulation is predominant compared with up regulation. The framed sub-network represents proteins associated with the NCI disease index (http://www.cancer.gov/), and they were selected using the Cytoscape-implemented Reactom FI plugin. Almost all of the selected proteins were found to be involved in neoplasms (Figure 50 B). A number of these proteins have also been found in female reproductive system neoplasms (Figure 50 C), particularly in ovarian cancer neoplasms (Figure 50 D). Among the up-regulated proteins, we found chaperones, cell structure proteins and proteins involved in DNA replication. The down-regulated proteins correspond to other types of chaperone, adhesion and structural proteins.

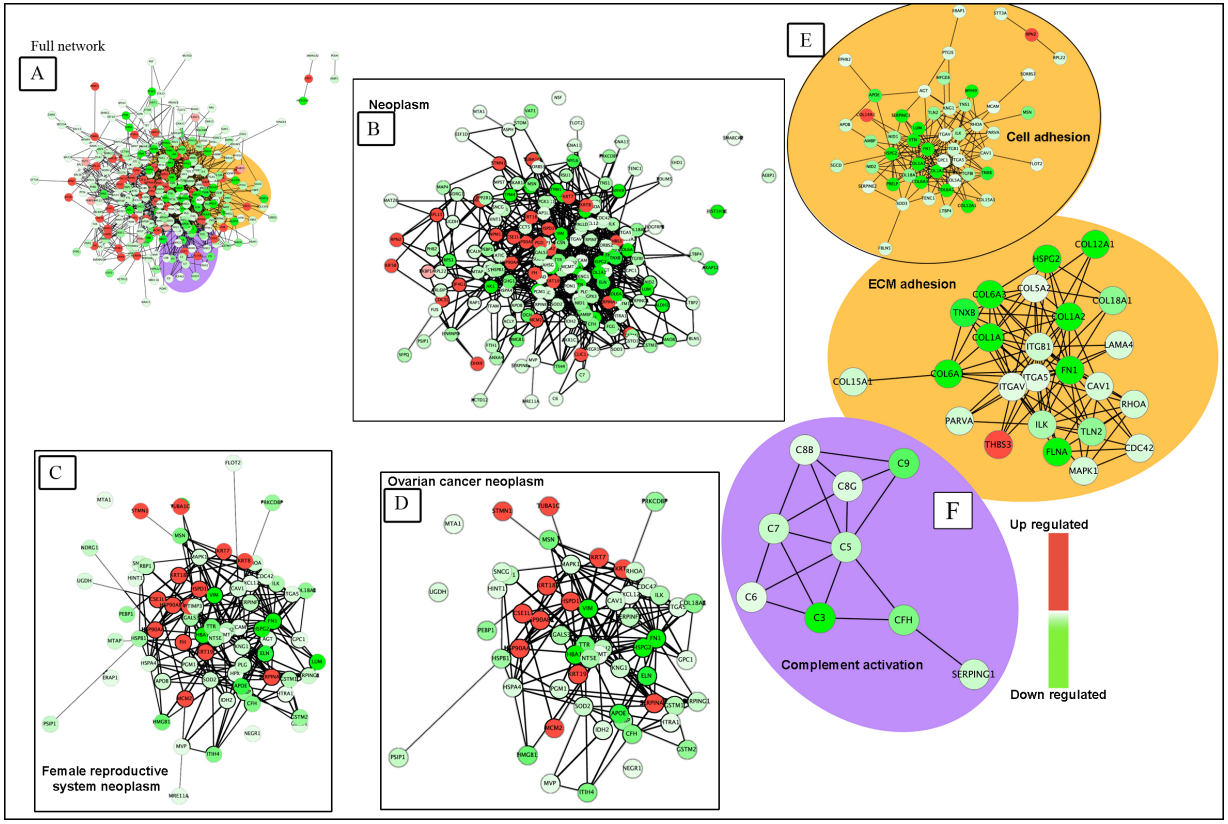

Figure 50 Interaction networks of proteins common between serous ovarian and tubal cancers.

Interactions were retrieved using gene names in the STRING network database (A). A full network was then constructed using Cytoscape with relative expression data as the Id mapper; the score based on the up and down regulation of each of the common proteins between ovarian and tubal cancers compared with the normal ovary is represented by a color code with the green shade representing negative score changes and the red shade positive score changes. The Reactome NCI plugin was then used to draw sub networks for neoplastic proteins (B), female reproductive neoplasm proteins (C) and ovarian cancer proteins (D). Blast2GO molecular functions were then used to represent networks for cell adhesion (E) and innate immune system proteins (F).

From these data, the molecular functions of interest were selected to construct sub-networks (Figure 50, insets at right). We decided to draw the networks of the proteins for which the functions were mainly represented, namely cellular adhesion (yellow-orange inset, Figure 50 E, supplementary Table S 2). Many of these proteins appear down regulated. This corresponds to the metastatic behavior of the cancerous cells (47). Indeed, in a spatio-temporal context, an EOC cell can detach from its tissue environment and attach to a new site. During these events, the plasma membrane of the cell loses its surface adhesion proteins for detachment. These observations highlight the common process mechanisms of ovarian and fallopian tube cancer tissues. According to the ectopic origin of ovarian cancer theory, a tubal cancerous cell could detach from its tumor site and attach in the ovarian environment. Another interesting molecular function observed in this network representation is complement activation (purple inset, Figure 50 F). We also found proteins associated with this function that was down regulated in the ovarian and tubal cancer contexts. This down regulation is also in agreement with previous discoveries. Previous work has shown that there is an immunosuppression phenomenon associated with ovarian cancer (47, 48). Here, complement activation proteins, namely the complement proteins C3, C5, C6, C7, C9, the complement component C8 gamma and beta chains (C8B, C8G), the complement factor H (CFH), and the plasma protease C1 inhibitor (SERPING1) (Supplementary Table S 3) were down regulated in the ovarian cancer context. Assuming that EOC has a Müllerian origin, it is not difficult to imagine that the suppression of the innate immune response is mandatory for a tubal cell settling in the ovary. A foreign cell could then act as an undetectable parasite in the ovarian immune environment. This mechanism would also be necessary for the evolution of these same cancerous cells in the fallopian tube environment.

To confirm the biological mechanistic found between ovarian and tubals cancer, we aimed to evaluate the proteins that were specifically found in both cancers but not in normal ovarian tissue. The distribution of the cellular processes was almost the same. Moreover we found an overexpression of cytosqueletal proteins in ovarian cancer samples. We also found immunoproteasome activators, such as PA28 alpha, which are known to be overexpressed and degraded in the ovarian cancer context (29, 48).

In addition to the inspection of the common molecular mechanisms of ovarian and tubal cancers, we examined the specific molecular mechanisms of ovarian and tubal cancers. Two arguments support this investigation. First, the analysis of tubal cancer proteins may provide insight into the underlying events in the fallopian tube environment that could lead to the metastasis of cancerous cells in the ovarian environment. In addition, investigation of specific serous ovarian cancer proteins may elucidate the mechanisms for cancer cell evolution in the ovarian environment. The second argument is that this analysis may provide a list of highly specific biomarkers for each cancer. Indeed, this specific workflow allows for the comparison of the tissue types in their anatomical context. Each protein then is found in only one tissue and not in the other two. The confidence of this specificity is even higher because we compared gynecological tissues with each other. Indeed, it is difficult to attribute a gynecological disease biomarker to a specific organ.

We first determined the gene ontology of each protein specifically identified in serous or ovarian tissues and evaluated their molecular function. Figure 51 A, B, C and D show the molecular functions and cellular processes of serous ovarian cancer and the molecular functions and the cellular processes of tubal cancer. We found that the molecular functions were not drastically different between the two tissues. The relative distributions of the functions were similar between the two cancers. This suggests that, although different proteins are implicated in fallopian tube tumorigenesis, the same biological mechanisms contribute to both neoplasms.

For example, molecular binding was highly represented in the two tissues. However, other molecular functions were listed for ovarian cancer including transmembrane transport and the peptidase function. Actin modeling, proliferation, and intercellular adhesion are the primary functions found in serous cancer. Here again, the most represented function was molecular binding.

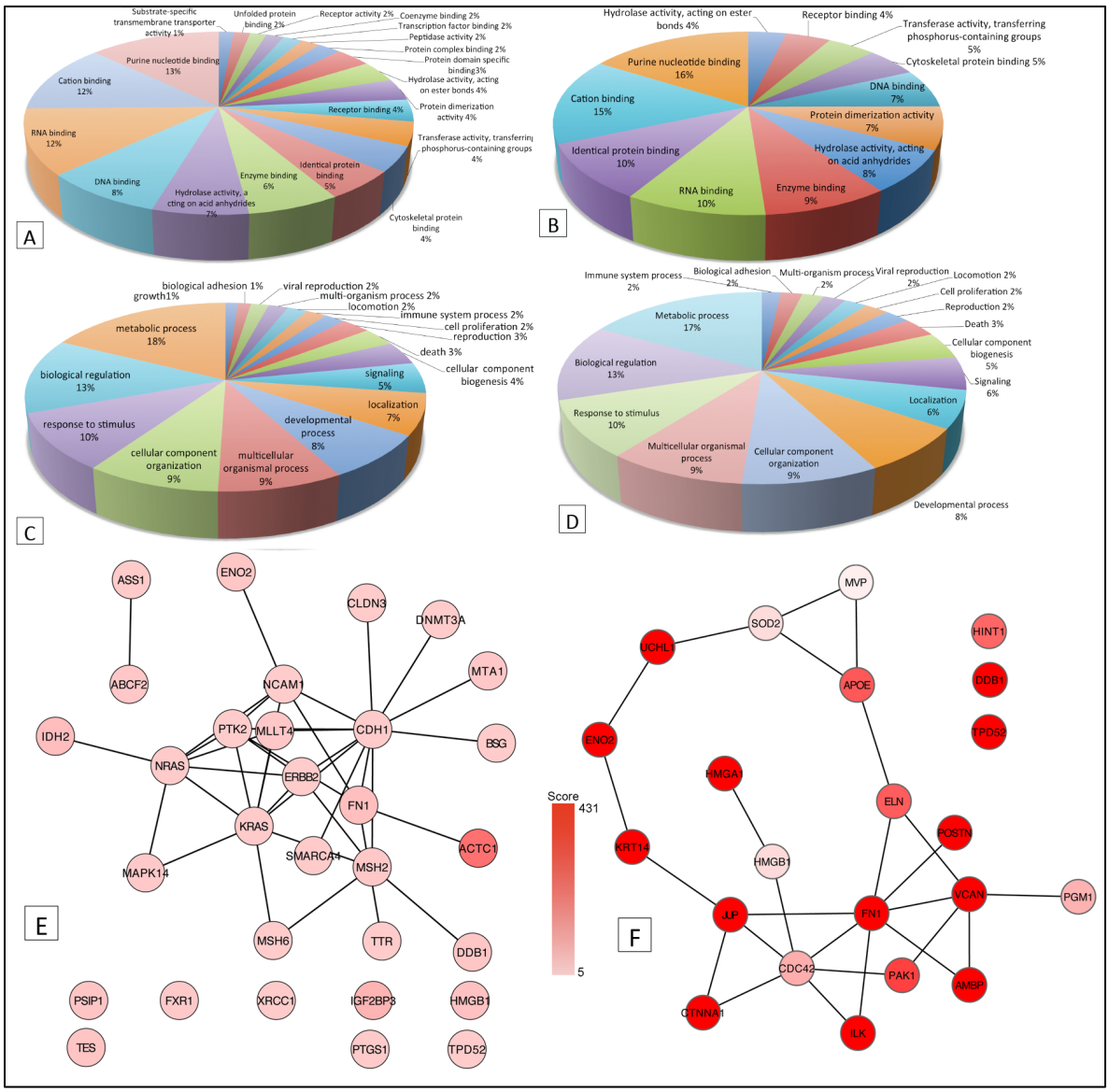

Figure 51 Analysis of specific proteins from fallopian tube and serous ovarian cancers.

From Blast2GO annotations, pie charts representing the molecular functions of ovarian cancer proteins (A) and tubal cancer proteins (B), and the cellular processes of ovarian cancer proteins (C) and tubal cancer proteins (D) were drawn. Using the Reactome NCI plugin, known ovarian cancer marker networks were traced from the ovarian cancer (E) and tubal cancer networks (F).

However, by close inspection of the nature of the proteins specifically identified in serous ovarian cancer (Supplementary Table S 1), we observed that the proteins bearing binding functions were drastically different from the proteins found in common between ovarian and tubal cancer. Indeed, we found that the adhesion proteins overexpressed in ovarian tissue were proteins corresponding to epithelial differentiation. For example, cell-cell adhesion proteins, cell-cell adherent junction proteins, homophilic and homotypic cell adhesion proteins were highly represented functions in this histological context. Some proteins implicated in cellular adhesion with the extracellular matrix were also found. The second striking observation was the high content of proteins implicated in cellular proliferation. Finally, many proteins associated with actin modeling appeared as an important overrepresented function among those proteins. These observations provide insights into the specific mechanisms we found in ovarian cancers. In fact, serous ovarian carcinogenesis appears to be controlled by highly specific mechanisms. These mechanisms may consist of the acquisition of epithelial characteristics combined with a great modeling of the cell shape and a greater proliferation potential. Other represented proteins are implicated in metabolism, HSP binding, lipid transport and catabolism, and MAPK network activation. All of these events are in agreement with previous findings in ovarian cancer research (47).

We also used the Reactome NCI plugin to determine whether the proteins were previously characterized in ovarian neoplasms. The network of these proteins is presented in, Figure 50 E (Supplementary Table S 4). Among these, we found the GTPases KRas (KRAS) (49) and NRas (NRAS) (50), mitogen-activated protein kinase 1 (MPK1) (51, 52), and receptor tyrosine-protein kinase erbB-2 (53, 54), which are involved in the EGF receptor signaling pathway that greatly promotes ovarian cancer (55-57), resulting in cancer progression. Focal adhesion kinase 1 (58) is involved is the VEGF receptor pathway, which promotes angiogenesis and the integrin pathway and induces the mitogen-activated protein kinase (ERK) pathway (52), resulting in cancer progression. Fibronectin (FN1) (59) is the extracellular component that activates the integrin pathway. The integrin pathway also induces actin polymerization for cellular remodelling (60). In addition, metastasis-associated protein is involved in activating the p53 pathway (61).

Supplementary Table 1 lists the proteins specifically identified in serous ovarian cancer, from the highest to lowest score. In this table, we determined that the most prevalent proteins corresponded to proteins associated with cellular shape changes (62), including cytoskeletal proteins, namely actin, beta actin like protein and microtubule-associated proteins. Proteins associated with nuclear modeling constituted another group of well-represented proteins, including histone H2B, histone H3 and heterochromatin protein 1-binding protein. The epigenetic modification of histones results in the repression of some genes and tumorigenesis events (63). Among the highest scoring proteins, we also found those implicated in metabolism such as transketolase (64), which is implicated in the pentose-phosphate pathway that is often used in metastatic processes (47). We also found proteins involved in glycolysis, which is another preferred metabolic pathway (65), including 6-phosphofructokinase and enolase. As previously mentioned, proteins involved in cell-cell interactions are represented, including zyxin (66) and desmoglein. Finally, we found that the majority of proteins implicated in RNA and protein synthesis were among the highest scoring. Among these proteins, we found heterogeneous nuclear ribonucleoproteins, ribosome-binding protein, eukaryotic translation initiation factor, protein disulfide-isomerase, 60 kDa SS-A/Ro ribonucleoprotein, and regulation of nuclear pre-mRNA domain-containing protein. All of these proteins had high scores in this analysis and may be considered for further analysis and validation by other methods using a large patient cohort. In this study, we determined the most important proteins specifically expressed in serous ovarian cancer.

We then investigated the specific tubal cancer biomarkers. The aim of this part of the study was to evaluate the relevance of the ovarian biomarkers for serous ovarian cancers. Indeed, if the ovarian cancer origin theory is valid, then tubal precursor markers may be appropriate for screening large cohorts of patients for the diagnosis of highly prevalent serous ovarian cancer. To do so, we used the Reactome NCI plugin to determine whether biomarkers initially discovered in the ovarian cancer context were expressed in fallopian tube tissues (Figure 51 F, Supplementary Table S 5). We observed that highly scoring proteins that were previously assigned to ovarian neoplasm were found in the fallopian tube tissue. This finding is the first clue that some biomarkers normally found in an ovarian cancer context may actually be tubal cancer biomarkers. Among these proteins, we found Fibronectin 1

(FN1), which is implicated in the integrin pathway for actin remodeling (59); cell division control protein 42 (CDC42), which is involved in cell migration (67); the glycolysis enzyme gamma-enolase (ENO2); high-mobility group protein 1 (HMGB1) (68), which is involved in the facilitation of transcription, replication, recombination, and DNA repair. We also found some cell-cell junction proteins such as junction plakoglobin (JUP) and alpha catenin a1 because tubal cancer is also an epithelial cancer; and serine/threonine-protein kinase PAK 1 (69) and integrin-linked protein kinase (ILK), which are involved in cytoskeleton remodelling (70).

This network is striking evidence that biomarkers initially found in the ovarian cancer context are also fallopian tube cancer biomarkers. This finding is reinforced by the fact that the Reactome NCI Plugin did not allow us to find tubal cancer biomarkers in the tubal cancer environment. Ovarian and tubal cancers evidently share biological functions in their development. However, the anatomical context provides a more accurate insight of the biomarkers for each gynecological disease.

Finally, we closely investigated the biological relevance of the highest scoring biomarkers in the fallopian tube environment to highlight the gynecological markers that the Reactome NCI Plugin may have missed.

Among all of the high scoring proteins found in the tubal tumoral environment, the most striking is periostin. This protein has been reported to be present in the environment of many cancer cells types. Periostin is a component of the extracellular matrix, and in cancer, it acts as a ligand for alpha-V/beta-3 and alpha-V/beta-5 integrins to support the adhesion and migration of epithelial cells (71). The binding of this ligand also promotes the recruitment of the epidermal growth factor receptor (EGFR) and the activation of the Akt/PKB- and FAK-mediated signaling pathways (70). Periostin-activated signaling pathways also promote cellular survival, angiogenesis, and resistance to hypoxia-induced cell death. In ovarian cancer, periostin promotes ovarian cancer angiogenesis and metastasis (71, 72). In this particular case, we found periostin specifically expressed in the fallopian tube cancer environment and not in that of ovarian cancer. This is a highly important point for the understanding of the relevance of the adapted workflow. This specific approach, relying on tissue proteomics in an anatomical context, allowed us to determine that periostin was a tubal cancer protein that was not present in ovarian cancer.

This also allows us to identify another response element to the question of ovarian cancer cellular origin. Here, we can speculate that periostin, which is highly expressed in tubal cancer, may induce the metastasis of fallopian tube cancer cells and promote their metastasis to a host tissue, which includes the ovary.

Osteopontin is another biomarker of the same type that promotes cell migration via integrin binding, and it has been previously found in epithelial ovarian cancers and was selected together with five other biomarkers for the multiplexed screening of epithelial ovarian cancers (73).

In this manner, ovarian serous cancers may develop after early metastasis events in the fallopian tube context from tubal cancer cells settling in the ovary. This theory is in agreement with the relative anatomical position of the fallopian tubes and the ovaries in the gynecological tracts. The fallopian tubes and the ovaries are physiologically closely related. For example, during reproduction events after ovulation, the female gamete migrates from the ovary to the endometrium through the fallopian tube. From this point of view, it is not surprising that the preferred hosting site for a migrating tubal cancer cell would be the ovary.

It is now possible to link the events that we observed that are shared by the fallopian tubes and ovaries and specific ovarian cancer events. We found that the events shared between ovarian and fallopian tube cancers consisted of the down regulation of many proteins. Assuming that a serous ovarian cancer could be derived from a fallopian tube cancerous cell, it appears that in both cases, this cell may need to act as a molecular phantom in its anatomical context, which results from the suppression of immune proteins in the cancerous context. The adhesion of the cell to the extracellular matrix must then be suppressed for detachment for its tumoral context. This detachment would be promoted by extracellular matrix elements. In the ovarian environment, cell proliferation greatly increases. In addition, the cell may undergo many changes to acquire epithelial characteristics. This event is transduced by an important remodeling of the actin network of the cell and the expression of proteins mostly involved in cell-cell interactions. All of the proteins specifically found in the ovarian cancer context may represent pathological biomarkers. Indeed, membrane proteins that are in close contact with the extracellular

milieu, which could easily be found in circulating fluids, must have a particular role in the transformation process.

We also demonstrated that some ovarian cancer biomarkers are actually fallopian tube cancer biomarkers. This discovery highlights the relevance of the anatomical context in the biomarkers research field. At the same time, this discovery suggests new methods for investigating the clinical screening of ovarian cancer.

Conclusion

Many questions remain regarding the origin of EOC and its mechanisms of progression. The emergence of proteomic technologies that identify potential biomarkers in body fluids and tissues allows biologists and clinicians to access pathological analysis on the molecular scale.

Here we proposed a two-step strategy for the study of specific proteins in their histological context. The first step is a quick examination of the molecular profiles found in tissues that are of a different nature. The PCA calculation is based on a global comparison of multidimensional data. We applied these analyses to spectra groups using the relative intensities of the detected peaks in tissue sections. This experiment is a quick way to provide the complete molecular content trends of the histological regions of interest on a single or a few biopsied sections. PCA was used for the comparison of tissues in the same patient to avoid inter-patient tissue variability. We speculated that the analysis of a small number of tissues may gain confidence when the patient is considered as the control in the experiment. The 2D representations provided by PCA allowed us to classify these in a way that our findings support the Müllerian origin of endometrioid and serous cancer hypothesis.

The second step consisted of a deeper investigation of the molecular actors in the tissues of interest. To do so, we performed a shotgun proteomics analysis of the tryptic digests analyzed on tissues with the MALDI source. The subsequent analyses using the Blast2GO and Cytoscape software gave us a global view of the potential biological events that may occur during serous cancer development. If we assume that serous epithelial ovarian cancers originate from a fallopian tube cancerous precursor, then cell detachment mechanisms from the tumor site may be involved as an immunosuppression mechanism for a cell that is considered a foreign element in the physiological context. In the ovarian environment, additional specific events may occur. The newly settled and undifferentiated

cell may differentiate into an epithelial cell to form an epithelial cancer in the ovarian host site.

This type of experiment can provide important insights into the histological specificity of the proteins of each pathology. We introduce a new concept that consists of providing new evidence for a clinical problem while assessing the molecular specificity of the pathological proteins. Based on the relative scores of the proteins found in different tissues, we were able to assess the relative specificity of the proteins in each tissue. We then provided the first proteomic insight into the degree of similarity of the serous ovarian cancer tissues with its possibly related Müllerian tissue. This comparison allowed us to elucidate the possible molecular mechanisms found in the appearance of ovarian cancer and its development.

Determining the specific serous epithelial ovarian cancer markers is only possible using this specific tissue profiling workflow. This may be considered for specific tissue biomarkers studies. The proteins up-regulated in each tissue may be selected for their specificity against two or more tissues from the same patient. Indeed, the clinical value of a biomarker that is useable for a diagnostic test is its specificity for one cancer type as opposed to another. Here we propose a list of specific serous ovarian cancer proteins that are found in their anatomical context and guaranteed to be absent in normal ovarian tissue and another type of gynecological cancer from the same patient, *i.e.*, the fallopian tube. Thus, these proteins are specific to the cancerous pathological status and are specific for the ovary as opposed to other gynecologic neoplasms.

The scope of this type of analysis is to evaluate the most appropriate biomarkers for serous ovarian cancer. If the fallopian tube is the cause of ovarian cancer, a large campaign identifying the fallopian tube cancer biomarkers may be performed. This may provide an insight into the early development of this specific neoplasm and identify the precise time when radical fimbriectomy may be performed for at-risk or even non-suspecting patients.

To definitively validate the hypotheses and biomarkers found, it will be necessary to repeat this experiment in a large cohort of tissues and interpret the results using statistical analyses. However, using the same patient for a comparison analysis is an excellent internal control for the experiment. At this time, we speculate that the observations made after this study may be the cornerstone of the Müllerian origin of serous ovarian cancer theory.

In conclusion, this workflow is an example of the potential of the mass spectrometric profiling method for biomarker research and for specific clinical application. We have been able to prove the feasibility of this method while providing the first proteomic evidence of the potential tubal origin of serous ovarian cancer We also introduced a new research method for the investigation of gynecological cancer biomarkers. On-tissue proteomics allowed us to determine that ovarian cancer biomarkers may actually derive from fallopian tube cancer precursors; it may then be relevant to compare whether biomarkers found in fallopian tube cancers have good predictive values for ovarian cancer screening in large patient cohorts. This type of investigation may be highly relevant for the early detection of ovarian cancers.

Acknowledgements

This research was supported by a collaboration between The Fundamental and Applied Biology Mass Spectrometry laboratory (MS) and Thermofisher (Bremen, KS) and grants from the Centre National de la Recherche Scientifique (CNRS), Ministère de L'Education Nationale, de L'Enseignement Supérieur et de la Recherche, Agence Nationale de la Recherche (ANR PCV to IF), Canadian Institutes of Health Research (CIHR to MS & RD), Ministère du Développement Économique de l'Innovation et de l'Exportation (MDEIE to RD), Fonds de Recherche du Québec - Santé (FRQS to R.D), CHRU of Lille (to CB), CNRS for HG and Région Nord-Pas de Calais and Université de Sherbrooke (to RL). R.D. is a member of the Centre de Recherche Clinique Etienne-Le Bel (Sherbrooke, Qc, Canada).

References

1. Dubeau L. The cell of origin of ovarian epithelial tumours. Lancet Oncol 2008; 9: 1191-7.
2. Shih Ie M, Kurman RJ. Ovarian tumorigenesis: a proposed model based on morphological and molecular genetic analysis. Am J Pathol 2004; 164: 1511-8.
3. Bell DA, Scully RE. Early de novo ovarian carcinoma. A study of fourteen cases. Cancer 1994; 73: 1859-64.
4. Leblanc E, Narducci F, Farre I, et al. Radical fimbriectomy: a reasonable temporary risk-reducing surgery for selected women with a germ line mutation of BRCA 1 or 2 genes? Rationale and preliminary development. Gynecol Oncol; 121: 472-6.
5. Callahan MJ, Crum CP, Medeiros F, et al. Primary fallopian tube malignancies in BRCA-positive women undergoing surgery for ovarian cancer risk reduction. J Clin Oncol 2007; 25: 3985-90.
6. Carcangiu ML, Radice P, Manoukian S, et al. Atypical epithelial proliferation in fallopian tubes in prophylactic salpingo-oophorectomy specimens from BRCA1 and BRCA2 germline mutation carriers. Int J Gynecol Pathol 2004; 23: 35-40.
7. Colgan TJ, Murphy J, Cole DE, Narod S, Rosen B. Occult carcinoma in prophylactic oophorectomy specimens: prevalence and association with BRCA germline mutation status. Am J Surg Pathol 2001; 25: 1283-9.
8. Finch A, Shaw P, Rosen B, Murphy J, Narod SA, Colgan TJ. Clinical and pathologic findings of prophylactic salpingo-oophorectomies in 159 BRCA1 and BRCA2 carriers. Gynecol Oncol 2006; 100: 58-64.
9. Kindelberger DW, Lee Y, Miron A, et al. Intraepithelial carcinoma of the fimbria and pelvic serous carcinoma: Evidence for a causal relationship. Am J Surg Pathol 2007; 31: 161-9.
10. Piek JM, van Diest PJ, Zweemer RP, Kenemans P, Verheijen RH. Tubal ligation and risk of ovarian cancer. Lancet 2001; 358: 844.
11. Piek JM, Verheijen RH, Kenemans P, Massuger LF, Bulten H, van Diest PJ. BRCA1/2-related ovarian cancers are of tubal origin: a hypothesis. Gynecol Oncol 2003; 90: 491.
12. Shaw PA, Rouzbahman M, Pizer ES, Pintilie M, Begley H. Candidate serous cancer precursors in fallopian tube epithelium of BRCA1/2 mutation carriers. Mod Pathol 2009; 22: 1133-8.
13. Staebler A. [Preneoplasias of ovarian carcinoma : Biological and clinical aspects of different pathways of tumorigenesis.]. Pathologe 2011.
14. Leonhardt K, Einenkel J, Sohr S, Engeland K, Horn LC. p53 Signature and Serous Tubal In-situ Carcinoma in Cases of Primary Tubal and Peritoneal Carcinomas and Serous Borderline Tumors of the Ovary. Int J Gynecol Pathol; 30: 417-24.
15. Chen EY, Mehra K, Mehrad M, et al. Secretory cell outgrowth, PAX2 and serous carcinogenesis in the Fallopian tube. J Pathol; 222: 110-6.
16. Carlson JW, Jarboe EA, Kindelberger D, Nucci MR, Hirsch MS, Crum CP. Serous tubal intraepithelial carcinoma: diagnostic reproducibility and its implications. Int J Gynecol Pathol 2010; 29: 310-4.
17. Wei CF, Hwang SH, Ho CM, Shih BY, Chien TY. Malignant mixed mullerian tumors of the ovary. Zhonghua Yi Xue Za Zhi (Taipei) 2000; 63: 344-8.

18. Roh MH, Kindelberger D, Crum CP. Serous tubal intraepithelial carcinoma and the dominant ovarian mass: clues to serous tumor origin? Am J Surg Pathol 2009; 33: 376-83.
19. Jarboe E, Folkins A, Nucci MR, et al. Serous carcinogenesis in the fallopian tube: a descriptive classification. Int J Gynecol Pathol 2008; 27: 1-9.
20. Stoeckli M, Chaurand P, Hallahan DE, Caprioli RM. Imaging mass spectrometry: a new technology for the analysis of protein expression in mammalian tissues. Nat Med 2001; 7: 493-6.
21. Callesen AK, Vach W, Jorgensen PE, et al. Reproducibility of mass spectrometry based protein profiles for diagnosis of breast cancer across clinical studies: a systematic review. J Proteome Res 2008; 7: 1395-402.
22. Franck J, Arafah K, Elayed M, et al. MALDI imaging mass spectrometry: state of the art technology in clinical proteomics. Mol Cell Proteomics 2009; 8: 2023-33.
23. Schwartz SA, Weil RJ, Thompson RC, et al. Proteomic-based prognosis of brain tumor patients using direct-tissue matrix-assisted laser desorption ionization mass spectrometry. Cancer Res 2005; 65: 7674-81.
24. Fournier I, Day R, Salzet M. Direct analysis of neuropeptides by in situ MALDI-TOF mass spectrometry in the rat brain. Neuro Endocrinol Lett 2003; 24: 9-14.
25. Fournier I, Wisztorski M, Salzet M. Tissue imaging using MALDI-MS: a new frontier of histopathology proteomics. Expert Rev Proteomics 2008; 5: 413-24.
26. El Ayed M, Bonnel D, Longuespee R, et al. MALDI imaging mass spectrometry in ovarian cancer for tracking, identifying, and validating biomarkers. Med Sci Monit 2010; 16: BR233-45.
27. Franck J, Longuespee R, Wisztorski M, et al. MALDI mass spectrometry imaging of proteins exceeding 30,000 daltons. Med Sci Monit 2010; 16: BR293-9.
28. Lemaire R, Lucot,J.P.,Collinet,P.,Vinatier,D.,Tabet,J.C.,Salzet,M.,Fournier, I. New developments in direct analyses by MALDI mass spectrometry for study ovarian cancer. Mol Cell Proteomics 2005; 4: S305-S8.
29. Lemaire R, Menguellet SA, Stauber J, et al. Specific MALDI imaging and profiling for biomarker hunting and validation: fragment of the 11S proteasome activator complex, Reg alpha fragment, is a new potential ovary cancer biomarker. J Proteome Res 2007; 6: 4127-34.
30. Longuespée RB, C.;Castellier, C.; Jacquet, E.; Desmons, A.;Kerdraon, O.;Vinatier, D., Day, R., Fournier, I.; Salzet, M. The C-terminal fragment of the immunoproteasome PA28S (Reg Alpha) as an early diagnosis and tumor-relapse biomarker: evidence from mass spectrometry profiling
Histochem Cell Biol 2012; in press: D.O.I. 10.1007/s00418-012-0953-0.
31. Stauber J, Lemaire, R., Wisztorski, M., Ait-Menguellet, S., Lucot, J.P., Vinatier, D., Desmons, A., Deschamps, M., Proess, G., Rudolf, I., Salzet, M., Fournier, I. . New developments in MALDI imaging mass spectrometry for pathological proteomic studies; Introduction to a novel concept, the specific MALDI imaging. Mol Cell Proteomics 2006; 5: S247-S9.
32. Bonnel D, Legouffe R, Willand N, et al. MALDI imaging techniques dedicated to drug-distribution studies. Bioanalysis; 3: 1399-406.
33. Bonnel D, Longuespee R, Franck J, et al. Multivariate analyses for biomarkers hunting and validation through on-tissue bottom-up or in-source decay in MALDI-MSI: application to prostate cancer. Anal Bioanal Chem 2011; 401: 149-65.

34. Gustafsson JO, Oehler MK, McColl SR, Hoffmann P. Citric acid antigen retrieval (CAAR) for tryptic peptide imaging directly on archived formalin-fixed paraffin-embedded tissue. J Proteome Res; 9: 4315-28.
35. Franck J, Arafah K, Barnes A, Wisztorski M, Salzet M, Fournier I. Improving tissue preparation for matrix-assisted laser desorption ionization mass spectrometry imaging. Part 1: using microspotting. Anal Chem 2009; 81: 8193-202.
36. Lemaire R, Desmons A, Tabet JC, Day R, Salzet M, Fournier I. Direct analysis and MALDI imaging of formalin-fixed, paraffin-embedded tissue sections. J Proteome Res 2007; 6: 1295-305.
37. Deininger SO, Ebert MP, Futterer A, Gerhard M, Rocken C. MALDI Imaging Combined with Hierarchical Clustering as a New Tool for the Interpretation of Complex Human Cancers. J Proteome Res 2008.
38. Colinge J, Chiappe D, Lagache S, Moniatte M, Bougueleret L. Differential proteomics via probabilistic peptide identification scores. Anal Chem 2005; 77: 596-606.
39. Nanduri B, Lawrence ML, Vanguri S, Pechan T, Burgess SC. Proteomic analysis using an unfinished bacterial genome: the effects of subminimum inhibitory concentrations of antibiotics on Mannheimia haemolytica virulence factor expression. Proteomics 2005; 5: 4852-63.
40. Searle BC. Scaffold: a bioinformatic tool for validating MS/MS-based proteomic studies. Proteomics 2010; 10: 1265-9.
41. Conesa A, Gotz S, Garcia-Gomez JM, Terol J, Talon M, Robles M. Blast2GO: a universal tool for annotation, visualization and analysis in functional genomics research. Bioinformatics 2005; 21: 3674-6.
42. Szklarczyk D, Franceschini A, Kuhn M, et al. The STRING database in 2011: functional interaction networks of proteins, globally integrated and scored. Nucleic Acids Res 2011; 39: D561-8.
43. Smoot ME, Ono K, Ruscheinski J, Wang PL, Ideker T. Cytoscape 2.8: new features for data integration and network visualization. Bioinformatics 2011; 27: 431-2.
44. Djidja MC, Carolan V, Loadman PM, Clench MR. Method development for protein profiling in biological tissues by matrix-assisted laser desorption/ionisation mass spectrometry imaging. Rapid Commun Mass Spectrom 2008; 22: 1615-8.
45. Trim PJ, Henson CM, Avery JL, et al. Matrix-assisted laser desorption/ionization-ion mobility separation-mass spectrometry imaging of vinblastine in whole body tissue sections. Anal Chem 2008; 80: 8628-34.
46. Prat J. New insights into ovarian cancer pathology. Ann Oncol; 23 Suppl 10: x111-x7.
47. Longuespee R, Boyon C, Desmons A, et al. Ovarian cancer molecular pathology. Cancer Metastasis Rev.
48. Longuespee R, Boyon C, Castellier C, et al. The C-terminal fragment of the immunoproteasome PA28S (Reg alpha) as an early diagnosis and tumor-relapse biomarker: evidence from mass spectrometry profiling. Histochem Cell Biol; 138: 141-54.
49. Ratner ES, Keane FK, Lindner R, et al. A KRAS variant is a biomarker of poor outcome, platinum chemotherapy resistance and a potential target for therapy in ovarian cancer. Oncogene.
50. Meunier L, Puiffe ML, Le Page C, et al. Effect of ovarian cancer ascites on cell migration and gene expression in an epithelial ovarian cancer in vitro model. Transl Oncol; 3: 230-8.

51. Nonaka M, Itamochi H, Kawaguchi W, et al. Activation of the mitogen-activated protein kinase kinase/extracellular signal-regulated kinase pathway overcomes Cisplatin resistance in ovarian carcinoma cells. Int J Gynecol Cancer; 22: 922-9.
52. Roberts PJ, Der CJ. Targeting the Raf-MEK-ERK mitogen-activated protein kinase cascade for the treatment of cancer. Oncogene 2007; 26: 3291-310.
53. Wilken JA, Badri T, Cross S, et al. EGFR/HER-targeted therapeutics in ovarian cancer. Future Med Chem; 4: 447-69.
54. Felip E, Del Campo JM, Rubio D, Vidal MT, Colomer R, Bermejo B. Overexpression of c-erbB-2 in epithelial ovarian cancer. Prognostic value and relationship with response to chemotherapy. Cancer 1995; 75: 2147-52.
55. Zhou C, Qiu L, Sun Y, et al. Inhibition of EGFR/PI3K/AKT cell survival pathway promotes TSA's effect on cell death and migration in human ovarian cancer cells. Int J Oncol 2006; 29: 269-78.
56. Kandala PK, Wright SE, Srivastava SK. Blocking epidermal growth factor receptor activation by 3,3'-diindolylmethane suppresses ovarian tumor growth in vitro and in vivo. J Pharmacol Exp Ther; 341: 24-32.
57. Sheng Q, Liu J. The therapeutic potential of targeting the EGFR family in epithelial ovarian cancer. Br J Cancer; 104: 1241-5.
58. Judson PL, He X, Cance WG, Van Le L. Overexpression of focal adhesion kinase, a protein tyrosine kinase, in ovarian carcinoma. Cancer 1999; 86: 1551-6.
59. Xing H, Weng D, Chen G, et al. Activation of fibronectin/PI-3K/Akt2 leads to chemoresistance to docetaxel by regulating survivin protein expression in ovarian and breast cancer cells. Cancer Lett 2008; 261: 108-19.
60. Vicente-Manzanares M, Choi CK, Horwitz AR. Integrins in cell migration--the actin connection. J Cell Sci 2009; 122: 199-206.
61. Li DQ, Divijendra Natha Reddy S, Pakala SB, et al. MTA1 coregulator regulates p53 stability and function. J Biol Chem 2009; 284: 34545-52.
62. Creekmore AL, Silkworth WT, Cimini D, Jensen RV, Roberts PC, Schmelz EM. Changes in gene expression and cellular architecture in an ovarian cancer progression model. PLoS One; 6: e17676.
63. Seeber LM, van Diest PJ. Epigenetics in ovarian cancer. Methods Mol Biol; 863: 253-69.
64. Krockenberger M, Honig A, Rieger L, et al. Transketolase-like 1 expression correlates with subtypes of ovarian cancer and the presence of distant metastases. Int J Gynecol Cancer 2007; 17: 101-6.
65. Karantanis D, Allen-Auerbach M, Czernin J. Relationship among glycolytic phenotype, grade, and histological subtype in ovarian carcinoma. Clin Nucl Med; 37: 49-53.
66. Grunewald TG, Kammerer U, Winkler C, et al. Overexpression of LASP-1 mediates migration and proliferation of human ovarian cancer cells and influences zyxin localisation. Br J Cancer 2007; 96: 296-305.
67. Mythreye K, Blobe GC. The type III TGF-beta receptor regulates epithelial and cancer cell migration through beta-arrestin2-mediated activation of Cdc42. Proc Natl Acad Sci U S A 2009; 106: 8221-6.
68. Chen J, Xi B, Zhao Y, Yu Y, Zhang J, Wang C. High-mobility group protein B1 (HMGB1) is a novel biomarker for human ovarian cancer. Gynecol Oncol; 126: 109-17.

69. Siu MK, Wong ES, Chan HY, et al. Differential expression and phosphorylation of Pak1 and Pak2 in ovarian cancer: effects on prognosis and cell invasion. Int J Cancer; 127: 21-31.
70. Lin SW, Ke FC, Hsiao PW, Lee PP, Lee MT, Hwang JJ. Critical involvement of ILK in TGFbeta1-stimulated invasion/migration of human ovarian cancer cells is associated with urokinase plasminogen activator system. Exp Cell Res 2007; 313: 602-13.
71. Gillan L, Matei D, Fishman DA, Gerbin CS, Karlan BY, Chang DD. Periostin secreted by epithelial ovarian carcinoma is a ligand for alpha(V)beta(3) and alpha(V)beta(5) integrins and promotes cell motility. Cancer Res 2002; 62: 5358-64.
72. Zhu M, Fejzo MS, Anderson L, et al. Periostin promotes ovarian cancer angiogenesis and metastasis. Gynecol Oncol; 119: 337-44.
73. Kim K, Visintin I, Alvero AB, Mor G. Development and validation of a protein-based signature for the detection of ovarian cancer. Clin Lab Med 2009; 29: 47-55.

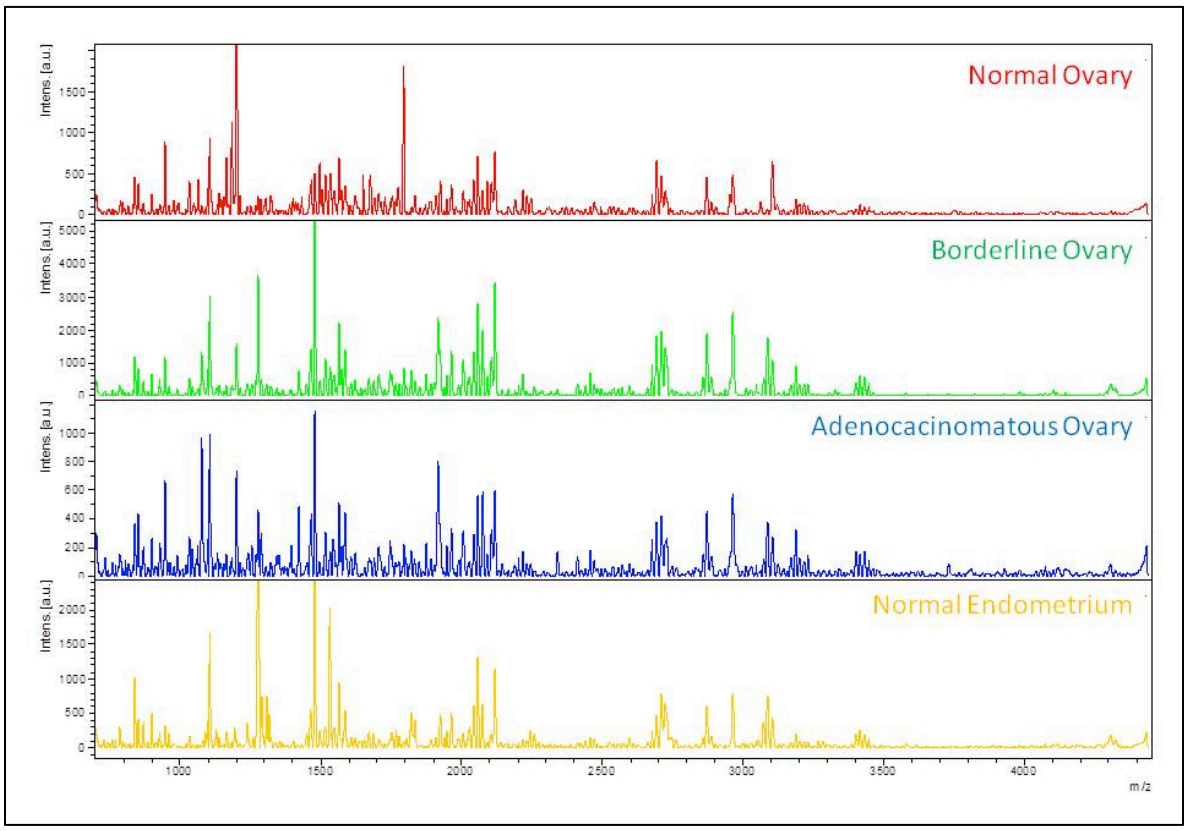

Figure S 13 Mass spectra observed in normal, borderline, and adenocarcinoma ovarian tissues.

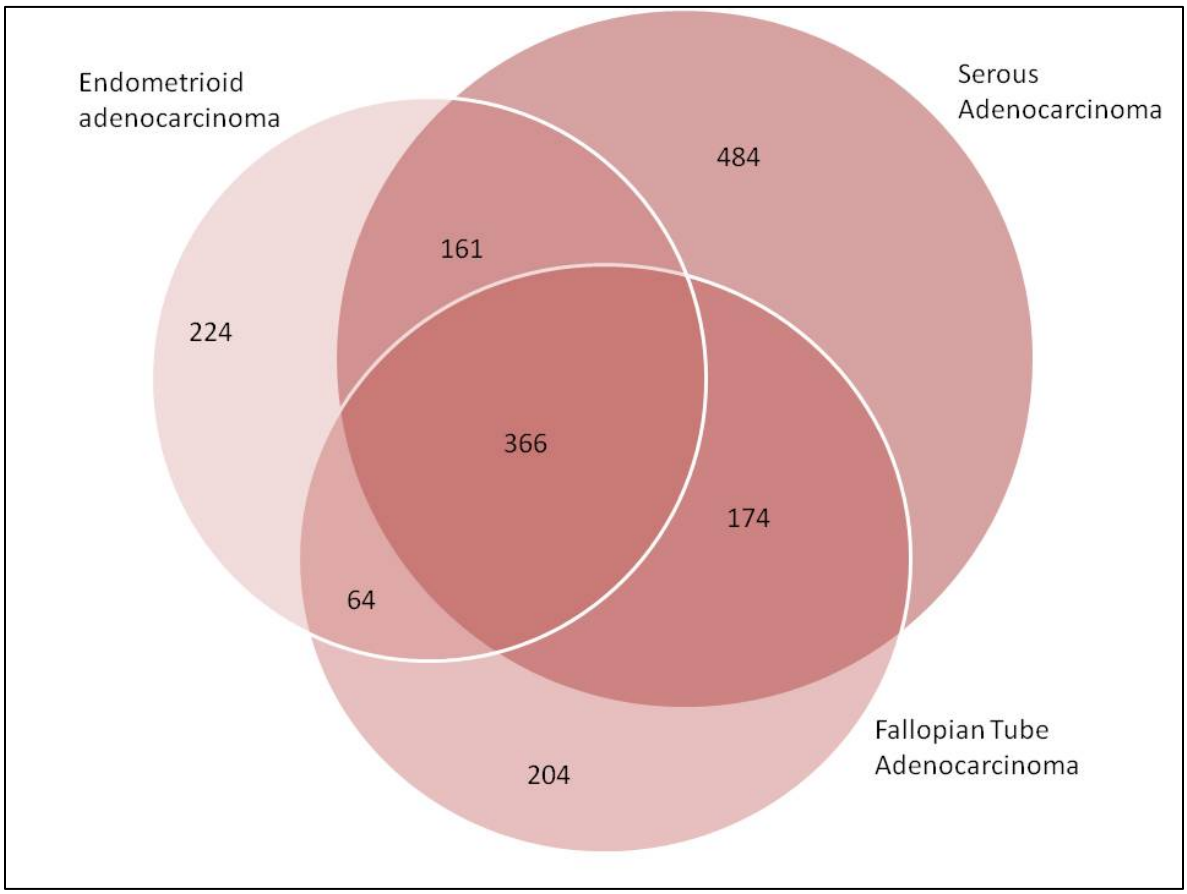

Figure S 14 Venn diagram illustration of protein identification between each cancer tissue.

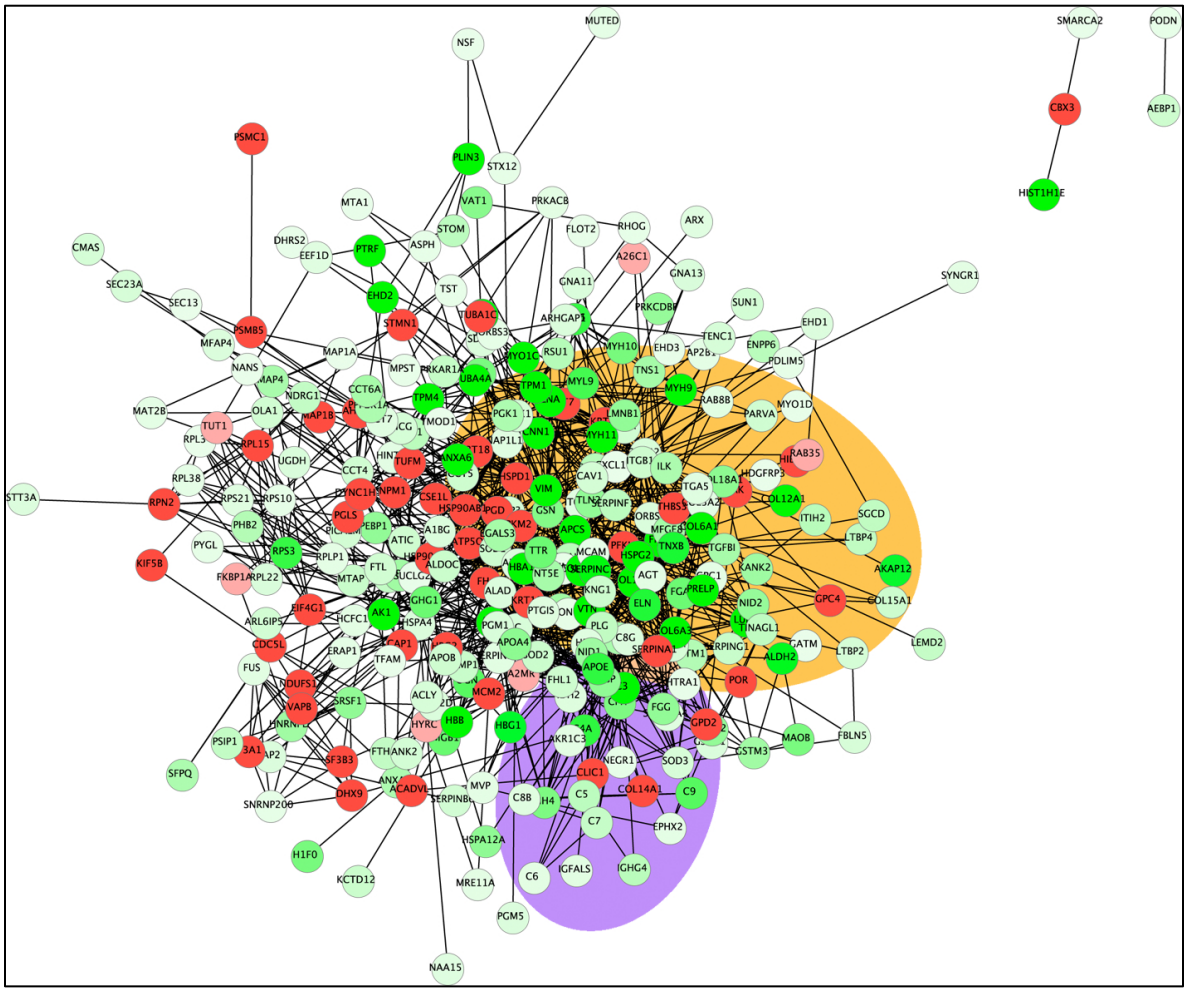

Figure S 15 Enlarged full network from Figure 50.

Table S 1 Protein identification, score and distributions across tissues.

Cette table contient une quantité de données trop grande pour être insérée dans un document imprimé et a été retirée.

Table S 2 Gene name, accession number, fold change and function of cell adhesion specific network in Figure 50.

Cell adhesion

Gene name	Acc	Fold	Function
MYH9	P35579	-98	Cellular myosin that appears to play a role in cytokinesis, cell shape, and specialized functions such as secretion and capping
PRPH	P41219	-97	Class-III neuronal intermediate filament protein
VTN	P04004	-86	Vitronectin is a cell adhesion and spreading factor found in serum and tissues. Vitronectin interact with glycosaminoglycans and proteoglycans. Is recognized by certain members of the integrin family and serves as a cell-to-substrate adhesion molecule. Inhibitor of the membrane-damaging effect of the terminal cytolytic complement pathway
PRELP	P51888	-77	May anchor basement membranes to the underlying connective tissue (By similarity)
LUM	P51884	-61	Binds to laminin
SERPINC1	P01008	-47	Most important serine protease inhibitor in plasma that regulates the blood coagulation cascade. AT-III inhibits thrombin as well as factors IXa, Xa and XIa. Its inhibitory activity is greatly enhanced in the presence of heparin
APOE	P02649	-40	Mediates the binding, internalization, and catabolism of lipoprotein particles. It can serve as a ligand for the LDL (apo B/E) receptor and for the specific apo-E receptor (chylomicron remnant) of hepatic tissues
HMGB1	Q5T7C4	-32	Binds preferentially single-stranded DNA and unwinds double stranded DNA (By similarity)
MSN	P26038	-29	Probably involved in connections of major cytoskeletal structures to the plasma membrane
MAOB	B7Z5H3	-28	Catalyzes the oxidative deamination of biogenic and xenobiotic amines and has important functions in the metabolism of neuroactive and vasoactive amines in the central nervous system and peripheral tissues. MAOB preferentially degrades benzylamine and phenylethylamine
CFH	P08603	-28	Factor H functions as a cofactor in the inactivation of C3b by factor I and also increases the rate of dissociation of the C3bBb complex (C3 convertase) and the (C3b)NBB complex (C5 convertase) in the alternative complement pathway
VAT1	Q99536	-26	Plays a part in calcium-regulated keratinocyte activation in epidermal repair mechanisms. Has no effect on cell proliferation. Negatively regulates mitochondrial fusion in cooperation with mitofusin proteins (MFN1-2).
AMBP	P02760	-24	Inter-alpha-trypsin inhibitor inhibits trypsin, plasmin, and lysosomal granulocytic elastase. Inhibits calcium oxalate crystallization
NID2	Q14112	-23	Cell adhesion glycoprotein which is widely distributed in basement membranes. Binds to collagens I and IV, to perlecan and to laminin 1. Does not bind fibulins. It probably has a role in cell-extracellular matrix interactions
NID1	P14543	-21	Sulfated glycoprotein widely distributed in basement membranes and tightly associated with laminin. Also binds to collagen IV and perlecan. It probably has a role in cell- extracellular matrix interactions
MFGE8	Q08431	-20	Specific ligand for the alpha-v/beta-3 and alpha-v/beta- 5 receptors. Also binds to phosphatidylserine-enriched cell surfaces in a receptor-independent manner. Zona pellucida-binding protein which may play a role in gamete interaction. Binds specifically to rotavirus and inhibits its replication

TNS1	E9PGF5	-20	May be involved in cell migration, cartilage development and in linking signal transduction pathways to the cytoskeleton
TGFBI	Q15582	-20	Binds to type I, II, and IV collagens. This adhesion protein may play an important role in cell-collagen interactions. In cartilage, may be involved in endochondral bone formation
PALLD	Q8WX93	-16	Cytoskeletal protein required for organization of normal actin cytoskeleton. Roles in establishing cell morphology, motility, cell adhesion and cell-extracellular matrix interactions in a variety of cell types. May function as a scaffolding molecule with the potential to influence both actin polymerization and the assembly of existing actin filaments into higher-order arrays. Binds to proteins that bind to either monomeric or filamentous actin. Localizes at sites where active actin remodeling takes place, such as lamellipodia and membrane ruff [...]
ENPP6	Q6UWR7	-16	Choline-specific glycerophosphodiester phosphodiesterase. Hydrolyzes the classical substrate for phospholipase C, p-nitrophenyl phosphorylcholine, while it does not hydrolyze the classical nucleotide phosphodiesterase substrate, p-nitrophenyl thymidine 5'-monophosphate. Hydrolyzes lysophosphatidylcholine (LPC) to form monoacylglycerol and phosphorylcholine but not lysophosphatidic acid, showing it has a lysophospholipase C activity. Has a preference for LPC with short (12:0 and 14:0) or polyunsaturated (18:2 and 20:4) fatty acids. Als [...]
LTBP4	E7EUU1	-14	May be involved in the assembly, secretion and targeting of TGFB1 to sites at which it is stored and/or activated. May play critical roles in controlling and directing the activity of TGFB1. May have a structural role in the extra cellular matrix (ECM) (By similarity)
SGCD	Q92629	-14	Component of the sarcoglycan complex, a subcomplex of the dystrophin-glycoprotein complex which forms a link between the F-actin cytoskeleton and the extracellular matrix
KNG1	B4DPP8	-12	(1) Kininogens are inhibitors of thiol proteases
AEBP1	Q8IUX7	-11	May positively regulate MAP-kinase activity in adipocytes, leading to enhanced adipocyte proliferation and reduced adipocyte differentiation (By similarity). May also positively regulate NF-kappa-B activity in macrophages by promoting the phosphorylation and subsequent degradation of I-kappa-B-alpha (NFKBIA), leading to enhanced macrophage inflammatory responsiveness (By similarity). Can act as a transcriptional repressor (By similarity)
APOB	P04114	-11	Apolipoprotein B is a major protein constituent of chylomicrons (apo B-48), LDL (apo B-100) and VLDL (apo B-100). Apo B-100 functions as a recognition signal for the cellular binding and internalization of LDL particles by the apoB/E receptor
ANK2	E9PHW9	-10	Attaches integral membrane proteins to cytoskeletal elements. Also binds to cytoskeletal proteins. Required for coordinate assembly of Na/Ca exchanger, Na/K ATPase and InsP3 receptor at sarcoplasmic reticulum sites in cardiomyocytes. Required for the coordinated expression of the Na/K ATPase, Na/Ca exchanger and beta-2-spectrin (SPTBN1) in the inner segment of rod photoreceptors. Required for expression and targeting of SPTBN1 in neonatal cardiomyocytes and for the regulation of neonatal cardiomyocyte contraction rate
SUN1	O94901	-10	Component of SUN-protein-containing multivariate complexes also called LINC complexes which link the nucleoskeleton and cytoskeleton by providing versatile outer nuclear membrane attachment sites for cytoskeletal filaments.
TENC1	Q63HR2	-10	Regulates cell motility and proliferation. May have phosphatase activity. Reduces AKT1 phosphorylation. Lowers AKT1 kinase activity and interferes with AKT1 signaling
FBLN5	Q9UBX5	-9	Promotes adhesion of endothelial cells through interaction of integrins and the RGD motif. Could be a vascular ligand for integrin receptors and may play a role in vascular development and remodeling
SOD3	P08294	-9	Protect the extracellular space from toxic effect of reactive oxygen intermediates by converting superoxide radicals into hydrogen peroxide and oxygen
RPL22	P35268	-9	
MFAP4	P55083	-8	Could be involved in calcium-dependent cell adhesion or intercellular interactions
PGM5	Q15124	-8	Component of adherens-type cell-cell and cell-matrix junctions. Lacks phosphoglucomutase activity
STT3A	E9PNQ1	-8	Component of the N-oligosaccharyl transferase enzyme which catalyzes the transfer of a high mannose oligosaccharide from a lipid-linked oligosaccharide donor to an asparagine residue within an Asn-X-Ser/Thr consensus motif in nascent polypeptide chains. N-glycosylation occurs cotranslationally and the complex associates with the Sec61 complex at the channel-forming translocon complex that mediates protein translocation across the endoplasmic reticulum (ER). SST3A seems to be involved in complex substrate [...]
PTGIS	Q16647	-8	Catalyzes the isomerization of prostaglandin H2 to prostacyclin (= prostaglandin I2)

IGFALS	P35858	-7	Involved in protein-protein interactions that result in protein complexes, receptor-ligand binding or cell adhesion
SERPINE2	P07093	-7	Serine protease inhibitor with activity toward thrombin, trypsin, and urokinase. Promotes neurite extension by inhibiting thrombin. Binds heparin
AGT	P01019	-7	Essential component of the renin-angiotensin system (RAS), a potent regulator of blood pressure, body fluid and electrolyte homeostasis. In response to lowered blood pressure, the enzyme renin cleaves angiotensinogen to produce angiotensin-1 (angiotensin 1-10). Angiotensin-1 is a substrate of ACE (angiotensin converting enzyme) that removes a dipeptide to yield the physiologically active peptide angiotensin-2 (angiotensin 1-8). Angiotensin-1 and angiotensin-2 can be further processed to generate angiotensin-3 (angiotensi [...]
SYNGR1	A2A283	-6	Involved in the regulation of short-term and long-term synaptic plasticity (By similarity)
ERAP1	Q9NZ08	-6	Aminopeptidase that plays a central role in peptide trimming, a step required for the generation of most HLA class I- binding peptides. Peptide trimming is essential to customize longer precursor peptides to fit them to the correct length required for presentation on MHC class I molecules. Strongly prefers substrates 9-16 residues long. Rapidly degrades 13-mer to a 9-mer and then stops. Preferentially hydrolyzes the residue Leu and peptides with a hydrophobic C-terminus, while it has weak activity toward peptides with charged C-terminus. May play [...]
GPC1	P35052	-6	Cell surface proteoglycan that bears heparan sulfate (By similarity)
EPHX2	B4E1M2	-6	Acts on epoxides (alkene oxides, oxiranes) and arene oxides. Plays a role in xenobiotic metabolism by degrading potentially toxic epoxides. Also determines steady-state levels of physiological mediators. Has low phosphatase activity
MCAM	P43121	-6	Plays a role in cell adhesion, and in cohesion of the endothelial monolayer at intercellular junctions in vascular tissue. Its expression may allow melanoma cells to interact with cellular elements of the vascular system, thereby enhancing hematogeneous tumor spread. Could be an adhesion molecule active in neural crest cells during embryonic development. Acts as surface receptor that triggers tyrosine phosphorylation of FYN and PTK2, and a transient increase in the intracellular calcium concentration
SORBS3	O60504	-6	Vinexin alpha isoform promotes up-regulation of actin stress fiber formation. Vinexin beta isoform plays a role in cell spreading and enhances the activation of JNK/SAPK in response to EGF stimulation by using its third SH3 domain
STX12	B1AJQ6	-6	SNARE that acts to regulate protein transport between late endosomes and the trans-Golgi network (By similarity)
NEGR1	Q8N440	-6	May be involved in cell-adhesion. May function as a trans-neural growth-promoting factor in regenerative axon sprouting in the mammalian brain (By similarity)
PODN	E7EPG6	-6	Negatively regulates cell proliferation and cell migration.
FLOT2	E7EMK1	-5	May act as a scaffolding protein within caveolar membranes, functionally participating in formation of caveolae or caveolae-like vesicles. May be involved in epidermal cell adhesion and epidermal structure and function
VAPB	E5RK64	18	May play a role in vesicle trafficking
RPN2	Q5JYR4	20	Essential subunit of N-oligosaccharyl transferase enzyme which catalyzes the transfer of a high mannose oligosaccharide from a lipid-linked oligosaccharide donor to an asparagine residue within an Asn-X-Ser/Thr consensus motif in nascent polypeptide chains
COL14A1	Q05707	80	Plays an adhesive role by integrating collagen bundles. It is probably associated with the surface of interstitial collagen fibrils via COL1. The COL2 domain may then serve as a rigid arm which sticks out from the fibril and protrudes the large N-terminal globular domain into the extracellular space, where it might interact with other matrix molecules or cell surface receptors (By similarity)
ECM (part of cell adhesion)			
FLNA	P21333	-411	Promotes orthogonal branching of actin filaments and links actin filaments to membrane glycoproteins. Anchors various transmembrane proteins to the actin cytoskeleton and serves as a scaffold for a wide range of cytoplasmic signaling proteins. Interaction with FLNA may allow neuroblast migration from the ventricular zone into the cortical plate. Tethers cell surface- localized furin, modulates its rate of internalization and directs its intracellular trafficking (By similarity)
COL6A3	E9PCV6	-409	Collagen VI acts as a cell-binding protein

COL12A1	Q99715	-170	Type XII collagen interacts with type I collagen- containing fibrils, the COL1 domain could be associated with the surface of the fibrils, and the COL2 and NC3 domains may be localized in the perifibrillar matrix (By similarity)
COL6A1	P12109	-128	Collagen VI acts as a cell-binding protein
COL1A2	P08123	-109	Type I collagen is a member of group I collagen (fibrillar forming collagen)
HSPG2	P98160	-95	This protein is an integral component of basement membranes. It is responsible for the fixed negative electrostatic charge and is involved in the charge-selective ultrafiltration properties. It serves as an attachment substrate for cells
COL1A1	P02452	-91	Type I collagen is a member of group I collagen (fibrillar forming collagen)
FN1	F8W7G7	-65	Fibronectins bind cell surfaces and various compounds including collagen, fibrin, heparin, DNA, and actin. Fibronectins are involved in cell adhesion, cell motility, opsonization, wound healing, and maintenance of cell shape
TNXB	B0UYX3	-42	Appears to mediate interactions between cells and the extracellular matrix. Substrate-adhesion molecule that appears to inhibit cell migration. Accelerates collagen fibril formation. May play a role in supporting the growth of epithelial tumors.
COL18A1	F8WDA7	-25	COLA18A probably plays a major role in determining the retinal structure as well as in the closure of the neural tube
TLN2	Q9Y4G6	-24	As a major component of focal adhesion plaques that links integrin to the actin cytoskeleton, may play an important role in cell adhesion. Recruits PIP5K1C to focal adhesion plaques and strongly activates its kinase activity (By similarity)
ILK	B7Z418	-19	Receptor-proximal protein kinase regulating integrin- mediated signal transduction. May act as a mediator of inside-out integrin signaling. Focal adhesion protein part of the complex ILK-PINCH. This complex is considered to be one of the convergence points of integrin- and growth factor-signaling pathway. Could be implicated in mediating cell architecture, adhesion to integrin substrates and anchorage-dependent growth in epithelial cells. Phosphorylates beta-1 and beta-3 integrin subunit on serine and threonine residues, but also AKT1 and GSK3B
ITGB1	P05556	-12	Integrins alpha-1/beta-1, alpha-2/beta-1, alpha-10/beta- 1 and alpha-11/beta-1 are receptors for collagen. Integrins alpha- 1/beta-1 and alpha-2/beta-2 recognize the proline-hydroxylated sequence G-F-P-G-E-R in collagen. Integrins alpha-2/beta-1, alpha- 3/beta-1, alpha-4/beta-1, alpha-5/beta-1, alpha-8/beta-1, alpha- 10/beta-1, alpha-11/beta-1 and alpha-V/beta-1 are receptors for fibronectin. Alpha-4/beta-1 recognizes one or more domains within the alternatively spliced CS-1 and CS-5 regions o [...]
COL15A1	P39059	-11	Structural protein that stabilizes microvessels and muscle cells, both in heart and in skeletal muscle (By similarity)
PARVA	Q9NVD7	-11	Probably plays a role in the regulation of cell adhesion and cytoskeleton organization
RHOA	P61586	-11	Regulates a signal transduction pathway linking plasma membrane receptors to the assembly of focal adhesions and actin stress fibers. Serves as a target for the yopT cysteine peptidase from Yersinia pestis, vector of the plague, and Yersinia pseudotuberculosis, which causes gastrointestinal disorders. May be an activator of PLCE1. Activated by ARHGEF2, which promotes the exchange of GDP for GTP
CAV1	Q03135	-10	May act as a scaffolding protein within caveolar membranes. Interacts directly with G-protein alpha subunits and can functionally regulate their activity (By similarity)
MAPK1	A8CZ64	-10	Involved in both the initiation and regulation of meiosis, mitosis, and postmitotic functions in differentiated cells by phosphorylating a number of transcription factors such as ELK1. Phosphorylates EIF4EBP1
LAMA4	Q16363	-10	Binding to cells via a high affinity receptor, laminin is thought to mediate the attachment, migration and organization of cells into tissues during embryonic development by interacting with other extracellular matrix components
CDC42	P60953	-9	Plasma membrane-associated small GTPase which cycles between an active GTP-bound and an inactive GDP-bound state. In active state binds to a variety of effector proteins to regulate cellular responses. Involved in epithelial cell polarization processes. Causes the formation of thin, actin-rich surface projections called filopodia
ITGA5	P08648	-7	Integrin alpha-5/beta-1 is a receptor for fibronectin and fibrinogen. It recognizes the sequence R-G-D in its ligands. In case of HIV-1 infection, the interaction with extracellular viral Tat protein seems to enhance angiogenesis in Kaposi's sarcoma lesions

ITGAV	E7EWZ6	-7	The alpha-V integrins are receptors for vitronectin, cytotactin, fibronectin, fibrinogen, laminin, matrix metalloproteinase-2, osteopontin, osteomodulin, prothrombin, thrombospondin and vWF. They recognize the sequence R-G-D in a wide array of ligands. In case of HIV-1 infection, the interaction with extracellular viral Tat protein seems to enhance angiogenesis in Kaposi's sarcoma lesions
COL5A2	P05997	-7	Type V collagen is a member of group I collagen (fibrillar forming collagen). It is a minor connective tissue component of nearly ubiquitous distribution. Type V collagen binds to DNA, heparan sulfate, thrombospondin, heparin, and insulin. Type V collagen is a key determinant in the assembly of tissue- specific matrices (By similarity)
THBS3	P49746	10	Adhesive glycoprotein that mediates cell-to-cell and cell-to-matrix interactions. Can bind to fibrinogen, fibronectin, laminin and type V collagen

Table S 3 Gene name, accession number, fold change and function of complement activation specific network in Figure 50.

Complement activation

Gene name	acc	Fold	function
C3	P01024	-150,5386999	C3 plays a central role in the activation of the complement system. Its processing by C3 convertase is the central reaction in both classical and alternative complement pathways. After activation C3b can bind covalently, via its reactive thioester, to cell surface carbohydrates or immune aggregates
C4A	A6H8M8	-40,23928869	C4 plays a central role in the activation of the classical pathway of the complement system. It is processed by activated C1 which removes from the alpha chain the C4a anaphylatoxin.
C5	P01031	-15,06295156	Activation of C5 by a C5 convertase initiates the spontaneous assembly of the late complement components, C5-C9, into the membrane attack complex. C5b has a transient binding site for C6. The C5b-C6 complex is the foundation upon which the lytic complex is assembled
C6	P13671	-6,482959509	Constituent of the membrane attack complex (MAC) that plays a key role in the innate and adaptive immune response by forming pores in the plasma membrane of target cells
C7	P10643	-13,11090875	Constituent of the membrane attack complex (MAC) that plays a key role in the innate and adaptive immune response by forming pores in the plasma membrane of target cells. C7 serves as a membrane anchor
C8B	F5GY80	-7,311434984	Constituent of the membrane attack complex (MAC) that plays a key role in the innate and adaptive immune response by forming pores in the plasma membrane of target cells
C8G	P07360	-8,20296526	C8 is a constituent of the membrane attack complex. C8 binds to the C5B-7 complex, forming the C5B-8 complex. C5-B8 binds C9 and acts as a catalyst in the polymerization of C9. The gamma subunit seems to be able to bind retinol
C9	P02748	-34,61516929	Constituent of the membrane attack complex (MAC) that plays a key role in the innate and adaptive immune response by forming pores in the plasma membrane of target cells. C9 is the pore-forming subunit of the MAC
CFH	P08603	-27,86143541	Factor H functions as a cofactor in the inactivation of C3b by factor I and also increases the rate of dissociation of the C3bBb complex (C3 convertase) and the (C3b)NBB complex (C5 convertase) in the alternative complement pathway
SERPING1	B4E1H2	-12,62042332	Activation of the C1 complex is under control of the C1- inhibitor. It forms a proteolytically inactive stoichiometric complex with the C1r or C1s proteases. May play a potentially crucial role in regulating important physiological pathways including complement activation, blood coagulation, fibrinolysis and the generation of kinins. Very efficient inhibitor of FXIIa. Inhibits chymotrypsin and kallikrein

Table S 4 Ovarian cancer Ids specific to ovarian cancer associated proteins.

Gene name	Score	Description
PTK2	6	PTK2 protein tyrosine kinase 2; Non-receptor protein-tyrosine kinase implicated in signaling pathways involved in cell motility, proliferation and apoptosis. Activated by tyrosine-phosphorylation in response to either integrin clustering induced by cell adhesion or antibody cross-linking, or via G-protein coupled receptor (GPCR) occupancy by ligands such as bombesin or lysophosphatidic acid, or via LDL receptor occupancy. Plays a potential role in oncogenic transformations resulting in increased kinase activity
NCAM1	6	neural cell adhesion molecule 1; This protein is a cell adhesion molecule involved in neuron-neuron adhesion, neurite fasciculation, outgrowth of neurites, etc
ERBB2	6	v-erb-b2 erythroblastic leukemia viral oncogene homolog 2, neuro/glioblastoma derived oncogene homolog (avian); Essential component of a neuregulin-receptor complex, although neuregulins do not interact with it alone. GP30 is a potential ligand for this receptor. Not activated by EGF, TGF- alpha and amphiregulin
BSG	6	basigin (Ok blood group); Plays pivotal roles in spermatogenesis, embryo implantation, neural network formation and tumor progression. Stimulates adjacent fibroblasts to produce matrix metalloproteinases (MMPS). May target monocarboxylate transporters SLC16A1, SLC16A3 and SLC16A8 to plasma membranes of retinal pigment epithelium and neural retina. Seems to be a receptor for oligomannosidic glycans. In vitro, promotes outgrowth of astrocytic processes (By similarity)
DNMT3A	7	DNA (cytosine-5-)-methyltransferase 3 alpha; Required for genome wide de novo methylation and is essential for the establishment of DNA methylation patterns during development. DNA methylation is coordinated with methylation of histones. It modifies DNA in a non-processive manner and also methylates non-CpG sites. May preferentially methylate DNA linker between 2 nucleosomal cores and is inhibited by histone H1. Plays a role in paternal and maternal imprinting. Required for methylation of most imprinted loci in germ cells. Acts as a transcriptional corepressor for ZNF238. Can actively ..." "
TTR	7	transthyretin; Thyroid hormone-binding protein. Probably transports thyroxine from the bloodstream to the brain
MSH6	8	mutS homolog 6 (E. coli); Component of the post-replicative DNA mismatch repair system (MMR). Heterodimerizes with MSH2 to form MutS alpha, which binds to DNA mismatches thereby initiating DNA repair. When bound, MutS alpha bends the DNA helix and shields approximately 20 base pairs, and recognizes single base mismatches and dinucleotide insertion-deletion loops (IDL) in the DNA. After mismatch binding, forms a ternary complex with the MutL alpha heterodimer, which is thought to be responsible for directing the downstream MMR events, including strand discrimination, excision, and resyn ..." "

CLDN3	8	claudin 3; Plays a major role in tight junction-specific obliteration of the intercellular space, through calcium- independent cell-adhesion activity (By similarity)
TPD52	8	tumor protein D52
SMARCA4	8	SWI/SNF related, matrix associated, actin dependent regulator of chromatin, subfamily a, member 4; Transcriptional coactivator cooperating with nuclear hormone receptors to potentiate transcriptional activation. Also involved in vitamin D-coupled transcription regulation via its association with the WINAC complex, a chromatin-remodeling complex recruited by vitamin D receptor (VDR), which is required for the ligand-bound VDR-mediated transrepression of the CYP27B1 gene
PTGS1	8	prostaglandin-endoperoxide synthase 1 (prostaglandin G/H synthase and cyclooxygenase); May play an important role in regulating or promoting cell proliferation in some normal and neoplastically transformed cells
XRCC1	8	X-ray repair complementing defective repair in Chinese hamster cells 1; Corrects defective DNA strand-break repair and sister chromatid exchange following treatment with ionizing radiation and alkylating agents
ASS1	9	argininosuccinate synthetase 1
KRAS	9	v-Ki-ras2 Kirsten rat sarcoma viral oncogene homolog; Ras proteins bind GDP/GTP and possess intrinsic GTPase activity
NRAS	9	neuroblastoma RAS viral (v-ras) oncogene homolog; Ras proteins bind GDP/GTP and possess intrinsic GTPase activity
CDH1	10	cadherin 1, type 1, E-cadherin (epithelial); Cadherins are calcium-dependent cell adhesion proteins. They preferentially interact with themselves in a homophilic manner in connecting cells; cadherins may thus contribute to the sorting of heterogeneous cell types. CDH1 is involved in mechanisms regulating cell-cell adhesions, mobility and proliferation of epithelial cells. Has a potent invasive suppressor role. It is a ligand for integrin alpha-E/beta-7

FXR1	10	fragile X mental retardation, autosomal homolog 1; RNA-binding protein required for embryonic and postnatal development of muscle tissue. May regulate intracellular transport and local translation of certain mRNAs (By similarity)
MAPK14	12	mitogen-activated protein kinase 14; Responds to activation by environmental stress, pro- inflammatory cytokines and lipopolysaccharide (LPS) by phosphorylating a number of transcription factors, such as ELK1 and ATF2 and several downstream kinases, such as MAPKAPK2 and MAPKAPK5. Plays a critical role in the production of some cytokines, for example IL-6. May play a role in stabilization of EPO mRNA during hypoxic stress. Isoform Mxi2 activation is stimulated by mitogens and oxidative stress and only poorly phosphorylates ELK1 and ATF2. Isoform Exip may play a role in the early onset o ..." "
MSH2	13	mutS homolog 2, colon cancer, nonpolyposis type 1 (E. coli); Component of the post-replicative DNA mismatch repair system (MMR). Forms two different heterodimers: MutS alpha (MSH2- MSH6 heterodimer) and MutS beta (MSH2-MSH3 heterodimer) which binds to DNA mismatches thereby initiating DNA repair. When bound, heterodimers bend the DNA helix and shields approximately 20 base pairs. MutS alpha recognizes single base mismatches and dinucleotide insertion-deletion loops (IDL) in the DNA. MutS beta recognizes larger insertion-deletion loops up to 13 nucleotides long. After mismatch binding, ..." "
MTA1	15	metastasis associated 1; May be involved in the regulation of gene expression by covalent modification of histone proteins. Isoform Long is a corepressor of estrogen receptor (ER). Isoform Short binds to ER and sequesters it in the cytoplasm and enhances non-genomic responses of ER
MLLT4	16	myeloid/lymphoid or mixed-lineage leukemia (trithorax homolog, Drosophila); translocated to, 4; Belongs to an adhesion system, probably together with the E-cadherin-catenin system, which plays a role in the organization of homotypic, interneuronal and heterotypic cell-cell adherens junctions (AJs). Nectin- and actin-filament-binding protein that connects nectin to the actin cytoskeleton
ABCF2	16	ATP-binding cassette, sub-family F (GCN20), member 2
ENO2	17	enolase 2 (gamma, neuronal); Has neurotrophic and neuroprotective properties on a broad spectrum of central nervous system (système nerveux central) neurons. Binds, in a calcium-dependent manner, to cultured neocortical neurons and promotes cell survival (By similarity)
DDB1	18	damage-specific DNA binding protein 1, 127kDa; Required for DNA repair. Binds to DDB2 to form the UV- damaged DNA-binding protein complex (the UV-DDB complex). The UV- DDB complex may recognize UV-induced DNA damage and recruit proteins of the nucleotide excision repair pathway (the NER pathway) to initiate DNA repair. The UV-DDB complex preferentially binds to cyclobutane pyrimidine dimers (CPD), 6-4 photoproducts (6-4 PP), apurinic sites and short mismatches. Also appears to function as a component of numerous distinct DCX (DDB1-CUL4-X-box) E3 ubiquitin-protein ligase complexes which ..." "
PSIP1	19	PC4 and SFRS1 interacting protein 1; Transcriptional coactivator involved in neuroepithelial stem cell differentiation and neurogenesis. Involved in particular in lens epithelial cell gene regulation and stress responses. May play an important role in lens epithelial to fiber cell terminal differentiation. May play a protective role during stress-induced apoptosis. Isoform 2 is a more general and stronger transcriptional coactivator. Isoform 2 may also act as an adapter to coordinate pre-mRNA splicing. Cellular cofactor for lentiviral integration

TES	20	testis derived transcript (3 LIM domains); Scaffold protein that may play a role in cell adhesion, cell spreading and in the reorganization of the actin cytoskeleton. May act as a tumor suppressor. Inhibits tumor cell growth
HMGB1	29	high-mobility group box 1; Binds preferentially single-stranded DNA and unwinds double stranded DNA (By similarity)
FN1	32	fibronectin 1; Fibronectins bind cell surfaces and various compounds including collagen, fibrin, heparin, DNA, and actin. Fibronectins are involved in cell adhesion, cell motility, opsonization, wound healing, and maintenance of cell shape
IDH2	37	isocitrate dehydrogenase 2 (NADP+), mitochondrial; Plays a role in intermediary metabolism and energy production. It may tightly associate or interact with the pyruvate dehydrogenase complex
IGF2BP3	56	insulin-like growth factor 2 mRNA binding protein 3; RNA-binding protein that act as a regulator of mRNA translation and stability. Binds to the 5'-UTR of the insulin-like growth factor 2 (IGF2) mRNAs. Binds to sequences in the 3'-UTR of CD44 mRNA
ACTC1	195	actin, alpha, cardiac muscle 1; Actins are highly conserved proteins that are involved in various types of cell motility and are ubiquitously expressed in all eukaryotic cells (By similarity)

Table S 5 Fallopian tube Ids specific to Ovarain cancer related proteins.

Gene Name	Score	Function
CTNNA1	22.68	catenin (cadherin-associated protein), alpha 1, 102kDa; Associates with the cytoplasmic domain of a variety of cadherins. The association of catenins to cadherins produces a complex which is linked to the actin filament network, and which seems to be of primary importance for cadherins cell-adhesion properties. May play a crucial role in cell differentiation
KRT14	52.35	keratin 14; The nonhelical tail domain is involved in promoting KRT5-KRT14 filaments to self-organize into large bundles and enhances the mechanical properties involved in resilience of keratin intermediate filaments in vitro
ELN	8.21	elastin; Major structural protein of tissues such as aorta and nuchal ligament, which must expand rapidly and recover completely. Molecular determinant of the late arterial morphogenesis, stabilizing arterial structure by regulating proliferation and organization of vascular smooth muscle (By similarity)
VCAN	15.23	versican; May play a role in intercellular signaling and in connecting cells with the extracellular matrix. May take part in the regulation of cell motility, growth and differentiation. Binds hyaluronic acid
HMGB1	5.81	high-mobility group box 1; Binds preferentially single-stranded DNA and unwinds double stranded DNA (By similarity)
DDB1	10.6	damage-specific DNA binding protein 1, 127kDa; Required for DNA repair. Binds to DDB2 to form the UV- damaged DNA-binding protein complex (the UV-DDB complex). The UV- DDB complex may recognize UV-induced DNA damage and recruit proteins of the nucleotide excision repair pathway (the NER pathway) to initiate DNA repair. The UV-DDB complex preferentially binds to cyclobutane pyrimidine dimers (CPD), 6-4 photoproducts (6-4 PP), apurinic sites and short mismatches. Also appears to function as a component of numerous distinct DCX (DDB1-CUL4-X-box) E3 ubiquitin-protein ligase complexes which "..."
TPD52	13.35	tumor protein D52

UCHL1	24.46	ubiquitin carboxyl-terminal esterase L1 (ubiquitin thiolesterase); Ubiquitin-protein hydrolase involved both in the processing of ubiquitin precursors and of ubiquitinated proteins. This enzyme is a thiol protease that recognizes and hydrolyzes a peptide bond at the C-terminal glycine of ubiquitin. Also binds to free monoubiquitin and may prevent its degradation in lysosomes. The homodimer may have ATP-independent ubiquitin ligase activity
PAK1	8.75	p21 protein (Cdc42/Rac)-activated kinase 1; The activated kinase acts on a variety of targets. Likely to be the GTPase effector that links the Rho-related GTPases to the JNK MAP kinase pathway. Activated by CDC42 and RAC1. Involved in dissolution of stress fibers and reorganization of focal complexes. Involved in regulation of microtubule biogenesis through phosphorylation of TBCB. Activity is inhibited in cells undergoing apoptosis, potentially due to binding of CDC2L1 and CDC2L2
MVP	5.42	major vault protein; Required for normal vault structure. Vaults are multi- subunit structures that may act as scaffolds for proteins involved in signal transduction. Vaults may also play a role in nucleo- cytoplasmic transport. Down-regulates INFG-mediated STAT1 signaling and subsequent activation of JAK. Down-regulates SRC activity and signaling through MAP kinases
AMBP	11.74	alpha-1-microglobulin/bikunin precursor; Inter-alpha-trypsin inhibitor inhibits trypsin, plasmin, and lysosomal granulocytic elastase. Inhibits calcium oxalate crystallization
APOE	8.3	apolipoprotein E; Mediates the binding, internalization, and catabolism of lipoprotein particles. It can serve as a ligand for the LDL (apo B/E) receptor and for the specific apo-E receptor (chylomicron remnant) of hepatic tissues
HINT1	8.04	histidine triad nucleotide binding protein 1; Hydrolyzes adenosine 5'-monophosphoramidate substrates such as AMP-morpholidate, AMP-N-alanine methyl ester, AMP-alpha- acetyl lysine methyl ester and AMP-NH2 (By similarity)
POSTN	40.96	periostin, osteoblast specific factor; Binds to heparin. Induces cell attachment and spreading and plays a role in cell adhesion. May play a role in extracellular matrix mineralization
FN1	22.37	fibronectin 1; Fibronectins bind cell surfaces and various compounds including collagen, fibrin, heparin, DNA, and actin. Fibronectins are involved in cell adhesion, cell motility, opsonization, wound healing, and maintenance of cell shape
PGM1	6.57	phosphoglucomutase 1; This enzyme participates in both the breakdown and synthesis of glucose

CDC42	6.68	cell division cycle 42 (GTP binding protein, 25kDa); Plasma membrane-associated small GTPase which cycles between an active GTP-bound and an inactive GDP-bound state. In active state binds to a variety of effector proteins to regulate cellular responses. Involved in epithelial cell polarization processes. Causes the formation of thin, actin-rich surface projections called filopodia
ENO2	13.01	enolase 2 (gamma, neuronal); Has neurotrophic and neuroprotective properties on a broad spectrum of central nervous system (système nerveux central) neurons. Binds, in a calcium-dependent manner, to cultured neocortical neurons and promotes cell survival (By similarity)
ILK	10.73	integrin-linked kinase; Receptor-proximal protein kinase regulating integrin- mediated signal transduction. May act as a mediator of inside-out integrin signaling. Focal adhesion protein part of the complex ILK-PINCH. This complex is considered to be one of the convergence points of integrin- and growth factor-signaling pathway. Could be implicated in mediating cell architecture, adhesion to integrin substrates and anchorage-dependent growth in epithelial cells. Phosphorylates beta-1 and beta-3 integrin subunit on serine and threonine residues, but also AKT1 and GSK3B
HMGA1	11.68	high mobility group AT-hook 1; HMG-I/Y bind preferentially to the minor groove of A+T rich regions in double stranded DNA. It is suggested that these proteins could function in nucleosome phasing and in the 3'-end processing of mRNA transcripts. They are also involved in the transcription regulation of genes containing, or in close proximity to A+T-rich regions
SOD2	5.77	superoxide dismutase 2, mitochondrial; Destroys radicals which are normally produced within the cells and which are toxic to biological systems (By similarity)
JUP	49.47	junction plakoglobin; Common junctional plaque protein. The membrane- associated plaques are architectural elements in an important strategic position to influence the arrangement and function of both the cytoskeleton and the cells within the tissue. The presence of plakoglobin in both the desmosomes and in the intermediate junctions suggests that it plays a central role in the structure and function of submembranous plaques. Acts as a substrate for VE-PTP and is required by it to stimulate VE- cadherin function in endothelial cells (By similarity)

CHAPITRE 6 - TARGETED MASS SPECTROMETRY IMAGING: SPECIFIC TARGETING MASS SPECTROMETRY IMAGING TECHNOLOGIES FROM HISTORY TO PERSPECTIVE

Auteurs de l'article : Hugo Gagnon, Julien Franck, Maxence Wisztorski, Robert Day, Isabelle Fournier, Michel Salzet

Statut de l'article : publié dans *Progress in Histochemistry and Cytochemistry*, 1–42. (2012) doi:10.1016/j.proghi.2012.08.002.

Avant-propos : Cet article est une revue approfondie de la littérature avec description méthodologique. J'ai participé à l'écriture, révision et correction du texte.

Résumé : Depuis son introduction au cours de la dernière décennie, l'imagerie par spectrométrie de masse (MSI) MALDI est maintenant une technique de routine en biologie. Néanmoins, un chaînon manquant existe dans l'approche MALDI-MSI. Les lipides, les peptides/protéines, les métabolites et les drogues peuvent être facilement cartographiés par cette méthode d'imagerie, mais la cartographie du transcriptome; comprenant les microARN, les siRNA et d'autres composants n'a pas encore été réalise en MALDI-MSI. Étant donné que l'étude du transcriptome est aujourd'hui un champ de recherche clinique d'importance et il doit être exploré par MALDI-MSI. Afin d'étudier le transcriptome, une nouvelle technique d'imagerie a été développée, appelée l'imagerie par spectrométrie de masse Tag-Mass. Le but de cette revue est de discuter de cette technique, de son histoire et de sa place dans l'avenir de l'imagerie par spectrométrie de masse.

TARGETED MASS spectrometry Imaging: Specific Targeting Mass Spectrometry imaging technologies from history to perspective

Hugo Gagnon[1,2], Julien Franck[1], Maxence Wisztorski[1], Robert Day[2], Isabelle Fournier[1*], Michel Salzet[1*]

Running headline: TARGETED MASS spectrometry Imaging

Corresponding authors :

Michel Salzet, Laboratoire de Spectrométrie de Masse Biologique Fondamentale et Appliquée, EA 4550, Université de Lille 1, Cité Scientifique, 59650 Villeneuve D'Ascq, email :Michel.salzet@univ-lille1.fr, Tel : +33 3 2043 41 94 ; Fax : +33 3 2043 4057

Isabelle Fournier, Laboratoire de Spectrométrie de Masse Biologique Fondamentale et Appliquée, EA 4550, Université de Lille 1, Cité Scientifique, 59650 Villeneuve D'Ascq, email :isabelle.fournier@univ-lille1.fr, Tel : +33 3 2043 41 94 ; Fax : +33 3 2043 4057

Hugo Gagnon[1,2] M.Sc. candidate for Ph.D., Julien Franck[1] Ph.D., Maxence Wisztorski[1] Ph.D. Robert Day[2] Ph.D., Isabelle Fournier[1*] Ph.D., Michel Salzet[1*] Ph.D.

1 : Université Lille Nord de France, Laboratoire de Spectrométrie de Masse Biologique Fondamentale et Appliquée, EA 4550, Université de Lille 1, Cité Scientifique, 59650 Villeneuve D'Ascq

2 : Institut de pharmacologie de Sherbrooke, Département de chirurgie/service d'urologie, Faculté de medicine et des sciences de la santé, Université de Sherbrooke, Sherbrooke, Québec, J1H 5N4, Canada

Acknowledgements

Supported by grants from Agence Nationale de la Recherche (IF), Région Nord-Pas-de Calais (to IF, MS), Université de Lille 1, and the Ministère de la recherche et de l'enseignement supérieur (to IF and MS). Also supported by grants from Canadian Institutes of Health Research (CIHR to RD), the Ministère du Développement Économique de l'Innovation et de l'Exportation (MDEIE to RD) and the Fond de recherche du Québec-Santé (FRQ-S to R.D). R.D. is a member of the Centre de Recherche Clinique Etienne-Le Bel (Sherbrooke, Qc, Canada). H.G. holds a BDI from CNRS and received Frontenac mobility grant for joint thesis Franco-Quebec from FQRNT and France consulate.

Abstract

Since its introduction during the last decade, MALDI mass spectrometry imaging (MSI) is now a routine technique in biology. Nevertheless, a missing link exists in MALDI MSI. Lipids, peptides/proteins, metabolites and drugs can easily be mapped using MALDI-MSI, but this technique has not yet been used to map the transcriptome, which includes microRNA, siRNA and other components. This latter field of research is now one of the major fields in clinical research and needs to be explored using MALDI-MSI. To investigate the transcriptome, a novel imaging technique has been developed called Tag-Mass imaging mass spectrometry. The aim of this review is to discuss this technique from its history to its place in the future of mass spectrometric imaging.

Abbreviation list

1,1,1,3,3,3-hexafluoro-2-propanol or hexafluoroisopropanol (HFIP), 1,5-diaminonaphthalene (1,5-DAN), 2,2,2-trifluoroethanol (TFE), 2,4-dinitrophenylhydrazine (2,4-DNPH), 2,5-dihydroxybenzoic acid (2,5-DHB), 2,6-dihydroxyacetophenone DHAP, or 6-aza-2-thiothymine (ATT), a-cyano-4-hydroxycinnamic acid (CHCA), antigen retrieval (AR), atomic mass unit (amu), citric acid-antigen retrieval procedure (CAAR), desorption electrospray ionization (DESI), dried blood spots (DBS), electron capture dissociation (ECD), electro spay ionization (ESI), electron-transfer dissociation (ETD), enzyme-linked immunosorbent assays (ELISA), formalin-fixed paraffin-embedded (FFPE), fourier transform ion cyclotron resonance (FT-ICR), giga octet (Go), heptafluorobutyric acid (HFBA), immunohistochemistry (IHC), in situ hybridization (ISH), in source decay (ISD), ion mobility coupled to orthogonal (IM-o), ion trap (IT), infrared (IR), laser ablation inductively coupled plasma (LA-ICP), laser capture microdissection (LCM), laser desorption/ionization (LDI), laser microprobe mass analyzer (LMMA), linear trap quadrupole (LTQ), liquid chromatography (LC), liquid extraction surface analysis (LESA), mass spectrometry (MS), mass spectrometric imaging (MSI), matrix-assisted laser desorption/ionization (MALDI), N-hydroxysuccinimide (NHS), N-succinimidyloxycarbonylmethyl-tris (2,4,6-trimethoxyphenyl) phosphonium bromide (TMPP), number of pixels (N), paraformaldehyde (PFA), peptide mass fingerprint (PMF), photocleavable linkers (PC-linkers), phosphatidylserine (PS), principal component analysis (PCA), quadrupole (Q), regions of interest (ROI), resolution (R), scanning microprobe MALDI (SMALDI), sinapinic acid (SA,) sufatide (ST), secondary-ion mass spectrometry (SIMS), targeted mass spectrometric imaging (Tag-Mass MSI), time of flight (TOF), time-to-digital converter (TDC), tissue microarrays (TMAs).

1.1. Introduction

Since its introduction in the late 1980s, MALDI has become a tool of choice for the analysis of biomolecules, especially for large compounds. With a growing need for molecular information about peptides and proteins, matrix-assisted laser desorption/ionization (termed MALDI) was quickly adopted for the direct analysis of tissues because of the convenience of this ion source for the analysis of crude samples. This highly sensitive method has allowed for the analysis of a wide range of molecules in their tissue-specific context and has also been used for the analysis of a single cell. Direct analysis offers the advantages of studying cells in their original context and avoiding lengthy purification and separation steps. To achieve these benefits, MALDI has taken advantage of knowledge of mass spectrometry techniques to improve direct tissue analysis, thus leading to the development of MALDI-Mass Spectrometric Imaging (MSI). As is the case with other desorption techniques, MALDI was developed with the help of physics. Whereas other fields that use mass spectrometry (e.g., chemistry) generally study solutions for which morphological aspects are not important, surface imaging is very common in physics. Indeed, a number of different imaging techniques have emerged, but thanks to the groups of B. Spengler (1994) in Germany and R.M. Caprioli (1997) in the United States, the MALDI-MSI methodology was developed in the late 1990s. These groups reported the reconstruction of ion density curves and the construction of molecular images of biomolecules in tissue samples. The development of MALDI-MSI was innovative for fundamental biology, leading to new clinical applications. Nevertheless, a missing link exists in MALDI-MSI. Lipids, peptides/proteins, metabolites, drugs can easily be mapped using MALDI-MSI; however, the transcriptome, which includes microRNA and other RNA-related molecules, has not yet been mapped in this way. Because the transcriptome is now a major area of clinical research, it would certainly benefit from the use of MALDI-MSI. To address this important topic, a novel imaging technique has been developed, namely targeted mass spectrometric imaging (Tag-Mass MSI). This review discusses topics ranging from the history to the future of mass spectrometric imaging.

1.2. From lenses to Immunocytochemistry

The oldest lens made of polished glass has been dated back to 700 BC. This lens was discovered at Ninive, the last Assyrian establishment in Kurdistan. Ancient Roman writings

have mentioned some enlarging tools such as balls full of water or an emerald sharpened like a concave lens. Since ancient times, human curiosity has encouraged us to observe the infinitely small. The first documented scientific usage of lenses appeared in the seventeenth century; before that time, all lenses were used to correct vision. The origin of the first microscope is difficult to ascertain because several types of microscopes were built during the same time period. However, Antonie van Leeuwenhoek and Robert Hooke have recorded observations of the highest quality. In 1625, Robert Hooke published drawings of plant cells, fungi and lice observations in the journal “Micrographia”. The magnification he used was approximately 160x. Using his microscope, Robert Hooke also successfully demonstrated the circulation of the nettle poison in his finger. At the same time, Francesco Stelluti published a book describing his observations using microscopes, and Marcello Malpighi was the first biologist to conduct research on the machinery and embryology of the liver using a microscope. Additionally, van Leeuwenhoek was the first to describe bacteria living in the mouth, which he named the "levende dierkens", or living small animals. In 1650, the magnification of the microscope was increased due to the use of biconvex lenses, but chromatic aberrations caused by light dispersion (e.g., coma) limited the usable field of view. In the eighteenth century, John Dollond corrected this problem by adding a negative eyeball composed of two plane-convex lenses. In 1870, a microscope with an approximately 160-mm-long tube and optics developed by Hartnack was in standard use in Europe. Thereafter, Carl Zeiss and Ernst Abbe were the first to propose the wave theory of microscopic imaging. Combining his own efforts with the work of his predecessors, Abbe developed a mathematical treatment of the lens concept. Concurrent with the development of novel types of glasses, the resolving power of microscopes was pushed to the limit of what was physically possible. In 1890, microscopic images became more refined due to the development of coating techniques, and the field of view increased. Since that time, the basic microscope structure has not changed. To achieve higher resolution, it was necessary to develop the electron microscope, which was introduced in 1930 and has a magnification of 800,000x. Major advancements have been made in the microscope optics, mechanics and, most critically, the lighting. Since the invention of the microscope, an average magnification of 200x to 1500x has been used, which means that most of the objects studied are 200 to 400 times smaller than the image observed.

Immediately prior to World War II, two technical advances in optics were introduced: the phase contrast (invented by Zernike) and the interference contrast. These advances allowed for the observation of almost transparent objects, such as living cells. The most recent microscope developments include the use of probes to detect an electric field using a tunnel effect, magnetic force or atomic force. The limits of magnification are now approximately 1 billion times, permitting the observation of the surface of objects on the atomic scale.

1.3. From Immunohistochemistry to MALDI Mass Spectrometry imaging

In addition to the microscope, immunohistochemical techniques permitting the localization of antigens in tissues, cells, organisms, bacteria, viruses, etc. were introduced. Immunohistochemistry was developed in 1930. In 1940, Coons and collaborators developed an antibody labeled with the fluorescent tracer fluorescein (Coons 1941). The development of novel fixation procedures (ethanol, methanol, acetone, picric acid and paraformaldehyde) (Gabe 1964; Gabe and Saint Girons 1967; Gabe 1969, 1972; Petit and Sahli 1975; Steinbach 1977; Hayashi et al. 2004; Demeure et al. 2007) were then introduced along with a technique for embedding tissues in paraffin and procedures to retrieve antigens during immunocytochemistry studies (Curran and Gregory 1980; Beckstead 1994; Ino 2004) Currently, multiplex immunocytochemistry using quantum dots (Brocke et al. 2003) and multiple antisera are being developed (Furuya et al. 2004). In summary, tissue imaging using a microscope allows us to localize several molecules of interest at a cellular or sub-cellular resolution. The current limit of this technology is the simultaneous detection of almost 50 different antigens. The major limitations of this technology are the tissue itself and the methods of tissue preservation. All developments made during the last seven decades regarding tissue preparation are now becoming a foundation for MALDI-MSI. Currently, we are interested in determining whether we can use this background knowledge to improve the technology and what contributions MALDI-MSI will make to this field of tissue imaging.

1.4. MALDI Mass Spectrometric Imaging (MSI)

MALDI has become a tool of choice for the analysis of biomolecules, especially large compounds. Because MALDI is easy to use with crude samples, it allows for the direct analysis of a wide range of molecules in the tissues. This property made MALDI-MSI an

ideal technique to meet the growing need for molecular information about biomolecules. Various reports of the analysis of peptides from different invertebrate cells or organelles have been published since 1994 (Jimenez et al. 1994), and many of these concern the study of peptide processing from protein precursors. Taking advantage of the great sensitivity of MALDI mass spectrometry, the direct analysis of single cells was also successful and allowed for the study of specific cell types, including neurons (Jimenez et al. 1994; Li et al. 1994a; Li et al. 1994b; Li et al. 1994c; Jimenez et al. 1997; Jimenez et al. 1998; Li et al. 1998; Li et al. 1999; Rubakhin et al. 1999; Li et al. 2000a; Li et al. 2000b; Rubakhin et al. 2000; Li et al. 2001; Rubakhin et al. 2003; Jimenez et al. 2004; Jimenez et al. 2006; Rubakhin et al. 2006). To improve the direct analysis method, it was necessary to take advantage of the knowledge of other mass spectrometry techniques, such as laser desorption/ionization (LDI) (Verbueken et al. 1985) or secondary-ion mass spectrometry (SIMS) (Castaing 1962), to achieve better MALDI-MSI results. As with other desorption techniques, MALDI was physics-based, wherein the imaging of sample surfaces is very common. MALDI-MSI was not fully introduced until the late 1990s when R.M. Caprioli and co-workers (Caprioli et al. 1997; Chaurand et al. 1999; Stoeckli et al. 1999) reported that the data acquired from biological samples can be processed to reconstruct ion density curves or molecular images of biomolecules in tissue samples.

1.4.1. MALDI imaging and the basis of protein molecular imaging

In certain ways, MALDI-MSI is a simple concept. In MALDI sources, ions are produced by laser irradiation of the sample, which, theoretically, is a homogeneous solid solution consisting of a large excess of matrix molecules and the analyte molecules. Our understanding of the processes that lead to ion formation in MALDI has increased since the introduction of this technique; however, we are still unable to fully describe the underlying mechanisms involved. Unfortunately, this incomplete understanding indicates that an important part of our knowledge is empirical; therefore, it is difficult to predict the properties of a good matrix. Currently, it is understood that short pulses of photon irradiation induce energy transfer to the matrix molecules (Karas and Kruger 2003; Knochenmuss and Zenobi 2003) to generate excited states. The relaxation of these high-energy states involves the dissipation of part of the energy to the analytes. Basic studies performed to examine the irradiated area of simple matrix crystals (a solution of a single

molecule in a water/solvent mixture) demonstrated that the laser crater formed by the removal of material does not exceed the area of the incident beam (Fournier et al. 2002; Fournier et al. 2003). Thus, most of the laser energy is transferred deep inside the sample, with little surrounding spread. The irradiation of the sample at the punctate coordinate will then produce ions that define the impact area between the laser and the sample surface. Controlling the focus of the laser can change the resolution of this area. This control is an important consideration for MALDI-MSI because it allows for the correlation of the laser irradiation coordinates with the corresponding position in the sample. Thus, laser irradiation at regular steps across the entire sample allows for the generation of coordinated spectra that can be used for molecular image reconstitution. Each collected spectrum represents the average of several laser shots to obtain a statistical representation of the analyzed area. Thus, MALDI-MSI is basically a point-to-point analysis.

MALDI-MSI is composed of four main steps (Figure 52).

1- Tissue sectioning and preparation

2- Matrix deposition

3- Data acquisition

4- Data processing/image generation

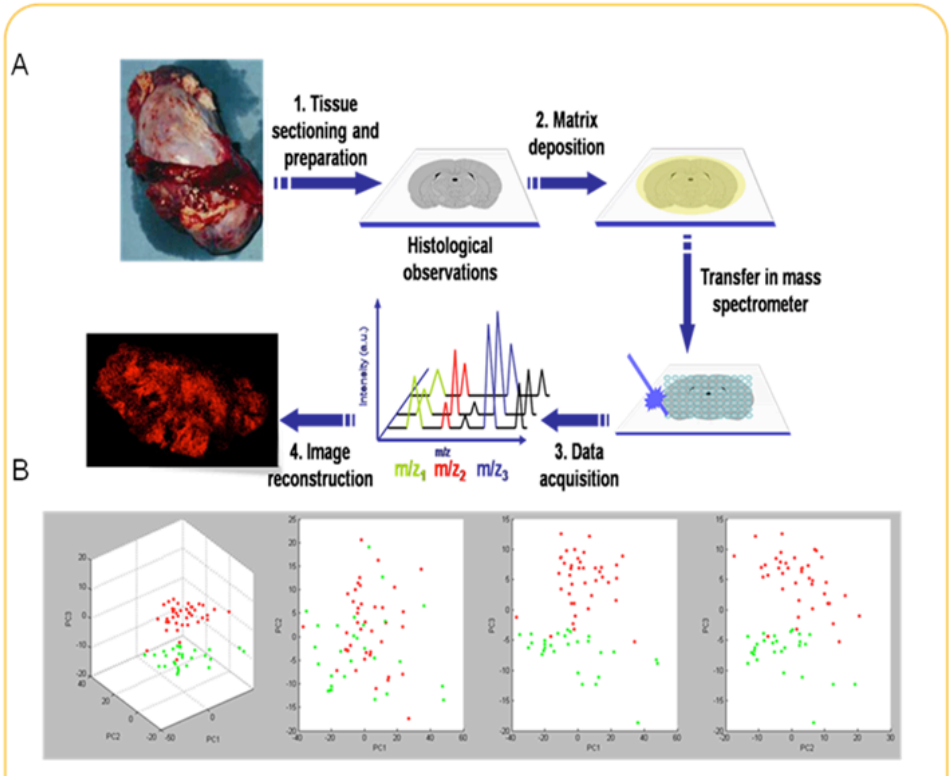

Figure 52 MALDI imaging workflow and data analysis.

A: The tissue preparation and analysis workflow for MALDI imaging. The resected organs or tissues were sliced with a microtome for FFPE tissues or with a cryostat for fresh frozen tissues. The sections were mounted on conductive slides, the matrix was applied dropwise onto the section, and the mass spectrometric analysis was performed over the area of the tissue. The positions and intensities of the ions are represented in a visual format called the "image". B: The corresponding PCA analysis of the tissue with normal and carcinomatous endometrium. The PC1/PC2, PC1/PC3, and PC2/PC3 analyses are shown, illustrating the best 2D-space separation of the ions.

The first step of MALDI-MSI involves tissue sectioning and preparation, which is performed using traditional procedures. The main concern is the preservation of tissue integrity while avoiding molecular composition changes, e.g., changes due to enzymatic activation. There is a subtle equilibrium that must be reached to preserve the molecular composition and molecular localization of the tissue from the time of dissection to the time of mounting on the experimental plate. As we will discuss later, the long-term storage of a tissue before analysis can be a problem. The second and third steps are based on MALDI-MS technology. The second step, which is crucial for analytical performance, consists of matrix deposition on the tissue section. It is known that the matrix is crucial for the quality of the mass spectra. The choice of an appropriate matrix and its proper preparation are key for a successful MALDI experiment. However, in the case of MALDI-MSI, it is important to ensure that matrix deposition does not induce any delocalization of the analytes across the sample. The minimum requirement is that delocalization must remain equal to or lower than the resolution of one laser shot. The third step is the automated acquisition of the data from the tissue, which depends on the mass analyzer and involves variable parameters that are set to achieve the best analytical capacity. The final step involves informatics tools that are designed to process the data, including algorithms to reconstruct images.

As with any technology, we must understand the limitations of MALDI-MSI. By drawing a simple parallel with photography, it is very easy to identify where developmental efforts should be directed. In photography, the expectation is to reflect an exact copy of a scene as observed by the human eye. The image must have enough definition to detect fine details and enough contrast to observe objects of different sizes, shapes, colors or brightness. Similarly, in MALDI-MSI, the pixel size and density in the image will define the acquisition of a highly resolved image. For MALDI-MSI, this limitation requires one to obtain the smallest irradiated area with the highest number of analysis spots while preserving analytical performance, i.e., a maximum of contiguous pixels should be used. For example, for a circular area, the distance between two spots should be minor relative to the diameter of the circle. Obtaining an exact molecular copy of whatever is being observed implies that we can analyze any class of molecule with the same capacities independently of its size, amount and localization within the system or origin. These are clearly challenges

for MALDI-MSI because this technique must be able to deal with all samples independently of their preparation and conservation process and to analyze a complete range of biomolecules, such as peptides, proteins, lipids, sugars and oligonucleotides at very low levels. Comparing one of the initially published images that was obtained using MALDI-MSI to a recent image directly addresses some of these concerns. Now, a decade after its introduction, MALDI-MSI has greatly improved its capacities and has overcome some of its challenges because of the constant efforts of several research groups involved in this field.

1.5. MALDI-MSI, a continuously evolving technology

1.5.1. Sample preparation: Tissue Conservation and Imaging Strategies

1.5.1.1. Frozen tissues

For molecular imaging technologies, the preparation and conservation of samples are crucial. Proper conservation ensures that molecules do not move or undergo degradation. Several well-established conservation methods can result in compatibility issues for MALDI-MSI, which are mainly analytical difficulties (Lemaire et al. 2006b). The samples can be preserved using three methods after dissection, including direct freezing (in isopentane for better structure integrity), freezing after the use of a fixative (e.g., formalin, Bouin, Bouin Hollande) and conservation after fixation followed by embedding in paraffin (Lemaire et al. 2007a) (Figure 53). The direct freezing approach results in the lowest number of analytical problems in the mass spectrometry analysis. However, frozen samples must be cut using a cryostat instrument and require storage in a freezer, preferably at -80°C. During long-term preservation at -80°C for more than 6 months, the lipids present in tissues move and mask the tissue sections. Specific washings, including washes with chloroform/methanol or acetone, are needed to remove these lipids (Lemaire et al. 2006b; Seeley et al. 2008).

1.5.1.2. Formalin-Fixed Paraffin-Embedded tissues

The most commonly used fixative for the long-term preservation of tissue sections is paraformaldehyde (PFA) or formalin (Figure 53). When PFA fixation is used prior to embedding the tissues in paraffin, the resulting samples are called formalin-fixed paraffin-

embedded (FFPE) tissues. The FFPE preparation not only increases sample stability over time but also results in better preservation of the fine structures of the tissue after tissue sectioning. The development of strategies for MALDI-MSI analyses also allows for retrospective studies of past clinical cases to be performed based on large collections of samples. Because FFPE samples can be stored for decades, many samples are available in hospital tissue banks, thus allowing for the creation of larger collections including rare pathologies or sub-pathologies (Lemaire et al. 2007a; Groseclose et al. 2008; Ronci et al. 2008; Stauber et al. 2008).

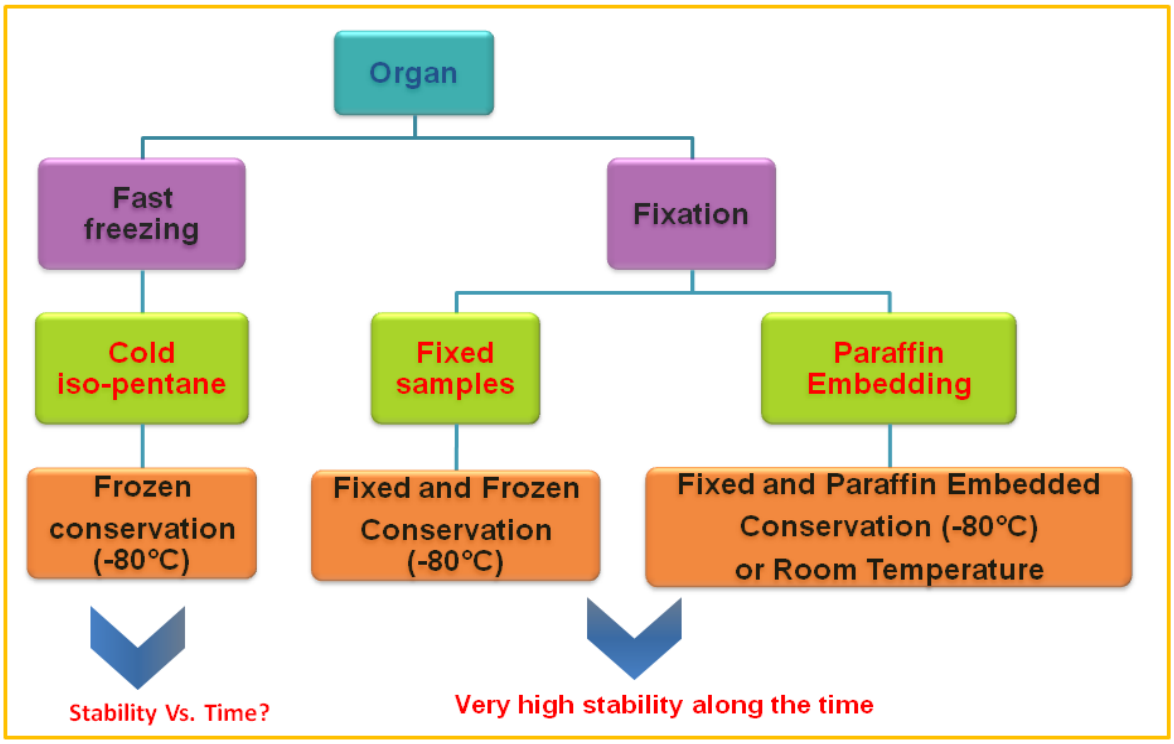

Figure 53 Scheme of the tissue conservation procedure as a function of the type of tissue considered, i.e., fresh or fixed.

However, although PFA fixation is ideal for conservation and structure preservation, it can also result in difficulties during the molecular analysis. For example, PFA fixation is known to induce molecular cross-linking, especially in peptides and proteins. The chemical reaction processes involved in PFA fixation are extremely complex. Although the protocols and outcomes of PFA fixation have been extensively studied, only a few literature reports directly address the molecular chemical reactions underlying the fixation process (Kieman 2000; Plenat et al. 2001; Plenat et al. 2006). To simplify, we can state that PFA reacts principally with free amine groups, binding amino acids tightly via the formation of methylene bridges. The primary reaction of the aldehyde with the protein involves rapid kinetics (Kieman 2000; Plenat et al. 2001; Plenat et al. 2006). In contrast, the second reaction leading to the formation of the methylene bridge is a much slower process that occurs over days (Kieman 2000; Plenat et al. 2001; Plenat et al. 2006). Thus, reactions are still occurring even after the tissues are embedded in the paraffin such that the proteins become further imprisoned over time as a result of the slow formation of methylene bridges. An MS analysis of such tissue samples after tissue sectioning and paraffin removal has generated very few results because the proteins are all cross-linked together. Because chemical reactions can still occur inside the paraffin blocks, the MS spectra generated from these samples are dependent on the storage time. For recently prepared FFPE blocks (~0-6 months), some ion signals can be retrieved (Lemaire et al. 2007a), which are mainly observed in the mass range of a peptide. A detailed study of the corresponding mass spectra indicates that the peaks exhibit broadened profiles with +12 amu adducts that increase with storage time as a result of the slow PFA secondary reaction (Redeker et al. 1998). However, more peptide signals could be observed when using very specific MALDI matrices, such as the reactive matrix 2,4-dinitrophenylhydrazine (2,4-DNPH) (Lemaire et al. 2007a). Surprisingly, with such a matrix, the MS spectra do not present any additional +12 amu adduct ions. This result could be explained by assuming that 2,4-DNPH reacts with the free aldehyde groups (PFA) remaining in the tissues. For samples stored for longer periods (> 1 y), the MS analyses do not allow for the retrieval of exploitable signals even with 2,4-DNPH. The cross-linking of proteins has also been shown to be problematic for immunohistochemistry (IHC) experiments because it hampers antibody access to the epitope of the antigen. To overcome such problems, pathologists have extensively studied

epitope-unmasking procedures. Different antigen retrieval (AR) protocols that are compatible with IHC are now well known and have been described elsewhere (Shi et al. 1997; Taylor and Shi 2000; Shi et al. 2001a, b; Shi et al. 2007a; Shi et al. 2007b; Xu et al. 2008). The most popular procedures include heating at high pressures (Shi et al. 1997; Taylor and Shi 2000; Shi et al. 2001a, b; Shi et al. 2007a; Shi et al. 2007b; Xu et al. 2008) and the citric acid-antigen retrieval procedure (CAAR) (Gustafsson et al. 2010; Bonnel et al. 2011b). However, although AR protocols result in epitope-unmasking, such procedures do not reverse protein cross-linking. AR protocols can be used prior to the MS analysis of tissues to improve the quality of the results, but this method is generally not sufficient because of the cross-linking of the proteins that renders these samples very difficult to analyze directly using MALDI and MALDI-MSI. New strategies are thus needed to analyze FFPE tissue sections in a very efficient manner that is independent of the storage period. Recently, we have developed an approach based on the enzymatic digestion of tissues that allows for the retrieval of pieces of proteins. In this strategy, digested peptides are generated and subsequently analyzed on the tissue or in the images. MALDI-MSI analysis following on-tissue enzymatic digestion is possible if the localization of the generated peptides can be retained, i.e., if the enzyme can be precisely deposited and localized onto the tissue. This requirement can be met by applying small droplets of enzyme in a controlled manner, i.e., by means of a reproducible automatic device (Lemaire et al. 2007a). If the localization of the digested peptides is sufficiently precise, then a MALDI-MSI analysis of the intact proteins can be deduced from the images generated from the ion signals of the digested peptides. This generation of peptides is also extremely interesting for identification purposes.

1.5.1.3. High-Mass protein accessibility

Proteins exceeding 25 kDa in size are not routinely detected using MALDI-MSI. This issue represents a significant methodological limitation because the size of most classes of proteins exceeds 25 kDa. Two previous articles reported sample preparation methods that enable MSI to be used for proteins with higher masses (Grey et al. 2009; Leinweber et al. 2009). The first method used extensive water washing procedures to remove the abundant soluble proteins, which was followed by the automated application of a matrix solution containing a high percentage of an organic solvent. This sample preparation allowed for the

detection of a 28 kDa integral crystalline lens membrane protein (Grey et al. 2009). In the second approach, a matrix application protocol using Triton X-100 was shown to enable the detection of proteins ranging from m/z 25 000 to 50 000 (Leinweber et al. 2009). These observations suggest several reasons for the lack of sensitivity of high-mass proteins that can be exploited for the further development of sample preparation methods. The use of organic solvents or Triton X-100 suggests that high-mass proteins may not be detected because they are not efficiently solubilized in the matrix solution. Consequently, these larger proteins are not extracted from the tissue. The detection of high-mass proteins after the removal of abundant soluble proteins suggests competition with the abundant proteins for incorporation into the matrix crystals and/or ionization in the MALDI process (ion suppression effects) (Cohen and Chait 1996). Ion suppression is most likely another effect that limits the routine detection of high-mass proteins. A new tissue sample preparation has been undertaken using hydrophobic solvents, e.g., hexafluoroisopropanol (1,1,1,3,3,3-hexafluoro-2-propanol, HFIP) (Redeby et al. 2004; Redeby et al. 2006) and 2,2,2-trifluoroethanol (TFE) (Redeby and Emmer 2005). These solvents have previously been used to extract membrane proteins (Ferro et al. 2000; Chertov et al. 2004; Wang et al. 2007b) and high-mass proteins (Thompson et al. 2008) and could aid in detecting high-mass proteins directly from the tissue. Using this method, proteins that are approximately 70 kDa in size have been detected (Franck et al. 2010). Coupling this procedure with the use of a specific high-mass detector has allowed for the detection of proteins with a molecular mass exceeding 100 kDa. Increasing the mass range of the detection is a key for developing direct tissue proteomics and, especially, for any potential functional investigation. These data will make possible a novel approach in mass spectrometric imaging (van Remoortere et al. 2010).

1.5.2. The MALDI matrix: The cornerstone of MALDI-MSI

1.5.2.1. What is the best matrix for MALDI-MSI?

There is insufficient knowledge available regarding the MALDI mechanisms to properly use theoretical and predictive considerations to choosing appropriate matrices; thus, we depend solely on empirical experimental data to establish the best matrix. At least three types of matrices are known for the MALDI analysis of biomolecules: sinapinic acid (SA),

a-cyano-4-hydroxycinnamic acid (CHCA) and 2,5-dihydroxybenzoic acid (2,5-DHB). Although all three of these matrices can be used for both peptide and protein analysis, SA is generally preferred for proteins in terms of signal intensity, resolution, signal-to-noise ratio and the number of detected compounds. CHCA is generally used for peptides, whereas 2,5-DHB offers a broader range for analysis and can be used for either peptides or proteins. For MALDI-MSI, the situation is more complex due to the interaction between the matrix and the tissue. Based on experimental data obtained following matrix deposition on tissue sections, CHCA appears to provide good signals for peptides up to m/z 5000, but only a few signals with weak intensities can be observed above this limit. SA yields better signals in the range of m/z 5000 to 30,000. However, although SA is better suited for high-mass proteins on tissues than it is for classical MALDI, the mass ranges are more limited on tissues. Thus, when comparing the classic solution analysis to the tissue analysis, proteins up to 100 kDa in size (e.g., antibodies) cannot be analyzed in tissues. This limitation in tissue sections is yet to be overcome. The most likely hypothesis to explain such a result is that it is difficult to readily extract high-mass proteins from tissues and incorporate them into the matrix crystals. The use of 2,5-DHB has been less than that of the other matrices, although it was initially employed for peptide/protein analysis because of the heterogeneous crystallization of this matrix. Indeed, spotted 2,5-DHB generally crystallizes in fine long needles at the rim of the spot, leaving small crystals in the inner region of the spots that contain high levels of salts. A MALDI signal is obtained by irradiating the rim of the sample. Moreover, 2,5-DHB is known to have “hot spots”, i.e., very strong signals in some parts of the crystals and no signals in other parts. This type of crystal behavior is very difficult to use for a MALDI direct tissue analysis for which signals must be reproducible for all studied spots of the sample. Nonetheless, satisfactory results may be obtained when 2,5-DHB is used in a spray or in a micro-spotting deposition procedure.

Although classic MALDI matrices are applicable for tissue analysis and have been shown to give good results, the search for new matrices that are better suited for MALDI-MSI remains a priority. Solid ionic matrices have been shown to provide good results in tissue analyses. Lemaire et al. (2006a) showed that novel solid ionic matrices were particularly well suited for the analysis of peptides up to 10 000 m/z. CHCA/aniline and CHCA/2-amino-4-methyl-5-nitropyridine were the best matrices for tissue analysis (compared with

CHCA), and these matrices resulted in increased signal intensities, improved signal-to-noise ratios and a larger number of detected compounds. Similarly, a solid ionic matrix consisting of SA and aniline was reported to be the best matrix for protein detection (Franck et al. 2010). For lipids, liquid ionic matrices such as DHB/aniline can also be used (Meriaux et al. 2010). The principal advantage of these matrices is their homogeneous crystallization (Figure 54), resulting in a very limited delocalization of peptides/proteins, although they are deposited without any specific system.

These studies also showed that ionic matrices are very stable under vacuum conditions and lead to very low material ablation rates under the source vacuum, thus allowing the sample to be used for an extended period inside the instrument to obtain several acquisitions with no decrease in performance.

Although classic MALDI matrices provide good performance, the analytical performance of MALDI-MSI must be maximized to increase the dynamic mass range and the number of analytes observed. Thus, the effort to find new matrices continues.

1.5.2.2. Which method is optimal for matrix deposition?

It is clear that adding a matrix on top of the tissue sample is a critical step in the sample preparation process, and several criteria must be fulfilled for successful MALDI-MSI. The first question is whether the solvent used for the matrix solubilization induces the delocalization of analytes during the crystallization process. In most cases, delocalization of the analytes does occur and must be limited. Deposition of the matrix solution onto a tissue section using a micropipette is thus not very satisfactory. Stoeckli et al. (2002) demonstrated that matrix crystals could migrate over 400 µm on the tissue section before solidification. In a typical preparation, the matrix crystals can range from 10 to 100 µm in size. Thus, the ideal matrix should have a minimal amount of solvent and produce the smallest size of crystals possible. This point is critical to obtain reliable image results and to achieve a better image resolution.

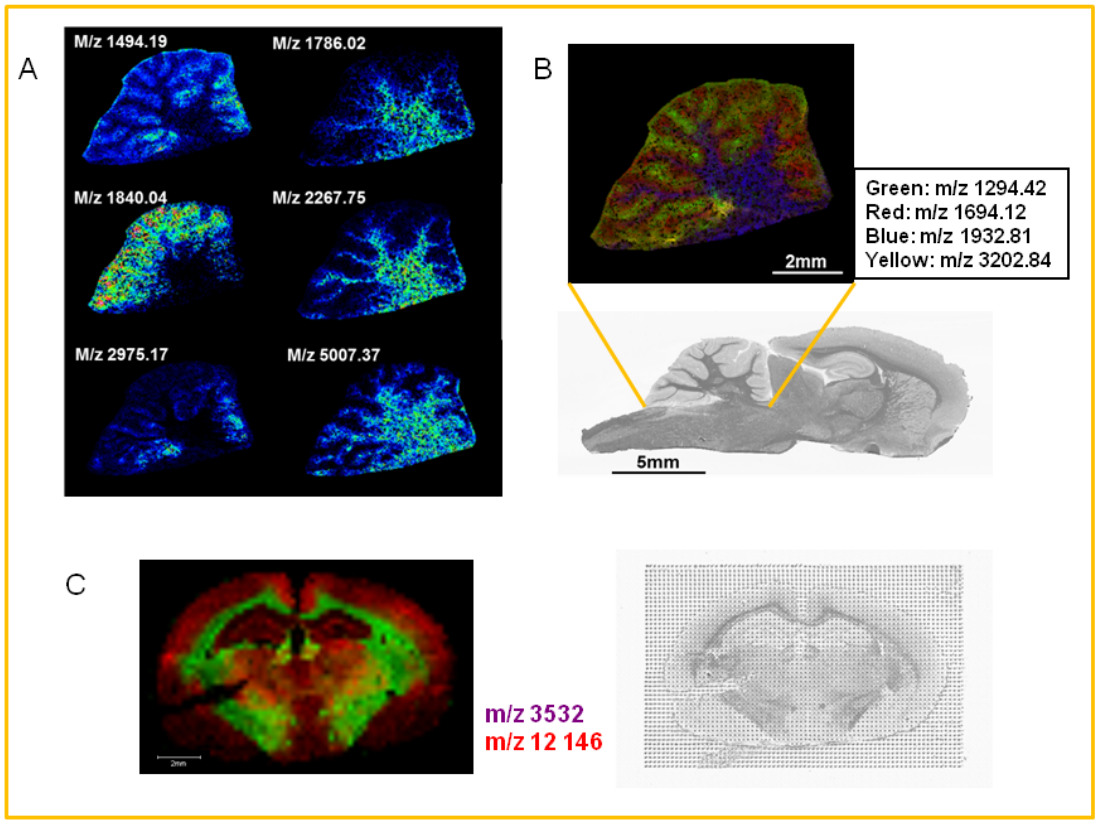

Figure 54 The matrix deposition procedure as a function of the type of instrument used.

A) Molecular images of a rat cerebellum section covered by CHCA/aniline using an automatic sprayer. B) Multiplex molecular image of 4 ions with different m/z values at the level of the rat cerebellum section covered by CHCA/aniline using an automatic sprayer. C) Multiplex molecular images of 2 ions of a rat brain section covered by SA/aniline using piezoelectric heads.

There are three different strategies to circumvent this problem: (1) spray the matrix solution, (2) deposit the matrix solution as discrete spots or (3) blot the analyte onto a membrane via passive or active transfer. Blotting was one of the first strategies to be tested (Chaurand and Caprioli 2002; Chaurand et al. 2002). With this method, the matrix can be easily deposited by adsorbing proteins on membranes. Conductive polyethylene membranes were successfully used for the direct analysis of a wide range of proteins up to 100 000 Da in size. The membrane transfer method is limited in terms of variability and transfer yields, especially when comparing different proteins. At present, analyses performed directly on the tissues are preferable to maximize the number of detected compounds and the sensitivity. The spraying technique and the application of discrete spots of the matrix are thus preferred. Spraying the matrix is now widely used because it is one of the easiest and cheapest methods for preparing samples for MALDI-MSI. Spraying is generally performed using a pneumatic sprayer, such as a TLC sprayer or an airbrush system. Such systems minimize the solvent quantities and the matrix crystal size, but they often lack reproducibility because the optimal spraying conditions are difficult to control. Because of the physicochemical proprieties of peptides/proteins, these species must be included in the matrix crystal for optimal ionization. This requirement leads to a paradox related to the correct spatial localization of molecules and their proper ionization. The proper incorporation of molecules into the matrix crystals is better achieved with a reasonable amount of solvent; however, experimental data have confirmed that an important loss of signal is observed even with low amounts of solvent. Thus, if the spraying conditions are not well controlled, the sample will be either too “dry” (not enough solvent) and will not permit sufficient incorporation of the analytes into the matrix crystals or too “wet”, leading to delocalization and heterogeneous crystallization. The distance between the sprayer and the sample, the flow rate of the spray, the duration of a spray cycle and the number of cycles applied are difficult to control by hand. Therefore, even if the microscopic observation of the deposited matrix layer is satisfactory, the resulting mass spectra can be of poor quality in terms of peak intensity, signal-to-noise or number of detected compounds. A robotic sprayer system that offers very good reproducibility of the MALDI mass spectra (Figure 54) was developed by Bruker Daltonics (Schuerenberg et al. 2007). This system monitors the growth of the matrix layer using an optical sensor that

monitors the light scattered from the matrix crystals and combines a fine control of all of the parameters to optimize the spraying conditions. The average droplet size is very small (~25 µm) in this system. Recent developments have also improved the discrete deposition method, which is more complex because it requires the deposition of picoliter amounts of matrix according to a regular raster to cover the entire tissue section (Figure 54). This strategy requires the use of a robotic system that can plot all of the matrix points. For example, to cover an entire 2 cm by 1 cm section of rat brain tissue, 5000 discrete matrix spots are required. Picoliter amounts of a matrix solution are generally insufficient to provide good extraction and incorporation of the analytes into the matrix crystals. Additionally, printing systems generally do not allow for the use of high concentrations of the matrix solution because this results in clogging of the system. It is therefore necessary to perform several deposition cycles to obtain good spectral quality, which results in an increased sample preparation time. Several commercial platforms are available to perform picoliter deposition of a solution. One of the simplest methods is to use a fused silicate capillary to generate a very small droplet that is gently deposited onto the samples, such as the systems used for nano-LC fraction collection. The solution volume and the spot size are then directly dependent on the internal diameter of the capillary. Piezoelectric systems, which are used for microarrays, can also be used for MALDI-MSI (Franck et al. 2009a). Finally, a system based on the acoustic ejection of solutions has the advantage of avoiding problems with clogs. Each of these strategies produces spot sizes ranging from 100 to 500 µm, which is sometimes higher than the typical resolution of 150-200 µm used for MALDI-MSI. The application of discrete spots can be quite time-consuming (several hours) and requires that the conditions are finely optimized for each solvent and matrix solution to obtain optimal MALDI spectra. Although it may appear that discrete deposition results in a lower resolution due to the spot size, this method does guarantee that the delocalization of a compound cannot exceed the size of the spots. Nonetheless, experimental results using discrete deposition do not exhibit any major differences in terms of image resolution when compared with the other matrix deposition methods. For a cheaper approach, an inkjet printer with ink cartridges filled with the matrix solution can be used for matrix application (Baluya et al. 2007). This approach yielded good results when monitoring lipids with 2,5-DHB as the matrix, but it was unsuccessful for the deposition of

CHCA, which needed to be solubilized in a high percentage of acetonitrile. Alternatively, matrix application via sublimation is also suitable for MALDI imaging (Hankin et al. 2007). This method was previously used to analyze polymers, and it has the advantage of being solvent-free. In this method, the matrix is applied by heating the solid matrix until sublimation occurs, and the matrix is then deposited by condensation onto the tissue sample. This strategy results in extremely fine and homogeneous layers of the matrix and avoids delocalization of the analytes, thus providing to highly resolved images. Although this method is well adapted for lipid detection, it is inappropriate for peptides and proteins because these latter molecules must be incorporated into the matrix crystals for the desorption/ionization process to be successful (i.e., peptides/proteins are too polar to be easily transferred into the gas phase).

1.5.3. Acquisition Time

The data acquisition time for the purpose of image reconstruction is a parameter sustained by the user with little choice. The acquisition time is principally dependent on the spatial resolution and the laser repetition rate, and it benefits from the developments of new lasers with higher performances.

Presently, lasers with repetition rates of up to 1000 Hz are available for commercial MALDI-TOF systems. However, the scan rate can also be limited by the mass analyzer duty cycle time and the number of duty cycles to be performed for good spectral quality. Only one cycle per laser shot is required for TOF analyzers, and the limitation in speed is linked to the capacity of the TDC (time-to-digital converter) system. Therefore, if a very broad mass range must be recorded, the repetition of laser shots may become faster than the time-to-digital conversion. In such cases, it is necessary to decrease either the acquisition mass range or the laser repetition rate. Using an ion trap (IT), the limitations of this method include the number of duty cycles necessary to record a mass spectrum.

MALDI-MSI typically works in a microprobe manner; therefore, the acquisition time is dependent on the size of the sample. The collection time of MALDI-MSI data can range from 15 min to greater than 24 hours depending on the size of the sample, the number of points to be acquired (i.e., the spatial resolution), the laser repetition rate and the time required to move the sample between each analysis point. For example, a 15 × 10 mm rat brain section with a raster of 100 μm in the x and y directions will result in 150 × 100 spots

(i.e., 15,000 spots to be analyzed). Using 300 laser shots for each spot to ensure good spectral quality and a laser repetition rate of 10 Hz, the acquisition time would be >20 hours. Using a laser repetition rate of 1000 Hz, the same spectra could be obtained in less than 1 hour. If better images are required, which can be achieved by decreasing the footstep between two points or by increasing the number of laser shots to be averaged, then the acquisition time will again increase. If MALDI-MSI is to be an important application in the pharmaceutical industry or in health-related research, the throughput must be optimized. The latest generation of MALDI-TOF/TOF spectrometers is now equipped with lasers with a repetition rate of 1000 Hz, and the next-generation MALDI laser could be 5000 Hz to 10.000 Hz.

1.5.4. Image Resolution

As mentioned earlier, the image resolution is dependent on the size of the image pixels and the number of pixels in the area studied. The number of pixels is limited by the precision of the (x,y) table that controls the sample plate, which result in very high precision that ensures good reproducibility within a sample of 1-2 µm. The image resolution is also limited by the data processing capacities. Indeed, each pixel that is added to a sequence corresponds to the data of a full mass spectrum that contains thousands of values for intensity vs. m/z. The amount of data collected will thus depend on the mass analyzer used for the MALDI-MSI sequence. Extremely large amounts of data are generated for an imaging sequence regardless of the type of instrument used. For example, an image of an entire rat brain section with a raster of 100 × 100 µm (approximately 1.5-2 cm by 1-1.5 cm) can result in more than 6 Go of data. Such a large data set requires a significant amount of computational power, which is not always provided by a standard mass spectrometer workstation.

Another challenge that must be overcome to improve MALDI-MSI resolution is to decrease the size of the pixel, i.e., to decrease the area irradiated by the laser. For a typical MALDI analysis, the irradiated area is not of great concern and does not need to be minimized. Thus, most existing systems, both home-made and commercial instruments, are generally equipped with a laser that can focus on an irradiated area with a diameter of approximately 100-150 µm, which produces images with a resolution (R) of 10000 pixels/cm^2. This resolution is a good starting point in the field of mass spectrometry, but it

is insufficient for biologists because this resolution corresponds at least to an irradiation area of 5 × 5 cells. To image a single cell using MALDI-MSI, a resolution of 20-25 µm would be required. Because the number of pixels (N) is proportional to R^2, doubling the resolution to collect the maximum amount of information leads to 4 times the number of pixels and data to be processed. The only direct way to decrease the size of the irradiated area is to use a better-focused laser beam, which may be a challenge but may be achievable for laser physicists. A very high-resolution system was developed by Spengler and Hubert (2002) for MALDI-MSI, namely the SMALDI (scanning microprobe MALDI). Using a very specific set-up of lenses that were incorporated both outside and inside the instrument along the laser beam pathway, a minimal resolution of ~0.5 µm per pixel is theoretically reachable. Experimentally, the resolution of the SMALDI system was very close to this theoretical value under classic conditions of laser flux (a measure of the energy delivered per unit area) and using a homogeneous laser beam. The resolution obtained (5 µm for lipids) is close to the size of an average cell (Römpp et al. 2010). The next step would be to develop systems capable of sub-cellular imaging and the relatively fine observation of organelles. Although such fine resolution is possible, obtaining data for peptides and proteins in tissue sections at such a resolution is another matter. To date, the best images have been obtained with an average resolution of 20 µm for highly abundant proteins (Lagarrigue et al. 2011). The first consideration is that decreasing the pixel size will also decrease the copy number of the ionized molecule being analyzed. Considering a fixed limit of detection, the amount of proteins available on such a surface is likely too low to be detected. Basic studies have shown a drastic decrease in the ion yield when the size of the irradiated area is decreased (Dreisewerd 1995). A 35-50 µm laser raster is reasonable, but the ion yields are well below their limits. MALDI is well known for its poor ability to produce ions because only a small fraction of the molecules ejected from the solid will reach the detector of the mass analyzer. Although our knowledge of MALDI processes has increased considerably over the past decade, we have not yet been able to increase the ion yield. Thus, the resolution of MALDI-MSI will only progress with increases in the fundamental understanding in this field. Presently, dedicated systems for MALDI-MSI provide better focusing systems for the laser beam, which are capable of reaching a pixel size as low as 10 µm and should at least provide pixels 30-50 µm in size while maintaining

good analytical capacities (Holle et al. 2006). Recently, Chaurand et al. (2007) designed a new system that allows for the collection of protein images at a resolution of 10 μm. Their experimental set-up combines a very carefully drawn system consisting of a focusing lens and an iris aperture to finely control the laser beam size. The source geometry also uses co-axial illumination of the sample, which reduces the radial distributions of the ejected molecules and ions formed, thus increasing the uptake of the ion into the mass analyzer. Although, such systems are currently only in a developmental phase and are not commercially available, other systems have been developed to increase the image resolution using alternate methods. One such alternative was proposed by Sweedler and collaborators (see: Jurchen et al. 2005) and involves the overlap of pixels during the acquisition of data. In this method, the sample is irradiated sufficiently to remove all matrix material from a spot, and the sample is then moved by only a fraction of the irradiated area diameter (e.g., half the diameter in a simple case). Thus, for consecutive spots, only half of the new material and ions can originate from an area that was not previously irradiated. This very simple method increases the spatial resolution up to approximately 25 μm and can be used on all existing instruments. However, this methodology results in a significant increase in acquisition time. Other methods designed to be applicable for all instruments are currently under study. Other authors have proposed the use of mask systems (Fournier 2007; Wisztorski et al. 2007; Wisztorski 2007) that involve covering the tissue with a mask, thus presenting a network of apertures of defined size and eliminating the need for a very complex system of laser focusing. The size of these apertures would limit the laser beam and control the size of the irradiated area. These systems reduce the pixel size up to 30 μm but maintain a sufficiently high ion yield for analysis of peptides and proteins. Mask systems are of great interest because they lead to an increase in the ion yield according to the specific shape of the apertures. Finally, Heeren et al. (see: Luxembourg et al. 2004) proposed a very different MALDI-MSI system that operates in ion microprobe mode: the so-called “stigmatic MALDI”. This specific instrument geometry is closely related to the old systems of the laser microprobe mass analyzer (LMMA) and is based on a correlation of the arrival positions of the ions with their original positions on the sample. In such a system, the laser is defocused to irradiate an area of approximately 200 × 200 μm with a very specific arrangement of extraction lenses and a position-sensitive detector that

independently treats data from each channel of its surface. Thus, the arrival positions of the ions allow for the calculation of their initial positions on the sample. A very fine lateral resolution of 4 µm can be achieved for an area of 200 × 200 μm^2 in a timeframe of less than 1 ms because only one-shot acquisition is needed for this surface. Reconstructing an entire image with high resolution would only require the contiguous acquisitions of small areas of the sample followed by the summation of these acquisitions. This technique also has great potential, as shown by the recently published reports (Altelaar et al. 2007) on the distribution of peptides in the rat pituitary tissues. This unique system has not yet been established for high-throughput applications.

1.5.5. MALDI-MSI and bioinformatics

As with all imaging technologies, data processing is vital for MALDI-MSI. Various types of software exist for image reconstruction, but there is no unique software for imaging. Even in the early years of MALDI-MSI, automation of the acquisition of data was proposed for most instruments. However, this automation was not suitable, and considerable time was lost in setting up the acquisition. Moreover, no tools were available for post-acquisition data processing. The simplest software would have to perform several tasks: acquisition of data using the specific instrumental settings according to a defined raster, creation of an average spectrum from all of the collected spectra, extraction of the intensity at a specific m/z value upon user inquiry and a report of the m/z intensities using a color scale as a function of the corresponding (x,y) coordinates. The first usable software able to perform these tasks was “Biomap” developed Martin Rausch with MSI additions by Markus Stoeckli. It allows full automation of the data acquisition for different MALDI-TOF instruments. “Biomap” is dedicated software that reconstructs images from whatever MALDI data are obtained. It offers many different functionalities and is available free of charge at http://www.maldi-msi.org/.

Optimal data processing can be the result of very different solutions that have the final goal of producing images that are closest to reality. Several questions must be answered when processing MALID-MSI data if the aim is to represent reality: Is reality better described by measuring peak intensity or peak areas? Must the mass spectra data be normalized? Must a minimum threshold of intensity be defined? Must a maximum intensity be defined? How well can mass calibration be performed? Can image resolution be increased by

extrapolation of a signal between two data points? What algorithms should be used? Can better tools be designed for biological applications using classification parameters? Overall, two different processing issues must be distinguished, including the need for the data processing to describe reality and the use of statistics for sample classification when performing a differential display analysis. Optimization of this work is balanced between increasing the extraction of information and reducing false information.

The influence of data processing in the classically used data process are discussed in a paper by Norris et al. (see: Klerk et al. 2007). Statistical analyses and clustering are already used to analyze proteomics data. Clustering methods were used in MALDI-MSI experiments and direct analyses to compare human glioma and other brain tumors with normal brain samples (Schwartz et al. 2004). This study demonstrated that tumor tissue could be easily discriminated from non-tumor tissue based on its very unique protein profiles, which were extracted using a statistical analysis. Moreover, a combination of molecular profiling and clustering also differentiated the different grades of tumors. An assessment of protein patterns in specific diseases was reviewed by Chaurand et al. (2004). Multivariable analyses and clustering can also be used to find regions of interest (ROI). A ROI represents the area on the sample in which some of the analyzed molecules are differentially expressed compared with other samples. An image can thus be reconstructed from the entire signal to identify the spatial correlation of the mass spectra with the tissue localization (McCombie et al. 2005). Recently, researchers demonstrated the applicability of principal component analysis (PCA) algorithms for MALDI-MSI (Van de Plas et al. 2007; Deininger et al. 2008; Walch et al. 2008).

1.5.6. MALDI-MSI: a general technology for all types of biomolecules?

Cells contain a large variety of molecules that constitute families ranging from peptides/proteins, oligonucleotides (DNA, RNA), saccharides, lipids, salts and small organic compounds, such as neurotransmitters, ATP, ADP and NO. Each of these families are themselves composed of molecules that can exhibit a large range of physico-chemical properties in terms of polarity, hydrophobicity, solubility, molecular mass, and acid/base properties. A perfect molecular imaging technique should be able to equally determine the distribution of all of these compounds. To date, none of the tools available is capable of such a task. However, a full understanding of living systems requires a better knowledge of

the interactions between these different families of biomolecules. It is thus worthwhile to use mass spectrometry to analyze these biomolecules.

1.5.6.1. Imaging of peptides and proteins

Due to its capacity to generate ions from compounds of various polarities and its ability to analyze molecules with very high molecular masses, MALDI-MSI is naturally well designed for monitoring peptides and proteins. Moreover, the analysis of peptides and proteins is currently the main field of application for such an ion source. The specificity of MALDI compared with other MSI techniques, such as SIMS-MSI, which affords very high resolution (1 µm lateral resolution routinely) but which is only well adapted for studying small organic compounds, such as lipids, and thus does not allow for peptide or protein analysis. Thus, it was natural that initial efforts were dedicated to improve MALDI-MSI in the field of proteomics. However, even in proteomics, MALDI-MSI has limitations, one of which is the mass range, which was observed in the direct MALDI-TOF/TOF analysis of proteins from tissue sections. These proteins had masses up to approximately 30 000-35 000 Da, which is outside the classic MALDI-TOF/TOF range. The reasons for this limitation are not clear. Reasonable hypotheses include difficulties in incorporating high-mass proteins in the matrix crystals because of their solubility in the solvent used for the matrix solubilization and a lower laser/matrix energy transfer to these proteins in tissue samples that does not allow the desorption process to occur.

1.5.6.2. Imaging of lipids

Small endogenous compounds can be difficult to analyze using MALDI for either practical or fundamental reasons. The matrix produces numerous and highly abundant signals in the Mw < 1000 Da spectral region that can interfere with the signals arising from the compounds of interest in this molecular range. However, some of these compounds are non-polar and exhibit low ionization rates. Saccharides are generally very difficult to analyze using MALDI and have not yet been analyzed using MALDI-MSI.

Besides proteins, lipids comprise the family of endogenous molecules that are the most studied using MALDI-MSI. Many efforts have been made by the groups of Woods (see: Jackson et al. 2005b, a; Jackson et al. 2005c; Wang et al. 2005; Wang et al. 2007a) and Yost (see: Garrett 2007; Hsieh et al. 2007) to improve the direct analysis of lipids using

MALDI. The identification of lipids from tissue sections is very complicated because there are only very small variations in the masses of different lipids, even those with very different compositions. For example, phosphatidylserine (PS) 40:6 (Mw=835.54 Da) and sufatide (ST) 20:0 (Mw=835.59 Da) are from very different families of lipids, but they exhibit a mass difference of only 0.05 Da. Moreover, several lipids present the same Mw and the same atomic composition but vary structurally because of differences in the position of an unsaturated bond. Moreover, the molecular weights of lipids generally range from 100 to 1000 Da, which, as previously explained, is where matrix interference occurs. The imaging protocols used for classic MALDI, e.g., using 2,5-DHB as the matrix or using more specific matrices, such as DHAP (2,6-dihydroxyacetophenone) or ATT (6-aza-2-thiothymine), has also been shown to be successful for the direct analysis of lipids. However, in the case of DHAP, the matrix was shown to be unstable under vacuum. Therefore, this matrix is not well suited for MALDI-MSI experiments (Wang et al. 2007a; Franck et al. 2009a). However, it was shown that the addition of heptafluorobutyric acid (HFBA) to the matrix solution increases the stability of DHAP under vacuum, thus making MALDI-MSI experiments with this matrix possible (Colsch and Woods). Recently, several groups have shown that the use of ionic matrices could improve the detection of some classes of lipids including gangliosides (Chan et al. 2009) and phospholipids (Meriaux et al. 2010). Regardless of the matrix used, the analyses were conducted in both positive and negative modes depending on the class of lipids being analyzed.

Great care must be taken for the lipids during matrix deposition because such small organic compounds are easily spread out on the tissue section. For this reason, the matrix is generally deposited using a pneumatic spray system or an airbrush to obtain a repartition of homogenous crystals and to avoid large quantities of solvents. Other strategies that were found to be efficient because they provided a homogeneous matrix coverage on tissues include solvent-free procedures (Puolitaival et al. 2008; Bouschen et al. ; Trimpin) and matrix application via sublimation (Hankin et al. 2007; Bouschen et al.). With respect to microspotting preparations, the use of liquid ionic matrices was found to greatly decrease the time needed for sample preparation, which is generally a significant issue with this procedure (Meriaux et al. 2010).

Finally, lipid imaging generally requires an MS^2 fragmentation analysis to confirm the identification and real assignment. As mentioned previously, lipids are very small in mass and are well adapted for a variety of mass analyzers. Thus, different instruments have been used for lipid analysis including Q-TOF, TOF-TOF, Ion Trap (IT), IM-o-TOF, orbitrap and FT-ICR. All analyzers that can function in MS^2 mode are suitable for lipids. The ion trap instrument does not result in high precision of the mass data, but it allows for MS^n fragmentation sequences and easy identification via structural elucidation. Conversely, FT-ICR provides highly resolved peaks with a high precision, but the instruments themselves remain very expensive and difficult to use. Recently, imaging and the direct identification of lipids were performed using an LTQ-Orbitrap instrument, leading to the detection of lipids with a very high mass-resolving power. Moreover, MS^n experiments were performed with a sub-ppm mass accuracy, allowing for a more accurate assignment of the lipids (Römpp et al. 2010).

1.5.6.3. Imaging of drugs

Imaging techniques for small exogenous compounds, such as drugs, have recently been developed (Schwartz et al. 2003; Reyzer et al. 2010; Bonnel et al. 2011a). Drugs are compounds that generally yield good MALDI data, although the same analytical problems observed for lipids can also be encountered with drugs. For drugs, the major difficulty is interference due to the matrix ions because the matrix peaks sometimes completely overlap with the drug peaks. Therefore, MS^2 is required to determine which part of the signal should be attributed to the drug. However, the ease of MALDI-MSI and its capacity to detect, identify and image both drugs and metabolites largely outweighs these analytical difficulties.

1.5.6.4. Imaging of oligonucleotides

Oligonucleotides are also very difficult to analyze using MALDI because they contain phosphate groups that complex with salts and induce a high instability during ionization. This situation leads to the observation of large and very weak peaks, and the signal intensity decreases significantly as the oligonucleotide mass increases. Under such conditions, the imaging of mRNA using MALDI is compromised, although some progress was made in this field by studying oligonucleotides under infrared (IR)-MALDI conditions.

1.5.7. One-point Images: Identification the Major point

The direct identification of biomolecules is the key to increasing the potential of MALDI-MSI. The most straightforward strategy consists of identifying molecules directly from tissue sections without the need for any procedures to extract and separate the molecules. In the case of small compounds including lipids and drugs, in situ identification can easily be achieved with the use of devices that provide high resolving power and MS^n capabilities. However, strategies for the direct identification of proteins have yet to be developed. The ideal procedure would involve the fragmentation of an intact protein on a time scale compatible with the mass spectrometer. For example, using an FT-ICR instrument equipped with an electro spay ionization (ESI) source, an electron capture dissociation (ECD) process (McLafferty et al. 1998; Zubarev et al. 2000) could fragment the intact protein, resulting in a highly charged state that is not compatible with MALDI sources in which even ions generated from proteins have a low charge.

Considering the instrumental specificities of the MALDI-TOF instrument, in-source decay (ISD) (Reiber et al. 1998a; Reiber et al. 1998b) is the only approach that allows for "Top-down" experiments to be performed. The second strategy requires the development of an in situ enzymatic digestion using micro-spotter, thus allowing for a "Bottom-up" experiment (Figure 55).

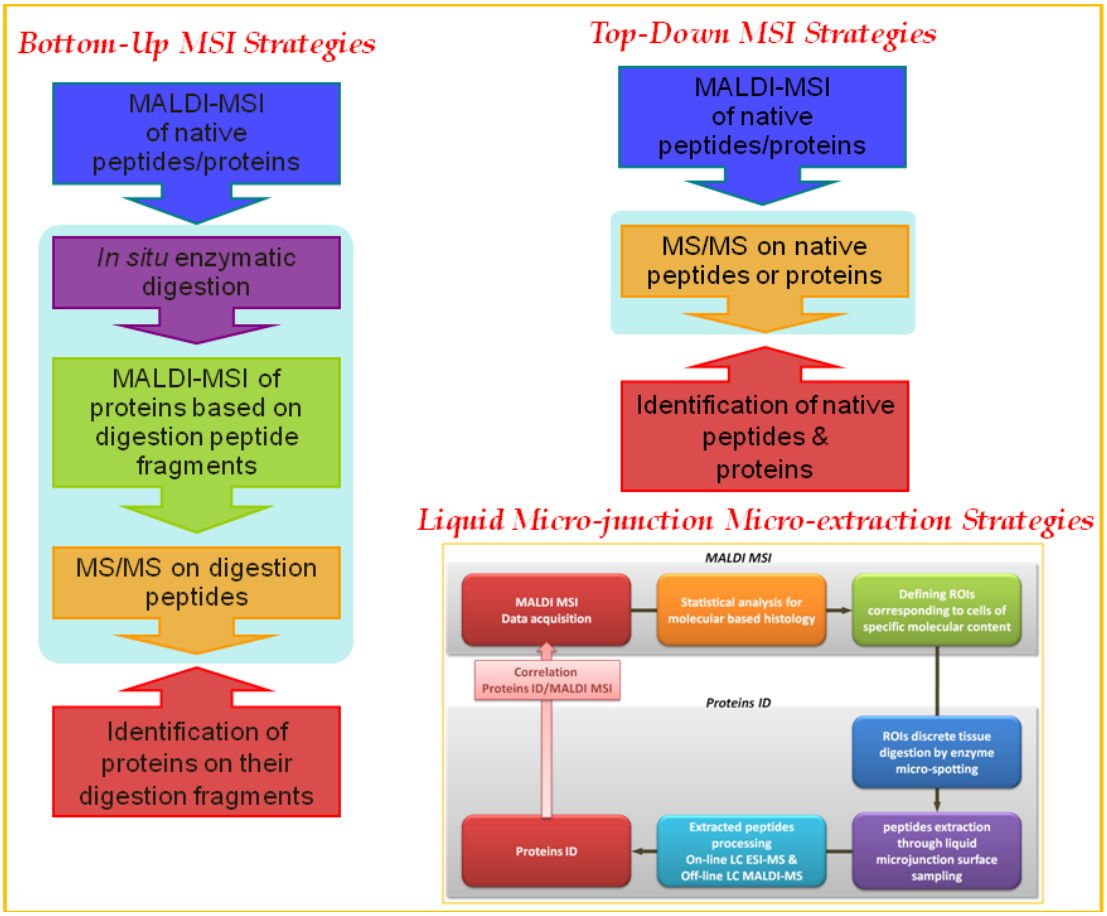

Figure 55 Scheme of the different procedures for identifying peptides and proteins from tissue sections using either bottom-up or Top-down analyses of liquid microjunction micro-extractions.

1.5.8. Top-down strategy

Fragmentation along the protein backbone in the MALDI source was first observed by the team of Brown and Lennon (see: Reiber et al. 1998a; Reiber et al. 1998b). The time scale between the ionization of the proteins and the extraction of the proteins from the source is large enough for the proteins to fragment and form z and c fragment ions, according to Roepstorff's nomenclature (Roepstorff and Fohlman 1984). The N or C-terminal moiety of the protein is then easily achieved; therefore, databank interrogation can be used to identify he corresponding protein. The main drawback of in source decay (ISD) is the lack of selectivity of the precursor ion. For this reason, the protein of interest must be purified to avoid detection of ISD fragment ions from several proteins in the same mass spectrum. However, because ISD fragment ions are detected as intact ions, a pseudo MS^3 analysis of these fragments, called T3 sequencing (Raska et al. 2002), can be performed, thus allowing the N-terminal or the C-terminal moiety of the protein to be sequenced. Moreover, this strategy can be adapted for MALDI-MSI experiments in which a mixture of proteins is detected on each pixel. The choice of the matrix is a very important parameter for the success of an ISD experiment. In fact, ISD involves the transfer of a radical proton from the matrix to the proteins, and 2,5-DHB was found to be efficient in performing this function (Reiber et al. 1998a). Recently, Demeure et al. (2007) showed that 1,5-diaminonaphthalene (1,5-DAN) was more efficient for ISD experiments because it provided a better fragmentation yield. Very recently, Debois et al. (2010) introduced the in situ identification of proteins directly from porcine eye lens and rat brain tissue sections using the ISD strategy. The beta-crystalline B2 protein was identified directly from a porcine eye lens by investigating the ISD fragment ions following data bank interrogation and T3 sequencing. Although software has recently been developed for on-tissue ISD identification (Demeure et al. 2011), this strategy suffers from an inability to study FFPE tissues containing cross-linked proteins. In contrast, the Bottom-Up strategy allows for the detection and the identification of proteins regardless of the mode of preservation used.

1.5.9. Bottom-up Strategy

The second approach that allows for the direct in situ identification of proteins is based on the classical Bottom-Up strategy. Basically, a solution of the enzyme is deposited on a region of interest or on an entire tissue section using a micro-spotter. Peptides are then

generated from the digestion of proteins, allowing for the localization and the identification of the corresponding proteins after the MALDI-MSI and MS^2 experiments. This strategy, introduced by Lemaire et al. (2007a), has been used to detect and identify proteins directly from FFPE tissue sections. Caprioli et al. (see: Groseclose et al. 2007) improved the procedure using a micro-spotter, thus leading to a better and more reproducible application of trypsin on a fresh rat brain tissue section. Several teams have used this procedure for clinical applications, including cancer research (Groseclose et al. 2008; Ronci et al. 2008; Djidja et al. 2009) and animal models of Parkinson disease (Stauber et al. 2008) from FFPE tissue sections. To date, the Bottom-Up strategy has been clearly demonstrated to be able to retrieve information from FFPE tissues. However, many efforts have been undertaken to improve the analysis of FFPE tissues that are difficult to process using in situ enzymatic digestion because of the residual hydrophobicity of the FFPE tissue after paraffin removal. Several strategies involving antigen retrieval were then developed and resulted in an improvement of the in situ enzymatic digestion of FFPE tissues (Gustafsson et al. 2010) and therefore, the detection and the identification of proteins.

However, due to the presence of many fragment ions from different precursors after MS^2 experiments, the corresponding protein is sometimes not identifiable using databank interrogation. Moreover, a mixture of digested proteins is detected at each position; therefore, no clear peptide mass fingerprint (PMF) can be observed from any specific protein. This result implies that the identification of proteins is based on the fragmentation of one or two peptides without any PMF. This result may explain why the corresponding protein is sometimes not clearly identified. To overcome this drawback, an in situ N-terminal derivatization strategy was recently introduced after in situ enzymatic digestion to orient the fragmentation toward a unique series (Franck et al. 2009c). Using this approach, the MS^2 spectra are easier to interpret, and the protein assignment is greatly improved. It was shown that N-succinimidyloxycarbonylmethyl-tris (2,4,6-trimethoxyphenyl) phosphonium bromide (TMPP) is a better derivatization candidate because it allows for a rapid N-terminal derivatization of tryptic peptides at room temperature. This reagent leads to the detection of a strong a_i^+ series of fragment ions after MS^2 experiments.

1.5.10. Liquid-microjunction micro-extraction strategy

A novel strategy consists of combining MALDI-MSI and LC-MS/MS in a single workflow to improve protein identification. Basically, proteins are digested in situ and then extracted prior to nano-LC separation, which is followed by an MS^2 analysis for databank interrogation (Stauber et al. 2008). This approach has demonstrated clear improvement in the number of identified proteins, but it was found to result in the loss of information about the localization of certain identified proteins because it is performed at the level of one or half of a tissue section. It was recently shown that intact proteins could be extracted from a tissue section prior to fractionation by ultracentrifugation. Moreover, in combination with high-resolution and very high-accuracy mass spectrometry, this approach has allowed for the detection of approximately one hundred proteins (Schober et al. 2011). A combination of protein extraction from tissues and MALDI-MSI data using various proteomics-based approaches, including Electron-transfer dissociation (ETD) fragmentation on intact proteins, was used for clinical applications in oncology and has led to the identification of several markers (Rauser et al. 2010; Elsner et al. 2012; Nipp et al. 2012). It is clear that these strategies are helpful for protein identification, but information about the localization of the proteins within the sample is lost. Moreover, the proteins of interest may be diluted in the complex extracts, which contain large amounts of abundant proteins. This problem is especially true if the region of interest is small in comparison to the size of the sample. Thus, there is a crucial need to develop a method that combines MALDI-MSI and LC-MS/MS to retain spatial information and avoid the dilution of low-abundance proteins. Recently, surface sampling using liquid microjunctions was introduced, demonstrating a possible liquid-microjunction micro-extraction technique that can be coupled to any ionization source (Van Berkel et al. 2008). The success of these methods as alternatives to typical ambient surface sampling/ionization sources is due to their greater extraction efficiency and larger surface sampling areas. For example, it has been shown that the metabolites of a drug could be detected using liquid-microjunction extraction, whereas these same metabolites were not detected using desorption electrospray ionization (DESI) (Kertesz and Van Berkel 2010a). In a method called liquid extraction surface analysis (LESA) (Kertesz and Van Berkel 2010b), the solvent can be brought into contact with the sample surface as a single droplet whose size and formation can be controlled by the

instrument. Because the sample extraction is independent of the ionization process, the liquid extraction surface sampling techniques permit further treatment of samples using coupled devices prior to their introduction into the mass analyzer. Currently, LESA has been demonstrated to be useful for the quantification of drugs on dried blood spots (DBS), the profiling of the total drug distribution in whole body tissue sections, and the extraction and quantification of samples on MALDI spots (Kertesz and Van Berkel 2010b). This technique has also recently been used to directly and rapidly identifies intact hemoglobin variants from DBS samples that are used for the neonatal screening of sickle cell and other hemoglobin-related diseases (Edwards et al. 2011). LESA has also been used to correlate the results obtained from MS imaging experiments (Marshall et al. 2011). Our group recently developed a new strategy to identify proteins from tissue sections that involves correlation of the spatial localization of the proteins based on liquid micro-junctions formed after on-tissue extraction and off-tissue LC-MS and MS^2 analyses. Specifically, we have evaluated the on-tissue enzymatic digestion of proteins with discrete localization, and this was followed by tissue micro-extraction and subsequent analysis using on-line nano-LC-ESI MS under high-spectral-resolution conditions. The results show that we can identify 1781 proteins from an original digestion spot of approximately 300 µm, which corresponds to 500-700 cells. All of the investigations were conducted using a MALDI-LTQ Orbitrap that provides a very high mass accuracy (<2 ppm), which is an important parameter for the unambiguous identification of proteins using the shotgun proteomics approach. This strategy will be integrated into the MALDI-MSI workflow to perform supervised profiling identification using defined cell groups with specific molecular profiles. This new strategy is more robust and faster than the laser capture microdissection (LCM) strategy and leads to the identification of a larger number of proteins with respect to the number of cells studied (Fournier et al., unpublished data, Figure 56).

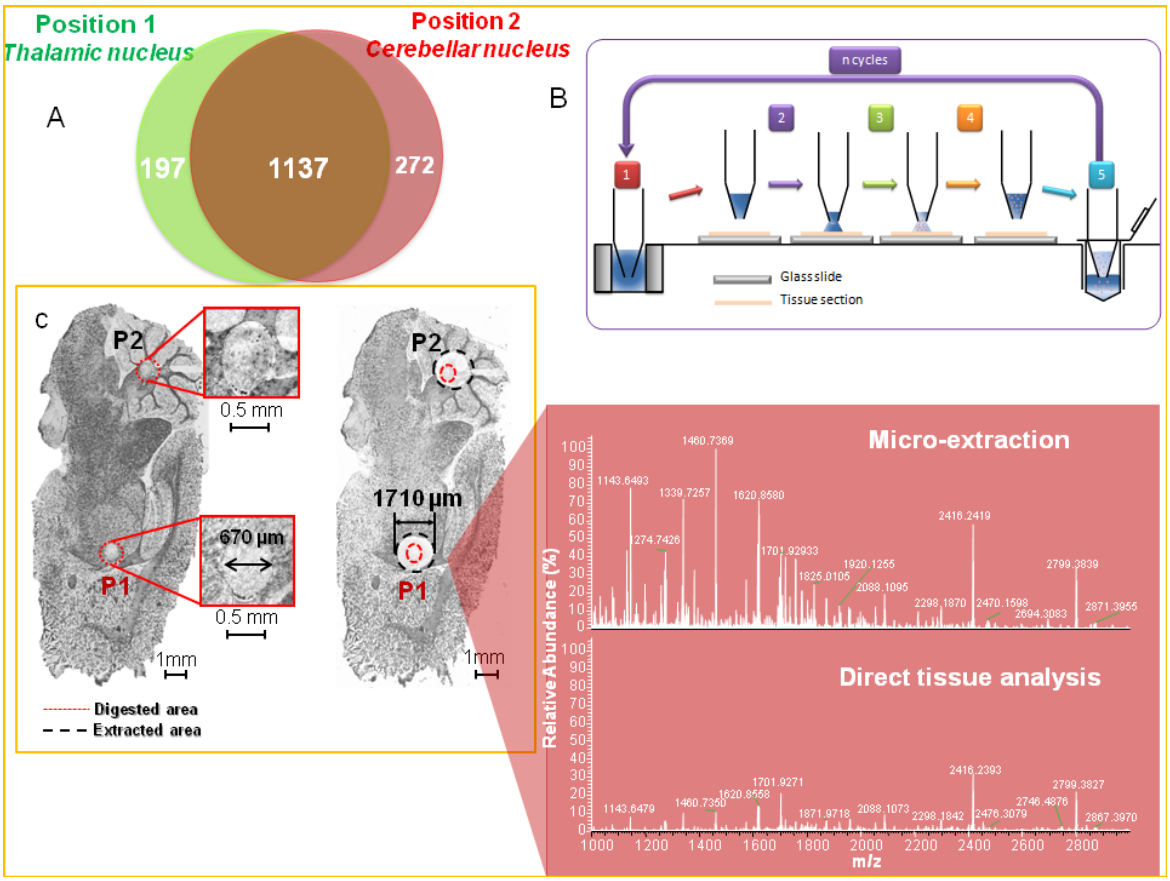

Figure 56 The liquid junction micro-extraction procedure for identifying peptides and proteins from tissue sections.

A: Protein identification from two different location within the rat brain section, i.e., thalamic and cerebellar nuclei.
B: On-tissue micro-extraction strategy for the identification of biomolecules using liquid micro-junction surface sampling. The micro-extraction consists of 5 steps: (1) solvent sampling, (2) solvent dispensing on the tissue section via the liquid micro-junction, (3) analyte extraction via liquid micro-junction to the tissue, (4) sampling of the extracted molecules, and (5) dispensing of the extract into a tube. Steps 1-5 can be reiterated several times to reach the optimized extraction yields.
C: Comparison of the MALDI-TOF MS spectra recorded in the linear positive mode from 2 consecutive sagittal tissue sections from rat brains at two distinct locations in two regions (1, 2) of the tissue after micro-extraction under the optimized conditions for the tryptic digestion peptides: a) micro-extraction of the undigested areas and b) micro-extraction after on-tissue digestion on 300-µm spots. The black circles indicate the micro-extraction areas that are approximately 771 µm in diameter, and the red circles define the position of the 300-µm trypsin digestion spots.

1.6. Photocleavable link and mass spectrometry

Biological processes involve many different signaling pathways from various classes of molecules. Multiplex techniques are necessary to provide tools for the diagnosis and prognosis of diseases. Tissue microarrays (TMAs) are being used more frequently to analyze a large number of diseased tissues, but new, fast and reproducible multiplex techniques are still indispensable (Walch et al. 2008). However, such technologies do not allow for the correlation of mRNA expression with the corresponding protein regulation, i.e., the correlation of the transcriptome with the proteome, which is of special interest for increasing our understanding of biological mechanisms. This correlation is an essential aspect of an analysis when studying pathologies to achieve earlier diagnosis by taking into account the non-coding RNAs that are emerging as important mediators of epigenetic regulation. Significant effort has been devoted to screening for miRNA signatures and identifying functional and clinical links between non-coding RNA expression patterns and various normal and disturbed physiological states (Diao et al. 2010; Enkelmann et al. 2011). However, some specific classes of biomolecules, such as oligonucleotides, are still barely accessible for direct analysis using MALDI. Ideally, oligonucleotides should be directly detected from tissues, although their large size, low abundance in cells and the associated salt adducts and gas phase instability render their analysis difficult (Nordhoff et al. 1994). To circumvent these problems, Olejnik et al. (1999) developed a new approach that combines the affinity purification and MALDI-MS analysis of biomolecules based on the use of photocleavable linkers. This method relies on the design of photocleavable linkers (PC-linkers) that can be incorporated into the target molecule either chemically (Olejnik et al. 1996, 1998a) or enzymatically (Olejnik et al. 1998b) using transcription (Hahner et al. 1999; Olejnik et al. 1999) or PCR (Stauber et al. 2009; Stauber et al. 2010). PC-linkers can be efficiently cleaved photochemically to release the target analyte with the aid of the near-UV desorption/ionization laser pulses used for MALDI (Figure 57).

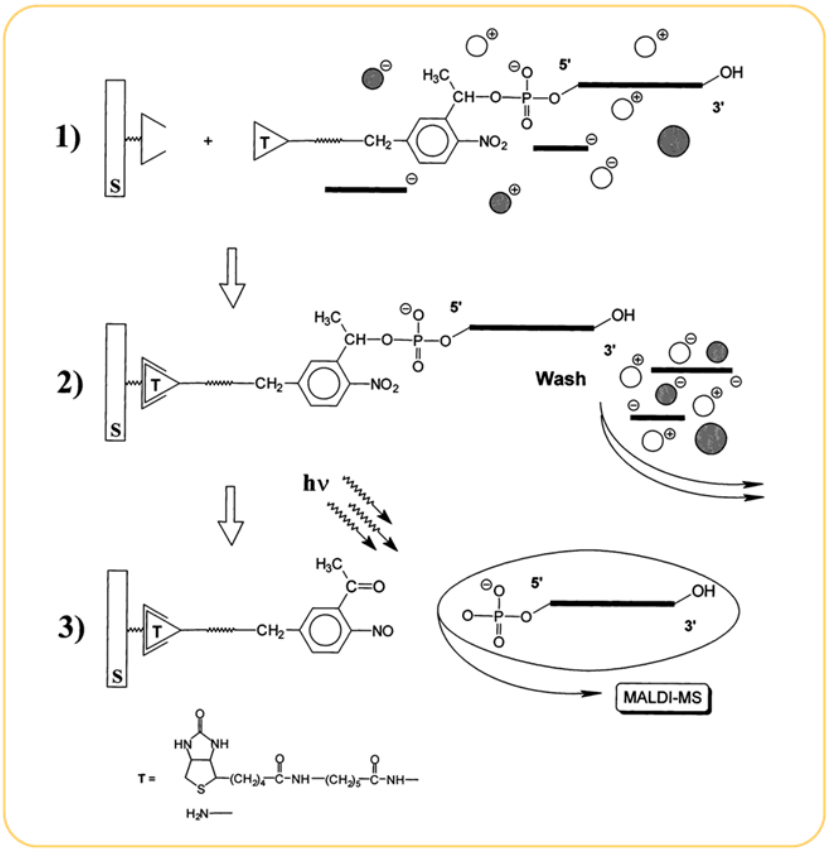

Figure 57 Photo-cleavage matrix-assisted laser desorption/ionization.

An outline of the photo-cleavage matrix-assisted laser desorption/ionization (PC-MALDI) method. Step 1: A reaction mixture containing DNA modified with a photocleavable affinity tag (T) is applied to the affinity support (S) and selectively bound; Step 2: Washing with a MALDI-compatible buffer removes contaminants and salts; Step 3: A UV light source, such as a UV-MALDI laser, cleaves the analyte, which is then analyzed in the mass spectrometer (Olejnik et al. 1999).

1.7. Targeted MALDI Mass Spectrometry Imaging (MSI)

Our team has proposed a new concept using PC-linkers for the multiplex, specific detection and localization of biomolecules. We have especially focused on mRNA and proteins for transcriptome/proteome correlations using MALDI-MSI. This concept, called Tag-Mass, relies on affinity detection using a specifically designed probe that is later detected using mass spectrometry (Lemaire et al. 2007c). Tag-Mass offers more selectivity and higher sensitivity during MALDI-MSI to specifically track known markers of physiological stages in collections of samples (Stauber 2006; Lemaire et al. 2007c; Franck et al. 2009b). The Tag-Mass method is an affinity-based strategy wherein a probe is directed against a specific target. The probe bears a reporter group (Tag) that can be later imaged using MALDI-MSI to report the localization of the probe (Stauber 2006; Lemaire et al. 2007c; Franck et al. 2009b). The reporter is designed to be a molecule of known molecular mass that is easily detectable under MALDI conditions but that does not correspond to an endogenous compound. To indirectly image a probe, the reporter must be linked to the probe and released in the final step immediately prior to or during the MALDI sequence. During Tag-Mass, the reporter group, which involves a photocleavable moiety that binds the reporter to the probe, is released via photodissociation as a result of the MALDI laser irradiation (Figure 58 A). Thus, the reporter is detached from the probe during the MALDI-MSI acquisition. Many different reporters can be used for this purpose, but peptides were often used. The photocleavable linker is selected to present a specific absorption band in the UV range at a wavelength (340 nm) that is very close to that of MALDI lasers (i.e., 337-355 nm). Thus, after hybridization of the modified probe to its target, a classical MALDI-MSI sequence is performed. At a specific point during the acquisition, the presence of a probe will be indicated by the presence of the reporter that was released due to the MALDI laser irradiation, which is evident by the observation of a peak at the m/z value expected for the reporter (Figure 58 B). Reconstruction of the reporter molecular image then yields the image of the probe, i.e., the image of the targeted molecule (Stauber 2006; Lemaire et al. 2007c; Franck et al. 2009b). Such a concept is compatible with all types of probes including mRNA probes, antibody probes, lectins and aptamers, which can be used to selectively obtain images of mRNA, antigens, oligosaccharides (including glycosylated proteins) and drugs, respectively, as targets. In the Tag-Mass workflow, MALDI-MSI is

combined with hybridization techniques including in situ hybridization (ISH) and IHC (Stauber 2006; Lemaire et al. 2007c; Franck et al. 2009b) (Figure 59). The procedures for imaging different targets (primer, antibody, dUTP) are presented in the legend of Figure 58.

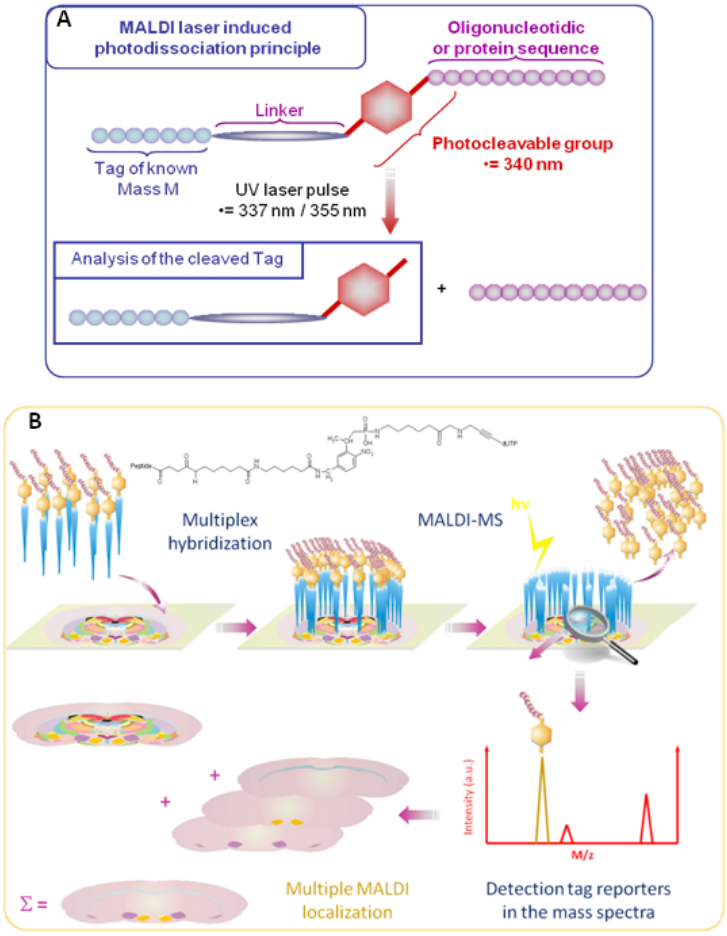

Figure 58 Targeted MALDI Mass Spectrometry Imaging.

A: Schematic representation of the reporter released via photodissociation as a result of irradiation from the MALDI laser using a photocleavable-reporter system coupled to the probe.
B: Scheme of the photocleavable linker/tag system for indirect detection following photodissociation via the MALDI UV laser. Specific tagged probes (see inset for the structure of the deoxyuracil-tagged nucleotide that was used to amplify the tagged riboprobe for in situ hybridization (ISH) to access the transcriptome) were hybridized to the tissue before the linker that was coupled to the reporter (PC-peptide) was released by photocleavage upon irradiation from the MALDI laser. The PC-peptide was then detected using mass spectrometry. Different reporters or different targets can be used simultaneously to perform multiplex analyses.

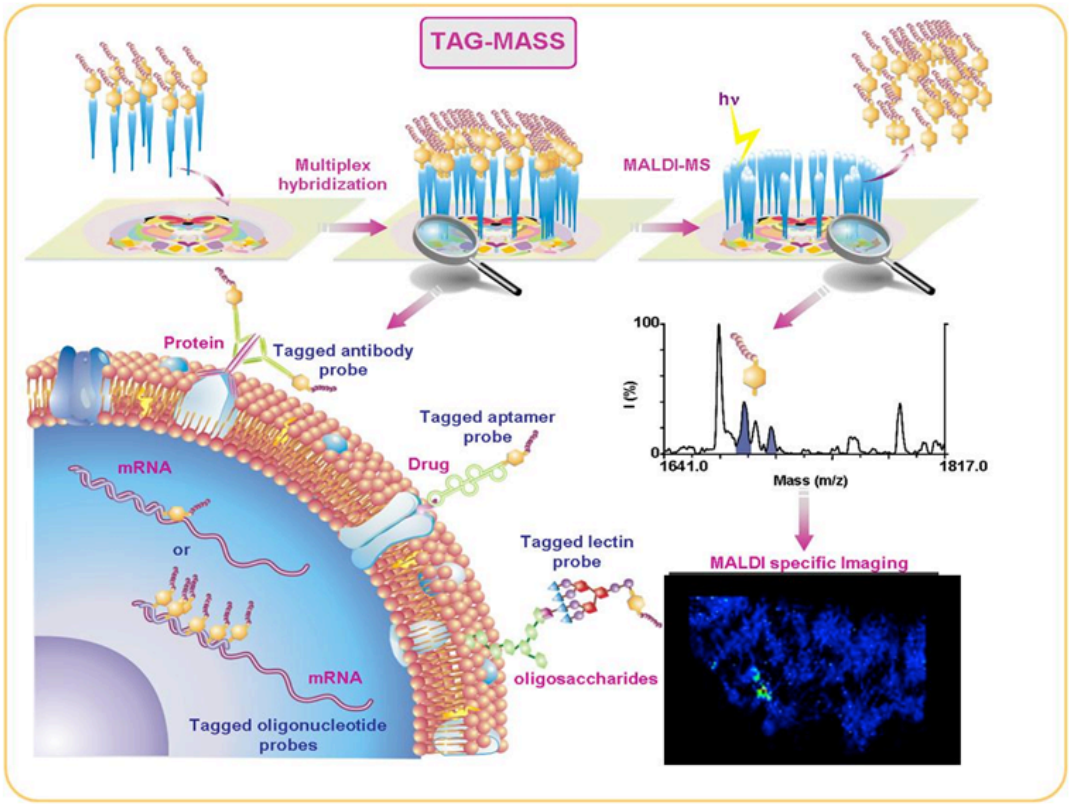

Figure 59 Workflow of the multiplex-specific MALDI MSI (Tag-Mass) method.

Workflow of the multiplex-specific MALDI MSI (Tag-Mass) method using either a tagged primer at the 5' end, tagged riboprobes containing tagged-dUTP, a tagged-antibody to study the peptidome and proteome, a tagged lectin to study the glycome, or a tagged aptamer for drug or metabolite targeting. The figure represents a molecular image of mannose and glucose in ovarian cancer using tagged-lectin (concavalin A type IV). The mass spectrum in the inset indicates the detection of the PC-peptide couple following the on-tissue laser shots. The procedure for the synthesis of these different targets is as follows: Photocleavable tagged oligonucleotide. The peptide was synthesized using a Symphony system (Protein Technologies, Inc.) and purified on a Delta-Pak C18, 15 µm, 100 Å column (Waters). The oligonucleotide was synthesized from the 3' end to the 5' end using an Expedite instrument (Applied BioSystem). The amine functional group with the photocleavable linker was added to the 5' region before cleavage and deprotection. These steps were performed using a 28% NH_4OH solution over 24 h in the dark. The amino oligonucleotide was then purified on a Delta-Pak C18, 15 µm, 300 Å column (Waters). The amino moiety of the oligonucleotide was coupled to a heterobifunctional reagent comprising a maleimide moiety. The maleimido oligonucleotide was solubilized in water and added to 1.2 equivalents of peptide in solution. The mixture was stirred for 16 h. The oligo-peptide conjugate was then purified on a Delta-Pak C18, 15 µm, 300 Å column (Waters) and characterized using MALDI-MS.

Photocleavable tagged antibody. The peptides were custom-made by Eurogentec S.A. using solid-phase peptide synthesis (SPPS) on a 0.25 mmol scale using Fmoc (9-fluorenylmethyloxycarbonyl amino-terminal protection) standard synthesis protocols (4 equiv. of Fmoc-AA) with double-coupling reactions (two reactions for 40 min each) using TBTU/NMM, which is used as an activator on a Symphony synthesizer (Rainin Instrument Co., Woburn, MA).

The photocleavable linker (4 equiv.) was introduced manually using DIPCDI/DIPEA (2 h) as an activator. The product was purified using RP-HPLC on a Waters (Milford, MA) Delta-Pak C18 [15 μm, 100 Å, 25 mm × 100 mm] column using a Waters liquid chromatography system consisting of a Model 600 solvent delivery pump, a Rheodine injector and an automated gradient controller (Solvent A, H_2O/0.125% TFA; Solvent B, CH_3CN/0.1% TFA; Gradients, 5-15% to 30-60% B over 20 min). The products were detected using a Model M2487 variable wavelength UV detector connected to the Waters Millennium software control unit. Quality control was performed using an analytical RP-HPLC system with a Waters Delta-Pak C18 [5 μm, 100 Å, 150 mm 3.9 mm] column (Solvent A, H_2O/0.125% TFA; Solvent B, CH_3CN/0.1% TFA; Gradient, 100% A to 60% B over 20 min) using a Waters Alliance 2690 Separation Module equipped with a Waters 996 Photodiode Array Detector and a MALDI-TOF MS. The antibody was functionalized with the photolinker-derivatized peptide A as follows: a solution of 0.5 mg of MBS in 300 μL of DMF was added to a solution of 4 mg of goat anti-rabbit IgG in 2 mL of PBS and mixed for 30 min. The solution was then desalted on a PD 10 column using 50 mM phosphate buffer at pH 6. To this desalted activated IgG, a solution of 1 mg of the photocleavable-derivatized peptide in 300 μL of DMF and 1 mL of PBS was added and stirred for 3 h at room temperature. The reaction mixture was then dialyzed overnight against PBS (membrane cutoff 12-14 000).

Synthesis of dUTP-peptide conjugates with a photocleavable linker. To prepare this triphosphate, an Fmoc-protected CPG resin was required. The succinylate was prepared from GT115A (100 mg). The sample was relatively pure but contained a small amount (by TLC) of a higher mobility nontritylated compound. Because it was not possible to purify the succinate, the reaction was modified slightly. A 1.5 equiv. aliquot was used because the exact purity of the product was undetermined. Based on a comparison of the intensity of the components on a TLC plate (visualized by UV irradiation at 254 nm) and the intensity of the DMT cation upon treatment with HCl fumes, it was concluded that the reaction did not proceed to completion (the completion was more than 50% as determined by TLC). Since the nonsuccinylated product would not react, the this mixture. The resin was prepared, but the loading was very low (5.4 μmol g^{-1}, 180 mg). The resin was detritylated using 2% TCA/DCM and washed with DCM until the DMT cation was completely removed. The resin was then dried (under argon) and soaked in 1:3 pyr/DMF (0.4 mL) for 5 min before a 0.1 M solution of Eckstein's reagent in dioxane was added (0.1 mL). The reaction was allowed to stand for 15 min. The resin was then washed (dioxane, MeCN) and dried (under argon). The resin was again soaked in a solution of 0.5 M bis(tributylammonium)pyrophosphate in anhydrous DMF and tri-*n*-butylamine for 20 min, and the resin was then washed (DMF, MeCN) and dried (under argon). The product was oxidized (iodine/water/pyridine/THF for 30 min), washed (MeCN) and dried (under argon). The Fmoc protecting group was removed (20% piperidine/DMF, 0.5 mL, 20 min), and the resin was washed thoroughly (DMF, MeCN) and dried (under argon). The resin was then washed with DCI, after which a solution of DCI/photolabile amino linker CEP (1:1, 0.5

mL) was added, and the reaction was allowed to stand for 20 min. The solution was removed, and the resin was washed (MeCN) and dried (under argon). A mixture of cap A/cap B (1:1, 0.5 mL) was added, and the resin was soaked for 5 min before removing the capping reagents and washing and drying the resin as described above. The product was oxidized (I_2/THF/pyr/H_2O, 5 min), and the resin was washed and dried as described above. The product was then cleaved from the resin with cNH_4OH at room temperature for 30 min and purified using anion exchange HPLC on a Dionex NucleoPac100 HPLC column with the following solvent system: Buffer A, 0.1 M NH_4Cl with 10% acetonitrile; Buffer B, 1 M NH_4Cl with 10% acetonitrile; flow rate 2.5 mL/min using 6Triphos.mth. This purification yielded 3 fractions (A, 7 min; B, 7.9 min; and C, 10.3 min). All 3 fractions were lyophilized overnight before being desalted by reverse-phase (RP) HPLC using the following solvents: Buffer A, water; Buffer B, acetonitrile; flow rate 4 mL/min. The 3 fractions were again lyophilized overnight before being suspended in 200 µL of water. An MS analysis indicated that CMM661A pk 1 was definitely not the desired triphosphate, but either CMM661 pk 2 or 3 might be the desired product (both exhibited very similar MS profiles). CMM662A was formed from CMM661A pk 2, and CMM663A was formed from CMM661A pk 3. Both samples were then used in the subsequent reaction. A bicarbonate buffer (10 µL) and the maleimide NHS ester (50 µL) were added to each sample, and the reactions were agitated overnight. The samples were diluted with milliQ water (500 µL) and filtered. The samples were purified by RP-HPLC (buffer A, 0.1 M TEAA; buffer B, MeCN; flow rate 4 mL/min) with MeCN50.mth, and the peptide was coupled in these fractions.

1.8. Tag-Mass MSI vs. TAM-SIM

Two types of photolinkers and reporters developed by two different teams.

Tag-Mass MSI

Our team developed the Tag-Mass concept in 2004 based on the 4-[4-[1-(Fmoc-amino)ethyl]-2-methoxy-5-nitrophenoxy]butanoic acid (photocleavable linker) coupled to a known peptide such as bradykinin (Figure 58 and Figure 59). Tag-Mass can also be used for semi-quantification under multiplex conditions if a reporter presenting the same physicochemical properties, i.e., the same analytical behavior, is used. For example, isotopically labeled reporters, such as differentially deuterated peptides, can be used. This concept can be extended by seeking alternate methods of releasing the reporter moiety, e.g. chemically induced release or prompt fragmentation pathways (i.e., before the end of the delay time period). The Tag-Mass concept was successful at detecting high-mass membrane proteins such as carboxypeptidase D (Figure 59), ovarian biomarkers in ovarian cancer in multiplex (Franck et al. 2009b; El Ayed et al. 2010) and intracellular enzymes (cathepsins-cystatins) in leech immune cells (Stauber et al. 2010). Such a photocleavable linker was used to develop tagged primers that can be used in PCR (Lemaire et al. 2007c). A second generation of tagged oligonucleotides has been generated and has allowed for the synthesis of modified uracil nucleotides (tagged-UTP) that can be easily used in PCR or for riboprobe synthesis. This tagged-UTP requires a specific synthesis to keep both the 3' and 5' termini of the nucleotide bases free. Thus, the modified nucleotide can be used during the probe amplification process. Previous experiments using modified primers, which were directly modified by the addition of a photocleavable-reporter system, were used to detect proenkephalin expression in rat brains (Figure 59) (Lemaire et al. 2007c; Stauber et al. 2009; Stauber et al. 2010). This approach revealed several disadvantages, including a lack of sensitivity (only one reporter per probe), a high cost (a specific synthesis is required for each mRNA to be localized) and the inability to amplify the probe via in vitro translation (because of the blockage of one terminus of the primer by the tagging agent). The development of modified uracil nucleotides is thus a significant advance. Modified nucleotides are available for the construction of all probes; the sensitivity of the probe is increased by the incorporation of several reporters in the probe sequence (amplification of the signal), and probes can be obtained via in vitro translation. Moreover, this method can

be applied to both transcriptome and proteome molecular imaging in the same tissue section using classical MALDI-MSI. A comparison between classical MALDI-MSI and tagged-multiplex MALDI-MSI (Figure 60) reveals the complementarity of these techniques. This new development now makes it possible to track mRNA or nonsense mRNA, such as miRNA, which are normally difficult to analyze using MALDI.

1.8.1. TAM-SIM

The second reporter designed to be observable under LDI conditions, TAM-SIM, was described in 2007 (Figure 9) and is based on an N-hydroxysuccinimide (NHS) linker coupled to 2,5-dioxopyrrolidin-1-yl-3-{[3-(6-(tertbutylamino)-6-oxohex-1-ynyl)-4-methoxyphenyl) bis (4-methoxyphenyl)] methylthio} propanoate, 2,5-dioxopyrrolidin-1-yl-3-{[3-(6-(benzylamino)-6-oxohex-1-ynyl)-4-methoxyphenyl) bis (4-methoxyphenyl)] methylthio} propanoate or 2,5-dioxopyrrolidin-1-yl-3-{[3-(6-(phenylamino)-6-oxohex-1-ynyl)-4-methoxyphenyl) bis (4-methoxyphenyl)] methylthio} propanoate reporters (Thiery et al. 2007; Thiery et al. 2008). Although this latest technique may be less sensitive than using MALDI, it would increase the spatial resolution of the images (Figure 61). This method can also be extended to other ion production sources. In SIMS (Touboul et al. 2004; Brunelle and Laprevote 2009) or laser ablation inductively coupled plasma mass spectrometry (LA-ICP-MS) (Becker et al. 2007; Becker et al. 2008; Becker et al. 2009), probes bearing a monoatomic element (e.g. gold) are easily detectable. However, this monoatomic element must be detectable with good analytical sensitivity and must not be naturally present on the surface under study. For example, gold-labeled secondary antibodies are useful for imaging antigens via LA-ICP-MS at a spatial resolution below 10 µm. The ionization techniques used for this method result in significant fragmentation yields, and the reporter element appears as a fragmentation product.

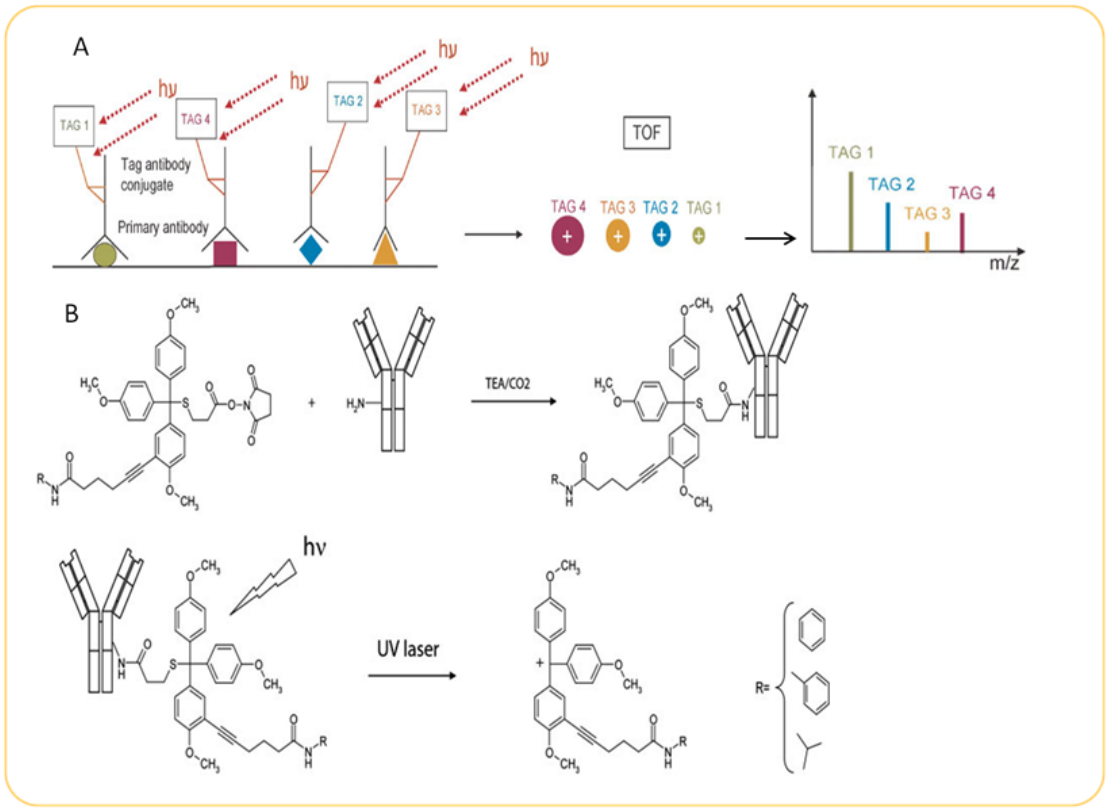

Figure 60 Workflow of multiplex TAM-SIM.

A: Four different primary antibodies were incubated with the sample to form complexes with the antigen in the tissue. Secondary antibodies, each carrying a specific mass tag, were specifically attached to each primary antibody. The slide containing the tissue section was mounted on a target plate and introduced into the source of the mass spectrometer. A pulsed UV laser cleaved the tags from their antibodies and released them into the gas phase. The m/z values of the antibodies were determined using a time-of-flight analyzer. The acquisition of the peak intensities over thousands of spots and mass spectra were used to reconstitute images at specific molecular weight values, each of which corresponds to the localization of a specific antigen. This procedure is identical to that used for Tag-Mass except for the fact that Tag-Mass uses matrix to amplify the signal to achieve better sensitivity, and Tag-Mass is a MALDI-MS procedure, whereas TAM-SIM does not use a matrix but instead uses laser desorption/ionization mass spectrometry. B: Conjugation of a mass tag to an antibody, photocleavage of the mass tag-conjugated antibody, and laser desorption. The tagging reagent contains an NHS-ester as the reactive group for covalent attachment to the primary amine groups of an antibody. In the mass spectrometer, the trityl groups absorb UV light, resulting in the cleavage of the C–S bond, creation of a stable carbocation and release of the tag.

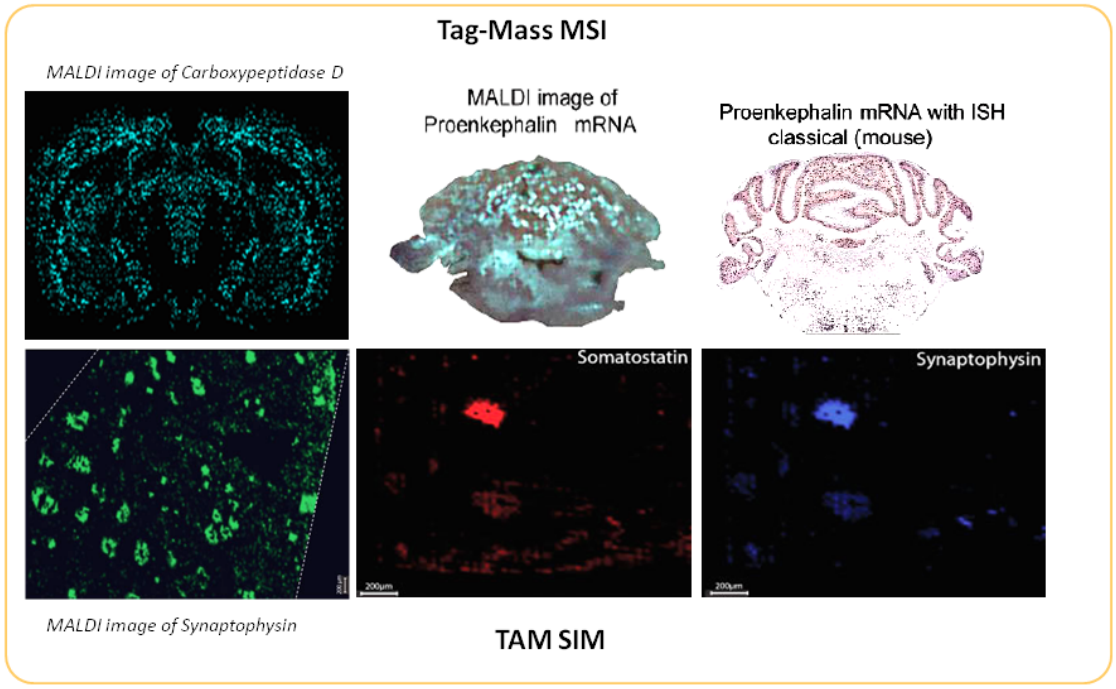

Figure 61 Image comparison between Tag-Mass and TAM-SIM.

The molecular images presented here that were obtained using Tag-Mass incorporated both the relevant tagged antibody and tagged dUTP. One image corresponds to the molecular image obtained using a tagged antibody. A molecular image of a 160-kDa membrane protein corresponding to the carboxypeptidase D localized in the rat brain is presented in A. B and C correspond to the transcriptome of the proenkephalin in the rat brain using either PC-tagged dUTP or deoxygenin dUTP in a mouse brain obtained from the brain atlas. A similar localization is observed in the two pictures. D corresponds to a TAM-SIM image of cells that were immunoreacted with a polyclonal anti-synaptophysin antibody in a healthy human pancreas using a monoclonal rabbit anti-synaptophysin conjugated with the tag, which was detected at 498 m/z. The false-colored green areas in the section indicate the presence of the tag, thus indicating synaptophysin-positive cells. E & F correspond to images of cells that were immunoreacted with a monoclonal rabbit anti-human somatostatin antibody (E) or a multiplex of 3 antibodies (anti-calcitonin, anti-somatostatin and anti-synaptophysin) (F) in the Islets of Langerhans using TAM-SIM technology.

1.9. Tag-Mass MSI vs. LA-ICP-MS

Gold clusters can be detected using LA-ICP-MS. Compared with single atoms, metal clusters increase the sensitivity based on the number of metal atoms in the cluster. Thus, gold cluster-labeled antibodies similar to those used in electronic microscopy immunogold technology (Molinari et al. 1984; He et al. 2001) can also be used in LA-ICP-MS (Becker et al. 2009; Becker et al. 2010) (Figure 11). This method is suitable for any protein presenting an epitope that is recognized by an available primary antibody. The applications of this technique include transgenic mouse models of Alzheimer's disease (Hutchinson et al. 2005) and cancer (Seuma et al. 2008). Multiplex analyses have also been performed (Seuma et al. 2008). In fact, the distribution of several breast cancer-associated proteins (Her 2, CK 7, and MUC 1) has been studied using multiple line rastering of tissue sections and the detection of relevant lanthanide-tagged antibodies bound to the tissue (Giesen et al. 2011). Compared with optical microscopy, the LA technique offers extremely high sensitivity and sufficiently good resolution to make fine scale feature mapping at the cellular level possible (Seuma et al. 2008). The size of the laser spot is 200 µm in LA-ICP-MS (Becker et al. 2009) and 20 µm (corresponding to the size of a cell) in MALDI-MS and LDI-MS (Thiery et al. 2008) (Figure 62).

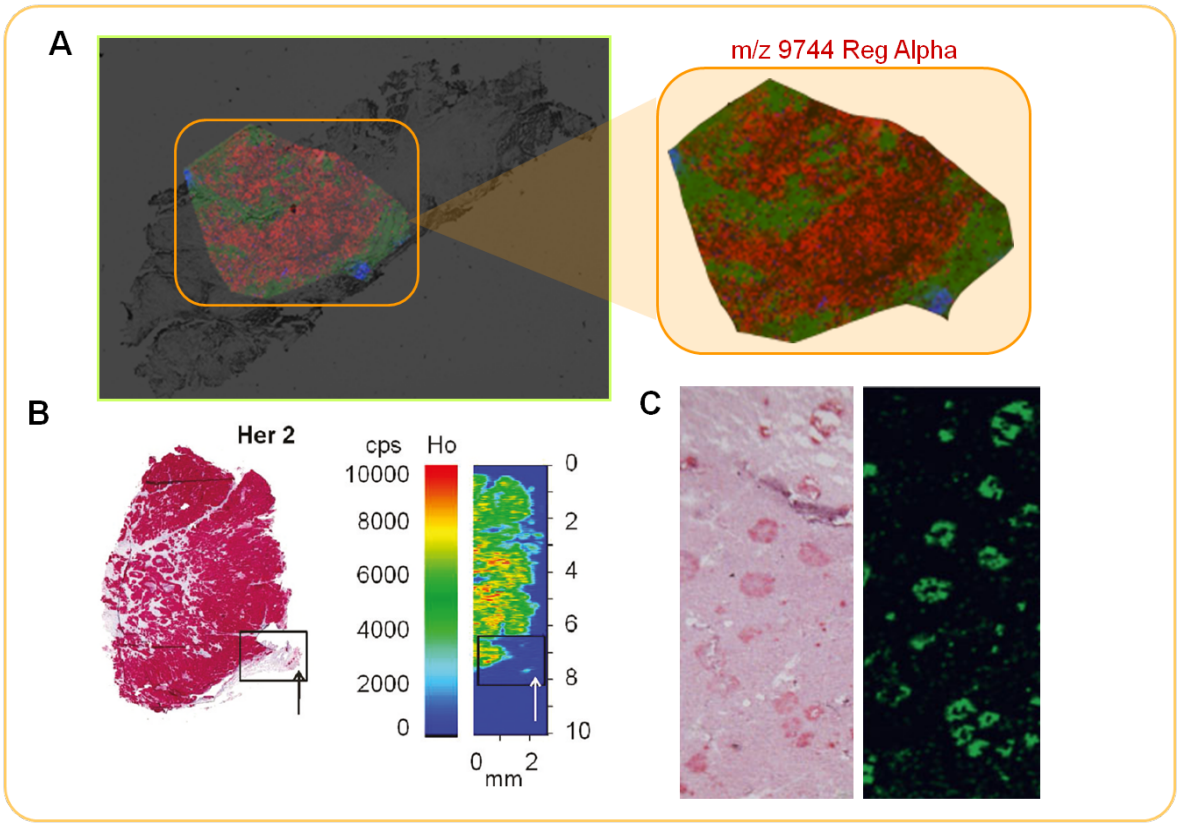

Figure 62 Comparison between MALDI-MSI, Tag-Mass imaging and LA-ICP-MSI.

A. A molecular image obtained using MALDI MSI of a specific biomarker detected in ovarian cancer, the C-terminal fragment of the immunoprotease activator PA28 alpha. The red color (a) corresponds to the ion at m/z 9744 in the tumor biopsy. The inset (b) corresponds to the detection of this biomarker at m/z 9744 using Tag-Mass MSI with an antibody directed against this biomarker in ovarian cancer (green color). (c) A comparison between Tag-Mass MSI and HES staining in a zoomed region. (d) HES staining of the ovarian cancer biopsy section. B. Immunohistochemical staining of 3 µm breast cancer tissue sections, which are positive for Her2 (scale bar, 2 mm), using a holmium-labeled antibody and analyzed using LA-ICPMS. Laser spot size, 200 µm; scan speed, 150 µm s^{-1}; repetition rate, 10 Hz; laser energy, 35%.

1.10.Discussion

Figure 62 shows that the three technologies discussed above are complementary. LA-ICP-MS provides an overview of the localization of a specific target, whereas MALDI-MSI and LDI-MSI provide localization information at the cellular level. Tag-Mass or TAM-SIM images can be clearly correlated with histological staining. The difference between these techniques is in the level of the signal intensity and the multiplex ability. Significantly, the Tag-Mass signal is higher than that of TAM-SIM due to the greater sensitivity of the matrix-assisted ionization. In fact, Tag-Mass can be used to track low-abundance proteins or to investigate some proteins involved in biological processes or mechanisms. Moreover, Tag-Mass technology presents the ability to perform highly multiplexed studies due to its ability to incorporate a variety of tag-like peptides or inorganic compounds (e.g., an 8 poly (amidoamine) dendrimer with 1024 amino groups (Yang et al. 2012)). Conversely, TAM-SIM multiplexing is limited to the rare monoatomic elements that are available. MALDI matrices and coumarins can also be used with the Tag-Mass method. Cellular localization can now be achieved using Tag-Mass as a result of the novel development by Spengler and co-workers of the SMALDI approach (Römpp et al. 2010). Laser spots smaller than 5 µm can been achieved, and the use of this technology with Tag-Mass MSI will provide access to minor proteins with a very high spatial resolution and a high accuracy at the single cell level (Figure 62). Another advantage of the Tag-Mass technology is the possibility to change the linker type according to the nature of the target under investigation. In fact, tagged deoxy-nucleotides can be used in PCR or qPCR for transcriptomics, antibodies can be used to detect antigens, lectins can be used for glycomics, aptamers can be used to detect drugs, ligands can be used to detect receptors and enzyme substrates can be used for enzyme tracking, as recently demonstrated by Caprioli and colleagues (Yang et al.). Clear results have already been obtained for transcriptomics, glycomics and the detection of antibodies using the Tag-Mass technology (Lemaire 2005; Fournier 2006; Stauber 2006; Lemaire et al. 2007b; Lemaire et al. 2007c; Franck et al. 2009b; Stauber et al. 2009; El Ayed et al. 2010; Stauber et al. 2010). An on-tissue microarray can be performed to simultaneously obtain molecular information. Targeted-MSI revolutionized the pharmacological domain with the introduction of whole-body MSI, which makes on-tissue target quantification possible. Targeted MSI can also be used to complement MALDI-MSI,

especially for clinical research. Figure 62 shows a good example of this complementarity. Using a potential ovarian cancer biomarker, the C-terminal fragment of the activator of the immunoproteasome PA28 alpha, it is possible to detect the protein and the mRNA encoding this protein in the same tissue section. This result reveals that the level of transcription is related to the abundance of the protein fragment. These data reflect the fact that cross-validation between the transcriptome and the proteome can be performed on the same tissue. Thus, this novel technology associated with classical IHC offers the ability to obtain a quick answer and a better molecular diagnosis for clinical surgery. Research using click chemistry to develop a novel generation of Tag-MASS reporters and linkers associated with novel signal amplification technology is now in progress. Moreover, this technology can also be applied to clinical diagnosis using enzyme-linked immunosorbent assays (ELISA) or PCR for biomarker quantification (Lemaire et al. 2007c; Stauber et al. 2009; Stauber et al. 2010). Several companies have recently developed their own "Tag-Mass" technology, such as the MassCode PCR available from Agilent or the isobaric TNT mass tags available from Trillion. This newly developed technology will soon be available in laboratories and will likely have significant impacts on the diagnosis and prognosis of diseases and on patient compliance.

1.11.References

Altelaar MAF, Taban IM, McDonnell LA, Verhaert PDEM, De Lange RPJ, Adanc RAH, Mooid WJ, Heeren RMA, S.R. P. (2007). "High-resolution MALDI imaging mass spectrometry allows localization of peptide distributions at cellular length scales in pituitary tissue sections." Int J Mass Spectrom **260**: 203-211.

Baluya DL, Garrett TJ, Yost RA. (2007). "Automated MALDI Matrix Deposition Method with Inkjet Printing for Imaging Mass Spectrometry." Anal Chem(79(17)): 6862-6867.

Becker JS, Zoriy MV, Dobrowolska J, Matucsh A. (2007). "Imaging mass spectrometry in biological tissues by laser ablation inductively coupled plasma mass spectrometry." Eur J Mass Spectrom (Chichester, Eng) **13**(1): 1-6.

Becker JS, Dobrowolska J, Zoriy M, Matusch A. (2008). "Imaging of uranium on rat brain sections using laser ablation inductively coupled plasma mass spectrometry: a new tool for the study of critical substructures affined to heavy metals in tissues." Rapid Commun Mass Spectrom **22**(18): 2768-2772.

Becker JS, Zoriy M, Matusch A, Wu B, Salber D, Palm C. (2009). "Bioimaging of metals by laser ablation inductively coupled plasma mass spectrometry (LA-ICP-MS)." Mass Spectrom Rev **29(1)** 156-175.

Becker JS, Matusch A, Palm C, Salber D, Morton KA. (2010). "Bioimaging of metals in brain tissue by laser ablation inductively coupled plasma mass spectrometry (LA-ICP-MS) and metallomics." Metallomics **2**(2): 104-111.

Beckstead JH. (1994). "A simple technique for preservation of fixation-sensitive antigens in paraffin-embedded tissues." J Histochem Cytochem **42**(8): 1127-1134.
Bonnel D, Legouffe R, Willand N, Baulard A, Hamm G, Deprez B, Stauber J. (2011a). "MALDI imaging techniques dedicated to drug-distribution studies." Bioanalysis **3**(12): 1399-1406.
Bonnel D, Longuespee R, Franck J, Roudbaraki M, Gosset P, Day R, Salzet M, Fournier I. (2011b). "Multivariate analyses for biomarkers hunting and validation through on-tissue bottom-up or in-source decay in MALDI-MSI: application to prostate cancer." Anal Bioanal Chem **401**(1): 149-165.
Bouschen W, Schulz O, Eikel D, Spengler B. (2010). "Matrix vapor deposition/recrystallization and dedicated spray preparation for high-resolution scanning microprobe matrix-assisted laser desorption/ionization imaging mass spectrometry (SMALDI-MS) of tissue and single cells." Rapid Commun Mass Spectrom **24**(3): 355-364.
Brocke T, Bootsmann MT, Tews M, Wunsch B, Pfannkuche D, Heyn C, Hansen W, Heitmann D, Schuller C. (2003). "Spectroscopy of few-electron collective excitations in charge-tunable artificial atoms." Phys Rev Lett **91**(25): 257401.
Brunelle A, Laprevote O. (2009). "Lipid imaging with cluster time-of-flight secondary ion mass spectrometry." Anal Bioanal Chem **393**(1): 31-35.
Caprioli RM, Farmer TB, Gile J. (1997). "Molecular imaging of biological samples: localization of peptides and proteins using MALDI-TOF MS." Anal Chem **69**(23): 4751-4760.
Castaing RaS, G. (1962). "Microanalyse par emission ioinque secondaire." Microscopie **1**: 395-410.
Chan K, Lanthier P, Liu X, Sandhu JK, Stanimirovic D, Li J. (2009). "MALDI mass spectrometry imaging of gangliosides in mouse brain using ionic liquid matrix." Anal Chim Acta **639**(1-2): 57-61.
Chaurand P, Stoeckli M, Caprioli RM. (1999). "Direct profiling of proteins in biological tissue sections by MALDI mass spectrometry." Anal Chem **71**(23): 5263-5270.
Chaurand P, Caprioli RM. (2002). "Direct profiling and imaging of peptides and proteins from mammalian cells and tissue sections by mass spectrometry." Electrophoresis **23**(18): 3125-3135.
Chaurand P, Schwartz SA, Caprioli RM. (2002). "Imaging mass spectrometry: a new tool to investigate the spatial organization of peptides and proteins in mammalian tissue sections." Curr Opin Chem Biol **6**(5): 676-681.
Chaurand P, Schwartz SA, Caprioli RM. (2004). "Assessing protein patterns in disease using imaging mass spectrometry." J Proteome Res **3**(2): 245-252.
Chaurand P, Schriver KE, Caprioli RM. (2007). "Instrument design and characterization for high resolution MALDI-MS imaging of tissue sections." J Mass Spectrom **42**(4): 476-489.
Chertov O, Biragyn A, Kwak LW, Simpson JT, Boronina T, Hoang VM, Prieto DA, Conrads TP, Veenstra TD, Fisher RJ. (2004). "Organic solvent extraction of proteins and peptides from serum as an effective sample preparation for detection and identification of biomarkers by mass spectrometry." Proteomics **4**(4): 1195-1203.
Cohen SL, Chait BT. (1996). "Influence of matrix solution conditions on the MALDI-MS analysis of peptides and proteins." Anal Chem **68**(1): 31-37.
Colsch B, Woods AS. (2010). "Localization and imaging of sialylated glycosphingolipids in brain tissue sections by MALDI mass spectrometry." Glycobiology **20**(6): 661-667.

Coons AH, Creech, H.J., Jones, R.N. (1941). "Immunological properties of an antibody containing a fluorescent group." Proc. Soc. Exp. Biol. **47**: 200-202.
Curran RC, Gregory J. (1980). "Effects of fixation and processing on immunohistochemical demonstration of immunoglobulin in paraffin sections of tonsil and bone marrow." J Clin Pathol **33**(11): 1047-1057.
Debois D, Bertrand V, Quinton L, De Pauw-Gillet MC, De Pauw E. (2010). "MALDI-in source decay applied to mass spectrometry imaging: a new tool for protein identification." Anal Chem **82**(10): 4036-4045.
Deininger SO, Ebert MP, Futterer A, Gerhard M, Rocken C. (2008). "MALDI Imaging Combined with Hierarchical Clustering as a New Tool for the Interpretation of Complex Human Cancers." J Proteome Res.
Demeure K, Quinton L, Gabelica V, De Pauw E. (2007). "Rational selection of the optimum MALDI matrix for top-down proteomics by in-source decay." Anal Chem **79**(22): 8678-8685.
Demeure K, Gabelica V, De Pauw EA. (2011). "New advances in the understanding of the in-source decay fragmentation of peptides in MALDI-TOF-MS." J Am Soc Mass Spectrom **21**(11): 1906-1917.
Diao S, Zhang JF, Wang H, He ML, Lin MC, Chen Y, Kung HF. (2010). "Proteomic identification of microRNA-122a target proteins in hepatocellular carcinoma." Proteomics **10**(20): 3723-3731.
Djidja MC, Francese S, Loadman PM, Sutton CW, Scriven P, Claude E, Snel MF, Franck J, Salzet M, Clench MR. (2009). "Detergent addition to tryptic digests and ion mobility separation prior to MS/MS improves peptide yield and protein identification for in situ proteomic investigation of frozen and formalin-fixed paraffin-embedded adenocarcinoma tissue sections." Proteomics **9**(10): 2750-2763.
Dreisewerd KS, M.; Karas,M.; Hillenkamp, F. (1995). "Influence of the laser intensity and spot size on the desorption ofmolecules and ions in matrix-assisted laser desorption/ionization with a uniform beam profile." Int J Mass Spectrom **141**: 127-148.
Edwards RL, Creese AJ, Baumert M, Griffiths P, Bunch J, Cooper HJ. (2011). "Hemoglobin variant analysis via direct surface sampling of dried blood spots coupled with high-resolution mass spectrometry." Anal Chem **83**(6): 2265-2270.
El Ayed M, Bonnel D, Longuespee R, Castelier C, Franck J, Vergara D, Desmons A, Tasiemski A, Kenani A, Vinatier D, Day R, Fournier I, Salzet M. (2010). "MALDI imaging mass spectrometry in ovarian cancer for tracking, identifying, and validating biomarkers." Med Sci Monit **16**(8): BR233-245.
Elsner M, Rauser S, Maier S, Schone C, Balluff B, Meding S, Jung G, Nipp M, Sarioglu H, Maccarrone G, Aichler M, Feuchtinger A, Langer R, Jutting U, Feith M, Kuster B, Ueffing M, Zitzelsberger H, Hofler H, Walch A. (2012). "MALDI imaging mass spectrometry reveals COX7A2, TAGLN2 and S100-A10 as novel prognostic markers in Barrett's adenocarcinoma." J Proteomics.
Enkelmann A, Heinzelmann J, von Eggeling F, Walter M, Berndt A, Wunderlich H, Junker K. (2011). "Specific protein and miRNA patterns characterise tumour-associated fibroblasts in bladder cancer." J Cancer Res Clin Oncol **137**(5): 751-759.
Ferro M, Seigneurin-Berny D, Rolland N, Chapel A, Salvi D, Garin J, Joyard J. (2000). "Organic solvent extraction as a versatile procedure to identify hydrophobic chloroplast membrane proteins." Electrophoresis **21**(16): 3517-3526.

Fournier I, Tabet JC, Bolbach G. (2002). "Irradiation effects in MALDI and surface modifications Part I : Sinapinic acid monocristals." Int JMS **219**: 1515-1523.
Fournier I, Marinach C, Tabet JC, Bolbach G. (2003). "Irradiation effects in MALDI, ablation, ion production, and surface modifications. Part II. 2,5-dihydroxybenzoic acid monocrystals." J Am Soc Mass Spectrom **14**(8): 893-899.
Fournier I, Lemaire, R., Wisztorski, M., Stauber, J., Jardin-Mathè, O., Van Camp, C., Deschamps, M., Proess, G., Day, R., Salzet, M. (2006). "New insight in sample preparation for MALDI imaging and new developments to approach specific MALDI imaging of the transcriptome." Proceedings of 54rd ASMS conference on Mass Spectrometry, Seattle, Wastington, May 30-June 2.
Fournier I, Thomy, V., Salzet, M., Wisztorski, M., Verplanck, N. (2007). "MASKS USEFUL FOR MALDI IMAGING OF TISSUE SECTIONS, PROCESSES OF MANUFACTURE AND USES THEREOF." PCT/EP2007/054253.
Franck J, Arafah K, Barnes A, Wisztorski M, Salzet M, Fournier I. (2009a). "Improving tissue preparation for matrix-assisted laser desorption ionization mass spectrometry imaging. Part 1: using microspotting." Anal Chem **81**(19): 8193-8202.
Franck J, Arafah K, Elayed M, Bonnel D, Vergara D, Jacquet A, Vinatier D, Wisztorski M, Day R, Fournier I, Salzet M. (2009b). "MALDI imaging mass spectrometry: state of the art technology in clinical proteomics." Mol Cell Proteomics **8**(9): 2023-2033.
Franck J, El Ayed M, Wisztorski M, Salzet M, Fournier I. (2009c). "On-tissue N-terminal peptide derivatizations for enhancing protein identification in MALDI mass spectrometric imaging strategies." Anal Chem **81**(20): 8305-8317.
Franck J, Longuespee R, Wisztorski M, Van Remoortere A, Van Zeijl R, Deelder A, Salzet M, McDonnell L, Fournier I. (2010). "MALDI mass spectrometry imaging of proteins exceeding 30,000 daltons." Med Sci Monit **16**(9): BR293-299.
Furuya T, Ikemoto K, Kawauchi S, Oga A, Tsunoda S, Hirano T, Sasaki K. (2004). "A novel technology allowing immunohistochemical staining of a tissue section with 50 different antibodies in a single experiment." J Histochem Cytochem **52**(2): 205-210.
Gabe M. (1964). "[Histochemistry of Secretion Products.]." Biol Med (Paris) **53**: 641-674.
Gabe M, Saint Girons H. (1967). "[Histological data on the tegument and cephalic epidermoid glands of Lepidosauria]." Acta Anat (Basel) **67**(4): 571-594.
Gabe M. (1969). "[Histological data on the endocrine pancreas of Protopterus annectens Owen]." Arch Anat Microsc Morphol Exp **58**(1): 21-40.
Gabe M. (1972). "[Relation between the abundance of glycol radicals and some tinctorial affinities of the product of hypothalamic neurosecretion]." C R Acad Sci Hebd Seances Acad Sci D **274**(4): 549-551.
Garrett TJP-C, M.C.;Kovtoun, V.;Bui, H.; Izgarian, N.; Stafford, G.; Yost, R.A. (2007). "Imaging of small molecules in tissue sections with a new intermediate-pressure MALDI linear ion trap mass spectrometer." Int J Mass Spectrom **260**: 166-176.
Giesen C, Mairinger T, Khoury L, Waentig L, Jakubowski N, Panne U. (2011). "Multiplexed immunohistochemical detection of tumor markers in breast cancer tissue using laser ablation inductively coupled plasma mass spectrometry." Anal Chem **83**(21): 8177-8183.
Grey AC, Chaurand P, Caprioli RM, Schey KL. (2009). "MALDI Imaging Mass Spectrometry of Integral Membrane Proteins from Ocular Lens and Retinal Tissue." J Proteome Res **8**(7): 3278-3283.

Groseclose MR, Andersson M, Hardesty WM, Caprioli RM. (2007). "Identification of proteins directly from tissue: in situ tryptic digestions coupled with imaging mass spectrometry." J Mass Spectrom **42**(2): 254-262.
Groseclose MR, Massion PP, Chaurand P, Caprioli RM. (2008). "High-throughput proteomic analysis of formalin-fixed paraffin-embedded tissue microarrays using MALDI imaging mass spectrometry." Proteomics **8**(18): 3715-3724.
Gustafsson JO, Oehler MK, McColl SR, Hoffmann P. (2010). "Citric acid antigen retrieval (CAAR) for tryptic peptide imaging directly on archived formalin-fixed paraffin-embedded tissue." J Proteome Res **9**(9): 4315-4328.
Hahner S, Olejnik J, Ludemann HC, Krzymanska-Olejnik E, Hillenkamp F, Rothschild KJ. (1999). "Matrix-assisted laser desorption/ionization mass spectrometry of DNA using photocleavable biotin." Biomol Eng **16**(1-4): 127-133.
Hankin JA, Barkley RM, Murphy RC. (2007). "Sublimation as a Method of Matrix Application for Mass Spectrometric Imaging." J Am Soc Mass Spectrom.
Hayashi H, Kimura N, Yamaguchi H, Hasegawa K, Yokoseki T, Shibata M, Yamamoto N, Michikawa M, Yoshikawa Y, Terao K, Matsuzaki K, Lemere CA, Selkoe DJ, Naiki H, Yanagisawa K. (2004). "A seed for Alzheimer amyloid in the brain." J Neurosci **24**(20): 4894-4902.
He PM, Zhang RX, Zhang DB, Zhao JH, Liang WQ. (2001). "[Immunogold localization of ribulose-1,5-bisphosphate carborylsae/oxygenase in chloroplasts of Chlorella]." Shi Yan Sheng Wu Xue Bao **34**(1): 18-23.
Holle A, Haase A, Kayser M, Hohndorf J. (2006). "Optimizing UV laser focus profiles for improved MALDI performance." J Mass Spectrom **41**(6): 705-716.
Hsieh Y, Chen J, Korfmacher WA. (2007). "Mapping pharmaceuticals in tissues using MALDI imaging mass spectrometry." J Pharmacol Toxicol Methods **55**(2): 193-200.
Hutchinson RW, Cox AG, McLeod CW, Marshall PS, Harper A, Dawson EL, Howlett DR. (2005). "Imaging and spatial distribution of beta-amyloid peptide and metal ions in Alzheimer's plaques by laser ablation-inductively coupled plasma-mass spectrometry." Anal Biochem **346**(2): 225-233.
Ino H. (2004). "Application of antigen retrieval by heating for double-label fluorescent immunohistochemistry with identical species-derived primary antibodies." J Histochem Cytochem **52**(9): 1209-1217.
Jackson SN, Wang HY, Woods AS. (2005a). "Direct profiling of lipid distribution in brain tissue using MALDI-TOFMS." Anal Chem **77**(14): 4523-4527.
Jackson SN, Wang HY, Woods AS. (2005b). "In situ structural characterization of phosphatidylcholines in brain tissue using MALDI-MS/MS." J Am Soc Mass Spectrom **16**(12): 2052-2056.
Jackson SN, Wang HY, Woods AS, Ugarov M, Egan T, Schultz JA. (2005c). "Direct tissue analysis of phospholipids in rat brain using MALDI-TOFMS and MALDI-ion mobility-TOFMS." J Am Soc Mass Spectrom **16**(2): 133-138.
Jimenez CR, van Veelen PA, Li KW, Wildering WC, Geraerts WP, Tjaden UR, van der Greef J. (1994). "Neuropeptide expression and processing as revealed by direct matrix-assisted laser desorption ionization mass spectrometry of single neurons." J Neurochem **62**(1): 404-407.
Jimenez CR, Li KW, Dreisewerd K, Mansvelder HD, Brussaard AB, Reinhold BB, Van der Schors RC, Karas M, Hillenkamp F, Burbach JP, Costello CE, Geraerts WP. (1997). "Pattern changes of pituitary peptides in rat after salt-loading as detected by means of

direct, semiquantitative mass spectrometric profiling." Proc Natl Acad Sci U S A **94**(17): 9481-9486.
Jimenez CR, Li KW, Dreisewerd K, Spijker S, Kingston R, Bateman RH, Burlingame AL, Smit AB, van Minnen J, Geraerts WP. (1998). "Direct mass spectrometric peptide profiling and sequencing of single neurons reveals differential peptide patterns in a small neuronal network." Biochemistry **37**(7): 2070-2076.
Jimenez CR, ter Maat A, Pieneman A, Burlingame AL, Smit AB, Li KW. (2004). "Spatio-temporal dynamics of the egg-laying-inducing peptides during an egg-laying cycle: a semiquantitative matrix-assisted laser desorption/ionization mass spectrometry approach." J Neurochem **89**(4): 865-875.
Jimenez CR, Spijker S, de Schipper S, Lodder JC, Janse CK, Geraerts WP, van Minnen J, Syed NI, Burlingame AL, Smit AB, Li K. (2006). "Peptidomics of a single identified neuron reveals diversity of multiple neuropeptides with convergent actions on cellular excitability." J Neurosci **26**(2): 518-529.
Jurchen JC, Rubakhin SS, Sweedler JV. (2005). "MALDI-MS imaging of features smaller than the size of the laser beam." J Am Soc Mass Spectrom **16**(10): 1654-1659.
Karas M, Kruger R. (2003). "Ion formation in MALDI: the cluster ionization mechanism." Chem Rev **103**(2): 427-440.
Kertesz V, Van Berkel GJ. (2010a). "Liquid microjunction surface sampling coupled with high-pressure liquid chromatography-electrospray ionization-mass spectrometry for analysis of drugs and metabolites in whole-body thin tissue sections." Anal Chem **82**(14): 5917-5921.
Kertesz V, Van Berkel GJ. (2010b). "Fully automated liquid extraction-based surface sampling and ionization using a chip-based robotic nanoelectrospray platform." J Mass Spectrom **45**(3): 252-260.
Kieman JA. (2000). "Formaldehyde, formalin, paraformaldehyde and glutaraldehyde: what they are and what they do " Microscopy Today(1): 8-14.
Klerk LA, Broersen A, Fletcher IW, van Liere R, Heeren RMA. (2007). "Extended data analysis strategies for high resolution imaging MS: New
methods to deal with extremely large image hyperspectral datasets." Int J Mass Spectrom **260**: 222-236.
Knochenmuss R, Zenobi R. (2003). "MALDI ionization: the role of in-plume processes." Chem Rev **103**(2): 441-452.
Lagarrigue M, Becker M, Lavigne R, Deininger SO, Walch A, Aubry F, Suckau D, Pineau C. (2011). "Revisiting rat spermatogenesis with MALDI imaging at 20-microm resolution." Mol Cell Proteomics **10**(3): M110 005991.
Leinweber BD, Tsaprailis G, Monks TJ, Lau SS. (2009). "Improved MALDI-TOF imaging yields increased protein signals at high molecular mass." J Am Soc Mass Spectrom **20**(1): 89-95.
Lemaire R, Tabet JC, Ducoroy P, Hendra JB, Salzet M, Fournier I. (2006a). "Solid ionic matrixes for direct tissue analysis and MALDI imaging." Anal Chem **78**(3): 809-819.
Lemaire R, Wisztorski M, Desmons A, Tabet JC, Day R, Salzet M, Fournier I. (2006b). "MALDI-MS direct tissue analysis of proteins: Improving signal sensitivity using organic treatments." Anal Chem **78**(20): 7145-7153.
Lemaire R, Desmons A, Tabet JC, Day R, Salzet M, Fournier I. (2007a). "Direct analysis and MALDI imaging of formalin-fixed, paraffin-embedded tissue sections." J Proteome Res **6**(4): 1295-1305.

Lemaire R, Menguellet SA, Stauber J, Marchaudon V, Lucot JP, Collinet P, Farine MO, Vinatier D, Day R, Ducoroy P, Salzet M, Fournier I. (2007b). "Specific MALDI imaging and profiling for biomarker hunting and validation: fragment of the 11S proteasome activator complex, Reg alpha fragment, is a new potential ovary cancer biomarker." J Proteome Res **6**(11): 4127-4134.
Lemaire R, Stauber J, Wisztorski M, Van Camp C, Desmons A, Deschamps M, Proess G, Rudlof I, Woods AS, Day R, Salzet M, Fournier I. (2007c). "Tag-mass: specific molecular imaging of transcriptome and proteome by mass spectrometry based on photocleavable tag." J Proteome Res **6**(6): 2057-2067.
Lemaire R, Fournier, I., Salzet, M., Deschamps, M.,Tabet, J.C.,Proess, G.,Rudloff, P., Lemaitre, C. (2005). "Use of Conjugates with linkers cleavable by photodissociation or fragmentation for mass spectromety analysis of tissue sections." US20050687848P.
Li KW, Hoek RM, Smith F, Jimenez CR, van der Schors RC, van Veelen PA, Chen S, van der Greef J, Parish DC, Benjamin PR, et al. (1994a). "Direct peptide profiling by mass spectrometry of single identified neurons reveals complex neuropeptide-processing pattern." J Biol Chem **269**(48): 30288-30292.
Li KW, Jimenez CR, Van Veelen PA, Geraerts WP. (1994b). "Processing and targeting of a molluscan egg-laying peptide prohormone as revealed by mass spectrometric peptide fingerprinting and peptide sequencing." Endocrinology **134**(4): 1812-1819.
Li KW, van Golen FA, van Minnen J, van Veelen PA, van der Greef J, Geraerts WP. (1994c). "Structural identification, neuronal synthesis, and role in male copulation of myomodulin-A of Lymnaea: a study involving direct peptide profiling of nervous tissue by mass spectrometry." Brain Res Mol Brain Res **25**(3-4): 355-358.
Li L, Moroz TP, Garden RW, Floyd PD, Weiss KR, Sweedler JV. (1998). "Mass spectrometric survey of interganglionically transported peptides in Aplysia." Peptides **19**(8): 1425-1433.
Li L, Garden RW, Romanova EV, Sweedler JV. (1999). "In situ sequencing of peptides from biological tissues and single cells using MALDI-PSD/CID analysis." Anal Chem **71**(24): 5451-5458.
Li L, Garden RW, Sweedler JV. (2000a). "Single-cell MALDI: a new tool for direct peptide profiling." Trends Biotechnol **18**(4): 151-160.
Li L, Romanova EV, Rubakhin SS, Alexeeva V, Weiss KR, Vilim FS, Sweedler JV. (2000b). "Peptide profiling of cells with multiple gene products: combining immunochemistry and MALDI mass spectrometry with on-plate microextraction." Anal Chem **72**(16): 3867-3874.
Li L, Floyd PD, Rubakhin SS, Romanova EV, Jing J, Alexeeva VY, Dembrow NC, Weiss KR, Vilim FS, Sweedler JV. (2001). "Cerebrin prohormone processing, distribution and action in Aplysia californica." J Neurochem **77**(6): 1569-1580.
Luxembourg SL, Mize TH, McDonnell LA, Heeren RM. (2004). "High-spatial resolution mass spectrometric imaging of peptide and protein distributions on a surface." Anal Chem **76**(18): 5339-5344.
Marshall P, Toteu-Djomte V, Bareille P, Perry H, Brown G, Baumert M, Biggadike K. (2011). "Correlation of skin blanching and percutaneous absorption for glucocorticoid receptor agonists by matrix-assisted laser desorption ionization mass spectrometry imaging and liquid extraction surface analysis with nanoelectrospray ionization mass spectrometry." Anal Chem **82**(18): 7787-7794.

McCombie G, Staab D, Stoeckli M, Knochenmuss R. (2005). "Spatial and spectral correlations in MALDI mass spectrometry images by clustering and multivariate analysis." Anal Chem **77**(19): 6118-6124.
McLafferty FW, Kelleher NL, Begley TP, Fridriksson EK, Zubarev RA, Horn DM. (1998). "Two-dimensional mass spectrometry of biomolecules at the subfemtomole level." Curr Opin Chem Biol **2**(5): 571-578.
Meriaux C, Franck J, Wisztorski M, Salzet M, Fournier I. (2010). "Liquid ionic matrixes for MALDI mass spectrometry imaging of lipids." J Proteomics **73**(6): 1204-1218.
Molinari A, Arancia G, Donelli G. (1984). "[Immunologic localizations in electronic microscopy]." Ann Ist Super Sanita **20**(2-3): 171-191.
Nipp M, Elsner M, Balluff B, Meding S, Sarioglu H, Ueffing M, Rauser S, Unger K, Hofler H, Walch A, Zitzelsberger H. (2012). "S100-A10, thioredoxin, and S100-A6 as biomarkers of papillary thyroid carcinoma with lymph node metastasis identified by MALDI imaging." J Mol Med (Berl) **90**(2): 163-174.
Nordhoff E, Kirpekar F, Karas M, Cramer R, Hahner S, Hillenkamp F, Kristiansen K, Roepstroff P, Lezius A. (1994). "Comparison of IR- and UV-matrix-assisted laser desorption/ionization mass spectrometry of oligodeoxynucleotides." Nucleic Acids Res **22**(13): 2460-2465.
Olejnik J, Krzymanska-Olejnik E, Rothschild KJ. (1996). "Photocleavable biotin phosphoramidite for 5'-end-labeling, affinity purification and phosphorylation of synthetic oligonucleotides." Nucleic Acids Res **24**(2): 361-366.
Olejnik J, Krzymanska-Olejnik E, Rothschild KJ. (1998a). "Photocleavable aminotag phosphoramidites for 5'-termini DNA/RNA labeling." Nucleic Acids Res **26**(15): 3572-3576.
Olejnik J, Krzymanska-Olejnik E, Rothschild KJ. (1998b). "Photocleavable affinity tags for isolation and detection of biomolecules." Methods Enzymol **291**: 135-154.
Olejnik J, Ludemann HC, Krzymanska-Olejnik E, Berkenkamp S, Hillenkamp F, Rothschild KJ. (1999). "Photocleavable peptide-DNA conjugates: synthesis and applications to DNA analysis using MALDI-MS." Nucleic Acids Res **27**(23): 4626-4631.
Petit J, Sahli F. (1975). "Cytochemical and electron-microscopic study of the paraoesophageal bodies and related nerves in Schizophyllum sabulosum (L.), Diplopoda Julidae." Cell Tissue Res **162**(3): 367-375.
Plenat F, Antunes L, Haller T, Piet-Ounnoughene M, Klein-Monhoven N, Champigneulle J, Chenal P, Bland V, Garcia-Pimenta F, Labouyrie E. (2001). "[Formaldehyde fixation in the third millennium]." Ann Pathol **21**(1): 29-47.
Plenat F, Montagne K, Weinbreck N, Corby S, Champigneulle J, Antunes L, Bonnet C, Maire C, Monhoven N. (2006). "[Molecular consequences of fixation and tissue processing: the examples of nucleic acids and proteins]." Ann Pathol **26**(1): 8-21.
Puolitaival SM, Burnum KE, Cornett DS, Caprioli RM. (2008). "Solvent-Free Matrix Dry-Coating for MALDI Imaging of Phospholipids." J Am Soc Mass Spectrom.
Raska CS, Parker CE, Huang C, Han J, Glish GL, Pope M, Borchers CH. (2002). "Pseudo-MS3 in a MALDI orthogonal quadrupole-time of flight mass spectrometer." J Am Soc Mass Spectrom **13**(9): 1034-1041.
Rauser S, Marquardt C, Balluff B, Deininger SO, Albers C, Belau E, Hartmer R, Suckau D, Specht K, Ebert MP, Schmitt M, Aubele M, Hofler H, Walch A. (2010). "Classification of HER2 receptor status in breast cancer tissues by MALDI imaging mass spectrometry." J Proteome Res **9**(4): 1854-1863.

Redeby T, Roeraade J, Emmer A. (2004). "Simple fabrication of a structured matrix-assisted laser desorption/ionization target coating for increased sensitivity in mass spectrometric analysis of membrane proteins." Rapid Commun Mass Spectrom **18**(10): 1161-1166.
Redeby T, Emmer A. (2005). "Membrane protein and peptide sample handling for MS analysis using a structured MALDI target." Anal Bioanal Chem **381**(1): 225-232.
Redeby T, Carr H, Bjork M, Emmer A. (2006). "A screening procedure for the solubilization of chloroplast membrane proteins from the marine green macroalga Ulva lactuca using RP-HPLC-MALDI-MS." Int J Biol Macromol **39**(1-3): 29-36.
Redeker V, Toullec JY, Vinh J, Rossier J, Soyez D. (1998). "Combination of peptide profiling by matrix-assisted laser desorption/ionization time-of-flight mass spectrometry and immunodetection on single glands or cells." Anal Chem **70**(9): 1805-1811.
Reiber DC, Brown RS, Weinberger S, Kenny J, Bailey J. (1998a). "Unknown peptide sequencing using matrix-assisted laser desorption/ionization and in-source decay." Anal Chem **70**(6): 1214-1222.
Reiber DC, Grover TA, Brown RS. (1998b). "Identifying proteins using matrix-assisted laser desorption/ionization in-source fragmentation data combined with database searching." Anal Chem **70**(4): 673-683.
Reyzer ML, Chaurand P, Angel PM, Caprioli RM. (2010). "Direct molecular analysis of whole-body animal tissue sections by MALDI imaging mass spectrometry." Methods Mol Biol **656**: 285-301.
Roepstorff P, Fohlman J. (1984). "Proposal for a common nomenclature for sequence ions in mass spectra of peptides." Biomed Mass Spectrom **11**(11): 601.
Römpp A, Guenther S, Schober Y, Schulz O, Takats Z, Kummer W, Spengler B. (2010). "Histology by Mass Spectrometry: Label-Free Tissue Characterization Obtained from High-Accuracy Bioanalytical Imaging." Angewandte Chemie International Edition **49**(22): 3834-3838.
Ronci M, Bonanno E, Colantoni A, Pieroni L, Di Ilio C, Spagnoli LG, Federici G, Urbani A. (2008). "Protein unlocking procedures of formalin-fixed paraffin-embedded tissues: application to MALDI-TOF imaging MS investigations." Proteomics **8**(18): 3702-3714.
Rubakhin SS, Li L, Moroz TP, Sweedler JV. (1999). "Characterization of the Aplysia californica cerebral ganglion F cluster." J Neurophysiol **81**(3): 1251-1260.
Rubakhin SS, Garden RW, Fuller RR, Sweedler JV. (2000). "Measuring the peptides in individual organelles with mass spectrometry." Nat Biotechnol **18**(2): 172-175.
Rubakhin SS, Greenough WT, Sweedler JV. (2003). "Spatial profiling with MALDI MS: distribution of neuropeptides within single neurons." Anal Chem **75**(20): 5374-5380.
Rubakhin SS, Churchill JD, Greenough WT, Sweedler JV. (2006). "Profiling signaling peptides in single mammalian cells using mass spectrometry." Anal Chem **78**(20): 7267-7272.
Schober Y, Schramm T, Spengler B, Römpp A. (2011). "Protein identification by accurate mass matrix-assisted laser desorption/ionization imaging of tryptic peptides." Rapid Commun Mass Spectrom **25**(17): 2475-2483.
Schuerenberg M, Luebbert C, Deininger SO, Ketterlinus R, Suckau D. (2007). "MALDI tissue imaging: mass spectrometric localization of biomarkers in tissue slices." Nature Methods(4).

Schwartz SA, Reyzer ML, Caprioli RM. (2003). "Direct tissue analysis using matrix-assisted laser desorption/ionization mass spectrometry: practical aspects of sample preparation." J Mass Spectrom **38**(7): 699-708.
Schwartz SA, Weil RJ, Johnson MD, Toms SA, Caprioli RM. (2004). "Protein profiling in brain tumors using mass spectrometry: feasibility of a new technique for the analysis of protein expression." Clin Cancer Res **10**(3): 981-987.
Seeley EH, Oppenheimer SR, Mi D, Chaurand P, Caprioli RM. (2008). "Enhancement of protein sensitivity for MALDI imaging mass spectrometry after chemical treatment of tissue sections." J Am Soc Mass Spectrom **19**(8): 1069-1077.
Seuma J, Bunch J, Cox A, McLeod C, Bell J, Murray C. (2008). "Combination of immunohistochemistry and laser ablation ICP mass spectrometry for imaging of cancer biomarkers." Proteomics **8**(18): 3775-3784.
Shi SR, Cote RJ, Taylor CR. (1997). "Antigen retrieval immunohistochemistry: past, present, and future." J Histochem Cytochem **45**(3): 327-343.
Shi SR, Cote RJ, Taylor CR. (2001a). "Antigen retrieval techniques: current perspectives." J Histochem Cytochem **49**(8): 931-937.
Shi SR, Cote RJ, Taylor CR. (2001b). "Antigen retrieval immunohistochemistry and molecular morphology in the year 2001." Appl Immunohistochem Mol Morphol **9**(2): 107-116.
Shi SR, Liu C, Young L, Taylor C. (2007a). "Development of an optimal antigen retrieval protocol for immunohistochemistry of retinoblastoma protein (pRB) in formalin fixed, paraffin sections based on comparison of different methods." Biotech Histochem **82**(6): 301-309.
Shi SR, Shi Y, Taylor CR. (2007b). "[Updates on antigen retrieval techniques for immunohistochemistry]." Zhonghua Bing Li Xue Za Zhi **36**(1): 7-10.
Spengler B, Hubert M, Kaufmann R. (1994). "MALDI ion imaging and biological ion imaging with a new scanning UV-laser microprobe." Proc. 42nd Annual Conf. Mass Spectrom. and Allied Topics: 1041.
Spengler B, Hubert M. (2002). "Scanning microprobe matrix-assisted laser desorption ionization (SMALDI) mass spectrometry: instrumentation for sub-micrometer resolved LDI and MALDI surface analysis." J Am Soc Mass Spectrom **13**(6): 735-748.
Stauber J, Lemaire R, Franck J, Bonnel D, Croix D, Day R, Wisztorski M, Fournier I, Salzet M. (2008). "MALDI imaging of formalin-fixed paraffin-embedded tissues: application to model animals of Parkinson disease for biomarker hunting." J Proteome Res **7**(3): 969-978.
Stauber J, El Ayed M, Wisztorski M, Day R, Fournier I, Salzet M. (2009). "Polymerase chain reaction and immunoassay--matrix assisted laser desorption mass spectrometry using tag-mass technology: new tools to break down quantification limits and multiplexes." Anal Chem **81**(22): 9512-9521.
Stauber J, Ayed ME, Wisztorski M, Salzet M, Fournier I. (2010). "Specific MALDI-MSI: Tag-Mass." Methods Mol Biol **656**: 339-361.
Stauber J, Lemaire, R., Wisztorski, M., Ait-Menguellet, S., Lucot, J.P., Vinatier, D., Desmons, A., Deschamps, M., Proess, G., Rudolf, I., Salzet, M., Fournier, I. . (2006). "New developments in MALDI imaging mass spectrometry for pathological proteomic studies; Introduction to a novel concept, the specific MALDI imaging." Mol Cell Proteomics **5**: S247-S249.

Steinbach P. (1977). "Granular cells in the connective tissue of Helix pomatia L. (gastropoda, pulmonata). Histochemistry, ultrastructure, and results of polyacrylamide electrophoretic investigations." Cell Tissue Res **181**(1): 91-103.
Stoeckli M, Farmer TB, Caprioli RM. (1999). "Automated mass spectrometry imaging with a matrix-assisted laser desorption ionization time-of-flight instrument." J Am Soc Mass Spectrom **10**(1): 67-71.
Stoeckli M, Staab D, Staufenbiel M, Wiederhold KH, Signor L. (2002). "Molecular imaging of amyloid beta peptides in mouse brain sections using mass spectrometry." Anal Biochem **311**(1): 33-39.
Taylor CR, Shi SR. (2000). "Antigen retrieval: call for a return to first principles." Appl Immunohistochem Mol Morphol **8**(3): 173-174.
Thiery G, Shchepinov MS, Southern EM, Audebourg A, Audard V, Terris B, Gut IG. (2007). "Multiplex target protein imaging in tissue sections by mass spectrometry--TAMSIM." Rapid Commun Mass Spectrom **21**(6): 823-829.
Thiery G, Anselmi E, Audebourg A, Darii E, Abarbri M, Terris B, Tabet JC, Gut IG. (2008). "Improvements of TArgeted multiplex mass spectrometry IMaging." Proteomics **8**(18): 3725-3734.
Thompson MR, Chourey K, Froelich JM, Erickson BK, Verberkmoes NC, Hettich RL. (2008). "Experimental Approach for Deep Proteome Measurements from Small-Scale Microbial Biomass Samples." Anal Chem **80**(24): 9517-9525.
Touboul D, Halgand F, Brunelle A, Kersting R, Tallarek E, Hagenhoff B, Laprevote O. (2004). "Tissue molecular ion imaging by gold cluster ion bombardment." Anal Chem **76**(6): 1550-1559.
Trimpin S. (2010). "A perspective on MALDI alternatives-total solvent-free analysis and electron transfer dissociation of highly charged ions by laserspray ionization." J Mass Spectrom **45**(5): 471-485.
Van Berkel GJ, Kertesz V, Koeplinger KA, Vavrek M, Kong AN. (2008). "Liquid microjunction surface sampling probe electrospray mass spectrometry for detection of drugs and metabolites in thin tissue sections." J Mass Spectrom **43**(4): 500-508.
Van de Plas R, Ojeda F, Dewil M, Van Den Bosch L, De Moor B, Waelkens E. (2007). "Prospective exploration of biochemical tissue composition via imaging mass spectrometry guided by principal component analysis." Pac Symp Biocomput: 458-469.
van Remoortere A, van Zeijl RJ, van den Oever N, Franck J, Longuespee R, Wisztorski M, Salzet M, Deelder AM, Fournier I, McDonnell LA. (2010). "MALDI imaging and profiling MS of higher mass proteins from tissue." J Am Soc Mass Spectrom **21**(11): 1922-1929.
Verbueken AH, Bruynseels FJ, Van Grieken RE. (1985). "Laser microprobe mass analysis: a review of applications in the life sciences." Biomed Mass Spectrom **12**(9): 438-463.
Walch A, Rauser S, Deininger SO, Hofler H. (2008). "MALDI imaging mass spectrometry for direct tissue analysis: a new frontier for molecular histology." Histochem Cell Biol **130**(3): 421-434.
Wang HY, Jackson SN, McEuen J, Woods AS. (2005). "Localization and analyses of small drug molecules in rat brain tissue sections." Anal Chem **77**(20): 6682-6686.
Wang HY, Jackson SN, Woods AS. (2007a). "Direct MALDI-MS analysis of cardiolipin from rat organs sections." J Am Soc Mass Spectrom **18**(3): 567-577.
Wang W, Guo T, Rudnick PA, Song T, Li J, Zhuang Z, Zheng W, Devoe DL, Lee CS, Balgley BM. (2007b). "Membrane proteome analysis of microdissected ovarian tumor

tissues using capillary isoelectric focusing/reversed-phase liquid chromatography-tandem MS." Anal Chem **79**(3): 1002-1009.
Wisztorski M, Lemaire R, Stauber J, Menguelet SA, Croix D, Mathe OJ, Day R, Salzet M, Fournier I. (2007). "New developments in MALDI imaging for pathology proteomic studies." Curr Pharm Des **13**(32): 3317-3324.
Wisztorski MV, N.;Thomy, V.;Stauber, J.;Camart, J.C.;Salzet, M.;Fournier, I. (2007). "Use of Masks in MALDI-MSI: an Easy Tool for Increasing Spatial Resolution of Images by Decreasing Irradiated Area." American Society of mass spectrometry, June 4-7, 2007, Indianapolis.
Xu H, Yang L, Wang W, Shi SR, Liu C, Liu Y, Fang X, Taylor CR, Lee CS, Balgley BM. (2008). "Antigen retrieval for proteomic characterization of formalin-fixed and paraffin-embedded tissues." J Proteome Res **7**(3): 1098-1108.
Yang J, Chaurand P, Norris JL, Porter NA, Caprioli RM. (2012). "Activity-Based Probes Linked with Laser-Cleavable Mass Tags for Signal Amplification in Imaging Mass Spectrometry: Analysis of Serine Hydrolase Enzymes in Mammalian Tissue." Anal Chem.
Zubarev RA, Horn DM, Fridriksson EK, Kelleher NL, Kruger NA, Lewis MA, Carpenter BK, McLafferty FW. (2000). "Electron capture dissociation for structural characterization of multiply charged protein cations." Anal Chem **72**(3): 563-573.

DISCUSSION

Par leurs importantes fonctions dans le développement de physiopathologies, les PC sont de plus en plus citées comme cibles thérapeutiques potentielles. Pour ces raisons, plusieurs études se sont attardées à démontrer les bénéfices d'inhiber les PC pour prévenir l'activation de pathogènes. L'approche présentée dans cette thèse préconise l'utilisation d'inhibiteurs peptidomimétiques pour y arriver. Ainsi, deux défis se posent : le premier est évidemment de développer un inhibiteur peptidique efficace contre les PC qui pourra être facilement administré pour traiter un éventail de pathogènes activés par les PC; le deuxième est plutôt la preuve de concept que l'inhibition des PC sera bénéfique chez les hôtes infectés.

1.1. Un inhibiteur peptidique ciblant les PC contre les infections

L'utilisation de peptides plutôt que de petites molécules synthétiques présente plusieurs avantages et certains inconvénients (Mason 2010). Les peptides sont faciles à modifier chimiquement et permettent aisément de développer des molécules avec une grande spécificité, une grande puissance d'inhibition et une faible toxicité. Toutefois, ils sont souvent rapidement éliminés ou métabolisés par le corps et parfois leur perméabilité cellulaire limite l'accès à la cible pharmacologique désirée. En suggérant d'utiliser un inhibiteur de furine, le nona-arginine et son dérivé dextrogyre, contre l'infection topique de l'œil causant la kératite par *Pseudomonas aeruginos,* une partie de ces inconvénients étaient évités (Cameron et al. 2000; Karicherla and Hobden 2009, 2010). Toutefois, cette avenue reste limitée en terme de champs thérapeutiques potentiels, puisque peu d'infections peuvent être traitées par une simple application topique d'un inhibiteur.

Le peptide que nous présentons, dérivé de la séquence de clivage de HA5, avait d'abord été présenté sous la séquence TPRARRRKKRT-NH_2 (Shiryaev et al. 2007) dans le but d'inhiber *in vivo* l'activation de pathogènes. Ce peptide montrait une certaine sélectivité pour furine avec un Ki de 23 nM et était efficace *in vivo* pour protéger contre une inhalation de spores d'anthrax, ainsi que contre une injection intrapéritonéale de la toxine Pseudomonas. Toutefois, le peptide devait être injecté de façon intrapéritonale quotidiennement à une forte dose (12.5 mg/kg). De plus, la protection contre l'anthrax

n'était observable qu'en présence d'une forte dose (25 mg/kg) de ciprofloxacin (un antibiotique). Le peptide lui-même n'était donc pas assez puissant pour protéger contre le développement de la physiopathologie. Dans le but d'augmenter son efficacité, le peptide a été optimisé sous la forme Ac-RARRRKKRT-NH_2 (Remacle et al. 2010). Sous cette forme, le peptide perdait de sa spécificité pour furine, mais enregistrait un gain significatif en puissance d'inhibition (Ki de 6,5 nM pour furine, de 2,6 nM pour PC5/6 et de 2,6 nM pour PACE4) (Remacle et al. 2010). De plus, le peptide avait été lié à un groupement aliphatique de huit carbones dans le but d'augmenter sa perméabilité cellulaire. Malgré tout, l'efficacité *in vivo* n'eut qu'un faible gain. En fait, les effets de protection du peptide contre le modèle d'inhalation d'anthrax nécessitaient toujours la présence de ciprofloxacin et une injection quotidienne du peptide à 5mg/kg.

Conséquemment, la stratégie d'optimisation du peptide devait être revue dans le but d'en arriver à un profil d'inhibition *in vivo* plus efficace. Cette thèse présente une approche qui a permis d'en arriver à des peptides inhibiteurs plus efficients dans deux essais cellulaires : l'essai de fusion cellulaire dépendant de HA5 et l'essai de protection de la toxicité de la toxine de Shiga. Toutefois, ces gains ne sont pas reliés à une augmentation de la puissance d'inhibition, mais principalement à la stabilisation du peptide contre les endoprotéases par la protection des extrémités N- et C-terminales avec des acides aminés non naturels Azaβ3. Il en découle qu'une stratégie d'optimisation utilisant des modèles cellulaires et des tests de stabilité *ex vivo* ont permis de mieux diriger les hypothèses de modifications de l'inhibiteur. De surcroît, l'importance du choix judicieux des modèles d'étude permet d'éviter des efforts inutiles avant d'en arriver au modèle *in vivo*. Particulièrement, l'essai de fusion a permis d'évaluer le potentiel des peptides optimisés contre l'activation du virus de l'influenza H5N1 et ce sans avoir à utiliser des installations spécialisées et hautement sécurisées. De plus, l'approche présentée vise à emprunter la voie d'administration intraveineuse, qui est plus réaliste pour des traitements pharmacologiques chez l'humain qu'une injection intrapéritonéale. Ainsi, nous démontrons que la stabilité et la faible toxicité prédominent sur la puissance d'inhibition et que l'ajout d'un groupement aliphatique n'est pas nécessaire pour inhiber l'activation de HA5 et de la toxine de Shiga en modèle cellulaire. Cette dernière observation est importante, car ces deux pathogènes utilisent des mécanismes d'activation différents. HA5 a été démontrée pour être clivée au

TGN durant sa synthèse (Stieneke-Grober et al. 1992), tandis que la toxine de Shiga est plutôt clivée durant son endocytose dans les endosmes (Sandvig 2001). D'ailleurs, des données préliminaires de pénétration cellulaire du peptide indiquent que l'inhibiteur entrerait par des mécanismes d'endocytose et qu'il s'accumulerait dans les voies de sécrétions des cellules analysées.

1.1.1. La spécificité, la puissance d'inhibition et la stabilité

Il est difficile de conclure si la perte de spécificité par la modification du peptide TPRARRRKKRT au peptide RARRRKKRT est bénéfique ou néfaste. D'un côté, l'inhibition générale des PC pourrait avoir des conséquences drastiques pour la physiologie normale de l'hôte, comme en témoigne la mortalité embryonnaire causée par les KO de furine (Roebroek et al. 1998; Kim et al. 2012), PC5/6 (Essalmani et al. 2008; Szumska et al. 2008) et PACE4 (Constam and Robertson 2000a). Toutefois, il est envisageable que l'inhibiteur en question soit utilisé qu'en traitements aigus de courtes durées, où le but serait de donner avantage au système immunitaire de patients hospitalisés conséquemment à une infection par un pathogène activé par les PC. Ainsi, les effets néfastes de l'inhibition des PC pourraient être minimisés. À ce point, les tests de toxicité aiguë nous indiquent que les peptides sont tolérés à de fortes doses chez la souris donnant espoir à la faisabilité de cette démarche. Jusqu'à maintenant, le seul KO de PC tissu spécifique chez les souris (et inductible) à l'âge adulte est le KO de furine dans le foie et celui-ci est parfaitement viable sans phénotype apparent (Roebroek et al. 2004), ce qui laisse croire que l'inhibition spécifique de furine chez les souris adultes n'aurait pas de conséquences néfastes. Toutefois, le résultat de l'inhibition à court terme des principales PC reste à déterminer. Ainsi, des études chez la souris, de pharmaco-distribution et de toxicologie à court terme des organes où le peptide est principalement retrouvé, doivent être envisagées. Par le fait même, certains substrats de PC bien définis pourraient alors être analysés.

D'un autre côté, les pathogènes sont capables de s'adapter rapidement (Walsh 2000; Coen and Whitley 2011) comme en témoignent l'apparition grandissante de résistances aux antiviraux (Coen and Whitley 2011) et aux antibiotiques (Coates and Hu 2007). Nos résultats de clivage *in vitro* appuient ce phénomène, car le virus H5N1 présente divers types de séquences pouvant être clivées par différentes PC. Il a même été démontré qu'une séquence multibasique serait clivée par d'autres protéases que les PC (Okumura et al.

2010). Cette équipe a montré que les protéases à sérine transmembranaires de type II (TMPRSS13 et MSPL) sont plus efficaces que furine et PC5/6 pour cliver les sites mutibasiques de HA7 qui ont une séquence de type K-K-K-R. Ainsi, le clivage spécifique par furine, que nous démontrons en modèle cellulaire à l'aide de shRNA, pourrait dériver et conférer une résistance à un inhibiteur trop spécifique à furine, d'où le bénéfice de développer un inhibiteur plus général des PC.

Toutefois, les modifications jusqu'ici apportées au peptide touchent principalement les positions P1 et P8, laissant place à d'autres modifications pour moduler divers paramètres de l'inhibiteur. D'ailleurs, diverses combinaisons au niveau de ces deux positions sont aussi envisageables pour obtenir un gain en puissance d'inhibition et en stabilité. Notamment, nous démontrons que l'ajout de mimétique d'Arg en P1, où le groupement fonctionnel présente une plus grande rigidité, permet d'augmenter la puissance d'inhibition. Cette observation corrèle avec celle des travaux de (Becker et al. 2010) qui observe une augmentation du pouvoir d'inhibition du peptide dec-RVKR où P1 est modifiée pour le mimétique AMBA. Ainsi, le mimétique AMBA ou ΔAgm en P1 pourrait être combiné à la modification AzaR en P8 pour obtenir un peptide plus stable et plus puissant. La spécificité est susceptible d'être optimisée en ajoutant un groupement P2' (Remacle et al. 2008). Toutefois, il n'est pas possible de combiner cet ajout en P2' avec les mimétiques AMBA ou ΔAgm en P1, car ceux-ci n'ont pas de groupement carboxyle pour former un nouveau lien peptidique. En outre, le criblage du peptide, des positions P7 à P3, avec les acides aminés Aza indique que cette modification en positions P6 a peu d'influence sur la puissance de l'inhibiteur, mais que le changement de conformation du peptide induit par le mimétique Aza en positions P5 à P3 et P7 engendre une perte importante de puissance d'inhibition envers furine. Ainsi, ces résultats proposent une conformation en feuillet β de la position P5 à P3 qui concorde avec les données structurelles décrites entre furine et ses substrats (Henrich et al. 2003; Henrich et al. 2005; Remacle et al. 2010). Par conséquent les liens peptidiques des positions P5 à P3 pourraient être modifiés pour augmenter la stabilité du peptide tout en conservant la conformation (Ruzza 2012). D'une autre part, la position P6 est connue pour un site potentiel de modulation de la sélectivité envers les PC (Remacle et al. 2008). Puisque cette position P6 semble avoir peu d'influence sur la puissance d'inhibition, il est tout à fait logique de la

modifier par un autre acide aminé si la spécificité de l'inhibiteur pour furine doit être augmentée.

1.2. L'inhibition des PC contre les pathogènes et la balance du système immunitaire

1.2.1. Le rôle de la réponse immunitaire innée dans le contrôle des infections H5N1

Dans l'éventualité où un virus H5N1 (ayant la boucle d'activation sensible aux PC) serait capable de se propager d'homme à homme, ce nouveau virus pourrait causer l'une des pires pandémies d'influenza de l'histoire (Webby and Webster 2003). Les PC deviennent donc une cible thérapeutique de choix pour bloquer l'entrée cellulaire de ce virus. Toutefois, cette approche doit permettre de suffisamment ralentir l'entrée virale pour permettre au système immunitaire de se débarrasser du virus sans qu'il cause le choc de cytokine normalement associé à la réponse contre H5N1. La question se pose donc, quel est l'effet de l'inhibition des PC sur la réponse immunitaire et sera-t-elle bénéfique dans un traitement contre H5N1 ciblant les PC? Mais d'abord, pour évaluer les bénéfices d'une modulation de la réponse immunitaire dans le cadre d'une infection par H5N1, il faut bien comprendre pourquoi celui-ci induit une réponse immunitaire non contrôlée. Les travaux de (Peiris et al. 2009) expliquent bien le paradoxe de l'équilibre entre une réponse immunitaire appropriée et les dommages que cette même réponse peut causer lors d'une infection par H5N1. En plus de l'infection systémique, le virus H5N1 réussit à retarder la réponse immunitaire innée de l'hôte qui au final entraine un choc de cytokine mortel. Les processus exacts qui mènent à cette réponse extrême restent flous. Toutefois, il a été démonté que la protéine virale NS1 inhibe des voix de signalisation de la réponse immunitaire, que l'infection par H5N1 des dérégule les fonctions des macrophages, que l'infection par H5N1 induit une apoptose précoce des cellules dendritiques et que l'infection par H5N1 induit une réponse Th1 aberrante et un débalancement de la réponse par les cellules T CD8 (Peiris et al. 2009; Peiris et al. 2010; Fukuyama and Kawaoka 2011; Karpala et al. 2011; Friesenhagen et al. 2012). Ainsi, une modulation précoce de la réponse immunitaire innée permet de mieux répondre au virus (Szretter et al. 2009). Ce genre de mécanisme est aussi observable chez les bactéries (Chin et al. 2012).

1.2.2. L'inhibition des PC et la réponse immunitaire

Malgré le peu d'études qui se sont penchées sur cette problématique, on peut en tirer quelques conclusions. L'utilisation du peptide nona-D-arginine, dans un modèle de kératite de l'œil par *Pseudomonas aeruginosa*, est capable de bloquer la sécrétion de cytokines (TNF-α, IFN-γ, IL-10, et le GM-CSF) dès le début de l'infection (Karicherla et al. 2010). Toutefois, le mécanisme exact par lequel se produisent ces évènements n'est pas décrit par les auteurs. Ceux-ci proposent que le peptide chargé positivement puisse lier le LPS chargé négativement ou que le peptide empêche la signalisation par le TLR9 en liant les ilots CpG de l'ADN bactérien (Lingnau et al. 2002). Toutefois, la littérature montre plutôt que la délétion de furine spécifique aux cellules T entraine une dérégulation de la voie Th1, l'augmentation de la sécrétion de cytokines inflammatoires et que notamment furine régule la sécrétion d'IFN-γ (Pesu et al. 2006; Pesu et al. 2008). Il y a donc une différence marquante entre ces deux observations qui pourrait être reliée au fait que l'un s'intéresse à une fonction locale de l'immunité et l'autre systémique et spécifique aux cellules T. Dans le cas d'un traitement par injection intraveineuse la fonction systémique s'avère plus probable. Récemment, les travaux de (Lin et al. 2012) se sont attardés sur le rôle systémique de furine dans la régulation de la réponse immunitaire. Malgré qu'ils utilisent un inhibiteur non spécifique pour furine (Fugere and Day 2005), il est clairement démontré que l'injection intrapéritonéale d'α1-PDX induit une réponse Th1 caractérisée par une augmentation des cytokines pro-inflammatoires (TNFα, IL-1β) et une diminution de la réponse des Treg. Ainsi, dans le contexte de l'inhibition de furine contre une infection H5N1 on pourrait conclure qu'un traitement rapide avec un inhibiteur de PC ciblant furine permettrait à la fois de réduire l'entrée virale, mais aussi d'induire une réponse rapide Th1 pour permettre à l'hôte de combattre le virus.

Un modèle d'étude qui permettrait d'évaluer à la fois le rôle d'un inhibiteur contre l'activation d'un pathogène et la modulation de l'immunité serait possible dans le cas de l'inhibition de la toxine de Shiga. Ce modèle consiste en l'injection combinée de la toxine de Shiga et du LPS de façon intrapéritonéale à des souris, permet de mimer une infection par la bactérie O157:H7 (Keepers et al. 2006). Puisque nous démontrons l'efficacité de nos peptides pour bloquer la toxicité cellulaire induite par la toxine de Shiga, ce modèle permettrait de mesurer les bénéfices d'une injection des peptides modifiés de Ac-

RARRRKKRT-NH_2 pour inhiber l'activation de la toxine et pour moduler une réponse immunitaire appropriée. Conséquemment, une expérience où l'on injecterait les peptides inhibiteurs à des souris (en présence de toxine ou de toxine et du LPS) permettrait de mesurer correctement l'efficacité de ces inhibiteurs à bloquer une infection bactérienne produisant la toxine de Shiga.

1.3. PC1/3 une protéase du système immunitaire

Jusqu'ici, le rôle de PC1/3 comme activateur de neuropeptides anti-inflammatoires (Gonzalez-Rey 2010) était principalement associé à une communication entre le système neuroendocrinien et les cellules du système immunitaire qui expriment les récepteurs de ces neuropeptides (Lasaga et al. 2008). Seulement une poignée d'études démontre l'expression et la maturation de neuropeptides dans les cellules et les tissus immunitaires (Saravia et al. 1993; Vindrola et al. 1994; LaMendola et al. 1997; Saravia et al. 1998; Lansac et al. 2006). Elles montrent que PC1/3 est principalement exprimée dans les macrophages, alors que PC2 se trouve plutôt dans les lymphocytes. De surcroit, les travaux des groupes de (Saravia et al. 1993; Saravia et al. 1998; Lansac et al. 2006) présentent une modulation de certains neuropeptides exprimés par les macrophages suite à une stimulation du système immunitaire innée avec le LPS. En présentant le phénotype immunitaire des souris PC1/3 KO stimulées au LPS, en montrant que ce phénotype se rattachait aux macrophages isolés de ces souris et en démontrant qu'un modèle cellulaire (où toutes fonctions paracrines ou juxtacrines avec d'autres types cellulaires étaient éliminées) pouvait reproduire en partie ce phénotype, nous pouvons conclure que PC1/3 a un rôle important comme modulateur de l'immunité au sein même des macrophages. Des plus intéressants, le phénotype observé par (Lin et al. 2012) en traitant les souris de façon intrapéritonéale avec l'α1-PDX (un inhibiteur de furine, mais aussi de PC1/3 (Fugere and Day 2005)) ressemble au phénotype immunitaire des souris PC1/3 KO. Cette étude montre que le traitement à l'α1-PDX induit une augmentation du rapport Th1/Th2 et une diminution des Treg notamment corrélées avec une augmentation de la sécrétion du TNF-α et de l'IL-1β et une diminution de l'IL-10 et de l'IL-4. Donc, PC1/3 pourrait avoir une contribution dans le phénotype observé par (Lin et al. 2012). On pourrait ainsi émettre l'hypothèse que les convertases en général auraient un rôle de régulatrices de la voie Th1.

Grâce aux approches par spectrométrie de masse nous avons pu associer des observations physiologiques à des voies moléculaires, ou même émettre des hypothèses sur les fonctions physiologiques à partir des observations moléculaires. La puissance de ces approches peut facilement être transférée d'un modèle d'étude à un autre, ce qui démontre les bénéfices d'utiliser cette technologie comme outil d'investigation. De plus, l'étude des tissus de patientes atteintes du cancer de l'ovaire démontre la complémentarité de l'approche d'imagerie par spectrométrie de masse et celle d'identification protéique à haut débit. Il est clair qu'une approche bio-informatique appropriée est essentielle pour tirer avantage des approches par spectrométrie de masse et pour ainsi établir des liens entre les phénotypes physiologiques et les caractéristiques moléculaires observés. Malgré tout, le plan de travail qui a été utilisé sur le modèle PC1/3 KO n'a pas permis de déterminer le mécanisme exact par lequel PC1/3 module la réponse immunitaire. L'hypothèse la plus évidente était que PC1/3 modulerait l'immunité par le biais de substrats. Les voies de signalisation qui semblent être affectées par le KO de PC1/3 supportent cette hypothèse. Toutefois, le phénotype d'hypercytokinémie observé chez les souris PC1/3 KO stimulé au LPS est drastique et il est difficile de croire que quelques neuropeptides qui pourraient être exprimés dans les macrophages (Saravia et al. 1993; Saravia et al. 1998; Lansac et al. 2006) puissent avoir un aussi grand effet. On peut supposer que d'autres substrats de PC1/3, encore inconnus, sont exprimés dans le système immunitaire. Toutefois, la localisation intracellulaire de PC1/3 indique que l'enzyme serait retenue au TGN et que PC1/3 (jusqu'ici observée) s'y trouve sous la forme non maturée. Ainsi, l'activité catalytique de PC1/3 serait toute de même présente (Jean et al. 1993), mais plus faible que si l'enzyme se trouvait sous la forme courte dans un compartiment acide (Jutras et al. 1997; Rabah et al. 2007). Malgré tout, le changement de localisation de PC1/3 induit par le LPS vers des compartiments plus acides laisse présager que PC1/3 pourrait être activée et cliver des substrats de façon stimulus dépendant. À ce point, deux procédés devront être étudiés. 1) La biologie cellulaire de PC1/3 devra être revue dans les macrophages, et ce en incluant divers stimulis immunitaires tels des ligands des TLR (ex. LPS, CpG-ODN) ou autres (tel l'IFN-γ). Ainsi, les mécanismes de régulation du trafic intracellulaire, en utilisant divers mutants de PC1/3, devront être déterminés (ex. mutation des acides aminés responsable du trafic vers les DCSG dans le domaine P (Ueda et al. 2003a; Dikeakos et al. 2007; Dikeakos

et al. 2009)). Parallèlement, la maturation de PC1/3 dans ces mêmes conditions devra être étudiée. De plus, d'autres protéines normalement acheminées aux DCSG devraient être exprimées dans les macrophages. Ceci permettrait de déterminer si le mécanisme de rétention de PC1/3 au TGN fait partie d'un mécanisme général qui définirait une nouvelle voie de sécrétion régulée chez les macrophages. 2) Des approches de découverte de substrats de PC1/3 dans les macrophages devront être mises au point. Les approches par spectrométrie de masse présentées dans cette thèse avaient comme but de permettre l'identification de substrats, mais n'ont pas été fructueuses. D'abord, l'approche peptidomique d'imagerie par spectrométrie de masse n'a pas permis l'identification de peptides sur coupe de tissus. Ensuite, l'approche protéomique sur gel aurait théoriquement pu permettre la découverte de substrats par une cartographie sur le gel SDS des changements des profils de migration engendrés par des clivages (Dix et al. 2008), mais les données obtenues ne permettaient pas de détecter avec une grande précision ces évènements de clivages. Deux nouvelles approches expérimentales qui utilisent la spectrométrie de masse sont donc proposées. Une première approche qui permettrait de cartographier dans leur contexte anatomique les substrats peptidiques de PC1/3 dans les tissus immunitaires (Figure 63). Une deuxième approche qui permettrait d'identifier les substrats protéiques sécrétés ou intracellulaires de PC1/3 dans les macrophages, nommée TAILS (*Terminal Amino acid Isotopic Labeling of Substrat*) (Figure 64) (Prudova et al. 2010).

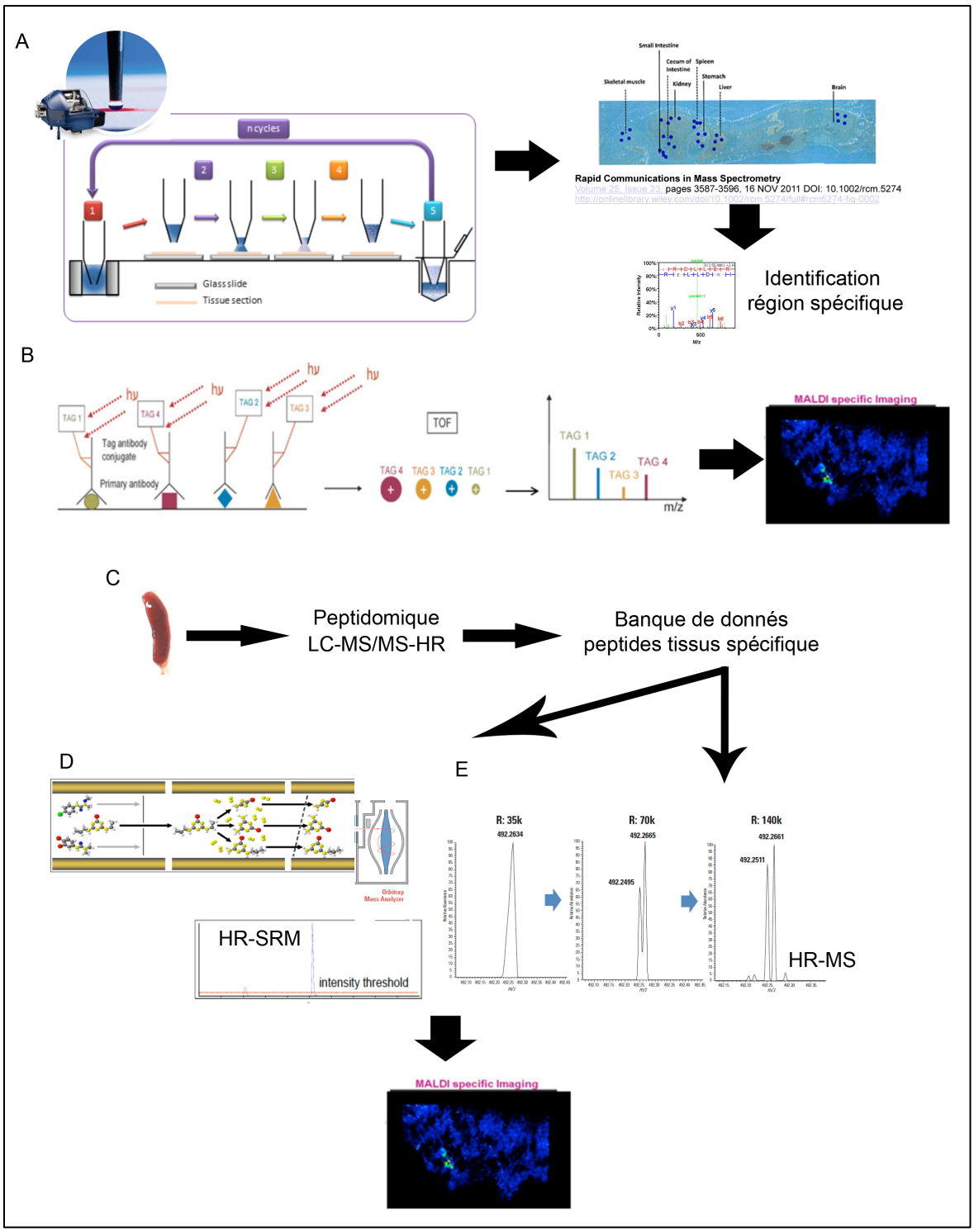

Figure 63 Approche d'identification peptidomique et d'imagerie des substrats de PC1/3 dans les tissus immunitaires

A) Une méthode de micro-extraction sur tissu qui utiise un système robotisé microfluidique permettrait d'extraire les peptides des coupes de tissus et d'en faire l'identification LC-MS/MS. Cette approche permettrait de déterminer la localisation des peptides avec une

résolution spatiale d'environ 1 mm, telle que présentée à la Figure 56. B) Une approche dirigée, en utilisant des anticorps ciblant des substrats connus de PC1/3, permettrait de faire de l'imagerie en multiplexe sur tissu TAG-MASS tel que présenté à la Figure 59. C) Une approche peptidomique, telle que précédemment utilisée sur les souris PC1/3 KO et PC2 (Pan et al. 2006; Wardman et al. 2010), pourrait être utilisée pour dresser une banque de données contenant les peptides différemment maturés dans les tissus immunitaires des souris PC1/3 KO. D) Cette banque de données pourrait être utilisée pour faire de l'imagerie par spectrométrie de masse en mode SRM (*Selected Reaction Monitoring*) sur un spectromètre de masse opérant en haute résolution (HR). Le mode HR-SRM permet d'abord de faire la sélection de l'ion d'intérêt dans une première section de l'appareil et ensuite d'un fragment MS/MS spécifique au peptide est détecté dans un analyseur haute résolution, tel un Orbitrap. L'image de l'ion signature de la molécule d'intérêt pourrait ensuite être reconstruite. E) La même base de données pourrait être utilisée pour faire de l'imagerie MS en mode haute résolution (HR-MS). Cette approche utilise plutôt les propriétés de haute résolution et de grande précision du spectromètre de masse (tels un LTQ-Orbitrap ou un FT-ICR) pour corréler les masses observées avec celles contenues dans la base de données.

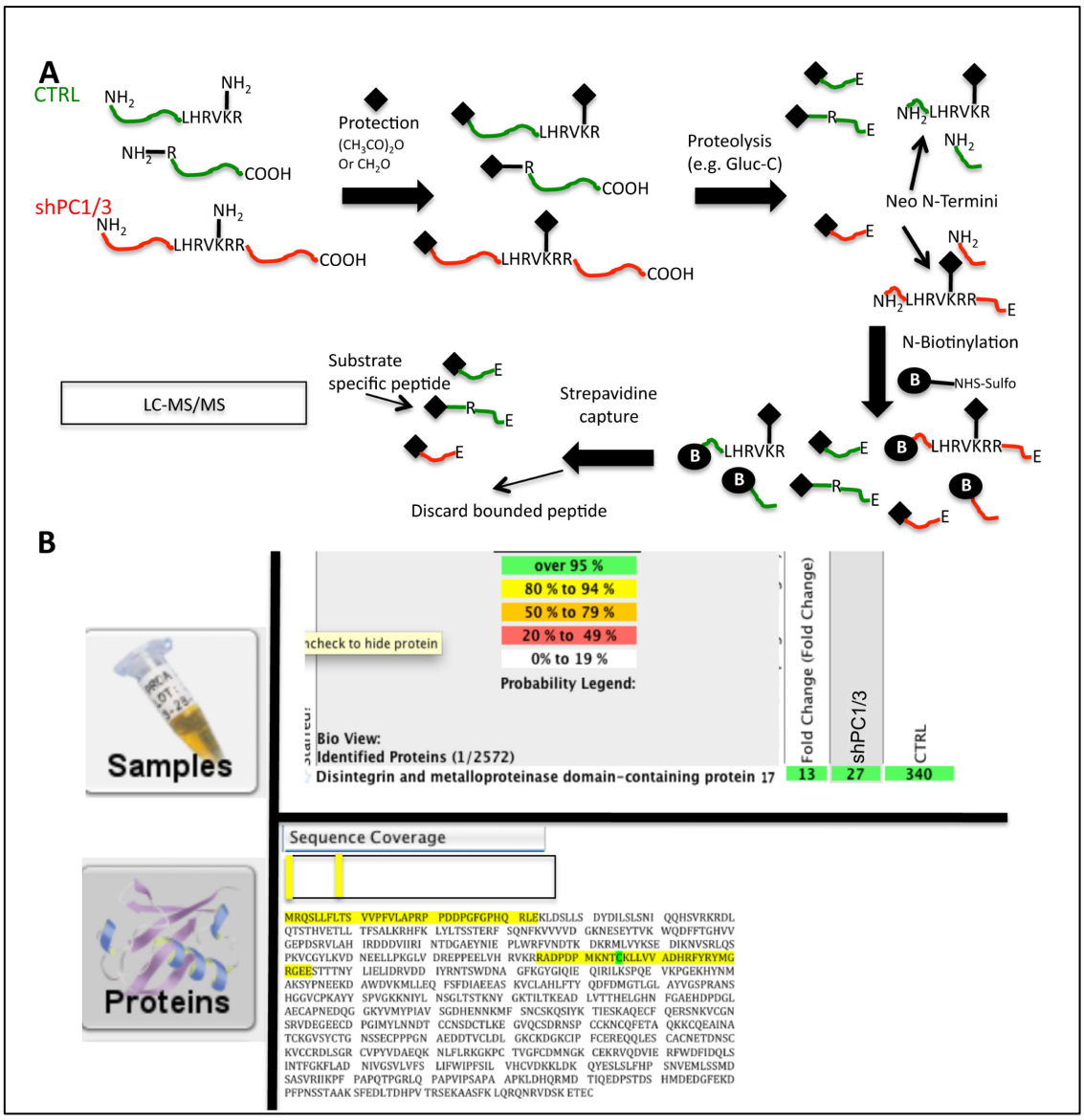

Figure 64 Étude de substrats protéiques par TAILS.

A) La méthode est en fait un protocole qui permet de simplifier le protéome pour en extraire les fragments N-terminaux naturels et les N-terminaux induits par la protéolyse. Brièvement, les amines primaires et secondaires de deux protéomes, un contrôle (CTRL) et un protéome où la protéine d'intérêt est inactivée (shRNA PC1/3), sont d'abord protégées en introduisant un tag isotopique ou isobarique qui permet de différencier et de quantifier les deux protéomes une fois combinés. Les deux protéomes combinés sont par la suite digérés à la trypsine, ce qui entraine la formation de nouvelles amines libres qui pourront être éliminées à l'aide de billes fonctionnalisées avec un groupement réactif aux amines. Aux finales, seulement les domaines N-terminaux naturels et induits par la protéolyse seront analysés par LC-MS/MS. B) Les peptides identifiés pourront être associés à leurs séquences protéiques et quantifiés. Une diminution de la présence d'un peptide précédé par un site de clivage reconnu par la protéase étudiée indiquera la détection d'un substrat.

L'hypothèse la plus probable reste que PC1/3 agit grâce à des substrats. Toutefois, les résultats des études de microscopie confocale sur le modèle NR8383, de la microscopie électronique sur les macrophages isolés des souris KO et l'étude protéomique sur les extrudâts péritonéaux de souris KO indiquent tous un grand dérèglement des protéines Rab et de la voie de sécrétion. Ainsi, une autre fonction de PC1/3 pourrait être en jeu. Des études suggèrent que PC1/3 aurait un rôle de protéine cargo, notamment en liant des sites contenant des paires de résidus basiques afin de les acheminer au DCSG (Brechler et al. 1996; Jackson et al. 1997; Kuliawat et al. 2000; Bundgaard et al. 2004; Mulcahy et al. 2005). Ces études montrent que plusieurs précurseurs protéiques (ex. proinsuline (Kuliawat et al. 2000), progastrine (Bundgaard et al. 2004), proneurotensine (Brechler et al. 1996; Jackson et al. 1997)) nécessitent la présence de PC1/3 pour être acheminés aux DCSG. Le simple fait de muter le site de clivage de ces précurseurs pour un site reconnu par furine modifie leur trafic intracellulaire vers la voie constitutive de sécrétion (Brechler et al. 1996). D'ailleurs, les travaux de (Feliciangeli et al. 2001) démontrent que des résidus dibasiques, en C-terminal, servent de signal pour acheminer des précurseurs protéiques dans la voie de sécrétion régulée. De plus, une mutation humaine de PC1/3, qui engendre une rétention au réticulum endoplasmique de PC1/3, entraine une hypersécrétion de proinsuline (Jackson et al. 1997), comme si elle ne pouvait plus être retenue dans la voie de sécrétion régulée. Ces observations sont d'ailleurs corroborées par les études sur le modèle de souris PC1/3 KO, où une sécrétion aberrante de certains neuropeptides est observée (Wardman et al. 2010). Si l'on ajoute le fait que PC1/3 a un profil enzymatique qui présente une phase de latence (Hoshino et al. 2011; Icimoto et al. 2011), PC1/3 pourrait contribuer à la rétention de certaines protéines dans divers compartiments cellulaires au sein des macrophages. Une autre hypothèse serait que PC1/3 pourrait masquer certains substrats à d'autres PC en les retenant, ce qui semble le cas entre PC2 et PC1/3 pour certains neuropeptides (Wardman et al. 2010). Dans les deux cas, l'identification des partenaires d'interaction de PC1/3, par spectrométrie de masse en immunoprécipitant PC1/3, permettrait d'identifier des pistes mécanistiques du rôle de PC1/3 dans les macrophages.

1.4. Conclusion

La famille des PC reste d'une grande complexité et l'inhibition des PC à des fins thérapeutiques est une approche en évolution aux applications diverses. Les deux domaines les plus prometteurs sont le cancer (où certaines PC semblent avoir un rôle spécifique dans le développement de maladie (Levesque et al. 2012)) et les maladies infectieuses activées par les PC (où les traitements sont souvent de courtes durées et qui permettrait ainsi d'éviter les effets néfastes à long terme de l'inhibition des PC). Le système immunitaire joue un rôle important, tant pour la réponse immunitaire contre les pathogènes que dans le développement de métastases et de la récurrence dans le cancer (Grivennikov et al. 2010). Ainsi, le choix des modèles d'études demeure important afin de prendre la réponse immunitaire en compte (Pienta et al. 2008). Par le fait même, une plus grande compréhension du rôle des PC dans le système immunitaire permettrait une meilleure intégration des connaissances et des choix expérimentaux plus judicieux. De surcroit, la découverte des mécanismes d'action des PC dans le système immunitaire par l'identification des substrats a tout à gagner, car ces substrats peuvent eux-mêmes devenir des outils thérapeutiques ou des cibles pharmacologiques. Cette tâche complexe peut tirer avantage d'une technologie comme la spectrométrie de masse qui (combinée à des analyses bio-informatiques) permet l'identification, la quantification, la cartographie des voies d'activation cellulaire et la localisation dans un contexte anatomique.

REMERCIEMENTS

Je tiens d'abord à remercier mes deux directeurs de recherche le Dr Robert Day et le Dr Michel Salzet. Merci Robert de m'avoir dirigé avec un grand respect, de m'avoir fait confiance en me laissant une grande liberté dans le cheminement de mes projets et de m'avoir impliqué dans tous les aspects de la démarche scientifique académique. Grâce à quoi, j'ai pu cheminer si bien en tant que scientifique, qu'en tant que personne. Merci Michel de m'avoir agréablement accueilli au sein de ton unité, mes séjours en France furent très intenses et formateurs. J'ai pu y apprécier ta passion et ton dévouement lors de nos très enrichissantes discussions et j'y ai appris un domaine passionnant qu'est la spectrométrie de masse. Je tiens aussi à remercier les membres de mon jury de thèse le Dr Martin Bisaillion, le Dr Philipe Bulet et la Dre Annik Prat. Votre temps et vos commentaires ont été un précieux aide pour améliorer cet ouvrage. Un merci aussi aux évaluateurs de mon examen pré doctoral, le Dr Xavier Roucou et le Dr Claude Lazure, ce dernier avec qui j'ai pu collaborer et apprécier ses connaissances en protéomique.

Les travaux de cette thèse n'auraient pas été possibles sans l'incroyable collaboration entre et au sein des laboratoires du Dr Robert Day et du Dr Michel Salzet. Merci à tous les membres de mon laboratoire d'accueil à Lille. Votre chaleureuse hospitalité m'a permis de me sentir intégré de l'équipe à chacun de mes séjours. Je tiens à souligner l'incroyable travail de l'équipe d'imagerie, Isabelle Fournier, Maxence Wisztorski, Julien Frank, Jusal Quanico, David Bonel et Rémi Longuespée. Merci David pour ton amitié, de m'avoir transmis ton savoir-faire en imagerie MALDI et de m'avoir généreusement hébergé chez toi et ta conjointe Céline lors de mon premier voyage en France. Merci Rémi de m'avoir si humblement permis de collaborer à tes travaux de recherche, ton amitié reste et restera très appréciée. Merci aux membres du laboratoire du Dr Day, François D'Anjou, Sophie Beauchemin, Frederic Couture, Roxane Dejardins, Fredirik Dufour, Sandra Gagnon, Anna Kwiatkowska, Christine Levesque, Keven Ly, Philippe Moussette, Sarah Refaie, Sophie Routier et Xue-Wen Yuan. Votre amitié et votre camaraderie ont fait de ces années de thèse des moments agréables. Vous avez tous contribué de près ou de loin aux travaux de cette thèse qui ont pu bénéficier de votre rigueur et de votre esprit critique. Je tiens cependant à souligner le travail extraordinaire de Sandra et Sarah, sans qui le projet PC1/3 immunité

n’en serait pas là où il en est. Et je tiens à mentionner le temps et la patience que Roxane m’a accordée lors de mon intégration au sein du laboratoire.

Finalement, je remercie mes parents, Benoit et Danielle, qui m’ont toujours encouragé à la poursuite de mes études. Et je garde ces derniers mots pour ma conjointe Karine et mes enfants Édouard et Liliane. Vous avez été mon équilibre et mon bonheur. Votre patience, votre amour, vos encouragements et parfois vos sacrifices ont été mon inspiration tout au long de ces années durant lesquelles j’ai grandi en tant que père et en tant que scientifique. Merci, je vous aime.

RÉFÉRENCES

Aaronson DS, Horvath CM. (2002). "A road map for those who don't know JAK-STAT." Science **296**(5573): 1653-1655.

Abell A. (1997). Advances in Amino Acid Mimetics and Peptidomimetics, Elsevier Science.

Abrami L, Fivaz M, Decroly E, Seidah NG, Jean F, Thomas G, Leppla SH, Buckley JT, van der Goot FG. (1998). "The pore-forming toxin proaerolysin is activated by furin." J. Biol. Chem. **273**(49): 32656-32661.

Akira S, Uematsu S, Takeuchi O. (2006). "Pathogen recognition and innate immunity." Cell **124**(4): 783-801.

Anderson CF, Mosser DM. (2002). "Cutting edge: biasing immune responses by directing antigen to macrophage Fc gamma receptors." J. Immunol. **168**(8): 3697-3701.

Anderson ED, VanSlyke JK, Thulin CD, Jean F, Thomas G. (1997). "Activation of the furin endoprotease is a multiple-step process: requirements for acidification and internal propeptide cleavage." EMBO J. **16**(7): 1508-1518.

Angliker H, Wikstrom P, Shaw E, Brenner C, Fuller RS. (1993). "The synthesis of inhibitors for processing proteinases and their action on the Kex2 proteinase of yeast." Biochem. J. **293 (Pt 1)**: 75-81.

Asara JM, Christofk HR, Freimark LM, Cantley LC. (2008). "A label-free quantification method by MS/MS TIC compared to SILAC and spectral counting in a proteomics screen." Proteomics **8**(5): 994-999.

Baird PA, Anderson TW, Newcombe HB, Lowry RB. (1988). "Genetic disorders in children and young adults: a population study." Am J Hum Genet **42**(5): 677-693.

Basak A, Cooper S, Roberge AG, Banik UK, Chretien M, Seidah NG. (1999). "Inhibition of proprotein convertases-1, -7 and furin by diterpines of Andrographis paniculata and their succinoyl esters." Biochem. J. **338 (Pt 1)**: 107-113.

Basak A, Zhong M, Munzer JS, Chretien M, Seidah NG. (2001). "Implication of the proprotein convertases furin, PC5 and PC7 in the cleavage of surface glycoproteins of Hong Kong, Ebola and respiratory syncytial viruses: a comparative analysis with fluorogenic peptides." Biochem. J. **353**(Pt 3): 537-545.

Bassi DE, Mahloogi H, Klein-Szanto AJP. (2000). "The proprotein convertases furin and PACE4 play a significant role in tumor progression." Mol. Carcinog. **28**(2): 63-69.

Bassi DE, Lopez De Cicco R, Mahloogi H, Zucker S, Thomas G, Klein-Szanto AJ. (2001). "Furin inhibition results in absent or decreased invasiveness and tumorigenicity of human cancer cells." Proc. Natl. Acad. Sci. U. S. A. **98**(18): 10326-10331.

Bassi DE, Mahloogi H, Lopez De Cicco R, Klein-Szanto A. (2003). "Increased furin activity enhances the malignant phenotype of human head and neck cancer cells." Am. J. Pathol. **162**(2): 439-447.

Bassi DE, Fu J, Lopez de Cicco R, Klein-Szanto AJ. (2005a). "Proprotein convertases: "master switches" in the regulation of tumor growth and progression." Mol. Carcinog. **44**(3): 151-161.

Bassi DE, Lopez De Cicco R, Cenna J, Litwin S, Cukierman E, Klein-Szanto AJ. (2005b). "PACE4 expression in mouse basal keratinocytes results in basement membrane disruption and acceleration of tumor progression." Cancer Res. **65**(16): 7310-7319.

Bassi DE, Zhang J, Cenna J, Litwin S, Cukierman E, Klein-Szanto AJ. (2010). "Proprotein convertase inhibition results in decreased skin cell proliferation, tumorigenesis, and metastasis." Neoplasia **12**(7): 516-526.

Becker GL, Sielaff F, Than ME, Lindberg I, Routhier S, Day R, Lu Y, Garten W, Steinmetzer T. (2010). "Potent inhibitors of furin and furin-like proprotein convertases containing decarboxylated P1 arginine mimetics." J. Med. Chem. **53**(3): 1067-1075.

Benjannet S, Rhainds D, Essalmani R, Mayne J, Wickham L, Jin W, Asselin MC, Hamelin J, Varret M, Allard D, Trillard M, Abifadel M, Tebon A, Attie AD, Rader DJ, Boileau C, Brissette L, Chretien M, Prat A, Seidah NG. (2004). "NARC-1/PCSK9 and its natural mutants: zymogen cleavage and effects on the low density lipoprotein (LDL) receptor and LDL cholesterol." J. Biol. Chem. **279**(47): 48865-48875.

Bergeron F, Leduc R, Day R. (2000). "Subtilase-like pro-protein convertases: from molecular specificity to therapeutic applications." J. Mol. Endocrinol. **24**(1): 1-22.

Bertram S, Glowacka I, Steffen I, Kuhl A, Pohlmann S. (2010). "Novel insights into proteolytic cleavage of influenza virus hemagglutinin." Rev Med Virol **20**(5): 298-310.

Bissonnette L, Charest G, Longpre JM, Lavigne P, Leduc R. (2004). "Identification of furin pro-region determinants involved in folding and activation." Biochem. J. **379**(Pt 3): 757-763.

Blackwell TS, Christman JW. (1997). "The role of nuclear factor-kappa B in cytokine gene regulation." Am. J. Respir. Cell Mol. Biol. **17**(1): 3-9.

Blanchet MH, Le Good JA, Mesnard D, Oorschot V, Baflast S, Minchiotti G, Klumperman J, Constam DB. (2008). "Cripto recruits Furin and PACE4 and controls Nodal trafficking during proteolytic maturation." EMBO J. **27**(19): 2580-2591.

Bonnel D, Longuespee R, Franck J, Roudbaraki M, Gosset P, Day R, Salzet M, Fournier I. (2011). "Multivariate analyses for biomarkers hunting and validation through on-tissue bottom-up or in-source decay in MALDI-MSI: application to prostate cancer." Anal Bioanal Chem **401**(1): 149-165.

Bowie AG, Haga IR. (2005). "The role of Toll-like receptors in the host response to viruses." Mol. Immunol. **42**(8): 859-867.

Braun P. (2012). "Interactome mapping for analysis of complex phenotypes: insights from benchmarking binary interaction assays." Proteomics **12**(10): 1499-1518.

Brechler V, Chu WN, Baxter JD, Thibault G, Reudelhuber TL. (1996). "A protease processing site is essential for prorenin sorting to the regulated secretory pathway." J. Biol. Chem. **271**(34): 20636-20640.

Brown J, Wang H, Hajishengallis GN, Martin M. (2011). "TLR-signaling networks: an integration of adaptor molecules, kinases, and cross-talk." J. Dent. Res. **90**(4): 417-427.

Bundgaard JR, Birkedal H, Rehfeld JF. (2004). "Progastrin is directed to the regulated secretory pathway by synergistically acting basic and acidic motifs." J. Biol. Chem. **279**(7): 5488-5493.

Burgess BJ, Roberts LM. (1993). "Proteolytic cleavage at arginine residues within the hydrophilic disulphide loop of the Escherichia coli Shiga-like toxin I A subunit is not essential for cytotoxicity." Mol. Microbiol. **10**(1): 171-179.

Cameron A, Appel J, Houghten RA, Lindberg I. (2000). "Polyarginines are potent furin inhibitors." J. Biol. Chem. **275**(47): 36741-36749.

Caprioli RM, Farmer TB, Gile J. (1997). "Molecular imaging of biological samples: localization of peptides and proteins using MALDI-TOF MS." Anal. Chem. **69**(23): 4751-4760.

Cardo-Vila M, Giordano RJ, Sidman RL, Bronk LF, Fan Z, Mendelsohn J, Arap W, Pasqualini R. (2010). "From combinatorial peptide selection to drug prototype (II): targeting the epidermal growth factor receptor pathway." Proc. Natl. Acad. Sci. U. S. A. **107**(11): 5118-5123.

Chaineau M, Danglot L, Proux-Gillardeaux V, Galli T. (2008). "Role of HRB in clathrin-dependent endocytosis." J. Biol. Chem. **283**(49): 34365-34373.

Chen J, Lee KH, Steinhauer DA, Stevens DJ, Skehel JJ, Wiley DC. (1998). "Structure of the hemagglutinin precursor cleavage site, a determinant of influenza pathogenicity and the origin of the labile conformation." Cell **95**(3): 409-417.

Cheng M, Watson PH, Paterson JA, Seidah NG, Chrétien M, Shiu RP. (1997). "Pro-protein convertase gene expression in human breast cancer." Int. J. Cancer **71**(6): 966-971.

Chin CY, Monack DM, Nathan S. (2012). "Delayed activation of host innate immune pathways in streptozotocin-induced diabetic hosts leads to more severe disease during infection with Burkholderia pseudomallei." Immunology **135**(4): 312-332.

Chretien M, Li CH. (1967). "Isolation, purification, and characterization of gamma-lipotropic hormone from sheep pituitary glands." Can. J. Biochem. **45**(7): 1163-1174.

Coates ARM, Hu Y. (2007). "Novel approaches to developing new antibiotics for bacterial infections." Br. J. Pharmacol. **152**(8): 1147-1154.

Coen DM, Whitley RJ. (2011). "Antiviral drugs and antiviral drug resistance." Curr Opin Virol **1**(6): 545-547.

Constam DB, Robertson EJ. (2000a). "SPC4/PACE4 regulates a TGFbeta signaling network during axis formation." Genes Dev. **14**(9): 1146-1155.

Constam DB, Robertson EJ. (2000b). "Tissue-specific requirements for the proprotein convertase furin/SPC1 during embryonic turning and heart looping." Development **127**(2): 245-254.

Cooray SN, Clark AJ. (2011). "Melanocortin receptors and their accessory proteins." Mol. Cell. Endocrinol. **331**(2): 215-221.

Cope A, Le Friec G, Cardone J, Kemper C. (2011). "The Th1 life cycle: molecular control of IFN-γ to IL-10 switching." Trends immunol **32**(6): 278-286.

Couture F, D'Anjou F, Day R. (2011). "On the cutting edge of proprotein convertase pharmacology: from molecular concepts to clinical applications." Biomol Concepts **2**(5): 421-438.

Creemers JW, Groot Kormelink PJ, Roebroek AJ, Nakayama K, Van de Ven WJ. (1993). "Proprotein processing activity and cleavage site selectivity of the Kex2-like endoprotease PACE4." FEBS Lett. **336**(1): 65-69.

Creemers JW, Khatib AM. (2008). "Knock-out mouse models of proprotein convertases: unique functions or redundancy?" Front. Biosci. **13**: 4960-4971.

Creemers JW, Choquet H, Stijnen P, Vatin V, Pigeyre M, Beckers S, Meulemans S, Than ME, Yengo L, Tauber M, Balkau B, Elliott P, Jarvelin MR, Van Hul W, Van Gaal L, Horber F, Pattou F, Froguel P, Meyre D. (2012). "Heterozygous mutations

causing partial prohormone convertase 1 deficiency contribute to human obesity." Diabetes **61**(2): 383-390.

D'Anjou F, Routhier S, Perreault J, Latil A, Bonnel D, Fournier I, Salzet M, Day R. (2011). "Molecular Validation of PACE4 as a Target in Prostate Cancer." Transl Oncol **4**(3): 157-172.

Das K, Aramini JM, Ma LC, Krug RM, Arnold E. (2010). "Structures of influenza A proteins and insights into antiviral drug targets." Nat Struct Mol Biol **17**(5): 530-538.

Day R, Salzet M. (2002). "The neuroendocrine phenotype, cellular plasticity, and the search for genetic switches: redefining the diffuse neuroendocrine system." Neuro Endocrinol Lett **23**(5-6): 447-451.

De Clercq E. (2002). "Strategies in the design of antiviral drugs." Nat Rev Drug Discov **1**(1): 13-25.

De Clercq E. (2006). "Antiviral agents active against influenza A viruses." Nat Rev Drug Discov **5**(12): 1015-1025.

de Jong JC, Claas EC, Osterhaus AD, Webster RG, Lim WL. (1997). "A pandemic warning?" Nature **389**(6651): 554.

Decha P, Rungrotmongkol T, Intharathep P, Malaisree M, Aruksakunwong O, Laohpongspaisan C, Parasuk V, Sompornpisut P, Pianwanit S, Kokpol S, Hannongbua S. (2008). "Source of high pathogenicity of an avian influenza virus H5N1: why H5 is better cleaved by furin." Biophys. J. **95**(1): 128-134.

Dikeakos JD, Mercure C, Lacombe MJ, Seidah NG, Reudelhuber TL. (2007). "PC1/3, PC2 and PC5/6A are targeted to dense core secretory granules by a common mechanism." Febs J **274**(16): 4094-4102.

Dikeakos JD, Reudelhuber TL. (2007). "Sending proteins to dense core secretory granules: still a lot to sort out." J. Cell Biol. **177**(2): 191-196.

Dikeakos JD, Di Lello P, Lacombe M-J, Ghirlando R, Legault P, Reudelhuber TL, Omichinski JG. (2009). "Functional and structural characterization of a dense core secretory granule sorting domain from the PC1/3 protease." Proc. Natl. Acad. Sci. U. S. A. **106**(18): 7408-7413.

Dix MM, Simon GM, Cravatt BF. (2008). "Global mapping of the topography and magnitude of proteolytic events in apoptosis." Cell **134**(4): 679-691.

Dores RM, Baron AJ. (2011). "Evolution of POMC: origin, phylogeny, posttranslational processing, and the melanocortins." Ann. N. Y. Acad. Sci. **1220**: 34-48.

Doria M, Salcini AE, Colombo E, Parslow TG, Pelicci PG, Di Fiore PP. (1999). "The eps15 homology (EH) domain-based interaction between eps15 and hrb connects the molecular machinery of endocytosis to that of nucleocytosolic transport." J. Cell Biol. **147**(7): 1379-1384.

Dreyer GB, Metcalf BW, Tomaszek TA, Jr., Carr TJ, Chandler AC, 3rd, Hyland L, Fakhoury SA, Magaard VW, Moore ML, Strickler JE, et al. (1989). "Inhibition of human immunodeficiency virus 1 protease in vitro: rational design of substrate analogue inhibitors." Proc. Natl. Acad. Sci. U. S. A. **86**(24): 9752-9756.

Dubois CM, Blanchette F, Laprise MH, Leduc R, Grondin F, Seidah NG. (2001). "Evidence that furin is an authentic transforming growth factor-beta1-converting enzyme." Am. J. Pathol. **158**(1): 305-316.

Edwards DR, Handsley MM, Pennington CJ. (2008). "The ADAM metalloproteinases." Mol. Aspects Med. **29**(5): 258-289.

Ehrchen JM, Sunderkotter C, Foell D, Vogl T, Roth J. (2009). "The endogenous Toll-like receptor 4 agonist S100A8/S100A9 (calprotectin) as innate amplifier of infection, autoimmunity, and cancer." J. Leukoc. Biol. **86**(3): 557-566.

Elagoz A, Benjannet S, Mammarbassi A, Wickham L, Seidah NG. (2002). "Biosynthesis and cellular trafficking of the convertase SKI-1/S1P: ectodomain shedding requires SKI-1 activity." J. Biol. Chem. **277**(13): 11265-11275.

Elgert KD. (2009). Immunology: Understanding The Immune System, John Wiley & Sons.

Essalmani R, Zaid A, Marcinkiewicz J, Chamberland A, Pasquato A, Seidah NG, Prat A. (2008). "In vivo functions of the proprotein convertase PC5/6 during mouse development: Gdf11 is a likely substrate." Proc. Natl. Acad. Sci. U. S. A. **105**(15): 5750-5755.

Fanjul-Fernandez M, Folgueras AR, Cabrera S, Lopez-Otin C. (2010). "Matrix metalloproteinases: evolution, gene regulation and functional analysis in mouse models." Biochim. Biophys. Acta **1803**(1): 3-19.

Farooqi IS, Volders K, Stanhope R, Heuschkel R, White A, Lank E, Keogh J, O'Rahilly S, Creemers JWM. (2007). "Hyperphagia and early-onset obesity due to a novel homozygous missense mutation in prohormone convertase 1/3." J. Clin. Endocrinol. Metab. **92**(9): 3369-3373.

Feliciangeli S, Kitabgi P, Bidard JN. (2001). "The role of dibasic residues in prohormone sorting to the regulated secretory pathway. A study with proneurotensin." J. Biol. Chem. **276**(9): 6140-6150.

Feliciangeli SF, Thomas L, Scott GK, Subbian E, Hung CH, Molloy SS, Jean F, Shinde U, Thomas G. (2006). "Identification of a pH sensor in the furin propeptide that regulates enzyme activation." J. Biol. Chem. **281**(23): 16108-16116.

Fiorentino DF, Zlotnik A, Mosmann T, Howard M, O'garra A. (1991). "IL-10 inhibits cytokine production by activated macrophages." J. Immunol. **147**(11): 3815.

Follis KE, York J, Nunberg JH. (2006). "Furin cleavage of the SARS coronavirus spike glycoprotein enhances cell-cell fusion but does not affect virion entry." Virology **350**(2): 358-369.

Friesenhagen J, Boergeling Y, Hrincius E, Ludwig S, Roth J, Viemann D. (2012). "Highly pathogenic avian influenza viruses inhibit effective immune responses of human blood-derived macrophages." J. Leukoc. Biol. **92**(1): 11-20.

Fugere M, Limperis PC, Beaulieu-Audy V, Gagnon F, Lavigne P, Klarskov K, Leduc R, Day R. (2002). "Inhibitory potency and specificity of subtilase-like pro-protein convertase (SPC) prodomains." J. Biol. Chem. **277**(10): 7648-7656.

Fugere M, Day R. (2005). "Cutting back on pro-protein convertases: the latest approaches to pharmacological inhibition." Trends Pharmacol. Sci. **26**(6): 294-301.

Fugere M, Appel J, Houghten RA, Lindberg I, Day R. (2007). "Short polybasic peptide sequences are potent inhibitors of PC5/6 and PC7: Use of positional scanning-synthetic peptide combinatorial libraries as a tool for the optimization of inhibitory sequences." Mol. Pharmacol. **71**(1): 323-332.

Fukuyama S, Kawaoka Y. (2011). "The pathogenesis of influenza virus infections: the contributions of virus and host factors." Curr. Opin. Immunol. **23**(4): 481-486.

Furuta M, Yano H, Zhou A, Rouillé Y, Holst JJ, Carroll R, Ravazzola M, Orci L, Furuta H, Steiner DF. (1997). "Defective prohormone processing and altered pancreatic islet morphology in mice lacking active SPC2." Proc. Natl. Acad. Sci. U. S. A. **94**(13): 6646-6651.

Furuta M, Zhou A, Webb G, Carroll R, Ravazzola M, Orci L, Steiner DF. (2001). "Severe defect in proglucagon processing in islet A-cells of prohormone convertase 2 null mice." J. Biol. Chem. **276**(29): 27197-27202.

Garred O, van Deurs B, Sandvig K. (1995). "Furin-induced cleavage and activation of Shiga toxin." J. Biol. Chem. **270**(18): 10817-10821.

Gauthier DJ, Sobota JA, Ferraro F, Mains RE, Lazure C. (2008). "Flow cytometry-assisted purification and proteomic analysis of the corticotropes dense-core secretory granules." Proteomics **8**(18): 3848-3861.

Gil-Torregrosa BC, Raul Castano A, Del Val M. (1998). "Major histocompatibility complex class I viral antigen processing in the secretory pathway defined by the trans-Golgi network protease furin." J. Exp. Med. **188**(6): 1105-1116.

Gil-Torregrosa BC, Castano AR, Lopez D, Del Val M. (2000). "Generation of MHC class I peptide antigens by protein processing in the secretory route by furin." Traffic **1**(8): 641-651.

Giordano RJ, Cardo-Vila M, Salameh A, Anobom CD, Zeitlin BD, Hawke DH, Valente AP, Almeida FC, Nor JE, Sidman RL, Pasqualini R, Arap W. (2010). "From combinatorial peptide selection to drug prototype (I): targeting the vascular endothelial growth factor receptor pathway." Proc. Natl. Acad. Sci. U. S. A. **107**(11): 5112-5117.

Glickman MH, Ciechanover A. (2002). "The ubiquitin-proteasome proteolytic pathway: destruction for the sake of construction." Physiol. Rev. **82**(2): 373-428.

Glish GL, Vachet RW. (2003). "The basics of mass spectrometry in the twenty-first century." Nat Rev Drug Discov **2**(2): 140-150.

Gluschankof P, Fuller RS. (1994). "A C-terminal domain conserved in precursor processing proteases is required for intramolecular N-terminal maturation of pro-Kex2 protease." EMBO J. **13**(10): 2280-2288.

Gonzalez-Rey E. (2010). "Keeping the balance between immune tolerance and pathogen immunity with endogenous neuropeptides." Neuroimmunomodulation **17**(3): 161-164.

Gordon VM, Rehemtulla A, Leppla SH. (1997). "A role for PACE4 in the proteolytic activation of anthrax toxin protective antigen." Infect. Immun. **65**(8): 3370-3375.

Grivennikov SI, Greten FR, Karin M. (2010). "Immunity, inflammation, and cancer." Cell **140**(6): 883-899.

Gross JH, Roepstorff P. (2011). Mass Spectrometry: A Textbook, Springer.

Gu M, Gordon VM, Fitzgerald DJ, Leppla SH. (1996). "Furin regulates both the activation of Pseudomonas exotoxin A and the Quantity of the toxin receptor expressed on target cells." Infect. Immun. **64**(2): 524-527.

Gu R, Huang YX, Luo YJ. (2010). "Anxiety and feedback negativity." Psychophysiology **47**(5): 961-967.

Hajdin K, D'Alessandro V, Niggli FK, Schafer BW, Bernasconi M. (2010). "Furin targeted drug delivery for treatment of rhabdomyosarcoma in a mouse model." PLoS One **5**(5): e10445.

Hallenberger S, Bosch V, Angliker H, Shaw E, Klenk HD, Garten W. (1992). "Inhibition of furin-mediated cleavage activation of HIV-1 glycoprotein gp160." Nature **360**(6402): 358-361.

Han X, Aslanian A, Yates JR, 3rd. (2008). "Mass spectrometry for proteomics." Curr. Opin. Chem. Biol. **12**(5): 483-490.

Harrison SC. (2008). "Viral membrane fusion." Nat Struct Mol Biol **15**(7): 690-698.
Hatta M, Gao P, Halfmann P, Kawaoka Y. (2001). "Molecular basis for high virulence of Hong Kong H5N1 influenza A viruses." Science **293**(5536): 1840-1842.
Hatta M, Hatta Y, Kim JH, Watanabe S, Shinya K, Nguyen T, Lien PS, Le QM, Kawaoka Y. (2007). "Growth of H5N1 influenza A viruses in the upper respiratory tracts of mice." PLoS Pathog **3**(10): 1374-1379.
Hedstrom L. (2002). "Serine protease mechanism and specificity." Chem. Rev. **102**(12): 4501-4524.
Helmby H, Grencis RK. (2004). "Interleukin 1 plays a major role in the development of Th2-mediated immunity." Eur. J. Immunol. **34**(12): 3674-3681.
Hendrickson EL, Xia Q, Wang T, Leigh JA, Hackett M. (2006). "Comparison of spectral counting and metabolic stable isotope labeling for use with quantitative microbial proteomics." Analyst **131**(12): 1335-1341.
Henrich S, Cameron A, Bourenkov GP, Kiefersauer R, Huber R, Lindberg I, Bode W, Than ME. (2003). "The crystal structure of the proprotein processing proteinase furin explains its stringent specificity." Nat. Struct. Biol. **10**(7): 520-526.
Henrich S, Lindberg I, Bode W, Than ME. (2005). "Proprotein convertase models based on the crystal structures of furin and kexin: explanation of their specificity." J. Mol. Biol. **345**(2): 211-227.
Hilleman MR. (2002). "Realities and enigmas of human viral influenza: pathogenesis, epidemiology and control." Vaccine **20**(25-26): 3068-3087.
Horimoto T, Nakayama K, Smeekens SP, Kawaoka Y. (1994). "Proprotein-processing endoproteases PC6 and furin both activate hemagglutinin of virulent avian influenza viruses." J. Virol. **68**(9): 6074-6078.
Hosaka M, Nagahama M, Kim WS, Watanabe T, Hatsuzawa K, Ikemizu J, Murakami K, Nakayama K. (1991). "Arg-X-Lys/Arg-Arg motif as a signal for precursor cleavage catalyzed by furin within the constitutive secretory pathway." J. Biol. Chem. **266**(19): 12127-12130.
Hoshino A, Kowalska D, Jean F, Lazure C, Lindberg I. (2011). "Modulation of PC1/3 activity by self-interaction and substrate binding." Endocrinology **152**(4): 1402-1411.
Hou JC, Min L, Pessin JE. (2009). "Insulin granule biogenesis, trafficking and exocytosis." Vitam. Horm. **80**: 473-506.
Hutagalung AH, Novick PJ. (2011). "Role of Rab GTPases in membrane traffic and cell physiology." Physiol. Rev. **91**(1): 119-149.
Icimoto MY, Barros NM, Ferreira JC, Marcondes MF, Andrade D, Machado MF, Juliano MA, Judice WA, Juliano L, Oliveira V. (2011). "Hysteretic behavior of proprotein convertase 1/3 (PC1/3)." PLoS One **6**(9): e24545.
Inocencio NM, Moehring JM, Moehring TJ. (1994). "Furin activates Pseudomonas exotoxin A by specific cleavage in vivo and in vitro." J. Biol. Chem. **269**(50): 31831-31835.
Jackson RS, Creemers JW, Ohagi S, Raffin-Sanson ML, Sanders L, Montague CT, Hutton JC, O'Rahilly S. (1997). "Obesity and impaired prohormone processing associated with mutations in the human prohormone convertase 1 gene." Nat. Genet. **16**(3): 303-306.
Jean F, Basak A, Rondeau N, Benjannet S, Hendy GN, Seidah NG, Chretien M, Lazure C. (1993). "Enzymic characterization of murine and human prohormone convertase-1

(mPC1 and hPC1) expressed in mammalian GH4C1 cells." Biochem. J. **292 (Pt 3)**: 891-900.

Jean F, Stella K, Thomas L, Liu G, Xiang Y, Reason AJ, Thomas G. (1998). "alpha1-Antitrypsin Portland, a bioengineered serpin highly selective for furin: application as an antipathogenic agent." Proc. Natl. Acad. Sci. U. S. A. **95**(13): 7293-7298.

Jean F, Thomas L, Molloy SS, Liu G, Jarvis MA, Nelson JA, Thomas G. (2000). "A protein-based therapeutic for human cytomegalovirus infection." Proc. Natl. Acad. Sci. U. S. A. **97**(6): 2864-2869.

Jiao GS, Cregar L, Wang J, Millis SZ, Tang C, O'Malley S, Johnson AT, Sareth S, Larson J, Thomas G. (2006). "Synthetic small molecule furin inhibitors derived from 2,5-dideoxystreptamine." Proc. Natl. Acad. Sci. U. S. A. **103**(52): 19707-19712.

Johnson RS, Martin SA, Biemann K, Stults JT, Watson JT. (1987). "Novel fragmentation process of peptides by collision-induced decomposition in a tandem mass spectrometer: differentiation of leucine and isoleucine." Anal. Chem. **59**(21): 2621-2625.

Julius D, Brake A, Blair L, Kunisawa R, Thorner J. (1984). "Isolation of the putative structural gene for the lysine-arginine-cleaving endopeptidase required for processing of yeast prepro-alpha-factor." Cell **37**(3): 1075-1089.

Jutras I, Seidah NG, Reudelhuber TL, Brechler V. (1997). "Two activation states of the prohormone convertase PC1 in the secretory pathway." J. Biol. Chem. **272**(24): 15184-15188.

Karicherla P, Hobden JA. (2009). "Nona-D-arginine therapy for Pseudomonas aeruginosa keratitis." Invest. Ophthalmol. Vis. Sci. **50**(1): 256-262.

Karicherla P, Aras S, Aiyar A, Hobden JA. (2010). "Nona-D-arginine amide suppresses corneal cytokines in Pseudomonas aeruginosa keratitis." Cornea **29**(11): 1308-1314.

Karicherla P, Hobden JA. (2010). "Nona-D-arginine amide for prophylaxis and treatment of experimental Pseudomonas aeruginosa keratitis." Curr. Eye Res. **35**(3): 220-224.

Karpala AJ, Bingham J, Schat KA, Chen LM, Donis RO, Lowenthal JW, Bean AG. (2011). "Highly pathogenic (H5N1) avian influenza induces an inflammatory T helper type 1 cytokine response in the chicken." J. Interferon Cytokine Res. **31**(4): 393-400.

Kawaguchi A, Nagata K. (2006). "[Molecular mechanism of replication and transcription of the influenza virus genome and host factors]." Uirusu **56**(1): 99-108.

Kawai T, Akira S. (2007). "TLR signaling." Semin. Immunol. **19**(1): 24-32.

Keepers TR, Psotka MA, Gross LK, Obrig TG. (2006). "A murine model of HUS: Shiga toxin with lipopolysaccharide mimics the renal damage and physiologic response of human disease." J. Am. Soc. Nephrol. **17**(12): 3404-3414.

Khoury GA, Baliban RC, Floudas CA. (2011). "Proteome-wide post-translational modification statistics: frequency analysis and curation of the swiss-prot database." Sci Rep **1**.

Kim W, Essalmani R, Szumska D, Creemers JW, Roebroek AJ, D'Orleans-Juste P, Bhattacharya S, Seidah NG, Prat A. (2012). "Loss of endothelial furin leads to cardiac malformation and early postnatal death." Mol. Cell. Biol. **32**(17): 3382-3391.

Klenk HD, Rott R, Orlich M. (1977). "Further studies on the activation of influenza virus by proteolytic cleavage of the haemagglutinin." J. Gen. Virol. **36**(1): 151-161.

Klimpel KR, Molloy SS, Thomas G, Leppla SH. (1992). "Anthrax toxin protective antigen is activated by a cell surface protease with the sequence specificity and catalytic properties of furin." Proc. Natl. Acad. Sci. U. S. A. **89**(21): 10277-10281.

Komiyama T, Coppola JM, Larsen MJ, van Dort ME, Ross BD, Day R, Rehemtulla A, Fuller RS. (2009). "Inhibition of furin/proprotein convertase-catalyzed surface and intracellular processing by small molecules." J. Biol. Chem. **284**(23): 15729-15738.

Korn T, Bettelli E, Oukka M, Kuchroo VK. (2009). "IL-17 and Th17 Cells." Annu. Rev. Immunol. **27**: 485-517.

Kowalska D, Liu J, Appel JR, Ozawa A, Nefzi A, Mackin RB, Houghten RA, Lindberg I. (2009). "Synthetic small-molecule prohormone convertase 2 inhibitors." Mol. Pharmacol. **75**(3): 617-625.

Kuliawat R, Prabakaran D, Arvan P. (2000). "Proinsulin endoproteolysis confers enhanced targeting of processed insulin to the regulated secretory pathway." Mol. Biol. Cell **11**(6): 1959-1972.

Kuo CT, Leiden JM. (1999). "Transcriptional regulation of T lymphocyte development and function." Annu. Rev. Immunol. **17**: 149-187.

Lamb RA, Takeda M. (2001). "Death by influenza virus protein." Nat. Med. **7**(12): 1286-1288.

LaMendola J, Martin SK, Steiner DF. (1997). "Expression of PC3, carboxypeptidase E and enkephalin in human monocyte-derived macrophages as a tool for genetic studies." FEBS Lett. **404**(1): 19-22.

Lansac G, Dong W, Dubois CM, Benlarbi N, Afonso C, Fournier I, Salzet M, Day R. (2006). "Lipopolysaccharide mediated regulation of neuroendocrine associated proprotein convertases and neuropeptide precursor processing in the rat spleen." J. Neuroimmunol. **171**(1-2): 57-71.

Lasaga M, Debeljuk L, Durand D, Scimonelli TN, Caruso C. (2008). "Role of alpha-melanocyte stimulating hormone and melanocortin 4 receptor in brain inflammation." Peptides **29**(10): 1825-1835.

Laurent V, Jaubert-Miazza L, Desjardins R, Day R, Lindberg I. (2004). "Biosynthesis of proopiomelanocortin-derived peptides in prohormone convertase 2 and 7B2 null mice." Endocrinology **145**(2): 519-528.

Lea N, Lord JM, Roberts LM. (1999). "Proteolytic cleavage of the A subunit is essential for maximal cytotoxicity of Escherichia coli O157:H7 Shiga-like toxin-1." Microbiology **145 (Pt 5)**: 999-1004.

Leduc R, Molloy SS, Thorne BA, Thomas G. (1992). "Activation of human furin precursor processing endoprotease occurs by an intramolecular autoproteolytic cleavage." J. Biol. Chem. **267**(20): 14304-14308.

Leitner A, Lindner W. (2009). "Chemical tagging strategies for mass spectrometry-based phospho-proteomics." Methods Mol. Biol. **527**: 229-243, x.

Lemeer S, Hahne H, Pachl F, Kuster B. (2012). "Software tools for MS-based quantitative proteomics: a brief overview." Methods Mol. Biol. **893**: 489-499.

Leonhardt RM, Fiegl D, Rufer E, Karger A, Bettin B, Knittler MR. (2010). "Post-endoplasmic reticulum rescue of unstable MHC class I requires proprotein convertase PC7." J. Immunol. **184**(6): 2985-2998.

Levesque C, Fugere M, Kwiatkowska A, Couture F, Desjardins R, Routhier S, Moussette P, Prahl A, Lammek B, Appel JR, Houghten RA, D'Anjou F, Dory YL, Neugebauer W, Day R. (2012). "The Multi-Leu Peptide Inhibitor Discriminates Between

PACE4 And Furin And Exhibits Antiproliferative Effects On Prostate Cancer Cells." J. Med. Chem.

Li CH, Barnafi L, Chretien M, Chung D. (1965). "Isolation and amino-acid sequence of beta-LPH from sheep pituitary glands." Nature **208**(5015): 1093-1094.

Li M, Nakayama K, Shuto Y, Somogyvari-Vigh A, Arimura A. (1998). "Testis-specific prohormone convertase PC4 processes the precursor of pituitary adenylate cyclase-activating polypeptide (PACAP)." Peptides **19**(2): 259-268.

Li M, Mbikay M, Nakayama K, Miyata A, Arimura A. (2000). "Prohormone convertase PC4 processes the precursor of PACAP in the testis." Ann. N. Y. Acad. Sci. **921**: 333-339.

Lin H, Ah Kioon MD, Lalou C, Larghero J, Launay JM, Khatib AM, Cohen-Solal M. (2012). "Protective role of systemic furin in immune response-induced arthritis." Arthritis Rheum. **64**(9): 2878-2886.

Lindberg I. (1994). "Evidence for cleavage of the PC1/PC3 pro-segment in the endoplasmic reticulum." Mol. Cell. Neurosci. **5**(3): 263-268.

Lingnau K, Egyed A, Schellack C, Mattner F, Buschle M, Schmidt W. (2002). "Poly-L-arginine synergizes with oligodeoxynucleotides containing CpG-motifs (CpG-ODN) for enhanced and prolonged immune responses and prevents the CpG-ODN-induced systemic release of pro-inflammatory cytokines." Vaccine **20**(29-30): 3498-3508.

Liu J, Afroza H, Rader DJ, Jin W. (2010). "Angiopoietin-like protein 3 inhibits lipoprotein lipase activity through enhancing its cleavage by proprotein convertases." J. Biol. Chem. **285**(36): 27561-27570.

Lloyd DJ, Bohan S, Gekakis N. (2006). "Obesity, hyperphagia and increased metabolic efficiency in Pc1 mutant mice." Hum. Mol. Genet. **15**(11): 1884-1893.

Lopez-Otin C, Overall CM. (2002). "Protease degradomics: a new challenge for proteomics." Nat Rev Mol Cell Biol **3**(7): 509-519.

Lusson J, Benjannet S, Hamelin J, Savaria D, Chretien M, Seidah NG. (1997). "The integrity of the RRGDL sequence of the proprotein convertase PC1 is critical for its zymogen and C-terminal processing and for its cellular trafficking." Biochem. J. **326 (Pt 3)**: 737-744.

Madala PK, Tyndall JD, Nall T, Fairlie DP. (2010). "Update 1 of: Proteases universally recognize beta strands in their active sites." Chem. Rev. **110**(6): PR1-31.

Malfait AM, Arner EC, Song RH, Alston JT, Markosyan S, Staten N, Yang Z, Griggs DW, Tortorella MD. (2008). "Proprotein convertase activation of aggrecanases in cartilage in situ." Arch. Biochem. Biophys. **478**(1): 43-51.

Malfait AM, Seymour AB, Gao F, Tortorella MD, Le Graverand-Gastineau MP, Wood LS, Doherty M, Doherty S, Zhang W, Arden NK, Vaughn FL, Leaverton PE, Spector TD, Hart DJ, Maciewicz RA, Muir KR, Das R, Sorge RE, Sotocinal SG, Schorscher-Petcu A, Valdes AM, Mogil JS. (2012). "A role for PACE4 in osteoarthritis pain: evidence from human genetic association and null mutant phenotype." Ann. Rheum. Dis. **71**(6): 1042-1048.

Marchesi C, Essalmani R, Lemarie CA, Leibovitz E, Ebrahimian T, Paradis P, Seidah NG, Schiffrin EL, Prat A. (2011). "Inactivation of endothelial proprotein convertase 5/6 decreases collagen deposition in the cardiovascular system: role of fibroblast autophagy." J Mol Med (Berl) **89**(11): 1103-1111.

Mason JM. (2010). "Design and development of peptides and peptide mimetics as antagonists for therapeutic intervention." Future Medicinal Chemistry **2**(12): 1813-1822.

Mbikay M, Tadros H, Ishida N, Lerner CP, De Lamirande E, Chen A, El-Alfy M, Clermont Y, Seidah NG, Chretien M, Gagnon C, Simpson EM. (1997). "Impaired fertility in mice deficient for the testicular germ-cell protease PC4." Proc. Natl. Acad. Sci. U. S. A. **94**(13): 6842-6846.

McClatchy DB, Yates JR, 3rd. (2008). "Stable Isotope Labeling of Mammals (SILAM)." CSH Protoc **2008**: pdb prot4940.

McDonald JL, D G. (2005). "Opioid receptors." Continuing Education in Anaesthesia, Critical Care & Pain **5**(1): 22-25.

Medzhitov R, Janeway CA, Jr. (1997). "Innate immunity: the virtues of a nonclonal system of recognition." Cell **91**(3): 295-298.

Medzhitov R. (2001). "Toll-like receptors and innate immunity." Nat Rev Immunol **1**(2): 135-145.

Molloy SS, Bresnahan PA, Leppla SH, Klimpel KR, Thomas G. (1992). "Human furin is a calcium-dependent serine endoprotease that recognizes the sequence Arg-X-X-Arg and efficiently cleaves anthrax toxin protective antigen." J. Biol. Chem. **267**(23): 16396-16402.

Morris CG, Maisto AA. (2004). Psychology: an introduction, Prentice Hall.

Mostafavi S, Morris Q. (2012). "Combining many interaction networks to predict gene function and analyze gene lists." Proteomics **12**(10): 1687-1696.

Muceniece R, Dambrova M. (2010). "Melanocortins in brain inflammation: the role of melanocortin receptor subtypes." Adv. Exp. Med. Biol. **681**: 61-70.

Mulcahy LR, Vaslet CA, Nillni EA. (2005). "Prohormone-convertase 1 processing enhances post-Golgi sorting of prothyrotropin-releasing hormone-derived peptides." J. Biol. Chem. **280**(48): 39818-39826.

Munster VJ, Schrauwen EJ, de Wit E, van den Brand JM, Bestebroer TM, Herfst S, Rimmelzwaan GF, Osterhaus AD, Fouchier RA. (2010). "Insertion of a multibasic cleavage motif into the hemagglutinin of a low-pathogenic avian influenza H6N1 virus induces a highly pathogenic phenotype." J. Virol. **84**(16): 7953-7960.

Murphy KP, Travers P, Walport M, Janeway C. (2008). Janeway's immunobiology, Garland Science.

Naffakh N, Tomoiu A, Rameix-Welti MA, van der Werf S. (2008). "Host restriction of avian influenza viruses at the level of the ribonucleoproteins." Annu. Rev. Microbiol. **62**: 403-424.

Nagata K, Kawaguchi A, Naito T. (2008). "Host factors for replication and transcription of the influenza virus genome." Rev Med Virol **18**(4): 247-260.

Neilson KA, Ali NA, Muralidharan S, Mirzaei M, Mariani M, Assadourian G, Lee A, van Sluyter SC, Haynes PA. (2011). "Less label, more free: approaches in label-free quantitative mass spectrometry." Proteomics **11**(4): 535-553.

Nour N, Mayer G, Mort JS, Salvas A, Mbikay M, Morrison CJ, Overall CM, Seidah NG. (2005). "The cysteine-rich domain of the secreted proprotein convertases PC5A and PACE4 functions as a cell surface anchor and interacts with tissue inhibitors of metalloproteinases." Mol. Biol. Cell **16**(11): 5215-5226.

Okumura Y, Takahashi E, Yano M, Ohuchi M, Daidoji T, Nakaya T, Böttcher E, Garten W, Klenk H-D, Kido H. (2010). "Novel type II transmembrane serine proteases,

MSPL and TMPRSS13, proteolytically activate membrane fusion activity of hemagglutinin of highly pathogenic avian influenza viruses and induce their multicycle replication." J. Virol.

Old WM, Meyer-Arendt K, Aveline-Wolf L, Pierce KG, Mendoza A, Sevinsky JR, Resing KA, Ahn NG. (2005). "Comparison of label-free methods for quantifying human proteins by shotgun proteomics." Mol Cell Proteomics **4**(10): 1487-1502.

Ong SE, Foster LJ, Mann M. (2003). "Mass spectrometric-based approaches in quantitative proteomics." Methods **29**(2): 124-130.

Ozden S, Lucas-Hourani M, Ceccaldi PE, Basak A, Valentine M, Benjannet S, Hamelin J, Jacob Y, Mamchaoui K, Mouly V, Despres P, Gessain A, Butler-Browne G, Chretien M, Tangy F, Vidalain PO, Seidah NG. (2008). "Inhibition of Chikungunya virus infection in cultured human muscle cells by furin inhibitors: impairment of the maturation of the E2 surface glycoprotein." J. Biol. Chem. **283**(32): 21899-21908.

Pan H, Che F-Y, Peng B, Steiner DF, Pintar JE, Fricker LD. (2006). "The role of prohormone convertase-2 in hypothalamic neuropeptide processing: a quantitative neuropeptidomic study." J. Neurochem. **98**(6): 1763-1777.

Parks WC, Wilson CL, Lopez-Boado YS. (2004). "Matrix metalloproteinases as modulators of inflammation and innate immunity." Nat Rev Immunol **4**(8): 617-629.

Peinado JR, Laurent V, Lee SN, Peng BW, Pintar JE, Steiner DF, Lindberg I. (2005). "Strain-dependent influences on the hypothalamo-pituitary-adrenal axis profoundly affect the 7B2 and PC2 null phenotypes." Endocrinology **146**(8): 3438-3444.

Peiris JS, Cheung CY, Leung CY, Nicholls JM. (2009). "Innate immune responses to influenza A H5N1: friend or foe?" Trends immunol **30**(12): 574-584.

Peiris JS, Hui KP, Yen HL. (2010). "Host response to influenza virus: protection versus immunopathology." Curr. Opin. Immunol. **22**(4): 475-481.

Perdue ML, Suarez DL. (2000). "Structural features of the avian influenza virus hemagglutinin that influence virulence." Vet. Microbiol. **74**(1-2): 77-86.

Pesu M, Muul L, Kanno Y, O'Shea JJ. (2006). "Proprotein convertase furin is preferentially expressed in T helper 1 cells and regulates interferon gamma." Blood **108**(3): 983-985.

Pesu M, Watford WT, Wei L, Xu L, Fuss I, Strober W, Andersson J, Shevach EM, Quezado M, Bouladoux N, Roebroek A, Belkaid Y, Creemers J, O'Shea JJ. (2008). "T-cell-expressed proprotein convertase furin is essential for maintenance of peripheral immune tolerance." Nature **455**(7210): 246-250.

Pienta KJ, Abate-Shen C, Agus DB, Attar RM, Chung LW, Greenberg NM, Hahn WC, Isaacs JT, Navone NM, Peehl DM, Simons JW, Solit DB, Soule HR, VanDyke TA, Weber MJ, Wu L, Vessella RL. (2008). "The current state of preclinical prostate cancer animal models." Prostate **68**(6): 629-639.

Piper DE, Jackson S, Liu Q, Romanow WG, Shetterly S, Thibault ST, Shan B, Walker NP. (2007). "The crystal structure of PCSK9: a regulator of plasma LDL-cholesterol." Structure **15**(5): 545-552.

Plaimauer B, Mohr G, Wernhart W, Himmelspach M, Dorner F, Schlokat U. (2001). "'Shed' furin: mapping of the cleavage determinants and identification of its C-terminus." Biochem. J. **354**(Pt 3): 689-695.

Prudova A, auf dem Keller U, Butler GS, Overall CM. (2010). "Multiplex N-terminome analysis of MMP-2 and MMP-9 substrate degradomes by iTRAQ-TAILS quantitative proteomics." Mol Cell Proteomics **9**(5): 894-911.

Puente XS, Sanchez LM, Overall CM, Lopez-Otin C. (2003). "Human and mouse proteases: a comparative genomic approach." Nat Rev Genet **4**(7): 544-558.

Qian WJ, Liu T, Monroe ME, Strittmatter EF, Jacobs JM, Kangas LJ, Petritis K, Camp DG, 2nd, Smith RD. (2005). "Probability-based evaluation of peptide and protein identifications from tandem mass spectrometry and SEQUEST analysis: the human proteome." J Proteome Res **4**(1): 53-62.

Rabah N, Gauthier D, Dikeakos JD, Reudelhuber TL, Lazure C. (2007). "The C-terminal region of the proprotein convertase 1/3 (PC1/3) exerts a bimodal regulation of the enzyme activity in vitro." Febs J **274**(13): 3482-3491.

Raiborg C, Rusten TE, Stenmark H. (2003). "Protein sorting into multivesicular endosomes." Curr. Opin. Cell Biol. **15**(4): 446-455.

Rawlings ND, Barrett AJ, Bateman A. (2012). "MEROPS: the database of proteolytic enzymes, their substrates and inhibitors." Nucleic Acids Res **40**(Database issue): D343-350.

Remacle AG, Shiryaev SA, Oh ES, Cieplak P, Srinivasan A, Wei G, Liddington RC, Ratnikov BI, Parent A, Desjardins R, Day R, Smith JW, Lebl M, Strongin AY. (2008). "Substrate Cleavage Analysis of Furin and Related Proprotein Convertases: A COMPARATIVE STUDY." J. Biol. Chem. **283**(30): 20897-20906.

Remacle AG, Gawlik K, Golubkov VS, Cadwell GW, Liddington RC, Cieplak P, Millis SZ, Desjardins R, Routhier S, Yuan XW, Neugebauer WA, Day R, Strongin AY. (2010). "Selective and potent furin inhibitors protect cells from anthrax without significant toxicity." Int. J. Biochem. Cell Biol. **42**(6): 987-995.

Richards RM, Lowy DR, Schiller JT, Day PM. (2006). "Cleavage of the papillomavirus minor capsid protein, L2, at a furin consensus site is necessary for infection." Proc. Natl. Acad. Sci. U. S. A. **103**(5): 1522-1527.

Robertus JD, Kraut J, Alden RA, Birktoft JJ. (1972). "Subtilisin; a stereochemical mechanism involving transition-state stabilization." Biochemistry (Mosc). **11**(23): 4293-4303.

Robinson DR, Wu YM, Lin SF. (2000). "The protein tyrosine kinase family of the human genome." Oncogene **19**(49): 5548-5557.

Roebroek AJ, Umans L, Pauli IG, Robertson EJ, van Leuven F, Van de Ven WJ, Constam DB. (1998). "Failure of ventral closure and axial rotation in embryos lacking the proprotein convertase Furin." Development **125**(24): 4863-4876.

Roebroek AJ, Taylor NA, Louagie E, Pauli I, Smeijers L, Snellinx A, Lauwers A, Van de Ven WJ, Hartmann D, Creemers JW. (2004). "Limited redundancy of the proprotein convertase furin in mouse liver." J. Biol. Chem. **279**(51): 53442-53450.

Rojek JM, Pasqual G, Sanchez AB, Nguyen NT, de la Torre JC, Kunz S. (2010). "Targeting the proteolytic processing of the viral glycoprotein precursor is a promising novel antiviral strategy against arenaviruses." J. Virol. **84**(1): 573-584.

Rousselet E, Benjannet S, Hamelin J, Canuel M, Seidah NG. (2011). "The proprotein convertase PC7: unique zymogen activation and trafficking pathways." J. Biol. Chem. **286**(4): 2728-2738.

Ruzza P. (2012). Peptides and Peptidomimetics in Medicinal Chemistry. Medicinal Chemistry and Drug Design. D. Ekinci, InTech**:** 406.

Salomon R, Webster RG. (2009). "The influenza virus enigma." Cell **136**(3): 402-410.
Salzet M, Tasiemski A. (2001). "Involvement of pro-enkephalin-derived peptides in immunity." Dev. Comp. Immunol. **25**(3): 177-185.
Sandvig K. (2001). "Shiga toxins." Toxicon **39**(11): 1629-1635.
Saravia F, Ase A, Aloyz R, Kleid MC, Ines M, Vida R, Nahmod VE, Vindrola O. (1993). "Differential posttranslational processing of proenkephalin in rat bone marrow and spleen mononuclear cells: evidence for synenkephalin cleavage." Endocrinology **132**(4): 1431-1437.
Saravia F, Padros MR, Ase A, Aloyz R, Duran S, Vindrola O. (1998). "Differential response to a stress stimulus of proenkephalin peptide content in immune cells of naive and chronically stressed rats." Neuropeptides **32**(4): 351-359.
Scamuffa N, Siegfried G, Bontemps Y, Ma L, Basak A, Cherel G, Calvo F, Seidah NG, Khatib AM. (2008). "Selective inhibition of proprotein convertases represses the metastatic potential of human colorectal tumor cells." J. Clin. Invest. **118**(1): 352-363.
Schechter I, Berger A. (1967). "On the size of the active site in proteases. I. Papain." Biochem. Biophys. Res. Commun. **27**(2): 157-162.
Schluesener HJ, Su Y, Ebrahimi A, Pouladsaz D. (2012). "Antimicrobial peptides in the brain: neuropeptides and amyloid." Front Biosci (Schol Ed) **4**: 1375-1380.
Schroder K, Hertzog PJ, Ravasi T, Hume DA. (2004). "Interferon-gamma: an overview of signals, mechanisms and functions." J. Leukoc. Biol. **75**(2): 163-189.
Scott MJ, Godshall CJ, Cheadle WG. (2002). "Jaks, STATs, Cytokines, and Sepsis." Clin. Diagn. Lab. Immunol. **9**(6): 1153-1159.
Searle BC. (2010). "Scaffold: a bioinformatic tool for validating MS/MS-based proteomic studies." Proteomics **10**(6): 1265-1269.
Seidah NG, Day R, Hamelin J, Gaspar A, Collard MW, Chretien M. (1992). "Testicular expression of PC4 in the rat: molecular diversity of a novel germ cell-specific Kex2/subtilisin-like proprotein convertase." Mol. Endocrinol. **6**(10): 1559-1570.
Seidah NG, Hamelin J, Mamarbachi M, Dong W, Tardos H, Mbikay M, Chretien M, Day R. (1996). "cDNA structure, tissue distribution, and chromosomal localization of rat PC7, a novel mammalian proprotein convertase closest to yeast kexin-like proteinases." Proc. Natl. Acad. Sci. U. S. A. **93**(8): 3388-3393.
Seidah NG, Benjannet S, Hamelin J, Mamarbachi AM, Basak A, Marcinkiewicz J, Mbikay M, Chretien M, Marcinkiewicz M. (1999a). "The subtilisin/kexin family of precursor convertases. Emphasis on PC1, PC2/7B2, POMC and the novel enzyme SKI-1." Ann. N. Y. Acad. Sci. **885**: 57-74.
Seidah NG, Chretien M. (1999). "Proprotein and prohormone convertases: a family of subtilases generating diverse bioactive polypeptides." Brain Res. **848**(1-2): 45-62.
Seidah NG, Mowla SJ, Hamelin J, Mamarbachi AM, Benjannet S, Toure BB, Basak A, Munzer JS, Marcinkiewicz J, Zhong M, Barale JC, Lazure C, Murphy RA, Chretien M, Marcinkiewicz M. (1999b). "Mammalian subtilisin/kexin isozyme SKI-1: A widely expressed proprotein convertase with a unique cleavage specificity and cellular localization." Proc. Natl. Acad. Sci. U. S. A. **96**(4): 1321-1326.
Seidah NG, Benjannet S, Wickham L, Marcinkiewicz J, Jasmin SB, Stifani S, Basak A, Prat A, Chretien M. (2003). "The secretory proprotein convertase neural apoptosis-regulated convertase 1 (NARC-1): liver regeneration and neuronal differentiation." Proc. Natl. Acad. Sci. U. S. A. **100**(3): 928-933.

Seidah NG, Khatib AM, Prat A. (2006). "The proprotein convertases and their implication in sterol and/or lipid metabolism." Biol. Chem. **387**(7): 871-877.

Seidah NG, Mayer G, Zaid A, Rousselet E, Nassoury N, Poirier S, Essalmani R, Prat A. (2008). "The activation and physiological functions of the proprotein convertases." Int. J. Biochem. Cell Biol. **40**(6-7): 1111-1125.

Seidah NG. (2011). "The proprotein convertases, 20 years later." Methods Mol. Biol. **768**: 23-57.

Seidah NG, Prat A. (2012). "The biology and therapeutic targeting of the proprotein convertases." Nat Rev Drug Discov **11**(5): 367-383.

Shimazu R, Akashi S, Ogata H, Nagai Y, Fukudome K, Miyake K, Kimoto M. (1999). "MD-2, a molecule that confers lipopolysaccharide responsiveness on Toll-like receptor 4." J. Exp. Med. **189**(11): 1777-1782.

Shiryaev SA, Remacle AG, Ratnikov BI, Nelson NA, Savinov AY, Wei G, Bottini M, Rega MF, Parent A, Desjardins R, Fugere M, Day R, Sabet M, Pellecchia M, Liddington RC, Smith JW, Mustelin T, Guiney DG, Lebl M, Strongin AY. (2007). "Targeting host cell furin proprotein convertases as a therapeutic strategy against bacterial toxins and viral pathogens." J. Biol. Chem. **282**(29): 20847-20853.

Siezen RJ, Leunissen JA. (1997). "Subtilases: the superfamily of subtilisin-like serine proteases." Protein Sci. **6**(3): 501-523.

Sim RB, Tsiftsoglou SA. (2004). "Proteases of the complement system." Biochem. Soc. Trans. **32**(Pt 1): 21-27.

Smoot ME, Ono K, Ruscheinski J, Wang PL, Ideker T. (2011). "Cytoscape 2.8: new features for data integration and network visualization." Bioinformatics **27**(3): 431-432.

Spengler B, Hubert M, Kaufmann R. (1994). "MALDI ion imaging and biological ion imaging with a new scanning UV-laser microprobe." Proc. 42nd Annual Conf. Mass Spectrom. and Allied Topics: 1041.

Srour N, Lebel A, McMahon S, Fournier I, Fugere M, Day R, Dubois CM. (2003). "TACE/ADAM-17 maturation and activation of sheddase activity require proprotein convertase activity." FEBS Lett. **554**(3): 275-283.

Stawowy P, Fleck E. (2005). "Proprotein convertases furin and PC5: targeting atherosclerosis and restenosis at multiple levels." J Mol Med (Berl) **83**(11): 865-875.

Steiner DF. (1967). "Evidence for a precursor in the biosynthesis of insulin." Trans. N. Y. Acad. Sci. **30**(1): 60-68.

Steiner DF, Cunningham D, Spigelman L, Aten B. (1967). "Insulin biosynthesis: evidence for a precursor." Science **157**(3789): 697-700.

Steiner DF. (2011). "On the discovery of precursor processing." Methods Mol. Biol. **768**: 3-11.

Stieneke-Grober A, Vey M, Angliker H, Shaw E, Thomas G, Roberts C, Klenk HD, Garten W. (1992). "Influenza virus hemagglutinin with multibasic cleavage site is activated by furin, a subtilisin-like endoprotease." EMBO J. **11**(7): 2407-2414.

Suderman M, Hallett M. (2007). "Tools for visually exploring biological networks." Bioinformatics **23**(20): 2651-2659.

Sukharev SA, Pleshakova OV, Sadovnikov VB. (1997). "Role of proteases in activation of apoptosis." Cell Death Differ. **4**(6): 457-462.

Susan-Resiga D, Essalmani R, Hamelin J, Asselin MC, Benjannet S, Chamberland A, Day R, Szumska D, Constam D, Bhattacharya S, Prat A, Seidah NG. (2011). "Furin is the major processing enzyme of the cardiac-specific growth factor bone morphogenetic protein 10." J. Biol. Chem. **286**(26): 22785-22794.

Szklarczyk D, Franceschini A, Kuhn M, Simonovic M, Roth A, Minguez P, Doerks T, Stark M, Muller J, Bork P, Jensen LJ, von Mering C. (2011). "The STRING database in 2011: functional interaction networks of proteins, globally integrated and scored." Nucleic Acids Res **39**(Database issue): D561-568.

Szretter KJ, Gangappa S, Belser JA, Zeng H, Chen H, Matsuoka Y, Sambhara S, Swayne DE, Tumpey TM, Katz JM. (2009). "Early control of H5N1 influenza virus replication by the type I interferon response in mice." J. Virol. **83**(11): 5825-5834.

Szumska D, Pieles G, Essalmani R, Bilski M, Mesnard D, Kaur K, Franklyn A, El Omari K, Jefferis J, Bentham J, Taylor JM, Schneider JE, Arnold SJ, Johnson P, Tymowska-Lalanne Z, Stammers D, Clarke K, Neubauer S, Morris A, Brown SD, Shaw-Smith C, Cama A, Capra V, Ragoussis J, Constam D, Seidah NG, Prat A, Bhattacharya S. (2008). "VACTERL/caudal regression/Currarino syndrome-like malformations in mice with mutation in the proprotein convertase Pcsk5." Genes Dev. **22**(11): 1465-1477.

Taams LS, van Amelsfort JM, Tiemessen MM, Jacobs KM, de Jong EC, Akbar AN, Bijlsma JW, Lafeber FP. (2005). "Modulation of monocyte/macrophage function by human CD4+CD25+ regulatory T cells." Hum. Immunol. **66**(3): 222-230.

Takeda K, Kaisho T, Akira S. (2003). "Toll-like receptors." Annu. Rev. Immunol. **21**: 335-376.

Takeda K, Akira S. (2005). "Toll-like receptors in innate immunity." Int. Immunol. **17**(1): 1-14.

Taubenberger JK, Morens DM. (2008). "The pathology of influenza virus infections." Annu Rev Pathol **3**: 499-522.

Trinchieri G, Sher A. (2007). "Cooperation of Toll-like receptor signals in innate immune defence." Nat Rev Immunol **7**(3): 179-190.

Tscherne DM, Garcia-Sastre A. (2011). "Virulence determinants of pandemic influenza viruses." J. Clin. Invest. **121**(1): 6-13.

Tsuji A, Sakurai K, Kiyokage E, Yamazaki T, Koide S, Toida K, Ishimura K, Matsuda Y. (2003). "Secretory proprotein convertases PACE4 and PC6A are heparin-binding proteins which are localized in the extracellular matrix. Potential role of PACE4 in the activation of proproteins in the extracellular matrix." Biochim. Biophys. Acta **1645**(1): 95-104.

Tsuneoka M, Nakayama K, Hatsuzawa K, Komada M, Kitamura N, Mekada E. (1993). "Evidence for involvement of furin in cleavage and activation of diphtheria toxin." J. Biol. Chem. **268**(35): 26461-26465.

Turpeinen H, Raitoharju E, Oksanen A, Oksala N, Levula M, Lyytikainen LP, Jarvinen O, Creemers JW, Kahonen M, Laaksonen R, Pelto-Huikko M, Lehtimaki T, Pesu M. (2011). "Proprotein convertases in human atherosclerotic plaques: the overexpression of FURIN and its substrate cytokines BAFF and APRIL." Atherosclerosis **219**(2): 799-806.

Ueda K, Lipkind GM, Zhou A, Zhu X, Kuznetsov A, Philipson L, Gardner P, Zhang C, Steiner DF. (2003a). "Mutational analysis of predicted interactions between the

catalytic and P domains of prohormone convertase 3 (PC3/PC1)." Proc. Natl. Acad. Sci. U. S. A. **100**(10): 5622-5627.

Ueda K, Ohta Y, Hosoya H. (2003b). "The carboxy-terminal pleckstrin homology domain of ROCK interacts with filamin-A." Biochem. Biophys. Res. Commun. **301**(4): 886-890.

UniProt C. (2012). "Reorganizing the protein space at the Universal Protein Resource (UniProt)." Nucleic Acids Res **40**(Database issue): D71-75.

Vindrola O, Mayer AM, Citera G, Spitzer JA, Espinoza LR. (1994). "Prohormone convertases PC2 and PC3 in rat neutrophils and macrophages. Parallel changes with proenkephalin-derived peptides induced by LPS in vivo." Neuropeptides **27**(4): 235-244.

Vogt L, Schmitz N, Kurrer MO, Bauer M, Hinton HI, Behnke S, Gatto D, Sebbel P, Beerli RR, Sonderegger I, Kopf M, Saudan P, Bachmann MF. (2006). "VSIG4, a B7 family-related protein, is a negative regulator of T cell activation." J. Clin. Invest. **116**(10): 2817-2826.

Volchkov VE, Feldmann H, Volchkova VA, Klenk HD. (1998). "Processing of the Ebola virus glycoprotein by the proprotein convertase furin." Proc. Natl. Acad. Sci. U. S. A. **95**(10): 5762-5767.

Volchkov VE, Volchkova VA, Stroher U, Becker S, Dolnik O, Cieplik M, Garten W, Klenk HD, Feldmann H. (2000). "Proteolytic processing of Marburg virus glycoprotein." Virology **268**(1): 1-6.

Walker JA, Molloy SS, Thomas G, Sakaguchi T, Yoshida T, Chambers TM, Kawaoka Y. (1994). "Sequence specificity of furin, a proprotein-processing endoprotease, for the hemagglutinin of a virulent avian influenza virus." J. Virol. **68**(2): 1213-1218.

Walsh C. (2000). "Molecular mechanisms that confer antibacterial drug resistance." Nature **406**(6797): 775-781.

Walsh PN, Ahmad SS. (2002). "Proteases in blood clotting." Essays Biochem. **38**: 95-111.

Wardman JH, Zhang X, Gagnon S, Castro LM, Zhu X, Steiner DF, Day R, Fricker LD. (2010). "Analysis of peptides in prohormone convertase 1/3 null mouse brain using quantitative peptidomics." J. Neurochem. **114**(1): 215-225.

Watanabe M, Hirano A, Stenglein S, Nelson J, Thomas G, Wong TC. (1995). "Engineered serine protease inhibitor prevents furin-catalyzed activation of the fusion glycoprotein and production of infectious measles virus." J. Virol. **69**(5): 3206-3210.

Watts C. (2012). "The endosome-lysosome pathway and information generation in the immune system." Biochim. Biophys. Acta **1824**(1): 14-21.

Webby RJ, Webster RG. (2003). "Are we ready for pandemic influenza?" Science **302**(5650): 1519-1522.

Webster RG, Rott R. (1987). "Influenza virus A pathogenicity: the pivotal role of hemagglutinin." Cell **50**(5): 665-666.

Wells JA, Estell DA. (1988). "Subtilisin--an enzyme designed to be engineered." Trends Biochem. Sci. **13**(8): 291-297.

Whitley RJ. (2010). "Of ferrets and humans: influenza pathogenesis." J. Infect. Dis. **201**(7): 976-977.

Williams RA, Peterson AT. (2009). "Ecology and geography of avian influenza (HPAI H5N1) transmission in the Middle East and northeastern Africa." Int J Health Geogr **8**: 47.

Writing Committee of the Second World Health Organization Consultation on Clinical Aspects of Human Infection with Avian Influenza AV, Abdel-Ghafar AN, Chotpitayasunondh T, Gao Z, Hayden FG, Nguyen DH, de Jong MD, Naghdaliyev A, Peiris JS, Shindo N, Soeroso S, Uyeki TM. (2008). "Update on avian influenza A (H5N1) virus infection in humans." N. Engl. J. Med. **358**(3): 261-273.

Xiao Y, Chen G, Richard J, Rougeau N, Li H, Seidah NG, Cohen EA. (2008). "Cell-surface processing of extracellular human immunodeficiency virus type 1 Vpr by proprotein convertases." Virology **372**(2): 384-397.

Yamamoto T, Lu C, Ryan RO. (2011). "A two-step binding model of PCSK9 interaction with the low density lipoprotein receptor." J. Biol. Chem. **286**(7): 5464-5470.

Yates JR, Ruse CI, Nakorchevsky A. (2009). "Proteomics by mass spectrometry: approaches, advances, and applications." Annu Rev Biomed Eng **11**: 49-79.

Zambon MC. (2001). "The pathogenesis of influenza in humans." Rev Med Virol **11**(4): 227-241.

Zanoni I, Granucci F. (2009). "Dendritic cells and macrophages: same receptors but different functions." Curr Immunol Rev **5**: 311-325.

Zapala B, Kaczynski L, Kiec-Wilk B, Staszel T, Knapp A, Thoresen GH, Wybranska I, Dembinska-Kiec A. (2010). "Humanins, the neuroprotective and cytoprotective peptides with antiapoptotic and anti-inflammatory properties." Pharmacol Rep **62**(5): 767-777.

Zhang X, Fugere M, Day R, Kielian M. (2003). "Furin processing and proteolytic activation of Semliki Forest virus." J. Virol. **77**(5): 2981-2989.

Zhang X, Pan H, Peng B, Steiner DF, Pintar JE, Fricker LD. (2010). "Neuropeptidomic analysis establishes a major role for prohormone convertase-2 in neuropeptide biosynthesis." J. Neurochem. **112**(5): 1168-1179.

Zhou A, Martin S, Lipkind G, LaMendola J, Steiner DF. (1998). "Regulatory roles of the P domain of the subtilisin-like prohormone convertases." J. Biol. Chem. **273**(18): 11107-11114.

Zhou A, Webb G, Zhu X, Steiner DF. (1999). "Proteolytic processing in the secretory pathway." J. Biol. Chem. **274**(30): 20745-20748.

Zhu X, Orci L, Carroll R, Norrbom C, Ravazzola M, Steiner DF. (2002a). "Severe block in processing of proinsulin to insulin accompanied by elevation of des-64,65 proinsulin intermediates in islets of mice lacking prohormone convertase 1/3." Proc. Natl. Acad. Sci. U. S. A. **99**(16): 10299-10304.

Zhu X, Zhou A, Dey A, Norrbom C, Carroll R, Zhang C, Laurent V, Lindberg I, Ugleholdt R, Holst JJ, Steiner DF. (2002b). "Disruption of PC1/3 expression in mice causes dwarfism and multiple neuroendocrine peptide processing defects." Proc. Natl. Acad. Sci. U. S. A. **99**(16): 10293-10298.

ANNEXES

Liste des publications

Publiées

Gagnon, H., Franck, J., Wisztorski, M., Day, R., Fournier, I., & Salzet, M. (2012). TARGETED MASS spectrometry Imaging: Specific Targeting Mass Spectrometry imaging technologies from history to perspective. *Progress in Histochemistry and Cytochemistry*, 1–42. doi:10.1016/j.proghi.2012.08.002

Refaie, S., Gagnon, S., Gagnon, H., Desjardins, R., D'Anjou, F., D'Orléans-Juste, P., Zhu, X., et al. (2012). Disruption of proprotein convertase 1/3 (PC1/3) expression in mice causes innate immune defects and uncontrolled cytokine secretion. *Journal of Biological Chemistry*, *287*(18), 14703–14717. doi:10.1074/jbc.M111.323220

Accepté

Dans Proteomics clinical application 2013

Proteomic analyses of serous and endometrioid epithelial ovarian cancers: cases studies :molecular insights of a possible histological etiology of serous ovarian cancer

Rémi Longuespée[*], Hugo Gagnon[*], Charlotte Boyon, Kurstin Strupat, Claire Dauly, Olivier Kerdraon[5], Adesuwa Ighodaro, Annie Desmons, Jocelyn Dupuis, Maxence Wisztorski, Denis Vinatier, Isabelle Fournier, Robert Day, Michel Salzet

Soumises

À PlosOne

Proprotein convertase 1/3 (PC1/3) in the rat alveolar macrophage cell line NR8383: localization, trafficking and effects on cytokine secretion

Hugo Gagnon, Sarah Refaie, Sandra Gagnon, Roxane Desjardins, Michel Salzet, Robert Day

À Journal of Medicinal Chemistry

Optimization of furin inhibitors to protect against the activation of influenza Hemagglutinin H5 and Shiga toxin.
Hugo Gagnon, Sophie Beauchemin, Anna Kwiatkowska, François D'Anjou, Frederic Couture, Christine Lévesque, Frederik Dufour, Adamy Roberge Desbiens, Rolland Vaillancourt, Sylvain Bernard, François Malouin, Yves L. Dory, Robert Day

Communications orales

Journée Phare 2011 (prix meilleur présentation par affiche de sa catégorie)
Rôle de PC1/3 dans l'immunité innée : une approche protéomique
Hugo Gagnon, Sandra Gagnon, Sarah Refaie, Claude Lazure, Michel Salzet et Robert Day.
Journée scientifique de la FMSS 2011
Rôle de PC1/3 dans l'immunité innée : une approche protéomique
Hugo Gagnon, Sandra Gagnon, Sarah Refaie, Claude Lazure, Michel Salzet et Robert Day.